Comparison of Rotliegend sandstone diagenesis from the northern and southern margin of the North German Basin, and implications for the importance of organic maturation and migration

Dissertation

zur Erlangung des akademischen Grades doctor rerum naturalium

(Dr. rer. nat.)

vorgelegt dem Rat der Chemisch-Geowissenschaftlichen Fakultät der Friedrich-Schiller-Universität Jena

von Dipl.-Geol. Robert Schöner

geboren am 11.01.1974 in München

Gutachter:

1. Prof. Dr. Reinhard Gaupp, Jena

2. Dr. Richard Worden, Liverpool

3. Prof. Dr. Lothar Viereck-Götte, Jena

Tag der öffentlichen Verteidigung: 08.03.2006

Abstract

Rotliegend sandstones (Permian) are important reservoir rocks in the North German Basin (NGB). The diagenetic evolution of these rocks is the result of fluid-rock interactions proceeding subsequent to deposition and during burial. Although Rotliegend diagenesis has been studied previously, the interactions of organic maturation products and red bed sandstones are still not well understood. Major objective of this study is to compare the diagenetic evolution of Rotliegend sandstones from areas with and without hydraulic contact to petroleum source rocks, and to evaluate the importance of organic maturation and migration for diagenetic mineral reactions. Target areas are the northern and the southern margin of the North German Basin (central part of the Central European Basin System), where Rotliegend sandstones were buried to about 3500-5200 m depth. Core and data material of three deep exploration wells from Schleswig-Holstein (northern basin margin) were used to carry out petrographic and geochemical investigations on Rotliegend sandstones, and to simulate burial and thermal evolution of source and reservoir rocks. Existing data sets from the southern basin margin (mainly the area north of Hannover) were compiled, re-evaluated, and complemented where necessary.

Petroleum source rocks are omnipresent beneath the Rotliegend of the southern basin margin, but absent in large parts of the northern study area. Local relics of Carboniferous shales at the northern margin of the NGB, containing low contents of organic carbon, were heated rapidly to temperatures of about 200°C in the Triassic. Minor oil generation was confined to a narrow time interval shortly after deposition of the Rotliegend. In contrast, thick coal-bearing Carboniferous source rocks at the southern basin margin produced CO_2, oil, and gas over long periods of time, starting in the Upper Carboniferous. Major generation of liquid hydrocarbons in upper source rock horizons (Westphalian) took place in Triassic to Early Jurassic times.

Early diagenetic processes are comparable at both basin margins. They include the formation of hematite and tangential illite grain coatings, minor quartz and albite, locally the growth of pore-lining Mg-rich chlorite, and abundant precipitation of pore-filling carbonate and sulphate cements. Early red bed diagenesis was mainly controlled by the depositional environment, and by the proximity to the basin margin. There are major differences in mesodiagenetic evolution between sandstones from the southern and northern study area. Eodiagenetic iron oxide grain coatings may have been preserved down to maximum burial depths, e.g. in the northern part of the NGB. At the southern basin margin, red beds were partly bleached by reduction and dissolution of hematite, and reduced iron was incorporated into chlorite and carbonate cements during burial diagenesis. Many Rotliegend sandstones of the southern basin margin were affected by major mesodiagenetic dissolution of unstable detrital grains (mainly feldspar) and intergranular cements (carbonates/sulphates). Dissolution was followed by pervasive formation of meshwork illite. Kaolinite/dickite precipitated locally in close proximity to Carboniferous source rocks. Clay minerals were impregnated by solid bitumen, which represent a relic of former liquid hydrocarbons. Illite growth took place in Late Triassic to Early Jurassic times, contemporaneously to the period of main oil generation in underlying source rocks. Locally, inter- and intragranular pore space was cemented by large volumes of late quartz. The spatial coincidence of these diagenetic patterns from the southern basin margin and their occurrence in Rotliegend sandstones with hydraulic contact to organic-rich source rocks suggest that they trace pathways of former petroleum migration. Apart from minor, very localised authigenic illite, these mesodiagenetic features are lacking in Rotliegend sandstones from the northern basin margin. Instead, relatively early cementation patterns are preserved down to maximum burial depths.

Results of diagenetic investigations and basin modelling indicate that major mesodiagenetic mineral reactions are related to the presence or absence of maturing petroleum source rocks. Reducing, hydrocarbon-bearing pore fluids were most likely responsible for bleaching of red beds. Leaching processes may have been caused by acidic, CO_2-bearing fluids, which were expelled during maturation of Carboniferous coals, or generated due to hydrocarbon oxidation within the red beds. K-feldspar dissolution provided the ions necessary for illite formation. Secondary pore space was partly filled by cements incorporating reduced iron. Such processes are apparently absent in areas, where red beds were not affected by petroleum migration during burial. The results of this study may help to interpret the diagenetic evolution of red bed sandstones, and migration pathways of organic maturation products in complex basin settings.

Kurzfassung

Rotliegend-Sandsteine (Perm) sind wichtige Speichergesteine des Norddeutschen Beckens (NDB). Die diagenetische Entwicklung dieser Gesteine ist die Folge von Fluid-Gesteins-Wechselwirkungen, die unmittelbar nach der Ablagerung der Sedimente und während ihrer Versenkung ablaufen. Obwohl die Diagenese des Rotliegenden bereits früher Gegenstand von Untersuchungen war, sind Wechselwirkungen zwischen organischen Reifungsprodukten und Rotfazies-Sandsteinen bisher nur unzureichend verstanden. Ziel der vorliegenden Studie ist es, die Diageneseentwicklung von Rotliegend-Sandsteinen mit und ohne hydraulischem Kontakt zu Kohlenwasserstoff-Muttergesteinen zu untersuchen, und die Bedeutung der organischen Reifung und Migration für diagenetische Mineralreaktionen zu bewerten. Die Arbeitsgebiete liegen am Nord- und Südrand des Norddeutschen Beckens (zentraler Teil des Zentraleuropäischen Beckensystems). Rotliegend-Sandsteine wurden in diesen Gebieten bis in etwa 3500-5200 m Tiefe versenkt. Kern- und Datenmaterial von drei tiefen Explorationsbohrungen aus Schleswig-Holstein (nördlicher Beckenrand) wurde verwendet, um petrographische und geochemische Untersuchungen an Rotliegend-Sandsteinen durchzuführen, und um die Versenkungsgeschichte und thermische Entwicklung von Mutter- und Speichergesteinen zu simulieren. Vorhandene Datensätze vom südlichen Beckenrand (v. a. aus der Gegend nördlich von Hannover) wurden zusammengestellt, neu bewertet und ergänzt.

Kohlenwasserstoff-Muttergesteine, vor allem kohleführende Schichten aus dem Karbon, sind am südlichen Beckenrand überall unter dem Rotliegenden vorhanden, fehlen aber in weiten Teilen des nördlichen Arbeitsgebietes. Dort wurden lokal vorkommende Karbon-Tonsteine mit niedrigen Gehalten an organischem Kohlenstoff noch während der Trias bis auf Temperaturen um 200°C aufgeheizt. Ölgenerierung in geringfügigem Ausmaß blieb auf einen kurzen Zeitabschnitt nach der Ablagerung des Rotliegenden beschränkt. Am südlichen Beckenrand dagegen generierten seit dem späten Karbon mächtige kohleführende Muttergesteine über lange Zeiträume hinweg CO_2, Öl, und Gas. Die Bildung flüssiger Kohlenwasserstoffe in den oberen Muttergesteinshorizonten (Westphal) fand hauptsächlich in der Trias und im frühen Jura statt.

Die frühdiagenetischen Prozesse in Rotliegend-Sandsteinen beider Beckenränder sind vergleichbar. Sie umfassen die Bildung kornumhüllender Hämatit-Illit-Kutane und geringer Mengen an Quarz bzw. Albit, das lokale Wachstum Mg-reicher, kornrandständiger Chlorite sowie die häufige Ausfällung porenfüllender Karbonat- und/oder Sulfat-Zemente. Der Ablagerungsraum und die relative Lage zum Beckenrand waren wichtige Einflussfaktoren der Frühdiagenese. Bei der Entwicklung der Mesodiagenese gibt es wesentliche Unterschiede zwischen den untersuchten Sandsteinen des südlichen und des nördlichen Beckenrandes. Eodiagenetische Eisenoxid-Kutane können bis zur maximalen Versenkungstiefe erhalten sein, beispielsweise im Nordteil des NDB. Am südlichen Beckenrand wurden primär rote Sandsteine teilweise durch Reduktion und Lösung von Hämatit gebleicht. Reduziertes Eisen wurde in mesodiagenetische Chlorite und Karbonate eingebaut. In vielen Rotliegend-Sandsteinen des südlichen Arbeitsgebietes wurden instabile detritische Komponenten (v.a. Feldspat) und intergranulare Zemente (Karbonate/Sulfate) während der Mesodiagenese gelöst. Auf diese Lösungsphase folgte eine den gesamten offenen Porenraum erfassende Ausfällung maschenförmiger Illite. Am direkten Kontakt von Rotliegend-Sandsteinen zu kohleführendem Karbon bildete sich lokal Kaolinit/Dickit. Die Oberflächen der Tonminerale erfuhren eine Imprägnierung mit Festbitumina, die als Relikte flüssiger Kohlenwasserstoffe gedeutet werden können. Die Illitbildung erfolgte in der späten Trias bzw. im frühen Jura, zeitgleich mit der Hauptphase der Ölgenerierung in den unterlagernden Muttergesteinen. Lokal wurden im Inter- und Intragranularraum späte Quarzzemente ausgefällt, die z. T. große Volumina ausfüllen. Diese mesodiagenetischen Diagenesephänomene am südlichen Beckenrand treten typischerweise gemeinsam auf und sind besonders in den Rotliegend-Sandsteinen verbreitet, die in hydraulischem Kontakt zu organikreichen Muttergesteinen stehen. Das deutet darauf hin, dass die beschriebenen Diagenesemuster Migrationsbahnen ehemaliger Kohlenwasserstoffe nachzeichnen. Abgesehen von geringfügiger, sehr lokaler Illitbildung fehlen solche mesodiagenetischen Diagenesephänomene im Rotliegenden des nördlichen Arbeitsgebietes. Dort sind stattdessen relativ frühe Zementationsmuster bis zur maximalen Versenkungstiefe erhalten geblieben.

Die Ergebnisse der Diageneseuntersuchungen und der Beckenmodellierungen deuten darauf hin, dass es einen Zusammenhang zwischen wesentlichen mesodiagenetischen Mineralreaktionen und der An- oder Abwesenheit reifender Kohlenwasserstoff-Muttergesteine gibt. Reduzierende, Kohlenwasserstoff-führende Porenwässer waren höchstwahrscheinlich für die Bleichung von roten Sandsteinen verantwortlich. Lösungsprozesse können durch saure, CO_2-führende Fluide verursacht worden sein, die entweder während der Reifung des kohleführenden Karbons freigesetzt wurden und in das Rotliegende migrierten, oder durch Oxidation von Kohlenwasserstoffen innerhalb des Rotliegenden entstanden. Die Lösung von K-Feldspat lieferte die Ionen, die zur Bildung der authigenen Illite erforderlich waren. Sekundäre Lösungsporen wurden teilweise mit Zementen gefüllt, die reduziertes Eisen enthalten. Solche Prozesse fehlen offensichtlich in Bereichen, die während der Versenkung nicht von Kohlenwasserstoff-Migration betroffen waren. Die Ergebnisse dieser Studie können dabei helfen, die diagenetische Entwicklung von Rotfazies-Sandsteinen und ehemalige Migrationswege organischer Reifungsprodukte in komplexen Sedimentbecken besser zu verstehen.

Acknowledgments

Prof. Dr. Reinhard Gaupp initiated and supervised this project, and encouraged me in many ways during the work progress. My sincere thanks go to him for his support.

I am grateful to the German Research Foundation (DFG), who funded this project (grant Ga 457/8) within the frame of the research program SPP 1135 (Dynamics of Sedimentary Systems under varying Stress Conditions by example of the Central European Basin-System).

The companies ExxonMobil Production Germany GmbH (formerly BEB Erdöl und Ergas GmbH, Hannover) and Gaz de France (formerly Preussag Energie, Lingen) are kindly acknowledged for supplying core and data material from Schleswig-Holstein, and for the permission to publish the results of the investigations.

At the Institut für Geowissenschaften in Jena, Sigrid Bergmann and Frank Linde carried out extensive sample preparation work and did not flinch from familiarising with new techniques. Michael Ude and Ursula Rudakoff accomplished the measurements of my X-ray fluorescence and X-ray diffraction samples. Prof. Dr. Klaus Heide enabled the DEGAS analyses, which were carried out by Stefan Lenk. The development of a suitable analytical procedure and interpretation of the DEGAS results benefited from discussions with Dr. Christian Schmidt.

I am particular grateful that I had the opportunity to use numerous analytical facilities from other institutions, and that I could profit from the skills of scientists in these institutions. Dr. Andreas Kronz (Geowissenschaftliches Zentrum Universität Göttingen) introduced me into electron microprobe analytics and supported me during the measurements in Göttingen. Dr. Jens Götze helped me with the hot cathodoluminescence microscopy at the Institut für Mineralogie in Freiberg. Isotope measurements were carried out by Dr. Michael Joachimski, Institut für Geologie und Mineralogie in Erlangen. Dr. Günther Völksch assisted me with the scanning electron microscopy, which I could accomplish at the Institut für Glaschemie in Jena. Dr. Andreas Bauer (Forschungszentrum Karlsruhe) and Dr. Rainer Dohrmann (BGR Hannover) helped me with questions on X-ray diffraction analyses.

My thanks go to Danny Schwarzer (RWTH Aachen), who kindly allowed me to use his basin modelling data from the area north of Hannover. I also like to thank Dr. Bernd Krooss (RWTH Aachen) and Stefan Graßmann (BGR Hannover) for supplying me with Rock-Eval pyrolysis data, and Dr. Georg Nover (Universität Bonn) for providing me petrophysical data from the Rotliegend of Schleswig-Holstein.

My understanding of diagenetic processes benefited significantly from numerous discussions with my fellow Robert Lippmann (Jena), and with Dr. Robert Ondrak (GFZ Potsdam), who also helped me with questions on basin modelling. I also am very grateful for stimulating discussions on various geological, diagenetic, or basin modelling problems with Dr. Hans-Jürgen Brink (formerly BEB, Hannover), Dr. Rolando di Primio (GFZ Potsdam), Marion Geißler (TU Bergakademie Freiberg), Nicola Hug (HLUG Wiesbaden), and with all my fellows of the Geology Group in Jena, especially Goska Rusek and Dr. Thomas Voigt. Finally, I thank my wife Angelika for helping me with numerous questions, and for backing me all the way.

I thank all those for their interest in my work and the time they spent on helping me.

Contents

List of abbreviations

apfu	atoms per formula unit
BEB	BEB Erdöl und Erdgas GmbH (Hannover)
BGR	Bundesanstalt für Geowissenschaften und Rohstoffe (Hannover)
BSE	back-scattered electron
CEB	Central European Basin
CL	cathodoluminescence
DEGAS	directly coupled evolved gas analysis system
DFG	German Research Foundation (Deutsche Forschungsgemeinschaft)
EDX	energy dispersive X-ray microanalysis
EMP	electron microprobe
EMPG	ExxonMobil Production Germany GmbH
GDF	Gaz de France
GFZ	GeoForschungsZentrum
GR	gamma-ray
HC	hydrocarbon(s)
IES	Integrated Exploration Systems (Aachen)
NGB	North German Basin
PDB	reference standard for carbonate isotopes (belemnite of the Pee Dee Formation)
RWTH	Rheinisch-Westfälische Technische Hochschule (Aachen)
SE	secondary electron
SEM	scanning electron microscopy
SPP	research program (Schwerpunktprogramm)
TOC	total organic carbon
V-PDB	Vienna-PDB, reference standard for carbonate isotopes, defined by its relationship to the limestone material NBS19
XRD	X-ray diffraction
XRF	X-ray fluorescence

Abbreviations of detrital minerals, authigenic minerals, and petrographic features are explained in table A7 (appendix).

1 Introduction

1.1 Objective of the study

Deeply buried red bed sandstones are important reservoir rocks worldwide. Paleozoic red beds of the North German Basin (NGB), especially the Permian Rotliegend deposits, were explored since many decades by the petroleum industry (e.g. Boigk, 1981b; Bender and Hedemann, 1983; Glennie, 2001). The NGB is part of the Central European Basin (CEB), which extends from England to Poland (see section 2.1). A number of Rotliegend reservoirs in about 3500-5000 m depth comprise gas charges, which were sourced from coal-bearing Carboniferous strata in most cases. The diagenetic evolution of these red beds is the result of complex fluid-rock interactions proceeding subsequent to deposition and during burial. Major controls on diagenetic processes include (1) the mineralogic and granulometric composition of the rock, (2) the type of fluids interacting with the host rock, (3) the timing of fluid migration, and (4) the concurrent temperature of the system. The diagenetic alterations not only affect the reservoir properties, but provide important information on paleo-fluid composition and thus contribute to the understanding of basin evolution.

Much effort was put into research on the clastic Rotliegend along the main gas fairway in the southern part of the NGB (compare Lokhorst, 1998; Pasternak et al., 2004). Deeply buried red bed sandstones in the northern part of the basin, in contrast, were never investigated in detail. Many studies concentrated on sedimentary facies, depositional system and stratigraphy of Rotliegend deposits (e.g. Glennie, 1972; Katzung, 1975; Falke, 1976; Katzung et al., 1977; Plein, 1978; Gralla, 1988; Gast, 1991; Kiersnowski et al., 1995; Plein, 1995; Gaupp et al., 2000; Rieke, 2001). Petrographic investigations were carried out to characterise the distribution of diagenetic patterns, often with regard to porosity, permeability and reservoir quality (e.g. Glennie et al., 1978; Hancock, 1978; Drong, 1979; Almon, 1981; Rossel, 1982; Seemann, 1982; Goodchild and Whitaker, 1986; Pye and Krinsley, 1986; Gaupp, 1996; Leveille et al., 1997). The importance of pore fluid evolution for diagenetic reactions in Rotliegend sandstones was recognised from multidisciplinary approaches including petrography, mineral chemistry, fluid inclusion analyses, K-Ar dating and basin modelling (Lee et al., 1989; Gaupp et al., 1993; Platt, 1993; Ziegler, 1993; Platt, 1994; Lanson et al., 1996; Zwingmann et al., 1999; Wolfgramm and Schmidt-Mumm, 2002). However, the reasons for contrasting diagenetic evolution in different basin compartments are still not well understood.

There have been intense discussions in past whether or not organic-rich fluids from petroleum source rocks are a major control on red bed diagenesis. Gaupp et al. (1993) concluded that in the southern part of the NGB, fluids expelled from Carboniferous Coal Measures strongly influenced diagenesis in adjacent Rotliegend sandstones. Liquid HC entered the mineralogically complex sandstone horizons, as evident from widespread traces of solid bitumen in Permian reservoirs. A number of well documented case studies from other areas clearly indicate that sandstone diagenesis may be influenced by organic-rich fluids, if they are in close proximity to petroleum source rocks (e.g. Burley, 1986; Parnell and Eakin, 1987; Saigal et al., 1992; Macaulay et al., 1998; van Keer et al., 1998). The discussion about the role of organic maturation products in clastic diagenesis mostly concentrated on the generation of secondary porosity and on metal-organic interactions (e.g. Schmidt and McDonald,

1979; Bjørlykke, 1984; Surdam et al., 1984; Crossey et al., 1986b; Edman and Surdam, 1986; Giles and Marshall, 1986; Kharaka et al., 1986; Lundegard and Land, 1986; Meshri, 1986; Eglinton et al., 1987; Kawamura and Kaplan, 1987; Bjørlykke et al., 1989; Harrison and Thyne, 1992; Muchez et al., 1992; Parnell, 1994). In spite of all these studies, the importance of organic-inorganic reactions during the burial of sandstones remains controversial.

The objective of this study is to test the hypothesis that major diagenetic mineral reactions of Permian red bed sandstones in the NGB are influenced or controlled by the presence or absence of organic maturation products. This shall be accomplished by comparing quantified diagenetic phenomena in these sandstones from areas with and without hydraulic contact to petroleum source rocks. The comparative study is based on two contrasting margins of the NGB in Germany. At the southern margin, thick coal-bearing Carboniferous rocks are present beneath Rotliegend reservoirs, while source rocks are limited or completely absent in northern Schleswig-Holstein, at the northern basin margin. The difference in source rock distribution is supposed to influence dramatically the pore fluid evolution in these two areas. The main steps to evaluate the importance of organic maturation and migration during red bed diagenesis are:

(1) to compile the distribution of potential petroleum source rocks and their spatial relation to Rotliegend sandstones (section 3);
(2) to examine the burial and thermal evolution of reservoir and source rocks, to evaluate the hydrocarbon (HC) generation potential of the source rocks, and the timing of organic maturation and migration (section 4);
(3) to investigate the diagenetic evolution of Rotliegend red beds from the northern basin margin (Schleswig-Holstein), using petrographic and geochemical methods (section 5);
(4) to compile and re-evaluate Rotliegend diagenesis at the southern basin margin (mainly North-Hannover area) from existing large data sets and to complement these data by further petrographic and geochemical investigations (section 6);
(5) to compare the diagenetic evolution and organic maturation/migration from the two basin margins, and to work out mineralogical processes which are related to the presence of maturing petroleum source rocks (section 7).

This study is part of the research program SPP 1135 of the German Research Foundation (DFG). Selected results have been published in Schöner and Gaupp (2005a), and in several conference proceedings (e.g. Schöner and Gaupp, 2004a, b, c, 2005b; Schöner et al., 2005).

1.2 Study areas

This study concentrates on the diagenetic evolution of Upper Rotliegend red beds in the German part of the NGB. Few deep exploration wells were drilled in the northern part of this basin. Core and data material of four wells in Schleswig-Holstein that penetrate Rotliegend sediments (figure 1) was released by the German petroleum industry for the research program (SPP) 1135 of the German Research Foundation (DFG). Only three wells, Flensburg Z1, Schleswig Z1, and Fehmarn Z1, comprise sandstone horizons in the lower part of the clastic Rotliegend succession (Havel Subgroup). The sandstones were buried to 4200-

5200 m depth. Rotliegend diagenesis of the rocks of these wells was investigated in detail for the first time during this project.

Petroleum exploration activities in northern Germany mainly followed the highly prospective Rotliegend eolian facies belt along the southern margin of the NGB. An extensive data set could be used from that area, including diagenetic data of 67 wells. The wells are located in different parts of northern Lower Saxony (figure 1): in the area north of Hannover (55 wells), around Bremen (10 wells), and in the Ems estuary (2 wells). They were investigated in previous PhD, Diploma and research projects (Platt, 1991; Deutrich, 1993; Gaupp et al., 1993; Cord, 1994; Hartmann, 1997; Baunack, 2002; Gaupp and Solms, 2005) and cover a variety of Upper Rotliegend facies types, tectonic settings and burial depths (~3500-5000 m). Well locations cannot be specified here, and well names have been encoded as in the original papers to comply with the requirements of confidentiality for industry data.

In this project, the two study areas in (1) northern Schleswig-Holstein and (2) northern Lower Saxony, as outlined in figure 1, will be referred to as (1) northern margin of the NGB and (2) southern margin of the NGB, respectively.

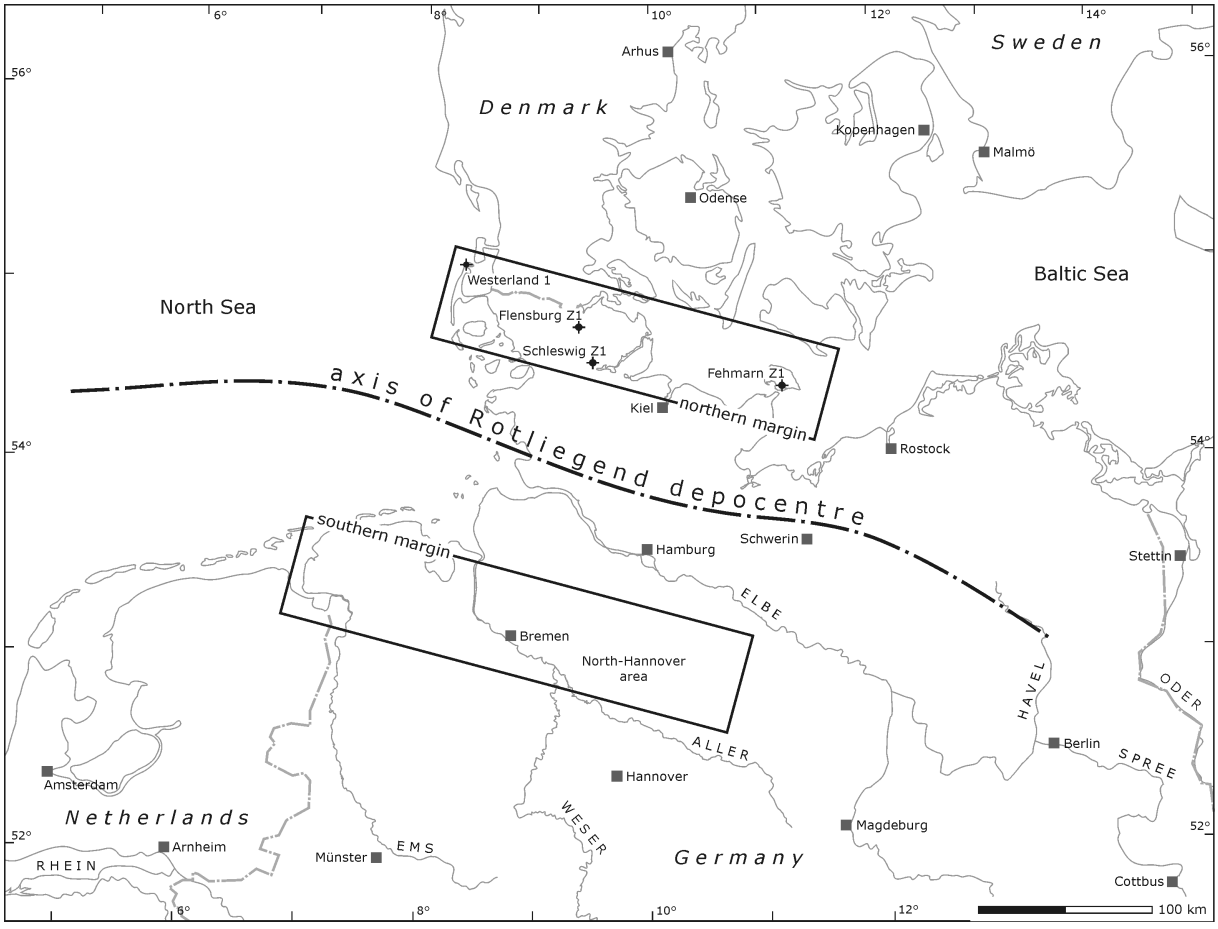

Figure 1: Map of northern Germany and surrounding countries. The two study areas (rectangles) are located in Schleswig-Holstein (northern margin of the NGB) and in Lower Saxony (southern margin of the NGB). Rotliegend sandstones of the three wells from Schleswig-Holstein (Fehmarn Z1, Schleswig Z1, Flensburg Z1) were investigated in this study. Detailed diagenetic data are available for the Rotliegend of 67 wells from the southern basin margin. Most of these wells are located in the North-Hannover area.

1.3 Methodology

This study is based on petrographic, geochemical and basin modelling work. Core and data material from Schleswig-Holstein was used to carry out diagenetic investigations on Rotliegend sandstones, and to simulate burial and thermal evolution (1D). Large data sets from the southern part of the NGB, which are available from earlier studies (see above), were compiled, re-evaluated, and complemented where necessary. The outline of this project is shown in figure 2. Table A1 and A2 (appendix) provide an overview of the wells and samples investigated, and the methods applied.

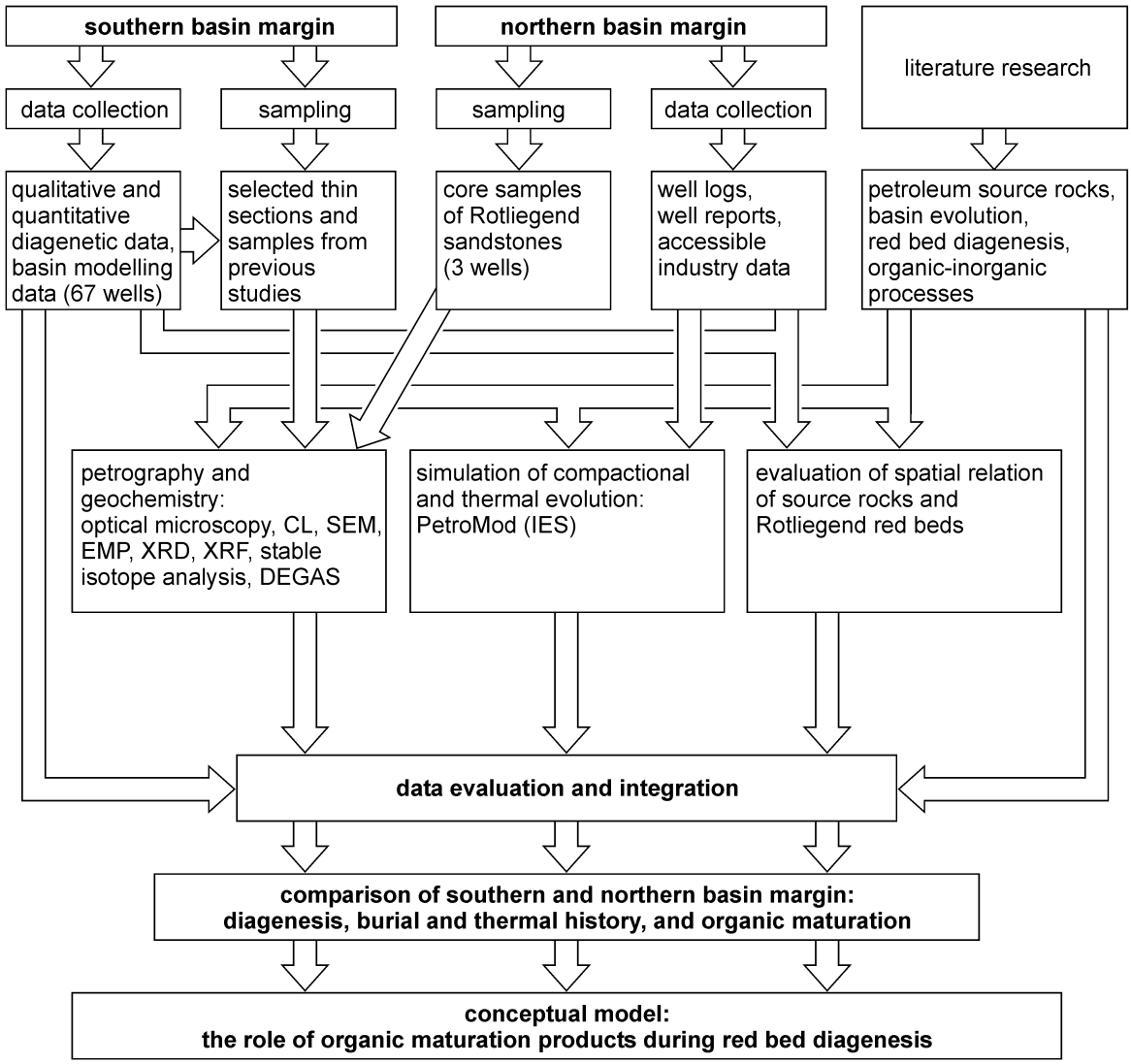

Figure 2: Schematic outline of the work flow of this study.

1.3.1 Sampling

Rotliegend cores from Schleswig-Holstein were surveyed in the core magazines of Nienhagen (wells Fehmarn Z1, Schleswig Z1), Lingen (well Flensburg Z1), and Wietze (well Westerland 1). Fine to medium grained sandstones and sandy conglomerates were sampled on a metre scale (table A1, appendix). Such lithologies were available from about 14, 24, and

40 core metres in the wells Fehmarn Z1, Schleswig Z1, and Flensburg Z1, respectively. Only one thin sandstone layer close to the top of the Rotliegend was present in well Westerland 1. Core slices up to a few 100 g in weight were used for petrographic and geochemical investigations. Additional samples were taken from Rotliegend mudstones and volcanics, from other sandstone horizons (Buntsandstein, Carboniferous, Devonian), and from basement rocks.

Remnant Rotliegend core material from the southern basin margin was available from previous PhD studies (especially Deutrich, 1993; Cord, 1994). These samples could be used to complement the existing diagenetic data set (table A2, appendix).

1.3.2 Optical microscopy

After digital photo documentation, thin-sections were prepared from 79 Rotliegend sandstone samples from Schleswig-Holstein. Core segments documented by thin-section were also used for other methods to be able to compare the results. Pores were impregnated with blue-dyed epoxy resin. Thin-sections were either polished or covered with glass after staining half of the thin-section with Alizarin Red-S for calcite determination. The ExxonMobil Production Germany GmbH (EMPG) provided additional thin-sections of well Schleswig Z1 and Flensburg Z1 (31 and 42 samples, respectively). Complementary thin-sections were prepared from some Rotliegend volcanics and mudstones, and from the samples of other stratigraphic horizons.

Optical microscopy studies on 152 Rotliegend sandstone samples focused on detrital and authigenic mineralogy, porosity, and textural relationships. Thin-sections were examined under plane and cross polarised light, polished thin-sections additionally under reflected light, using a ZEISS Axioplan 2 microscope and a HITACHI HV-C20 digital colour camera. Quantification of 69 samples was accomplished by point-counting 300 points per thin-section (automatic point counter PRIOR Model G). Coarse grained and well sorted layers were preferred for quantification if layers with different grain size or sorting were present in one thin-section. Several samples were crosschecked after some weeks. The error was within the range of the statistical 95% confidence interval of point counting data (figure 3; compare Howarth, 1998).

Polymineralic detrital grains with minerals >63 µm were counted as lithic fragments, in contrast to the Gazzi-Dickinson method (Ingersoll et al., 1984; Zuffa, 1985), to provide data comparable to that of the southern basin margin. Furthermore, the Gazzi-Dickinson method has a number of disadvantages (compare Decker and Helmold, 1985; von Eynatten and Gaupp, 1999): Quartz and feldspar phenocrysts of abundant volcanic grains, e.g., would not be counted as lithic fragments, in contrast to the fine crystalline matrix, and oxidised mafic phenocrysts would have to be counted as opaque minerals.

The abundance of diagenetic grain coatings may be overestimated in thin-section. Similarly, the fine platy or hairy crystal structure of authigenic clay minerals hampers a reliable volumetric quantification. Hence, diagenetic information that was difficult to characterise by point counting (grain coatings, clay minerals, feldspar dissolution/alteration, bitumen impregnation) was classified semi-quantitatively on a four class scale (table A7, appendix).

The long diameters of 100 grains per thin-section were measured along a number of random lines perpendicular to the bedding plane using a projection macroscope (MINOX Petroscope®). Clearly defined layers of different grain size within one thin-section were measured separately. Mean and median diameter were calculated from Φ-values, and re-transformed into the µm-scale, which is easier to imagine. Calculations on a metric scale would overemphasise large grain sizes (compare Tucker, 1996). The mode of the grain sizes is stated as midpoint of the most abundant class in bar charts with a class width of 0.5 Φ. Statistical calculations were carried out with the MATLAB® 6.0 software. Standardised charts were used to semi-quantitatively determine sorting (Beard and Weyl, 1973), roundness (Powers, 1953; in Füchtbauer, 1988), and grain contacts (Pettijohn et al., 1987).

Qualitative diagenetic data from the southern margin of the NGB are available from previous studies for more than 3000 thin-sections of 67 deep exploration wells (Platt, 1991; Deutrich, 1993; Cord, 1994; Hartmann, 1997; Gaupp and Solms, 2005). Point-counting data (mostly 300 points per section) of almost 900 samples from 47 wells could be used in this project. Re-evaluation of this data set included compilation and homogenisation of point counting data, and complementary optical microscopy on about 300 thin-sections from 16 wells in total. These thin-sections were partly available during the DGMK project 593-8 (Tight Gas Reservoirs, Gaupp et al., 2005), and were partly prepared from selected samples of earlier projects (table A2, appendix). The EMPG provided 77 thin-sections from one well north of Bremen. The main target of these petrographic investigations was to bring together the results of previous studies, and to specify the most characteristic diagenetic phenomena and their distribution.

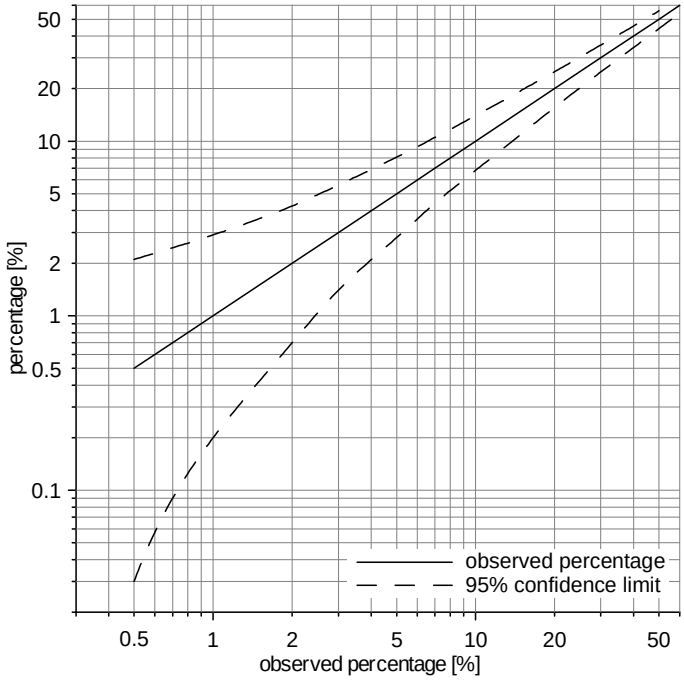

Figure 3: 95% confidence interval of point counting data for a total of N = 300 counts (according to Howarth, 1998).

1.3.3 Scanning electron microscopy

Cement textures, crystal habit of authigenic minerals and detrital feldspars, and the morphology of pores were examined by scanning electron microscopy (SEM) and combined qualitative chemical analysis (energy dispersive system, EDX). Investigations were carried out on

broken rock chip surfaces and on polished thin-sections of 17 samples from Schleswig-Holstein. The samples were coated with carbon for combined SEM-EDX analyses. Gold coating, which allows a better resolution but impedes chemical analysis, was used for some broken rock surfaces. The Zeiss DSM 940A SEM was operated with 20 kV and 0.01-0.1 nA for image acquisition, and ~0.3 nA for EDX (eXL10 Oxford Instruments). The working distance was adjusted between 6-25 mm, depending on the requirements of image quality or chemical analysis, respectively. SEM micrographs were recorded digitally in back-scattered (BSE) as well as in secondary electron (SE) mode. Typical EDX spectra were also recorded digitally.

1.3.4 Cathodoluminescence microscopy

A hot-cathode luminescence (CL) device at the TU Bergakademie Freiberg (model HC1-LM) was used to visualise different generations within carbonate and quartz cements and veins. Eight polished thin-sections from the northern basin margin were carbon coated and studied under standard conditions of $<10^{-6}$ bar vacuum, acceleration voltage of 14 kV, and a current density of 10 µA/mm^2. CL images were recorded with a digital camera (KAPPA 961-1138 CF 20 CXC). Weak luminescence colours of quartz were difficult to observe in most samples due to abundant bright luminescing carbonate cements.

1.3.5 X-ray diffraction analysis

Supplementary to the microscopic investigations, 14 whole rock sandstone samples from the northern basin margin were powdered manually and analysed routinely by X-ray diffraction analysis (XRD) from 4° to 70° 2 θ (0.02° 2 θ steps, counting time 2 s), using Ni-filtered Cu-*Kα* radiation at 40 kV and 40 mA. The evaluation was based on the *Powder Diffraction File* of the JCPDS-ICDD and has been carried out using the program *MacDiff* of Dr. R. Petschick (e.g. Petschick, 2002).

Five samples across the sandstone sequence of well Flensburg Z1, containing 0.3-1.7 vol.-% authigenic chlorite, were selected for clay mineral separation. Clean pieces of about 500 g in weight were carefully crushed in a hydraulic press to grain sizes <2 mm. The crushed material was filled in a 2 l beaker with deionised water and stirred slowly with an automatic mixer for 2 hours. After decanting the suspension the procedure was repeated until the water remained almost clear. The clay size fraction (<2 µm) was separated by gravity settling. 15 ml of Na-pyrophosphate solution (20 g/l $Na_4P_2O_7$ x 10 H_2O) were added to avoid flocculation. Oriented samples were prepared directly from concentrated suspensions on a porous ceramic disk (compare Shaw, 1972). A vacuum generated by a water jet pump sucked the liquid through the ceramic within 2-3 minutes and thus effectively reduced sedimentation within the suspension. Oriented samples were analysed from 4° to 40° 2 θ in 0.02° 2 θ steps. All samples were measured first under air-dried conditions, then glycol-solvated, and finally after heating to 550°C for one hour. The program *MacDiff* was used for evaluation, combined with references on XRD analysis of clay minerals (Brindley and Brown, 1980; Moore and Reynolds, 1997; Bouchet et al., 2000). Since the <2 µm fractions were strongly contaminated (amongst others quartz, albite, dolomite), clay fractions <0.4 µm were separated by ultra-centrifugation. This subdivision was chosen since the <0.6 µm fraction still contained a relatively high percentage of contaminations and the <0.2 µm fraction contained too little

material to be analysed. The <0.4 µm fractions were analysed from 4 to 40° 2 θ for arid-dried oriented preparations. The chlorite fractions were investigated additionally by EMP.

1.3.6 Electron microprobe analysis

A JEOL JXA 8900 RL electron microprobe (EMP) equipped with five wavelength dispersive spectrometers at the Geowissenschaftliches Zentrum Göttingen was used to determine quantitatively the mineral chemistry of carbonates, feldspars and clay minerals. Minerals unidentifiable with other methods were also investigated by the EMP. BSE images from typical petrographic textures could be recorded digitally. In total, 18 polished thin-sections from the three wells of the northern basin margin were selected for this method. Three chlorite fractions <0.4 µm separated from sandstone samples were analysed additionally, since the chlorite crystals were mostly too small to be measured directly in thin-section. The chlorite samples were prepared on glass slides from clay suspensions. All samples had to be coated with carbon prior to EMP analysis. The operational conditions are summarised in table 1.

Table 1: Operational conditions of EMP analyses. The detection limits are calculated as 2σ background signals.

carbonate programm	acceleration voltage [kV]		beam current [nA]		beam diameter [µm]			used for		calibration	
	15		12		10-15			carbonates		CO_2	
elements	**Sr**	**Mg**	**Ca**	**Ba**	**Mn**	**Si**	**Fe**				
counting time peak [s]	30	15	15	30	30	15	15				
background [s]	15	5	5	15	15	5	5				
standard	strontia-nite	dolomite	calcite	baryte	rhodo-nite	wollasto-nite	siderite				
detection limit [ppm]	280	340	410	460	270	440	500				

silicate programm	acceleration voltage [kV]		beam current [nA]		beam diameter [µm]			used for		calibration	
	15		15		5-10 25-30 (<0.4µm clay fractions)			feldspars, clay minerals		O	
elements	**Si**	**Na**	**Ca**	**K**	**Fe**	**Al**	**Mg**	**Ti**	**Sr**	**Mn**	**Ba**
counting time peak [s]	15	10	15	15	15	15	15	15	30	15	30
background [s]	5	5	5	5	5	5	5	5	15	5	15
standard	anorthite	albite	wollasto-nite	sanidin	hematite	anorthite	MgO	TiO_2	coeles-tine	rhodo-nite	celsian
detection limit [ppm]											
feldspars	450	380	280	220	410	300	210	420	630	370	530
clay minerals	410	300	270	290	410	280	250	410	460	400	520

1.3.7 X-ray fluorescence analysis

49 Rotliegend samples of the northern basin margin were selected for whole rock geochemical analysis by X-ray fluorescence (XRF) analysis. Sample preparation included powdering of about 35 g in a thoroughly cleaned agate ring mill, preparation of glass discs for main element and pressed powder tablets for trace element analysis. Glass discs were made from 0.4 g of the annealed sample powder and 4 g Li-tetra/metaborate (MERCK Spectromelt® A12). 1 g binder (HOECHST Wax C) was added to 6 g sample material to prepare the

pressed powder tablets. The measurements were conducted on an sequential, wavelength dispersive XRF spectrometer (PHILIPS PW 2400), working with a rhodium tube. The machine was calibrated by 51 international rock standards appropriate for quartz-rich sediments. The relative error (1 σ) is approximately ±1% for main elements and ±5% for trace elements.

1.3.8 Stable isotope analysis

Carbonate cements were analysed with respect to their carbon and oxygen isotopic composition. 29 samples were chosen after petrographic characterisation of the thin-sections. Preferred samples for isotope analyses contained >4 vol.-% of carbonate cements and only one dominant type of carbonate. However, bulk rock analyses can not avoid mixing of different calcite respectively dolomite generations, especially if they are zoned. In addition to Rotliegend cements, some calcite veins and Carboniferous carbonate cements were analysed. The measurements were carried out by Dr. Michael Joachimski at the University of Erlangen. Carbonate powders were reacted with 100% phosphoric acid (density >1.9, Wachter and Hayes, 1985) at 75°C using a Kiel III online carbonate preparation line connected to a ThermoFinnigan 252 mass spectrometer. The values are reported in ‰ relative to V-PDB by assigning a $\delta^{13}C$ value of +1.95‰ and a $\delta^{18}O$ value of -2.20‰ to the standard NBS19. Oxygen isotopic compositions of dolomite were corrected using the fractionation factors given by Rosenbaum and Sheppard (1986). The reproducibility was checked by replicate analysis of laboratory standards and was better than ±0.03 ‰ (1σ).

1.3.9 Evolved gas analysis (DEGAS)

The degassing behaviour of Rotliegend sandstones was investigated using a directly coupled evolved gas analysis system (DEGAS), mainly to characterise traces of organic material present in the rocks. The system consists of a vacuum thermoanalyser (NETZSCH STA 429) coupled directly with a Balzer quadrupol mass spectrometer (figure 4). The configuration and operating mode are described in detail in Stelzner and Heide (1996), Heide et al. (2000), and Schmidt (2004). The sample material is heated under vacuum conditions (10^{-3}-10^{-4} Pa) from room temperature to 1450°C using a linear heating rate of 10 K min^{-1}. Volatile species up to mass numbers m/z = 200 can be recorded online. Ionisation of released volatiles occurs in the ion source of the mass spectrometer. Reverse reactions can be neglected since the degassing process occurs under highly non-equilibrated conditions. Turbomolecular pumps were used to prevent oil from the vacuum devices to contaminate the system.

Five sandstone samples from the northern and ten samples from the southern margin of the NGB were chosen for this method. The samples from the southern basin margin comprise different degrees of bitumen impregnation and different intensity of illite formation. There are no data available suggesting that the samples were in contact with oil or other organic liquids during the drilling process or later sample preparation. However, it must be noted that the wells were drilled up to 40 years ago and the record is partly incomplete. First tests indicated that carbonates are problematic since carbonate decomposition reactions dominate the degassing profiles between 400 and 700°C. Hence, about 5 g dry sample material from the inner part of core pieces were powdered manually, and carbonates were dissolved in 7% HCl until the reaction ceased. The samples were neutralised by washing with deionised water.

Further tests were carried out using 10-40 mg sample material and a rapid scanning mode over the entire mass spectrum during heating. Based on these preliminary investigations, the measurements were conducted on 40 mg sample material and the mass numbers m/z 2, 12-18, 28, 29, 32, 39, 43, 44, 48, 51, 54, 57, 64, 65, 71, 78, 85, 91, and 191 (multiple ion detection mode). Additional analyses examined blank samples and clay mineral standards. The gas release curved were interpreted considering fragmentation of molecules (table 4, section 5.7), isotopic abundances, and the background of the system.

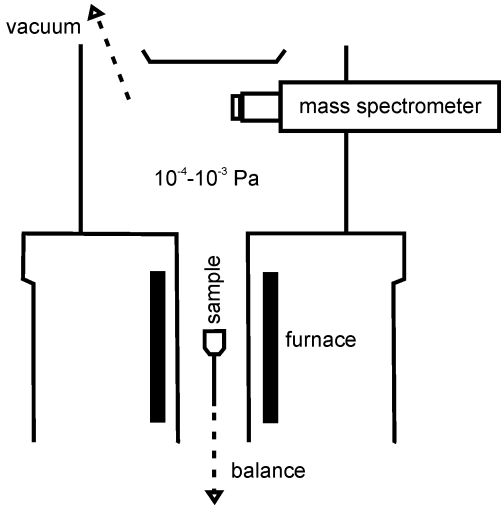

Figure 4: Schematic outline of the main components of the DEGAS-device (from Heide et al., 2000).

1.3.10 Basin modelling

Subsidence histories and temperature evolution for three wells of the northern basin margin (Fehmarn Z1, Schleswig Z1, Flensburg Z1) were simulated using the program PetroMod® 1D 8.0 (IES, Aachen). PetroMod® is a commercial software package which is mainly designed for the needs of the petroleum industry, but is equally suitable for academic purposes. The numerical simulation is a tool to evaluate the time-depth-temperature frame in which diagenetic processes took place. Furthermore, the simulations allow to calculate the maturation history and the timing of HC generation. Two-dimensional models, which are available for the southern basin margin (Neunzert, 1997; Schwarzer and Littke, 2005), also allow conclusions on hydrocarbon expulsion and accumulation.

The PetroMod® software is based on a deterministic finite-element forward modelling approach and uses mathematical equations to describe the processes controlling sediment accumulation and temperature evolution in space and time. The theoretical approach and the basic equations used for the numerical simulation have been described in detail in past (e.g. Welte and Yükler, 1981; Welte and Yalçin, 1988; Allen and Allen, 1997; Yalçin et al., 1997). Important input data for the models are the well reports, vitrinite reflectance values and bore-hole temperatures supplied by the petroleum industry. Total organic carbon (TOC) contents and Rock-Eval pyrolysis data for the Carboniferous of well Schleswig Z1 was provided by B. Krooss, RWTH Aachen (pers. comm.) and S. Grassmann, BGR Hannover (pers. comm.). Additional information was compiled from literature (regional geology, sedimentary facies and stratigraphy, paleogeographic reconstructions).

2 Geological setting

2.1 Tectonic and stratigraphic evolution

The Central European Basin (CEB) is the most prominent intracontinental basin structure in Middle Europe and passed through a complex history of deposition, and periods of uplift and erosion. The basin, which may be subdivided into several sub-basins, extends from England to Poland and is bordered by the Sorgenfrei-Tornquist/Teysseire-Tornquist Zone in the north and by the Variscan mountains in the south. Two large sub-basins, the Northern and Southern Permian Basins, are separated by the Mid-North-Sea and Ringkøbing-Fyn trend of highs (figure 7). The Southern Permian Basin may be subdivided into the Southern North Sea, the North German, and the Polish sub-basins. This study focusses on the Rotliegend deposits of the North German Basin (NGB), which is the main depocentre in Rotliegend times.

Intensive research has been carried out on the geology of the CEB in past, especially in the North Sea and North German areas. A substantial overview of the geological and tectonic history of that area is given in Ziegler (1990), Glennie (1998), and Evans et al. (2003). Detailed structural maps, subcrop maps, geochemical maps and geological cross sections are available from the atlas volumes of Baldschuhn et al. (1996; 2001) and Lokhorst (1998). In this section, the complex geological history of the NGB will be sketched briefly.

The main basement units beneath the sedimentary fill of the NGB are from north to south the Baltic Shield, the North German Caledonides, and the Variscan fold and thrust belt (figure 5, 6). The Baltic Shield comprises crystalline rocks and undeformed Cambro-Silurian sediments. The Caledonides are composed of the northern thrust and accretion belt and the southern Lüneburg Massif (Cadomian or older crust). This basement configuration is a result of the collision of East Avalonia with Laurussia in the Silurian (Caledonian Orogeny; see Franke and Oncken, 1990; Ziegler, 1990; Berthelsen, 1992a; Torsvik et al., 1993; Meissner et al., 1994; Franke et al., 1995). In post-Caledonian times, the Rhenohercynian basin opened to the south of the "Old Red Continent" and gave rise to Devonian and Early Carboniferous shelf sedimentation. The northern fluvial and deltaic facies, approximately in the area of southern Denmark and northernmost Germany, passed southwards into a carbonate platform and finally into a basinal facies (Franke, 1990). Docking of Gondwana and Gondwana-derrived terranes at the southern border of East Avalonia took place during the Carboniferous (Varican Orogeny). A foreland basin with northward migrating basin axis developed in the Upper Carboniferous north of the rising Varican orogen (Hedemann and Teichmüller, 1971; Katzung, 1988). Sand, shale and coal were deposited on a large, low relief paralic plain. The facies changed gradually from dominantly marine to paralic, limnic-fluvial and finally continental during the Upper Carboniferous (Franke, 1995). The transition from coal-bearing facies types to barren red beds is diachronous and took place in the Westphalian C-D in most areas (Hedemann and Teichmüller, 1971). The source rock distribution in the Carboniferous will be discussed in more detail in section 3. Major changes of the tectonic setting in the Late Carboniferous and Early Permian resulted in fragmentation of the European Variscides and their foreland (Katzung and Krull, 1984; Dvorák and Paproth, 1988). Pre-Permian sediments were deeply truncated over large areas.

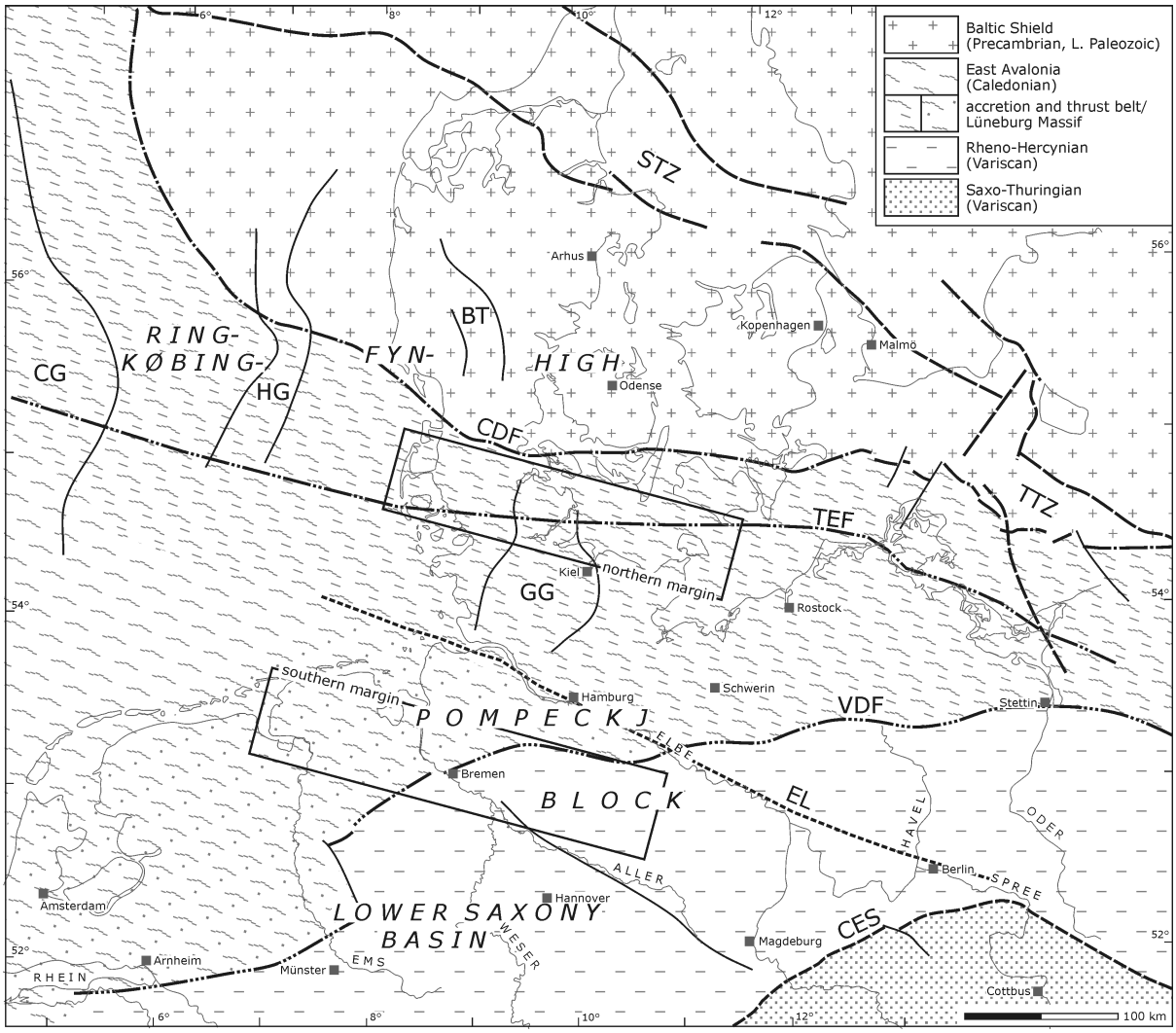

Figure 5: Schematic map of the basement beneath the central part of the NGB and main structural elements. BT = Brande Trough, CDF = Caledonian Deformation Front, CES = Central European Suture, CG = Central Graben, EL = Elbe Line, GG = Glückstadt Graben, HG = Horn Graben, STZ = Sorgenfrei-Tornquist Zone, TEF = Trans-European Fault, TTZ = Teysseire-Tornquist Zone, VDF = Variscan Deformation Front. Compiled from Blundell et al. (1992), Pharaoh (1999), Baldschuhn et al. (2001), and Frisch and Kockel (2004).

It is widely accepted that the emergence of the NGB started during this period, following the termination of the Variscan orogeny. The basin initiation was accompanied by wrench-related deformation and extensive volcanic activity (Ziegler, 1990; Hoth et al., 1993; Marx et al., 1995; Benek et al., 1996; Breitkreuz and Kennedy, 1999). A dextral shear system is inferred from basin subsidence patterns (compare figure 7). Early Rotliegend deposition was restricted to local fault-bounded basins (e.g. Drong et al., 1982; Gast, 1988). Rapid subsidence in the NGB started in Upper Rotliegend times and declined throughout the Early Mesozoic (Menning, 1991; van Wees et al., 2000). Purely extensional/transtensional models for crustal thinning prior to the main phase of subsidence (e.g. Bachmann and Grosse, 1989; Brink et al., 1990) are problematic since evidence for active tectonics during the period of maximal accommodation is very limited. Van Wees et al. (2000) suggest that a significant component of the Late Permian and Triassic tectonic subsidence can be explained by thermal relaxation of Early Permian lithospheric thinning, and by delayed infilling of topog-

raphic depressions. Sediment accumulation was concentrated in two large continental drainage basins (figure 7). Red-coloured Upper Rotliegend clastics and evaporites were deposited under semi-arid conditions (see below). Marine conditions were re-established in the Zechstein, when thick carbonates, evaporites and minor shales accumulated. The Zechstein represents the most important seal for the Rotliegend gas reservoirs (Glennie, 1998).

The Triassic in northern Germany is characterised by dominantly fluvial and lacustrine (Lower-Middle Buntsandstein), marine (Upper Buntsandstein-Muschelkalk), and fluvio-lacustrine or partly marine (Keuper) depositional environments (e.g. Röhling, 1991; Aigner and Bachmann, 1992; Gaupp et al., 1998; Beutler et al., 1999). Sand- and mudstones prevail in the lower part, carbonates and evaporites in the middle part, and pelites as well as evaporites in the upper part of the Triassic sequence. The break up of the super-continent Pangea since the Triassic was manifested by rifting in the North and Central Atlantic domain, in the Mediterranean, and in the Gulf of Mexico (Ziegler, 1990). In the NGB, extensional tectonics led to the formation of several troughs, e.g. the N-S oriented Horn Graben offshore Denmark, and the Glückstadt Graben in Schleswig-Holstein (figure 5, 7). These Graben systems probably developed along pre-existing faults which were active already during the Permian or Late Paleozoic (Best et al., 1983). The Glückstadt Graben accommodated up to 9000 m of Triassic sediments (Baldschuhn et al., 1996). In areas where thick Permian evaporites had been deposited, salt mobilisation strongly influenced the basin evolution since the Triassic (e.g. Trusheim, 1957; Jaritz, 1973; Brink, 1984; Scheck et al., 2003; Mohr et al., 2005). Tectonic events and salt migration are closely interrelated and cannot be treated independently.

In the Late Triassic to Early Jurassic, tectonic activity intensified along the Tethys-Central Atlantic-Caribbean rift/wrench system and subsequently led to the opening of new oceanic basins by the Middle to Late Jurassic (Ziegler, 1990). The Rhaetian to Early Jurassic marine transgression in Central Europe was followed by shale and sandstone sedimentation. Lower Jurassic organic-rich shales are important oil source rocks for Meso- and Cenozoic reservoirs (Bentz, 1958). The Mid-Jurassic thermal doming in the central North Sea brought about uplift of a large region of the North Sea and adjacent onshore areas (Underhill and Partington, 1993). The NGB differentiated into several blocks with distinct uplift/subsidence history. In northern Germany, the Lower Saxony Basin accommodated sediments throughout the Jurassic and Cretaceous, while the Ringkøbing-Fyn and Pompeckj Highs were subjected to uplift and erosion from the Middle/Late Jurassic to the Early Cretaceous (Jaritz, 1969; Betz et al., 1987). Elevated accumulation rates in the Upper Cretaceous in many parts of the NGB can be related to a global eustatic sea level high (Haq et al., 1987). Marl and chalk were deposited in a large epicontinental sea during that time.

Major tectonic activity is evident again for the Late Cretaceous and Early Paleogene, when NW-SE-trending areas were uplifted, e.g. the Lower Saxony Basin. This uplift is interpreted as tectonic inversion of former depocentres and is probably related to compressional stress induced by the Alpine continent-continent-collision (Ziegler, 1990; Gemmer et al., 2003). The North Atlantic continental margin was characterised by rifting and igneous activity at the beginning of the Paleogene. Rapid subsidence during that period is evident from the North Sea and adjacent onshore areas in the Netherlands and NW Germany (Hall and White, 1994; Scheck-Wenderoth and Lamarche, 2005). The Paleogene and Neogene succession in

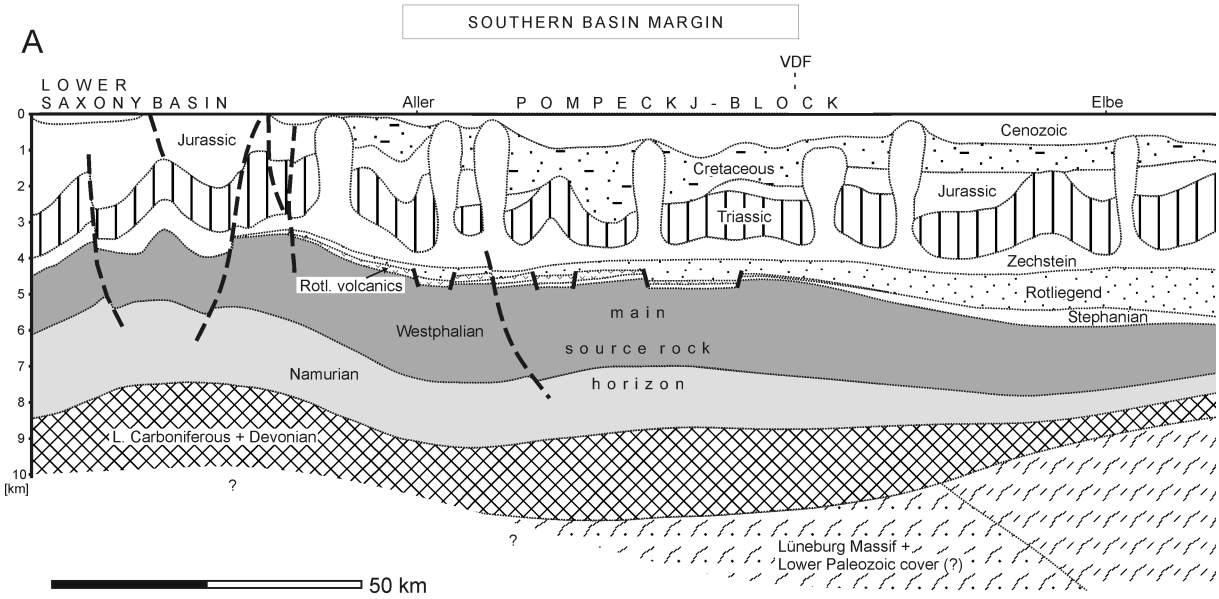
A
SOUTHERN BASIN MARGIN
VDF
LOWER SAXONY BASIN
Aller
POMPECKJ-BLOCK
Elbe
Jurassic
Cretaceous
Triassic
Cenozoic
Jurassic
Zechstein
Rotliegend
Stephanian
Rotl. volcanics
Westphalian
main source rock horizon
Namurian
L. Carboniferous + Devonian
Lüneburg Massif + Lower Paleozoic cover (?)
[km]
50 km

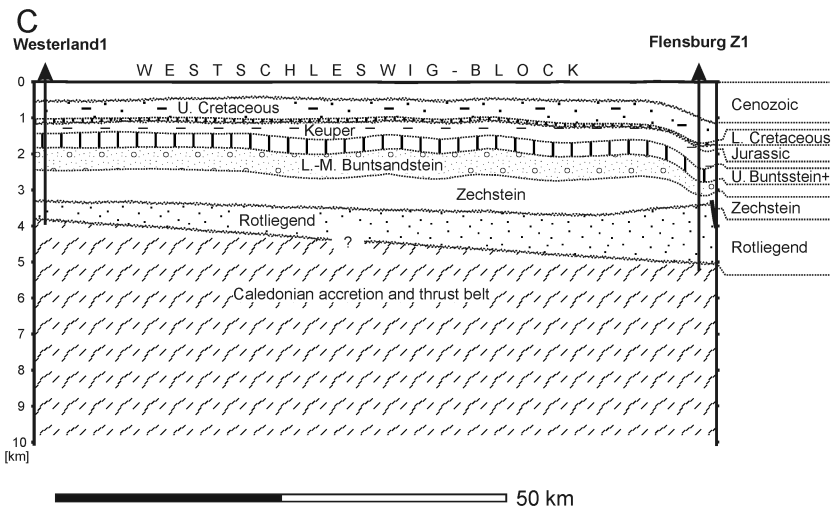
C
Westerland1
Flensburg Z1
WESTSCHLESWIG-BLOCK
U. Cretaceous
Keuper
L.-M. Buntsandstein
Zechstein
Rotliegend
Caledonian accretion and thrust belt
Cenozoic
L. Cretaceous
Jurassic
U. Buntsstein+
Zechstein
Rotliegend
[km]
50 km

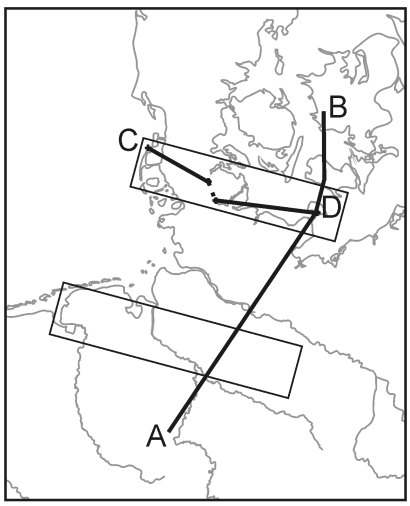
A
B
C
D

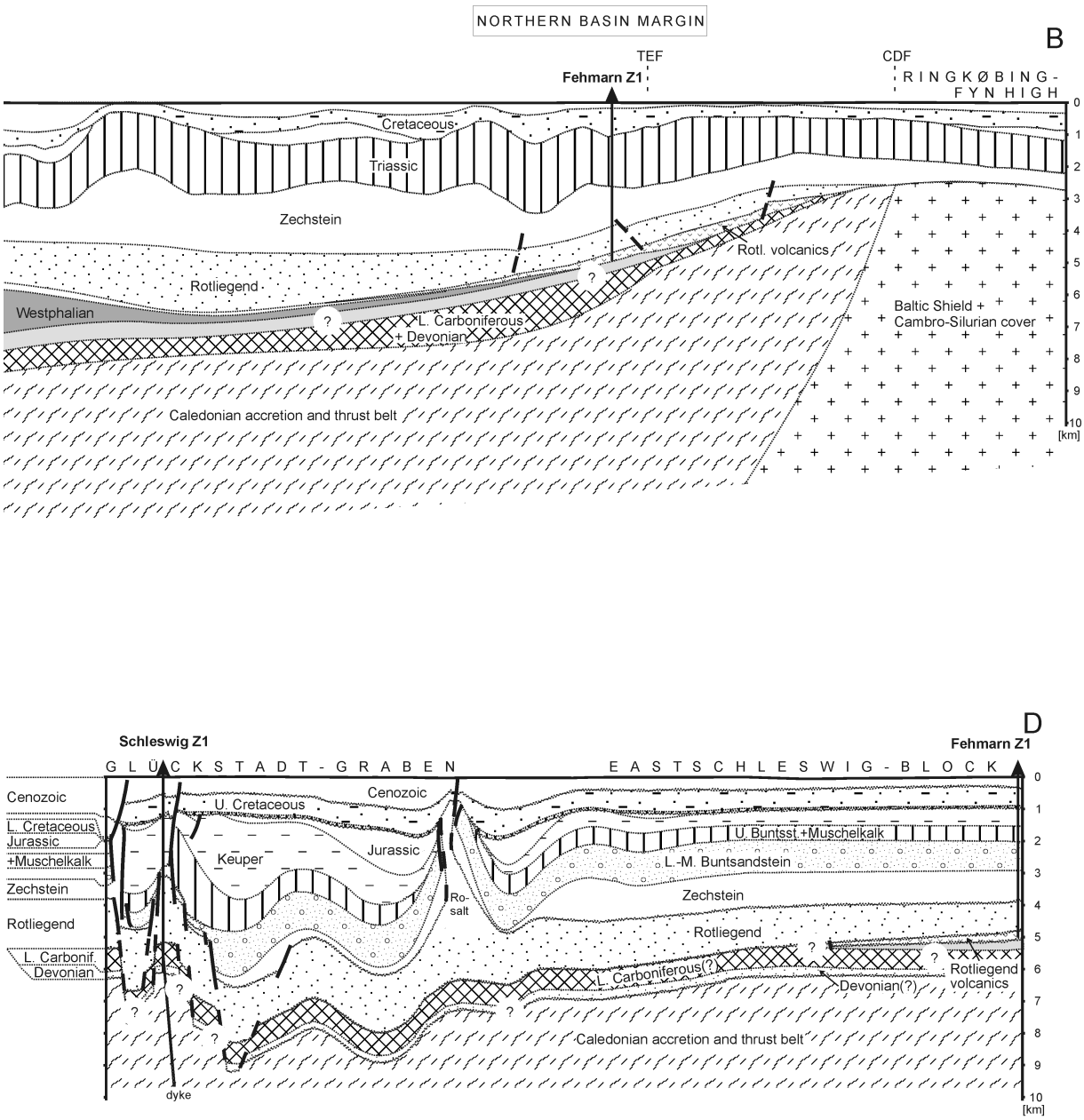

Figure 6: Schematic geological SSW-NNE cross section across the NGB (A-B), and E-W cross section along the northern margin of the basin (C-D). Section A-B illustrates the increasing erosion of Carboniferous rocks towards the north. The two study areas are indicated as "southern basin margin" and "northern basin margin". The distribution of pre-Permian rocks in the northern part of the basin is not well confined. Lower Carboniferous and Devonian was only drilled in well Schleswig Z1 (section C-D). Cross section A-B modified from Plein (1978), Boik (1981), and Berthelsen (1992b). Cross section C-D modified from Baldschuhn et al. (1996).

northern Germany is composed of shales, sandstones and some brown coal horizons (Miocene). Apart from the stress pattern, sedimentation was strongly influenced by sea level fluctuations (Haq et al., 1987; Gramann and Kockel, 1988) and salt movements (Jaritz, 1973; Hinsch, 1986). The area was repeatedly covered by the Pleistocene ice shield. Pleistocene and Holocene sediments comprise mostly logement tills, sand and gravel.

2.2 Rotliegend sedimentology and reservoir rocks

The Rotliegend volcanics and sediments rest unconformably on Carboniferous, Lower Paleozoic, deformed Caledonian or Precambrian rocks (figure 10). They were deposited under semi-arid to arid climatic conditions in a large intracontinental, internally drained basin system of the super-continent Pangea. The subdivision of the Rotliegend is mainly based on lithostratigraphy, while biostratigraphic approaches were successful only locally (e.g. Hoffmann et al., 1989; Schneider and Gebhardt, 1993). The commonly accepted stratigraphic subdivision of the German Rotliegend (Schröder et al., 1995, table 2) is based on earlier concepts in East and West Germany (Katzung et al., 1977; Hedemann et al., 1984).

Table 2: Stratigraphy of the Rotliegend in Germany. Stratigraphic subdivision according to Schröder et al. (1995) and Plein (1995), numerical ages according to Menning (1995).

Group		Subgroup	Formation	Member	Lithology	Age
Rotliegend	Upper Rotliegend	Elbe	Hannover	Heidbeck	evaporite/shale/sandstone	258
				Munster	evaporite/shale/sandstone	
				Niendorf	evaporite/shale/sandstone	
				Dambeck	evaporite/shale/sandstone	
				Bahnsen	evaporite/shale/sandstone	
				Wustrow	evaporite/shale/sandstone/basalt	
				Ebsdorf	evaporite/shale/sandstone	
			Dethlingen	Einloh	evaporite/shale/sandstone	260
				Strackholt	evaporite/shale/sandstone	
				Schmarbeck	evaporite/shale/sandstone	
				Wettenbostel	evaporite/shale/sandstone	
				Gralstorf	evaporite/shale/sandstone	
				Findorf	shale/sandstone	
				Sande	evaporite/shale/sandstone	
		Havel	Mirow		evaporite/shale/sandstone ("Schneverdingen sandstone")	262
			Parchim		evaporite/shale/sandstone ("Schneverdingen sst.", "Büste sst.") /conglomerate/basalt	264
		Müritz			shale/sandstone/conglomerate	266
	Lower Rotliegend				rhyolite/andesite sediments	296

2.2.1 Lower Rotliegend

Lower Rotliegend volcanic rocks are widespread in the German and Polish part of the basin as well as in several minor troughs, e.g. the Oslo Graben and the Saar-Nahe Basin (compare Lokhorst, 1998; Evans et al., 2003). The volcanic suite comprises mainly rhyolites, andesites and minor basalts and reaches its maximal thickness in NE Germany (~2500 m). SiO_2-rich lava flows and ignimbrites are dominant; tuffs and volcaniclastics may be intercalated (Marx et al., 1995; Benek et al., 1996). Rare Lower Rotliegend clastic sediments may occur at the base of the volcanic succession (mostly coarse grained clastics), or may be interbedded with volcanic rocks (Schneider and Gebhardt, 1993; Gaitzsch et al., 1995). Andesitic volcanics up

to ~500 m thickness are widespread east of Bremen, in the southern study area (Marx et al., 1995). In Schleswig-Holstein, volcanic rocks of more than 200 m thickness are present around Fehmarn. Several intrusive bodies and caldera-like structures were recognised in the NGB (Gast, 1988; Benek et al., 1996). Hoth et al. (1993) distinguished five stages of extrusive activity in the late Stephanian and Lower Rotliegend, based on the lithostratigraphic succession: (1) andesite stage, (2) explosive ignimbrite stage, (3) post-ignimbrite eruptive stage (ryholites > andesites > basalts), (4) late rhyolite stage, (5) late basalt stage. U/Pb dating of magmatic zircons from NE Germany, however, indicates a comparably short period of volcanic activity at the Carboniferous-Permian boundary (Breitkreuz and Kennedy, 1999). The upper part of the Rotliegend volcanics was mostly eroded prior to the onset of Upper Rotliegend deposition (Bachmann and Hoffmann, 1997).

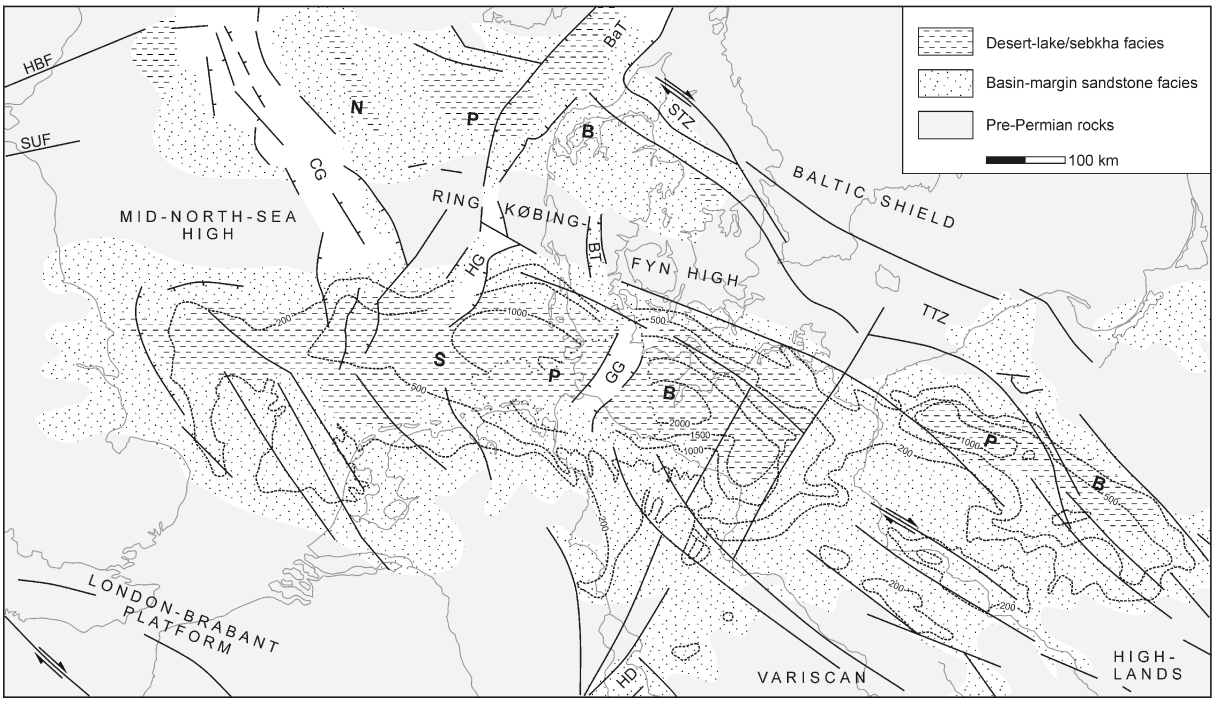

Figure 7: Rotliegend deposits in the Central European Basin System, with schematic outline of the basin-centre desert lake/sebkha facies, the basin-margin sandstone facies, and the pattern of major faults believed to have been active during the Permian. The main depocentres in Rotliegend times are the Southern Permian Basin (SPB) / Polish Basin (PB), and the Northern Permian Basin (NPB). BaT = Bamble Trough, BT = Brande Trough, CG = Central Graben, GG =Glückstadt Graben, HBF = Highland Boundary Fault, HD = Hessian Depression, HG = Horn Graben, STZ = Sorgenfrei-Tornquist Zone, SUF = Southern Uplands Fault, STZ/TTZ = Sorgenfrei-/ Teysseire-Tornquist Zone; contours in meters. Compiled mainly from Glennie (1997) and Ziegler (1990); Rotliegend isopachs according to Lokhorst (1998).

2.2.2 Upper Rotliegend

Thick continental, red-coloured sediments accumulated in the Southern Permian (>2200 m) and Polish Basin (>1400 m), in the Northern Permian Basin (probably >300 m), and in several minor sub-basins (figure 7). Magneto- and biostratigraphy indicate a Tartarian age for the Upper Rotliegend (Menning et al., 1988; Gebhardt et al., 1991; Menning, 1995; Schneider et al., 1995). The following overview concentrates on the main depocentre in the German part of the basin system.

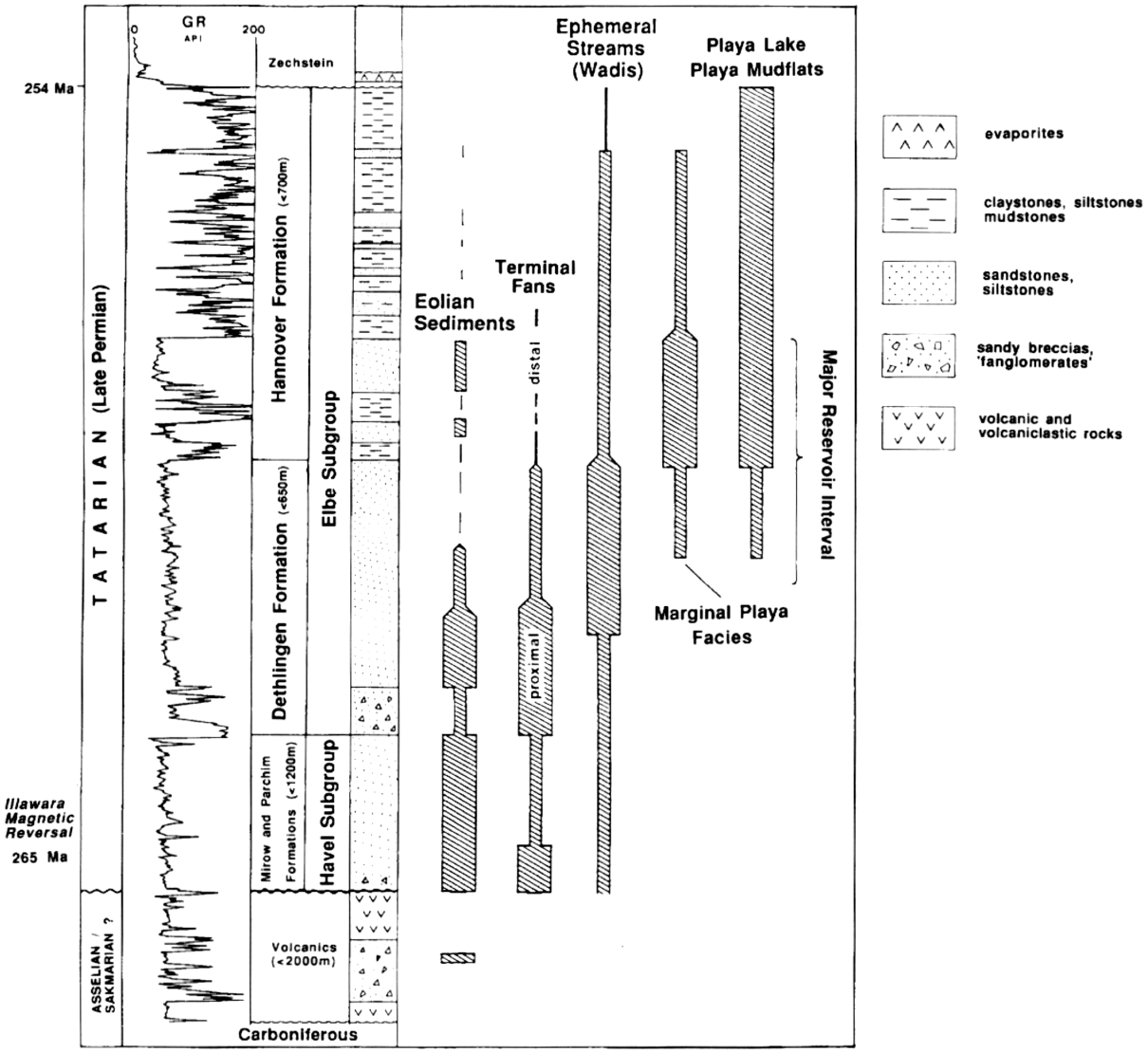

Figure 8: Generalised Rotliegend stratigraphy and distribution of major depositional facies types (from Gaupp et al., 2000). The column is representative for marginal to medial areas in the central southern part of the NGB.

The oldest sediments of the Upper Rotliegend, which are summarised to the Müritz subgroup, were deposited locally in fault-bounded depressions on top of the volcanic sequence (Hoffmann et al., 1989; Gebhardt et al., 1991). The succession comprises mostly fine grained fluvial to lacustrine clastics.

During the deposition of the Havel subgroup, isolated basins were connected to a basin-wide sedimentation area. The Parchim- and Mirow-Formation are characterised by two fining-upward cycles (Gebhardt et al., 1995). At the southern basin margin, sedimentation was strongly influenced by a rift system with N-S trending Horst and Graben structures (Gast, 1988). Wadis, which developed in the Graben structures, acted as feeder channels. Coarse grained alluvial fan sediments, mainly debris flows and sheetfloods, are widespread at the base of the Havel subgroup (figure 8). They interfinger with fluvial and eolian sandstones, which are dominant in the upper part of the succession. Fluvial sandstones at the southern basin margin mostly represent ephemeral stream environments (Glennie, 1972).

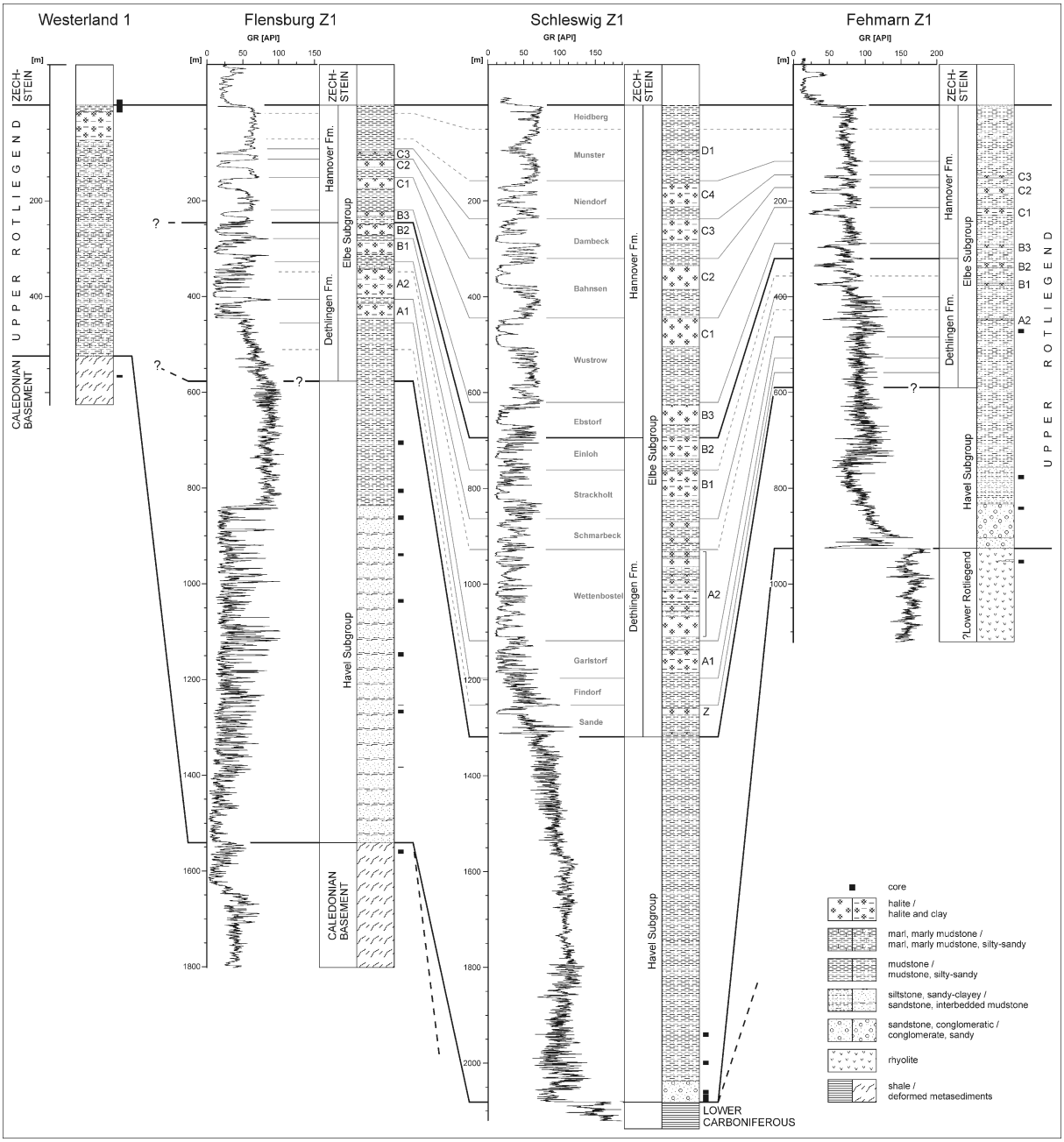

Figure 9: Rotliegend lithology and stratigraphy in Schleswig-Holstein, close to the northern margin of the NGB. The sampled core intervals are marked by grey bars. Stratigraphic subdivision of well Schleswig Z1 according to Schröder et al. (1995); correlation of the other wells in analogy by using gamma-ray (GR) logs and lithological information from the well reports. The correlation lines within the Rotliegend indicate maximum inundation phases (lake level highstands).

Corresponding to the paleogeographic position, the predominant paleo-wind direction was from NE-E towards SW-W (Glennie, 1972; Katzung, 1975; Nairn and Smithwick, 1976). Eolian sandstones up to 400 m thickness, e.g. the "Schneverdingen" and "Büste" sandstone, accumulated along the southern basin margin in Graben structures and in the vicinity of paleo-morphological highs (Drong et al., 1982; Gast, 1988; Rieke, 2001). Most of the Early Rotliegend relief was compensated during the deposition of the Parchim Formation (Schneider and Gebhardt, 1993). Towards the basin centre, pelite-dominated sediments were deposited in mudflat/sandflat and ephemeral lake environments. Salt deposition was limited

to local basin-central depressions (Gralla, 1988; Plein, 1993). Sediments were transported into the basin from uplifted highlands in the south (mainly the Variscan mountains). Much less sediment was supplied from the Ringkøbing-Fyn-High and the Fennoscandian hinterland (Plein, 1978). The sandy and conglomeratic alluvial facies belt bordering the Rotliegend basin in the north is comparably narrow, and eolian facies types are very subordinate.

The Elbe subgroup can be divided into the Dethlingen and Hannover Formation, which are each composed of seven Members (table 2). Regional subsidence and expansion of the sedimentation area, probably related to thermal contraction of the lithosphere, are evident for the beginning of the Dethlingen Formation. The greatest extension of the Rotliegend basin, however, was reached in the upper Hannover Formation (Plein, 1993, 1995). Up to 200 m of fluvial and minor eolian sandstones, locally referred to as "(Slochteren) Hauptsandstein", were deposited at the southern basin margin at the beginning of this period (Dethlingen formation). They represent large terminal fan and ephemeral stream systems, which advanced into the Rotliegend basin and were partly reworked by wind action (Plein, 1978; Gaupp et al., 2000; Rieke, 2001). The basin centre is characterised by cyclic sedimentation of pelites and evaporites in a perennial saline lake, and evaporitic mudstones/muddy sandstones on adjacent, periodically flooded mud- and sandflats (Gralla, 1988; Gast, 1991; Gaupp et al., 2000). Cyclic sand, shale and salt deposits dominate the Hannover formation and can be correlated almost over the entire basin. The clastic input from the hinterland gradually decreased (Plein, 1993). Well sorted eolian and beach sandstones were deposited along the shore line of the central lake. Climatic changes and episodic marine incursions were responsible for water level fluctuations and migration of facies boundaries (Gast, 1991; Schneider and Gebhardt, 1993; Gaupp et al., 2000; Legler et al., 2005). At the northern basin margin, fine grained clastic and evaporitic sediments are dominant throughout the Elbe subgroup (figure 9). Important sandstone horizons have not been drilled here so far.

The dominant sediment supply from the south throughout the Upper Rotliegend resulted in an asymmetrical facies distribution (figure 7). Northwards directed alluvial and SW-W directed eolian transport led to the development of a broad fluvial-eolian facies belt along the southern basin margin. The most important reservoir rocks of the Rotliegend are the eolian dominated sandstones of the Havel subgroup and the eolian/beach sandstones along the playa lake shoreline (Elbe Subgroup, figure 8). The sandy facies belt at the northern basin margin, in contrast, is comparably narrow and rapidly interfingers with muddy deposits of the central desert lake. Potential reservoir rocks are restricted to the basal Rotliegend sandstone interval. The thickness of these sandstone successions varies from 0 to almost 700 m at different locations (figure 9).

3 Distribution of petroleum source rocks

3.1 Potential source rocks in the NGB: overview

Substantial petroleum source rocks are lacking within the Rotliegend. Oxidising conditions during deposition consumed almost any organic material which may have been deposited primarily. Maturing organic matter from the overlying Zechstein possibly influenced the Rotliegend locally, especially if source and reservoir rocks were juxtaposed along fault zones. Mesozoic source rocks can be neglected due to the Zechstein evaporite seal, except for very complex tectonic settings. The majority of the HC deposits in Rotliegend sandstones were sourced from underlying Carboniferous sediments. The pre-Permian subcrop therefore illustrates the distribution of the most important source rocks in the NGB on a regional scale (figure 10). This subcrop is a result of the Caledonian orogeny, the Variscan orogeny and foreland basin evolution, and tectonic and igneous processes around the Carboniferous-Permian boundary. Carboniferous rocks are not exposed at the surface in most parts of the NGB, but buried deeply under Permian to Cenozoic sediments. Most data on the Carboniferous derive from the exposures and coal mines in the Ruhr district, the Lower Rhine and Aachen area. Additionally, a number of deep wells in northern Germany and the Southern North Sea encountered Carboniferous sediments. According to this data base, organic rich rocks were deposited in marine shelf and continental to paralic environments. Sedimentary facies, thickness and coal content of the Upper Carboniferous are supposed to be relatively constant over large areas, while different facies belts can be mapped out for the Lower Carboniferous (Franke, 1990; Lokhorst, 1998). Upper parts of the sequence have been eroded in consequence of the foreland deformation north of the Variscan nappe complex. The intensity of deformation decreases from the Variscan belt towards N-NW, although the location of the Variscan deformation front (VDF) is debatable (Blundell et al., 1992; Franke et al., 1995, 1996; Drozdzewski and Wrede, 1997; Baldschuhn et al., 2001; Frisch and Kockel, 2004). Tectonic movements at Late Hercynian fault systems disrupted the Carboniferous foreland basin (Ziegler, 1990). The Ringkøbing-Fyn-High and Southern North Sea area were uplifted and deeply truncated prior to Rotliegend sedimentation (van Wees et al., 2000). The distribution of Carboniferous source rocks is thus controlled by the primary extent of depositional environments that accumulated organic matter, and by the intensity of pre-Upper Rotliegend erosion.

3.2 Source rocks at the northern margin of the NGB

Petroleum source rocks are largely absent beneath the Rotliegend of northern Schleswig-Holstein. Well data from the northernmost basin margin indicate deformed metasediments below the clastic Rotliegend succession (wells Flensburg Z1, Westerland 1), which record Late Ordovician to Silurian metamorphic ages (Ziegler, 1978). These rocks can be interpreted as part of the Caledonian marginal thrust belt of East Avalonia (Berthelsen, 1992; Meissner et al., 1994; Torsvik and Rehnström, 2003). Devonian and Lower Carboniferous sediments underlie the Rotliegend further to the south (well Schleswig Z1). In the area of Fehmarn (well Fehmarn Z1), Rotliegend volcanics were drilled below clastic Rotliegend sediments, but the pre-Permian succession is unknown.

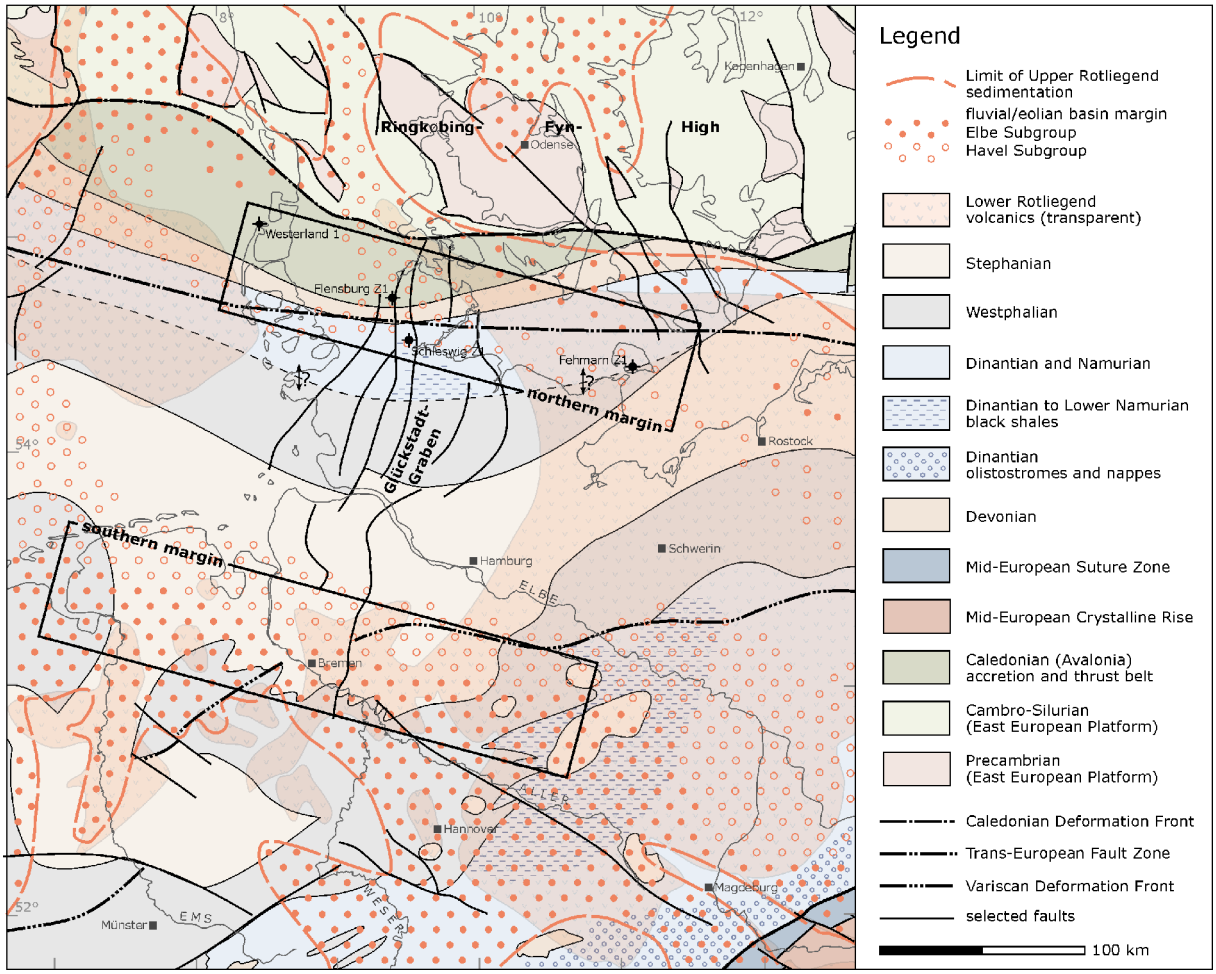

Figure 10: Schematic map of pre-Upper Rotliegend geology in the NGB, with superimposed Rotliegend volcanics (transparent) and Upper Rotliegend sandy sediments (modified from Ziegler, 1990; Plein, 1995; Lokhorst, 1998; Baldschuhn et al., 2001; Hoffmann et al., 2005). The northern limit of Upper Carboniferous source rocks is not well confined. The Rotliegend of the wells at the northern basin margin is underlain by Caledonian rocks or by Dinantian/Namurian sediments. Westphalian (±Stephanian) rocks are present beneath the Rotliegend of the southern basin margin.

The northern limit of Upper Carboniferous source rocks in northern Germany is not well confined due to few deep wells and poor quality of seismic data below the Zechstein evaporites. Neither Westphalian nor Namurian sediments were drilled in Schleswig-Holstein so far. A likely extension for Upper Carboniferous rocks – according to present knowledge – is drawn in figure 10. The Upper Carboniferous probably covered primarily entire northern Germany and much of southern Denmark, but was eroded during pre-Stephanian respectively pre-Rotliegend to Early Rotliegend times (Katzung and Krull, 1984; Katzung, 1988; Franke, 1990). Evidence for subaerial exposure is provided by red and brown colours at the top of the Lower Carboniferous shales of well Schleswig Z1, which can be interpreted as result of oxidative weathering. The increasing erosion of the Carboniferous towards the northern margin of the NGB and the absence of Westphalian source rocks in central and northern Schleswig-Holstein (figure 6) has been illustrated in the profiles drawn by e.g. Plein (1978), Boigk (1981) and Stancu-Kristoff and Stehn (1984). It is not clear, however, to what extent this erosion has removed Carboniferous rocks, hence the northern margin of Westphalian rocks may even be further south than shown in figure 6 and 10. Considering the

wells investigated in this study, Namurian and relics of Westphalian sediments may be only present in the subsurface of Fehmarn, where Rotliegend volcanics of more than 200 m thickness separate red bed clastics from pre-Permian strata. However, seismic lines record no strong reflectors below the volcanics, which could be interpreted as Upper Carboniferous Coal horizons (Brink 2004, pers. comm.). Similarly, Westphalian rocks in Mecklenburg, east of Fehmarn, are almost free of coal (Franke, 1990).

Coal bearing rocks are absent in the deep wells of Schleswig-Holstein. However, almost 400 m of Dinantian sediments, intersected by quartz porphyry dykes, were drilled in well Schleswig Z1 beneath the clastic Rotliegend. Limestones and shales are dominant in the lower part. They are overlaid by minor sandstones, followed again by shales. Traces of coal, although extremely rare, suggest the import of terrestrial organic material, while the shales possibly contain marine organic matter. The high maturity of the sediments (vitrinite reflectance: 2.4-4.4% R_o) makes the classification of organic matter from Rock-Eval pyrolysis data impossible. Organic carbon contents of dark grey and black pelites range from 0.2% to 2% TOC, with an average of about 1% TOC (Krooss 2004, pers. com.; Grassmann 2004, pers. com.). The vitrinite reflectance values indicate that these rocks almost completely realised their HC generation potential, so the primary TOC was distinctly higher. Since grey to black shales account for about 250 m thickness, the total amount of organic material may have been about $6 \cdot 10^6$ t/km² originally (figure 11).

Paleogeographic reconstructions suggest that the Lower Carboniferous facies at the southern rim of the Ringkøbing-Fyn-High was dominated by littoral and terrestrial-fluvial deposits of braided rivers (lower part) and deltaic to shallow marine deposits (upper part), passing southwards into a regionally extended carbonate platform (Lokhorst, 1998). Gerling et al. (1999b) pointed out that the northern facies belt may correlate to the Yordale facies of Scotland and NE England. Limestones of the carbonate platform ("Kohlenkalk") covered probably most of Schleswig-Holstein, with increasing continental influence towards the north (Ziegler, 1990; Franke, 1995; McCann, 1996). However, there is some evidence for local, probably fault-controlled facies differentiations. In NE Germany (Rügen aera), Lower Carboniferous sedimentation started with carbonate-rich deposits in tectonically controlled basins, followed by platform carbonates, which are partly replaced by marine deeper water clastics (McCann, 1999). Recent magnetotelluric measurements in Schleswig-Holstein indicate low resistivity zones in the Glückstadt Graben area south of well Schleswig Z1 (Hoffmann et al., 2005). These highly conductive layers can be interpreted as deeply buried carbon-rich black shales in the Lower Carboniferous. Black shale deposition may have been restricted to a pre-Permian depression along the later Glückstadt Graben, while limestones were deposited on the platform areas. It is not unlikely that the Dinantian shales, drilled in well Schleswig Z1, correlate with the (more distal?) black shale facies proposed by Hoffman et al. (2005). The possible existence of local basins in various parts of the Kohlenkalk platform was proposed by e.g. Franke (1990) and Gerling et al. (1999a). Examples have been found in central and northern England, where marine, turbiditic sediments within such deep sub-basins may have source rock potential (Fraser et al., 1990).

Devonian rocks were drilled in clastic, barren facies in well Schleswig Z1. Similar lithologies may be expected in the area of Fehmarn. Lower Paleozoic organic-rich sediments are not present in the northern study area (Ziegler, 1990; Gerling et al., 1999b; Hoffmann et al., 2001). Potential Zechstein source rocks include the Kupferschiefer (~0.5 m) and the

Zechstein 2 carbonate (~10-25 m). However, the effect of post-Permian source rocks is negligible for the three case studies, since 700-1400 m Rotliegend shales and evaporites separate the Zechstein from Rotliegend reservoirs. Even in well Schleswig Z1, which is located close to fault zones, a direct hydraulic contact between the Zechstein and basal Rotliegend sandstones is very unlikely (figure 6).

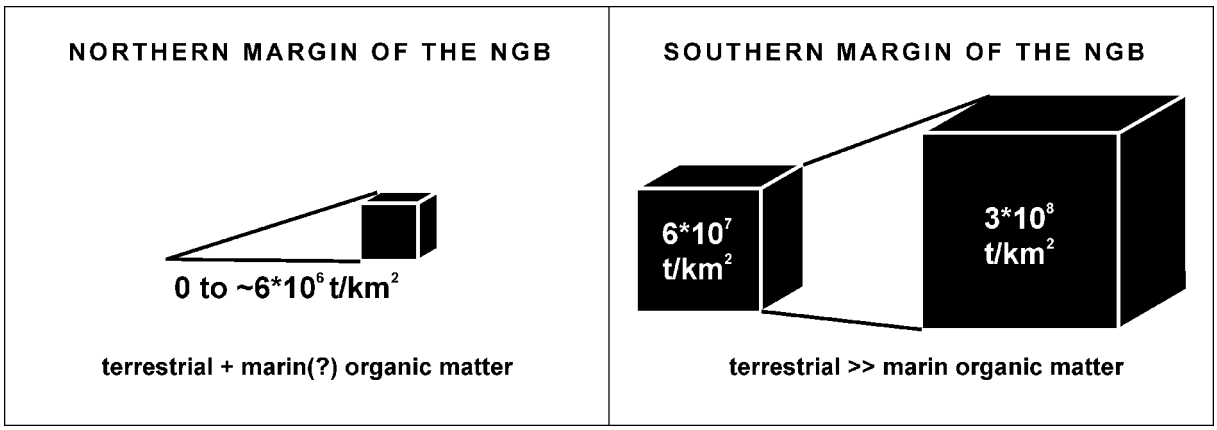

Figure 11: Illustration of the range of organic matter present in the two study areas. Data for the northern basin margin cover the Lower Carboniferous and were estimated from well reports and TOC measurements. Only the main source rock horizons (Namurian C to lower Westphalian C) were taken into account at the southern basin margin. The density of organic material is assumed as 1.6 t/m³. Minimum and maximum values were estimated from literature (see text).

3.3 Source rocks at the southern margin of the NGB

It is widely accepted that coal-bearing Upper Carboniferous sediments, dominantly the Westphalian Coal Measures beneath the Rotliegend deposits, are the most important source rocks for natural gas in the NGB. This is evident from the paleogeographic distribution (figure 1), thickness and lithology of the Carboniferous (e.g. Hedemann and Teichmüller, 1971; Hedemann et al., 1984; Teichmüller et al., 1984; Lokhorst, 1998) as well as from isotopic studies (e.g. Stahl, 1968; Boigk et al., 1971; Faber et al., 1979). Nevertheless, pre- or post-Westphalian source rocks may locally have contributed to gas accumulations in Rotliegend reservoirs (Müller, 1990; Gerling et al., 1999a; Hoffmann et al., 2001).

Westphalian Coal Measures, up to 2500 m in thickness, underlie the Rotliegend succession in the southern part of the NGB (Hedemann et al., 1984; Katzung and Krull, 1984; Stancu-Kristoff and Stehn, 1984). Coal seams are frequent in the Westphalian A-C, and rapidly decrease in number and thickness towards the top (upper Westphalian C, Westphalian D). In addition to coal seams, organic-rich, partly marine pelites have source rock potential. The Westphalian A-C comprises 3-5% coal on average, with a maximum of more than 6% in the Early Westphalian of the Ruhr area (Hedemann et al., 1984; Strack and Freudenberg, 1984; Drozdzewski, 1992). Philipp and Reinicke (1982) assumed about the same range for coal seams plus dispersed coal in Upper Carboniferous sediments of the region NE of Hannover. In the same area, Neunzert (1997) used averages of 2-3% TOC for the Westphalian A to lower Westphalian C as input data for a basin modelling study. His values, however, are dominantly based on interpretation of sonic and gamma ray logs and are likely to neglect dispersed organic material.

In the area investigated, the underlying Namurian sediments with an assumed thickness of 1500-2000 m (Katzung and Krull, 1984; Frisch and Kockel, 2004) comprise coal and partly marine source rocks. Coal seams are sporadically present since the Namurian B and became abundant in the Namurian C (Hedemann et al., 1984). During the early Namurian, deep basins accommodated bituminous shales of type I and II kerogen, while turbidites filling these basins from the south supplied terrestrial organic material (Gerling et al., 1999a; Frisch and Kockel, 2004). Deposition of marine black shales in starved basins (Culm facies) prevailed since Dinantian times (Franke, 1990; Lokhorst, 1998). Magnetotelluric measurements of Hoffmann et al. (1998; 2001; 2005) indicate that Dinantian to Early Namurian black shales cover large areas of NW Germany, including the southern study area (compare figure 10). These source rocks contributed locally to Rotliegend gas accumulations, in particular if the Westphalian had been (partly) eroded prior to Rotliegend deposition (Müller, 1990; Gerling et al., 1999b; Hoffmann et al., 2001). According to Gerling et al. (1999a), TOC-contents of bituminous shales range from 0.5% to 12% in the Dinantian and from 2% to almost 60% in the Namurian. Regional studies in northern Germany mostly assumed averages of 1-2% TOC for the Dinantian and Namurian (Hedemann and Teichmüller, 1971; Müller, 1990; Neunzert, 1997).

It can be expected that any potential Devonian or Lower Paleozoic source rocks (e.g. organic-rich shales, compare Gerling et al. 1999b) had realised most of their HC generation potential at the end of the Carboniferous due to deep burial under Dinantian to Westphalian/Stephanian sediments. Results from basin modelling support this assumption (section 4.2). Pre-Carboniferous source rocks will therefore not be regarded here.

The influence of marine Zechstein source rocks is possible, if a hydraulic contact to Rotliegend reservoirs exists, especially for the uppermost sandstone horizons of the Hannover Formation. Potential oil and gas source rocks with limited thickness are the Kupferschiefer and organic-rich carbonates and mudstones in the Zechstein 2 cycle (Stassfurt). The Kupferschiefer contains about 5% TOC on average, but is mostly less than 1 m thick (Frisch and Kockel, 2004). The Stassfurt source rocks are some metres to few decametres thick and comprise commonly less than 1.2 % TOC of type I, II or III kerogen, depending on sedimentary facies (Gerling et al., 1996). A mixture of Westphalian and minor Zechstein sources was suggested for some Rotliegend reservoirs of northwest Germany (Littke et al., 1996; Gerling et al., 1999a). Nevertheless, Upper Carboniferous Coal Measures are in most cases the dominant source for HC in the southern study area.

To estimate the order of magnitude of organic material present beneath the Rotliegend in the southern part of the NGB, average TOC-values of 3-5% are assumed for the Westphalian, and 1-2% for the Namurian and Dinantian. Zechstein source rocks are omitted for this calculation. Taking minimum and maximum thickness for the Carboniferous from literature (e.g. Hedemann and Teichmüller, 1971; Stancu-Kristoff and Stehn, 1984), approximately 0.6-$3 \cdot 10^8$ t organic material per km² can be expected. This volume is 10 to 50 times as much as the maximum value assumed for the northern study area (figure 11). Terrestrial, gas-prone source rocks of kerogen type III are dominant, especially in the coal-rich succession from the Namurian C to Westphalian C. Nevertheless, sapropelic cannel and boghead coals as well as marine type I and II kerogen shales may be relevant as oil source rocks. Marine source rocks are not only abundant in the Dinantian to Early Namurian, but may be locally present in Late Namurian and Westphalian sediments too. Kettel (1989) pointed out that sapropelic

facies realms prevailed in marine and lacustrine influenced environments in the NW part of the Upper Carboniferous basin, while dominantly humic organic matter was accumulated in flood plain deposits of the German onshore region. However, differential subsidence, the positions of sediment input, and sea level fluctuations induced migration of facies boundaries and periodic flooding of the basin (Süss et al., 2000). Marine influence is evident from several horizons of the German Westphalian (e.g. Teichmüller, 1955; Dahm, 1966; Rabitz, 1966). Sapropelic shales developed especially in limnic environments (Süss et al., 2000). In addition to potential type I or II kerogen, however, oil generation from terrestrial source rocks has to be considered. Leythaeuser et al. (1985) demonstrated that thin shales of the Westphalian A and B, containing <1% TOC of type III kerogen, had expelled oil into inter-bedded sandstone horizons (primary migration). Coal seams themselves contain varying amounts of petroleum producing compounds and are poor to moderate oil source rocks (Boigk et al., 1971; Teichmüller, 1974; Durand et al., 1983; Horsfield et al., 1988; Boreham and Powell, 1993; Littke and Leythaeuser, 1993; Pepper and Corvi, 1995). Although liquid HC are mostly retained within the coal seams, they may be expelled into reservoir rocks, especially along zones of high porosity (Radke et al., 1985; Littke et al., 1989; Forbes et al., 1991; Littke and Leythaeuser, 1993).

4 Numerical simulation of burial history, thermal evolution, and hydrocarbon generation

The numerical simulation of burial and thermal evolution allows to test geological hypotheses of basin evolution and to asses HC generation through time. Main targets in the context of this diagenetic study are to evaluate the burial and thermal history of Rotliegend sandstones, and the timing of HC generation from Carboniferous source rocks. 1D-models have been developed for the wells Fehmarn Z1, Schleswig Z1, and Flensburg Z1 at the northern margin of the NGB (section 4.1). Although 1D-models of well Fehmarn Z1 and Schleswig Z1 were also established by Rodon and Littke (2005), the simulations were carried out independently here for several reasons: (1) Rodon and Littke (2005) concentrated on the post-Zechstein sedimentary succession, while pre-Zechstein rocks are investigated here; (2) HC generation from pre-Rotliegend rocks was not calculated; (3) pre-Upper Rotliegend erosion, which affects the maturity of Carboniferous rocks, was not taken into account (see below); (4) the thermal effects of the dyke intrusion in well Schleswig Z1 were not considered during calibration of the model (see below). Burial history, thermal evolution, and HC generation at the southern margin of the NGB are covered by 1D- and 2D-modelling studies carried out in earlier studies (e.g. Neunzert et al., 1996; Schwarzer and Littke, 2005). The results of these studies are briefly reviewed here (section 4.2).

The principles of numerical simulation of sedimentary basins are explained in Welte and Yükler (1981), Tissot and Welte (1984), Yalçin (1991), Waples (1994), and Welte et al. (1997). Figure 12 shows the work flow of the simulation and the required input parameters for the model. Precondition to set up a numerical model is to define a conceptual model (e.g. Welte and Yükler, 1981; Poelchau et al., 1997). The conceptual model is based on all available geological and geochemical data of the study area. The basin evolution has to be subdivided into consecutive lithological units ("events"). Each event represents a period of sedimentation, non-sedimentation or erosion. Each sedimentary unit ("layer") is characterised by a specific lithology, including all petrophysical properties necessary for the numerical simulation. The heat flow at the base of the model and the temperature at the sediment-water interface together with the paleobathymetry define the lower and upper boundary conditions. The simulation starts with the oldest layer (decompacted), adding successively younger events and calculating compaction, burial history and temperature evolution. Finally, oil and gas generation is simulated based on the thermal history and on reaction kinetic models. The calibrated model has to match the observed thickness of the sedimentary units, the measured present day temperatures, and the measured vitrinite reflectance data. If the simulation does not match the calibration data, the boundary conditions and/or the parameters of the conceptual model have to be modified, and the simulation has to be performed again (figure 12). This procedure is repeated until the result is satisfactory. It should be noted that there may be not only one model, which is geologically reasonable and well calibrated. The sensitivity of the models with respect to various input parameters and the results of different alternative models are discussed in section 4.1.3.

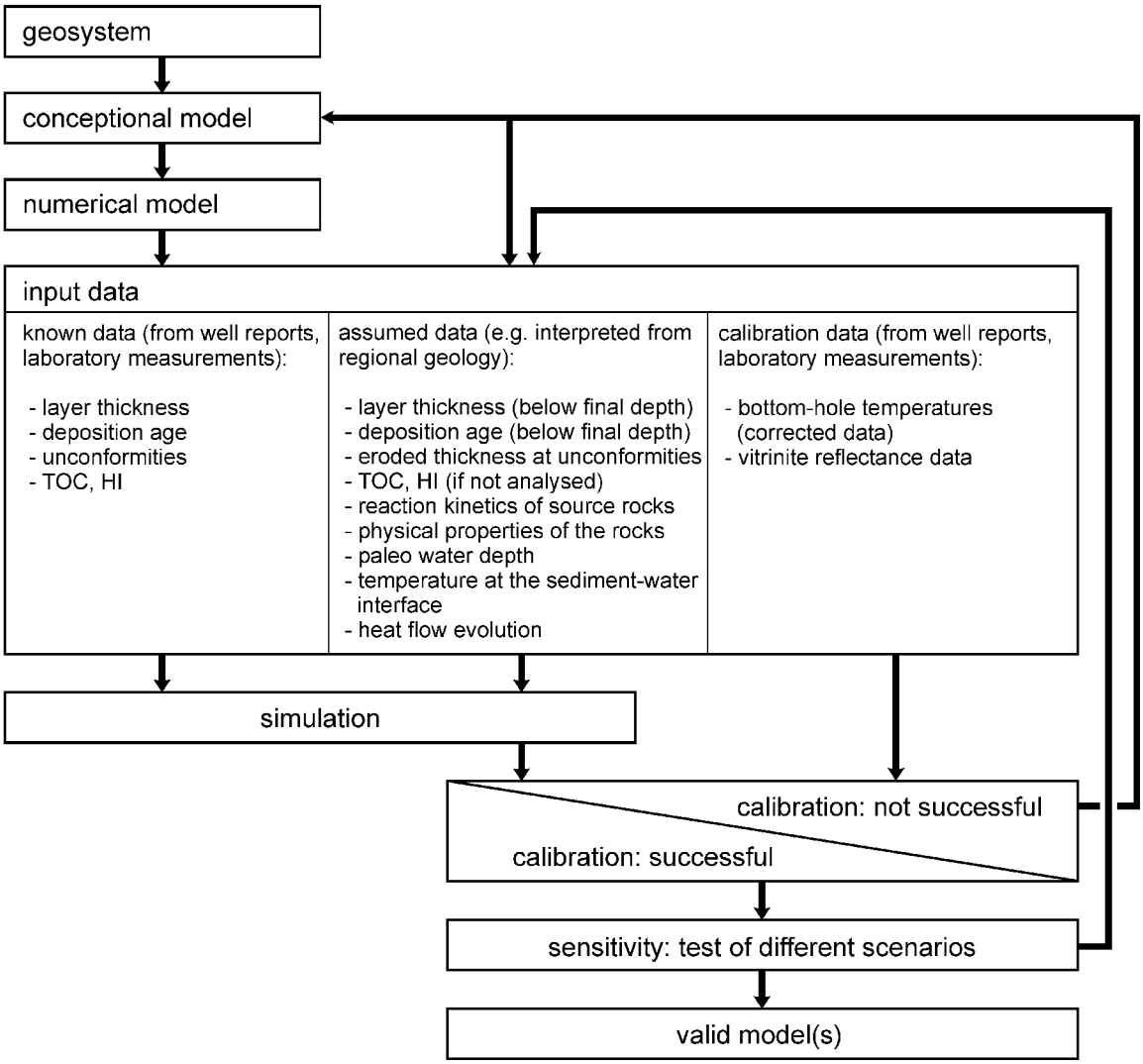

Figure 12: Schematic outline of the work flow during 1D basin modelling. Modified from Welte and Yükler (1981).

4.1 1D-simulations at the northern margin of the NGB

4.1.1 Conceptual and numerical model

The conceptual model for the northern basin margin includes following main assumptions:

- Sediments were deposited from the Devonian until the Westphalian, and locally eroded during the uppermost Carboniferous to Lower Rotliegend.
- Sedimentation started again in Upper Rotliegend times and continued until the Middle Jurassic. Jurassic sediments were eroded during a Middle Jurassic-Lower Cretaceous period of uplift.
- The following phase of sedimentation persisted until the Miocene, when the maximal burial depth was reached. It was interrupted only locally by minor Cenozoic unconformities. The Pliocene-Pleistocene was a phase of non-sedimentation or erosion.

- The sediments were deposited in terrestrial, lacustrine or shallow marine environments, with maximal water depths of a few hundred metres during the Zechstein, Lower Jurassic, Upper Cretaceous, and Paleogene. Surface temperatures varied between ~20-25°C from the Devonian until the Paleogene, then rapidly decreased to present-day values.
- A considerable thermal disturbance combined with a high heat flow occurred around the Carboniferous-Permian boundary simultaneously to crustal thinning and extensive volcanism. In the Glückstadt Graben area, increased heat flow can be assumed again during Triassic rifting.

Events

The definition of sedimentation and non-sedimentation events, and the characterisation of lithologies is mainly based on the well reports provided by the petroleum industry. The input data are summarised in table A3-A5 (appendix). Absolute ages of the lithological units (= events) were assigned according to the time scale of the Deutsche Stratigraphische Kommission (2002). Detailed well information was generalised to layers of some tens to hundreds of metres in thickness.

The deepest horizons encountered by the wells available for this study are deformed metasediments below Rotliegend clastics (well Flensburg Z1, Westerland 1), Rotliegend volcanics (well Fehmarn Z1), and Upper Devonian sediments (well Schleswig Z1, figure 6). Primary thickness and lithology of the pre-Rotliegend horizons in the models was compiled from the rock record of well Schleswig Z1, from deep wells in NE Germany (McCann, 1998, 1999) and in Denmark (Michelsen, 1971; Nielsen and Japsen, 1991). Previous basin-wide paleogeographic reconstructions were also taken into consideration (e.g. Katzung and Krull, 1984; Franke, 1990; Ziegler, 1990). Nevertheless, the estimated thickness and lithology of Lower Paleozoic rocks is hypothetical (table A3-A5, appendix). Erosion up to several thousands of metres in the Late Carboniferous to Early Permian is evident for the Ringkøbing-Fyn-Møn trend of highs and for the Southern North Sea (van Wees et al., 2000). Katzung and Krull (1984) assumed no or very little Namurian sedimentation and a thickness of 0-1000 m for the Westphalian in northern Schleswig-Holstein and around Fehmarn. Drozdzewski (1992) proposed much higher Westphalian thicknesses for the same area (1500-2500 m). Franke (1990) suggested a more or less stable northern margin of the basin in central Denmark/southern Sweden throughout the Carboniferous. In the conceptual model of the present study, 400 m Namurian and 1000 m Westphalian sediments were primarily deposited all over northern Schleswig-Holstein. To satisfy the uncertainty of the pre-Permian geological history in the area of Schleswig-Holstein, different alternative scenarios have been tested (section 4.1.3). The intrusion of the rhyolite dykes (drilled thickness up to 270 m), which crosscut the Lower Carboniferous of well Schleswig Z1, was defined as an event at the Carboniferous-Permian boundary. 800°C were assumed as intrusion temperature.

Rotliegend sediments were subdivided into four layers to allow for different lithologies and to avoid extremely thick layers (> 1000 m). The layer "Havel sst." contains the core intervals sampled during this project. No evidence of mobilised Rotliegend salt has been found in the salt domes next to investigated wells (Baldschuhn et al., 1996). The primary thickness of the Zechstein in northern Schleswig-Holstein was probably 900-1100 m (Weber, 1977; Clark and Tallbacka, 1980). Zechstein equal or similar to the likely primary thickness was drilled in well Fehmarn Z1 (942 m). Only minor salt movement is known from that area (Jaritz, 1973;

Weber, 1977; Baldschuhn et al., 1996). The other two wells, which comprise Zechstein of significantly less thickness, are located close to salt diapirs (Flensburg-Sieverstedt and Langsee salt diapir). The original thickness of the Zechstein was defined as 1000 m for all three wells. The timing of salt migration was assigned according to Jaritz (1973, see table A3-A5, appendix). The uppermost part of the Zechstein salt in well Schleswig Z1 was probably removed by subrosion during the Triassic, since Lower Keuper sediments rest directly upon the Zechstein. Subrosion was handled as erosion in the numerical model.

The Buntsandstein, which was only drilled in well Fehmarn Z1 and Flensburg Z1, was subdivided into three layers. Several unconformities are evident for this period of dominantly continental and lacustrine sedimentation (Geluk and Röhling, 1997). Rifting in the central part of the Glückstadt Graben started in the Middle Buntsandstein, although local tectonic movements were already active in the uppermost Zechstein (Kockel, 2002). Brink et al. (1992) suggested that faulting was accompanied by wrench deformation, particularly in the northern part of the Graben. Reduced Lower Triassic sequences are preserved on uplifted Graben shoulders. Up to hundreds of metres may have been eroded at the Hardegsen (pre-Solling) unconformity (Röhling, 1991; Geluk and Röhling, 1997). However, thickness variations in the Buntsandstein could also be a result of syn-sedimentary faulting in a low-relief landscape (Radies et al., 2005). For well Flensburg Z1, 200 m erosion was estimated at the Hardegsen unconformity in accordance with the concept of Röhling (1991). Other unconformities were neglected with regard to the time-scale of the model, and continuous sedimentation was assumed. It is not clear if Buntsandstein sediments were deposited primarily on the structural high explored by well Schleswig Z1, which was located close to the western boundary fault of the central Glückstadt Graben during the Early Triassic (Baldschuhn et al., 1996; Kockel, 2002, figure 6). For modelling purposes, it was assumed that sedimentation terminated and subrosion of Zechstein evaporites started at the Zechstein-Buntsandstein boundary. Muschelkalk, which is 200-270 m thick in the other two wells, is also missing in well Schleswig Z1. Again, it was assumed that no sediments were accumulated there. During the Keuper, 500-550 m of clastic and evaporitic sediments were deposited east and west of the Glückstadt Graben area (well Fehmarn Z1, Flensburg Z1). Three times as much are recorded in well Schleswig Z1. This sediment distribution reflects the period of rapid subsidence in the Glückstadt Graben, which was related to extensional tectonics and to strong salt movements (Brink et al., 1992; Baldschuhn et al., 1996; Maystrenko et al., 2005).

Jurassic sediments of limited thickness (65 m) are only preserved in well Flensburg Z1. However, regional geological data suggest continued sedimentation at least until the end of the Lower Jurassic in most parts of Schleswig-Holstein (Ziegler, 1990). Up to 2000 m of Jurassic sediments accumulated in deep troughs in NW Germany, which are related to salt migration (Trusheim, 1957; Bentz, 1958; Brand and Hoffmann, 1963; Baldschuhn et al., 1996). In the area investigated, paleogeographic reconstructions indicate a thickness of ≤500 m for the Lower Jurassic and termination of sedimentation probably in the Middle Jurassic (Brand and Hoffmann, 1963; Boigk, 1981; Ziegler, 1990). Jaritz (1969; 1980) postulated uplift of 700 m or more for most parts of Schleswig-Holstein in the Late Jurassic and Early Cretaceous. From regional seismic profiles published in Baldschuhn et al. (1996), 100-200 m remnant Jurassic thickness is evident in the vicinity of the wells studied here (figure 6). The localities are located close to the margin of the Jurassic sedimentation area at the rim of the Ringkøbing-Fyn High (Ziegler, 1990), so a moderate primary thickness of

Jurassic sediments appears to be likely. For modelling purposes, an original thickness of 200 m and 400 m was assumed for well Fehmarn Z1 and for the wells in the Glückstadt Graben area, respectively.

A large area of the Ringkøbing-Fyn-High and the Pompeckj-Block was uplifted during the Upper Jurassic and the lowermost Cretaceous (Jaritz, 1969; Ziegler, 1981). Sediment accumulation started again in the Hauterivian (well Schleswig Z1, Flensburg Z1) or Aptian (well Fehmarn Z1), when the uplifted areas were successively flooded (Schott et al., 1967). Deposition rates, however, remained very low throughout the Early Cretaceous. Increased sedimentation rates in the Upper Cretaceous (~600 m chalk deposition in total) correspond to the global sea level highstand during that time (Haq et al., 1987).

The Paleocene was a phase of condensed sedimentation or non-sedimentation. Parts of the uppermost Cretaceous and/or Lower Paleocene were eroded locally (Baldschuhn, 1979; Fahrion, 1984). Thin Danian sediments, which were only drilled in well Flensburg Z1, were added to the youngest Cretaceous unit. The thickness of Upper Paleocene to Miocene sediments varies between 270 to 960 m in the three wells. Enhanced sediment accumulation in well Flensburg Z1 can be related to contemporaneous salt migration (Jaritz, 1973; Hinsch, 1974, 1986). Only parts of the Paleogene and Neogene sequence are preserved in well Fehmarn Z1 and Schleswig Z1. Although several unconformities are evident, which were caused by local salt migration and by basin-wide transgressive-regressive cycles (e.g. Hinsch, 1974; Kockel, 1980; Gramann and Kockel, 1988), it is not reasonable to resolve them on the scale of this modelling approach. Erosion of the upper part of the Miocene sequence is likely for well Schleswig Z1, where brown coal horizons are directly underlying the Peisto-/Holocene, and for well Fehmarn Z1, where the Oligocence to Pliocene is completely missing. Potential other intra-Paleogene/Neogene periods of non-sedimentation or erosion were neglected. Thin clastic sediments on top of each sequence were summarised as deposits of the last 1 Ma of earth history.

Lithology, source rocks and hydrocarbon generation kinetics

Petrophysical properties of the layers were taken from PetroMod® standard lithologies, since no other data were available. A suitable lithology was assigned to each event using the descriptions of cores and drill cuttings in the well reports. In some cases, complex lithofacies associations required the definition of new lithologies by mixing of existing standard lithologies (table A6, appendix).

As described in section 3, lithologies with major source rock potential for Rotliegend reservoirs are absent or rare in the area investigated. No source rocks are evident in well Flensburg Z1. HC generation was calculated for the Lower Carboniferous of well Schleswig Z1 and for assumed Lower Carboniferous and Namurian rocks in well Fehmarn Z1. Kinetic data for HC generation in these rocks are not existent, and the maturity of the samples in well Schleswig Z1 is too high to determine kinetic data experimentally. In other areas of the NGB, the Upper Carboniferous was investigated for the methane and nitrogen generation potential (e.g. Krooss et al., 1995; Littke et al., 1995). In this study, the early periods of organic maturation including oil generation are of special interest, since early maturation products (e.g. organic acids, CO_2, liquid HC) are likely to react with inorganic components in source and reservoir rocks (e.g. Surdam et al., 1989; Barclay and Worden, 2000; Seewald, 2003,

compare section 7). These products are generated before and during the main phase of oil generation (compare Hunt, 1979; Surdam et al., 1984). Therefore, the timing of oil generation was calculated using established kinetic data sets with different oil generation and oil degradation characteristics (table 3). These data sets are available in the PetroMod® software. The kinetic model of Burnham (1989), determined from laboratory experiments, suggests little oil generation for type III kerogen. Pepper and Corvi (1995) determined oil and gas generation for source rocks deposited on coastal plains using field and laboratory data from several sites and stratigraphic intervals, including the Westphalian (type III/IV, organofacies F). Their model implies relatively high oil generation rates. The possibility that the Lower Carboniferous of well Schleswig Z1 may contain a significant portion of marine organic matter was taken into account by simulating HC generation additionally with appropriate kerogen type II kinetics (table 3). Other kinetic approaches were tested in a sensitivity study (section 4.1.3).

Table 3: Kinetic models used for simulation of HC generation in the Lower Carboniferous of well Schleswig Z1 and well Fehmarn Z1. The kinetic data are available in the PetroMod software.

Primary oil and gas reaction	HI_{Oil} [mg/g_{TOC}]	HI_{Gas} [mg/g_{TOC}]	secondary cracking
well Schleswig Z1 and Fehmarn Z1:			
Burnham (1989) TIII	50	110	Burnham (1989) TIII
Pepper and Corvi (1995) TIII-IV (F)	158	70	Schenk et al. (1997) TIII (Mahakam)
additionally (well Schleswig Z1 only):			
Burnham (1989) TII	350	65	Burnham (1989) TII
Pepper and Corvi (1995) TIIS (A)	617	105	Schenk et al. (1997) TII (Smackover)
alternative kinetic models tested during sensitivity analysis:			
Behar et al. (1997) TIII (Mahakam)	72	28	Schenk et al. (1997) TIII (Mahakam)
Behar et al. (1997) TIII (Dogger)	155	57	Schenk et al. (1997) TIII (Mahakam)
Vandenbroucke et al. (1999) TIII (Brent)	155	78	Schenk et al. (1997) TIII (Mahakam)
additionally (well Schleswig Z1 only):			
Behar et al. (1997) TII-S(MontSh)	490	70	Schenk et al. (1997) TII (Smackover)
Vandenbroucke et al. (1999) TII (KCF)	501	77	Schenk et al. (1997) TII (Tuscaloosa)

Calibration data

Calibration data were available from unpublished industry reports. They comprise vitrinite reflectance data (well Schleswig Z1, Fehmarn Z1) and temperature measurements (3 wells). The provided temperature values are bottom-hole temperatures corrected partly by the Horner method (compare e.g. Dowdle and Cobb, 1975; Kutasov and Eppelbaum, 2005), and partly by other methods, which were not specified in the well reports. Additional virtinite measurements of well Flensburg Z1 were taken from Rodon and Littke (2005). Vitrinite reflectance is an indicator for the maximal maturity of the sediments; measured temperatures should reflect the present-day temperature gradient. Calibration of the model was accomplished by comparing calculated maturity and temperature data with measured values. The vitrinite reflectance was calculated using the EASY%R_o approach (Sweeny and Burnham, 1990), which is valid for the maturity range of 0.3-4.5% R_o.

Paleo water depths and temperature at the sediment-water interface

The paleo water depths are based on a combination of data compiled from the well reports, global sea level cycles (Haq et al., 1987), and studies on the depositional environment of different stratigraphic units in NW Germany (Brand and Hoffmann, 1963; Schott et al., 1967; Jaritz, 1969; Hedemann and Teichmüller, 1971; Hinsch, 1974; Weber, 1977; Clark and Tallbacka, 1980; Franke, 1990; Ziegler, 1990; Röhling, 1991; Beutler et al., 1996; McCann, 1996; Glennie, 1998; Beutler and Szulc, 1999). Only long term trends could be considered and fluctuations of water depth had to be strongly generalised to allow for the precision of the simulation. Maximal water depths of 200-300 m were defined for the Zechstein, Early Jurassic, Late Cretaceous and Paleogene (figure 13).

The temperature at the sediment-water interface, which designates the upper temperature boundary of the model, was calculated with an automatic PetroMod® routine. This calculation is based on the evolution of global surface temperatures and on plate movements through earth's history, corrected for the paleo water depth (Wygrala, 1989). The temperatures mostly vary around 25°C until the Cretaceous, and decrease from the Early Paleogene onwards to values of about 5°C in the Neogene (figure 13).

Heat flow

The temperature input at the base of model is defined by the heat flow (lower temperature boundary). Only the present day heat flow and the heat flow during the time of maximal maturity can be deduced from the calibration data. The remaining heat flow history has to be estimated from the geological and geotectonic evolution of the study area. The mean continental heat flow in Europe is about 65 mW/m² (Cermak, 1979; Kappelmeyer, 1985), which is within the range of the global average of 60-70 mW/m² (Allen and Allen, 1997). However, it is not likely that the NGB was characterised by a constant heat flow through time. The initiation of basin formation in Late Carboniferous-Early Permian times involved thermal thinning of the mantle-lithosphere combined with crustal extension (van Wees et al., 2000). Lithospheric thinning and the extensive contemporaneous magmatism (e.g. Benek et al., 1996; Breitkreuz and Kennedy, 1999) indicate a heat flow increase during that period. Average values for active rift basins range from 65-110 mW/m², with an average of 80 mW/m² (Allen and Allen, 1997). The recent surface heat flow in the Upper Rhine valley reaches values of 90 to locally >150 mW/m² in the Graben centre, and it exceeds 100 mW/m² in areas around active volcanoes, e.g. in Italy (Cermák, 1979; Hurtig et al., 1992).

The conceptual model of this study assumes a constant heat flow of 65 mW/m² for the Paleozoic, modified by a thermal perturbation at the Carboniferous-Permian boundary (figure 13). This results in a maximal heat flow of 80 mW/m² in areas devoid of volcanic deposits (Schleswig Z1, Flensburg Z1), and 90 mW/m² in areas closer to presumable volcanic centres (Fehmarn Z1). Previous basin modelling studies in the NGB mostly applied similar heat flow values for this time period (Neunzert, 1997; Friberg, 2001; Schwarzer and Littke, 2005). For the Glückstadt Graben, increased heat flow (maximal 75 mW/m²) was assumed again during the Triassic extensional phase (figure 13). The conceptual model further involves a heat flow decrease to about 60 mW/m² in the Early Jurassic and a constant heat flow since then. To account for the uncertainty of heat flow evolution, especially for the

periods which can not be controlled by calibration data, different scenarios were tested during the simulation (see section 4.1.3).

well Fehmarn Z1

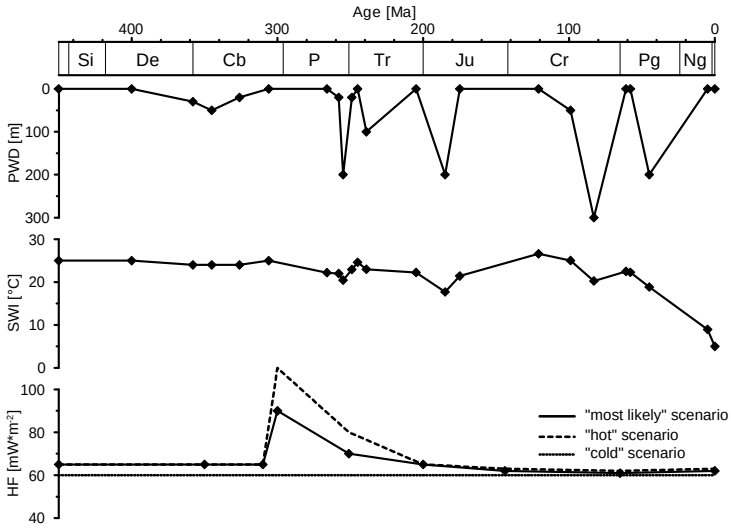

well Schleswig Z1

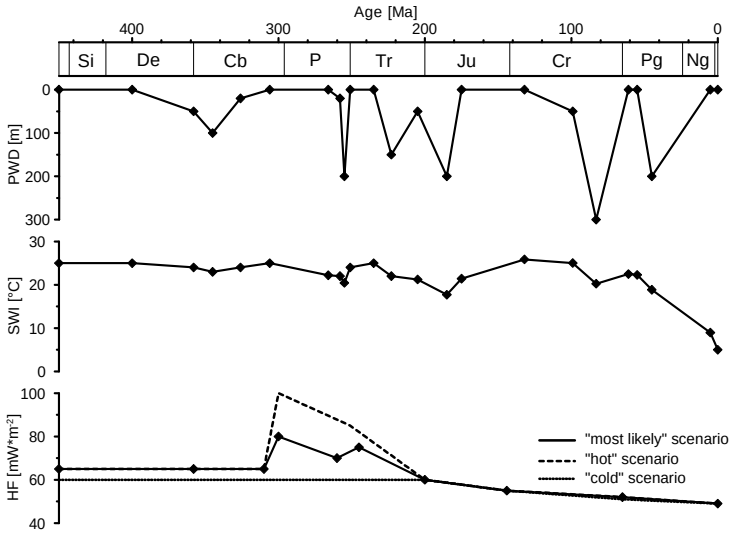

well Flensburg Z1

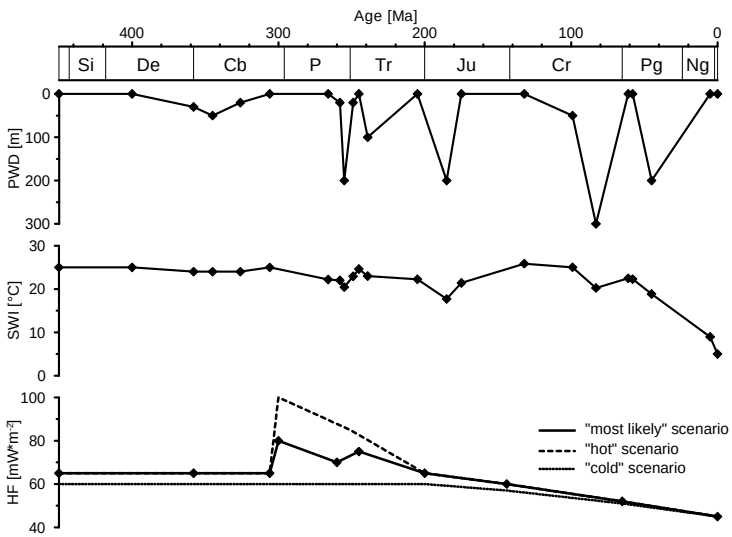

Figure 13: Boundary conditions for the calibrated models of well Fehmarn Z1, Schleswig Z1, and Flensburg Z1. PWD = paleo water depth, SWI = temperature at the sediment-water interface, HF = heat flow. The heat flow was modified for the simulation of different scenarios, as well as the thickness of eroded sediments (see text).

4.1.2 Results of the 1D-simulations

Test simulations have been run with a cell thickness of 100 m, the final simulations with 50 m cell thickness. Successful simulations had a relative difference <1% between the numerical input model and the calculated model. All simulations started with a constant heat flow of 65 mW/m² and no erosion throughout the model. Both parameters were then adapted to the initial conceptual model. The present day heat flow, the heat flow at the time of maximal maturity of the sediments and the potential thickness of eroded strata during the same time interval are results of the simulation and were adjusted iteratively during calibration of the model (see figure 12). This section presents the results of the preferred 1D-models. Alternative scenarios and their significance are discussed in section 4.1.3.

Simulation of well Fehmarn Z1

Five major phases may be defined in the burial history of well Fehmarn Z1 (figure 14A). Devonian to Westphalian sedimentation (phase 1) was followed by uplift, erosion and dominantly non-sedimentation during the latest Carboniferous and Lower Rotliegend (phase 2). Only Rotliegend volcanics were deposited during that time. Sedimentation started again in the Upper Rotliegend with high accumulation rates, which declined throughout the Triassic and Jurassic (phase 3). The post-Mid-Jurassic uplift removed any Jurassic strata (phase 4). Increased sedimentation rates in the Upper Cretaceous slowed down in the Cenozoic and were interrupted by short periods of uplift and erosion in the Paleocene and Late Neogene (phase 5).

Simulation with a constant heat flow of 65 mW/m² resulted in almost acceptable vitrinite reflectance and temperature profiles, although the calculated temperatures above 3000 m are slightly higher than the measured temperatures, and the calculated vitrinite reflectance is slightly above the mean measured value from the Zechstein (~3750 m, figure 14B). The heat flow scenario as described in the conceptual model produced similar results. The resulting model includes 100 m erosion of Upper Cretaceous plus Danian, and 100 m Eocene sediments, together with a present day heat flow of 62 mW/m². Minor erosion during the Paleogene has been defined due to the lack of Danian sediments and relatively thin Maastrichtian deposits, but hardly affects the calibration. The calibration data do not allow to control the amount of Mesozoic or Paleozoic erosion. The calibrated model is only in accordance with the lowest vitrinite reflectance values above 1600 m depth (figure 14B). It is impossible to obtain a better fit unless assuming at least 1500 m eroded Eocene to Miocene sediments together with a very low heat flow (~45 mW/m²) during that time. This would imply a heat flow increase of about 20 mW/m² in the Neogene to match the present day temperature data. There is no evidence from the geotectonic history for major erosion and major heat flow changes in the Neogene, so this scenario was discarded. The relatively high maturities measured for some vitrinites of Triassic, Cretaceous and Paleogene sediments can be explained by the detrital origin of the organic material. Vitrinite may be inherited from older stratigraphic horizons, or oxidation during sediment transport may be responsible for an increase in vitrinite reflectance. Only the lowest values are therefore likely to reflect the actual maturity of the sediments.

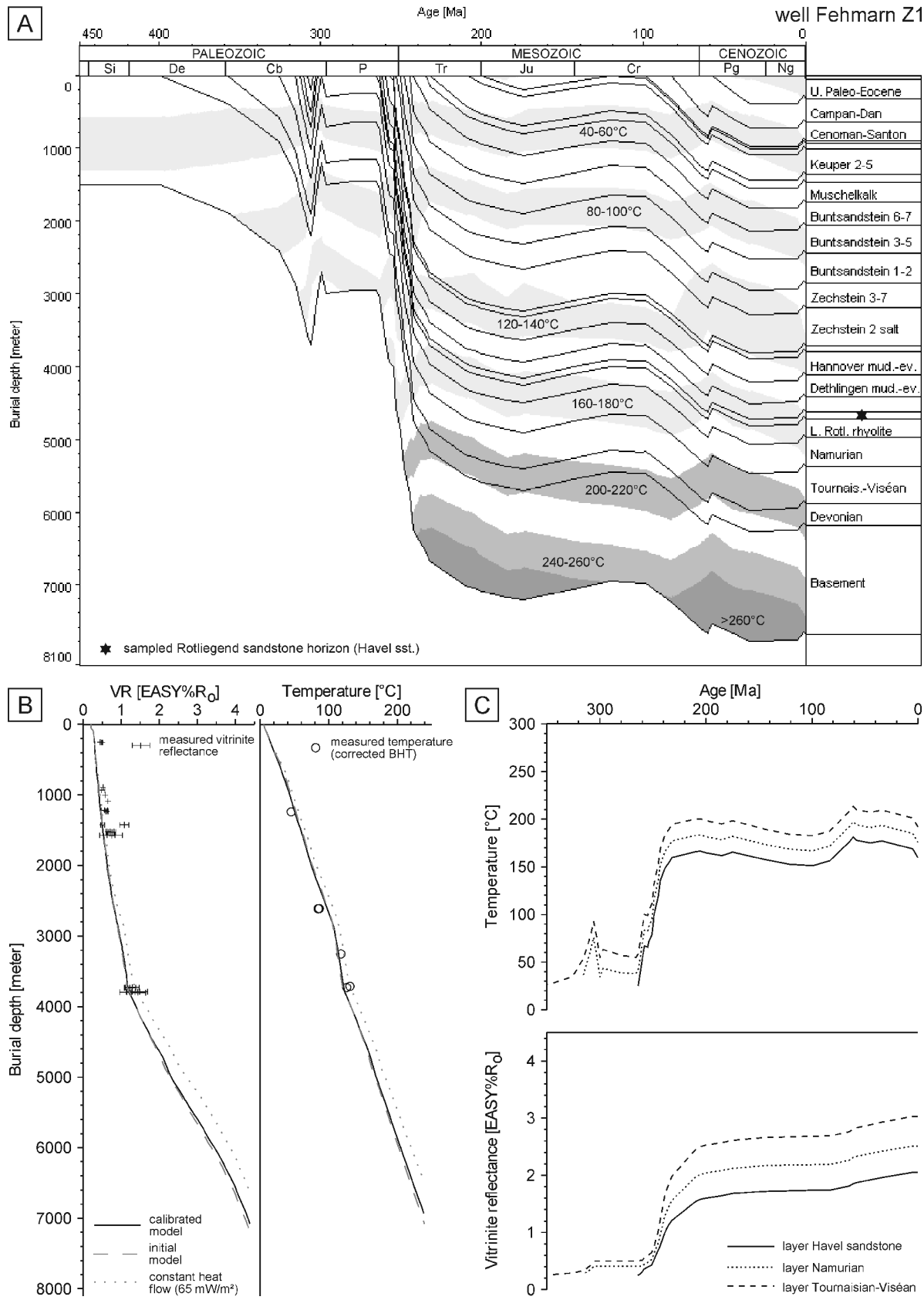

Figure 14: A) Burial history and temperature evolution for the calibrated model of well Fehmarn Z1. Temperature isolines are indicated by white and grey bars of 20°C temperature intervals. B) Measured and calculated vitrinite reflectance and temperature of well Fehmarn Z1. The calibrated model matches the measured data. C) Calculated temperature and maturity evolution of the sampled Rotliegend horizon (Havel sst.), the Namurian, and the Tournaisian-Viséan (well Fehmarn Z1, calibrated model).

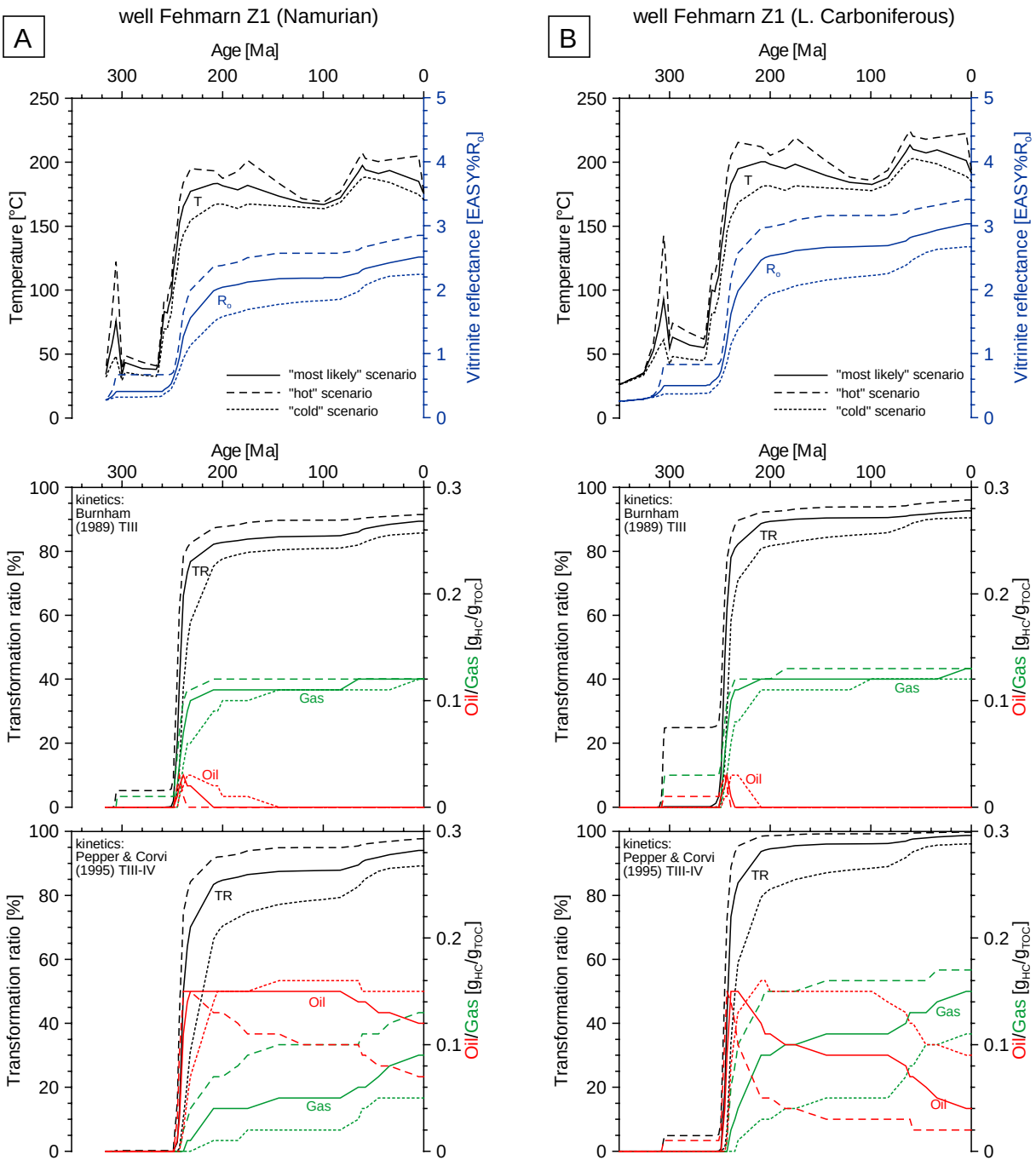

Figure 15: Evolution of temperature, maturity and HC generation for the Carboniferous of well Fehmarn Z1. HC generation was calculated using the kinetic models of Burnham (1989) TIII, and Pepper and Corvi (1995) TIII-IV(F) (see text). Additionally to the "most likely scenario", two calibrated models for a "hot" (dashed line) resp. "cold" (dotted line) scenario are shown. Note that the calculations remain hypothetical since no information on the thickness of Carboniferous rocks is available in that area. A) Layer Namurian (assumed top Carboniferous). B) Layer Tournaisian-Viséan (base Carboniferous).

The highest temperature and maturity was reached during the Paleogene to Neogene, but a first temperature maximum is evident during the Late Triassic to Early Jurassic (figure 14C). The temperature of basal Rotliegend clastics rapidly increased during the Late Permian and Early Triassic to about 165°C in Late Triassic times. Late Jurassic to Early Cretaceous uplift caused only minor cooling (~10°C), before further burial resulted in maximum temperatures of about 185°C for the base of the Rotliegend sediments. The Namurian was heated up to approximately 185°C (Late Triassic) and 200°C (Paleogene). The temperature maxima of the layer Tournaisian-Viséan were still 15°C above these values. The first maturation of Carboniferous strata occurred during the Late Carboniferous, when the Tournaisian-Viséan reached vitrinite reflectance values in the range of 0.5% R_o (figure 14C). The major period of maturation was the Late Permian and Triassic. By Early Jurassic times, vitrinite reflectance had increased to ~2.1% R_o in the Namurian and ~2.6% R_o in the Tournaisian-Viséan. A slow but continuous maturity rise is evident throughout the Jurassic and earliest Cretaceous. Late Cretaceous-Cenozoic subsidence brought about further maturation up to present day values of approximately 2.7% and 3.2% R_o (Namurian and Tournaisian-Viséan).

Figure 15 shows the calculated HC generation of the preferred model (solid lines) and of two alternative models ("hot" and "cold" scenario), which will be discussed in section 4.1.3. In Namurian and Tournaisian-Viséan sediments, the first significant transformation of organic material into HC started in Early Triassic times with both the kinetic model of Burnham (1989) and Pepper and Corvi (1995). 70-85% of the HC generation potential of these horizons were realised during the Lower to Middle Triassic, and 80-95% before the end of the Triassic. A minor pulse in HC generation is evident during the Late Cretaceous to Paleogene. Present day transformation ratios range from 90% to 96% for the Namurian, and from 94% to 99% for the Tournaisian-Viséan according to the kinetic data for type III kerogen of Burnham (1989) and Pepper and Corvi (1995). Oil was generated only during a short time interval from the Early to Middle Triassic. Using the kinetic data of Burnham (1989), most gas was also produced during that period, but slow gas generation prevailed until the Late Triassic. A minor second gas production occurred in the Late Cretaceous/Cenozoic. Simulations with the kinetics of Pepper and Corvi (1995) resulted in major gas generation during the Middle to Late Triassic and Late Cretaceous to Cenozoic, while minor amounts of gas were also produced in the Jurassic.

Simulation of well Schleswig Z1

Similar to well Fehmarn Z1, the burial history can roughly be subdivided into five phases (figure 16A). The first phase involves a increase in subsidence rates from the Devonian to the Westphalian. Erosion and non-deposition prevailed during the uppermost Carboniferous and Lower Rotliegend (phase 2). The third phase is characterised by most accelerated burial during the Upper Rotliegend, Zechstein and Lower to Middle Keuper, which slowed down in Middle to Upper Keuper and Lower Jurassic times. Sedimentation was interrupted by a period of non-deposition and subrosion/erosion in the Early Triassic. Upper Jurassic-Lower Cretaceous uplift and erosion (phase 4) was followed by relatively high Upper Cretaceous and moderate Cenozoic sedimentation rates, including times of non-deposition and minor erosion (phase 5, see also section 4.1.1). The maximum burial was reached in the Neogene.

Simulation with constant heat flow (65 mW/m²) and without erosion produced a misfit between calculated and calibration data (figure 16B). Applying the parameters of the conceptual model resulted in a better match of the maturity data, but also a poor fit of simulated versus measured temperatures. The latter require a present day heat flow of 49 mW/m². Almost the same result (50 mW/m²) was obtained by Rodon and Littke (2005). An good match between calculated and measured vitrinite reflectance could be achieved by assuming 400 m of eroded Jurassic sediments and a heat flow decrease from 60 mW/m² at the Triassic-Jurassic boundary to present day values (compare figure 13). An acceptable calibration would also be possible by increasing the eroded thickness of the Lower Jurassic (e.g. 800 m) and slightly decreasing the coeval heat flow. However, the scenario pointed out in the conceptual model has been preferred here. This model is not sensitive to thickness changes of eroded Upper Carboniferous, Early Triassic, or Cenozoic rocks, as long as they remain geologically reasonable. There is also almost no control on Paleozoic, Early Triassic and Cenozoic heat flow from the calibration data.

Figure 16C shows the calculated temperature and maturation history for the horizons Tournaisian a (lowermost source rock horizon), Viséan b (uppermost source rock horizon), and Havel sandstone (sampled reservoir horizon). The rocks experienced two temperature maxima during the Late Triassic to Lower Jurassic, and during the Early Paleogene. In Late Triassic times, Rotliegend sandstones heated up to about 190°C, while the Lower Carboniferous reached temperatures between 190°C and 215°C according to this model. Lower Carboniferous temperature and maturity were strongly affected by the intrusion of dykes, which were assumed to be 297-300 Ma in age (table A4, appendix). Most of the Lower Carboniferous was overmature with respect to HC generation by that time. For the uppermost layer (Viséan b), the program calculated an average vitrinite reflectance of ~1.9% R_o in the Early Permian. Further maturation took place during the rapid Late Permian and Triassic burial and temperature rise. The top Carboniferous had almost reached its present day maturity of about 2.8% R_o by Jurassic times.

Using the temperature and maturation history of this model, the ratios of kerogen to HC transformation in the Carboniferous would be 50-100% in different layers immediately after the rhyolite intrusion. However, it is likely that these intrusions only locally affected the temperature field, and that the calculation does not represent the average HC generation history in this area. Hence, simulations were carried out omitting the temperature effect of the intrusions. The results of these calculations are displayed in figure 17 (solid lines) together with alternative scenarios (see section 4.1.3). Major periods of maturation were the Late Permian and the Late Triassic. At least 70-80% of the HC generation potential of the basal Carboniferous layer was realised by Early Triassic times, while transformation ratios >90% were reached at the end of the Triassic. There is almost no HC generation in post-Jurassic times. Assuming dominantly type III organic matter, different kinetic approaches result in variable transformation ratios in layer Viséan b in the Early Triassic (30-60 %), while 85-90 % were transformed at the Triassic-Jurassic boundary. If marine type II kerogen was present, it had lost its HC generation potential almost completely at the end of the Permian in all horizons of the Carboniferous. For the base of the Carboniferous (layer Tournaisian a), main oil generation took place in Late Permian respectively Late Permian to Early Triassic times, depending on the kinetic data. Gas generation started in the Late Permian or at the beginning of the Triassic, and prevailed - with interruptions - until Late Triassic to Early Jurassic. The top Carboniferous (layer Viséan b) generated oil in the Late Permian, and again during

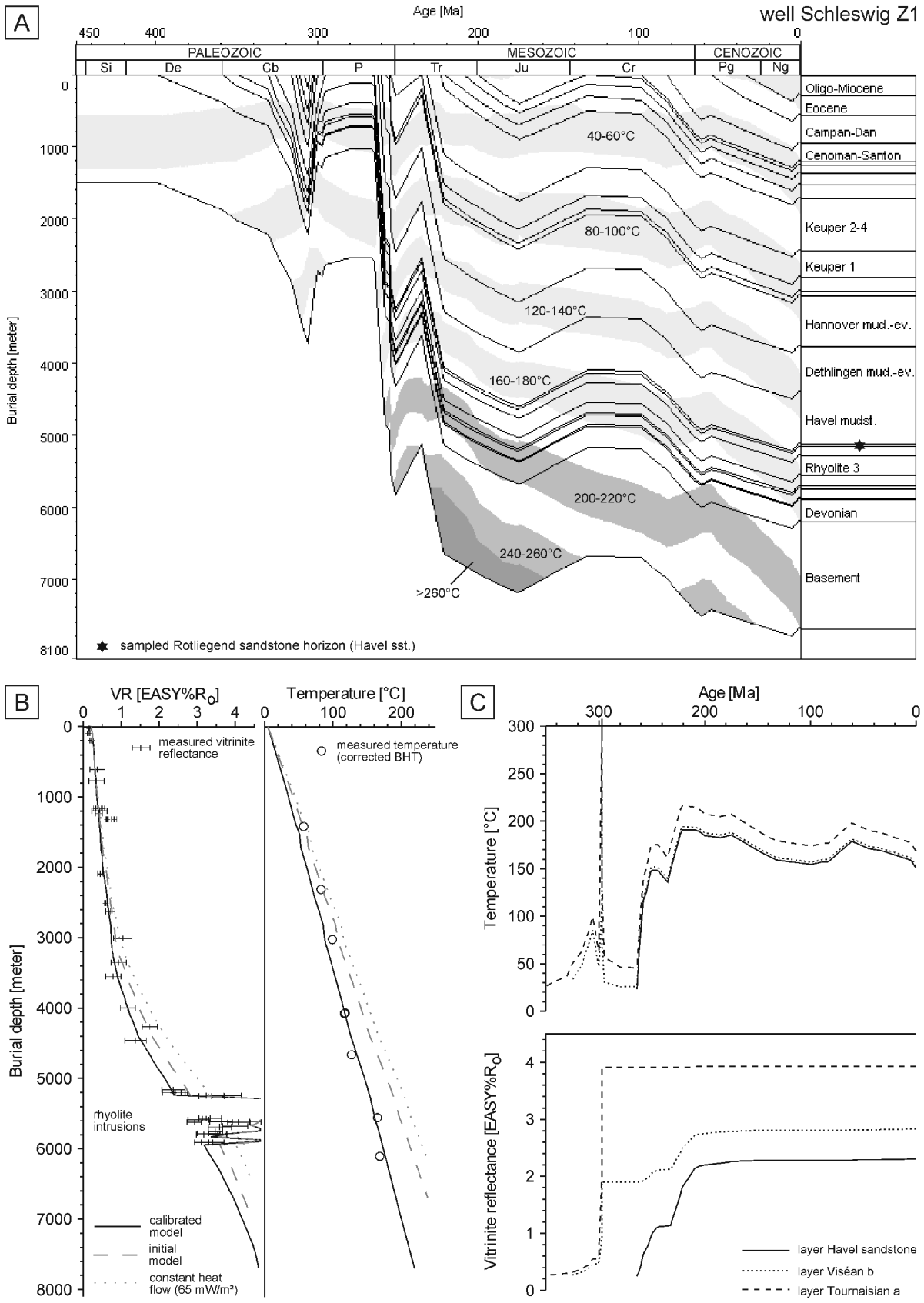

Figure 16: A) Burial history and temperature evolution for the calibrated model of well Schleswig Z1. Temperature isolines are indicated by white and grey bars of 20°C temperature intervals. B) Measured and calculated vitrinite reflectance and temperature of well Schleswig Z1. The calibrated model matches the measured data. C) Calculated temperature and maturity evolution of the sampled Rotliegend horizon (Havel sst.) and the top (Viséan b) and base (Tournaisian a) of the Carboniferous (well Schleswig Z1, calibrated model).

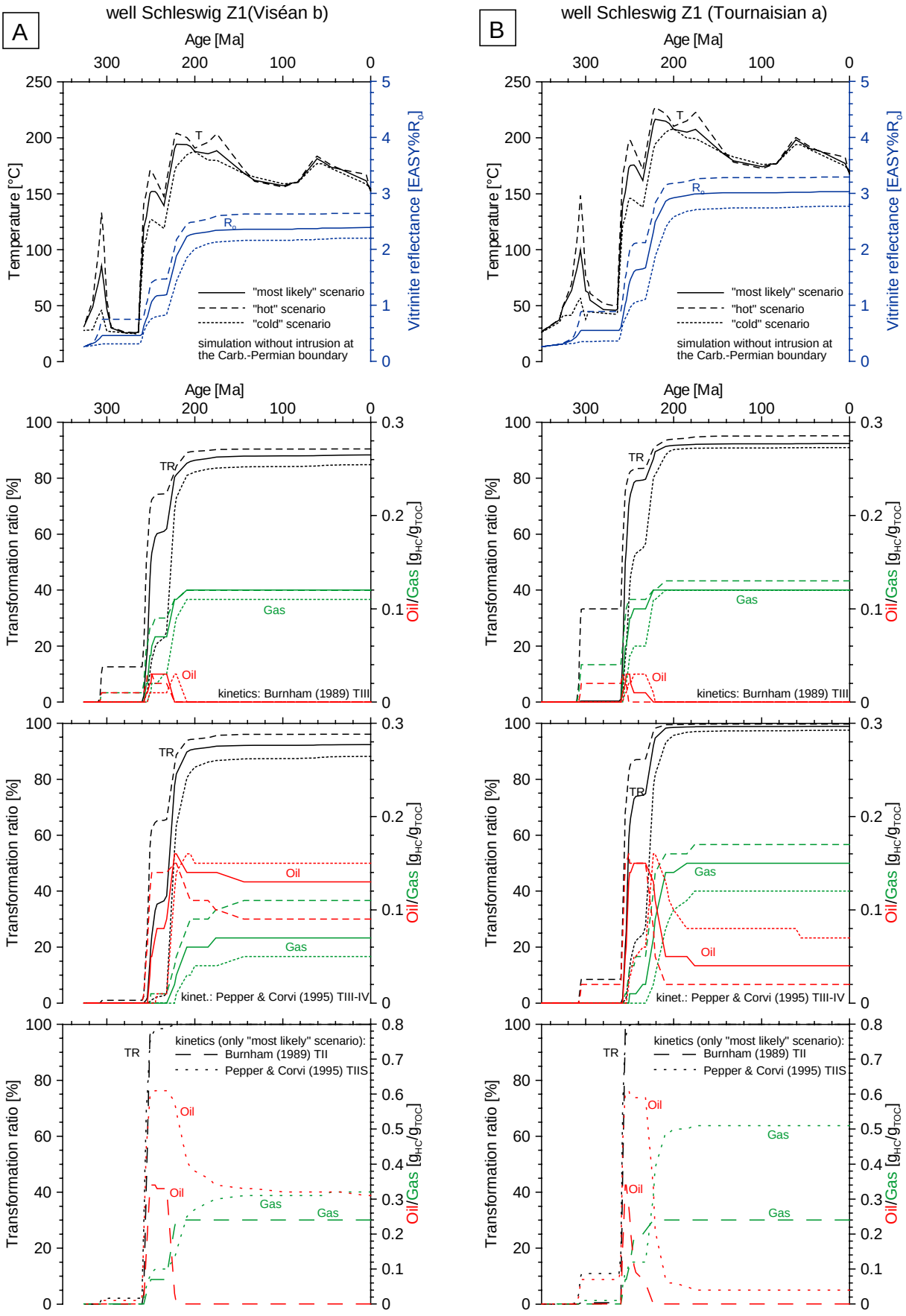

Figure 17: Evolution of temperature, maturity and HC generation for the Carboniferous of well Schleswig Z1. HC generation was calculated using different kinetic models of Burnham (1989) and Pepper & Corvi (1995, see text). The temperature effect of Permian-Carboniferous intrusions was omitted. Additionally to the "most likely scenario", two calibrated models for a "hot" (dashed line) resp. "cold" (dotted line) scenario are shown. A) Layer Viséan b (top Carboniferous). B) Layer Tournaisian a (base Carboniferous).

the Keuper, following the kinetic data of Pepper and Corvi (1995) for terrestrial organic matter. Applying the kinetics of Burnham (1989), gas was dominantly produced in the Late Permian and Keuper, while the kinetics of Pepper and Corvi (1995) suggest that Keuper and Lower Jurassic were the periods of main gas generation.

Simulation of well Flensburg Z1

The general trend of the burial history is comparable to the other two wells from Schleswig-Holstein (figure 18A). Three periods of subsidence, the Devonian to Westphalian, the Upper Rotliegend to Early Jurassic, and the Late Cretaceous to Neogene, are separated by two major periods of uplift and erosion. Paleozoic, post-Caledonian sediments were completely stripped off during the uppermost Carboniferous and Early Permian. Upper parts of the Jurassic were eroded in Late Jurassic to Early Cretaceous times. A short phase of uplift and minor erosion is likely in the Buntsandstein.

A good fit of the model to the calibration data has been achieved by using a declining heat flow after the thermal event at the Carboniferous-Permian boundary (figure 13, solid line), and erosion of 600 m Jurassic strata. Constant heat flow of 65 mW/m² as well as the parameters of the conceptual model resulted in too high present day temperatures (figure 18B). The heat flow trend is similar to that of well Schleswig Z1. Late Carboniferous and intra-Buntsandstein erosion has been applied as described in the conceptual model (section 4.1.1). There is no evidence for significant erosion during the Cenozoic. However, since there are only very few vitrinite reflectance data, the results of this model need to be interpreted with caution.

Highest temperatures were reached in the Early Jurassic (figure 18C). The top and base of the thick Rotliegend sandstone unit (layer Havel sst.) heated up to approximately 160°C and 190°C, respectively. A minor period of cooling during Late Jurassic to Cretaceous was followed by a second, less pronounced temperature maximum in the Paleogene. The maturation history is characterised by a rapid Late Permian to Triassic increase in vitrinite reflectance up to ~1.7 $\%R_o$ (Havel sst.) in the Early Jurassic. There is only very little further maturation in post-Jurassic times. Paleozoic HC source rocks are absent, as pointed out in section 3. The basement consists of folded, low-grade metamorphic pelites.

4.1.3 Alternative scenarios and discussion

The simulation of burial history, thermal evolution, and HC generation is based on a series of assumptions, which are reasonable in the geological context according to present knowledge. However, there is room for modification of some parameters, and some alternatives have significant influence on the results of the simulation. As demonstrated above, the use of e.g. different kinetic models leads to different timing and quantity of oil and gas generation. It is important to evaluate the sensitivity of the models with respect to controlling parameters and to test different geological hypotheses. The main focus in the context of this study is to assess the possible variation in thermal evolution and HC generation, especially for the major period of maturation (Late Paleozoic to Early Mesozoic).

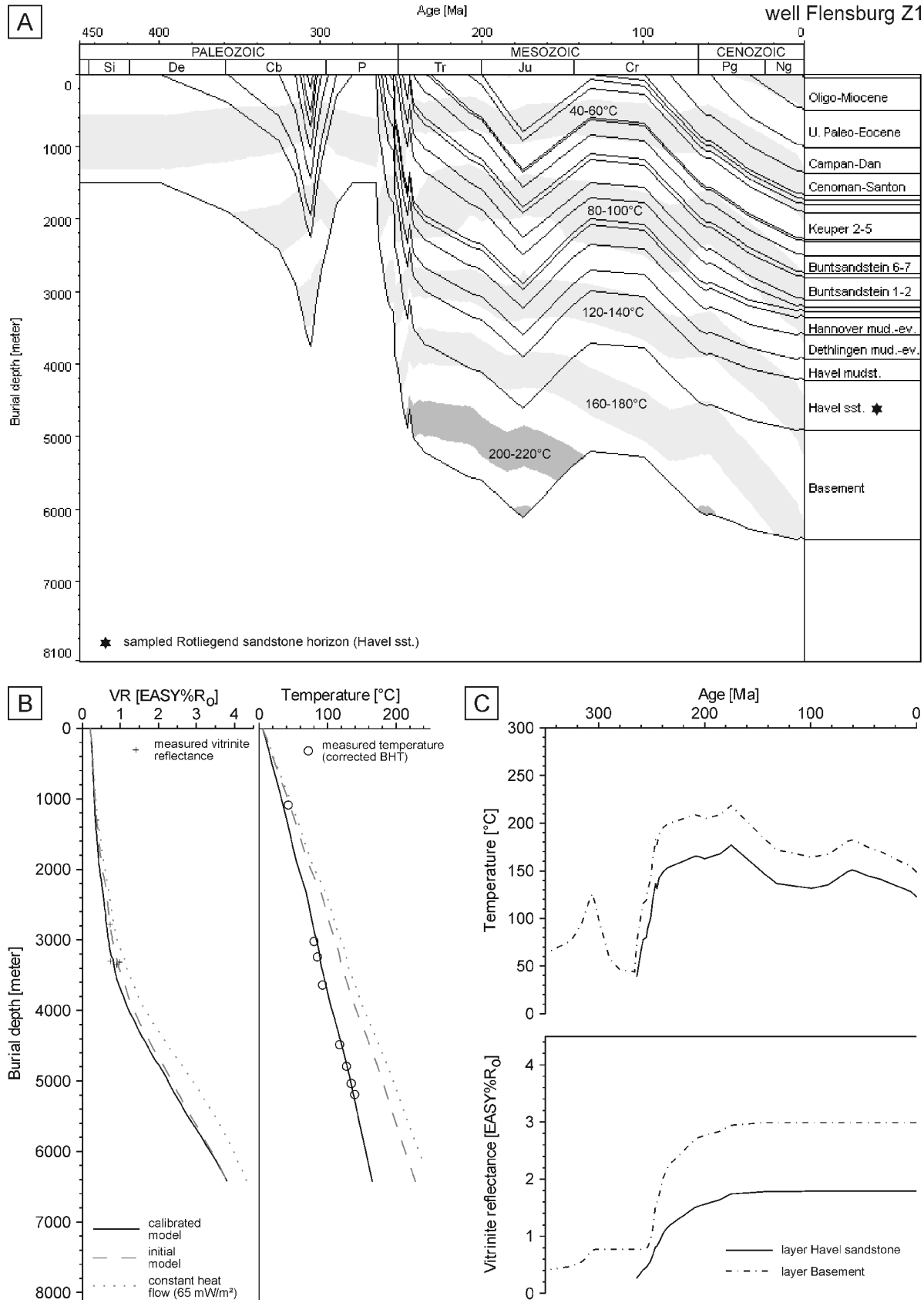

Figure 18: A) Burial history and temperature evolution for the model of well Flensburg Z1. Temperature isolines are indicated by white and grey bars of 20°C temperature intervals. B) Calculated and measured vitrinite reflectance and temperature of well Flensburg Z1. The calibrated model matches the measured temperature data. C) Calculated temperature and maturity evolution of the sampled Rotliegend horizon (Havel sst.) and the Basement layer (well Flensburg Z1, calibrated model).

The calculated present day heat flow is lower than the surface heat flow predicted by the Geothermal Atlas of Europe (Hurtig et al., 1992). Similar results have been found in other parts of the basin, where the calculated present day heat flow ranges between 41-75°mW/m² (Neunzert, 1997; Friberg, 2001). One source of error are temperature anomalies induced by the drilling process. If the time between drilling and temperature measurement was too short to allow complete temperature re-equilibration, which is almost always the case, the geothermal gradient given by bottom-hole temperatures is too low. Large scale circulation of water can also cause temperature anomalies (e.g. Andrews-Speed et al., 1984; Littke et al., 1994; Magri et al., 2005). Groundwater circulation may be especially important in the vicinity of salt domes (well Schleswig Z1, Flensburg Z1). According to Andrews-Speed et al. (1984), regional heat flow maps in complex sedimentary basins are generally of very limited significance.

The calibration of the models demonstrated that the simulations are sensitive to changes in heat flow (see above). Thickness changes of eroded strata are important too, at least if some hundreds of metres are involved. Both parameters are poorly confined by available geological data. The use of different lithologies for eroded strata of the models, e.g. different mixtures of sandstone, silt and shale for the Westphalian, has a small but noticeable effect on the thermal and burial evolution of the rock sequence. Similarly, modification of petrophysical properties, e.g. the thermal conductivity, affects the calibration results, especially if very thick layers are involved (e.g. Zechstein evaporite). However, with respect to subsidence and temperature history, heat flow and thickness of eroded sediments are probably the dominant controlling parameters to be modified in the models of this study. Maximum and minimum values of these two parameters were used to define different scenarios.

Minimum and maximum scenarios for the heat flow history can be based on Allen and Allen (1997), who suggested 60-70 mW/m² as global average. Active extensional basins are usually characterised by higher heat flows, while thermally subsiding basins comprise heat flows around 50 mW/m². Crustal extension and igneous activity around the Permian-Carboniferous boundary indicate a temperature pulse during that time. Although the heat flow in recent Graben settings may exceed 150°mW/m² (e.g. Hurtig et al., 1992), values above 90°mW/m² are unlikely for most areas of the NGB apart from the centres of igneous activity (Hoth, 1993; Neunzert, 1997; Friberg, 2001). The assumption of low heat flows in the Mesozoic (50-55 mW/m²) would imply a heat flow increase to 60-65 mW/m² in the Paleogene to explain the measured vitrinite reflectance data. This would slow down the organic maturation in the Mesozoic and increase the maturation in the Early Cenozoic. Neunzert (1997) and Friberg (2001) argued that the best calibration of their 1D-models can be achieved by assuming elevated heat flows of 60-74 mW/m² in the Paleogene. Hall and White (1994) suggested that rapid Paleogene subsidence in the North Sea may have been caused by either basaltic melts trapped within the lithosphere, or by a minor episode of lithospheric stretching. Both mechanisms create a heat flow increase. It is not likely, however, that this had a significant influence on the northern margin of the NGB. In the area investigated, elevated accumulation rates are not evident for the Paleogene, nor is there evidence for tectonic subsidence (Scheck-Wenderoth and Lamarche, 2005). The scenario of heat flows <60 mW/m² in the Mesozoic and a minor heat flow peak in the Paleogene has therefore not been taken into account, although it cannot be excluded completely.

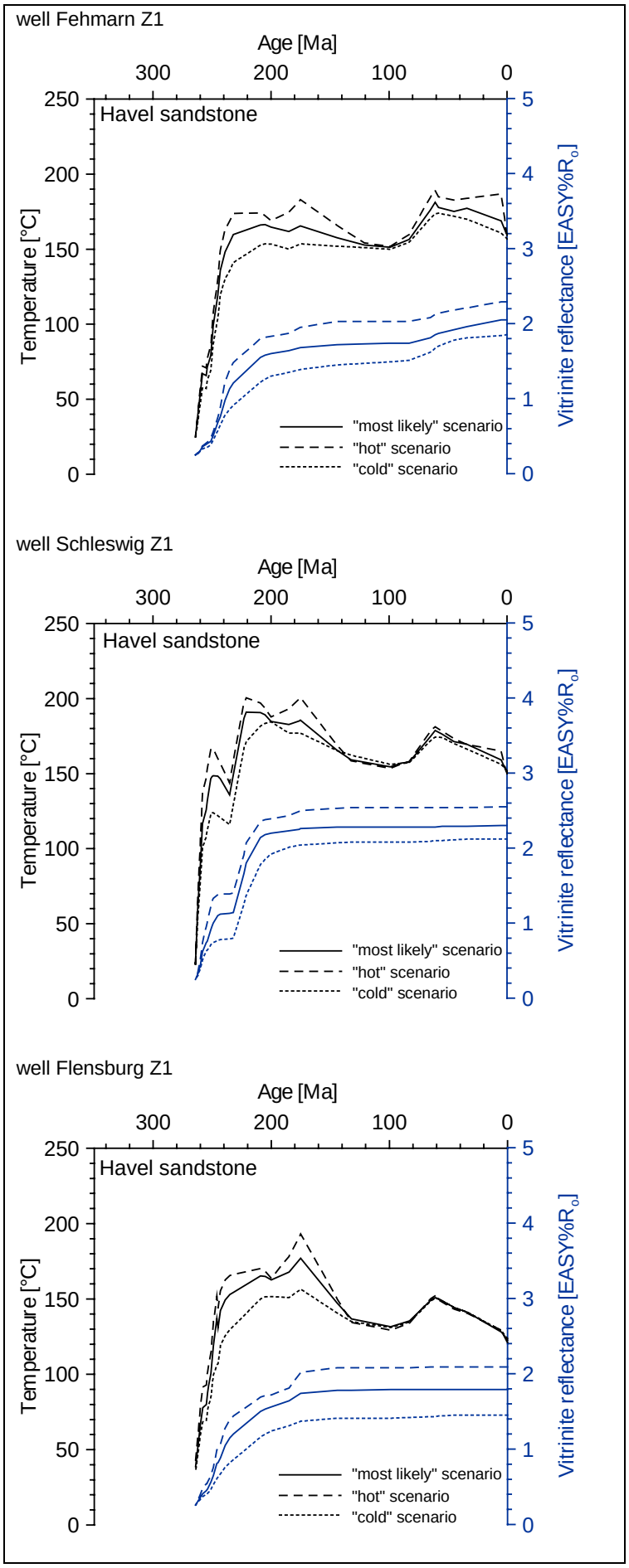

Figure 19: Effect of different scenarios on thermal evolution and maturity, illustrated by the calculated temperature and vitrinite reflectance for the Rotliegend sandstones (layer Havel sst.) of the three wells at the northern basin margin. The solid line indicates the model which has been preferred in this study ("most likely" senario). Additionally, two calibrated models for a "hot" (dashed line) respectively "cold" scenario (dotted line) are shown.

Based on these considerations, "cold" and "hot" scenarios were calculated for each model additionally to the results presented above ("most likely" scenarios). The additional models were built by modifying stepwise heat flow or thickness of eroded sediments. Only the final results are shown here, including modifications of both parameters. To define a lower limit for the Late Paleozoic to Early Mesozoic evolution, a constant heat flow of 60 mW/m² was assumed, adjusted only during the Cenozoic to fit the calibration data ("cold" scenario). The "cold" scenario further includes minor Carboniferous erosion (no Namurian, 500 m Westphalian), reduced Lower Jurassic thickness (100-300 m), and no further erosion throughout the Meso- and Cenozoic. In the "hot" scenario, +20 mW/m² were added to the initial heat flow peak of the "most likely" scenario at the Carboniferous-Permian boundary (figure 13). The elevated heat flow was assumed to decay until the Jurassic. Additionally, the "hot" scenario involves high eroded Carboniferous thickness (500 m Namurian, 2000 m Westphalian), and strong erosion at Mesozoic and Cenozoic unconformities (800-1000 m eroded Lower Jurassic, 900-1100 m total Paleogene+Neogene thickness). The reaction kinetics already applied above were used to calculate HC generation (Burnham, 1989; Pepper and Corvi, 1995). These different approaches were chosen since they are contrasting with respect to oil generation and thermal degradation. The influence of other standard kinetic models available in PetroMod® (table 3) was tested additionally, since the HC generation kinetics of the Carboniferous in Schleswig-Holstein are unknown.

The results of these simulations are displayed in the figures 15, 17, 19 and 20. The calculated temperature differences between the "cold" and "hot" scenario mostly vary between 20-40°C, partly up to 50°C in the Late Permian to Jurassic, and are much less in the Cretaceous and Cenozoic. The maximal temperatures of the Rotliegend sandstones investigated in this study range 170-190°C (well Fehmarn Z1), 185-200°C (well Schleswig Z1), and 150-200°C (well Flensburg Z1; see figure 19). Maturity differences up ~1% R_o were calculated in Carboniferous rocks of well Schleswig Z1 and Fehmarn Z1. These differences influence the timing and rate of HC generation. If 2000 m Westphalian sediments were deposited primarily, the Lower Carboniferous started to generate HC already during the late Westphalian. Transformation ratios vary from 5% to 35% for the deepest Carboniferous layers in well Schleswig Z1 and Fehmarn Z1 according to different kinetic models for terrestrial source rocks (figure 15, 17). The data of Burnham (1989) suggest generation of oil and gas, while only oil generation was calculated by the kinetics of Pepper and Corvi (1995). The major period of HC generation was the Late Permian to Triassic in all scenarios. However, while the main oil generation took place in Late Permian to Early Triassic times in both the "hot" and "most likely" scenarios, it extends or completely shifts to the Late Triassic if the parameters of the "cold" scenario are applied. Similarly, the main gas generation is slightly retarded in the "cold" scenario.

Simulations with the kinetic data of Pepper and Corvi (1995, type III/IV) generally result in higher oil generation rates compared to the kinetics of Burnham (1989). In the latter model, terrestrial source rocks are dominantly gas-generative, and any oil is subject to rapid thermal degradation. In contrast, Pepper and Corvi (1995) pointed out that almost all source rocks initially generate oil, with gas yield exceeding oil only at an exceptionally low primary hydrogen index. Other kinetic models for terrestrial source rocks (Behar et al., 1997; Vandenbroucke et al., 1999) produced results comparable to those of Pepper and Corvi (1995), or intermediate between those of Pepper and Corvi (1995) and Burnham (1989), at

least with respect to oil generation (figure 20A). The same can be stated for the reaction kinetics for type II kerogen (figure 20B). According to Burnham (1989), oil is completely transformed into gas by Late Triassic times (partly Lower Jurassic in the "cold" model), before the Carboniferous reached its maximum temperature (190-215°C in the "most likely" model). All other models used the data of Schenk et al. (1997) for secondary cracking reactions, which were determined experimentally for petroleum in reservoirs. In these models, secondary cracking is much slower and not completed until today. These comparisons show that in the present study, the two kinetic data sets of Burnham (1989) and Pepper and Corvi (1995) can be regarded as suitable "end member" models with respect to oil generation for typical type III as well as type II organic material.

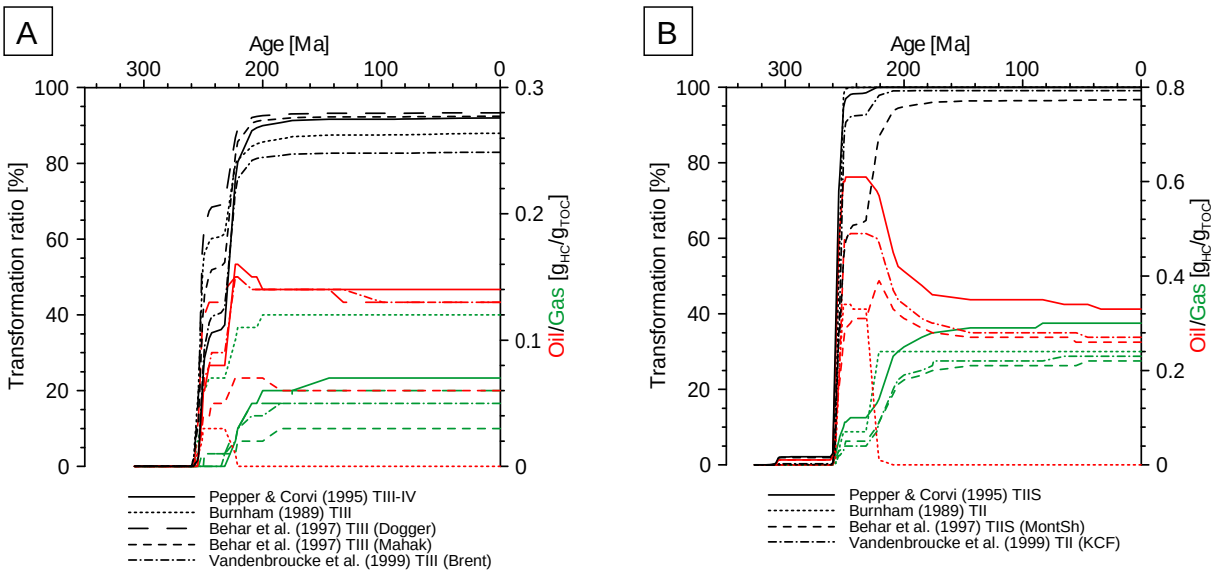

Figure 20: Comparison of the effect of different kinetic models by example of the layer Viséan b in well Schleswig Z1. The models of Pepper and Corvi (1995) and Burnham (1989) are suitable to represent the variability of oil generation rates depending of the kinetic data. A) Different models for terrestrial type III kerogen. B) Different models for marine type II kerogen.

4.2 1D- and 2D-simulations at the southern margin of the NGB

Results from basin modelling at the southern margin of the NGB, dominantly in the area north of Hannover, are available from previous studies. The most important findings are briefly reviewed here and evaluated with respect to oil and gas generation.

A coalification-map of the top Carboniferous was first compiled by Teichmüller et al. (1979) and subsequently improved (Teichmüller et al., 1984; Koch et al., 1997; Lokhorst, 1998). This map reflects regional maturity trends in the NGB. The mean vitrinite reflectance ranges from 1% to more than 3% R_o at the top Carboniferous of the southern study area. The highest values are evident from the eastern part and from the area around Bremen.

Philipp and Reinicke (1982) calculated the burial history of the Munster area north of Hannover and estimated gas volumes generated from the coal-bearing Carboniferous. The authors concluded that the main periods of gas generation were the Late Permian to Triassic, the Late Cretaceous to Paleogene, and the Neogene, when maximum burial was

reached. Bandlowa (1990; 1998) investigated burial evolution and gas generation for various gas fields of the NGB. According to her model for the area north of Hannover, main coalification took place in the two periods Permian to Jurassic, and Upper Cretaceous to recent. The Upper Rotliegend was buried to more than 2000 m depth in the Triassic, and to more than 4000 m in the Cenozoic. In contrast to the model of Philipp and Reinicke (1982), main gas generation started in Early Jurassic times. The use of different wells from different tectonic compartments may be responsible for these variations. During the Triassic, gas may have migrated into the North-Hannover area from deeper parts of the basin (Bandlowa, 1990).

Numerical simulations of burial and thermal history were carried out along two profiles of approximately 70 km and 90 km length, one running from Bremen eastwards, the second from the North-Hannover gas province towards NNE, crossing the axis of the NGB (Neunzert et al., 1996; Neunzert, 1997). According to these models, elevated subsidence rates are evident in the Upper Carboniferous, the Upper Rotliegend to Triassic, the Upper Cretaceous, and the Paleogene. First coalification took place in the Upper Carboniferous, but main periods of maturation were the Triassic and Cenozoic. However, Carboniferous burial depths vary by several 1000 m depending on the structural position and the relative position with respect to the basin axis. During the Jurassic, the maturity at the top of the Carboniferous varied between ~2% R_o distant from the basin axis and in Horst positions, and ≥3% R_o in Graben settings and in central parts of the basin (Neunzert, 1997). During the Cenozoic, vitrinite reflectance increased by additional 0.3-1.4% R_o. The base of the Rotliegend experienced temperatures of about 90-120°C in the Upper Jurassic, and 160-200°C in present times. Westphalian source rocks entered the main stage of methane generation (>1.2% R_o) in Triassic times and, depending on their structural position, generated gas until the Paleogene or partly until today.

The burial histories of numerous wells on the Pompeckj Block were investigated by Gerling et al. (1999). The authors deduced a systematic burial and uplift pattern, including Stephanian to Early Rotliegend uplift and erosion, the onset of rapid burial in the Upper Rotliegend, and declining burial rates throughout the Triassic and Early Jurassic. Minor erosion is interpreted to occur at the Hardegsen (pre-Solling) unconformity. The area was uplifted during the middle Dogger to Albian, and erosion may have removed up to 1000 m of sediments. Rapid sedimentation is evident again in the Upper Cretaceous and Paleogene, interrupted by a short erosional period at the Cretaceous/Paleogene boundary. Burial rates slowed down in the Oligocence and Miocene.

Most recently, HC generation, migration and accumulation were investigated by 1D- and 2D-modelling in the area of the North-Hannover gas fields, at the southern rim of the Pompeckj Block (Schwarzer et al., 2003; Schwarzer and Littke, 2005). The general trend of the burial histories is similar to that presented by previous workers for the same region, but in contrast to Neunzert et al. (1996), Schwarzer and Littke (2005) assumed substantial erosion at Late Carboniferous to Early Permian, and Late Jurassic to Early Cretaceous unconformities (figure 21). Both periods of erosion were postulated earlier for this part of the NGB (compare Jaritz, 1969; Ziegler, 1978; Teichmüller et al., 1984). The base of the Upper Rotliegend sediments heated up to 100-130°C in the Early Jurassic, and experienced maximum temperatures of 150-170°C in the Paleogene or Neogene. Rapid maturation is evident in the Triassic and again in the Cenozoic, interrupted by the Late Jurassic to Early Cretaceous uplift.

At the top of the coal-bearing Carboniferous (Lower Westphalian C), the calculated vitrinite reflectance increased up to 1.3% R_o in the Early Jurassic, and up to 2.5% R_o in the Neogene. The maturity at the base of the coal-bearing sequence (Namurian C) partly exceeded 3% R_o in Jurassic times. The 2D-simulations demonstrated that the maturity is strongly influenced by the structural position (Horst vs. Graben), and by evolving salt accumulations (Schwarzer and Littke, 2005).

Two examples taken from the 2D-profiles are given in figure 21 and 22. The localities are identical to wells investigated by Gaupp and Solms (2005) and used in this study (well TG 4, TG 35; see also table A2, appendix). In lower parts of the coal-bearing Carboniferous (Namurian C), main transformation of kerogen into HC took place during the Late Carboniferous to Early Permian and the Triassic. Rocks of Lower Carboniferous and Namurian A-B age had already realised most of their HC generation potential before the deposition of Rotliegend sediments. The Westphalian generated HC during Triassic-Jurassic and Late Cretaceous-Paleogene times in most areas. During the latter period, kerogen transformation was most intense on horst blocks (figure 22B). Liquid HC generation started in the Carboniferous (Namurian and older rocks) and Early-Middle Triassic (Westphalian rocks). Figure 22A illustrates that oil generation continued throughout the Triassic and Lower-Middle Jurassic in different horizons of the Westphalian. A second period of oil generation in the Late Cretaceous to Paleogene is suggested by the kinetic model of Pepper and Corvi (1995), while the model of Burnham (1989) indicates oil to gas cracking during the same time period. On horst blocks, however, main oil generation took place consistently during this youngest maturation phase, although some liquid HC were already generated in the Early Mesozoic (figure 22B). Schwarzer and Littke (2005) pointed out that oil migration proceeded slowly due to low permeabilities of the Upper Carboniferous, but was improved along faults. The simulated oil saturation in Rotliegend reservoirs is very low, but the calculated composition points to Upper Carboniferous sources.

Gas generation from the Westphalian depends on the kinetic data used in the model, but probably started in the Middle-Late Triassic (figure 22). Parts of the Upper Carboniferous source rocks still have gas generation potential today, while the Namurian became overmature in the Late Triassic to Jurassic in most areas. According to 2D-modelling, accumulation of methane in uppermost Carboniferous and Rotliegend reservoirs started after deposition of the Zechstein evaporites, but tectonic movements during the Upper Triassic, Late Jurassic and Cretaceous caused flushing of many structures (Schwarzer and Littke, 2005). Volumetric calculations indicate that only a small amount of the HC generated during basin subsidence is trapped in today's gas reservoirs (e.g. Philipp and Reinicke, 1982; Hedemann, 1985; Krooss et al., 1995; Neunzert, 1997). Present Rotliegend gas reservoirs were filled mainly during the Cenozoic, while large amounts of Late Paleozoic to Mesozoic HC must have escaped to the atmosphere (Teichmüller et al., 1984; Littke et al., 1995).

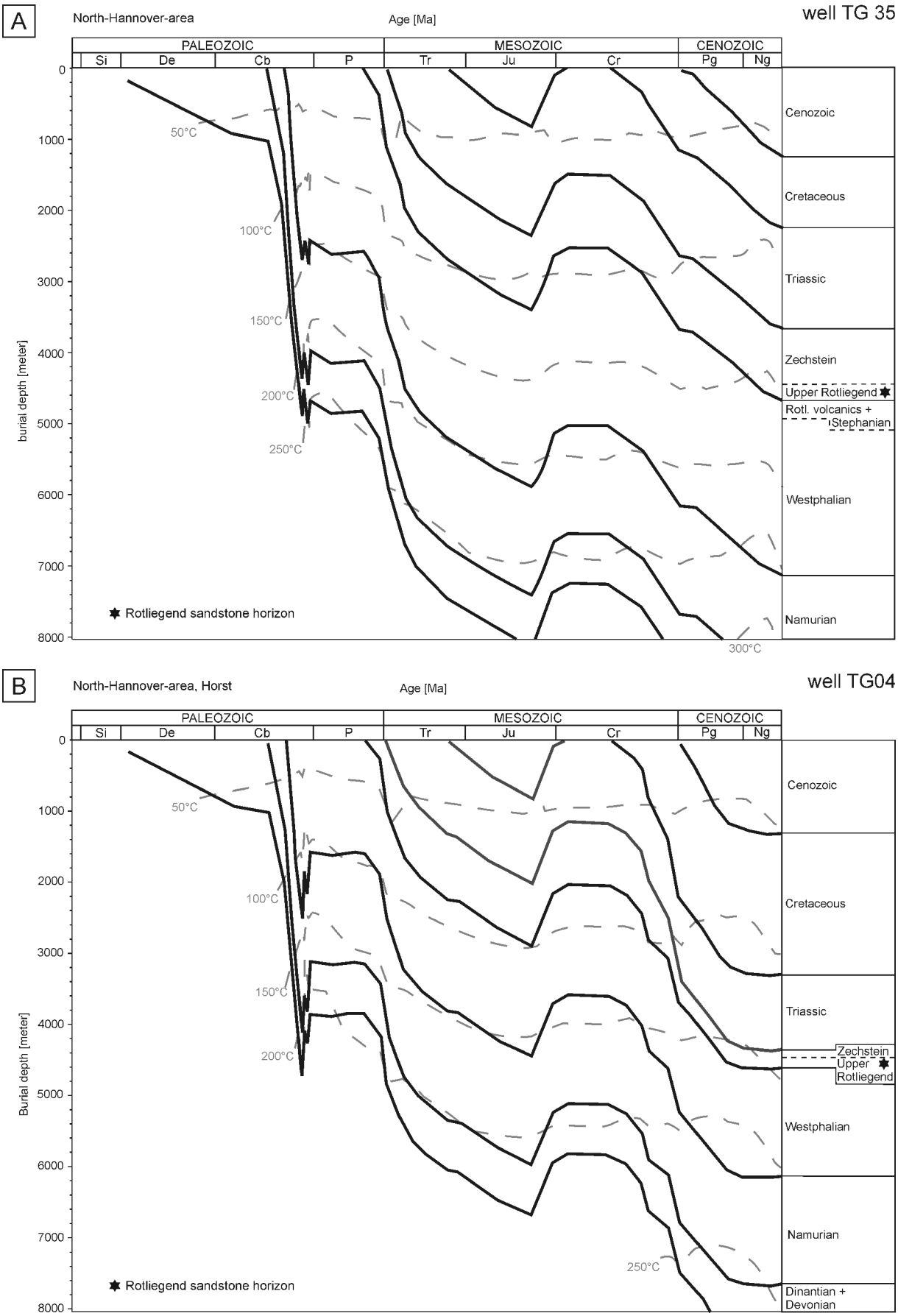

Figure 21: Two examples of burial and thermal history at the southern basin margin, North-Hannover area. The two wells are part of 2D basin models (modified from Schwarzer and Littke, 2005). A) Well TG 35 illustrates the typical pattern in many parts of the North-Hannover area. B) Well TG04 is located on a horst block.

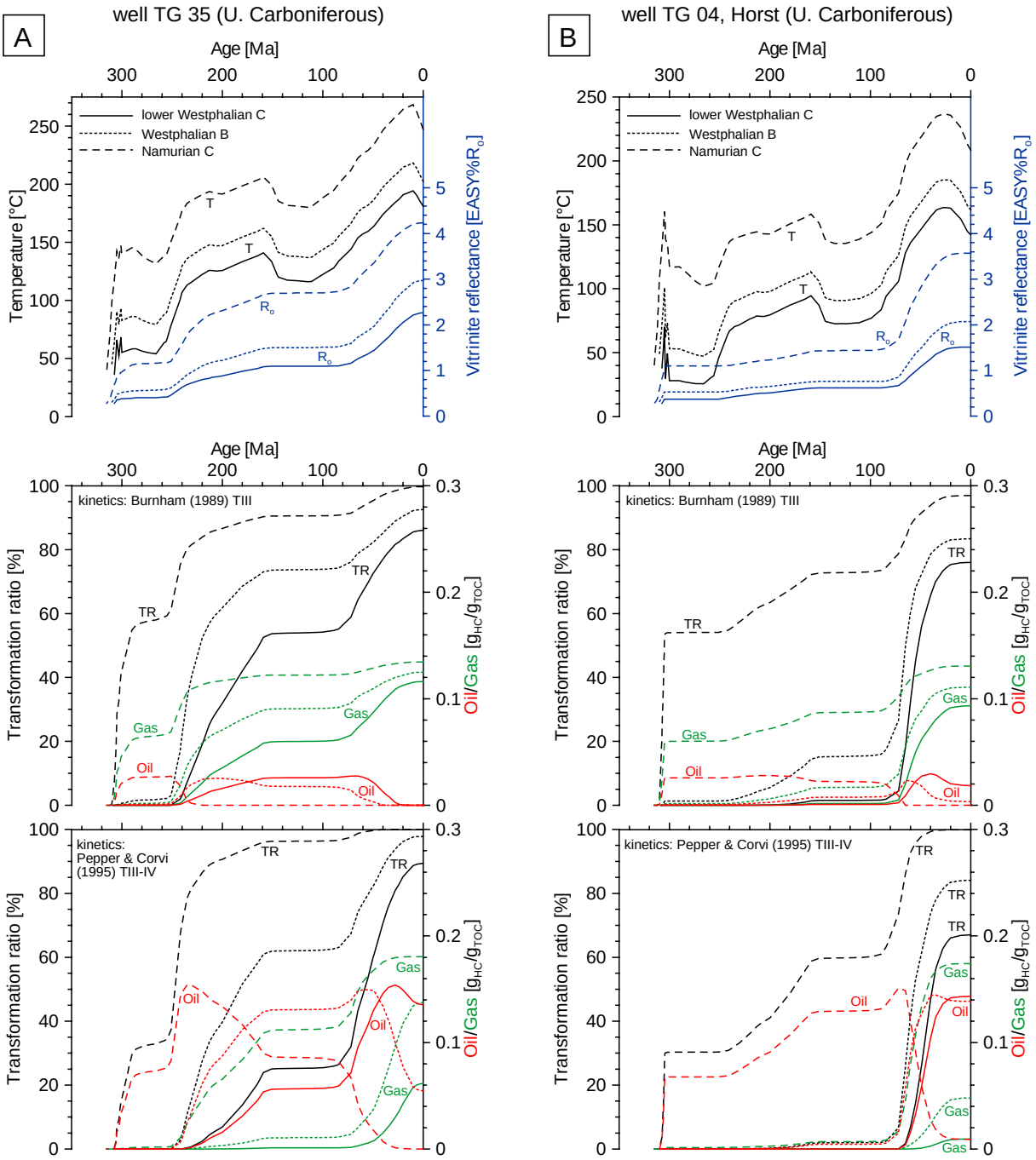

Figure 22: Two examples illustrating the evolution of temperature, maturity and HC generation of the Upper Carboniferous from the North-Hannover area (southern basin margin). The lines indicate the upper (lower Westphalian C), the middle (Westphalian B) and the lower layer (Namurian C) of the main source rock interval. HC generation was calculated using the kinetic models of Burnham (1989) TIII and Pepper and Corvi (1995) TIII-IV(F). Data from Schwarzer and Littke (2005). A) Well TG 35 is representative for many parts of the North-Hannover area. B) Well TG 04 is situated on a horst block; maturation and HC generation are retarded in comparison to well TG 35.

4.3 Comparison of early organic maturation in the southern and northern study area

The comparison of basin modelling results from the southern basin margin with the case studies at the northern basin margin clearly demonstrates major differences in organic maturation and HC generation. Where remnant Carboniferous rocks are present in the north, most of their genetic potential was realised before the beginning of the Jurassic. It can be concluded that oil generation started in Late Carboniferous times if thick Upper Carboniferous source rocks had been deposited. Main oil generation took place in the Late Permian to Early Triassic, or possibly until Late Triassic, if relatively cold conditions are assumed. Regardless of the kinetic model used, oil generation was completed before the end of the Triassic. Much of the liquid HC generated may have been thermally cracked within the source rocks due to rapid heating to temperatures around 200°C in the Triassic. If any oil was expelled, it probably migrated along fault zones active during the Permian and Triassic (compare figure 6). Well Schleswig Z1 was drilled on a Triassic horst structure. In the adjacent, deeply subsiding parts of the Glückstadt Graben, HC generation must have been even more rapid. It is likely that in those areas oil generation was completed by Middle Triassic times. These results are in clear contrast to Rodon and Littke (2005), who mention a possibility for oil generation in Tertiary times from Paleozoic source rocks in northern Schleswig-Holstein, although the calculated maturity at the base Zechstein of their model is almost identical to the results presented here. The interpretation of Rodon and Littke (2005) can only be related to the fact that their study concentrates on the post-Zechstein succession, and that they did not consider the thickness of Rotliegend deposits.

Complex structural evolution and salt migration at the southern basin margin do not allow to generalise the timing of HC generation and migration over large areas. However, the considerable thickness of Carboniferous source rocks ensures HC generation over long periods of time, starting in the Late Carboniferous and continuing until the Cenozoic. Although most studies carried out so far concentrated on gas generation and accumulation, liquid HC were generated during early periods of maturation, mainly during the Triassic and Early Jurassic. Lower Carboniferous and Namurian rocks were oil-generative already during the Late Carboniferous and Early Permian. On the other hand, areas located on horst blocks still generated liquid HC in the Late Cretaceous and Paleogene. Significant thermal degradation of oil in the Westphalian probably started not before the Late Cretaceous. Vertical oil migration through thick Carboniferous shale, silt- and sandstone sequences was slow, but may have been focused along faults. This implies that oil migration was enhanced especially during periods of tectonic activity.

So far, the simulations only provide information on the timing of oil and gas generation, independent from the percentage of kerogen present in the source rocks. However, the quantity of produced oil and earlier organic maturation products would be important to evaluate their influence on sandstone diagenesis. Early organic maturation products preceding oil generation include organic acids and CO_2. The maximum of carboxylic acids is assumed to be generated just prior to liquid HC (Surdam et al., 1984). Humic source rocks, especially coals, can produce large quantities of CO_2 (e.g. Hunt, 1979; Tissot and Welte, 1984; Littke et al., 1989). This is important especially for the coal-bearing Upper Carbonifer-

ous at the southern basin margin. Assuming 50-100°C as temperature range of main CO_2 production from humic source rocks (compare Hunt, 1979; Barclay and Worden, 2000), CO_2 generation occurred mainly in the Carboniferous to Early Triassic in more rapidly subsiding parts of the southern basin margin. On horst blocks, however, it may have lasted until the Lower Jurassic, possibly even until the Late Cretaceous (figure 21, 22). CO_2 production at the northern basin margin was most likely not important owing to the apparent absence of coal in that area (compare section 3).

A reliable quantification of organic maturation products would require the knowledge of their generation potential and reaction kinetics from field data and/or laboratory experiments. Such data are not available for the source rocks of the study areas. Simple hypothetical calculations shall nevertheless illustrate the order of magnitude of CO_2 and oil generation. The estimation of the cumulative CO_2 generation is based on following assumptions: (1) the amount of organic material at the northern basin margin ranges between 0 and $6*10^6$ t/km² (figure 11), (2) only the coal horizons of the main source rock horizons at the southern basin margin are considered (Namurian C to lower Westphalian C), and an average of $1.5*10^8$ t coal per km² is applied (compare figure 11), (3) the CO_2 generating capacity of the source rocks is approximately 100 mg CO_2/g TOC at the northern basin margin, and 150 mg CO_2 /g TOC at the southern basin margin (see also Krooss et al., 1995). The calculated values range from 0 to ≤0.6 t CO_2/m² at the northern basin margin, and add up to more than 20 t CO_2/m² at the southern basin margin. The two examples in figure 23 highlight the differences between the two study areas with respect to oil generation. For the Lower Carboniferous of well Schleswig Z1, two scenarios with 100% type III kerogen and mixture of 50% type II and 50% type III kerogen have been calculated. Initial TOC values of 0.5%, 1.0% and 1.25% were assigned to the three horizons Tournaisian a, Tournaisian b-Viséan a, and Viséan b in well Schleswig Z1. For the example of the southern basin margin (well TG 35), only the main source rock horizons were summarised, and 100% type III kerogen was assumed. TOC contents of 1.5% (Namurian C), 2% (Westphalian A), 2.5% (Westphalian B), and 3% (lower Westphalian C) were applied as suggested by Neunzert (1997). In these examples, the cumulative oil generation potential at the southern basin margin is about one order of magnitude higher than at the northern basin margin, if the same type of kerogen is present throughout the basin. This difference decreases, if the Lower Carboniferous in the area of Schleswig Z1 contains significant proportions of marine type II kerogen. Note that the calculations still ignore any influence of sapropelic coals or marine kerogen in the Upper Carboniferous of the southern basin margin. Therefore, they probably still underestimate the oil generation potential of that area. The kinetic model of Pepper and Corvi (1995) may be more suitable to account for the organic material present in the thick Carboniferous sequence, while the model of Burnham (1989) most likely underestimates oil generation from terrestrial kerogen. This interpretation is supported by other kinetic models as well as by studies showing that liquid HC are generated and expelled from terrestrial shaly and coaly source rocks (see above and section 3).

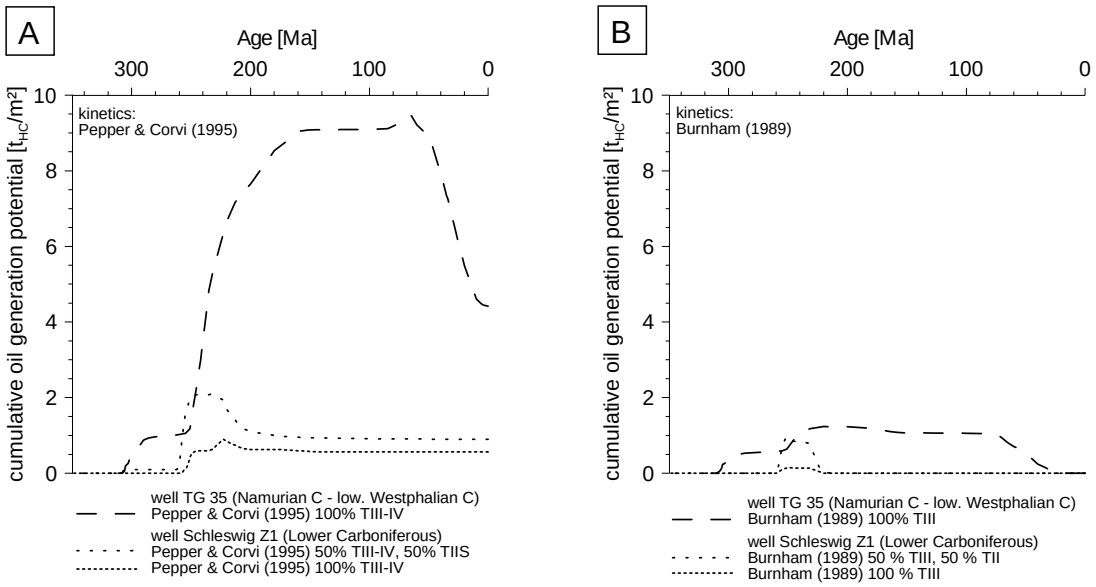

Figure 23: Two examples illustrating the cumulative oil generation potential through time at the northern basin margin (well Schleswig Z1) and the southern basin margin (well TG 35 from the North-Hannover area, data from Schwarzer and Littke, 2005). These calculations are hypothetical, since the actual oil generation potential of the Upper Carboniferous is unknown. Only the main source rock horizon of the southern basin margin (Namurian C to lower Westphalian C) has been used for the calculation. The cumulative oil generation potential of the Lower Carboniferous of well Schleswig Z1 was calculated for 100% type III kerogen, and for 50% type II and type III kerogen, respectively. The strong effect of different reaction kinetics is demonstrated in A) vs B). Note that well Schleswig Z1 is likely to represent the maximum possible oil generation potential of the northern study area.

Summary

1D-simulations of three wells from the northern margin of the NGB show rapid and deep burial of Rotliegend sandstones in Late Permian times, and declining burial rates in the Triassic and Early Jurassic. Moderate rates of subsidence are evident from the Late Cretaceous and Paleogene. Non-sedimentation and/or erosion prevailed in latest Carboniferous to Lower Permian, and in Mid-Jurassic to Lower Cretaceous times. Burial history in the North-Hannover area (southern basin margin) follows in general a similar trend, but shows less rapid and deep burial during the Late Permian to Early Triassic, and higher sedimentation rates in the Cenozoic. There are significant differences in organic maturation between the northern and southern margin of the NGB, both in timing and quantity. Where relics of Carboniferous rocks are preserved at the northern basin margin, minor generation of oil and preceding maturation products (CO_2, organic acids) was confined to a narrow time interval shortly after deposition of the Rotliegend. Rapid heating to temperatures of ~200°C in the Triassic suggests that much of the early maturation products were rapidly cracked, probably even before they were expelled. At the southern basin margin, in contrast, thick coal-bearing source rocks were heated more gently and produced much larger volumes of organic maturation products (CO_2, oil, CH_4) over much longer periods of time. The coal-rich horizons generated significant quantities of CO_2 from the Carboniferous to the Triassic in many areas. Most intense liquid HC generation occurred during the Triassic and Early Jurassic. Organic acids must be expected prior to oil generation. It is likely that these organic components were partly expelled, especially during periods of tectonic activity.

5 Rotliegend sedimentology, petrography and geochemistry: northern margin of the NGB

5.1 Sedimentology and stratigraphy of the horizons investigated

Along the northern margin of the NGB, coarse grained clastic sediments were deposited only at the base of the Upper Rotliegend. Basal sandstones and conglomerates are approximately 40 m (Schleswig Z1), 100 m (Fehmarn Z1), and 700 m thick (Flensburg Z1), while comparable lithologies are lacking in well Westerland 1. Correlation of the Rotliegend successions on the basis of gamma-ray logs and lithology indicates that the sandy Rotliegend sediments are part of the Havel Subgroup (figure 9). However, stratigraphic correlation in case of well Flensburg Z1 is not univocal. There is no clear evidence for either Rotliegend or pre-Rotliegend age of the ~700 m thick coarse grained sediments below the Rotliegend mudstones and evaporites. The possible age of the sandstones at the northern basin margin will be discussed at the end of this section.

5.1.1 Well Fehmarn Z1

The sedimentary Rotliegend in well Fehmarn Z1 rests upon porphyric volcanics with quartz, feldspar, and strongly altered mafic phenocrysts. Their emplacement age is close to the Carboniferous/Rotliegend boundary (Breitkreuz 2004, pers. comm.). The volcanic deposits are dominantly rhydodacites (Geißler 2005, pers. comm.) and contain sporadically sandstone lenticles or diffuse sandy frazzles, at least in the upper part of the volcanic succession. Clastic deposition started with alluvial conglomerates and sandstones. The cored section (~6 m) comprises medium to coarse grained conglomerates, interbedded with thin, sometimes pebbly sandstones (plate 1C). The conglomerates are poorly to moderately sorted, clast- to matrix-supported, and contain sandy matrix. Coarsest components (<10 cm) are not concentrated at the base, but within the conglomerate layers. Abundant clast types are subangular to well rounded siltstones, fine grained sandstones, volcanic rocks, and to a minor degree quartz, low-grade metasediments, cherts, and shales. Conglomerates may show a sub-horizontal clast imbrication, and most sandstone horizons are horizontally laminated. Erosive surfaces are rare in the cored section. These rocks are overlaid by approximately 75 m of siltstones to fine grained sandstones, which contain subordinate clay and coarse grained sand (figure 9). They are characterised by poor sorting and diffuse lamination, although some layers are horizontally laminated or low-angle cross-bedded (plate 1G). Desiccation cracks are evident from rare thin mudstone layers. Mudstones with minor sand content and evaporites are predominant in the upper part of the Rotliegend (~760 m in total). According to available core material, the mudstones may be massive, diffuse bedded or rarely laminated, and occasionally contain anhydrite concretions. Similar lithofacies types were described in detail recently from the Upper Zechstein in the Hessian Depression (Hug, 2004). The colour of the Rotliegend clastics of well Fehmarn Z1 is red to red-brown throughout.

I n t e r p r e t a t i o n

The abundance of (sub)rounded pebbles and the clast-supported, moderately sorted fabric of some conglomerates argues for deposition from stream flow. Other sedimentary textures suggest that the lower, conglomeratic part was more likely deposited from hyper-concentrated flow, e.g. the concentration of large clasts in central or upper parts of conglomerate layers. Evidence for cross-bedding and clearly defined channel floors, which would be expected in a typical braided fluvial system, is lacking. The relatively regular alternation of conglomerates and flat laminated sandstones in dm- to m-scale could have been generated by a largely unconfined, non- or poorly channelised system. Blair and McPherson (1994), e.g., described planar stacked sheets of gravel and laminated sand as typical facies of sheetflood-dominated alluvial fans. It must be noted, however, that the limited, "one-dimensional" core material is not suitable to ascertain the mechanisms of sedimentation beyond doubt. The overlying silty-sandy succession may be interpreted as sandflat environment, which was repeatedly affected by aquatic deposition, probably from unconfined sheetflood events. Mudflat and saline lake environments prevailed since the upper Havel Subgroup (compare Gaupp et al., 2000).

5.1.2 Well Schleswig Z1

In well Schleswig Z1, red to red-brown coloured Rotliegend sediments overlie weathered Lower Carboniferous shales (compare section 3.1). The coarse grained clastic rocks consist of approximately 60% conglomerates and 40% sandstones. (Sub)angular volcanic fragments up to ~10 cm size are by far the most frequent clast type, so the term breccia is adequate for some clast-rich sections (plate 1A). Angular to subrounded pelites, fine grained sandstones, low-grade metapelites, and carbonates form minor constituents. The (very) poorly sorted conglomerates/breccias contain varying portions of sand matrix. Elongate clasts are often imbricated. Sandstones directly above or interbedded with conglomerate layers are massive, or horizontally to low-angle cross-bedded, and partly contain pebbles (plate 1F). Several erosive surfaces are evident from the cores. Some sandstone horizons of 0.5-1 m thickness are uniformly cross-bedded (~25-30°) and consist of alternating laminae of fine grained and fine-medium grained, moderately to well sorted sand (plate 1E). The coarse grained basal succession is overlaid by about 700 m of mudstones with variable sand content and anhydrite concretions, and in turn by more than 1300 m of pelites and evaporites (figure 9). Most frequent lithotypes in the cored sections are massive mudstones, diffuse bedded sandy mudstones, and poorly sorted, diffuse bedded silt- and clay-rich sandstones. Small scale cross-bedding, rippel cross-lamination and faint parallel lamination are evident from some sandstone lenses.

I n t e r p r e t a t i o n

The basal ~40 m of coarse grained sediments record dominantly, but not exclusively, subaqueous conditions. The alternation of matrix-supported gravel and massive, flat- or cross-bedded sand could have originated in a braided fluvial environment. However, poorly sorted conglomerates to pebbly sandstones without clearly defined base, and large clasts floating in finer grained matrix suggest deposition by gravity-flow processes. Eolian origin can be assumed for the planar cross-bedded sandstone horizons. The basal succession may thus represent an ephemeral stream environment with intercalation of gravity-flow deposits

and minor eolian reworking. More detailed interpretations would require information on the geometry of the sedimentary units. Similar lithologies were interpreted as wadi deposits by e.g. Glennie (1972) and Plein (1978). Mudflat and saline lake conditions persisted during the remaining Rotliegend interval. Although some sand-rich horizons occur within the mudflat succession, there is no evidence for a sandflat development comparable to that in well Fehmarn Z1.

5.1.3 Well Flensburg Z1

The 700 m thick basal succession in well Flensburg Z1 is composed of fine- to coarse grained sandstones plus minor conglomerates, and interstratified mudstones. The colour of the sandstones is brown-grey, grey, or red-brown, while mudstones including thin interbedded sandstones horizons are red to red-brown. Cross-bedded and flat laminated sandstones are particularly abundant, although horizontally laminated and massive sandstones are present as well (plate 1D). The lamination is partly due to heavy mineral layers. The sandstones often contain well rounded pebbles and mud flakes. Clast-supported, fine to medium grained conglomerates, mostly less than 20 cm thick, are often incorporated in cross-bedding sets of several decimetres thickness (plate 1B). Conglomerates may be graded and may have erosive contacts to the underlying sediments. They are composed of well rounded quartz/quartzite pebbles, and less frequently pelite, fine grained sandstone or dolomite clasts, mud flakes, and sandy matrix. Mudstone horizons, which may be few decimetres to few metres thick according to the gamma-ray log, are regularly interbedded with the sandstones. Additionally, thin mudstone layers (mm-cm) may also occur within the sand-dominated sections. The sandstone-mudstone succession is followed by pelites and evaporites similar to those of well Schleswig Z1 (~840 m in total).

I n t e r p r e t a t i o n

The lower part of the succession can be interpreted as sand-dominated fluvial deposits, most likely from braided rivers. The abundance of mud flakes in the sandstones and conglomerates points to desiccation of mud layers, reworking and rapid deposition in a highly mobile fluvial system. Ephemeral conditions are suggested by the repeated occurrence of thin mudstone layers, e.g. on top of channel-facies conglomerates (plate 1B). There is no clear evidence for eolian deposition from the available core material. The sandstones were probably deposited in a relatively stable fluvial drainage system, considering the thickness of the succession and the facies continuity. Similar to well Schleswig Z1, the upper part of the Rotliegend is characterised by mudflat and saline lake conditions, which can be correlated over large parts of the basin (compare figure 8 and 9, and Legler et al., 2005).

5.1.4 Discussion of the age of the sandstones investigated

Rotliegend age of basal sandstones and conglomerates is indicated by onset of deposition above Late Carboniferous to Early Rotliegend volcanics (cored in well Fehmarn Z1), and above a subaerial unconformity on top of Lower Carboniferous sediments (cored in well Schleswig Z1). Rotliegend age is also evident from the abundance of reworked volcanic detritus in well Fehmarn Z1 and Schleswig Z1, which derives most likely from volcanics similar to those in well Fehmarn Z1 (compare section 5.3). Assuming continuous deposition

during the Upper Rotliegend, the coarse grained sediments are part of the Havel Subgroup (figure 9), although the presence of older Rotliegend relics cannot be excluded. The age of the basal sediments in well Flensburg Z1 is less clear. Compared to the other two wells, the sandstone-mudstone succession of well Flensburg Z1 is very thick and shows significant differences in detrital composition (section 5.3). Four scenarios appear to be possible: The almost 700 m thick sandy succession on top of the basement is

(1) Devonian and/or Carboniferous in the lower part, and Rotliegend in the upper part;
(2) entirely Devonian ("Old Red") in age, while Carboniferous rocks as well as basal Rotliegend sandstones are missing;
(3) Carboniferous (most likely upper Westphalian or Stephanian) in age, while older sediments and basal Rotliegend sandstones are missing;
(4) entirely Rotliegend in age.

Scenario (1) can be ruled out based on the results of the present study. The relative continuity of sedimentary facies, gamma-ray patterns, detrital composition (section 5.3), diagenesis (section 5.4), and geochemistry (section 5.6) from base to top does not support the assumption of a major hiatus within the succession. Devonian and Carboniferous rocks in the region of Schleswig-Holstein are only known from well Schleswig Z1. The Devonian consists of ≥215 m fine to medium grained, homogeneous quartzarenites, which are strongly compacted and cemented by quartz and minor carbonate. The Lower Carboniferous succession of well Schleswig Z1, which has been briefly described in section 3.2, is very different from the basal sediments in well Flensburg Z1. The occurrence of thick Upper Carboniferous sandstones would be in contrast to the absence of any Upper Carboniferous rocks in wells of northernmost Germany and southern Denmark (compare Nielsen and Japsen, 1991). Scenario (2) and (3) would also imply that no coarse grained Rotliegend clastics were deposited, but sedimentation started with pelites, similar to well Westerland 1. However, in contrast to the latter, well Flensburg Z1 is located south of the Brande Trough, a presumed connection between Southern and Northern Permian Basin (figure 7, Plein, 1995). It is not likely that coarse grained clastics are missing completely at the base of the Rotliegend in that area. The explanation which is favoured here is that the entire sedimentary sequence between the basement and the Zechstein in well Flensburg Z1 is Rotliegend in age. Drong et al. (1982) and Gast (1988) showed that the early Upper Rotliegend at the southern basin margin was characterised by fault-controlled sedimentation, and correspondingly by significant thickness variations. A similar concept probably applies to the northern basin margin too. The sedimentology of the basal clastics in well Flensburg Z1 is consistent with high sedimentation rates in a fault-bounded basin. A possible connection between the rift system in Lower Saxony and the Glückstadt and Horn Graben was proposed already by Gast (1988). Fault-controlled sedimentation in Schleswig-Holstein may explain differences in thickness, lithofacies and detrital composition (section 5.3) of early Upper Rotliegend deposits.

5.2 Rock texture

The granulometric data of the samples from the northern basin margin are included in table A7 (appendix). Dominantly medium to fine grained sandstone samples were selected for petrographic investigations. The average mean grain diameter measured in thin-section is about 140 µm (well Fehmarn Z1, Schleswig Z1) and 180 µm (well Flensburg Z1). The

average median is equal or slightly higher. Figure 24 illustrates the abundance of mean grain sizes. Grains of 125-180 µm (3-2.5 F) diameter are most abundant in well Schleswig and Fehmarn Z1, while grain sizes of 90-250 µm (3.5-2 F) are frequent in well Fehmarn Z1. The bar charts (0.5 F class width) of some samples indicate bimodal grain size distribution, especially in pebbly fluvial sandstones, and in eolian sandstones with alternating fine and medium grained laminae (well Fehmarn Z1, Schleswig Z1; see table A7, appendix). It must be noted that the thin-section derived grain size values are not equivalent to the true grain size owing to the random sectioning of the grains (compare Harrel and Eriksson, 1979). However, they can be compared to the data from the southern basin margin, which were also measured in thin-section.

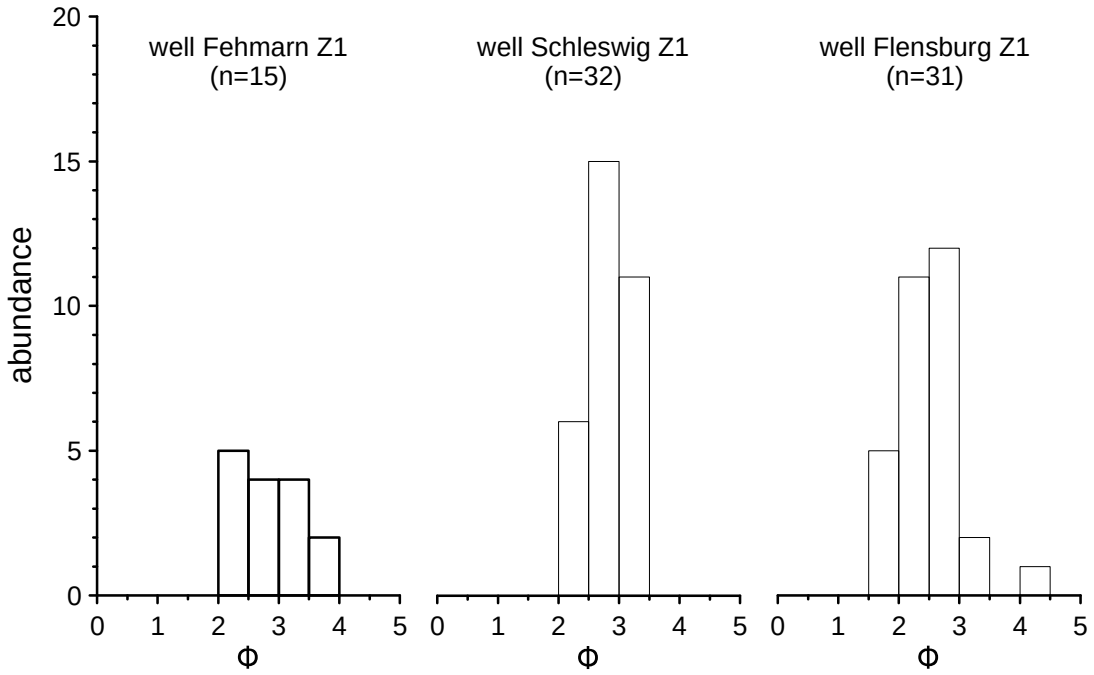

Figure 24: Distribution of mean grain sizes in Rotliegend sandstones of the northern basin margin, calculated from n samples. Grain size classes 3.5-2.0 F (90-250 µm) are abundant in well Fehmarn Z1. The class 3.0-2.5 F (125-180 µm) is most abundant in well Schleswig and Flensburg Z1.

Comparison of thin-sections with charts provided by Beard and Weyl (1973) indicates that the Trask sorting coefficients (compare Trask, 1932) in well Fehmarn Z1 are mostly between 1.4 and 2.7, in well Schleswig Z1 between 1.2 and 2.7, and in well Flensburg Z1 between 1.1 and 2.0. This is equivalent to moderately to poorly sorted (well Fehmarn Z1), well to poorly sorted (well Schleswig Z1), and well to moderately sorted sandstones (well Flensburg Z1) according to the widely used Folk and Ward (1957) sorting scale. Following Ehrenberg (1995), the Trask sorting coefficient may be used to deduce the "wet-packed original porosity", which represents not the condition of depositional sand, but of moderate mechanical compaction reached at very shallow levels of burial. This wet-packed original porosity can be estimated to be 33±4 vol.-%, 36±3 vol.-%, and 38±3 vol.-% for the samples of well Fehmarn Z1, Schleswig Z1, and Flensburg Z1 (compare Ehrenberg, 1995).

The sand grains are mostly subrounded to subangular. The determination of grain contacts in thin-sections is problematic since grains are sectioned at random positions, which may not represent the true relation to the adjacent grains. For example, an apparently floating grain in

thin-section may well have point or long contacts to other grains outside the visible plane. Grain contacts were therefore estimated by considering the closest contact of each grain to its adjacent grains. On average, concavo-convex grain contacts are most abundant in well Fehmarn Z1, while long to concavo-convex contacts are dominant in well Schleswig Z1 and Flensburg Z1.

5.3 Detrital mineralogy

The sandstones contain mono- and polycrystalline quartz (17-70 vol.-%), non-quarzitic rock fragments (6-59 vol.-%), and feldspars (1-9 vol.-%; compare table A7, appendix). The dominant grain type in most samples is monocrystalline quartz, which shows straight or undulatory extinction, or subgrain formation. Detrital quartz with inclusions of vermicular chlorite ("helminth-chlorite", see Tröger, 1967) is a minor component in sandstones of all localities, especially in those of well Flensburg Z1. Quartz grains sometimes have syntaxial quartz overgrowths with rounded, uneven edges, which indicate transport and re-deposition of former sandy sediments. In some places, two generations of inherited quartz overgrowths have been detected.

Detrital feldspars are much less abundant than quartz: 82% of the samples contain <5 vol.-% feldspar. Plagioclase is more common than K-feldspar, which is almost completely absent in well Flensburg Z1. K-feldspar is an important constituent of felsic igneous grains. The composition of most plagioclases is close to pure albite, while Ca-rich plagioclase is apparently absent (figure 25 and table A8, appendix). Textural evidence suggests that detrital feldspars were partly affected by replacement, albitisation, and minor dissolution (section 5.4.4).

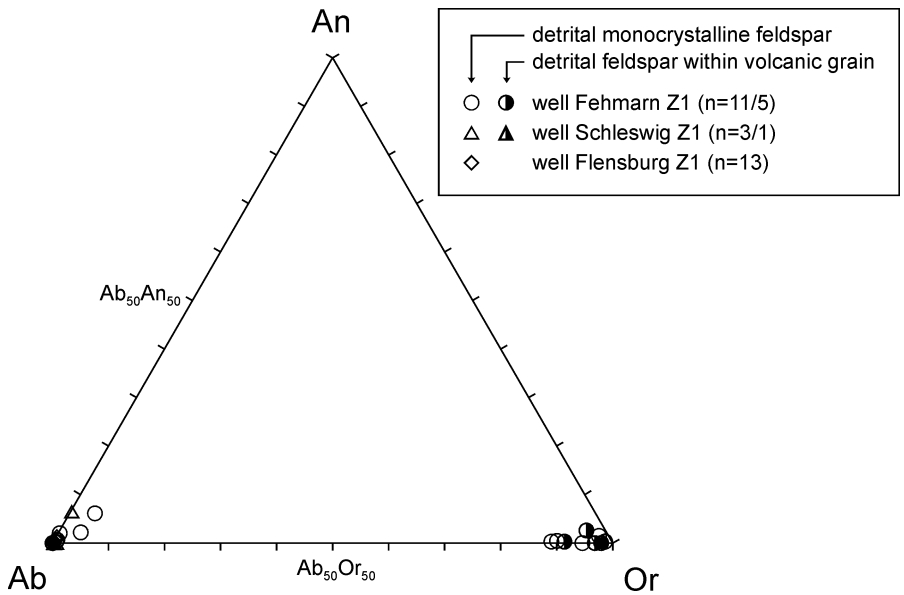

Figure 25: Chemical composition of detrital feldspars and feldspars within volcanic clasts for samples from the northern basin margin. Ba was considered to substitute for K. Mg, Sr, and Mn were considered to replace Ca (see Deer et al., 1992). Only albite was detected in well Flensburg Z1. Most albites are relatively pure ($Ab_{>99.0}An_{<0.8}Or_{<0.8}$). Four analyses have compositions between $Ab_{98.8}An_{0.6}Or_{0.5}$ and $Ab_{97.7}An_{2.0}Or_{0.3}$, three analysis indicate minor Ca- and/or K-enrichment (up to $Ab_{89.4}An_{6.2}Or_{4.5}$). The composition of detrital K-feldspars (partly within volcanic grains) ranges from relatively pure orthoclase ($Or_{98.5}Ab_{1.2}An_{0.3}$) to slightly Na-enriched orthoclase ($Or_{88.9}Ab_{10.8}An_{0.3}$). Composition in mol.-%.

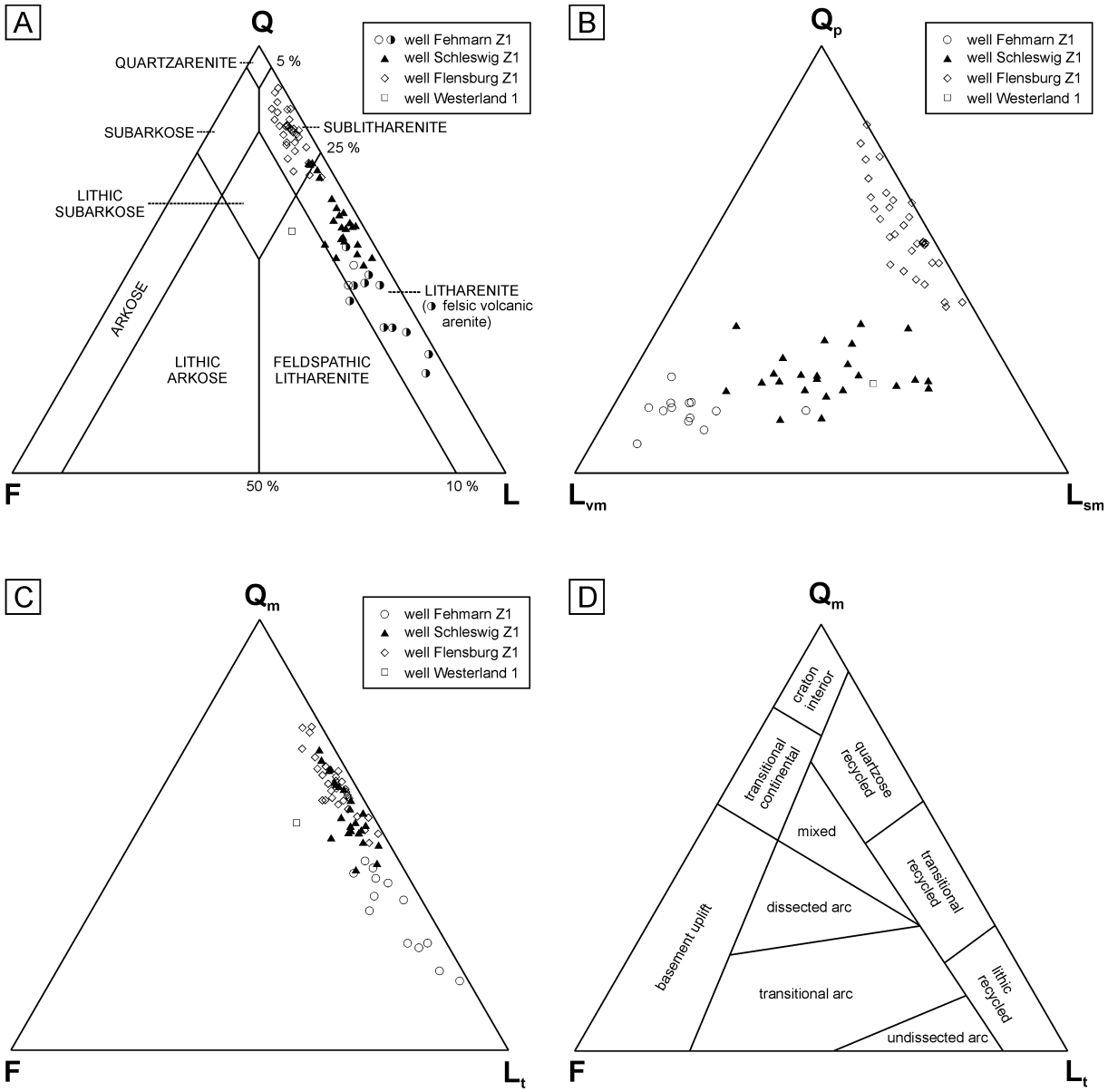

Figure 26: Detrital composition of Rotliegend sandstones from the northern margin of the NGB. A) Sandstone classification according to McBride (1963). Q = mono- and polycrystalline quartz + chert, F = feldspar, L = unstable rock fragments including extrabasinal carbonate clasts. The samples are mainly sublitharenites and litharenites, or felsic volcanic arenites. B) Abundance of rock fragments in the Q_p-L_{vm}-L_{sm} diagram. Q_p = polycrystalline quartz, L_{vm} = (meta-) volcanic rock fragments, L_{sm} = (meta-) sedimentary rock fragments. C) Detrital composition in the Q_m-F-L_t diagram. Q_m = monocrystalline quartz, F = feldspar, L_t =total lithic fragments, including extrabasinal carbonate clasts. D) Q_m-F-L_t provenance diagram after Dickinson (1985). All samples suggest a recycled orogen provenance.

The abundance of lithic rock fragments varies from locality to locality. Well Fehmarn Z1 contains 24-47 vol.-% of felsic volcanic grains. Most samples may thus be classified as felsic volcanic arenites (figure 26, compare McBride, 1963). Several different volcanic textures are evident from thin-section, including interlocked feldspar-quartz textures, porphyric textures with feldspar, quartz, and/or mafic phenocrysts, and spherulitic textures. Basaltic volcanics form a minor constituent (<2 vol.-%). Sedimentary clasts, often well rounded, were derived from shales, siltstones, sandstones, cherts, and carbonates. Metamorphic grains like slates, phyllites, quarzites, and quartz-chlorite- or quartz-mica-schists are less abundant. Polycrys-

talline quartz (3-10 vol.-%) may be of metamorphic or plutonic origin. Rock fragments in well Schleswig Z1 are qualitatively similar, but (meta-) sedimentary clasts are about as frequent as volcanics (5-25 vol.-%). The shape of large volcanic fragments and of red to brown mudstones is often subangular, while most other lithic grains are better rounded. Low-grade meta-pelites are partly abundant. Some of the detrital carbonates (>3 vol.-%) show biogenous origin: Fragments of echinoderms, foraminifera, and ostracod limestones could be identified in thin-section. Many carbonate grains, however, were replaced by diagenetic calcite. Rounded to well rounded polycrystalline quartz is the dominant rock fragment in well Flensburg Z1 (7-28 vol.-%). Metamorphic grains include slates, phyllites, quartz-chlorite-/quartz-mica-schists, quarzites, and gneiss (or granite) fragments. Sedimentary clasts, like (sandy) dolomite and subangular red to brown mudstones, are much less common. In contrast to the other two wells, grains of volcanic origin are very subordinate (0-3 vol.-%).

Some illite-rich, strongly deformed aggregates ("pseudomatrix") could not be unambiguously assigned to one of the grain types and have been separated from other rock fragments (group PM, see table A7). They may represent strongly altered volcanic as well as clay-rich (meta-) sedimentary or feldspar grains. Similarly, chlorite-rich aggregates of well Flensburg Z1 were included into this group. Fluvial sandstones locally contain pelitic matrix (<5 vol.-%).

Accessory components comprise Fe-oxide clasts, white mica, biotite, chlorite, and heavy minerals. There is good petrographic evidence that chlorite is at least partly an alteration product from biotite. Sporadically, bright green grains have been observed, which may consist of 7 Å or mixed-layer clay minerals like berthierine or corrensite. Odin et al. (1988) pointed out that such green clays often consist of several mineral species. Rare detrital sulphates were also counted as accessories. Non-opaque heavy minerals are with decreasing abundance: zircon, Ti-oxides, tourmaline and apatite. Ti-oxides and apatite are partly diagenetic in origin, however (section 5.4.9). Rare garnet was found in thin-sections of well Flensburg Z1. Opaque minerals are often altered to Fe-oxide or Fe-Ti-oxide aggregates, which provide no clear polished surfaces under reflected light. Some opaque minerals could be identified as magnetite, which partly contain Ti-rich exsolution lamellae (probably ilmenite).

The sandstone framework petrography can be classified in ternary diagrams (figure 26). Following von Eynatten and Gaupp (1999) and contrary to the original concept of McBride (1963), extrabasinal carbonate clasts were included into the L pole of the Q-F-L diagram, and in analogy into the and L_t and L_{sm} poles of the other two diagrams in figure 26 (see Mack, 1984; Dickinson, 1985; von Eynatten and Gaupp, 1999 for discussion). The effect remains subordinate, however, since the carbonate content does not exceed 3 vol.-%. According to the classification of McBride (1963), the samples can be characterised as dominantly litharenites/felsic volcanic arenites (well Fehmarn Z1), litharenites (well Schleswig Z1), and sublitharenites (well Flensburg Z1). The sample of well Westerland Z1 is a feldspathic litharenite. The three localities Fehmarn Z1, Schleswig Z1 and Flensburg Z1 can be distinguished by the abundance and types of rock fragments. The sandstones of well Flensburg Z1 are closest to the quartz pole of the Q-F-L diagram, those of well Fehmarn Z1 contain the most unstable rock fragments, and those of well Schleswig Z1 have intermediate compositions. The single sample of well Westerland 1 may not be representative and will not be considered further. The differences between well Schleswig Z1 and Flensburg Z1 diminish in the Q_m-F-L_t diagram, where all rock fragments including polycrystalline quartz and chert are

added to the L_t pole. The diagram Q_p-L_{vm}-L_{sm} shows most clearly the different importance of lithic fragments in the localities investigated. Samples of well Fehmarn Z1 are dominated by volcanic fragments. In well Schleswig Z1, grains of both volcanic and sedimentary/metamorphic origin may be abundant, while polycrystalline quartz is only a minor constituent. The sandstones of well Flensburg Z1, in contrast, are variable in terms of their Q_p/L_{sm} ratio, but the portion of volcanic grains remains minor throughout.

It should be noted that these diagrams represent the present detrital composition, which may differ from the primary composition. Replacement of detrital carbonates, pelites, feldspars, volcanics, and quartz by authigenic carbonates and/or sulphates may account for up to 7 vol.-% locally. Feldspar dissolution is not intense in most samples. However, intragranular porosities, which were most likely generated during diagenesis, can be in the order of 1 vol.-%. Feldspars affected by albitisation were still counted as detrital grains, if their detrital origin was evident from the grain shape and turbidity. The reduction of the original feldspar content by albitisation can thus be neglected.

P r o v e n a n c e

Applying the plate tectonic interpretation of Dickinson (1985), all sandstone samples suggest a recycled orogenic provenance (figure 26 C, D). They plot into the subcategories "quartzose + transitional recycled" (well Schleswig Z1, Fensburg Z1), or "transitional + lithic recycyled" (well Fehmarn Z1) of the Q_m-F-L_t diagram. Type, abundance, grain size and grain shape of felsic volcanic clasts in conglomerates and sandstones point to a nearby volcanic source area of acid to intermediate chemical composition. Large components in well Fehmarn Z1 are petrographically similar to the underlying volcanics. It is most likely that Late Carboniferous to Early Rotliegend igneous rocks were exposed and eroded at the northern margin of the deposition area. The abundance of volcanic detritus in the sandstones decreases from East (well Fehmarn Z1) to West (well Flensburg Z1), and supports the assumption that Rotliegend volcanics are thinning-out NW of Fehmarn (figure 10, Marx et al., 1995). The sample of the westernmost well (Westerland 1) contains again a higher percentage of volcanic material, however. Non-igneous rock fragments point to a mixed sedimentary-metamorphic hinterland. Clastic sediments and (biogenous) carbonate clasts may be derived from Carboniferous rocks and/or from Lower Paleozoic strata of the Baltic shield. Quartz grains containing inclusions of helminth-chlorite are typical in low-grade metamorphic rocks (Frank et al., 1992). Caledonian metasediments are a likely source for the observed low-grade metamorphic material. Elongate, angular shaped mud flakes, sulphate clasts, and some of the detrital carbonates and Fe-oxides are probably re-deposited intrabasinal components of the Rotliegend. Such material is available from mud deposits, near-surface sulphate or carbonate concretions, and from Fe-oxide incrustations.

In summary, the framework petrography is consistent with a mixed sedimentary-metamorphic-igneous source area to the north of the Rotliegend basin (Ringkøbing-Fyn/ Fennoscandian High). Significant compositional variations in the localities investigated suggest that the material was transported into the basin by individual alluvial systems with different drainage areas and point to a complex, heterogeneous hinterland.

5.4 Authigenic mineralogy

A range of authigenic minerals formed in the Rotliegend sandstones subsequent to deposition and during burial, including Fe-oxides, quartz, feldspar, carbonates, sulphates, and clay minerals. Carbonates are volumetrically dominant in most samples, although quartz cements may be locally abundant. The relative succession of diagenetic minerals is shown in figure 37A at the end of section 5.

Two main types of authigenic parageneses can be observed in the wells from Schleswig-Holstein. They are similar to the diagenesis types classified by Gaupp (1996; compare table 5 in section 6.4), but show some differences in detail. The most abundant type is dominated by early hematite-illite grain coatings and by calcite cements, which often fill large parts of the pore space. Authigenic quartz, feldspar and sulphates are volumetrically only locally important. This paragenesis occurs in well Fehmarn Z1, Schleswig Z1, and in some horizons of well Flensburg Z1. It is termed here "hematite-sebkha type" (H-SB; compare table 5). The second paragenesis, which is only evident from well Flensburg Z1, is characterised by dolomite, chlorite and quartz cements, although minor authigenic feldspar, calcite, and hematite are present as well. This diagenesis type is termed here "dolomite-chlorite type" (D-C; compare table 5).

The terms "eodiagenesis" and "mesodiagenesis" are used here in the sense of Schmidt and McDonald (1979): Eodiagenesis is defined as the regime at or near the surface of sedimentation, where the chemistry of the pore water was mainly controlled by the surface environment. Mesodiagenesis is defined as the subsurface regime during burial under strata that sealed the sandstones from a predominant influence of surface waters.

5.4.1 Fe-oxides/hydroxides

Hematite is almost omnipresent in sandstones from the northern part of the NGB, albeit with varying abundance. The presence of hematite in Rotliegend sandstones is evident from microscopic investigations and XRD analyses (compare plate 2, 5, 8), and has been confirmed by Raman spectroscopy (Hasner, 2004). In most sandstones, hematite occurs in sub-µm- to µm-thick coatings on grain surfaces (plate 2A, 2C, 2E, 5E, 5F). These grain coatings typically consist of a mixture of hematite and illite, partly together with minor Ti-oxides (see below). They are particularly well developed in diagenesis type H-SB, where they partly form dense opaque crusts. The grain framework was dominated by point contacts during the formation of these coatings, suggesting an early origin prior to significant mechanical compaction (plate 2E, 4B). Hematite is responsible for the red colour of the coatings and hence for the rubification of Rotliegend sandstones. Point-counting data indicate that the abundance of hematite-bearing coatings ranges from 0 to 7 vol.-% in most samples. Only few sandstones have exceptionally high hematite contents of 8-14 vol.-%. However, the quantification of coatings in thin-section is problematic, and these figures cannot be interpreted directly as the Fe-oxide content of the sandstones (section 5.6). Dark coatings are likely to be overestimated due to oblique grain surfaces in thin sections of ~25 µm thickness, and since they mostly contain some porosity, which is impossible to quantify. Furthermore, hematite and illite within these coatings cannot be separated during point counting. Investigations by transmission electron microscopy indicate that sheet silicates are more abundant than hematite crystals (Hasner, 2004). According to a semi-

quantitative classification, all samples contain at least traces of hematite (table A7, appendix).

Hematite grain coatings are subordinate in a number of sandstones of well Flensburg Z1, which were cemented by pore lining or radial chlorite, or by pore-filling early quartz and dolomite cements (diagenesis type D-C). Such sandstones have brown-grey or grey rock colours. Nevertheless, opaque minerals or mineral aggregates can often be found on grain surfaces, mostly beneath chlorite coatings (plate 2D, 4H). These aggregates are typically < 3µm in size and consist mainly of hematite and minor Ti-oxides according to optical microscopy and SEM-EDX. Hematite also precipitated on authigenic dolomite crystals in those rocks. Alternating layers of dolomite and hematite suggest that hematite formed contemporaneously to dolomite (plate 2B, 7A, 7B, 7C).

Grain embayments preserve hematite-rich aggregates in many samples investigated (plate 3C). Hematite staining is common in detrital grains, especially in volcanic and feldspar clasts holding (micro-) porosity. It also occurs in authigenic dolomites and rarely in authigenic calcite. If clay matrix is present, it mostly contains some hematite. Commonly, single Fe-oxide crystals can not be resolved under the optical microscope. However, hematite crystals up to 100 µm size, showing sharp crystal edges, have been detected sporadically.

I n t e r p r e t a t i o n

Thick hematite coatings in grain embayments and hematite staining of detrital grains may be inherited from weathering processes in the source area. Most hematite, however, is early diagenetic in origin. Textural evidence points to near-surface precipitation in uncompacted or poorly compacted sediments. Eodiagenetic near-surface formation of Fe-oxides or -hydroxides is characteristic for semi-arid clastic deposits (e.g. Walker, 1967; van Houten, 1968; Folk, 1976). Iron was released during the breakdown of unstable ferromanganese or Fe-oxide minerals within the sandstones under surface conditions. Mafic components of volcanic grains, e.g., were completely oxidised in most cases. Additionally, iron may have been transported into the basin by meteoric waters from weathering profiles at the adjacent basin margin. Various Fe-oxides/-hydroxides may have precipitated during fluctuation of the water table (redox changes) and transformed into hematite during burial of the sediments (Chukhrov, 1973; Walker, 1976).

The presence of tangential illite coatings apparently promoted the formation of relatively continuous hematite-illite coatings around grain surfaces. Where tangential illite is lacking, as in a number of sandstones of well Flensburg Z1, hematite precipitated preferentially as small aggregates. Absence of hematite is common in areas that were strongly cemented by early quartz and dolomite cements. Early cementation and/or rapid burial below the depth of ground water fluctuations may have been responsible for the inhibition of hematite formation in these cases. This assumption is consistent with the thickness and sedimentology of the sandstones in well Flensburg Z1, which suggest high sedimentation rates (see section 5.1.3). However, the precipitation of ferric oxides on authigenic dolomite crystals, which are probably early mesodiagenetic (section 5.4.5), points to local influence of oxygenated surface waters during early burial diagenesis.

5.4.2 Ti-oxides

Diagenetic Ti-oxides often occur close to opaque heavy minerals, e.g. magnetite, or volcanic grains. They partly replace detrital Ti-bearing components. Clusters of Ti-oxides ("leucoxene") are common, but single Ti-oxide crystals precipitated locally within the pore space too (plate 2C, 2D). They formed after hematite coatings, and they were often overgrown by later carbonate or sulphate cements. Raman analyses show that diagenetic anatase has formed in these rocks, and that minor anatase may also be associated with hematite-illite coatings (Hasner, 2004). However, the concomitance of rutile, brookite and other Ti-minerals cannot be excluded (compare Zimmerle and Tietze, 1971).

I n t e r p r e t a t i o n

The common clustering of authigenic Ti-oxides, e.g. around opaque heavy minerals or dissolved grains, suggests that they dominantly formed form local Ti-sources. However, isolated crystals suggest that Ti was mobile at least on thin-section scale. The most likely sources for Ti were mafic minerals of volcanic clasts, biotite, or detrital heavy minerals (e.g. Ti-bearing magnetite and ilmenite), which were altered/dissolved during diagenesis. Authigenic Ti-oxides probably precipitated during early mesodiagenesis, although anatase within hematite-illite coatings may have formed already during eodiagenesis. Late eodiagentic to early mesodiagenetic anatase formation has been recorded from other red bed sandstones previously (Burley, 1984; Weibel, 1998).

5.4.3 Quartz

Quartz cements are not abundant in the wells Fehmarn Z1 and Schleswig Z1 (0-2 vol.-%). In well Flensburg Z1, authigenic quartz is much more frequent and partly occludes the pore space (2-12 vol.-%, one sample 16 vol.-%). Early quartz precipitated as syntaxial overgrowth, i.e. with the same crystallographic orientation as the detrital quartz grain. Such overgrowths are locally present in all wells. The earliest generation formed prior to hematite coatings (plate 2E, 2F). However, early quartz overgrowths with rounded edges appear to be inherited (see section 5.3). Euhedral, prismatic quartz crystals are a widespread minor constituent. According to sharp crystal edges and almost perfect crystal habit they must have been growing into open pore space. Early quartz has often been overgrown by later pore-filling carbonate or sulphate cements, or by later generations of quartz. The pore-filling quartz cements of well Flensburg Z1 are mostly syntaxial (plate 3A, 3B). They preserve of intergranular volumes (IGV) up to 28%. In sandstones cemented by radial chlorite, some quartz cements pre-date, others post-date chlorite growth (plate 5D). Quartz precipitated also in veins intersecting the sandstones.

CL-colours are difficult to observe when carbonates are present. In some samples of well Flensburg Z1, however, CL petrography indicates a polyphase origin of quartz cements (plate 3D). Early quartz overgrowths are commonly non-luminescent. Later pore-filling cements are zoned and show areas of bright blue CL-colours and non-luminescent quartz. Blue luminescence colours, which fade within about one minute, were observed in a quartz vein of well Fehmarn Z1.

I n t e r p r e t a t i o n

Early syntaxial quartz overgrowths and euhedral quartz crystals are eodiagenetic cements, which formed prior to pore-filling cements. They are common in red beds of evaporitic sebkha/playa environments, where they typically occur together with authigenic sulphates (Platt, 1994). Early quartz precipitation is also possible from meteoric waters, which took up dissolved Si released from chemical weathering processes (compare Bjørlykke, 1983; McBride, 1989).

Pore-filling quartz-cements precipitated most likely during burial diagenesis. Based on fluid-inclusion studies, many authors suppose that the main quartz cementation in sandstones takes place at temperatures above 70-80°C (e.g. Burley et al., 1989; Walderhaug, 1994; Marchand et al., 2002). Considering the burial history of well Flensburg Z1 (figure 18), this temperature was reached in approximately 1500 m depth in Late Permian times. Although quartz cements in well Flensburg Z1 pre- and post-date authigenic chlorite growth, it is not clear whether there are separate generations of quartz or a more or less continuous quartz growth. The zonation visible by CL, however, does not support the assumption of a steady process. Blue and short-lived blue luminescence colours are very typical for authigenic quartz cements and quartz crystals from fractures and veins (Ramseyer et al., 1988). Likely sources for silica within the sandstone-mudstone succession were quartz dissolution at grain-grain-contacts ("pressure dissolution"), dissolution of amorphous volcanogenic Si, dissolution of feldspar, and clay mineral transformations. Additionally, compaction waters from shales of the central Rotliegend basin may have imported Si-oversaturated fluids into basin-margin sandstone horizons. Other possible sources of silica as well as the mechanisms of quartz precipitation in sandstones are discussed in more detail in Worden (2000).

5.4.4 Feldspar

Authigenic feldspar occurs as either syntaxial overgrowth on detrital feldspar grains, or euhedral crystals, which locally agglomerate to pore-filling aggregates (plate 2G, 3C, 6E). They are usually twinned and non-luminescent. Feldspar overgrowths are volumetrically not important (<1 vol.-%). Overgrowths may have formed pre- and post-hematite, while euhedral crystals commonly post-date hematite grain coatings. Carbonate or sulphate cements have typically overgrown authigenic feldspar. EMP measurements yield compositions close to stoichiometric albite (table A8, appendix). Authigenic albite has partly replaced detrital feldspar (plate 4A, 4B). This process is referred to as albitisation (see also Morad et al., 1990). It is evident from all localities, but more extensive in well Flensburg Z1. The total amount of authigenic feldspar is <2 vol.-% in well Schleswig Z1 and Flensburg Z1, but may locally reach 8 vol.-% in well Fehmarn Z1.

I n t e r p r e t a t i o n

Minor eodiagenetic albite is characteristic in SB-type cement assemblages (Gaupp, 1996, compare section 6.4). Higher contents of authigenic albite (>2 vol.-%) correspond to a higher abundance of volcanic material: felsic volcanic arenites of well Fehmarn Z1, which were deposited on top of Rotliegend volcanics, contain the most authigenic albite (figure 27, plate 6E). The abundance of albite in these rocks is probably related to surface weathering or

eodiagenetic alteration of volcanic rock fragments, and re-precipitation of the dissolved ions, mainly as albite and clay mineral grain coatings (see below).

Albitisation is a widespread diagenetic process in sandstones containing detrital feldspars, and has been focus of research over many years (e.g. Land and Milliken, 1981; Boles, 1982; Saigal et al., 1988; Aagaard et al., 1990; Morad et al., 1990; Baccar et al., 1993). K-feldspars as well as plagioclase may be affected by albitisation. These reactions consume Na, and release K or Ca. Possible Na-sources for albite growth in the Rotliegend were the formation water, or clay mineral transformations within the sandstones or adjacent shales. K and Ca may have been consumed by smectite to illite conversion reactions, and carbonate precipitation, respectively.

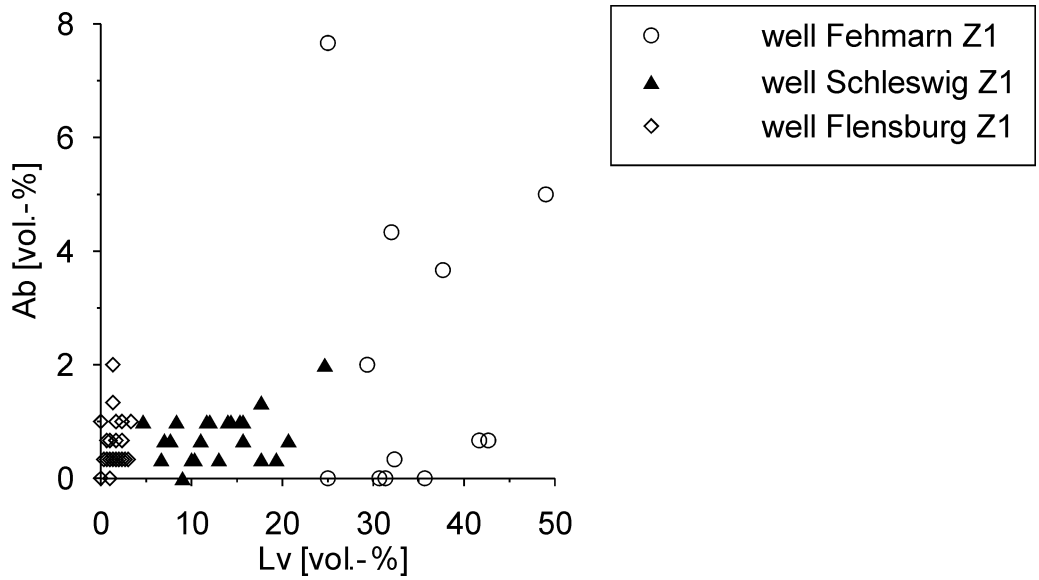

Figure 27: Abundance of detrital volcanic grains (Lv) vs. abundance of authigenic albite. Albite contents >2 vol.-% are only evident in samples with >25 vol.-% volcanic grains from well Fehmarn Z1.

5.4.5 Carbonates

Authigenic carbonates are the dominant pore-filling cements in the northern part of the NGB. Calcite is abundant in well Fehmarn Z1, Schleswig Z1, and in some horizons of well Flensburg Z1 (diagenesis type H-SB). Dolomite is only present in well Flensburg Z1 (diagenesis type D-C). Ankerite, siderite, or magnesite cements, which have been reported from Rotliegend deposits of other localities (Almon, 1981; Pye and Krinsley, 1986; Purvis, 1989; Gaupp et al., 1993), are apparently absent in the area investigated.

Calcite

Calcite typically occludes the pore space, but also replaces detrital feldspars, volcanics and carbonates, and partly authigenic dolomite. The earliest generation is often associated with sulphate cements and locally pre-dates major hematite formation. These cements may preserve large IGV (~30-35 vol%). However, most calcites post-date hematite-illite grain coatings and yield 1-17 vol.-% in H-SB type cemented sandstones (second generation). A clear determination between calcites of first and second generation is not possible in all

samples. Regular zoning is visible by bright orange to red or red/brown luminescence colours as well as by BSE microscopy (plate 3G, plate 6). Zoning is evident especially in large pores, while smaller pores (<100 µm) were often cemented by homogeneous calcite cement (plate 3E, 3F). EMP analyses indicate that different zones corresponds to different Mn contents. The earliest calcite crystals are often nearly pure $CaCO_3$. The composition of pore-filling, zoned calcites ranges from nearly $CaCO_3$ to $Ca_{0.91}Mg_{0.01}Mn_{0.08}CO_3$ (figure 28A, table A9, appendix). Some samples show a trend towards increasing Mn contents during crystal growth. The calcites may be enriched in magnesium (up to 2.5 mol.-% $MgCO_3$). The Fe content of these cements is below or little above the detection limit of the EMP (0.10 mol.-% $FeCO_3$). There are no systematic differences between samples from individual wells. Grain replacing calcites have similar chemical composition, although the Fe content may locally be higher (<0.6 mol.-% $FeCO_3$). Strontium and barium are mostly below the detection limit of the EMP.

At least one later generation, post-dating dolomite and chlorite formation, can be texturally distinguished from earlier pore-filling calcites (diagenesis type D-C). However, these late calcites are volumetrically only locally important (<2 vol.-%). They are commonly clear in microscopic image. The outer rim of these calcites shows orange CL colours, the centre is dull brown to non-luminescent (plate 3H). The orange luminescing areas are slightly enriched in Mn and/or Fe (<1.5 mol.-% $MnCO_3$, <0.6 mol.-% $FeCO_3$). Central areas are slightly enriched in Mg (<0.9 mol.-% $MgCO_3$), but Mn and Fe could not be detected there (plate 6G, 6H). Another type of late calcite is occurring within partly dissolved/albitised feldspars of any diagenesis type. Locally, calcite and albite have replaced feldspar grains almost completely (plate 4C). Calcite may have precipitated contemporaneously or subsequent to albitisation reactions.

Vein calcites of well Flensburg Z1 appear to have formed relatively late according to petrographic relationships, and they show similar chemical composition as late calcite cements (figure 28B). The veins of well Flensburg Z1 are partly open. Textural and CL evidence suggest that veins in well Fehmarn Z1 were cemented by calcite contemporaneously to early pore-filling calcite. One EMP analysis of a vein calcite yields 4.4 mol.-% $MnCO_3$.

The carbon and oxygen isotopic composition of calcite cements and vein calcites is shown in figure 29, 30 and table A15 (appendix). $d^{13}C$ values of calcite cements range from 0‰ to +0.4‰ V-PDB for well Fehmarn Z1 and from -2.9‰ to -1.3‰ V-PDB for well Schleswig Z1. One sample of well Flensburg Z1 yields -6.3‰ V-PDB. There is a trend towards lighter carbon isotopic ratios with increasing depth in well Schleswig Z1 (figure 30). A trend towards lighter oxygen isotopic ratios with increasing depth is evident from well Fehmarn Z1, where $d^{18}O$ values decrease from -9.5‰ to -11.7‰ V-PDB within 70 m. Calcites of well Schleswig Z1 have less negative $d^{18}O$ values (-8.4‰ to -7.4‰ V-PDB). The $d^{18}O$ value of the calcite sample of well Flensburg Z1 is -11.0‰ V-PDB. The isotopic composition of vein calcites is similar to the composition of cements in the individual wells (figure 29). Comparable isotopic compositions were found in calcites from other parts of the NGB (Rieken, 1988; Platt, 1991).

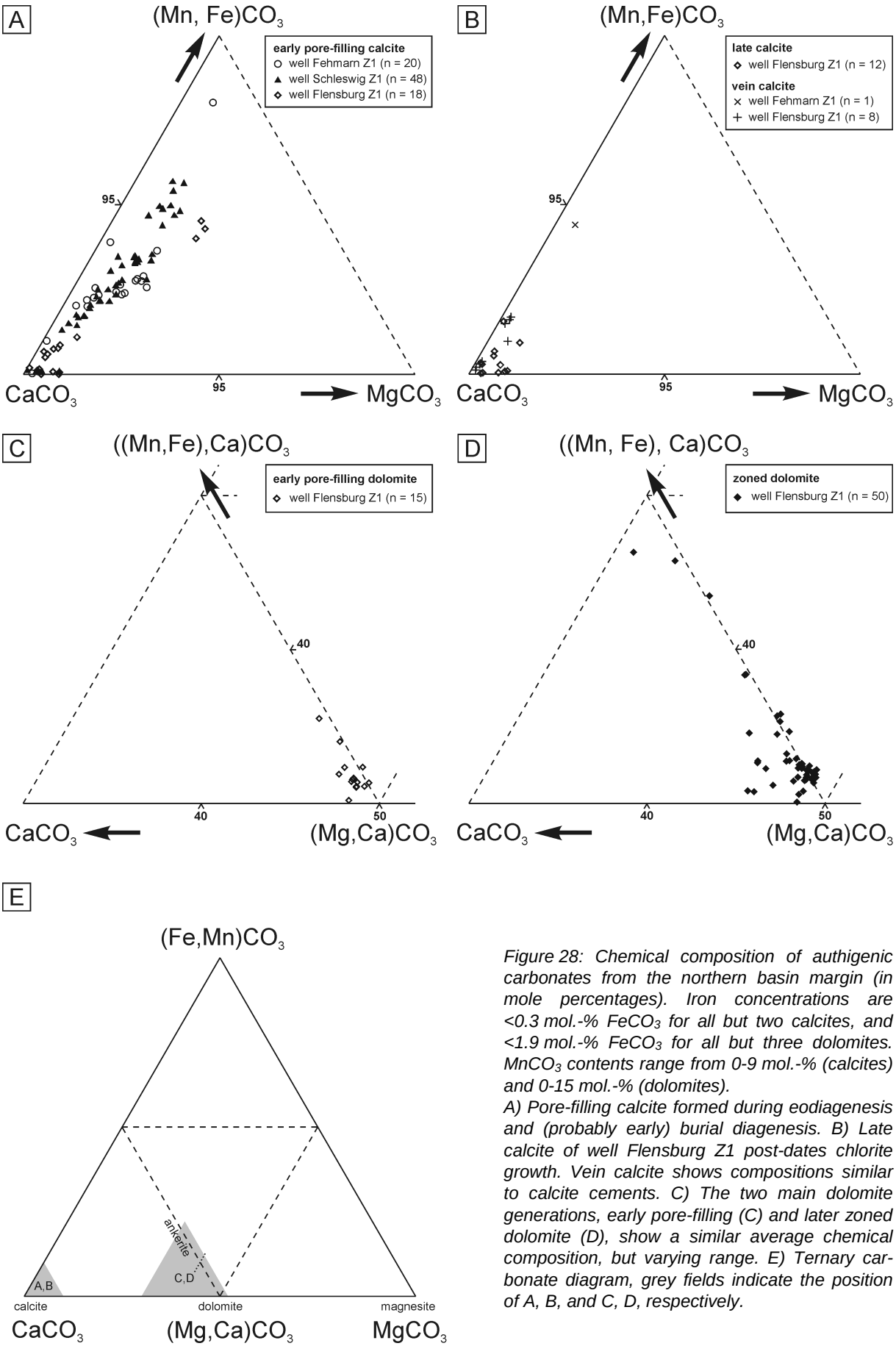

Figure 28: Chemical composition of authigenic carbonates from the northern basin margin (in mole percentages). Iron concentrations are <0.3 mol.-% $FeCO_3$ for all but two calcites, and <1.9 mol.-% $FeCO_3$ for all but three dolomites. $MnCO_3$ contents range from 0-9 mol.-% (calcites) and 0-15 mol.-% (dolomites).
A) Pore-filling calcite formed during eodiagenesis and (probably early) burial diagenesis. B) Late calcite of well Flensburg Z1 post-dates chlorite growth. Vein calcite shows compositions similar to calcite cements. C) The two main dolomite generations, early pore-filling (C) and later zoned dolomite (D), show a similar average chemical composition, but varying range. E) Ternary carbonate diagram, grey fields indicate the position of A, B, and C, D, respectively.

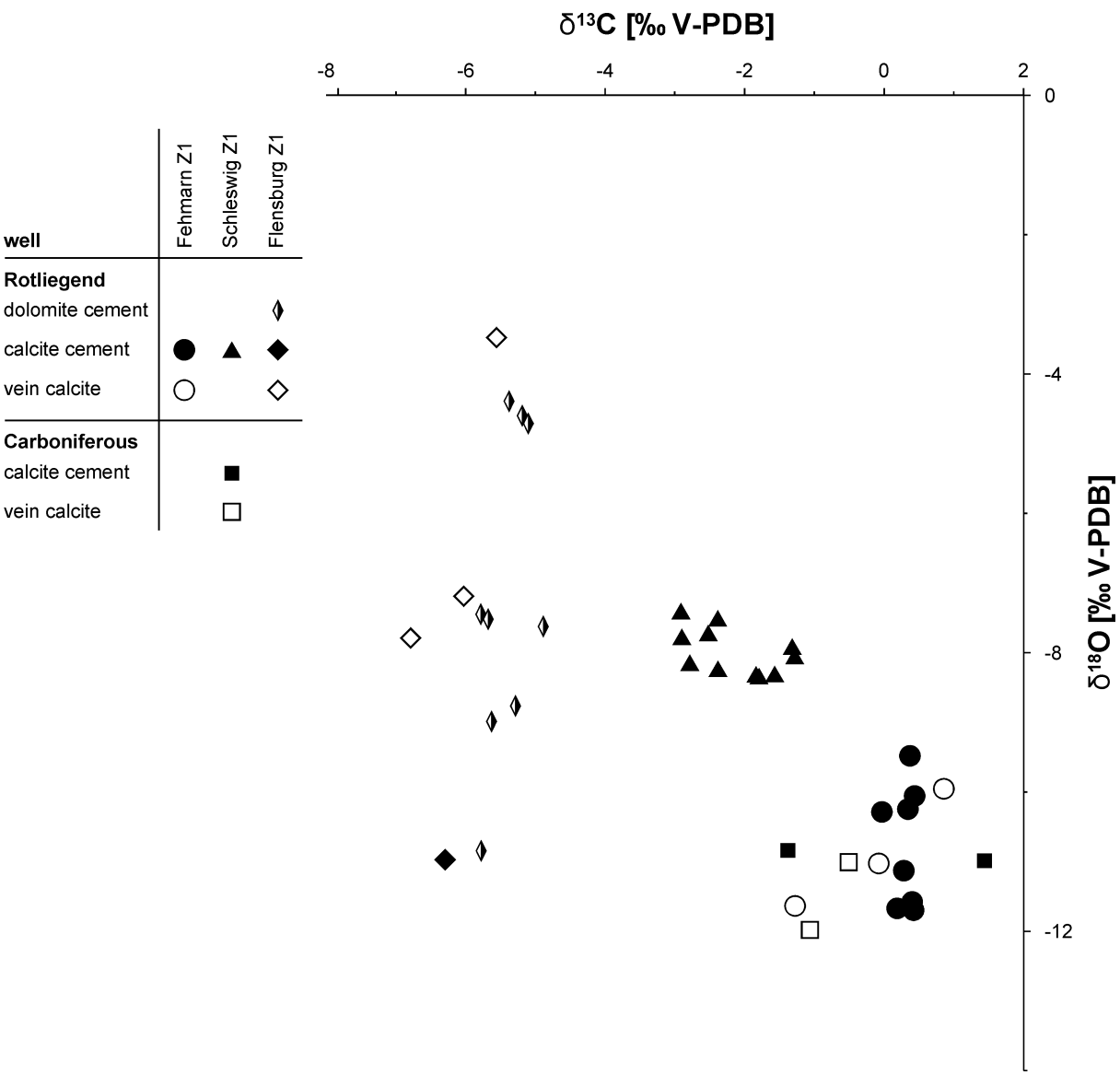

Figure 29: Plot of oxygen isotope ratio against carbon isotope ratio of calcite cements and vein calcites, and dolomite cements. Additionally to Rotliegend sandstones, two samples of calcite cements and vein calcites from Carboniferous sandstones were investigated (well Schleswig Z1). Samples from well Fehmarn Z1 have the most negative oxygen and most positive carbon isotopic values. Calcites and dolomites of well Flensburg Z1 can be distinguished by more negative carbon isotopic composition. Isotope ratios in Rotliegend samples of well Schleswig Z1 show intermediate composition.

Dolomite

Two main generations of dolomite can be distinguished from textural evidence. The first generation commonly precipitated directly on grain surfaces, partly post-dating syntaxial quartz overgrowths (plate 2F). Early dolomite may have grown corrosively against detrital grains, and has replaced mudstone, carbonate and feldspar grains (plate 2H). These dolomites are not clearly zoned, but exhibit a patchy growth pattern in BSE image and are often full of opaque inclusions. Dissolution textures are occasionally visible between first and second generation of dolomite.

The second generation comprises rhombohedral dolomite crystals, which are often zoned and may form overgrowths on earlier dolomites (plate 2B, 7A, 7C, 7E). Single growth bands can be separated by ferric iron layers. Dolomite may have been replaced by calcite and often shows minor dissolution textures, especially in the vicinity of hematite layers. The position of the most intense dolomite reflection in XRD traces ranges from 2.887 to 2.890 Å; ankerite was not detected by XRD (plate 8). Both dolomite generations have iron contents up to 1.9 mol.-% $FeCO_3$, except three samples (2.5-4.7 mol.-% $FeCO_3$; see table A10, appendix). Iron contents >2 mol.-% $FeCO_3$ were only obtained for rare narrow growth bands of the second dolomite generation. A contamination of these analyses by ferric iron crystals cannot be excluded. The manganese contents vary between 0.2-5.0 mol.-% $MnCO_3$ (early dolomites, figure 28C) and 0.1-15.2 mol.-% $MnCO_3$ (zoned dolomites, figure 28D). Volumetrically dominant parts of dolomite cements comprise relatively low manganese contents (<2 mol.-% $MnCO_3$). Higher values were measured preferentially in the outer rims of zoned dolomites and in small areas of early pore-filling dolomites (plate 7). It is possible that these Mn-rich spots within the earlier dolomite generation precipitated contemporaneously to the later zoned generation. Due to their high Mn+Fe content, three analyses plot into the ankerite field in figure 28D. However, the term ankerite can not be applied here, since it is commonly used for material with >20 mol.-% $(Fe,Mn)CO_3$ and Fe>Mn (compare Deer et al., 1992). Mn-dominated members of the dolomite group are termed kutnohorite, $Ca(Mn,Mg,Fe)(CO_3)_2$. There is probably a continuous series between dolomite and kutnohorite (Deer et al., 1992). Zoned dolomites partly show increasing calcium contents – up to 53.9 mol.-% $CaCO_3$ – towards the outer edge of the crystal (plate 7A-D). Pure dolomite has not been observed. Strontium and barium are mostly below the detection limit of the EMP. Despite their different chemistry, all dolomites investigated by CL microscopy have relatively uniform bright red to dull red-brown luminescence colours (plate 3H).

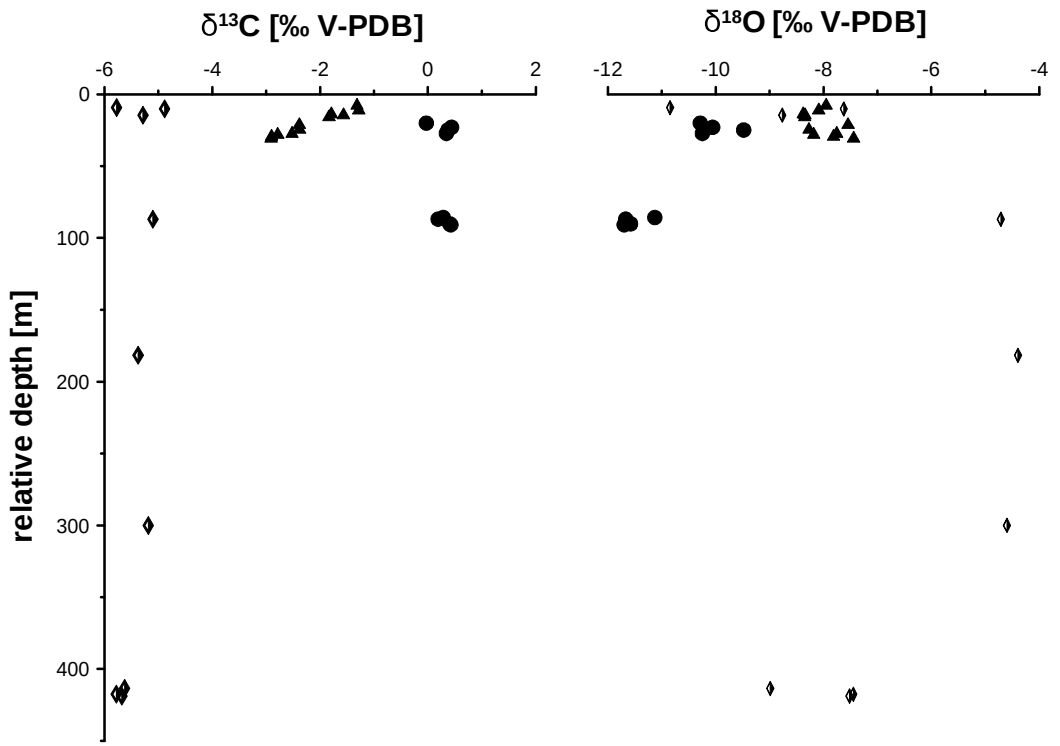

Figure 30: Plot of carbon and oxygen isotope ratio against depth; legend see figure 29. $d^{13}C$ values decrease from -1.3 to -2.9‰ V-PDB within 25 m in well Schleswig Z1. $d^{18}O$ values decrease from -9.5 to -11.7‰ V-PDB within 70 m in well Fehmarn Z1. Other isotope ratios show no depth related trends.

Oxygen isotopic ratios of dolomite cements show a much larger range than carbon isotopic ratios (figure 29, 30; table A15, appendix). The $d^{13}C$ values vary from -5.8‰ to -4.9‰ (V-PDB), the $d^{18}O$ values from -10.9‰ to -4.4‰ (V-PDB). There is no clear relation of isotopic composition to burial depth, although the succession investigated is about 410 m thick.

Interpretation of carbonate cements

Although there is some evidence for very early calcite and dolomite cements, which preserve large IGV and are likely to be eodiagenetic, most carbonates formed during mechanical compaction. However, a number of arguments indicate that the pore-filling carbonates dominantly precipitated from meteoric-type pore waters: (1) Carbonate-rich sandstones may still have IGV around 25 vol.-%, reduced from estimated original porosities of only 33-38 vol.-% (section 5.2). (2) Hematite layers interrupting dolomites growth point to relatively shallow burial depths, where oxygenated waters could percolate through the pore system. (3) Complex zoning requires multiple fluctuations in water composition, which is typical in near-surface environments. (4) Carbonates enriched in Mn have often been found in cements that originated from meteoric pore waters (Boles and Ramseyer, 1987). (5) Oxygen isotopic compositions are similar to those of eodiagenetic and shallow burial carbonates of the southern basin margin, which most likely precipitated from meteoric-type waters (Platt, 1994).

It is likely that recurrent carbonate growth started close to surface and continued during burial. Considering the rapid burial in Upper Permian (plus lowermost Triassic) times and the range of IGV preserved, this process may have taken place over the first 1000-2000 m of burial, where mechanical compaction is most intense (compare Füchtbauer, 1979). Calcite in sandstones with relatively low IGV may have formed by redistribution of earlier calcite cement without major changes in petrographic characteristics. Dissolution of early calcite cement has been suggested as one major source of carbonates precipitated during burial (Bjørlykke et al., 1989). Variations in oxygen isotopic composition probably date from different crystallisation temperatures, and thus represent several cement generations, which precipitated over a range of burial depths. Differences between the three localities may be related to differences in meteoric water supply versus evaporation. The primary $d^{18}O$ signature of waters in a semi-arid terminal lake basin becomes heavier towards the basin margin due to increasing evaporation (compare Platt, 1994). The carbon isotopic ratios range from values typically found in carbonates from continental desert environments (approximately -6‰ to -1‰ PDB; e.g. Pierre et al., 1984; Mertz and Hubert, 1990) to values similar to those assumed for Permian sea water (0‰ to 2‰ PDB; Sullivan et al., 1990). Although the decrease in $d^{13}C$ of calcite cements with increasing depth (well Schleswig Z1) could be interpreted as influx of relatively light carbon from the underlying Lower Carboniferous, the $d^{13}C$ values are still relatively heavy compared to the typical range of carbon isotopes from the Rotliegend of northwest Germany (Rieken, 1988; Platt, 1991). The supply of isotopically light carbon from thermal maturation or bacterial degradation of organic matter may result in $d^{13}C$ values of -40‰ to -10‰ PDB in carbonate cements (e.g. Irwin et al., 1977; Curtis and Coleman, 1986; Schwarzkopf, 1990; Macaulay et al., 2000; Campbell et al., 2002). Depth-related trends in isotopic composition could have been caused by e.g. changing ratios of earlier versus later cement generations with slightly different isotopic composition. It must be pointed out that isotope data were analysed from bulk carbonate cements and cannot

account for different generations in one sample, so the significance of this data is limited. The interpretation is also hampered by possible recrystallisation of carbonate cements.

Late calcites are one of the latest diagenetic phases in the samples investigated. There may be several phases of late calcite precipitation, which cannot be differentiated by the present petrographic data. These calcites grew in a stabilised grain framework after the main phase of mechanical compaction.

5.4.6 Sulphates

Minor amounts of sulphate cements are present only in some sandstones of diagenesis type H-SB. Well Flensburg Z1 does not contain any diagenetic sulphates. Anhydrite is rare (<1 vol.-%) in well Fehmarn Z1 and Schleswig Z1, but makes up 17% of the rock volume in the sample of well Westerland 1. Barite is rare (<0.5 vol.-%) in well Fehmarn Z1, but relatively widespread in well Schleswig Z1 (up to 5 vol.-%; see table A7, appendix).

Some detrital grains are composed of anhydrite or barite laths, which may be intergrown with small quartz crystals (well Fehmarn Z1, Schleswig Z1). Similar textures are found in sulphate nodules of overlying Rotliegend mudstones, and were also recorded in anhydrite nodules of other evaporitic environments (e.g. Kerr and Thomson, 1963; Dean et al., 1975). Evidence for the earliest generation of anhydrite, which precipitated after hematite formation and encloses relatively large IGV (40 vol.-% in well Westerland 1), comes from few samples only. Most sulphates form pore-filling aggregates in sandstones with moderate to low IGV (25-15 vol.-%) and post-date early calcite growth (plate 2E, 2G). Barite is typically found within coarse, well sorted laminae. Authigenic sulphate may have replaced detrital grains, especially feldspars, and also occurs in veins. EMP analyses of barite cements yield <1 mol.-% $CaCO_3$ and 3-5 mol.-% $SrSO_4$ (table A11, appendix), so they may be called "strontiobarites" (compare Deer et al., 1992). Sr enrichment is also evident from the position of the most intense barite reflections in the powder XRD patterns (021 reflection = 3.435 Å, 121 reflection = 3.098 Å; plate 8). These positions are not identical to pure barite, but slightly displaced in direction of strontian barite (see *Power Diffraction File*, 24-1035 and 39-1469). Semi-quantitative EDX-analyses of anhydrite indicate almost pure $CaSO_4$.

I n t e r p r e t a t i o n

Rare relics of early diagenetic anhydrite/barite and detrital sulphate grains suggest that eodiagenetic sulphate precipitation has taken place. However, it was probably not extensive in the coarse grained fluvial sandstone sequences of the northern study area. This would be consistent with the observation of other workers that fluvial sandstones at the margin of continental semi-arid to arid basins are typically dominated by early carbonate cementation, while anhydrite precipitation dominates closer to the basin centre (e.g. Hardie, 1968; Glennie, 1972; Morad et al., 2000). Anhydrite is much more common in the mudflat environment overlying the basal Rotliegend sandstones (see section 5.1). In these horizons, anhydrite nodules occur mainly in mudstones; anhydrite cements are frequent in interbedded fine grained sandstones (e.g. sample Wl001). Locally, anhydrite replaces fish-tale twins of gypsum in Rotliegend mudstones.

Minor mesodiagenetic sulphate cements are widespread in many reservoir sandstones (e.g. Füchtbauer, 1974; Almon, 1981; Weibel, 1998; Ramseyer et al., 2004). The abundance of

barite in some samples of the northern study area may be related to the release of barium during feldspar dissolution in sediments or Rotliegend volcanics of the nearby hinterland. Diagenetic dissolution/albitisation of feldspar may also have contributed to the supply of barium. Detrital K-feldspars analysed by EMP typically yield 0.2-0.6 wt.-% BaO (table A8, appendix). However, the barite content of the sandstones investigated does not correlate directly with the abundance of volcanic detritus. Barite precipitation due to infiltration of Zechstein fluids into Rotliegend sandstones was proposed by Pye and Krinsley (1986) for the southern North Sea. This process is unlikely for the northern study area, since 700-1400 m Rotliegend shales and evaporites separate the Zechstein from Rotliegend reservoirs.

Pore size apparently controls cementation patterns to some degree, as already noted by Füchtbauer (1979), Glennie et al. (1978), and others. In the present study, this is evident for authigenic barite, but has also been noted for zoned calcite cements (see above). Putnis and Mauthe (2001) argued that fluids in small pores can maintain a higher supersaturation with respect to crystallisation compared to large pores. This may explain why some cements precipitated in coarse grained, well sorted laminae, but are absent within finer grained layers. Considering such difference in crystallisation patterns within individual samples, the establishment of a precise paragenetic sequence becomes very difficult. It is almost impossible to interpret the timing of cementation of coarse versus fine grained layers. The paragenetic sequences shown in figure 37 are simplifications, which are mainly confined to the diagenetic evolution in the coarser grained layers.

5.4.7 Halite

Traces of halite have been observed in few samples of well Flensburg Z1 by EMP. Euhedral NaCl-crystals form loose aggregates in open pores (plate 4H). They are not post-dated by any other cement. Sandstone powders analysed by XRD do not show a detectable halite reflection, confirming that halite is a very minor phase in the rocks investigated.

I n t e r p r e t a t i o n

It is not clear whether halite formed during (late) burial diagenesis, or during drilling. Halite precipitation during burial diagenesis is common in the vicinity of salt domes, which cause high salinity in the brines of adjacent permeable rocks (Putnis and Mauthe, 2001). Halite may also precipitate from the formation water due to pressure or temperature decline during drilling, or from saturated drilling muds (compare Mauthe, 2001).

5.4.8 Clay minerals

Although illite and/or chlorite may be present in Rotliegend sandstones of the northern basin margin, clay minerals are not as abundant as in many other reservoir sandstones (compare Worden and Morad, 2003a). Minor illite can be found in sandstones of diagenesis type H-SB. Chlorite is partly abundant in D-C type sandstone diagenesis. Kaolinite is lacking in the Rotliegend, but may be present in Carboniferous rocks.

Kaolinite/dickite

Kaolinitic minerals have been observed in one sandstone sample at the top of the Lower Carboniferous (well Schleswig Z1). They are mainly found in secondary pore space and appear to almost quantitatively replace detrital feldspars. Directly overlying sandstones of the basal Rotliegend (~10 cm above) are free of kaolinitic minerals.

I n t e r p r e t a t i o n

The formation of kaolinite in this sandstone sample is probably related to subaerial weathering processes at the Upper Carboniferous to Lower Rotliegend unconformity. The present surface of the Lower Carboniferous in that locality was probably exposed for a long time prior to the onset of Rotliegend deposition, where climatic conditions may have been more humic to allow kaolinite formation. Formation of kaolinite by interaction of detrital aluminosilicate minerals with meteoric water is often observed below subaerial unconformities (Emery et al., 1990; Morad et al., 2000).

Illite

Illite occurs as tangential illite coatings in sandstones of diagenesis type H-SB. Thin illite rims (<1 µm) partly pre-date Fe-oxide formation (plate 4D). Thick illite layers on top of Fe-oxides coatings can be observed in well Fehmarn Z1 (plate 2A, 2B, 5E). In most cases, however, tangential illite is closely associated with hematite and forms red rims of few µm thickness around detrital grains (e.g. plate 2E, 4B, 5F). These coatings consist of dominantly lath-shaped illite crystals of 50-150 nm length, hexagonal hematite (≤200 nm) and minor anatase crystals of about 40 nm length (Hasner, 2004).

Well Fehmarn Z1 and Schleswig Z1 comprise locally dense meshworks of grain replacing or pore-filling illite. In well Fehmarn Z1, illite forms compact, pore-lining fringes, or replaces detrital grains (plate 4D). In well Schleswig Z1, altered relics of grains or their outlines are still visible in most places where authigenic illite occurs (plate 4E, 4F). Feldspars, volcanic grains, and (meta-) sedimentary grains can be identified locally. Pore-bridging platy or fibrous illites is only present in few samples. They are restricted to single pores, while adjacent open pores are free of clay minerals. These illites appear to be late in the diagenetic sequence and are not post-dated by other cements. The maximal illite content recorded by point-counting is 0.3 vol.-% for well Schleswig Z1 and 2 vol.-% for well Fehmarn Z1. The chemical composition of illite has been measured by EMP on polished thin sections of one sample per well (table A13, appendix). The loose fabric of illites in well Schleswig Z1 impeded accurate analyses and caused low subtotals of wt.-%. The illite analyses of well Fehmarn may be contaminated by minor hematite. The measured K contents are relatively high (1.5-1.7 apfu). Illites of well Fehmarn Z1 are slightly more Mg-rich and Al-poor compared to illites of well Schleswig Z1. The molar Si/Al ratios vary around 1.7 (well Fehmarn Z1), and 1.4 (well Schleswig Z1).

I n t e r p r e t a t i o n

The occurrence of grain-coating illite and their red staining by hematite is typical for continental red beds (e.g. Walker, 1976). They probably transformed from primary smectite or mixed-layer smectite/illite coatings, which are characteristic of sandstones deposited in arid

or semi-arid environments (McKinley et al., 2003; Worden and Morad, 2003b). Several mechanisms are discussed in the literature for the origin of these clay coatings. They may be inherited and form prior to the deposition of the grains (Wilson, 1992). On the other hand, grain-rimming clays have been interpreted to result from alteration of unstable lithic grains during early diagenesis (Glennie et al., 1978; Goodchild and Whitaker, 1986; Dixon et al., 1989). They can also form by adhesion of clay at wet or damp surfaces (Wilson, 1992; Gaupp, 1996), by infiltration of clay from suspensions (Walker, 1976; Walker et al., 1978; Matlack et al., 1989), or by pedogenic processes (e.g. Scheffer and Schachtschabel, 2002). Textural criteria for distinguishing different processes were reviewed by e.g. Matlack et al. (1989) and Wilson (1992). The origin of clay rims is related to depositional facies. Clay infiltration is a very likely process in ephemeral fluvial environments of semi-arid continental basins. Wilson (1992) pointed out that grain-rimming clays in eolian sandstones are inherited and initially formed in sebkha and interdune environments by infiltration of clay-charged water or by adhesion to wet surfaces. The clay rims in the Rotliegend sandstones of the northern basin margin are at least partly inherited, since they may be present at point contacts between grains and they are often thicker in grain embayments than along convex grain surfaces. However, continuous rim thickness without evidence of abrasion – not even at subangular grains – and absence of clay at point contacts in numerous samples clearly points to eodiagenetic formation.

Although the sandstones were buried to 4200-5200 m depth, meshwork illite is not pervasive but only locally present. Most of these illites are morphologically and chemically similar to type C (compact illite fringes) and D (illitic lithoclasts) of Deutrich (1993). They probably replaced detrital clay matrix in well Fehmarn Z1. They also precipitated in places where feldspars, volcanics, or mica-/clay-rich grains have been dissolved. In general, the distribution of illite is patchy, even in samples with porosities up to 9 vol.-%. There is no example where meshwork illite is present in dominant parts of the intergranular pore space of a sandstone. Since evidence for late dissolution of pore-filling cements is lacking, the patchy distribution of meshwork illite has to be primary. Local meshwork illite growth probably took place during mesodiagenesis in a relatively stabilised grain framework.

Chlorite

Authigenic chlorite is present only in sandstones of diagenesis type D-C, where it mostly accounts for less than 1.5% of the rock volume (point-counting data, table A7, appendix). Only three samples contain between 1.5 and 3.0 vol.-% chlorite. Early tangential chlorite coatings may encase grain surfaces (plate 4A, 5C). These coatings are colourless to pale green in linear polarised light and commonly less than 3 µm thick. Tangential chlorites record a grain framework that was dominated by point and long contacts. The second and more dominant type of chlorite formed in a slightly more compacted grain framework. Radial, pore-lining chlorite platelets, 5-10 µm in size, have been growing perpendicular to grain surfaces into open pore space. The crystallites are arranged in a boxwork or honeycomb texture and often show ragged edges (plate 5A, 5D). In some cases, chlorites are intergrown and form smooth, curved crystal faces (plate 5B). Optical properties are similar to the tangential type. Radial chlorite formed after a phase of quartz precipitation, and is also post-dated by authigenic quartz. The petrographic relationship to dolomite is ambiguous: Zoned dolomite partly pre-dates chlorite growth, but partly overgrows radial chlorite (plate 2B). Locally, platy green chlorite replaces detrital biotite, lithic grains, or rarely feldspar.

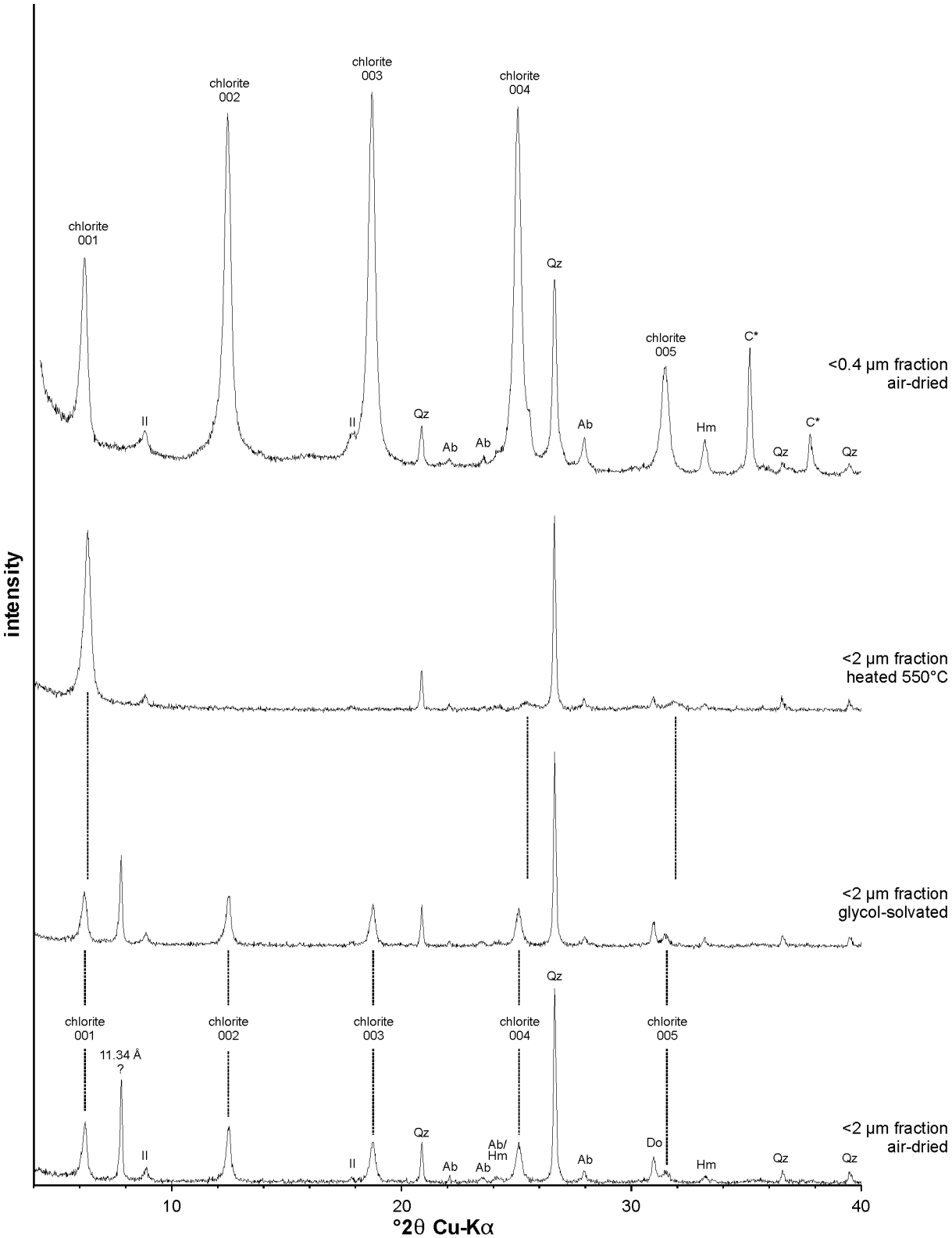

Figure 31: XRD patterns of chlorite fractions <2µm (air dried, glycolated, heated) and <0.4µm (air dried). Well Flensburg Z1, sample Fb057. The intensities were standardised relative to the intensity of the quartz reflection at 3.34 Å (26.67°2?). Odd- and even-order reflections of chlorite are sharp and narrow. The coarser fraction is strongly contaminated by quartz (qz), albite (Ab), illite (Il), dolomite (Do), hematite (Hm), and a 11.34 Å phase, probably a tobermorite-like phase. The reflections of the ceramic plate (C) are visible in the smallest clay fraction, since the amount of clay <0.4µm is very small.*

Available sandstone samples large enough to separate clay minerals contain 0.3-1.7 vol.-% chlorite only. Owing to the low percentage of chlorite, the <2 µm clay fractions are heavily contaminated by quartz, illite, albite, dolomite, and hematite (figure 31). Illite may be of detrital origin or may derive from drilling mud, since no authigenic illite could be observed by optical/SEM methods. Four air-dried samples (only <2 µm fractions) show a sharp reflection at 11.33-11.39 Å, which appears to be unaffected by glycolation, but disappears on heating. This could represent a tobermorite-like phase (compare McConnell, 1954), or alternatively a zeolite like erionite and offretite (see section 5.4.9). The XRD traces of oriented clay fractions show sharp and narrow even-order as well as odd-order chlorite reflections (figure 31). The relative intensities of the basal reflections indicate overall Fe-poor composition (compare Brindley and Brown, 1980; Moore and Reynolds, 1997). There is no systematic change with increasing burial depth. The basal spacing of the air-dried <2 µm specimens, calculated from the 004 reflection by using quartz as internal standard, falls within the range 14.15-14.19 Å. Glycol-solvated samples produce no detectable change of peak positions. Heating to 550°C (1 hour) results in a strong enhancement of the 001 reflection and a slight contraction to 13.90-13.99 Å as expected for chlorite (see Moore and Reynolds, 1997). The 002 and 003 reflections disappear on heating, the intensity of the 004 reflection is strongly reduced. The lack of a 3.57 Å reflection confirms the absence of kaolinite. The peak width at half height of the 001 reflection is 0.21-0.26°2? for the air-dried samples, indicating that the proportion of 7 Å layers must be clearly below the detection limit of ~5% (compare Hillier and Velde, 1992).

It was difficult to carry out EMP analyses on these chlorites due to their small size and the loose fabric of the crystals. Direct measurements were successful only on one thin-section. Additional analyses were performed on clay fractions <0.4 µm equivalent grain diameter, using a defocused beam (25-30 µm). The samples contain dominantly chlorite, but they are still contaminated by quartz and minor illite, albite, and hematite (figure 31). Mean values and standard deviations of the EMP analyses, and calculated chlorite formulas are given in table A12 (appendix). Chlorite formulas for clay fractions were calculated twice, firstly assuming 20% quartz contamination only, and secondly assuming contamination by 20% quartz, 5% illite, and 3% albite and hematite each. The calculated Fe/(Fe+Mg) ratios of the radial chlorites are ~0.1 on average, considering small hematite contaminations in the clay fractions (figure 32, 33). Grain replacing chlorites may have slightly higher Fe/(Fe-Mg) ratios. Following the AIPEA Nomenclature Committee (Bailey et al., 1980), the chlorites may be called clinochlores.

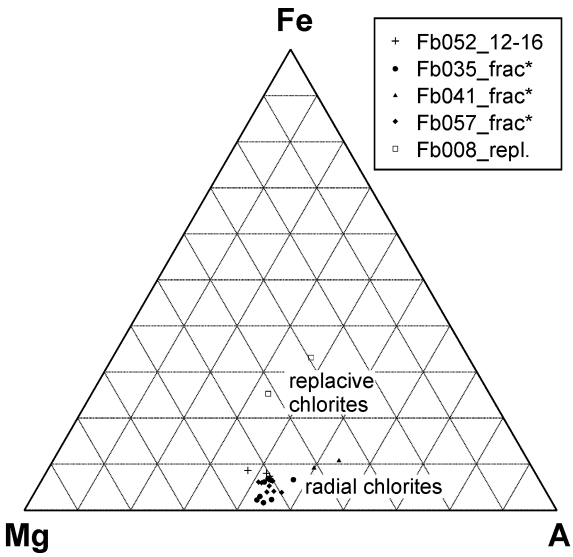

Figure 32: Chemical composition (mol.-%) of authigenic chlorites from the northern basin margin in the total Al-Mg-Fe diagram. Each point represents one single analysis. Samples marked by an asterisk (*) are clay fractions <0.4 µm equivalent grain diameter, which were analysed by defocused beam (25-30 µm). The scatter of the data of radial chlorites is due to inhomogeneous contaminations. Apart from grain replacing chlorites, all chlorites of the northern basin margin are Mg-rich. Their Al-contents are similar to those of other diagenetic chlorites (e.g. Humphreys et al., 1989; Hillier and Velde, 1991; Ryan and Hillier, 2002).

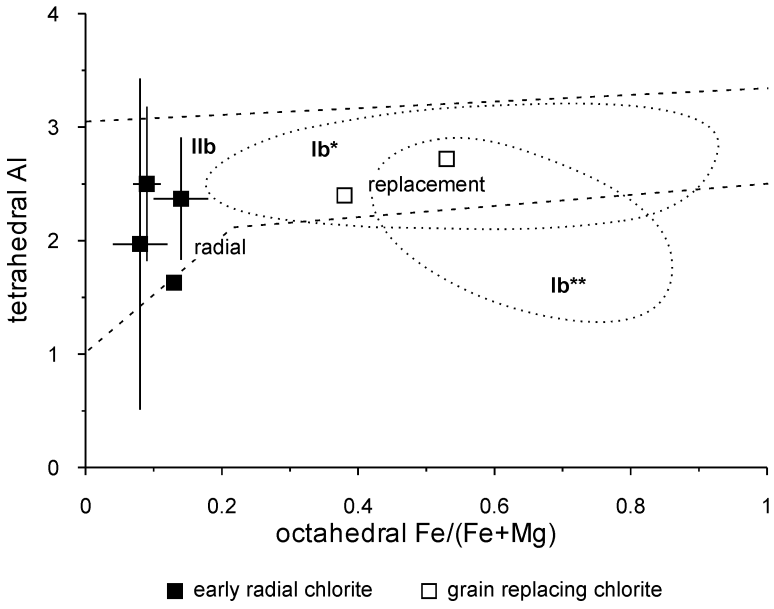

*Figure 33: Plot of tetrahedral Al versus Fe/(Fe+Mg) ratio of authigenic chlorites from the northern basin margin. Mean and standard deviation of each data point (each sample) were calculated from EMP analyses (see table A12; assuming contamination of 20% quartz , 5% illite, 3% albite, and 3% hematite contamination for clay fractions). Large standard deviations in tetraheral Al in three samples is due to contaminations in the clay fractions (see text for further explanation). Open squares are two single analyses of grain-replacing chlorites. Y-axis are formula units based on 28 oxygen equivalents. Compositional fields of typical diagenetic Ib** and metamorphic IIb chlorites taken from Curtis et al. (1985); field Ib* according to Brown and Bailey (1962).*

I n t e r p r e t a t i o n

The subtotals of wt.-% for chlorite analyses are low (here 83-88 wt.-%) owing to volatile OH-components (~10-13 wt.-%, see Deer et al., 1992), and analytical problems with EMP analyses of authigenic chlorites. These problems have been discussed in detail previously (Curtis et al., 1984; Humphreys et al., 1989; Hillier and Velde, 1991). They include the small size of the crystals (smaller than beam diameter/penetration depth), void spaces between individual crystals, and possible smectite or 7 Å mineral layers within the chlorite structure. Published chlorite analyses are often in the range of only 55 to 80 wt.-% oxide totals (e.g. Hillier, 1994; Humphreys et al., 1994). Direct EMP analysis on thin-sections may be contaminated, if the beam penetrated potential grain coatings (e.g. hematite, anatase) or the host grain. Although iron in most chlorites is dominantly ferrous (Curtis et al., 1985; Deer et al., 1992), the assumption that all iron is Fe^{2+} is an oversimplification (compare Hillier and Velde, 1991). However, the effect is insignificant here due to low total Fe contents. Despite all these problems, the calculated structural formulas are commonly believed to be fairly reliable (Humphreys et al., 1989; Hillier and Velde, 1991; Hillier, 1994). Another specific problem here is the contamination of the clay fractions. Assuming contaminations as stated above results in reasonable structural chlorite formula, although the error may be significant, especially for the Si content and Al distribution. However, the assumption of higher contaminations than about 5% illite, 3% albite, and 3% hematite would result in negative values for K, Na, and Fe in some analyses.

Chlorites do not form directly during eodiagenesis (Worden and Morad, 2003b). The most common mechanisms for formation of authigenic chlorite are (1) transformation of precursor kaolinite (Boles and Franks, 1979), (2) transformation of precursor smectite/swelling chlorite, e.g. corrensite (Curtis et al., 1985; Humphreys et al., 1994; Ryan and Hillier, 2002), (3) alteration of detrital or early diagenetic berthierine, or similar 7 Å minerals (Small et al., 1992; Hillier, 1994; Ryan and Reynolds, 1996; Aagaard et al., 2000), (4) reaction of HC with kaolinite or other clay minerals and hematite (Surdam et al., 1993), (5) reaction of kaolinite or illite with dolomite during burial (Hutcheon et al., 1980), or (6) direct precipitation from the

pore fluid (Hayes, 1970; Humphreys et al., 1989). Many diagenetic chlorites are Fe-rich, especially those formed by processes mentioned in (3) and (4). Fe-rich varieties of pore-lining chlorites are often interstratified with 7 Å layers and commonly occur in sandstones deposited at the transition between marine and non-marine environments (Hillier and Velde, 1992; Hillier, 1994; Grigsby, 2001). Mg-rich varieties are typically not interstratified with 7 Å layers and tend to be found in eolian and evaporitic environments (Hillier, 1994). However, diagenetic chlorites with Fe/(Fe+Mg)-ratios less than 0.3 are only very rarely reported in the literature (e.g. Hillier and Velde, 1991; Ramseyer et al., 2004).

In the samples investigated, radial chlorite is found only in places where it faces open pore space, but there is often a transition to tangential coatings along grain contacts. The curved, smooth crystal faces of some samples and the honeycomb fabric resemble the morphology of swelling chlorites (Tompkins, 1981; Humphreys et al., 1989; Small et al., 1992; Hillier, 1994; Humphreys et al., 1994), although their presence is not evident from XRD patterns. Hence, radial and tangential chlorite may have developed from the same precursor clay, e.g. from a Mg-rich smectite via the intermediate corrensite, as suggested by Hillier (1994). The low Fe content may indicate a high oxygen partial pressure during chlorite formation (oxidising conditions). Such conditions would favour precipitation of ferric iron and would not leave much Fe^{2+} available in the pore water. The slightly higher Fe/(Fe+Mg) ratio of grain replacing chlorite may be explained by incorporation of Fe directly from the detrital component (e.g. biotite).

5.4.9 Minor authigenic minerals

Mn-oxides/hydroxides

Veins intersecting Rotliegend volcanics and sandstones of well Fehmarn Z1 contain Mn-bearing calcite and a second Mn-rich phase (sample Fe011, Fe020). The latter is opaque in transmitted light. BSE images show that this phase is zoned and partly replaced by calcite (plate 4G). Volcanic grains along the vein are extensively replaced by these minerals and Mn-bearing calcite. One EMP analysis of a relatively homogeneous area yields about 62 wt.-% Mn, 2.7 wt.-% Si and <1 wt.-% Ca, Fe, and Al. However, at least two zones were encountered by the EMP beam. The composition is close to that of various Mn-oxides/hydroxides (amoung others, pyrolusite, braunite, manganite). The zoning indicates changes in mineral chemistry during crystal growth. Precipitation of Mn-oxides/hydroxides suggests oxidising conditions (compare Hartmann, 1963).

Ca-Al-Si-hydrate phases (?)

XRD patterns of some chlorite fractions (2-0.4 µm equivalent grain diameter) show the presence of a 11.3-11.4 Å phase (figure 31), which could be a tobermorite-like phase, or alternatively a zeolite like eroinite or offretite. Such zeolites may form at surface under arid to semiarid conditions, e.g. in alkaline lake environments, but they are commonly transformed into other zeolites and finally albite during burial (Hay and Sheppard, 2001; Utada, 2001). Authigenic Ca-Al-Si-hydrate phases like tobermorite were observed to form by interaction of alkaline solutions with clay minerals (Claret et al., 2002). 11 Å tobermorite is stable at temperatures between about 100-300°C (e.g. Miyake et al., 2000; Merlino et al., 2001) and

has often fibrous to honeycomb textures, similar to chlorite. This may have be the reason why a tobermorite-like mineral could not be identified by microscopic investigations of the sandstones from well Flensburg Z1. Further SEM-EDX investigations would help to characterise the chemical composition of this phase.

REE-phases

Euhedral, compact crystals rich in REE were detected in the pore space of one sample of well Flensburg Z1 (Fb 041). The crystals are smaller than 8 µm and could only be detected by SEM on broken rock chips. Qualitative EDX analyses indicate high Ce contents, moderate amounts of V, Ca, Si, P, and Al, and traces of K, Mg and Cl. However, high background signals must be expected (especially Si, Al, Mg, K from silicate minerals) owing to the small size of the minerals and the lack of optimal surfaces for EDX measurements. Ce-rich REE-phases have been described from diagenetic and hydrothermal environments (Williams-Jones and Wood, 1992; Gieré, 1996; Hartmann, 1997), but they commonly do not contain V. More detailed investigations would be necessary for an accurate characterisation of these minerals. Possible intraformational sources for REE are detrital REE-bearing components (e.g. apatite, titanite, zircon, feldspar, volcanics), shale horizons, and clay-hematite grain coatings (further discussion see Hartmann, 1997).

Apatite

Euhedral apatite crystals are occasionally present within or around altered volcanic grains. Their sharp crystal edges suggest authigenic origin.

5.5 Porosity, permeability and intergranular volume

The "wet-packed original porosity" of the sandstones investigated was probably about 33-38 vol.-% (section 5.2). Porosity has been reduced during burial by mechanical and chemical compaction, and cementation. Porosities derived from point-counting of thin-sections range from 0 to 1.3 vol.-% (well Fehmarn Z1), and 0 to 10 vol.-% (well Schleswig Z1 and Flensburg Z1). Measured core porosities of well Fehmarn Z1 show similar values, those of well Schleswig Z1 are higher on average (mostly 3-11 vol.-%, maximal 17 vol.-%; von der Gönna et al., 2003, Nover 2005, pers. comm., unpublished BEB report). Microfractures and microporosity, especially pores within the hematite and clay coatings, which cannot be resolved with standard microscopic methods, may account for this discrepancy. Most of the porosity is intergranular. Partial dissolution of feldspar, especially from volcanic rock fragments, may locally account for 1 vol.-% of intragranular porosity. The sandstones of well Fehmarn Z1 are essentially tight. The permeabilities of sandstones of well Schleswig Z1 show mostly values between 0.01 and 2 mD, with maximal values ranging up to 17 mD (unpublished BEB report). No permeability data are available for well Flensburg Z1.

The intergranular volume (IGV), which is composed of intergranular pore volume and volume of intergranular cements, reflects the compactional status and history of a sandstone. The IGV of Rotliegend sandstones from the northern basin margin ranges from 9 to 28 vol.-% (figure 34; table A7, appendix). Different degrees of sorting and mechanical compaction are responsible for this wide range of IGV. Low values are dominant in poorly sorted sandstones

and in samples with high portions of mechanically unstable rock fragments. IGV close to initial porosities were only detected in the sample of well Westerland 1, which was cemented by eodiagenetic sulphates and carbonates (40 vol.-%, SB-type cementation). All other samples show significant compaction prior to the growth of framework supporting cements. Long and concavo-convex contacts are abundant, suggesting that grain-grain-contact dissolution ("pressure solution") has taken place, especially in quartz-rich samples with low IGV. Volumes of intergranular cement account for 8 to 26 vol.-%. Different diagenesis types show in general similar IGV-porosity-cement relations (figure 34).

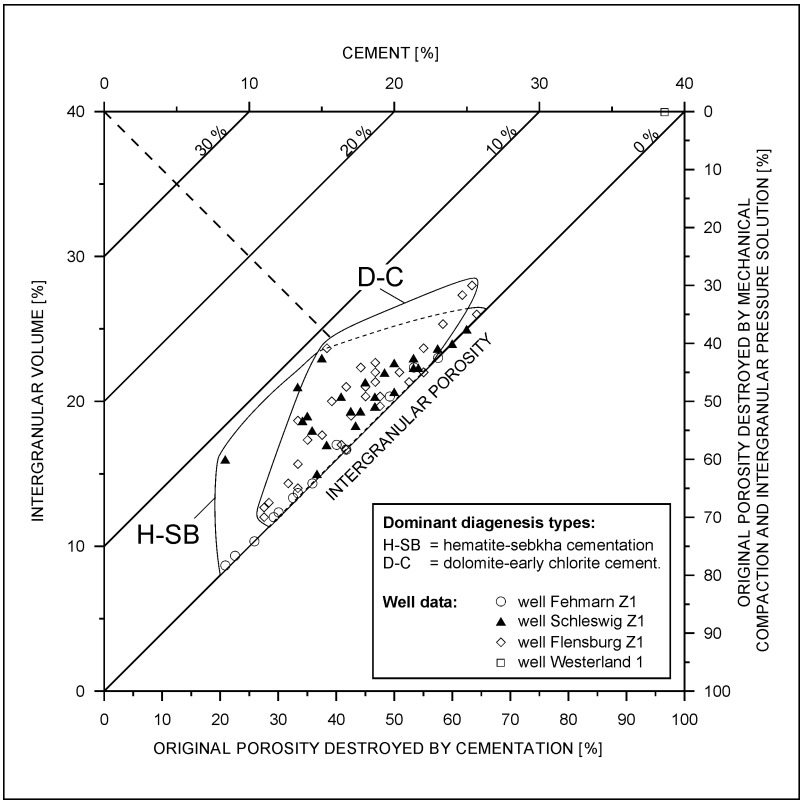

Figure 34: Intergranular volume versus volume of intergranular cements for sandstones from the northern margin of the NGB in the diagram according to Houseknecht (1987). Fields indicate characteristic IGV-cement-porosity relations for the dominant diagenesis types of the samples investigated.

There are some indications that minor dissolution of grains and cements have taken place during three periods of diagenesis (compare figure 37A): (1) Intragranular pore space of volcanic clasts is partially cemented by early carbonate. Feldspars within these grains may have been corroded already during weathering, or shortly after deposition. Detrital quartz and feldspar grains occasionally hold corrosion edges, which could have been produced by corrosive early cements (plate 2A, 3C). Partial dissolution of eodiagenetic cements would be coincident with their sporadic present-day distribution. (2) Minor leaching of zoned dolomites during early mesodiagenesis is only locally important (plate 2B, plate 7). (3) Partially dissolved feldspar grains that remain undeformed argue for a third phase of dissolution after stabilisation of the grain framework by pore-filling cements (plate 4B). However, apart from minor feldspar dissolution – which is partly associated with albitisation – there is no evidence for a mesodiagenetic generation of enhanced secondary porosity.

5.6 Bulk rock geochemistry

The bulk rock chemical composition of sandstones from the northern basin margin is given in table A14 (appendix). Samples of well Flensburg Z1 are relatively rich in Si (79-88 wt.-% SiO_2) and poor in Al (2-6 wt.-% Al_2O_3), compared to samples from well Fehmarn Z1 and Schleswig Z1 (62-82 wt.-% SiO_2; 4-10 wt.-% Al_2O_3). This compositional difference corresponds to the high percentage of detrital quartz and low percentage of volcanic material and feldspar in well Flensburg Z1 (section 5.3). The K contents of sandstones from that well are very low (<0.5 wt.-% K_2O) and confirm the petrographic observation that K-feldspars and illite are lacking almost completely (figure 35A). The typical range of K_2O in sandstones from well Schleswig Z1 and Fehmarn Z1 is 0.5-1.7 wt.-%. Only volcaniclastic sandstones contain up to 4 wt.-% K_2O.

Iron contents from 0.8 to 2.6 wt.-% Fe_2O_3 were measured in red and grey-red sandstones of well Flensburg Z1 (figure 35B). Higher iron contents are typical for red sandstones of the other two wells (1.7-5.8 wt.-% Fe_2O_3). They also show higher average contents of heavy metals (table A14). There is a positive correlation between iron content and both the intensity of hematite coatings and the percentage of volcanic material in the sandstones (figure 35C, 35D). All iron has been calculated as Fe_2O_3, since the only Fe^{2+}-bearing minerals observed are rare detrital magnetite, bitotite, and chlorite. The resultant error is probably small considering the low percentage of such minerals and the petrographic evidence for strongly oxidising conditions during deposition of the Rotliegend. Analyses of other red beds have also shown that the FeO content of red beds is commonly very low (Schluger and Roberson, 1975).

Bulk rock geochemistry also reflects the distribution of pore-filling carbonate and sulphate cements: calcite-cemented sandstones are relatively high in CaO (1.8-9.7 wt.-%) and low in MgO (0.3-3.0 wt.-%), dolomite-cemented sandstones are relatively low in CaO (1.8-3.6 wt.-%) and high in MgO (1.2-5.6 wt.-%). Samples containing abundant barite show exceptionally high BaO contents (up to 12 wt.-%) compared to most other sandstones (<<1 wt.-% BaO).

I n t e r p r e t a t i o n

The bulk rock geochemistry of sandstones is controlled by the detrital composition of the rocks and chemical alterations during diagenesis. The abundance of pore-filling cements, but also the occurrence of rare diagenetic phases like Mn-oxides/hydroxides, coincide with relatively high contents of the involved elements compared to sandstones in which such cements are absent. Significant variations of Ca, Mg, Ba, and Mn in sandstones with very similar detrital composition suggest that these elements were highly mobile during diagenesis.

The percentage of hematite determined by point-counting corresponds well to the measured iron content of the sandstones (figure 35C). However, the iron content is clearly related to the detrital composition, and point-counting values tend to overestimate hematite coatings (see section 5.4.1). Ferromagnesian components of volcanic rocks or their oxidised relics, Fe-oxide clasts, Fe-rich heavy minerals, and biotite or chlorite are the most important detrital Fe-bearing phases. Considering their abundance in the rocks investigated (table A7), and assuming an average Fe_2O_3 content of 3-5 wt.-% for the volcanic material (compare Benek

et al., 1996), authigenic hematite coatings can be estimated to account for about 0.5 to 2.0 wt.-% Fe_2O_3 on average.

Relatively high K_2O contents in well Schleswig Z1 and Fehmarn Z1 are mainly related to the abundance of K-rich volcanic material. Feldspars of well Flensburg Z1 show often textures of albitisation, but clear indications for the original feldspar chemistry are lacking. All samples investigated by EMP yield almost pure albite (table A8). If primary K-feldspars were present, they dissolved during diagenesis, and K may have been exported from the sandstone, since no diagenetic K-phase is present. Other case studies suggest that K released through albitisation of K-feldspar may be consumed by e.g. illitisation of smectites in interbedded mudstones (Aagaard et al., 1990).

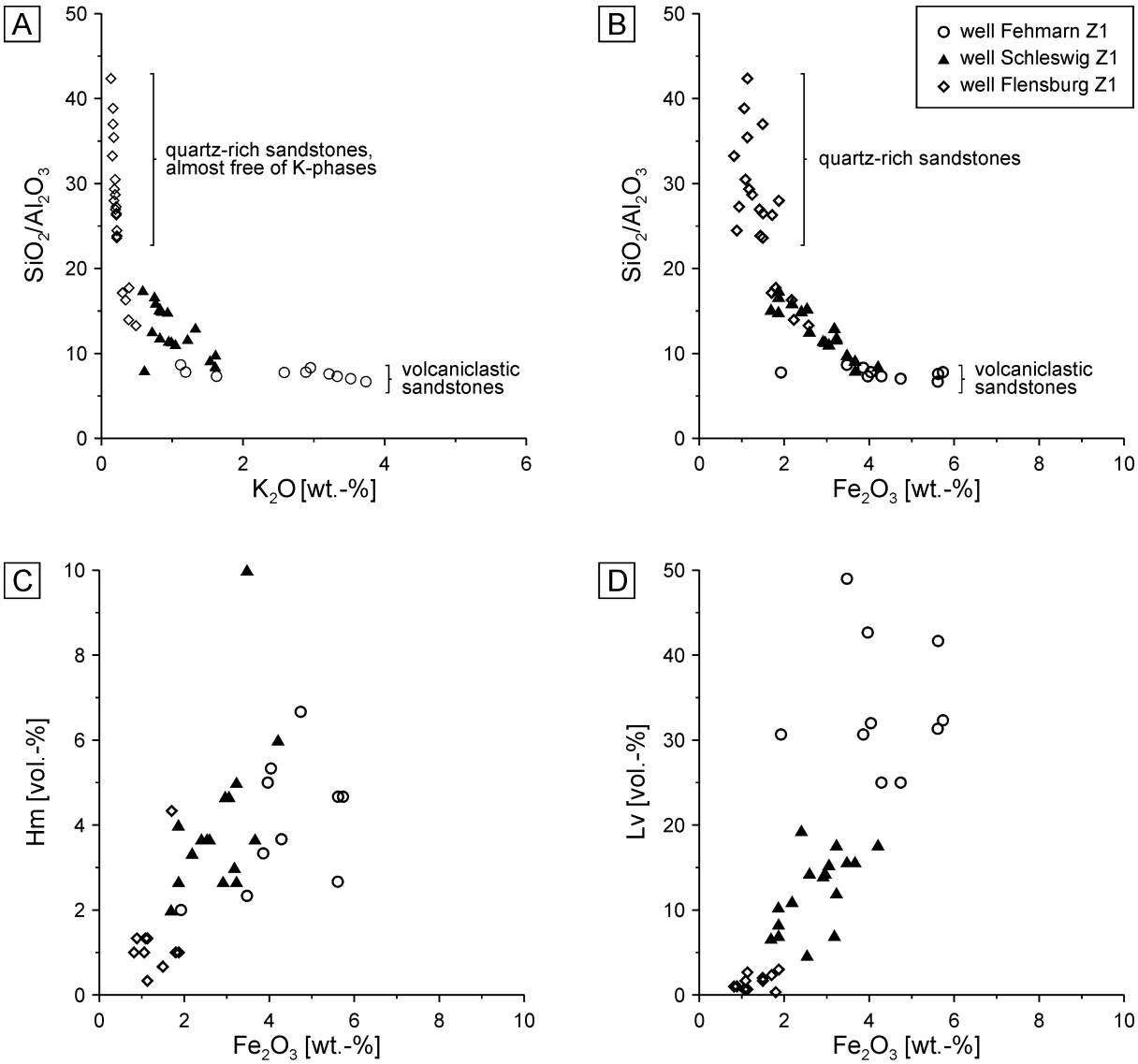

Figure 35: Chemical composition of sandstones from the northern basin margin (bulk rock XRF analyses, units in wt.-%). A) and B) SiO_2/Al_2O_3 ratio versus K_2O, and versus Fe_2O_3. C) and D) Bulk rock Fe_2O_3 (determined by XRF) versus percentage of hematite (Hm), and versus percentage of volcanic material (Lv) determined by point counting. Samples with thick hematite coatings show relatively high iron contents. Sandstones rich in volcanic detritus are also relatively rich in iron.

5.7 Organic inventory

No traces of solid bitumen (in the following often briefly "bitumen") have been detected in Rotliegend sandstones from the northern NGB by optical or fluorescence microscopy. Neither grain surfaces nor authigenic clay minerals show any visible bitumen impregnation. Furthermore, random thin-section samples from potential reservoir sandstones from the Triassic (well Fehmarn Z1), Carboniferous and Devonian (well Schleswig Z1), which were investigated for comparison, do not contain any bitumen, either.

DEGAS analysis can provide further information on the organic inventory of the rocks. The methyl fragment (m/z 15) is a good marker for HC release in the temperature range below 800-1000°C (Heide et al., 2000; Schmidt and Heide, 2001; Schmidt, 2004). Volatilisation of low-molecular organic material is commonly assumed to dominate at temperatures up to 300-400°C, while the temperature range of pyrolysis reactions is approximately 300-1000°C (Schmidt, 2004). Residual carbon is not released under normal conditions of pyrolysis, but is oxidised at temperatures above 1000°C in the vacuum. It probably reacts with residual water or oxygen from iron oxides, mainly to CO (Schmidt and Heide, 2001). High temperature release of the mass fragment m/z 28 can therefore be used here as indicator for the content of residual carbon in the rocks (compare Schmidt, 2004). The decomposition of water-bearing components is best identified using the mass fragment m/z 18 (water).

Table 4: Measured mass numbers, corresponding fragmentations, and potential origin (modified from Schmidt, 2004).

mass number (m/z)	fragmentations	potential origin
2	H_2^+, D^+	sheet silicates, hydroxides, organic matter
12	C^+	carbonates, organic matter
13	CH^+, $^{13}C^+$	organic matter, carbonates
14	N^+, CO^{++}, CH_2^+	organic matter, carbonates, gas inclusions
15	CH_3^+, NH^+, $^{15}N^+$	organic matter
16	O^+, CH_4^+, NH_2^+	sheet silicates, hydroxides, organic matter, oxides
18	H_2O^+	sheet silicates, hydroxides, organic matter, hydrates
28	N_2^+, $C_2H_4^+$, CO^+	carbonates, organic matter
32	O_2^+, $^{32}S^+$	hydroxides, oxides, sulphides, sulphates
44	CO_2^+, $C_3H_8^+$, N_2O^+	carbonates, organic matter
48	SO^+	sulphates, sulphides
64	S_2O^+	sulphates
78	$C_6H_6^+$	organic matter (aromatic compounds)
91	$C_7H_7^+$	organic matter (aromatic compounds)
191	unspecific	organic matter (e.g. hopane, unspecific)

Examples of degassing profiles of Rotliegend sandstones from the northern basin margin are shown in figure 36 (complete profiles see plate 12-14, appendix). The diagrams are in the same scale as in figure 46 (section 6.7) to be comparable to the results from the southern basin margin. The degassing profiles are dominated by release of water in the temperature range 300-700°C (see intensity of m/z 18). For m/z 18, the samples of well Schleswig Z1 and Fehmarn Z1 show two maxima between 470°C and 530°C. The maximum for the sample of well Flensburg Z1 (Fb050) is at 500°C, with a small shoulder at about 620°C. The signal of m/z 2 of all three samples largely corresponds to that of water, but it is much less intense (probably deuterium). Although there is no strong maximum of a methyl fragment (m/z 15) throughout entire temperature range, minor amounts of CH_3^+ were detected at temperatures between 60 and 300°C (Sw015), and around 500°C (Sw015, Fe030). Traces of m/z 15 at temperatures up to 500°C were also noticed in one sample of well Flensburg Z1 (not shown here). Traces of aromatic compounds (m/z 78, 91) were released at temperatures between 60°C and 600°C from some samples. The intensity of these signals is about one order of magnitude lower than that of m/z 15 (note the scale of the y-axis in figure 36). There is no major release of CO in samples from the northern margin of the NGB. The signals of the mass fragment m/z 28 are similar to that of the blank sample (figure 36). The spikes at temperatures above 1250°C are probably related to degassing from bubbles during partial melting (compare Schmidt, 2004). First investigations of samples containing carbonates had resulted in very strong release of CO_2 (m/z 44) in the temperature range 400-700°C. After carbonates had been dissolved, clear maxima below 700°C are lacking. The increase of m/z 44 at high temperatures (> 700°C) in some samples is difficult to interpret due to the relatively high background. Other components released at high temperatures (> 1000°C) are molecular oxygen, and locally sulphur species (m/z 32, 48, 64; see plate 12-14, appendix).

I n t e r p r e t a t i o n

After dissolution of carbonates, the main volatile component in the sandstones investigated is water from sheet silicates. Major water release at about 500°C in samples from well Fehmarn and Schleswig Z1 can be related to dehydration of illite (± mica), which is present in detrital rock fragments, as clay matrix, or as authigenic illite (mainly illite coatings). The temperatures are slightly lower than the average temperatures found by Schmidt (2004) for illite in shales (about 600°C). Different crystal size or chemical composition may be responsible for different reaction temperatures. The release of water at 500°C in sample Fb050 can be interpreted as the result of chlorite dehydration; illite is almost absent in the rocks of well Flensburg Z1.

The absence of solid bitumen in Rotliegend sandstones of the northern basin margin is confirmed by the lack of CO maxima during heating up to temperatures of 1400°C. The high-temperature area is dominated by the release of oxygen and sulphur of inorganic origin: Reduction of iron oxides is most likely responsible for the peaks in the degassing profiles of m/z 32 above 1000°C (plate 12-14, appendix). If sulphate cements are present (Sw015), m/z 32 may also represent a sulphur fragment (table 4). Decomposition of sulphates is indicated by maxima of m/z 48 and 64 (SO^+ and SO_2^+) at about 1100°C. However, traces of methyl fragments, and partly of aromatic organic compounds were analysed at relatively low temperatures (60 to 600°C), although their intensity is very low. Such traces were not only found in samples of well Schleswig Z1, where minor source rocks are present in the subsurface, but also in well Flensburg Z1, where Rotliegend sandstones rest on top of metapelites, and where no organic-rich rocks are available according to present data. Therefore, it

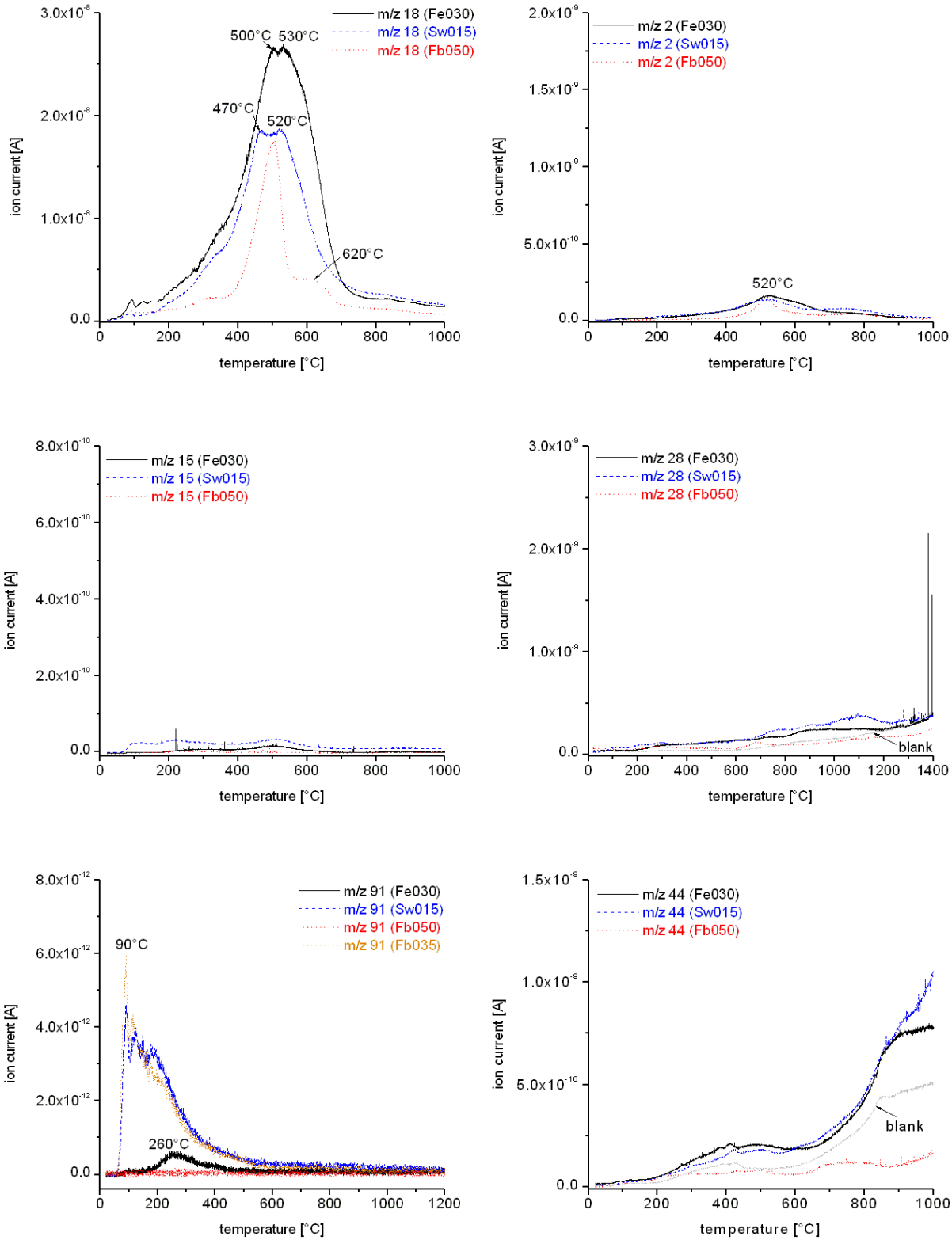

Figure 36: Degassing profiles of Rotliegend sandstones from the northern margin of the NGB. Release of m/z 18 (water), m/z 2 (here probably deuterium), m/z 15 (methyl fragment), m/z 44 (carbon dioxide), and m/z 91 (aromatic fragment) until 1000°C; m/z 28 (carbon monoxide or molecular nitrogen) until 1400°C. Note the different scale of the Y-axis. The samples are free of solid bitumen according to microscopic investigations. Sample Fe030 (well Fehmarn Z1) and Sw015 (well Schleswig Z1) contain clay-/mica-bearing detrital grains and eodiagenetic illite coatings, sample (Fe030) additionally abundant matrix clay. Sample Fb050 contains authigenic Mg-rich chlorite and chlorite-/mica-bearing detrital grains.

is more likely that these minor traces of organic compounds are contaminations caused during drilling or later sample treatment (see also section 6.7).

5.8 Summary and diagenetic sequence

Between 0 and 700 m of alluvial sandstones and conglomerates, and very subordinate eolian sandstones, were deposited at the northern margin of the NGB on top Caledonian basement, Lower Carboniferous sediments, or Early Rotliegend volcanics. The coarse grained clastics at the base of the Upper Rotliegend are probably part of the Havel Subgroup, and were deposited from alluvial systems draining the northern hinterland (Ringkøbin-Fyn/ Fenno-scandian High). Most rocks investigated are fine to medium grained sublitharenites and litharenites. Porosities <10 vol.-% and IGV in the range of 9-28 vol.-% reflect considerable mechanical compaction and mostly strong cementation of the sandstones. The relative succession of diagenetic minerals is summarised in figure 37A. Only cement generations that can be distinguished clearly by petrographic methods are shown. Eodiagenetic carbonate, sulphate, quartz and albite cements, preserving very high IGV, are only locally present. The occurrence of detrital grains of sulphate (+quartz) cement indicates recurrent sediment deposition, precipitation of cements, reworking and re-deposition. Early coating of grain surfaces by hematite and clay minerals is widespread in sandstones of the northern basin margin. The pore volume was cemented by minor late eodiagenetic to early mesodiagenetic quartz or albite, followed by carbonates and sulphates. Compaction often reduced IGV to around 20% prior to precipitation of framework supporting cements. Chlorite formed prior or simultaneously to early mesodiagenetic cements, but probably had earlier precursors. Locally, different generations of carbonate and quartz cements can be distinguished by the growth of radial chlorite. Dolomite and chlorite formed in fluvial channel sandstones that were probably deposited from braided rivers. Hematite-illite coatings, calcite and anhydrite cements are abundant in ephemeral stream, gravity-flow, and minor eolian deposits, and in sandstones of the sandflat environment. Petrographic observations, isotopic data and variations in IGV suggest that (early) mesodiagenetic cementation occurred in several phases, and over a distinct period of burial. Local precipitation of hematite on dolomites that formed during burial suggest that surface waters occasionally penetrated to considerable depths. Local feldspar alteration/dissolution and illite growth in mechanically stabilised grain framework were probably the latest diagenetic processes in these rocks. Altered feldspars may also comprise late authigenic albite and calcite. Major dissolution of grains or cements during burial is not obvious from the sandstones investigated.

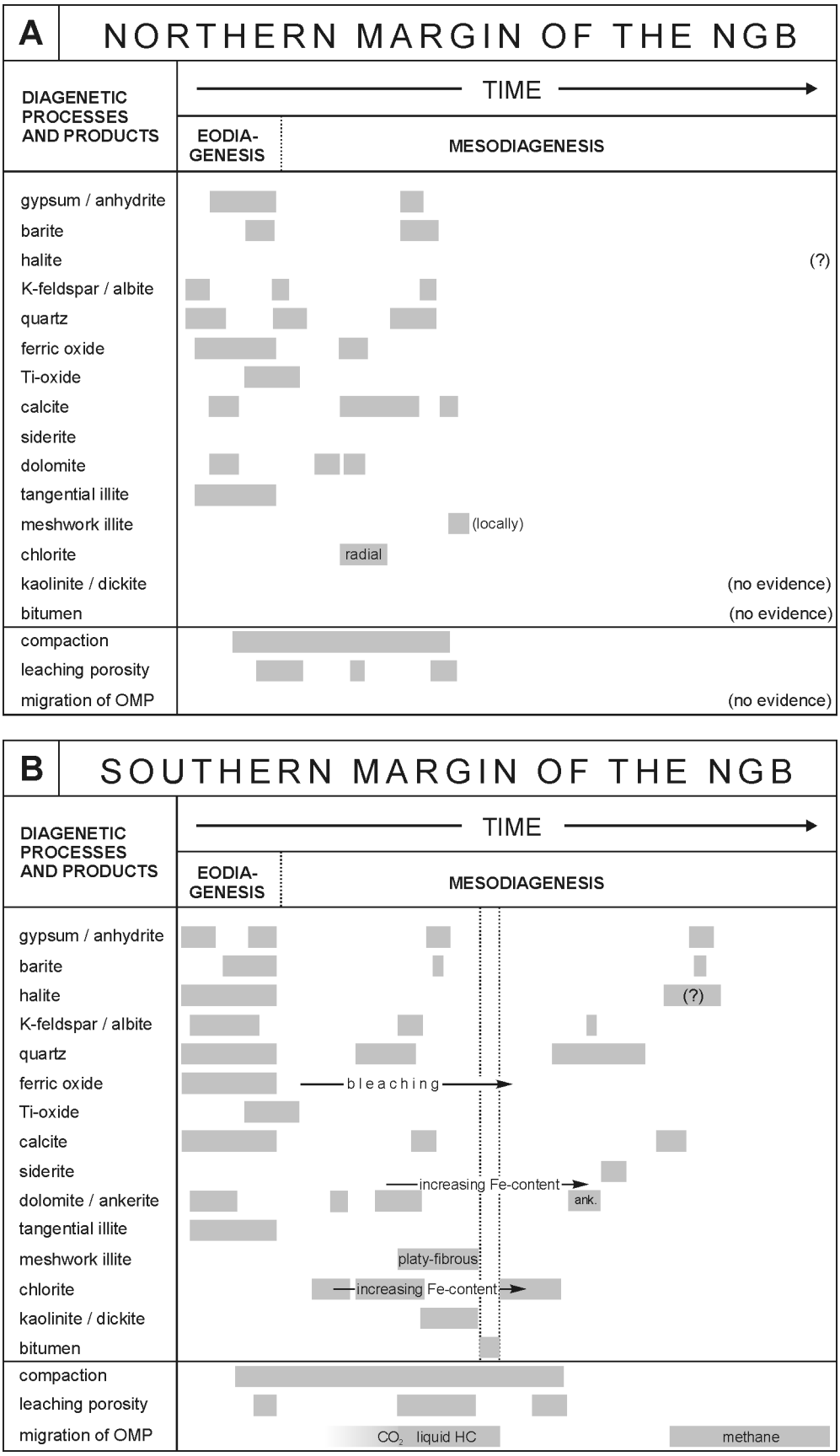

Figure 37: Schematic diagenetic sequence for Rotliegend red bed sandstones from the NGB. The diagrams for the northern (A) and southern (B) basin margin are summarized from 3 wells and from 67 wells, respectively. Note that these are composite diagrams and not all diagenetic events are present at one locality. The bars indicating the duration of cementation are simplified and represent the most prominent cement generations. Important mesodiagenetic processes, which are abundant at the southern basin margin (B), are absent in the case studies from the northern NGB (A).

6 Rotliegend sedimentology, petrography and geochemistry: southern margin of the NGB

Rotliegend diagenesis has been a focus of research over many years in the main gas fairway of northern Germany (Hancock, 1978; Drong, 1979; Budzinski and Judersleben, 1980; Platt, 1991; Deutrich, 1993; Gaupp et al., 1993; Platt, 1993; Cord, 1994; Platt, 1994; Gaupp, 1996; Hartmann, 1997; Gaupp et al., 2005) and in the southern North Sea (e.g. Glennie et al., 1978; Rossel, 1982; Seemann, 1982; Goodchild and Whitaker, 1986; Pye and Krinsley, 1986; Lee et al., 1989; Ziegler, 1993; Lanson et al., 1996; Glennie, 1997; Leveille et al., 1997). The following section provides a brief review of the petrography and geochemistry of Rotliegend sandstones from the southern part of the NGB, including introductory remarks on the sedimentology of the investigated horizons. This summary is mainly based on the more recent studies (since the 90'th) and own complementary investigations. Emphasis is placed on petrographic features, which are dissimilar from the northern basin margin, and which will be discussed in the context of organic-inorganic diagenesis later in this thesis (section 7).

6.1 Sedimentology and stratigraphy of the horizons investigated

The samples and the diagenetic data used for this study derive from all major sandstone horizons of the Upper Rotliegend at the southern margin of the NGB, i.e. from the Havel Subgroup ("Schneverdingen" sandstone), the Dethlingen Formation ("Hauptsandstein"), and the Hannover Formation (especially "Wustrow" sandstone). Sandstone samples were mainly taken from dry eolian, and to a minor degree from alluvial depositional environments (alluvial fan, fluvial channel, and sheetflood deposits). Detailed lithological descriptions of cored Rotliegend sediments are available from Platt (1991), Deutrich (1993), Cord (1994), and Gaupp and Solms (2005).

The sampled intervals of the Havel Subgroup consist dominantly of moderately to well sorted sandstones and sandy conglomerates. These rocks were deposited in alluvial fan and ephemeral stream environments within fault-bounded depressions (Drong et al., 1982; Gast, 1988), and were frequently affected by eolian reworking. Dry eolian dune and sandflat deposits are most widespread in the Dethlingen Formation. They are intercalated with damp eolian and sheetflood sediments. Conglomerates occur typically at the base of the succession. The abundance of mudflat deposits increases in the upper part of the Dethlingen Formation, and towards the basin centre. In the Hannover Formation, significant sandstone horizons accumulated during periods of shoreline stability along the margin of the central saline lake (Gast, 1991; Gaupp et al., 2000). They comprise mainly eolian sandstones with subordinate wave reworking. Fine grained mudflat and saline lake deposits dominate the Hannover Formation, however.

6.2 Rock texture

The textural features of Rotliegend sandstones from the southern basin margin are highly variable. Important factors controlling grain size, sorting and roundness are depositional facies, proximity to the basin margin, paleo-climate, and paleo-topography. Most petro-

graphic investigations were carried out on fine to medium grained, moderately to well sorted dry eolian sandstones. The distribution of mean grain sizes in different stratigraphic horizons is shown in figure 38. The most frequent grain size class decreases from 250-350 µm (2.0-1.5 F) in the Havel Subgroup to 180-250 µm (2.5-2.0 F) in the Dethlingen and Hannover Formations. Dry eolian rocks are usually better sorted than sandstones of damp depositional environments. Fluvial sandstones may have very similar texture than eolian sandstones, but they cover a greater range in grain size, and they are often moderately or poorly sorted. Sandstones of mudflat environments are mostly fine grained and poorly sorted, and may have clay matrix. In the North-Hannover area, there is an overall decrease in grain size from south to north (towards the basin centre), and also from older to younger stratigraphic intervals (Gaupp and Solms, 2005). The typical roundness of the grains varies from subangular to rounded, although some eolian and beach sands may be well rounded. Angular grain shapes are rare. Grains of eolian sands are commonly better rounded than grains deposited by fluvial processes. Deutrich (1993) pointed out that there is a positive relation between mean grain size and roundness. The type of grain contacts is highly variable and strongly related to depositional facies, detrital composition, and diagenesis. E.g., quartz rich, well sorted eolian sandstones are commonly less densely packed than poorly sorted fluvial sandstones with high portions of mechanically unstable rock fragments. Investigations of Cord (1994) indicate that grain fabrics range from point contacts to concavo-convex contacts on average, and that they are dominated by long contacts in many sandstones.

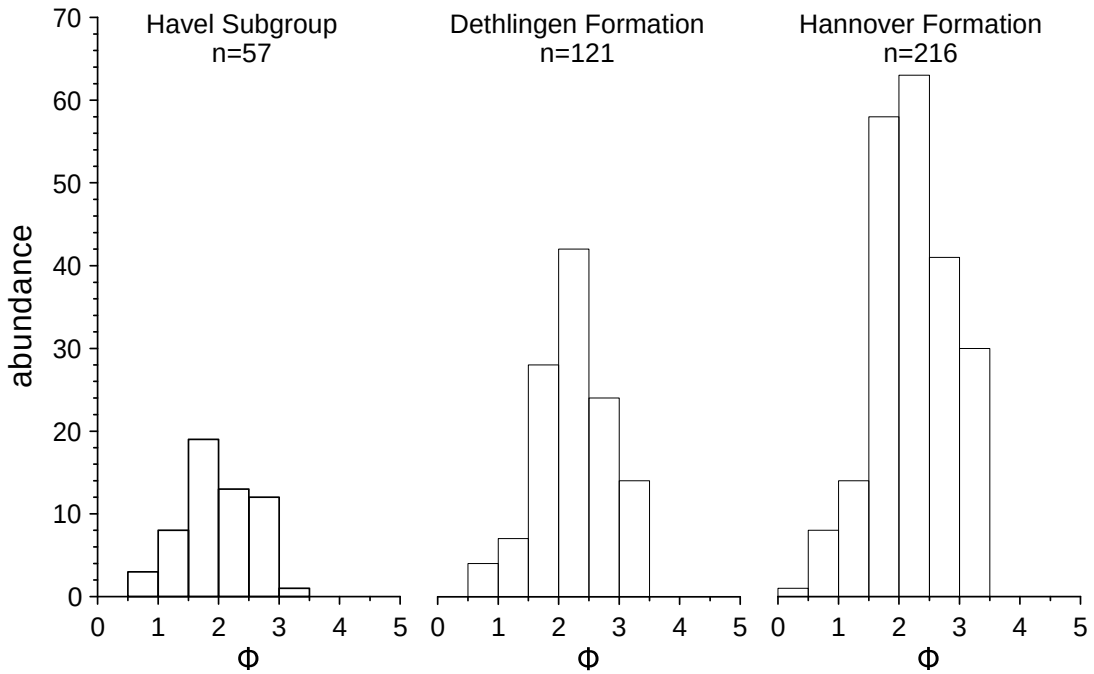

Figure 38: Distribution of mean grain sizes in Rotliegend sandstones of the southern basin margin, calculated from n wells. The most frequent grain size class decreases from 250-350 µm (2.0-1.5 F) in the Havel Subgroup to 180-250 µm (2.5-2.0 F) in the Dethlingen and Hannover Formations. Data from Platt (1991), Deutrich (1993), Cord (1994), and Gaupp and Solms (2005).

6.3 Detrital mineralogy

The detrital grains of the sandstones from the southern margin of the NGB are dominated by mono- and polycrystalline quartz (mostly 40-70 vol.-%), feldspar (0-18 vol.-%) and non-quartzitic lithic fragments (1-50 vol.-%). Monocrystalline quartz is often clear and may show undulatory extinction, or formation of subgrains. Detrital K-feldspar and albite are both common, while Ca-plagioclase is absent or extremely rare. Rock fragments comprise abundant polycrystalline quartz and volcanic grains of dominantly acidic-intermediate chemistry. Basic volcanics, grains of plutonic origin, clastic sediments, cherts, carbonates, and quartz-rich metamorphic fragments are much less frequent. Volcanic clasts may be very abundant (<50 vol.-%) in some alluvial or interstratified eolian deposits. Mud flakes and carbonate-cemented sand- or siltstones are probably intraformational (Gaupp et al., 1993). Accessory components, mostly <1 vol.-%, include white mica, biotite, which may be altered to Fe-rich chlorite, rare detrital chlorite, and heavy minerals (zircon, opaques > tourmaline, apatite). Matrix clay is only abundant in some samples of mudflat and alluvial fan deposits, but may be present in traces within sandstones.

Figure 39 shows the present detrital sandstone composition in the Q-F-L diagram (McBride, 1963). The sandstones can be classified as (lithic) subarkoses, sublitharenites, and partly as (feldspathic) litharenites and quartzarenites. Samples from different stratigraphic horizons all show a similar range in detrital composition (figure 39A). Eolian sandstones are overlapping with other facies types in the Q-F-L diagram (figure 39B). The overall composition of dry eolian Rotliegend sandstones at the southern basin margin is approximately $Q_{72}F_9L_{19}$. Lithic rock fragments are more frequent in alluvial sandstones ($Q_{67}F_{10}L_{23}$ on average). Sandstones deposited on mudflat or lake shoreline environments ($Q_{79}F_{10}L_{12}$ on average) contain more quartzitic material and less rock fragments than sandstones deposited in alluvial fans. It is not the objective of this study to investigate compositional trends in the Rotliegend. Such trends will be obscured in a composite diagram like figure 39, where samples from different positions within the basin, of different grain size, and of different stratigraphic age or depositional environment were plotted together. The dominance of samples from eolian in comparison to other depositional environments is also problematic. However, previous work has shown that the Hannover Formation contains more quarzitic material than older stratigraphic horizons. This trend may be related to the mean grain size decrease (see above), to increased reworking of the material, or to climatic reasons (Platt, 1991).

Diagenetic processes are also an important control on detrital sandstone composition, especially the dissolution and alteration of feldspars. Detrital feldspars and feldspar-bearing volcanics may have been replaced by diagenetic illite, carbonate, quartz, albite, and locally by kaolinite, or they may have been partially or completely dissolved. The process of plagioclase/K-feldspar dissolution and in-situ albite precipitation is called albitisation and results in a net volume reduction (e.g. Saigal et al., 1988; Aagaard et al., 1990; Morad et al., 1990). Feldspar leaching and illite formation is particular abundant in many sandstones of the southern basin margin (section 6.5). The present percentage of detrital feldspar is negatively related to the intensity of feldspar dissolution (Platt, 1991; Deutrich, 1993), any may be several vol.-% lower than the original feldpar content. Locally, diagenetic dissolution removed almost all feldspars.

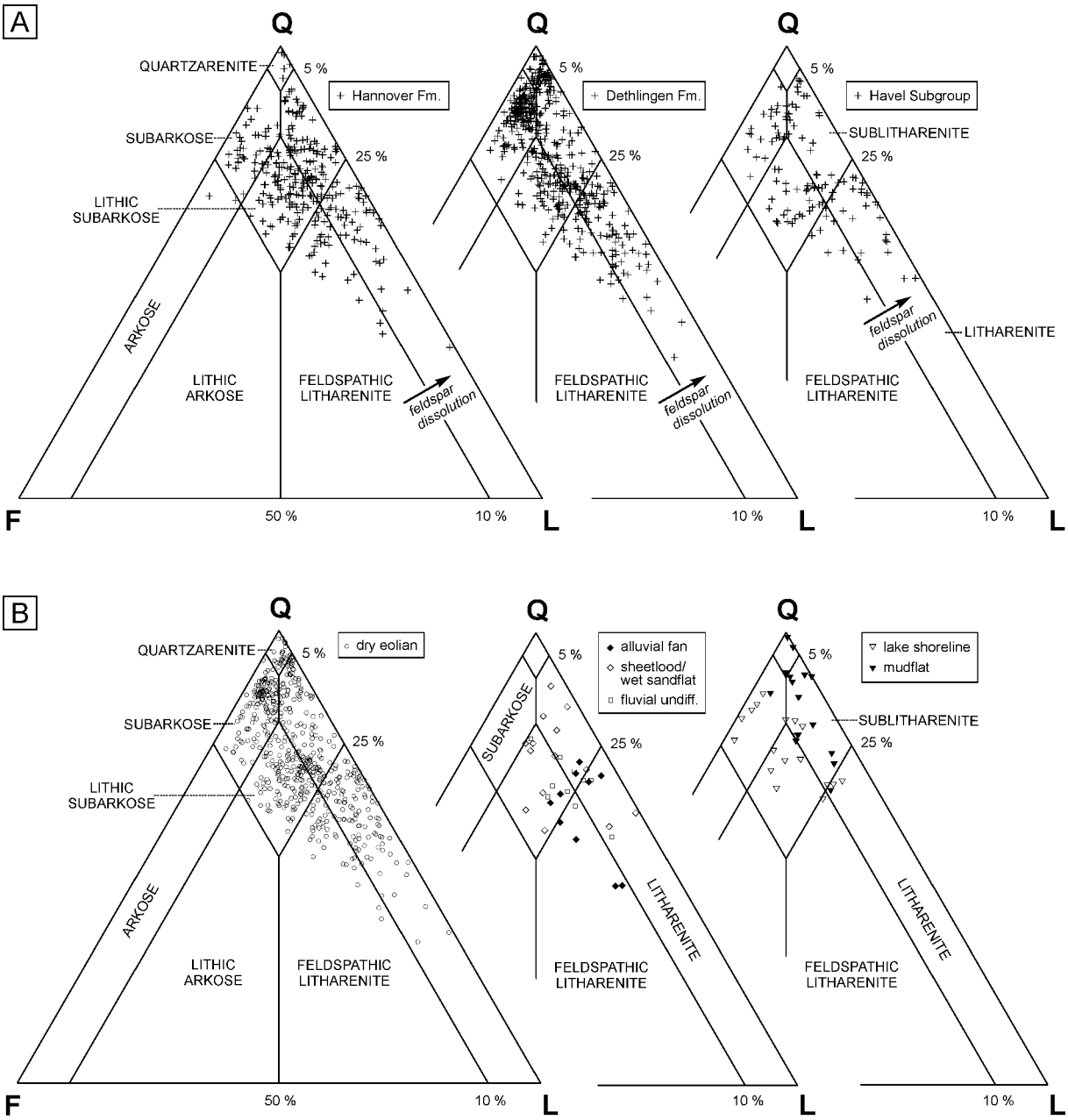

Figure 39: Detrital composition of Rotliegend sandstones from the southern basin margin in the diagram of McBride (1963). Q = mono- and polycrystalline quartz + chert, F = feldspar, L = unstable rock fragments including extrabasinal carbonate clasts. Feldspar dissolution often reduced the primary feldspar content. A) Sandstones of different stratigraphic horizons show a similar range in detrital composition. B) Influence of facies on detrital composition. Most samples are sandstones of dry eolian facies types, which overlap with the samples of other facies types. Sandstones in lake shoreline and mudflat environments are closer to the Q-pole of the diagram than alluvial fan sandstones. Data from Platt (1991), Deutrich (1993), Cord (1994) and Gaupp and Solms (2005).

P r o v e n a n c e

The detrital grains of the Rotliegend sandstones investigated represent typical recycled orogenic material (compare Dickinson, 1985). CL investigations of detrital quartz grains (Platt, 1991) and the types of rock fragments point to a mixed hinterland comprising a variety

of igneous, metamorphic, and minor sedimentary rocks. Volcanic rocks and eventually K-feldspar grains may derive from Lower Permian volcanics. These observations and the Upper Rotliegend paleogeography (figure 7) are consistent with a source area in the Variscan orogen to the south of the Rotliegend basin.

6.4 Authigenic mineralogy

The most abundant authigenic minerals in Rotliegend sandstones from the southern basin margin are quartz, various carbonates, sulphates, clay minerals, and hematite. The relative succession of diagenetic minerals is shown in figure 37B at the end of section 5. For definition of the terms eodiagenesis and mesodiagenesis compare section 5.4. Gaupp (1996) distinguished twelve diagenesis types, which cover the most important diagenetic alterations. A brief description of these types, slightly modified according to additional data, is given in table 5. However, the list is not exclusive and neglects e.g. minor mesodiagenetic quartz, calcite, anhydrite and Fe-chlorite cements. Sandstones cemented by only one "end-member" diagenesis type are rare, but combinations of several types are more common. Most typical are the association of H-IC, H-SB, and H-D during early diagenesis, and FL-K-A or FL-IM-B(-Q) during advanced mesodiagenesis. Note that the data presented here and summarised in figure 37B derive from numerous wells, and that not all of the diagenetic phases and reactions can be observed at one locality.

Table 5: Summary of the most abundant diagenesis types in Rotliegend sandstones of the southern basin margin. Modified from Gaupp (1996).

diagenesis type	**abbre-viation**	**description**
sebkha type	SB	extensive eodiagenetic cementation by pore-plugging sulphate, calcite, quartz, albite; originally defined to occur prior to H-type, but similar cement assemblages are also typical after hematite formation
illite coating type	IC	coating of grain surfaces by tangential eodiagenetic illite
hematite type	H	Gaupp et al. (1993) and Gaupp (1996) used this diagenesis type to describe sandstones containing grain coating aggregates of hematite and minor pore-filling cements only. However, H-type diagenesis often occurs together with other early diagenesis types.
dolomite type	D	precipitation of early diagenetic grain rimming or pore filling dolomite cement
radial chlorite type	C	early mesodiagenetic growth of radial Mg-rich chlorite on grain surfaces
feldspar leaching type	FL	mesodiagenetic feldspar dissolution, often associated with K- or IM-type diagenesis
kaolinite type	K	formation of kaolinite/dickite in sandstones in close proximity to Carboniferous Coal Measures, often together with Fe-rich chlorite and Fe-carbonate cement
illite meshwork type	IM	precipitation of mesodiagenetic platy and fibrous "meshwork" illite in inter- and intragranular pore space, often together with minor Fe-rich chlorite cement
ankerite/siderite type	A	precipitation of mesodiagenetic pore-plugging or vein-filling Fe-rich carbonates
bitumina type	B	impregnation of pore surfaces and clay minerals by solid bitumen
late quartz type	Q	occlusion of large pore spaces by late quartz cement (post bitumen)
late barite type	BA	growth of late lath-shaped barite, often together with anhydrite and calcite

6.4.1 Fe-oxides/hydroxides

Hematite may occur in matrix clay, as staining of detrital clasts, and as replacement of mafic components (mainly within volcanic clasts). More typical, ferric oxides are found directly on grains surfaces, mostly together with tangential illite coatings (H-type/H-IC-type diagenesis; plate 9A, 9D, 11H). Two generations of hematite coatings can be observed locally, separated by quartz overgrowths. Hematite-illite grain coatings are responsible for the "red bed" colour and are almost omnipresent within Rotliegend sandstones. The formation of these coatings is not related to a specific depositional environment, although the most intense hematite coatings were found in Rotliegend conglomerates (Deutrich, 1993). Red coloured coatings very rarely exceed 20% of the rock volume according to point counting, but they are mostly much less abundant (<<10%). The Fe content stored within these coatings is better characterised by chemical methods (section 6.6), since the quantification of these coatings in thin-section is problematic (see section 5.4.1).

Hematite precipitated early, but later than the first generation of SB-type cements (Gaupp, 1996). If the pore space was plugged by SB-type sulphate, carbonate and quartz cements, hematite may have been lacking primarily. However, hematite is absent from a number of reservoir horizons of the southern basin margin, which show no evidence for SB-type cementation (e.g. plate 10). Grey or locally almost white rock colours prevail in these sandstones. Grey horizons are typically some meters to some tens of meters thick. There may be a continuous transition from red to grey sandstones, corresponding to a decrease in hematite. Nevertheless, traces of hematite may still be present in grey sandstones, e.g. below authigenic quartz cements (plate 9B), or within small pores of detrital clasts.

I n t e r p r e t a t i o n

As described in section 5.4.1, Fe-oxide/hydroxide coatings formed during early near-surface diagenesis under semi-arid climatic conditions, owing to fluctuations of the water table. Early hydroxides transformed into hematite during burial. Although the grey colour of some sandstones may be due to primary inhibition of Fe-oxide/hydroxide precipitation, secondary removal of ferric iron is more likely in most cases. The relics of hematite coatings beneath early cements indicate that grey sandstones have been red originally, and that the grey colour was generated by iron reduction. The bleaching of red beds will be discussed in more detail in section 7.2.3.

6.4.2 Ti-Oxides

Authigenic Ti-oxides are found within or around altered volcanic grains or heavy minerals. Clustering of Ti-phases ("leucoxene") is common. Locally, individual euhedral Ti-oxides are also present in the pore space of sandstones. These crystals were often overgrown by pore-filling carbonate cements. The observation of Hartmann (1997), that Ti-oxide grew after fibrous illite, could not be verified here.

I n t e r p r e t a t i o n

The authigenesis of Ti-oxides was most likely related to the dissolution of Ti-bearing detrital components within the sandstones (e.g. mica, ilmenite, sphene, volcanics; compare Hart-

mann, 1997). A relatively early mesodiagenetic origin is proposed here on the basis of textural observations, similar to the northern basin margin (section 5.4.2).

6.4.3 Quartz

Early quartz cements mostly precipitated as syntaxial overgrowths on quartz grains. These overgrowths may pre- or post-date the formation hematite-illite grain coatings (plate 9B). Zoned eodiagenetic quartz with bright blue and green luminescence colours is particularly abundant in sandstones cemented by pore-filling anhydrite cements, or in the vicinity of anhydrite nodules (Gaupp et al., 1993).

Mesodiagenetic quartz cement is present in most parts of the southern study area and significantly reduces porosity in many samples. Two major phases can be recognised from textural evidence. The first, syn-compactional phase pre-dates major grain dissolution and fibrous illite authigenesis (plate 10E), and often forms syntaxial, pore-filling overgrowths. Blue luminescence colours prevail. Extensive late mesodiagenetic quartz cement post-dates grain/cement dissolution and meshwork illite growth and may locally occlude large inter- and intragranular pore spaces (Q-type diagenesis; plate 10E, 10F, 10G). This cement type may fill up to 20 vol.-% of the rock in single samples, and up to 9 vol.-% on average in discrete reservoir horizons. Late quartz is closely intergrown with fibrous illite and partly comprises bitumen staining and HC-inclusions (Gaupp, 1996; Gaupp et al., 1996). The luminescence colours are short-lived blue to bottle-green where quartz contains bitumen inclusions, and dull blue or brown in areas without bitumen impregnations (Gaupp et al., 1996). There is no recognisable relation of quartz cementation to the gas water contact (GWC).

95% of the samples investigated by point-counting contain up to 15 vol.-% of total quartz cement; samples with more than 20 vol.-% quartz are very rare. 13% of the sandstones are almost free of authigenic quartz (<1 vol.-%).

I n t e r p r e t a t i o n

The occurrence of several generations of quartz cements is typical for Rotliegend sandstone diagenesis. Some of the earliest quartz overgrowths may be inherited. Most early diagenetic quartz appears to be related to SB-type cements, which precipitated from continental pore waters, concentrated by evaporation, in a semi-arid to arid environment (compare Platt, 1994).

It has been suggested that the amount of quartz dissolved at grain-grain contact appears to be insufficient to account for the syn-compactional, (early) mesodiagenetic quartz generation (Platt, 1991). Silica may have been imported, e.g. by compactional waters from basin-central Rotliegend shales. However, a clear discrimination of early and late quartz cements is often difficult solely on petrographic observations, if meshwork illite is absent and no CL investigations are available. Possible internal sources for late (post-illite) quartz cement are feldspar dissolution and again quartz "pressure" solution. An additional external source of Si is claimed for this type of quartz cement, at least in sandstones with high IGV (Gaupp et al., 1993). According to fluid inclusion studies, mesodiagenetic quartz cements precipitated at elevated temperatures (T_h 130 to >160°C) from solutions with moderate to high salinities (Rieken, 1988; Gaupp et al., 1996). The base of the Rotliegend was heated up to temperatures of about 100-130°C prior to Late Jurassic-Early Cretaceous uplift. 150-170°C were

reached during Cenozoic burial (compare section 4.2). The observed quartz cements therefore represent either a very late phases, which formed mainly in Cenozoic times, or they precipitated earlier during relatively hot fluid events. Such hot fluids may have affected not the whole basin but only the most permeable layers. A discrepancy between formation temperatures from basin modelling and fluid inclusion data of cements, indicating hotter conditions, was observed in other cases studies too. Burley et al. (1989), e.g., reported evidence for multiple pulses of hot, compactional fluids into Jurassic sandstones of the North Sea.

6.4.4 Feldspar

Authigenic albite and locally K-feldspar form early syntaxial overgrowths on detrital feldspar grains. Albite, which can also be found as pore-filling cement, is more frequent than K-feldspar, but both minerals yield less than 1 vol.-% in about 80% of the samples. Only very few sandstones contain more than 4 vol.-% authigenic feldspar. Many detrital feldspars, however, have undergone significant albitisation (section 6.3). Diagenetic albite is non- or dull blue luminescent; the CL colour of K-feldspar overgrowths is palish blue (Platt, 1991).

I n t e r p r e t a t i o n

Formation of authigenic feldspar – K-feldspar as well as albite – is typical for early diagenesis of red bed sandstones (e.g. Baisert, 1975; Walker et al., 1978; Füchtbauer, 1979). Füchtbauer (1974) pointed out that albite precipitates preferentially in evaporitic or marine environments, while K-feldspar forms under meteoric freshwater conditions or in highly evaporitic environments, where halite precipitation led to elevated K/Na ratios. The predominance of albite versus K-feldspar in Rotliegend sandstones of northern Germany was recorded already by Hancock (1978). Possible causes for albitisation of K-feldspar and plagioclase during burial diagenesis have been discussed extensively in past (compare section 5.4.4).

6.4.5 Carbonates

Carbonates are volumetrically important cements in Rotliegend sandstones of the southern study area. Calcite, dolomite, ankerite and locally siderite can be observed in these rocks. The carbonates formed in several generations and exhibit complex textural relations to other diagenetic minerals. Their chemical and isotopic composition is shown in figure 40 and table 6.

Calcite

Calcite is one of the most abundant cement phase and may fill up to 17 vol.-% of the sandstones, in rare cases even more than 20 vol.-%. Apart from minor grain rimming crystals, early calcite forms commonly pore-filling cements, which precipitated directly on grain surfaces and partly replace detrital grains (SB-type diagenesis, plate 11A, 11B). Calcite post-dating hematite and tangential illite formation is also common. Zoning of the earliest calcite generation is evident from dull and bright yellow/orange CL colours, while most of the later calcites show relatively uniform yellow/orange luminescence (Platt, 1991; Hartmann,

1997). Early calcites are typically enriched in $MnCO_3$ (2-6 mol-%), but contain mostly less than 1 mol.-% $FeCO_3$ (figure 40; Platt, 1994).

At least one generation of late calcite post-dates meshwork illite formation and bitumen impregnation (plate 10E, 10H). In contrast to late quartz cement (see section 6.4.3), calcite is commonly not intergrown with fibrous illite. Late poikilotopic calcite crystals often grew in enlarged secondary pores. They have low $FeCO_3$ and $MgCO_3$ contents (mostly <0.5 mol.-%), and contain moderate amounts of $MnCO_3$ (0.5-2 mol.-%, figure 40; Gaupp et al., 1993). Compared to early calcite cements, late calcites show a tendency to more negative $d^{18}O$ values and a wider range in carbon isotopic composition (table 6).

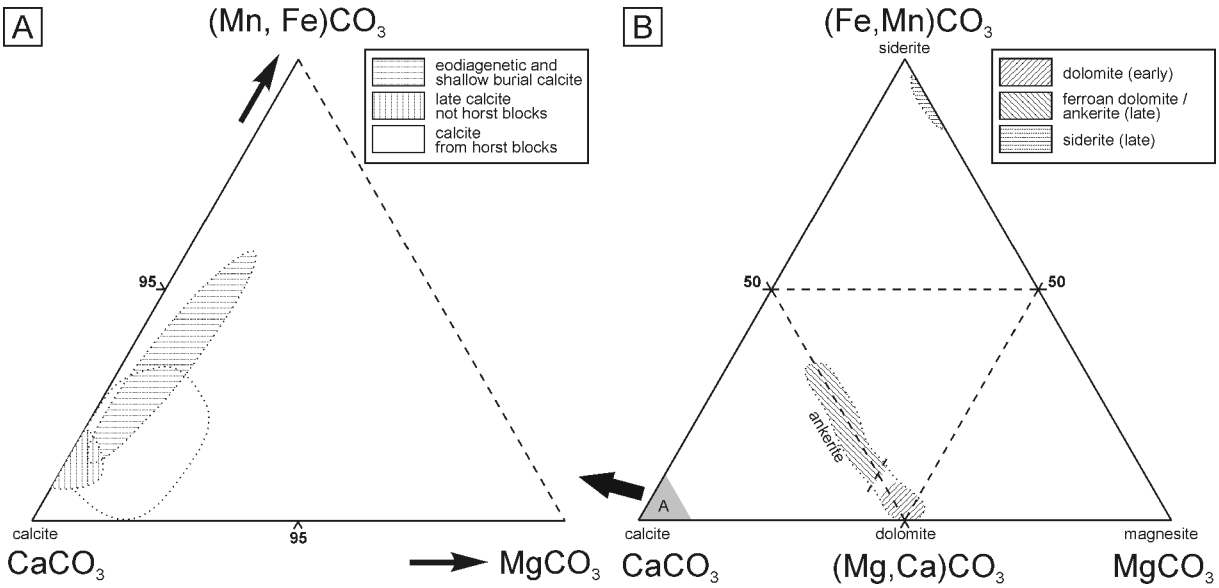

Figure 40: Chemical composition of authigenic carbonates from the southern basin margin (in mole percentages). Modified from Platt (1991) and Gaupp et. al (1993). A) Early and shallow burial calcites show moderate to high manganese and minor magnesium enrichment, but commonly contain <1 mol.-% $FeCO_3$. Late calcites have mostly low magnesium and moderate manganese contents. Calcite cements from horst blocks show often higher magnesium contents. B) Dolomites and Fe-poor ankerites may be enriched in manganese (<9 mol.-% $MnCO_3$). The iron content of ankerites ranges from 11 to 32 mol.-% $FeCO_3$. Measured siderite cements are Ca-poor, but contain 6-14 mol.-% $MgCO_3$ and 5-7 mol.-% $MnCO_3$.

Dolomite/ankerite

Authigenic dolomite is less widespread than calcite and only occurs in a limited number of wells, but may also fill up to 17 vol.-% of the rock (D-type diagenesis). Anhedral grain-rimming or poikilotopic dolomite crystals occur in sandy facies of ephemeral stream/wadi and alluvial terminal fan deposits (Gaupp, 1996). Rhombic crystals often grew within clay matrix or pelitic grains. Dolomite may be replaced by later calcite cements. Authigenic dolomites typically contain 2-4 mol.-% $MnCO_3$ (Platt, 1991).

Ferroan dolomite and ankerite grew on top of early dolomite cements, partly after a phase of dolomite dissolution. Fe-rich carbonates also occur as pore-filling rhombs or replace grains, and may be associated with siderite (A-type diagenesis). They formed after fibrous illite growth and often precipitated within dissolved grains. Ankerite is a common vein cement (Platt, 1991). Large zoned crystals show a typical trend from Mn-enriched dolomite cores to

increasingly Fe-rich carbonate towards the outer edge of the crystal (Platt, 1991; Gaupp et al., 1993). CL colours of dolomite are bright orange and partly dull red, while Fe-rich dolomites and ankerites are non-luminescent. Ankerites contain between 11 and 32 mol.-% $FeCO_3$ (figure 40). Fe-poor ankerites and ferroan dolomites are partly Mn-rich (<9 mol.-% $MnCO_3$; Platt, 1991). The $d^{18}O$ values of ankerites are on average more negative than those of dolomites, and ankerites show a wider range in carbon isotopic composition compared to dolomites (table 6).

Siderite

Siderite is only locally present and commonly fills veins, secondary pore space, or replaces grains. Platt (1991) observed a maximum of 6 vol.-% of siderite. This cement post-dates the main phase of grain dissolution and is typically associated with dickite and late Fe-rich chlorite (section 6.4.8). Siderite is low in calcium (<1.4 mol.-% $CaCO_3$), and contains 6-14 mol.-% $MgCO_3$, and 5-7 mol.-% $MnCO_3$ (figure 40; Platt, 1994). Carbon and oxygen isotope analyses from one locality give $d^{13}C$ values of about -2‰ PDB and $d^{18}O$ values of about -7‰ PDB (table 6).

Table 6: Carbon and oxygen isotopic composition of diagenetic carbonates from the southern basin margin. Summarised from Platt (1994).

cement type	**$d^{13}C$ [‰ PDB]**	**$d^{18}O$ [‰ PDB]**
early calcite cement	-5 to -3	-11 to -10
late calcite cement	-7 to -2	-13 to -11
early dolomite cement	-5 to -3	-8 to -3
late ankerite cement and mixtures with ankerite/dolomite ≥3	-6 to -2	-9 to -7
late siderite cement	about -2	about -7

Interpretation of carbonate cements

According to petrographic and isotopic evidence, the calcite generations pre-dating meshwork illite formation precipitated during eodiagenesis and shallow burial diagenesis from meteoric-type waters (Platt, 1994). Early carbonate cementation is typical in continental, evaporitic basins (e.g. Walker et al., 1978; Bjørlykke, 1983; Burley, 1984; Morad et al., 2000). These carbonates are typically non-ferroan due to oxidising groundwater conditions, and since ferric iron is not easily incorporated into the carbonate mineral structure (Metcalfe et al., 1994). They may have markedly high Mn-contents, however (Boles and Ramseyer, 1987). Evaporation of meteoric waters, which invade such basins during episodic flood events (Glennie, 1972), causes concentration of dissolved ions. Carbonates are commonly the first precipitates, and they have often been reported from basin margin fluvial deposits (Hardie, 1968; Strong and Milodowski, 1987; Garcia et al., 1998). In the Rotliegend basin, the abundance of early carbonates decreases from the basin margin towards the basin centre, where increasing evaporation resulted in sulphate and finally halite precipitation (Drong, 1979; Platt, 1994).

Later calcite generations and Fe-rich carbonate cements formed during deeper burial. They post-date the growth of fibrous illite, which has been dated to 180-200 Ma by the K-Ar system (e.g. Gaupp et al., 1993; Zwingmann et al., 1998). At that time, Rotliegend sandstones were buried to about 2000-3000 m in most areas (compare figure 21). Oxygen isotopic compositions of late carbonates point to a more negative $d^{18}O$ compared to early cements. Platt (1991; 1994) suggested that the later carbonate generations probably formed by dissolution and re-precipitation of earlier cements. Siderite (and ankerite) vein fillings indicate that the formation of Fe-rich carbonates is related to reducing fluids carrying ferrous iron. Such reducing fluids could have originated in underlying Carboniferous source rocks. However, the carbon isotopic composition of late carbonates is similar to that of early carbonate cements and does not allow univocal conclusions concerning the carbon origin (see also section 5.4.5). Influx of Zechstein fluids into Rotliegend sandstones may be possible in the vicinity to faults juxtaposing Rotliegend and Zechstein formations, as evident from isotopic analyses (Platt, 1994).

6.4.6 Sulphates

Authigenic sulphate cements include anhydrite as well as minor barite and gypsum. Anhydrite is a major pore-plugging cement that may fill up to 30% of the rock volume (plate 11A-D). Minor gypsum may be associated with anhydrite. Barite is much less abundant; it rarely exceeds 2 vol.-% of the sandstones. The earliest generation of sulphates is indicated by highest IGV (up to 40 %) and direct contact to grain surfaces (Budzinski and Judersleben, 1980; Gaupp, 1996). Nodular early anhydrite and replacement of grains by anhydrite or gypsum is common in sandstones of evaporitic sandflat and sandy mudflat environments (Platt, 1991; Gaupp, 1996). A second generation of sulphate precipitated after formation of hematite-illite grain coatings and minor compaction. They often form poikilotopic laths up to mm-size and enclose early quartz, albite and carbonate cements. Late anhydrite/barite cements fill pore spaces left after fibrous illite growth. They are among the latest diagenetic phases evident from Rotliegend sandstones of the southern basin margin (BA-type diagenesis, figure 37B). Semi-quantitative chemical analyses (SEM-EDX) of Platt (1991) indicate relatively pure $CaSO_4$ for anhydrites, and relatively high strontium contents for barites.

I n t e r p r e t a t i o n

Early sulphates are characteristic cements of the eodiagenetic SB-type diagenesis (Gaupp, 1996). Sandstones cemented by early anhydrite occur further to the basin centre than sandstones cemented by early carbonate (see above). There is abundant evidence for a comparable zoning of early diagenetic minerals from modern playa and sebkha systems, where both anhydrite and gypsum are widespread early precipitates (e.g. Hardie, 1968; Handford, 1982; Metcalfe et al., 1994). The fact that anhydrite is abundant but gypsum is absent or rare in most ancient continental evaporitic basins (e.g. Baisert, 1975; Glennie et al., 1978; Dixon et al., 1989; Purvis and Okkerman, 1996) is probably due to the dehydration of gypsum and conversion into anhydrite during burial. Remobilisation of eodiagenetic sulphates may be a source for later sulphate cements. Barium is released e.g. during feldspar dissolution. Infiltration of Zechstein brines has been hold responsible for late anhydrite/barite formation (Pye and Krinsley, 1986; Bath et al., 1987; Glennie and Provan, 1990). In the study area, however, Rotliegend sandstones and Zechstein evaporites are

separated by shales at the top of the Rotliegend. Isotopic analyses of Platt (1994) suggest very limited influence of Zechstein fluids in most parts of the German Rotliegend (southern basin margin), apart from localities in the vicinity of horst blocks, where a fluid mixing model implies up to 40% of Zechstein fluid.

6.4.7 Halite

Authigenic halite locally formed during early diagenesis, and preserves high IGV (Drong, 1979; Budzinski and Judersleben, 1980). Halite may rarely be a late authigenic phase with euhedral crystal shape (Platt, 1991; Gaupp et al., 1993).

I n t e r p r e t a t i o n

In the southern study area, the precipitation of eodiagenetic halite cements is related to lacustrine environments close to the centre of the Rotliegend basin (Drong, 1979; Gaupp et al., 1993). Similarly, early halite formation was recorded from basin central Rotliegend sandstones of eastern Germany (Baisert, 1990). It is possible that late halite precipitated during the drilling procedure (see section 5.4.7). Platt (1991) noted that halite was observed dominantly from samples which were cut and polished using petrol instead of water. Traces of halite may have been dissolved during sample preparation.

6.4.8 Clay minerals

Clay minerals are abundant in Rotliegend sandstones of the southern basin margin. Type and distribution of these minerals are decisive for the reservoir quality of the rocks. The most widespread authigenic clay is illite, which occurs in number of morphologies. Different types of chlorite with variable chemistry are also common. Kaolinite and dickite are only locally present.

Kaolinite/dickite

The sporadic occurrence of kaolinitic minerals was noted already by Hancock (1978), Drong (1979) and Budzinski and Judersleben (1980). Tabular and blocky plates of kaolinite and dickite have been observed in some shallow buried wells (<3.5 km) in the western part of the study area, partly not far from surface outcrops (Hancock, 1978; Platt, 1991). In these localities, kaolinite/dickite are most common around dissolved grains (Platt, 1993).

In deeply buried parts of the study area, kaolinitic minerals occur in narrow (<300 m) haloes around Carboniferous horst blocks (Gaupp et al., 1993; Gaupp, 1996). Drong (1979) showed that feldspar dissolution and formation of kaolinitic minerals is pervasive in the Carboniferous and in directly overlying Rotliegend sandstones, whereas the Rotliegend on top of volcanic rocks is not affected by these diagenetic processes. Dickite predominates in deeply buried sandstones according to XRD studies of Deutrich (1993) and Platt (1993). Coarse, blocky or vermicular dickite "booklets" may completely occlude the pore space, including secondary pores, and account for up to 20 vol.-% (Platt, 1993). Dickite is often associated with feldspar leaching, the formation of fibrous illite and Fe-dominated chlorites, and bitumen impregnation (see below). The distribution of kaolinitic minerals in deeply buried Rotliegend sandstones is not related to sedimentary facies (Deutrich, 1993).

I n t e r p r e t a t i o n

Kaolinitic minerals in diagenetic environments mostly form at the expense of feldspar or mica in pore waters with low pH (Bjørlykke et al., 1989). Kaolinite is dominant in low temperature environments, while both kaolinite and dickite are frequent in deep burial diagenetic settings (Lanson et al., 2002; Worden and Morad, 2003). Two mechanisms appear to be dominant for authigenic kaolinite precipitation: (1) Meteoric water flushing may be responsible for feldspar dissolution and kaolinite formation (Bjørlykke, 1984; Bjørlykke and Brendsdal, 1986; Wilkinson et al., 2004). (2) Fluids rich in organic acids or CO_2, derived from maturation of organic matter, can lead to a similar result (e.g. Curtis, 1983; Surdam et al., 1984; Meshri, 1986; Surdam et al., 1989). The first process is likely to dominate in eodiagenetic and shallow burial settings, where meteoric waters can flow through the sandstones. The second process occurs especially in deeper buried sandstones, which received acidic fluids expelled from organic-rich horizons. Flushing by meteoric fluids is very unlikely at depths greater than 2000 m (compare Giles and Marshall, 1986). Kaolinite precipitation during burial diagenesis has often been recorded from sandstones interbedded with coal or organic rich shales (e.g. Crossey and Larsen, 1992; van Keer et al., 1998; Cookenboo and Bustin, 1999). The transformation of kaolinite to dickite probably results from invasion by acidic fluids of organic origin (Clauer et al., 1999; Lanson et al., 2002).

In the Rotliegend of the southern study area, kaolinite formation in meteoric waters is possible only in few wells in shallow burial settings, especially if they are located close to Rotliegend outcrops. Platt (1991; 1993) argued that the oxygen isotopic composition of kaolinite from one of these wells does not support the meteoric water scenario. However, her isotope data may be not reliable due to contamination of the samples with 10-17% of quartz, feldspar, illite and carbonates. Furthermore, early kaolinite may be (partly) recrystallised and transformed into dickite during burial (compare Worden and Morad, 2003) and make interpretation of isotopic data difficult.

The formation of kaolinite/dickite in deeply buried Rotliegend sandstones is restricted to areas of close stratigraphic or tectonic proximity to Carboniferous Coal Measures (K-type diagenesis). Comparable authigenic dickite can be observed in Carboniferous sandstones (Sedat, 1992; Deutrich, 1993). It is obvious that feldspar dissolution and dickite formation were caused by the influx of acidic fluids expelled from adjacent coal-bearing Carboniferous rocks (Gaupp et al., 1993; Platt, 1993). Boles (1982) suggested that kaolinite can also form as a by-product of albitisation of plagioclases at temperatures above 100°C. However, there is no petrographic evidence from the sandstones investigated that albitisation is associated with kaolinite or dickite growth.

Illite

Illite is the dominant authigenic clay mineral in Rotliegend sandstones of the southern basin margin. Gaupp (1996) distinguished two main types of illite diagenesis: (1) tangential illite coatings covering grain surfaces formed early in the paragenetic sequence (IC-type diagenesis). (2) Illite meshworks are characterised by platy and hairy illite morphologies and precipitated during burial diagenesis (IM-type diagenesis).

Authigenic illite coatings range from sub-µm thin layers at the grain surface to µm-thick coatings encasing almost the entire grain (plate 9A, 9D). They are best developed in alluvial

fan and ephemeral stream deposits (Gaupp et al., 1993), but they are volumetrically only locally important. The red colour of many illite coatings is due to associated hematite.

The distribution of meshwork illite is not facies related, although strong illite formation is often found in sandstones with high paleo-permeability (Deutrich, 1993; Gaupp, 2005). Various morphologies of meshwork illite have been recorded and may be grouped chronologically (Deutrich, 1993; Liewig and Clauer, 2000). Most important are platy types and fibrous/hairy, partly pore bridging illites (plate 9C-G, 10A-C). The crystal size of authigenic illite is typically around 10 µm (max. 50 µm) perpendicular to the c-axis, and <1µm parallel to the c-axis (Deutrich, 1993). Illite commonly grew on grain surfaces, preferentially on pre-existing illite coatings. IM-type diagenesis is usually pervasive and affects the complete pore space connected to fluid flow (plate 10B, 11G). Dense illite meshworks may replace detrital clay matrix and fill the pore space affected by feldspar dissolution. Meshwork illite is particularly abundant around major fault zones and positively correlated to the degree of feldspar leaching (Platt, 1991; Deutrich, 1993; Gaupp et al., 1993). Illite is typically impregnated by solid bitumen (section 6.7). Quantification by point counting suggest that up to 20 vol.-% of the sandstones are composed of illite (mainly meshwork illite). However, the actual percentage of illite is probably lower (most likely <10 vol.-%), since there is significant porosity between the illite crystals, which is impossible to quantify under the microscope. Platt (1993) and Deutrich (1993) showed that diagenetic illites are commonly well crystallised and do not contain expandable components ("smectite") above the 5% detection limit of XRD analysis. Both authors observed that authigenic illites are typically K-rich (1.6-1.8 apfu) and show relatively low Fe and Mg contents (mostly ≤0.9 apfu in total). The molar Si/Al ratio ranges between 1.1 and 1.7, with most Al-rich illites occurring close to fault zones. The chemical composition of illite appears to be independent from burial depth and whole rock chemical composition. Based on K-Ar dating of illite separates, Zwingmann et al. (1999) suggested that distinct episodes of hydrothermal activity between 210 and 165 Ma were responsible for illitisation in Rotliegend reservoirs. Most K-Ar data of illite samples from various burial depths across southern basin margin record ages between 200 and 180 Ma (Gaupp et al., 1993; Platt, 1993; Zwingmann et al., 1998, 1999; Liewig and Clauer, 2000).

I n t e r p r e t a t i o n

Grain-rimming illites of the southern study area are probably both inherited and eodiagenetic in origin, similarly as discussed for the northern basin margin (section 5.4.8).

Deutrich (1993) summarised possible mechanisms of authigenic illite formation during burial diagenesis. These include the transformation of smectite or kaolinite to illite, the alteration or replacement of detrial feldspars, volcanic grains, and detrital micas, and the precipitation of illite directly from fluids. Illitisation of early diagenetic kaolinite is a process observed in many reservoir sandstones (e.g. Bjørlykke and Aagaard, 1992; Bjørlykke et al., 1995; Lanson et al., 1996; Lanson et al., 2002; Meunier and Velde, 2004). At the southern margin of the NGB, kaolinite is lacking apart from few exceptions (see above) and was not a direct precursor of illite. The absence of detectable smectite components, the hairy/fibrous morphology, and the fact that illitisation affects the complete pore space of the rocks indicate that pore-filling illites precipitated directly from the pore fluids. Lath-shaped illite crystallites can easily be produced in the laboratory using supersaturated KOH-solutions (Bauer et al., 2000). On the other hand, illite replacing detrital clay matrix may have been transformed from earlier smectite or

mixed-layer illite/smectite precursors. There is also textural evidence for in-situ replacement of feldspar and volcanic grains by illite. Hancock (1978) suggested that volcanic material is the major source of ions for authigenic clay minerals in the Rotliegend. However, there is no overall relationship of clay minerals to the abundance of volcanic detritus (Deutrich, 1993; Platt, 1993).

According to Deutrich (1993) and Gaupp et al. (1993), K-feldspar dissolution may provide the ions necessary for illite cementation in the sandstones investigated, and there is probably no need for an external source of K, as proposed for other case studies (Almon, 1981; Goodchild and Whitaker, 1986; Gluyas and Leonard, 1995). In contrast, it has been noted that K released during K-feldspar dissolution may be exported from reservoir sandstones into adjacent mudstones (Milliken et al., 1994; Thyne, 2001; Wilkinson et al., 2003). Field data and reactive transport modelling for Jurassic sandstones of the North Sea indicate that illite and quartz may precipitate rapidly in sandstones due to K-feldspar dissolution at temperatures of about 130-140°C (Thyne et al., 2001). Experimental studies and thermodynamic considerations show that illite is stable and may actually grow at temperatures of 50°C or less (Bjørkum and Gjelsvik, 1988; Bauer et al., 2000). However, the fundamental processes controlling meshwork/fibrous illite growth in reservoir sandstones are not understood, as discussed in Wilkinson and Haszeldine (2002). The latter authors suggested that the growth of authigenic, fibrous illite may be controlled by the kinetics of nucleation rather than by thermodynamics or growth kinetics. Their theory implies that illite growth requires unusual geological conditions such as abnormally high pore fluid supersaturations, high fluid flow velocities, high temperatures, or a catalyst (Wilkinson and Haszeldine, 2002). This idea is consistent with observations of many workers, showing that the growth of major authigenic illite is related to oil charging (e.g. Liewig et al., 1987; Glasmann et al., 1989; Hamilton et al., 1992; Clauer et al., 1999; Barclay and Worden, 2000), to episodic migration of hot fluids during tectonically active periods (e.g. Gaupp et al., 1993; Zwingmann et al., 1999; Liewig and Clauer, 2000), or to high fluid flow rates (e.g. Darby et al., 1997). Gaupp et al. (1993) pointed out that acidic fluids from coal-bearing Carboniferous strata migrated into Rotliegend sandstones at tectonic contacts between the two formations. These fluids caused feldspar destruction and illitisation in the Rotliegend, decreasing in intensity with increasing distance of fluid migration. Result of the present study suggest that major meshwork illite formation occurred contemporaneous to the main period of oil generation in the Westphalian (see section 4.3 and section 7.2.5 for discussion).

Chlorite

Four types of chlorite can be distinguished petrographically and/or chemically in Rotliegend sandstones from the southern study area.

(1a) Minor early tangential chlorite coatings have been observed locally (Deutrich, 1993; Gaupp et al., 2001; Gaupp and Solms, 2005). They are commonly 2-4 µm thick and not widespread. XRD analyses indicate Mg-rich composition (Gaupp and Solms, 2005).

(1b) A second type of relatively early Mg-dominated chlorite precipitated as pore-lining, radial rims on grain surfaces. The platy crystals, 10-20 µm across, and are arranged in a honeycomb fabric (Platt, 1993). They typically occur in texturally mature lake margin sandstones of the Hannover formation (Gaupp et al., 1993). Their Fe/(Fe+Mg) ratio commonly ranges from

0.23 to 0.46 (figure 42). This type of chlorite was often recorded in the German Rotliegend (Hancock, 1978; Platt, 1991; Deutrich, 1993; Gaupp et al., 1993; Platt, 1993; Cord, 1994; Gaupp and Solms, 2005) and has been described as C-type diagenesis by Gaupp (1996). Hillier (1994) pointed out that Mg-rich chlorites from the Rotliegend are exclusively the IIb polytype.

(2a) The third type forms platelets or small fan-like crystals of 10-20 µm in size. They may be arranged sub-parallel or perpendicular to grain surfaces and they are often overgrown by later meshwork illite (plate 9G). Fe/(Fe+Mg) ratios of this chlorite type are intermediate between early radial and late chlorites (figure 42; Deutrich, 1993).

(2b) Late chlorites, the fourth type, are rich in Fe and form pore-filling, coarse, often fan-like aggregates that post-date grain dissolution, meshwork illite formation, and bitumen impregnation (plate 9D-F). The length of single crystals perpendicular to the c-axis may exceed 50 µm. Such chlorites are a widespread minor component in sandstones of the southern basin margin. Close to the Carboniferous, fan-like chlorite locally replaces dickite (Platt, 1991). Late chlorite show Fe/(Fe+Mg) ratios between 0.60 and 0.95 (figure 42). Chlorites rich in Fe and Al are frequent in areas showing intense grain dissolution (Deutrich, 1993; Platt, 1993). Similar Fe-rich chlorites also occur within Carboniferous sandstones (Sedat, 1992; Deutrich, 1993).

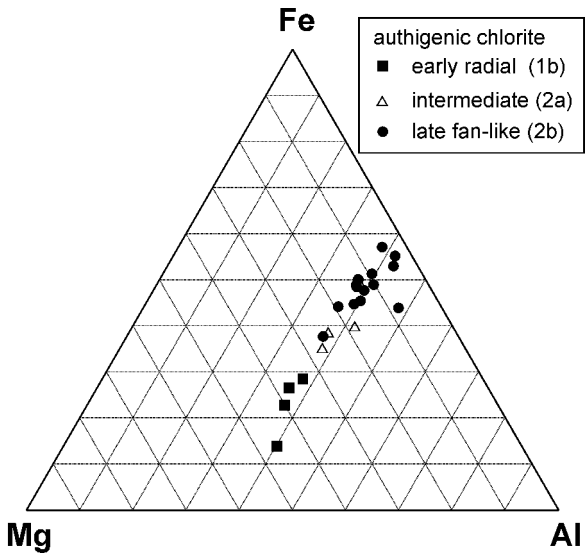

Figure 41: Chemical composition (mol.-%) of authigenic chlorites from the southern basin margin in the total Al-Mg-Fe diagram. Each point represents the average of one chlorite type per sample (data of Deutrich 1993), or per well (data of Platt 1993). There is much less variation in total Al than in the Fe/Mg ratio.

Most samples contain ≤5 vol.-% chlorite in total, both sandstones comprising Mg-rich and Fe-rich varieties. Few samples with up to 15 vol.-% chlorite are mostly alluvial fan or damp eolian deposits with relatively high contents of clay matrix, which appears to be partly replaced by Fe-rich chlorite. Locally, chlorite also replaces detrital biotite, volcanic grains, or feldspar. XRD analyses do not suggest the presence of expandable or 7 Å components in any of the chlorite types (Deutrich, 1993). The following "end-member" compositions can be deduced from EMP measurements (see Deutrich, 1993; Platt, 1993):

Mg-rich early chlorite: $(Mg_{6.0}\,Fe_{1.8}\,Al^{VI}_{3.3})\,(Si_{6.0}\,Al^{IV}_{2.0})\,O_{20}\,(OH)_{16}$
Fe-, Al-rich late chlorite: $(Mg_{0.7}\,Fe_{7.8}\,Al^{VI}_{3.3})\,(Si_{5.0}\,Al^{IV}_{3.0})\,O_{20}\,(OH)_{16}$

Following the AIPEA Nomenclature Committee (Bailey et al., 1980), radial chlorites (1b) may be called clinochlores, late chlorite generations (2a, 2b) are chamosites. There is much less variation in total the Al concentration than in the Fe and Mg concentrations (figure 41). In the diagram of tetrahedral Al versus Fe/(Fe+Mg), the chamosite composition is similar to other Ib ß = 90° and IIb ß = 97° chlorites (Brown and Bailey, 1962; Hayes, 1970; Curtis et al., 1985). Clinochlores tend to be slightly lower in tetrahedral Al (figure 42). There is a positive correlation ($R^2 = 0.73$) between the Fe/(Fe+Mg) ratio and tetrahedral Al (i.e. a negative correlation with Si, since tetrahedral Al has been calculated as 8 - Si).

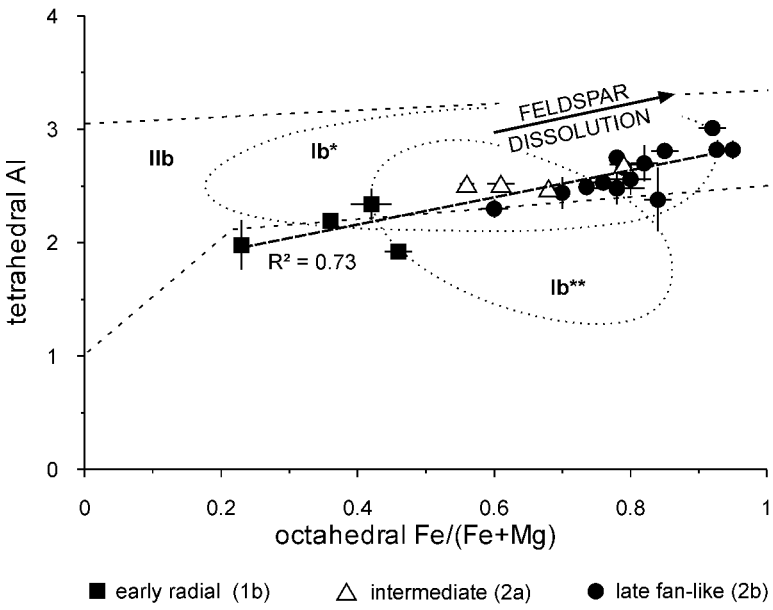

*Figure 42: Plot of tetrahedral Al versus Fe/(Fe+Mg) ratio of different types of authigenic chlorite from the southern basin margin. Mean and standard deviation of each data point (each sample/well) was calculated from 2-8 EMP analyses of Platt (1993) and Deutrich (1993). Y-axis are formula units based on 28 oxygen equivalents. Compositional fields of typical diagenetic Ib** and metamorphic IIb chlorites taken from Curtis et al. (1985); field Ib* according to Brown and Bailey (1962). (1b), (2a), and (2b) in the legend refer to the explanations in the text. Fe/(Fe+Mg) ratios of early radial chlorites are <0.5, those of intermediate and late chlorites are >0.5. The highest Fe/(Fe+Mg) ratios are found in late fan-like chlorites in areas of strong feldspar dissolution (compare Gaupp et al., 1993).*

Interpretation

Tangential chlorite and illite coatings may both originate form early clay coatings (compare section 5.4.8). During burial, dioctahedral smectites commonly transform to illite, trioctahedral smectites to chlorite (McKinley et al., 2003). However, tangential chlorite commonly records a more compacted grain framework compared to tangential illite in the sandstones investigated. Chlorite coatings (1a) probably formed during (early) mechanical compaction of the sediments. Radial chlorites (1b) also grew during early mesodiagenesis, prior to the main phase of mechanical compaction. The distribution of this chlorite type appears to be limited to shoreline sandstones, which are imbedded in mudflat and saline lake deposits (Deutrich, 1993; Gaupp et al., 1993). Radial chlorites most likely precipitated from alkaline, Mg-rich waters, which were expelled from the adjacent shales of the Rotliegend saline lake during compaction (Gaupp et al., 1993). Similarly, April (1981) demonstrated that alkaline lake waters favour the transformation of trioctahedral smectite to Mg-rich chlorite/smectite, which may transform to clinochlore during further burial. Although there is no evidence from XRD studies, the former presence of precursor phases like smectite/corrensite is possible. Honeycomb morphology, which is typical for the radial chlorites (1b) of the study area, is indeed characteristic for pore-lining authigenic corrensite (Tompkins, 1981; Hillier, 1994). A very similar type of chlorite has been described by Dixon et al. (1989) from desert sandstones of the Jurassic Norphlet Formation in Alabama. Early pore-lining chlorite cements

have been investigated intensely due to their apparent potential to preserve relatively high porosities (e.g. Heald and Larese, 1974; Pittman et al., 1992; Ehrenberg, 1993; Jahren and Ramm, 2000).

Textural evidence suggests that subparallel chlorite platelets (2a), the third type described here, formed during mesodiagenesis, probably later than radial chlorites, but earlier than meshwork illite. The increasing Fe^{2+}-content may be related to increasingly reducing conditions during burial. The fan-like Fe-rich variety (2b) is the latest mesodiagenetic chlorite type in the paragenetic sequence (figure 37B). The crystal morphology strongly suggests direct precipitation form the pore fluid, and not replacement of a precursor phase. In contrast to early facies-related chlorites, the late Fe-dominated variety grew independently from depositional environment after a phase of feldspar dissolution. Humphreys et al. (1989) presented comparable observations from Late Triassic sandstones of the Central Graben, North Sea. Late Fe-rich chlorite has often been reported to form at relatively deep burial after grain dissolution (e.g. Burton et al., 1987; Dutton and Land, 1988). Chloritisation of kaolinite has been described from medium to deep burial settings (about 2.5-4.5 km, Boles and Franks, 1979; Burton et al., 1987; Worden and Morad, 2003) and is discussed in more detail in Platt (1991). A positive correlation between Fe/(Fe+Mg) and Al is a common feature of diagenetic chlorites from may different settings (e.g. Brown and Bailey, 1962; Hillier and Velde, 1991). Jahren and Aagaard (1989) pointed out that the tetrahedral Al of diagenetic chlorites increases (i.e. Si decreases) with increasing formation temperature, but that the Fe/(Fe+Mg) ratio reflects the pore water composition and is not sensitive to P-T conditions. It has been suggested that the Fe incorporated in such chlorite cements may derive from reduction of ferric iron oxides (Curtis et al., 1985; Surdam et al., 1993). Similar processes may apply for the Rotliegend of the southern study area. The association of Fe-rich chlorite with grain dissolution, its abundance around faults juxtaposing Rotliegend and Carboniferous rocks, and decreasing Fe/Mg and Al/Si ratios away from such faults indicate that late chlorite precipitation is related to cross-formational fluid flow.

6.4.9 Minor authigenic minerals

REE-fluorocarbonates

Hartmann (1997) found minor authigenic REE fluorocarbonates (synchysite) in Rotliegend sandstones of two wells. The synchysites precipitated in the inter- or intragranular pore space, and may be associated with Ti-oxides. Hartmann (1997) concluded that they precipitated during mesodiagenesis, after formation of fibrous illite, and that underlying Rotliegend volcanics are the most likely source for the REE. He interpreted the formation of synchysite as result of focused fluid events causing locally relatively high fluid/rock ratios.

Apatite

Platt (1991) and Deutrich (1993) recorded traces of authigenic apatite, but were not able to determine the timing of formation with respect to other diagenetic minerals. Apatite occasionally occurs within altered volcanic grains, but also within the pore space of the sandstones. It may best be identified by its bright yellow CL colours (Platt, 1991).

Tourmaline

Detrital tourmaline grains may have syntaxial tourmaline overgrowths (Hancock, 1978; Platt, 1991). They formed either as one of the earliest phases during eodiagenesis, or they are relics which survived the grain transport, and thus represent pre-depositional processes.

6.5 Porosity, permeability and intergranular volume

The initial porosity of medium to fine grained, well sorted sandstones is commonly assumed to be about 40 vol.-% (Houseknecht, 1987). This appears to be a good approximation for average sandstones of the southern basin margin, since IGV around 40 vol.-% are the highest values preserved by eodiagenetic near-surface cements. Cord (1994) reported that the IGV may even be 40-50 vol.-% in some cases. However, he did not specify intergranular versus grain replacing cements, and it is more likely that including the latter resulted in these extreme IGV values. IGV, porosity and volume of cements correlate to different cementation types (figure 43), and partly to sedimentary facies in the southern part of the NGB (Gaupp et al., 1993). Highest porosities (up to ~20 vol.-%) and often high IGV can be found in eolian lake shore sandstones cemented by radial chlorite (C-type diagenesis). Sandstones comprising little cementation except hematite grain coatings and quartz overgrowths may preserve porosities above 10 %, but can also be strongly compacted (H-type diagenesis). Low porosity and strong compaction are dominant in sandstones containing detrital illitic clay or significant illite grain coatings (IC-type diagenesis). SB-type diagenesis is characterised by high cement volumes and low to moderate mechanical compaction. Samples cemented by meshwork illite show moderate to low porosities and varying IGV, and overlap with most other diagenesis types. Late cementation, especially extensive post-bitumen quartz, may have reduced porosity to almost zero. The highest permeabilities (about 1-100 mD) are found in the diagenesis types C and H (Gaupp and Solms, 2005). Most sandstones comprising significant meshwork illite have permeabilities less than 1 mD.

Leaching of feldspar and igneous rock fragments is the most important process that generated intragranular porosity, which may account for up to 5% of the total volume. However, only parts of the pore space generated by dissolution processes remained open until today. There is good petrographic evidence that significant secondary pore space was cemented again during diagenesis, mainly by clay minerals and quartz, but locally also by late generations of carbonates and sulphates. At least three leaching phases are evident from petrographic investigations (compare figure 37B): (1) Cement textures locally indicate that dissolution of anhydrite or carbonate took place during eodiagenesis. (2) Significant volumes of secondary porosity were generated prior (or contemporaneous) to illite formation and bitumen impregnation (plate 9D-F). Large oversized pores cemented by e.g. IM-B-Q-type diagenesis imply that destruction of feldspars or unstable rock fragments and early cements (carbonates/sulphates?) may have been extensive (plate 10G). Feldspar corrosion is greatest close to faults displacing the Rotliegend against Carboniferous Coal Measures (Gaupp et al., 1993). It is impossible to quantify the dissolution of early cements, but the co-occurrence of early and late diagenetic patterns in individual samples suggest that considerable cement dissolution has taken place (plate 11C-F, 11H). (3) Partly dissolved feldspars may have been coated by meshwork illite and solid bitumen along their outer grain surfaces, but may remained free of illite and bitumen in the intragranular pore space (plate 10D, 10H).

These textures imply a late dissolution stage, which post-dates bitumen impregnation. Gaupp (2005) proposed from a case study in the North-Hannover area that calcite and anhydrite cements were also affected by late dissolution in the vicinity of paleo oil migration pathways. Possible causes for mesodiagenetic periods of dissolution are discussed in section 7.2.4.

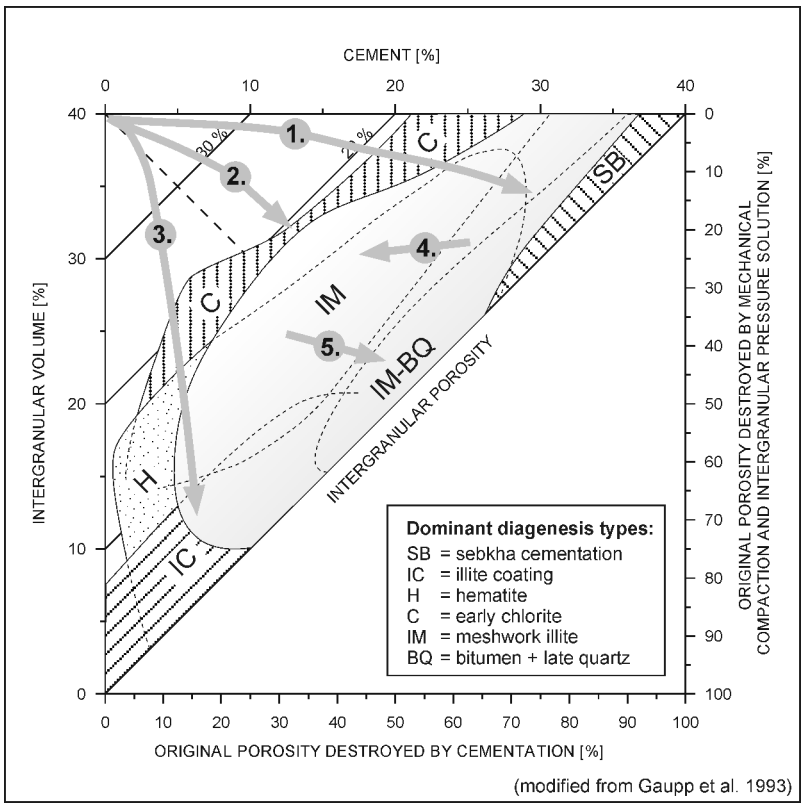

Figure 43: Intergranular volume versus volume of intergranular cements for sandstones from the southern margin of the NGB in the diagram according to Houseknecht (1987). Fields indicate characteristic IGV-cement-porosity relations for the dominant diagenesis types. Examples of typical compaction-cementation evolution are indicated by arrows: 1. low compaction, early cementation; 2. moderate compaction; 3. strong compaction, low cementation; 4. dissolution; 5. post-illite cementation.

6.6 Bulk rock geochemistry

Most Rotliegend sandstones investigated by XRF contain 70-90 wt-% SiO_2, 3-8 wt.-% Al_2O_3, 0.5-3.0 wt.-% K_2O, and up to 2.5 wt.-% Na_2O (Deutrich, 1993; Hartmann, 1997). These chemical variations are within the range which may be expected owing to alternating detrital composition of the sandstones (compare section 6.3). Grey sandstones show lower average K_2O contents than red sandstones (figure 44). SiO_2/Al_2O_3 ratios of typical sandstones range from 10 to 23. Only sandstones or conglomerates rich in volcanic rock fragments or clay matrix may have SiO_2/Al_2O_3 ratios around 5. These samples are often exceptionally rich in iron (3-10 wt.-% Fe_2O_3). The Fe contents of other sandstones of both red and grey colour range from 0.3 to 3.0 wt.-% Fe_2O_3, although the minimum Fe content measured in red sandstones is 0.5 wt.-% Fe_2O_3 (figure 44).

Chemical aspects of authigenic illite formation are illustrated in figure 45. The degree of illitisation was calculated by dividing the percentage of authigenic illite by the sum of K-Al components in the sandstones (illite + K-feldspar + approximate K-feldspar percentage of felsic volcanic rocks (33%), see Benek et al. 1996). Early tangential illite coatings and mesodiagenetic meshwork illite were not distinguished, but meshwork illite is dominant in all samples with high degree of illitisation. Chlorite and detrital mica were neglected after confirming that their abundance is not directly related to illitisation. The bulk rock Al_2O_3 is apparently independent from the percentage of authigenic illite, but shows a wide scatter.

However, the K_2O content and correspondingly the $K_2O/(K_2O+Al_2O_3)$ ratio tend to be lower in grey sandstones which are strongly cemented by illite compared to sandstones with minor authigenic illite. Similar results can be obtained if illitisation is referred to the total feldspar content instead of K-feldspar only (figure 45D).

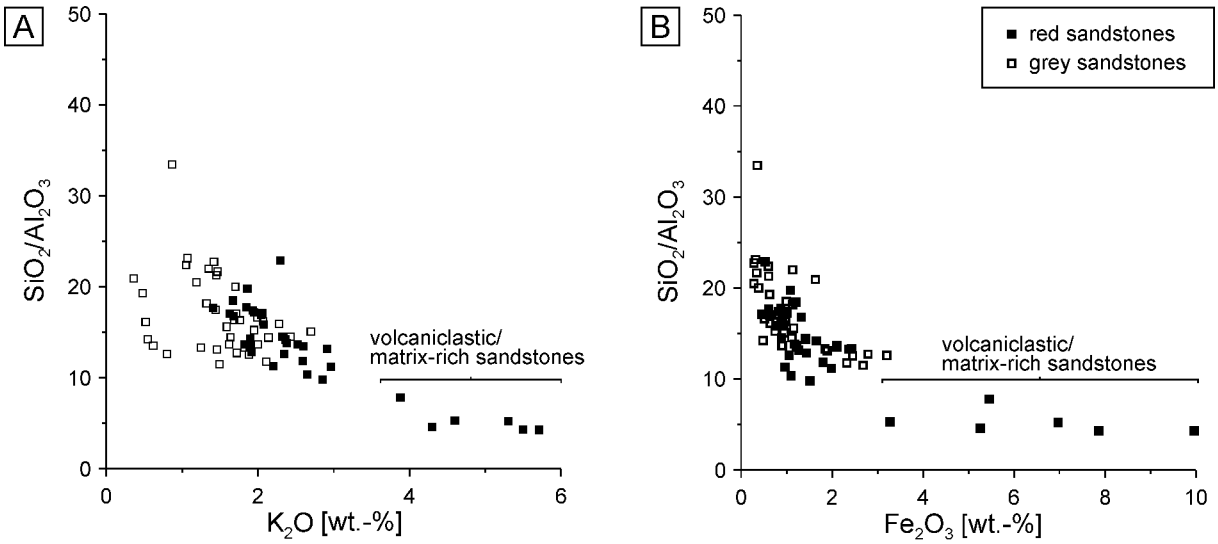

Figure 44: SiO_2/Al_2O_3 ratio versus K_2O (A), and versus Fe_2O_3 (B) of sandstones from the southern basin margin (bulk rock XRF analyses, units in wt.-%). Grey sandstones are on average lower in K_2O than red sandstones. Samples with low SiO_2/Al_2O_3 ratios are sandstones or conglomerates rich in volcanic rock fragments or clay matrix. Apart from the latter, which have Fe_2O_3 contents of 3 to 10 wt.-%, red and grey sandstones show a similar range in iron content (0.3-3 wt.-%). Data from Deutrich (1993) and Hartmann (1997).

Interpretation

Range and average of Fe_2O_3 are similar in most red and grey sandstones, apart from proximal alluvial deposits, which may be more Fe-rich. 0.5 wt.-% Fe_2O_3 appears to be the minimum Fe content of red sandstones with low percentage of Fe-bearing detrital material, and absence of Fe-bearing diagenetic phases other than hematite. Considering the amount of detrital iron as described in section 5.6, it can be estimated that 0.3 wt.-% hematite, distributed evenly within grain coatings, may be sufficient to cause rubification of sandstones. Hartmann (1963) proposed that some red sandstones may have total iron contents as low as 0.2 wt.-% Fe_2O_3. On the other hand, it not likely that grain coatings account for more than 2 wt.-% Fe_2O_3 of typical Rotliegend red beds.

Deutrich (1993) suggested that the illitisation of Rotliegend sandstones was probably a more or less isochemical process, and that the K and Al consumed through illite formation were provided by feldspar dissolution (see above). The trends shown in figure 45 are consistent with a conservative behaviour of Al. However, they indicate a net loss of K from grey sandstones in case of strong illitisation, assuming that illite was formed by dissolution of detrital feldspar. Red sandstones do not show evidence for K loss.

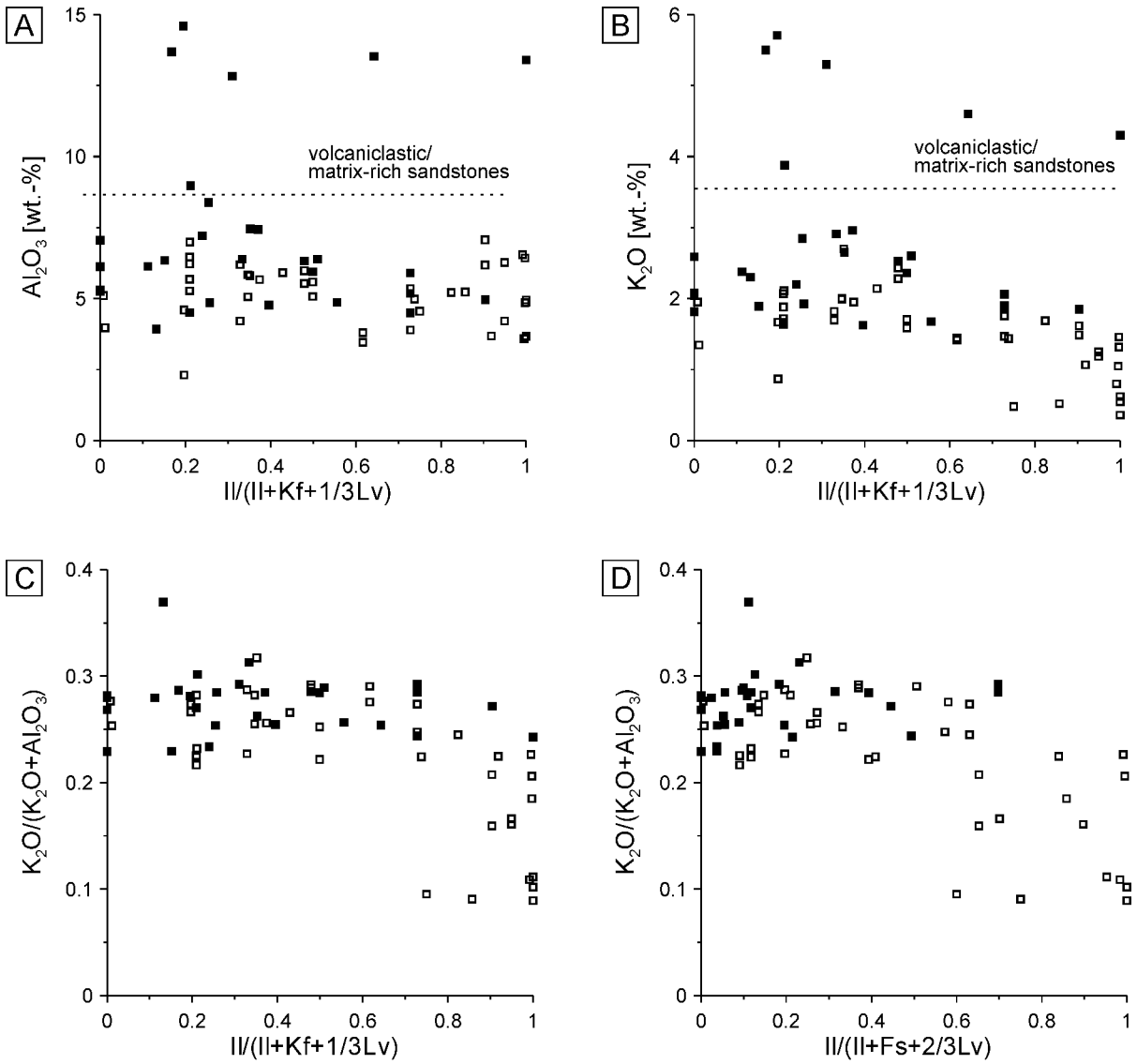

Figure 45: Plot of degree of illitisation versus (A) bulk rock Al_2O_3 content, (B) bulk rock K_2O content, and (C) the $K_2O/(K_2O+Al_2O_3)$ ratio. Degree of illitisation calculated by dividing the percentage of authigenic illite by the sum of K-Al components in the sandstones (Il = illite, Kf = K-feldspar, Fs = total feldspar, Lv = volcanic clasts, values in vol.-%). (D) Authigenic illite referred to the sum of illite plus the total detrital feldspar components. Symbols as in figure 44. Data from Deutrich (1993) and Hartmann (1997).

6.7 Organic inventory

Traces of solid bitumen are widespread in many Rotliegend sandstones from the southern NGB. Typically, the surfaces of clay minerals, particularly authigenic meshwork illite, are impregnated by bitumen (see plate 9, 10). In some samples without significant illite formation, grain surfaces may be directly coated by solid bitumen (plate 9H). The degree of impregnation ranges from extremely thin, greenish or brownish coatings to solid black pore-plugging aggregates (plate 10B-D). However, visible bitumen impregnations are not omnipresent, but often concentrated in distinct horizons, which are characterised by high paleopermeabilities (Gaupp, 2005). Zones of intense bitumen impregnation correlate with zones where initially red sandstones were bleached to grey colours (see section 7.2.3). In many cases, no later cements have been growing on surfaces impregnated by bitumen (plate 9C,

9G, 10A-D). In other cases, however, almost the entire pore space has been plugged by late quartz cement (see section 6.4.3). Late generations of carbonate, sulphate, or Fe-rich chlorite cements may also post-date bitumen impregnation (plate 9H, 10F, 10H).

DEGAS measurements were carried out to characterise the degassing behaviour of samples with different degree of bitumen impregnation. Measured mass numbers, corresponding mass fragments, and their potential origin are shown in table 4 (section 5.7). Figure 46 provides typical examples of degassing profiles of Rotliegend sandstones from the southern basin margin (complete profiles see plate 15-17, appendix). The three samples contain fibrous meshwork illite (IM) and partly mesodiagenetic Fe-rich chlorite (CF). Sample 36991 shows massive aggregates of solid bitumen in the pore space (plate 10D), sample 45908 is characerised by intense bitumen impregnation of clay mineral surfaces (plate 10B), and sample 42031 contains no visible bitumen (similar to plate 10A). Similar to the samples from the northern study area, the most intense signal was recorded for the mass fragment m/z 18 (water). Maxima are in the range 470°C to 660°C (figure 46). Release of hydrogen (m/z 2) occurs partly at similar temperatures, but a second and more intense maximum is evident at about 710-720°C from the samples 36991 and 45908. Although traces of m/z 15 (CH_3^+) were released at temperatures below 300°C, the maximum is at about 470-510°C for samples containing visible solid bitumen (36991, 45908). The same samples are also characterised by a strong release of CO (m/z 28) at high temperatures (maxima between 1000°C and 1180°C). A minor maximum of m/z 28 occurs at 430°C (only sample 36991). There are no corresponding signals in the degassing profile of carbon dioxide (m/z 44). Very low intensities of aromatic components (m/z 78, 91, note the scale in figure 46) were recorded for some samples in the temperature range 60-600°C. There is no relation of these signals to the visible intensity of bitumen impregnation for the samples measured by this method.

I n t e r p r e t a t i o n

The presence of solid bitumen in Rotliegend sandstones corresponds to a release of carbon monoxide at temperatures above 800-900°C; there is no significant overlap by nitrogen (compare m/z 14 in plate 15-17). This can be interpreted as reaction of residual carbon ("dead" carbon) with water or oxygen from other high-temperature reactions (section 5.7, Schmidt, 2004). Strong maxima of m/z 15 and m/z 2 in the temperature range of 300-1000°C can be explained release of methyl/methane and molecular hydrogen from solid bitumen. The fact that methane is released at lower and hydrogen at higher temperatures is typical for the degassing behaviour of kerogen and pyrobitumen (see discussion in Schmidt, 2004). The major water release can be explained by dehydration of sheet silicates. Most samples of the southern basin margin contain only very little detrital mica and mica/clay-bearing clasts, but abundant authigenic clay minerals. Samples containing abundant Fe-rich chlorite show a more intense maxima at 630-660°C than samples containing almost exclusively illite. This indicates that the Fe-chlorites in Rotliegend sandstones dehydrate dominantly at temperatures between 600 and 700°C. The absence of a correlation between the detected traces of aromatic compounds and the intensity of bitumen impregnation in the sandstones is difficult to explain, unless assuming some sort of contamination of the samples (see also section 5.7). This problem may be solved e.g. by future comparative investigations of outcrop samples, where contaminations can be excluded.

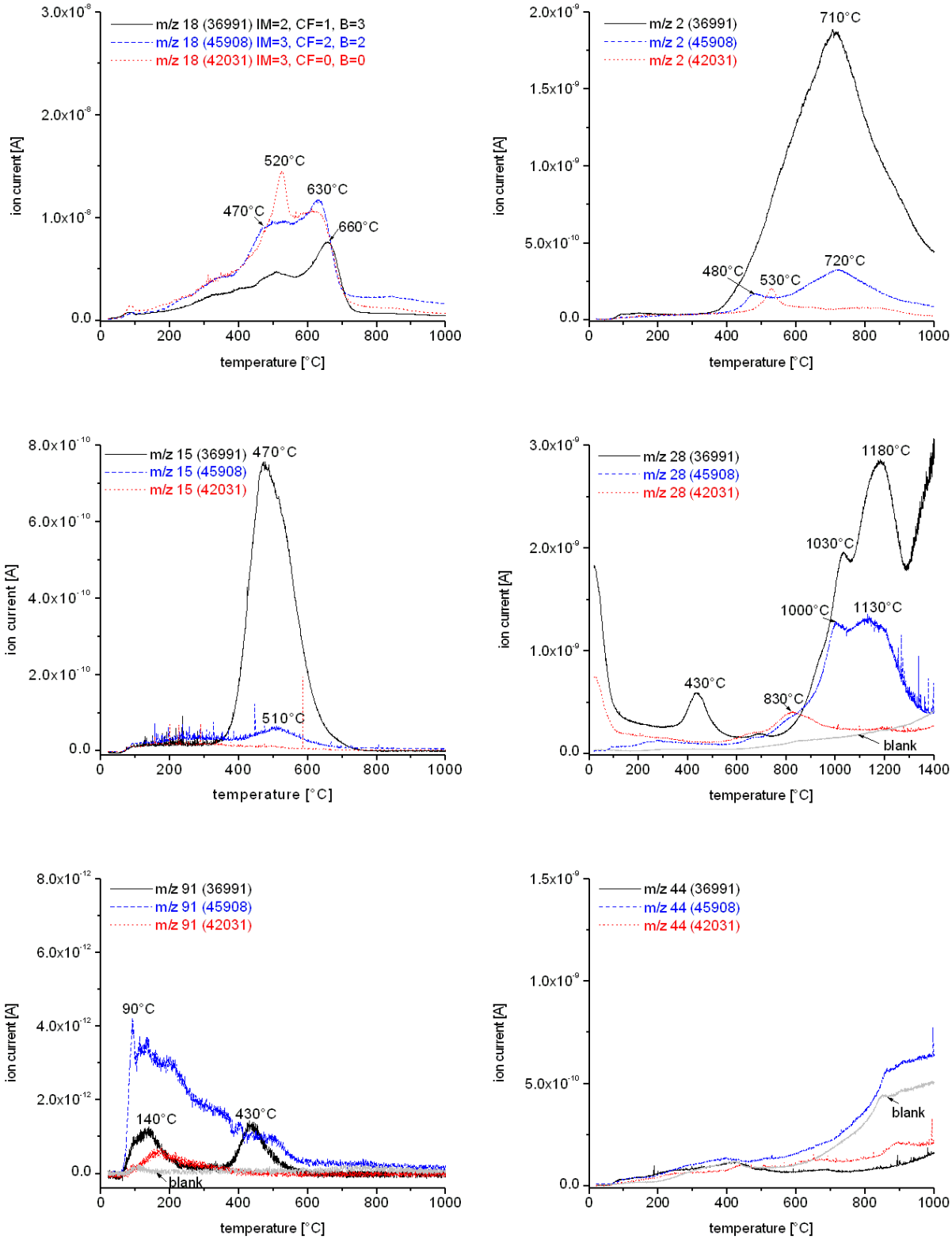

Figure 46: Degassing profiles of Rotliegend sandstones from the southern margin of the NGB. Release of m/z 18 (water), m/z 2 (deuterium/molecular hydrogen), m/z 15 (methyl fragment), m/z 44 (carbon dioxide), and m/z 91 (aromatic fragment) until 1000°C; m/z 28 (carbon monoxide or molecular nitrogen) until 1400°C. Note the different scale of the Y-axis. The intensity of authigenic meshwork illite formation (IM), late Fe-rich chlorite formation (CF), and bitumen impregnation (B) were classified in thin sections from 0 (not visible) to 3 (strong). Sample 36991 and 45908 are from well D-B9, sample 42031 is from well C-L (see table A2, appendix).

Solid bitumen in the pore space of sandstones reflects the former presence of liquid HC (Parnell, 1994; Littke et al., 1996). Littke et al. (1996) suggested that solid bitumen in north German Rotliegend reservoirs was a by-product of thermal cracking of oil to gas, when the sandstones reached higher temperatures upon further burial. However, major conversion of oil to gas in reservoir rocks is unlikely to occur at temperatures below 160°C (Horsfield et al., 1992; Schenk et al., 1997). Basin modelling results suggest that the maximal temperatures reached in the horizons investigated are about 150-170°C in the Cenozoic (figure 21, Schwarzer and Littke, 2005). These temperatures are probably insufficient to account for the observed widespread bitumen occurrence. Other mechanisms to generate solid bitumen include biodegradation of liquid HC (e.g. Connan, 1984; Machel, 2001; Larter et al., 2003), ashpaltene precipitation from oil e.g. due to gas influx (see Ehrenberg et al., 1995), or reaction of organic compounds with reservoir minerals or water (Shebl and Surdam, 1996). Biodegradation is not likely in case of the Rotliegend reservoirs of the southern study area, since the Rotliegend was buried to more than 2000 m during illite formation, which preceded bitumen emplacement. The corresponding formation temperatures were about 100-130°C. Although the available data do not allow to specify a process for bitumen formation, reactions of liquid HC with water or minerals could explain the presence of solid bitumen and the dominance of "dead carbon" in some horizons of the Rotliegend sandstones (see also section 7). However, ashpaltene precipitation may have been an important process to retain organic material in the rocks. The lack of later cements in many pores impregnated by bitumen could be related to hydrophobisation of pore surfaces.

6.8 Summary and diagenetic sequence

During the Upper Rotliegend (Havel Subgroup, Dethlingen and Hannover Formation), sandstone were deposited along the southern margin of the NBG, forming a broad alluvial-eolian facies belt. The clastic material was transported into the basin by ephemeral rivers that drained the Variscan hinterland to the south, and was frequently reworked by wind action. Most samples investigated are fine to medium grained, moderately to well sorted (lithic) subarkoses and (sub-) litharenites. There is a wide range of porosity (0-20 vol.-%), permeability (mostly 0.01-100 mD), and IGV (<10-40 vol.-%), depending mainly on depositional facies and diagenesis. The succession of diagenetic processes and products is summarised in figure 37B at the end of section 5. Eodiagenesis is characterised by formation of iron oxide and clay mineral grain coatings, and by precipitation of carbonates, sulphates, and minor quartz or feldspar in the pore space of the sandstones. Pore-filling eodiagenetic cements preserve large IGV and may be present as the only cementation type in certain horizons, or as relics in sandstones which are dominated by mesodiagenetic cementation patterns. Pore-lining Mg-dominated chlorite formed during early burial diagenesis, probably from earlier clay precursors. Textural evidence points to the presence of several mesodiagenetic generations of carbonate, sulphate, and quartz cements. Authigenic feldspar and halite as well as Ti-oxides are only locally important. Many sandstones at the southern basin margin contain abundant platy and fibrous illite (meshwork illite), which has been dated to about 180-200 Ma in various parts of the basin. Precipitation of meshwork illite was pervasive and usually affected the complete pore space connected to fluid flow. Kaolinite, dickite or chlorite locally formed at a similar paragenetic position. Clay mineral formation post-dates a major phase of grain dissolution and leaching of reversible cements (carbonates, sul-

phates). Mesodiagenetic illite is often impregnated by solid bitumen. The succession of these petrographic features is very typical and seems to be strongly interrelated. There is some evidence for late dissolution of feldspar grains and carbonate/sulphate cements subsequent to bitumen impregnation. Post-illite diagenetic minerals include Fe-rich chlorite, ankerite, siderite, quartz, sulphate and calcite cements. Pore-plugging authigenic quartz is particularly abundant in some areas. However, in many samples bitumen stained illite was not overgrown by any later cements.

7 Discussion: Comparison of diagenetic evolution at the northern and southern margin of the NGB

The main objective of this study is to compare the diagenetic evolution of Rotliegend sandstones from the northern and southern margin of the NGB, and to test the hypothesis that major diagenetic mineral reactions are influenced by the presence or absence of organic maturation products. Difference in source rock distribution and organic maturation between the two basin margins were described in section 3 and 4, Rotliegend diagenesis was characterised in section 5 and 6. This section specifies major differences in diagenetic evolution between northern and southern basin margin. The discussion concentrates mainly on the relation of diagenetic processes to organic maturation and migration. Other controls on diagenesis are treated only briefly, e.g. the influence of sedimentary facies, which has been discussed in detail previously (e.g. Glennie et al., 1978; Gaupp et al., 1993; Platt, 1994).

7.1 Eodiagenesis

7.1.1 Pore-filling early cements

The early, near-surface stages of diagenetic evolution are comparable at both basin margins, although pore-filling early cements are less common in the case studies from the north, compared to the southern study area. Eodiagenesis was mainly controlled by depositional environment and by the relative position within the basin during that period. Eodiagenetic carbonates, sulphates, locally halite, minor quartz, albite, and hematite precipitated from waters which were fed from the Variscan highland areas to the south, and the Ringkøbing-Fyn/Fennoscandian High to the North, respectively. Oxygen isotopic data of carbonates, and sulphur as well as strontium isotopic data of anhydrite are consistent with continental, meteoric-type waters (section 5.4.5 and 6.4.5, Platt, 1994). Early calcite and dolomite cements occur in alluvial deposits at both basin margins. In the southern NGB, waters became increasingly saline from the basin margin towards the basin centre owing to evaporation, and successively formed calcite/dolomite, anhydrite plus quartz, and halite (Drong, 1979; Platt, 1994). Only three wells at the much narrower northern margin of the NGB are not sufficient to trace a comparable trend. Early cements, e.g. dolomite, have partly replaced detrital grains. Replacement of silicate grains by carbonate cements during eodiagenesis of siliciclastic rocks has been reported previously, especially from areas with high evaporation (Watts, 1980; Colson and Cojan, 1996). Corrosion edges on detrital grains indicate that corrosive early cements could have been more widespread primarily than traceable today. Eodiagenetic carbonates and sulphates may have been re-dissolved, e.g. during periods of high fresh water supply. However, it is not clear whether grain corrosion has taken place during eodiagenesis or earlier, e.g. during weathering in the source area.

7.1.2 Hematite coatings

Hematite aggregates on grain surfaces may be partly inherited. This is likely especially for grain indentations, where iron oxides were protected from abrasion during transport. However, most hematite precipitated during eodiagenesis, when the grain framework was dominated by point contacts. Hematite is typically related to tangential illite coatings, which may represent mechanically infiltrated clay (Walker, 1976; Turner, 1980; Matlack et al., 1989). The eodiagenetic formation of ferric oxide/hydroxide and clay mineral grain coatings is characteristic for semi-arid clastic deposits, and responsible for their rubification (Walker, 1967; van Houten, 1968; Walker, 1976; Turner, 1980; Torrent and Schwertmann, 1987; Mücke, 1994). Ferrous iron was released by the breakdown of unstable Fe-bearing minerals (e.g. pyroxene, magnetite, biotite) within the sediment, or transported into the basin by meteoric waters from weathering profiles at the basin margins. Ferric oxide coatings can be interpreted as a result of repeated changes in wetting and drying of the sediment (desiccation cycles). Various early Fe-hydroxides may have transformed into hematite at higher temperatures via dehydration (e.g. van Houten, 1968; Chukhrov, 1973; Folk, 1976; Walker, 1976; Cornell and Schwertmann, 1996). Hematite crusts are locally absent in sandstones which were strongly cemented by the first generation of sebkha-type cements (Gaupp, 1996), and may be scarce in areas of rapid accumulation, where the sediments were not exposed to multiple redox changes near the surface (e.g. channel facies sandstones in well Flensburg Z1). In general, however, it can be assumed that Fe-oxide grain coatings were almost omnipresent in sandstones of the Rotliegend basin.

The iron content of hematite coatings may vary significantly. Hartmann (1963) proposed, based on chemical analyses of Permian and Triassic red beds in central Germany, that the minimum iron content necessary to cause red rock colour is about 0.2 wt.-% Fe_2O_3. The extractable free iron of bright red sandstones may be as low as 0.1 wt.-% Fe (Walker and Honea, 1969), but iron-rich red beds can also reach values around 6 wt.-% Fe (Schluger and Roberson, 1975). However, average values around 1 wt.-% Fe_2O_3 appear to be typical for hematite crusts in red bed sandstones (Walker and Honea, 1969). Bulk rock geochemical and petrographic investigations of Rotliegend sandstones from the southern and northern margin of the NGB support earlier findings and suggest that between 0.3 and 2.0 wt.-% Fe_2O_3 is stored in hematite coatings (section 5.6, 6.6).

7.2 Mesodiagenesis

7.2.1 Pore-lining radial chlorite

Mg-dominated radial chlorite and minor tangential chlorite coatings are evident from both basin margins. Radial chlorites formed typically later than eodiagenetic cements. They are common in lake-margin sandstones at the southern basin margin, and in fluvial channel sandstones at the northern basin margin. Following Gaupp et al. (1993), these chlorites precipitated from alkaline fluids that were expelled from basin-central Rotliegend shales during burial. At the northern margin, chlorite cemented sandstones are interbedded with Rotliegend shales, suggesting similar formation mechanisms. Further indication of Mg-rich early pore fluids comes from abundant dolomite cementation in chlorite-bearing sandstones

of the northern basin margin. Textural and morphological characteristics of radial chlorites point to precursor clay phases. The occurrence of trioctrahedral smectites, which are likely to be chlorite precursors, is typical in lithic sandstones of semi-arid to arid depositional environments (McKinley et al., 2003). Hillier (1994) suggested that Mg-rich chlorites formed by replacement of Mg-smectite precursors via the intermediate mineral corrensite. Berthierine has also been claimed as a precursor of pore-lining radial chlorite in reservoir sandstones (e.g. Curtis et al., 1985; Hillier, 1994; Aagaard et al., 2000). However, berthierine is typically found in marine or coastal environments, is relatively Fe-rich and commonly transforms to Fe-rich chlorite during burial. Former growth of early bertherine or similar Fe-dominated 7 Å minerals is therefore not likely for Permian red beds of the NGB. The low Fe content of radial chlorite cements and the precipitation of ferric oxides suggest high oxygen partial pressures during early diagenesis, leaving little Fe^{2+} available for incorporation in chlorites. Similarly, Weibel (1998) showed that chlorites from red areas of the Skagerrak Formation have higher Mg/Fe-ratios than chlorites from white areas, which reflect locally reducing conditions.

7.2.2 Pore-filling shallow burial cements

In the southern part of the NGB, quartz, carbonates, sulphates and locally feldspar formed during early burial (figure 37). They can be distinguished texturally from eodiagenetic cements, but still show dominantly meteoric fluid signature (Platt, 1994). It is possible that early mesodiagenetic carbonates and sulphates formed by redistribution of earlier cement generations. A comparable cement assemblage fills much of the pore volume in Rotliegend sandstones from the northern basin margin. Relatively low IGV preserved by these cements indicate that they grew not close to the surface but during burial. However, hematite layers interrupting early mesodiagenetic dolomite cementation (well Flensburg Z1) indicate precipitation at rather shallow burial depths, where oxygenated waters could occasionally percolate through the pore system. Elevated Mn-concentrations of carbonates, their often multiple zoning, and isotopic data also suggest that they originated from meteoric-type waters (compare Boles and Ramseyer, 1987; Platt, 1994). It should be noted that the sandstones of the northern study area were buried to 900-2000 m at the end of the Rotliegend, compared to less than 500 m in most areas of the southern study area. Rapid burial at the northern basin margin probably resulted in more pronounced mechanical compaction compared to early cementation. Variations in oxygen isotopic composition of eodiagenetic to shallow burial carbonates at both basin margins (section 5.4.5, 6.4.5) are consistent with the assumption that they represent a number of cement generations, which precipitated over a range of burial depths and temperatures.

7.2.3 Bleaching of red beds

While eodiagenetic and early mesodiagenetic processes characterised so far are comparable in both study areas, the evolution of Fe-bearing authigenic phases forms a major contrast between southern and northern margin of the NGB (table 7). Authigenic hematite is well preserved down to maximum burial depth in the wells from Schleswig-Holstein, and also at some localities of the southern basin margin. However, hematite grain coatings were removed during diagenesis from a significant number reservoir horizons in the southern NGB, which show grey rock colours today. The original presence of ferric iron is evident from hematite relics within these rocks. They may be preserved beneath quartz overgrowths,

which protected the Fe-oxides from pore fluids, and thus inhibited further mineral reactions (plate 9B). It is also evident from the distribution of grey colours, which is not facies related but correlates with zones of bitumen impregnation (figure 48A, B). Fe^{3+} is immobile in the diagenetic temperature range under normal pore fluid conditions, but reduced iron (Fe^{2+}) is mobile and may be transported in solution (figure 47, Drever, 1997). This implies that hematite was dissolved by reduction of Fe^{3+} to Fe^{2+}, and ferrous iron was removed or incorporated in other authigenic phases. A number of processes may be responsible for iron oxide reduction and bleaching of red beds, as discussed in the following.

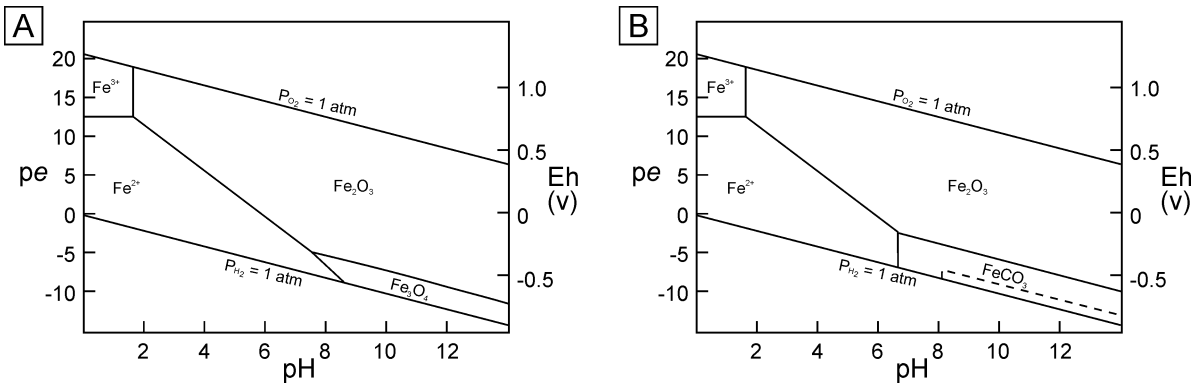

Figure 47: Eh-pH diagrams at 25°C with hematite as stable ferric oxide phase. Boundaries drawn for an activity of dissolved Fe species of $a_{Fe^{2+}} = 10^{-6}$. A) System Fe-O-H_2O. B) System Fe-O-H_2O-CO_2 for P_{CO_2} = 1 atm (solid line) and 10^{-3} atm (dashed line). Redrawn from Drever (1997).

(1) Many authors considered liquid HC as most likely reducing agents (Burley, 1984; Kilgore and Elmore, 1989; Surdam et al., 1989a; Surdam et al., 1993; Lee and Bethke, 1994; Garden et al., 2001; Parry et al., 2004). This is probably also relevant in the southern part of the NGB, since liquid HC were generated from Carboniferous source rocks during early burial of the Rotliegend (section 4). Bleaching of red beds was often recorded in the vicinity of faults and fractures, which are regarded as conduits for reducing petroleum fluids (e.g. Almon, 1981; Foxford et al., 1996; Rowe and Burley, 1997). Beitler et al. (2003) inferred from regional bleaching patterns in exhumed Jurassic sandstones on the Colorado Plateau that bleaching corresponds to the locations of structural traps for past petroleum reservoirs. Slow but long-continued microseepage of HC from petroleum reservoirs may lead to reduction of ferric oxides/hydroxides and formation of magnetite in the overlying formations (Donovan et al., 1979; Donovan et al., 1984). However, diagenetic magnetite is absent in the Rotliegend of the NGB according to present studies. Shebl and Surdam (1996) carried out oil-rock-water experiments at 200-360°C in order to simulate redox reactions in clastic petroleum reservoirs. In these experiments, iron oxides were reduced and liquid HC were oxidised to CO_2 and organic acids. Hematite may be reduced to pyrite, e.g. from sulfur-bearing oils:

$$0.15\ C_9H_{20} + 0.5\ Fe_2O_3 + 2\ S \rightarrow 0.675\ CH_3COOH + FeS_2 + 0.15\ H_2O$$

(Surdam et al., 1993).

An alternative possible summary reaction for iron reduction has been suggested, where CH_2O is used as a representative term for HC compounds:

$$CH_2O + 2\ Fe_2O_3 + 8\ H^+ \rightarrow CO_2 + 5\ H_2O + 4\ Fe^{2+}$$ (Chan et al., 2000).

Other experimental studies indicate that n-alkanes can be oxidised to carboxylic acids by formation water, and that mineral oxidants (e.g. hematite) may consume the molecular hydrogen generated by this reaction (Seewald, 2001a, 2003).

(2) A second possibility to remove hematite from red beds is iron reduction by dissolved organic acids (e.g. Kharaka et al., 1986; Muchez et al., 1992). McCollom and Seewald (2003) demonstrated by laboratory studies at 325°C and 350 bars that organic acids and acid anions like acetic acid and acetate, which are abundant in oil-field brines (Carothers and Kharaka, 1978; Kharaka et al., 1986), are oxidised rapidly in the presence of hematite. The authors concluded that the oxidation reaction produces CO_2 and is coupled to the reduction of hematite, which may lead to magnetite formation:

$CH_3COOH + H_2O \rightarrow 2\ CO_2 + 4\ H_2$

$3\ Fe_2O_3 + H_{2(aq)} \rightarrow 2\ Fe_3O_4 + H_2O$ (McCollom and Seewald, 2003).

(3) Iron reduction may be a consequence of bacterial (<80°C) or thermochemical sulphate reduction (>100-140°C). These processes produce hydrogen sulphide by reaction of various HC and dissolved sulphate, which commonly derives from dissolution of solid sulphate minerals like anhydrite (Machel et al., 1995; Worden et al., 1995; Machel, 2001). The reactions can be summarised as follows:

hydrocarbons + SO_4^{2-} → altered hydrocarbons + bitumen + HCO_3^- + H_2S

(Machel, 2001).

Consequently, authigenic pyrite or other Fe-sulphides may form as by-products of bacterial or thermochemical sulphate reduction, if iron oxides are available (Reynolds et al., 1993; Machel, 2001). Another typical result of these processes is calcite precipitation from reaction of HCO_3^- with Ca^+ from anhydrite (Machel et al., 1995; Worden et al., 1996). They absence of authigenic pyrite in Rotliegend sandstones of the NGB suggests that bacterial or thermochemical sulphate reduction did not play a major role here, although sulphate cements were locally abundant.

(4) As recently pointed out by Palandri and Kharaka (2005) and Haszeldine et al. (2005), bleaching can also occur by interaction of hematite with CO_2 fluids carrying H_2S and/or SO_2. It must be noted that in this case, no HC are involved directly or indirectly. Thermodynamic calculations, carried out to predict the potential of red beds for CO_2 sequestrations, indicate that hematite can be reduced according to the overall reactions:

$4\ Fe_2O_3 + 15\ H_2S + H_2SO_4 \rightarrow 8\ FeS_2 + 16\ H_2O$

$Fe_2O_3 + 2\ CO_{2(g)} + 2\ SO_{2(g)} + H_2O \rightarrow 2\ FeCO_3 + H_2SO_4$ (Palandri and Kharaka, 2005)

Although these reactions imply that iron is retained within the reservoir, field and petrographic data suggest transport of substantial volumes of iron (Chan et al., 2000; Haszeldine et al., 2005). Dissolution of hematite by H_2S requires fluids of relatively low pH as shown by the following equation:

$4\ Fe_2O_3 + H_2S + 14\ H^+ \rightarrow 8\ Fe^{2+} + SO_4^{2-} + 8\ H_2O$ (Metcalfe et al., 1994).

CO_2 was generated from Carboniferous Coal Measures at the southern margin of the NGB, but there is no evidence for H_2S- or SO_2-bearing fluids. Pyrite is absent, and Fe-

carbonates are only locally associated with bleached sandstones. It has also been hypothesised that groundwater rich in CO_2 could cause bleaching of red sandstones (Schumacher, 1996; Allis et al., 2001). Iron is mobile at very low pH (figure 47), and acidity is largely controlled by CO_2 (e.g. Giggenbach, 1997). Although the typical range of red bed brines appears to be between pH 5 and pH 9 (Bjørlykke et al., 1989; Metcalfe et al., 1994), pH 2.6 to 4 were occasionally reported from Rotliegend formation waters (Warren and Smalley, 1994). However, it has to be remembered that the measured pH may be different from the actual pH in the reservoir rock, e.g. due to temperature alterations or loss of volatile gases such as CO_2 and H_2S (see also Kharaka et al., 1986). Furthermore, acidic, CO_2-rich pore waters will be neutralised by reactions with carbonate and feldspar (Bjørlykke, 1983; Giles and Marshall, 1986).

(5) Several authors suggested, partly based on thermodynamic calculations, that methane may reduce hematite in red bed sandstones (Barker and Takach, 1992; Schumacher, 1996; Chan et al., 2000; Parry et al., 2004). One possible reaction is:

$Fe_2O_3 + CH_4 \; ? \;\; Fe_3O_4 + CO_2 + H_2$ (Barker and Takach, 1992).

The authors emphasised, however, that a thermodynamic approach can only be applied to very deeply buried sandstones (>7-8 km), and that kinetics are likely to control reactions at shallower depths. Following Giggenbach (1997), the most effective buffer controlling redox conditions in sedimentary fluid-rock systems is a reaction similar to that above:

$8\ Fe_2O_3 + 2\ CH_4 \; ? \; 2\ CO_2 + 16\ FeO + 4\ H_2O$ (Giggenbach, 1997).

He suggested that, above temperatures of about 160°C, the CH_4/CO_2 ratio is increasingly controlled by approach to equilibrium with Fe-bearing minerals of the host rock contacted by the fluid. Rotliegend sandstones of the northern study area were probably heated to 160-190°C during the Triassic, so iron reduction could have been possible theoretically according to the above reaction, if methane had migrated into the rocks during that time. In contrast, the Rotliegend of the southern basin margin were mostly less than 130°C during the time relevant for bleaching reactions (compare section 4.2).

(6) Microorganisms are capable of reducing Fe^{3+} in subsurface environments. Bleaching of Rotliegend red beds of the NGB may have taken place in a temperature range suitable for microbial activity, considering that Fe^{3+} reducing microorganisms have been reported to exist in hot sedimentary environments, up to temperatures of 121°C (Kashefi and Lovley, 2003; Kashefi et al., 2004). Reductive dissolution of Fe^{3+} oxides/hydroxides by dissimilatory iron-reducing bacteria appears to be most effective for amorphous or poorly crystalline phases (Lovley and Phillips, 1988; Lovley, 1991), but has also been proven for goethite and hematite in subsurface environments (Roden and Zachara, 1996; Zachara et al., 1998; Zachara et al., 2004). Important controls on the rate and extent of bacterial Fe^{3+} oxide reduction are crystallographic properties and specific surface area (Roden and Zachara, 1996; Zachara et al., 1998), nutrient conditions (Glasauer et al., 2003), the presence or absence of Fe^{3+} chelators, e.g. organic acids (Liang et al., 1993; Lovley and Woodward, 1996), and the removal of ferrous iron from solution (Roden and Urrutia, 1999; Hansel et al., 2004).

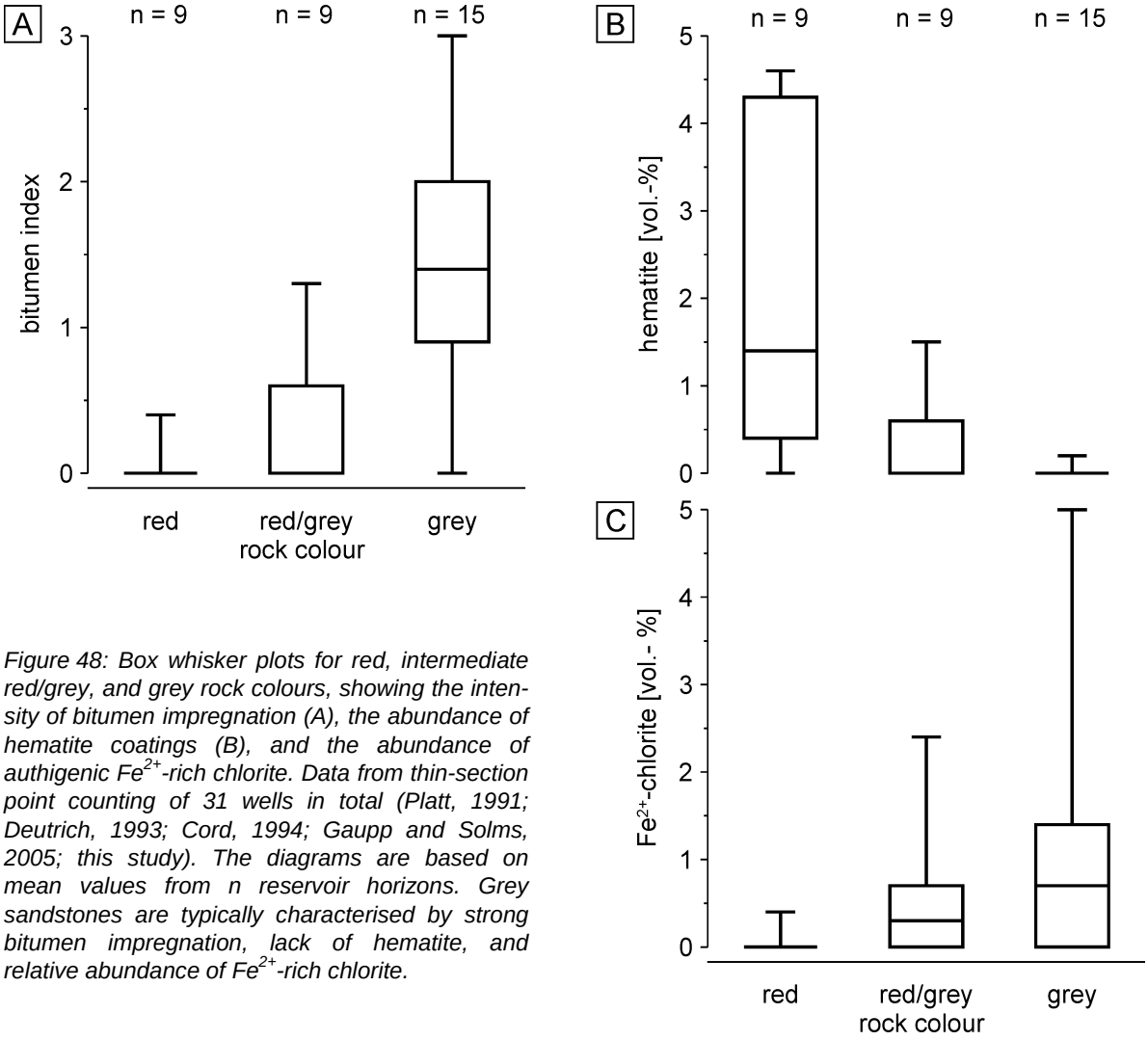

Figure 48: Box whisker plots for red, intermediate red/grey, and grey rock colours, showing the intensity of bitumen impregnation (A), the abundance of hematite coatings (B), and the abundance of authigenic Fe^{2+}-rich chlorite. Data from thin-section point counting of 31 wells in total (Platt, 1991; Deutrich, 1993; Cord, 1994; Gaupp and Solms, 2005; this study). The diagrams are based on mean values from n reservoir horizons. Grey sandstones are typically characterised by strong bitumen impregnation, lack of hematite, and relative abundance of Fe^{2+}-rich chlorite.

Petrographic investigations of bleached red beds from the southern margin of the NGB indicate that hematite was dissolved. There is no evidence for in-situ preservation of iron reduction products like pyrite or magnetite. These observations were confirmed by Raman spectroscopy (Hasner, 2004). Major bleaching occurred prior to the precipitation of meshwork illite and to bitumen impregnation. The timing of iron reduction probably corresponds to early periods of oil generation in the underlying Carboniferous source rocks (section 4). At least some parts of bleached horizons typically show strong bitumen impregnation. Rock colour and abundance of authigenic hematite correlate with the intensity of bitumen impregnation on a basin scale (figure 48A, B). In conclusion, although it is not possible to tell exactly which reaction was responsible for bleaching, or if a singe process or multiple processes caused hematite reduction, the data imply that bleaching was related to migration of early organic maturation products, most likely liquid HC or organic acids. Interaction with H_2S-bearing fluids and bacterial/thermochemical sulphate reduction is unlikely owing to the absence of Fe-sulphides. It is also questionable if the temperatures were high enough to enable reaction of methane with hematite. Whether or not microorganisms played a role in Fe-oxide reduction remains a question open to further research.

7.2.4 Dissolution of grains and cements

Dissolution processes generating "secondary porosity" during burial diagenesis have been discussed extensively in the past, since this porosity is of great economic importance for oil and gas exploration (among others, Schmidt and McDonald, 1979; Curtis, 1983; Bjørlykke, 1984; Surdam et al., 1984; Burley, 1986; Giles and Marshall, 1986; Kawamura and Kaplan, 1987; Surdam et al., 1989b; Shebl and Surdam, 1996). However, depending on the timing of diagenetic processes, parts of the porosity generated by mineral dissolution may have been filled by later cements. Abundant evidence for burial diagenetic leaching of grains and cements in the NGB is only available from the southern basin margin. Large oversized pores cemented by (late) mesodiagenetic cements, and relics of feldspar or volcanic grains, which have been replaced by meshwork illite, indicate corrosion and dissolution of unstable detrital grains. Mainly indirect evidence points to dissolution of intergranular cements: Pore networks cemented by meshwork illite are free of earlier cement generations, apart from minor grain coating clay/Fe-oxide and minor quartz/feldspar overgrowths. Illite meshwork (IM) formation has been dated to about 200-180 Ma. This implies that the sandstones remained either non-cemented throughout the Permian and Triassic, or that earlier cements were removed prior to illite growth. The lack of any early carbonate/sulphate cements is highly unlikely in a continental, evaporitic basin like the Permian Rotliegend basin of central Europe. Hence, dissolution of early reversible cements has probably taken place in the forefront of illitisation. This assumption is confirmed by the coexistence of early IM-free and later IM-dominated cementation patterns in close proximity, partly within one thin-section (plate 11). Such contrasting cementation patterns within individual samples are apparently not related – at least not confined – to textural changes (e.g. grain size, sorting), but often occur in patchy distribution in the rocks. Mesodiagenetic leaching may have removed several volume percent of detrital feldspar, locally even around 15 vol.-% (Platt, 1991). The amount of intergranular mineral dissolution is impossible to quantify from petrographic observations, but may have been substantial. Wilkinson and Haszeldine (1996) emphasise that optical identification generally tends to underestimate secondary porosity.

Possible mechanisms of mineral dissolution in the subsurface include (1) meteoric water flushing (Bjørlykke, 1983, 1984), (2) mixing corrosion (Plummer, 1975), (3) focused leakage of overpressured pore fluids (Wilkinson et al., 1997), (4) import of acidic products from clay mineral transformations in mudstones (Bjørlykke, 1983), (5) influx of acidic fluids generated from CO_2 or organic acids from maturing petroleum source rocks (Schmidt and McDonald, 1979; Surdam et al., 1984), and (6) generation of CO_2 and/or organic acids by oxidation of HC within the reservoir (e.g. Surdam and Crossey, 1985; Shebl and Surdam, 1996; Seewald, 2001a, 2003). A comprehensive review on mechanisms (1), (2), (4), and (5) is given in Giles and Marshall (1986). Dissolution of K-feldspar has also be interpreted to be controlled by temperature (e.g. Dutton and Land, 1988; Wilkinson et al., 2001). However, pure temperature control cannot be applied here, since feldspar corrosion is not related to burial depth in the sandstones investigated.

Meteoric waters may penetrate to considerable depths in sedimentary basins (e.g. Galloway, 1984). Magri et al. (2005a; 2005b) proposed density-driven convective fluid cells in the NE German Basin, reaching down to depths of approximately 3000 m. However, these cells are confined to the basin fill above the thick Zechstein evaporites, which can be regarded as major fluid barrier. The Rotliegend reservoirs at the southern margin of the NGB were buried

to around 2000 m in the Early Triassic (figure 21), and they were covered by evaporites of about 1000 m thickness originally (compare Schwarzer and Littke, 2005). Large scale post-Zechstein flushing by meteoric water is unlikely in this setting. Furthermore, isotopic evidence for Zechstein fluids from cements in Rotliegend sandstones are very rare in this area, and confined to wells lying on or near uplifted horst blocks (Platt, 1994).

Mixing corrosion is probably restricted to relatively low temperatures and therefore shallow burial, especially where meteoric water mixes with sea water or basinal brines (Giles and Marshall, 1986). In contrast, the mechanisms listed under (3) to (6) are more likely in deeper settings. Mineral dissolution by moving pore-fluids close to overpressure leak-off points (Wilkinson et al., 1997) could apply to certain localities, but cannot explain the widespread leaching patterns in Rotliegend sandstones of the southern basin margin.

Expulsion of organic maturation products like organic acids and carbon dioxide were interpreted to be responsible for major dissolution events in sandstone reservoirs (e.g. Schmidt and McDonald, 1979; Curtis, 1983; Surdam et al., 1984; Burley, 1986; Meshri, 1986). Blake and Walter (1996) demonstrated that carboxylic acid species significantly enhance the dissolution of orthoclase. Alternatively, conversion reactions of smectite and kaolinite to illite release protons, which may lead to expulsion of acidic compaction waters from shale horizons during burial (Bjørlykke, 1983). Giles and Marshall (1986) pointed out that acidic fluids will generally not be capable of causing significant leaching in sandstone reservoirs. Based on mass-balance calculations, they argued that CO_2, organic acids, or acids from clay mineral reactions will be neutralised already in the source rock. However, the authors also mention the potential of rich humic source rocks and coals to generate large quantities of CO_2, which may be sufficient to create some secondary porosity, if source and reservoir rocks are in close hydraulic contact. Van Keer et al. (1998) demonstrated that K-feldspar dissolution and clay mineral formation is enhanced at direct sandstone-coal contacts. Mass balance and fluid migration problems may argue against major influx of aggressive fluids, but there are mechanisms to generate organic acids and CO_2 within the reservoir. Oxidation of kerogen by ferric iron released during transformation of smectite to illite may produce organic acids (Surdam and Crossey, 1985; Crossey et al., 1986). Hematite coatings could also be reduced by liquid HC, resulting in the generation of organic acids and CO_2 (see section 7.2.3). Recent experimental studies suggest that oxidation of n-alkanes to organic acids may be pervasive in sedimentary environments, and that subsequent decarboxylation and/or oxidation reactions may produce substantial amounts of CO_2 (Seewald, 2001a, b; McCollom and Seewald, 2003; Seewald, 2003). Likely oxidising agents are reservoir minerals like iron oxides or sulphates, and formation water. HC decomposition may occur before, during, and after the peak oil generation (Seewald, 2001b, 2003).

Major mineral dissolution in Rotliegend sandstones from the southern margin of the NGB precedes illite formation and bitumen impregnation. The intensity of feldspar corrosion is greatest close to tectonic contacts between the Rotliegend and Carboniferous Coal Measures (Platt, 1991; Deutrich, 1993; Gaupp et al., 1993). Dissolution could be contemporaneous to major CO_2 generation in the underlying Westphalian coals (compare section 4.3). Close to direct hydraulic contacts of Rotliegend sandstones and Carboniferous Coal Measures, the influx of acidic fluids from coal-bearing source rocks is the most likely mechanism to explain the observed leaching processes, as proposed by Gaupp et al. (1993). However, organic acids and CO_2 produced from oxidation of HC compounds within the

sandstones may have been more effective in dissolution of feldspar and early cements, especially in sandstone horizons without close contact to the Carboniferous. Although water is an important oxidising agent, it is not unlikely that hematite coatings of Rotliegend red beds play an important role in HC decomposition, especially since bleached horizons contain less feldspar on average than red sandstones (figure 49). Thus feldspar corrosion was more pervasive in bleached sandstones compared to red sandstones, assuming that the original feldpar content was similar.

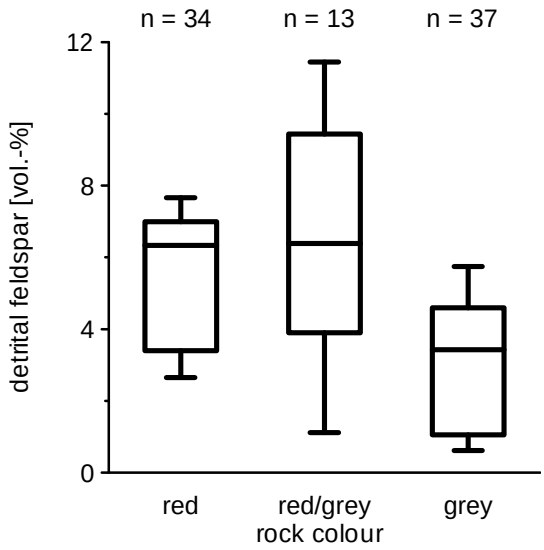

Figure 49: Box-whisker plot of the detrital feldspar content of Rotliegend sandstones (only southern basin margin) for red, intermediate red/grey, and grey rock colours. Feldspar contents derived from thin-section point counting data of 35 wells in total (Platt, 1991; Gaupp and Solms, 2005). The diagram is based on mean values from n reservoir horizons. On average, grey, i.e. bleached sandstones contain less detrital feldspar than red sandstones.

Late, post-bitumen dissolution processes (section 6.5) could again be related to acids generated by redox reactions between HC and reservoir minerals or water. Thermal cracking of HC would be an alternative mechanism to generate corrosive fluids during late diagenesis, although the modelled temperature evolution of the reservoirs is probably not high enough to cause severe oil-to gas cracking (compare section 6.7).

7.2.5 Meshwork illite and bitumen

In the southern study area, mesodiagenetic leaching of feldspar and cements is typically associated with the formation of pervasive meshwork illite, which is characteristically impregnated by solid bitumen (table 7). Kaolinit/dickite may form at the same paragenetic position in rocks with direct hydraulic contact to Carboniferous Coal Measures (Gaupp et al., 1993). Locally, platelets of chlorite with higher average Fe content than earlier radial chlorites pre-date fibrous illite growth. The succession: (1) leaching, (2) illite formation, (3) bitumen impregnation is very typical and appears to be strongly interrelated, although illite is more widespread than solid bitumen. The growth of fibrous illite apparently terminated after impregnation of pore surfaces by HC. As pointed out by Worden and Morad (2003), clay reactions slow down in a water-wet sandstone after oil immigration, and stop if the sandstone is oil-wet. Clay mineral growth has been most intense in areas, where a hydraulic contact to Carboniferous source rocks was available. In the case studies from the northern NBG, where bitumen is missing and no significant petroleum migration can be expected, authigenic illite was only locally observed. There, illite morphologies dominantly indicate replacement of clay matrix and detrital grains. Although fibrous illite is present sporadically, only small parts of the pore space connected to fluid flow were affected by illitisation. Illite formation appears to

have been a localised process, probably controlled by the availability of appropriate elements, which may have been supplied by local feldspar dissolution.

Although the fundamental processes controlling illitisation are poorly understood, the formation of fibrous/meshwork illite in reservoir sandstone appears to be an episodic process that requires relatively unusual geological conditions, as indicated by radiometric ages and theoretical considerations (Lee et al., 1989; Zwingmann et al., 1999; Liewig and Clauer, 2000; Wilkinson and Haszeldine, 2002). Many studies have shown that meshwork illite precipitates from increasingly acidic/CO_2-bearing pore waters during early stages of oil charging, although this is probably not the only mechanism (e.g. Cookenboo and Bustin, 1999; Barclay and Worden, 2000, see section 6.4.8). In the NGB, the timing of illite formation in the latest Triassic to Early Jurassic corresponds to the period of main oil generation in the underlying source rocks (figure 52). Although the onset of (post-Rotliegend) oil generation was much earlier, already in the Early Triassic, solid bitumen always post-dates illite formation. This implies that major oil migration was not directly controlled by the timing of oil generation, but more likely favoured by tectonically induced fluid events. Concordantly, basin modelling in the North Hannover area suggests that oil migration was mainly confined to permeable fault zones (Schwarzer and Littke, 2005). It can be concluded, in coincidence with earlier studies (Gaupp et al., 1993; Platt, 1994; Zwingmann et al., 1998) that pervasive illite and local kaolinite/dickite formation are the result of one or multiple fluid events, which were injecting organic-rich fluids from Carboniferous Coal Measures into Rotliegend red beds. Zwingmann et al. (1999) proposed on the basis of isotopic investigations that illite growth took place during distinct hydrothermal fluid pulses with fluid temperatures exceeding present-day formation temperatures. Liassic hydrothermal activity was most likely related to extensional tectonic activity (Ziegler, 1990; Gaupp et al., 1993). It is not restricted to the NGB but has been noted from several areas in Europe (e.g. Clauer et al., 1996).

Platt (1993) argued that the volume of dickite in Rotliegend sandstones close to the Carboniferous (up to 20%) is significantly greater than could have been produced by feldspar dissolution, and that Al must have been imported into these sandstones. Both Platt (1993) and Deutrich (1993) noted enhanced Al-contents of clay minerals in localities close to fault zones. It has been pointed out that organic acids are capable of dissolving and transporting significant concentrations of metal cations, including aluminium (Curtis, 1983; Surdam et al., 1984; Surdam et al., 1989b; Blake and Walter, 1996). Some workers proposed considerable mass transport of Al from sandstones to shales (Wilkinson and Haszeldine, 1996; Wilkinson et al., 2003), as well as import of Al into sandstones (Gluyas and Leonard, 1995). However, Al mobility in diagenetic environments is commonly considered as being very low, and the efficiency of organic acids to enhance this mobility has been doubted (e.g. Giles and De Boer, 1990; Bjørlykke et al., 1995; Worden and Morad, 2003). However, the pervasive distribution of authigenic illite in the pore system of Rotliegend sandstones, enhanced Al-contents of clay minerals close to fault zones, and the abundance of kaolinite/dickite around Carboniferous horst blocks point to enhanced Al mobility during one or more fluid events, at least on the scale of few hundred meters. On a basin scale, petrographic and geochemical data of Rotliegend sandstones from the southern basin margin provide no evidence for significant import or export of Al. The data suggest relatively conservative behaviour of Al, but export of K from bleached rocks showing strong illitisation (section 6.6). Loss of K has been observed frequently during sandstones diagenesis (Milliken et al., 1994; Thyne, 2001; Wilkinson et al., 2003).

7.2.6 Fe^{2+}-rich authigenic minerals

Fe^{2+}-rich cements are absent from all three case studies at the northern margin of the NGB, where ferric iron remains fixed in hematite. In contrast, mesodiagenetic Fe^{2+}-rich sheet silicates and carbonates are abundant at many localities of the southern NGB, and suggest that ferrous iron was mobile during advanced burial diagenesis. While Fe^{2+}-rich, fan-like chlorite is relatively widespread, ankerite and siderite are only locally important pore-filling cements, and partly fill fractures. Siderite, in particular, is associated with kaolinite/dickite precipitation (Platt, 1991).

Fe^{2+}-rich mesodiagenetic chlorites and ferroan carbonates that formed in deep (>2500 m) and relatively hot (>100°C) environments were found in many reservoirs sandstones (e.g. Burley, 1984; Burton et al., 1987; Dutton and Land, 1988; Burley et al., 1989; Ziegler, 1993; van Keer et al., 1998). Continuous dolomite-ferroan dolomite-ankerite cements may reflect a successively evolving pore fluid during burial (Ziegler, 1993). On the other hand, ferroan carbonates that fill intragranular and large intergranular pore space post-date a period of leaching and cannot be explained in the same way. Barclay and Worden (2000) demonstrated by geochemical modelling that dissolution of detrital K-feldspar may lead to precipitation of authigenic illite, ankerite, and quartz. Late, fan-like chlorite is also often found in secondary pore space (plate 9E). Two main sources of dissolved Fe^{2+} have been claimed: (1) smectite to illite reactions, which release Si, Ca, Na, Fe, and Mg (Boles and Franks, 1979; Boles, 1981); and (2) reduction of iron oxides (Curtis et al., 1985; Surdam et al., 1993). The first mechanism involves mass transport of elements from adjacent shales into sandstone horizons. Iron oxides are available from hematite coatings within the red beds.

Quantitative petrographic data from the southern margin of the NGB suggest that the percentage of Fe^{2+}-rich chlorite is higher in bleached sandstones than in red sandstones (figure 48C). Similar relationships were observed previously in other red bed sandstones containing bleached areas (Thompson, 1970). Furthermore, the abundance of Fe^{2+}-rich chlorite appears to be related to the intensity of bitumen impregnation. In areas of strong bitumen impregnation, which have to be interpreted as petroleum migration pathways, ferric iron is absent, but ferrous iron was incorporated in authigenic chlorite (figure 50A, B). Electron microprobe investigations have shown that the iron content of authigenic chlorite decreases with increasing distance to fault zones (Deutrich, 1993). These petrographic and geochemical data may be interpreted as evidence for injection of reducing, HC-bearing fluids via faults into Rotliegend red beds. The average bulk rock iron content of bleached sandstones is not significantly lower compared to red sandstones, although some red beds may be exceptionally rich in iron (figure 51). On a basin scale, bulk rock geochemistry argues against substantial mass transport of iron from/to the rocks investigated. The average iron content of chlorites in bleached sandstones can be balanced by dissolution of about 0.5 wt.-% Fe_2O_3 in the sandstones, as can be shown by simple mass balancing (table A16). This result corresponds to the estimated iron content stored in hematite coatings (0.3-2.0 wt.-% Fe_2O_3, see above). In conclusion, the formation of late Fe-rich chlorite may result from influx of reducing petroleum fluids, which caused bleaching of red beds by reduction and dissolution of hematite, and a major leaching event. These results support the view of Surdam et al. (1993), who suggested that once HC become part of the fluid phase, any subsequent iron-bearing diagenetic phases are ferroan rich.

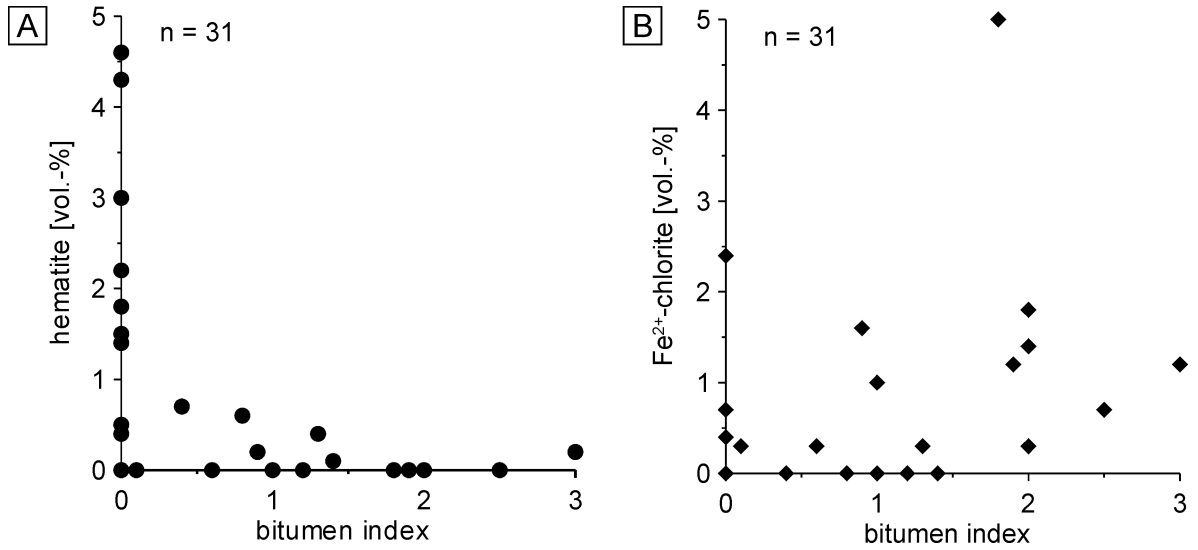

Figure 50: Solid bitumen index versus abundance of hematite coatings (A) and authigenic Fe^{2+}-rich chlorite. Each data point represents the mean of one reservoir horizon of on well, derived from point counting data of n wells in total (Platt, 1991; Deutrich, 1993; Cord, 1994; Gaupp and Solms, 2005). Bitumen index: 0 = no bitumen is present, 3 = strong bitumen impregnation. Sandstones impregnated by considerable bitumen are commonly free of hematite, but contain relatively high contents of Fe^{2+}-rich chlorite.

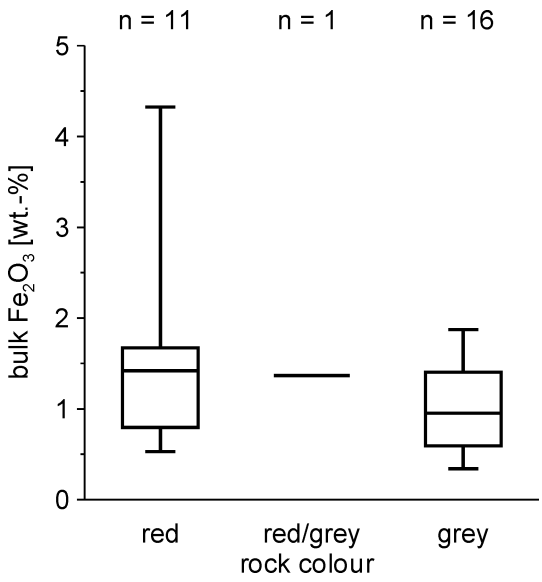

Figure 51: Box-whisker plot of bulk rock iron content of fine to medium grained Rotliegend sandstones for red, intermediate red/grey, and grey rock colours. Iron contents derived from XRF analysis (Deutrich, 1993; Hartmann, 1997; this study). The diagram is based on mean values from n reservoir horizons of 15 wells in total. On average, grey, i.e. bleached sandstones contain only slightly less iron than red sandstones.

7.2.7 Pore-filling late cements

Although clay minerals surfaces impregnated by bitumen were often not overgrown by later cements, there are a number of examples from the southern basin margin, where the pore space was occluded by late quartz cement. Close intergrowth of quartz and bitumen stained illite, HC-inclusions within quartz cements, and quartz volumes demanding an external source of silica suggest a relation of this late quartz generation to petroleum migration. Fluid inclusion studies (Rieken, 1988; Gaupp et al., 1996) indicate temperatures higher than the expected Mesozoic formation temperatures for the solutions that formed these quartz cements (>130°C). These elevated temperatures could be explained by episodic hot fluid events, which were also claimed by Zwingmann et al. (1999) based on isotopic investigations. Fluid inclusion studies from other areas have shown that authigenic quartz may precipitate from two-phase fluids containing petroleum and aqueous components (Parnell et

al., 1996; Wilkinson et al., 1998; Cookenboo and Bustin, 1999). Quartz cements grew even at high oil saturations under experimental condition (Teinturier and Pironon, 2004). Spötl et al. (2000) described late quartz cements that formed at temperatures of >150°C to at least 200°C and post-date liquid HC emplacement, and probably also thermal cracking of these HC. However, the origin and formation mechanism of this cement type is still not clear. No comparable diagenetic features were observed at the northern margin of the NGB.

Locally, late calcite, anhydrite, or barite cements fill the pore space after illitisation and bitumen impregnation. In contrast to late quartz cements, they are commonly not intergrown with fibrous illite. The ions required for these cements may derive from dissolution of earlier cement generations, from feldspar dissolution, or from smectite-illite reactions in adjacent mudstones (compare Boles and Franks, 1979). Influx of Zechstein fluids may locally also be responsible for late carbonate/sulphate cements in Rotliegend sandstones of the southern basin margin. However, Platt (1994) showed by isotopic investigations that significant influence of Zechstein fluids on Rotliegend diagenesis in northern Germany is only noted in wells lying on or close to uplifted horst blocks.

7.3 Possible causes for contrasting red bed diagenesis, and implications for the importance of organic maturation and migration

Comparison of diagenetic data from the southern and northern margin of the NGB indicates that the following phenomena are spatially related to the presence of organic-rich Carboniferous source rocks (table 7):

(1) bleaching of red bed sandstones by reduction of hematite grain coatings,

(2) massive dissolution of unstable grains and carbonates/sulphates during different stages of burial,

(3) formation of pervasive meshwork illite and locally kaolinite/dickite,

(4) impregnation of pore surfaces by solid bitumen,

(5) precipitation of late Fe^{2+}-rich sheet silicates and carbonates,

(6) local extensive late post-bitumen quartz cementation.

The spatial coincidence of these phenomena suggests a causal interrelation. Their occurrence can be interpreted as a result of the interaction of migrating petroleum-bearing fluids with red bed reservoirs, which is most obvious in cases where a direct hydraulic contact to petroleum source rocks exists (compare Gaupp et al., 1993; Gaupp et al., 2005). The temporal succession and the presence of paleo-oil (bitumen) denote the importance of liquid HC and their precursors in bleaching, feldspar/cement leaching and illite formation. It should be noted that the use of petrographic and geochemical data to reconstruct mineral reactions has limitations. As pointed out above, there are several possible mechanisms for most of the mesodiagenetic processes, which are inferred to be related to petroleum migration here. It is also not clear if the organic-inorganic reactions involved in this model are capable of explaining quantitatively the observed mineral reactions. Future experimental studies and quantitative diagenetic modelling may help to solve these problems. However, the easiest way to explain the spatial relationships of diagenetic patterns in Rotliegend sandstones from

Table 7: Summary of major differences between source rock distribution and red bed diagenesis at the southern and northern margin of the NGB.

SOUTHERN MARGIN	**NORTHERN MARGIN**	**OF THE NGB**
source rock distribution		
area-wide thick high quality Carboniferous source rocks present	source rocks absent, or only minor Lower Carboniferous source rocks with low TOC present	
diagenetic features		**inferred processes / possible organic-inorganic reactions**
widespread bleaching of red bed sandstones	no evidence for bleaching, hematite preserved down to maximum burial depth	reduction of hematite coatings by liquid HC or their precursors
(late) mesodiagenetic Fe-rich carbonates and sheet silicates	no Fe-rich mesodiagenetic cements	incorporation of ferrous iron into authigenic phases during mesodiagenesis
mesodiagenetic dissolution of grains (mainly feldspar) and reversible cements	only locally evidence for mesodiagenetic feldspar and cement leaching	influx of acid/CO_2-rich fluids from Carboniferous source rocks, generation of organic acids/CO_2 by HC oxidation within sandstones
formation of pervasive authigenic meshwork illite	only very locally meshwork illite formation	relation of strong illite formation to migration of organic maturation products into reservoirs
widespread solid bitumen impregnation	no evidence for solid bitumen	impregnation of pore surfaces by hydrocarbons (oil/asphaltene), and subsequent oxidation of hydrocarbons
frequently no further cementation after bitumen impregnation	not applicable	termination of sheet silicate growth and inhibition of further cementation by hydrophobisation
late feldspar and/or cement leaching after bitumen impregnation	very localised minor late feldspar leaching in stabilised grain framework	generation of acid fluids by HC oxidation in red bed reservoirs
locally pervasive late quartz cementation with HC-inclusions	no late quartz cementation	possible relation to late petroleum migration (?)

the southern part of the NGB, the co-occurrence of specific phenomena, and their relative timing with respect to organic maturation is to assume fluid import from Upper Carboniferous strata. These fluids may have reacted with red bed sandstones in multiple ways. The expulsion of aggressive acidic solutions from the source rocks should be considered at least for Rotliegend sandstones with direct hydraulic contact to the Carboniferous. Coal-rich rocks, which have a high CO_2 generation potential, are likely to release CO_2-bearing fluids into adjacent reservoir horizons. Organic acids or liquid HC are the most likely reducing agents for bleaching reactions. It has been noticed in other studies, too, that bleached sandstones are often affected by mesodiagenetic leaching processes (Muchez et al., 1992; Surdam et al., 1993). HC oxidation by ferric oxide or water within reservoir sandstones can create considerable amounts of organic acids and CO_2, which have the capacity to dissolve carbonate cements and detrital feldspars (Shebl and Surdam, 1996; Seewald, 2001a, 2003). Dissolution of K-feldspar, probably in combination with enhanced mobility of Al and Si in the

presence of organic compounds (Blake and Walter, 1996), was responsible for precipitation of pervasive meshwork illite, which occurred contemporaneously to the period of main oil generation the upper part of the Carboniferous.

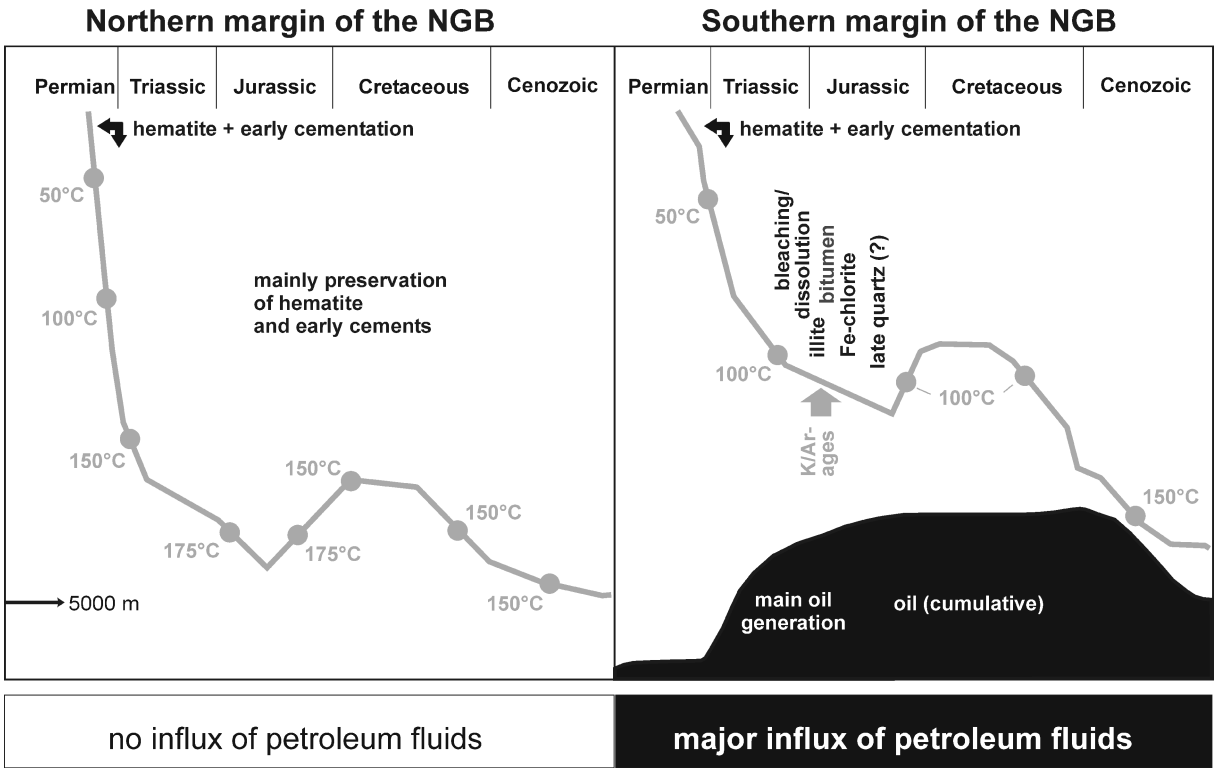

Figure 52: Schematic model of diagenetic evolution at the northern and southern margin of the NGB. Burial history and temperatures from the northern basin margin taken from well Flensburg Z1. Example of burial history and temperatures of the southern basin margin from Schwarzer and Littke (2005; well TG 35).

Areas that were not affected by petroleum influx from the Carboniferous may have retained cementation patterns dominated by early to shallow burial diagenetic processes. Such areas are e.g. horizons where sebkha-type cements are preserved. The fluid system obviously did not change significantly and therefore did not allow a major reorganisation of diagenetic patterns. The case studies from the northern margin of the NGB support this interpretation. The petrographic features listed above are absent there, except very localised grain dissolution and illite formation in relatively high porosity sandstones, which are stratigraphically overlying Lower Carboniferous rocks. Minor influence of Carboniferous fluids, potentially enriched in organic components, cannot be excluded in that case.

In conclusion, there is evidence from microscopic scale to basin scale that the type and distribution of mesodiagentic phases are influenced by the presence or absence of organic maturation products. The most important arguments supporting this conclusion are (1) the spatial relationship of specific diagenetic features to maturing petroleum source rocks on a basin scale, (2) the co-occurrences and relative timing of a suite of mesodiagenetic features, including bitumen relics, and (3) the timing of diagenetic reactions in relation to organic maturation. It is suggested that not only solid bitumen, but also specific diagenetic patterns can be used to trace paleo petroleum migration pathways.

8 Conclusions

The northern and southern margin of the North German Basin are contrasting with respect to distribution of petroleum source rocks and clastic diagenesis of deeply buried Rotliegend sandstones. Results from petrographic and geochemical investigations, and spatial patterns of specific petrographic phenomena suggest that major mesodiagenetic mineral reactions in red bed sandstones are controlled by the presence or absence of maturing petroleum source rocks. The main conclusions of the comparative study in the North German Basin are:

Source rocks, organic maturation, and migration

(1) At the northern basin margin (northern Schleswig-Holstein), it is unlikely that organic maturation products have affected Rotliegend sandstones to a great extent. The Upper Carboniferous was largely eroded in this area prior to Rotliegend deposition. Coals are absent according to data available. Lower Carboniferous rocks with poor source rock properties are present in the Glückstadt-Graben area, and probably around Fehmarn. Where remnant Carboniferous rocks are preserved, oil generation was completed before the end of the Triassic. Much of the liquid hydrocarbons generated may have been thermally cracked within the source rocks due to rapid heating to temperatures around 200°C in the Triassic.

(2) Carboniferous source rocks are omnipresent and thick beneath the Rotliegend of the southern basin margin (northern Lower Saxony). The Upper Carboniferous, which is the most important source rock interval, comprises predominantly gas-prone terrigenous organic material (coal), but also oil source rocks to a limited extent. Generation of CO_2 and liquid hydrocarbons started in the Late Carboniferous. The main cumulative oil generation from Westphalian rocks took place in the Triassic and Early Jurassic. It can be expected that expulsion of liquid hydrocarbons occurred mainly in this time interval, especially during phases of tectonic activity and elevated fluid flow.

Sedimentology

(3) In contrast to the southern margin of the North German Basin, where a broad alluvial-eolian sandstone belt developed during of the Upper Rotliegend, major sandstone horizons at the northern basin margin are confined to the base of the Upper Rotliegend (Havel Subgroup) in the wells investigated. 0 to 700 m of alluvial sandstones and conglomerates, and very subordinate eolian sandstones, were deposited at different localities of Schleswig-Holstein. The clastic material at the northern basin margin was supplied by local alluvial systems that were draining the northern hinterland (Ringkøbing-Fyn/Fennoscandian High). Substantial differences in thickness between individual localities suggest fault controlled sedimentation during the Early Upper Rotliegend of Schleswig-Holstein.

Diagenesis

(4) Eodiagenetic and early mesodiagenetic processes are comparable at both basin margins. They include the formation of hematite and tangential illite grain coatings, precipitation of minor quartz or albite, and growth of carbonate and sulphate cements, which partly fill the pore space. Grain rimming Mg-rich chlorite formed locally in lake

margin sandstones at the southern basin margin, and in fluvial channel sandstones at the northern basin margin. Early red bed diagenesis was mainly controlled by depositional environment, and by the relative position within the basin.

(5) Major mesodiagenetic features are spatially related to the occurrence of petroleum source rocks. Most important features are bleaching of red beds and precipitation of Fe^{2+}-rich cements, major dissolution of unstable grains and reversible cements, formation of pervasive meshwork illite, impregnation of pore surfaces by solid bitumen, and locally extensive late post-bitumen quartz cementation. The spatial coincidence of this suite of processes and their occurrence in red bed sandstones with hydraulic contact to organic-rich source rocks suggest that they trace paleo petroleum migration pathways. In areas where considerable source rocks are absent or scarce, like in the case studies from the northern basin margin, there is no evidence for a prominent mesodiagenetic rearrangement within the pore space of Rotliegend sandstones.

(6) Eodiagenetic Fe^{3+}-oxide grain coatings must have been almost omnipresent primarily due to Rotliegend facies and climate conditions. The iron content stored within these coatings is typically between 0.3 and 2 wt.-% Fe_2O_3. They can be preserved down to more than 4000 m of burial, which is the case in the northern part of the North German Basin. Bleaching of red staining by reduction of hematite coatings is recorded in sandstones, which have been affected by reducing fluids expelled from petroleum source rocks. The precipitation of mesodiagenetic, Fe^{2+}-rich chlorite is also related to bleaching and bitumen impregnation. The amount of iron within these chlorites can be balanced by dissolution of about 0.5 wt.-% hematite in the sandstones.

(7) Major dissolution of unstable detrital grains (mainly feldspar) as well as intergranular cements (carbonates/sulphates) was followed by pervasive meshwork illite formation and subsequent bitumen impregnation. Illite formation was contemporaneous to the period of main oil generation in the underlying source rocks. Leaching processes may have been caused by acidic fluids from CO_2 released during maturation of Carboniferous coals, and by organic acids and/or CO_2 that were generated due to oxidation of hydrocarbon compounds within the red beds.

(8) Although major oil generation in the Upper Carboniferous started in the Early Triassic, solid bitumen impregnation always post-dates illite formation, which has been dated to about 180-200 Ma. This implies that main oil migration was not directly controlled by the timing of oil generation, but more likely favoured by tectonically induced fluid events.

(9) In summary, the easiest model to explain the contrasting mesodiagenetic evolution in Rotliegend sandstones of the North German Basin is to assume that migration of liquid hydrocarbons and their precursors caused major rearrangement of cementation patterns in red beds with hydraulic contact to Carboniferous source rocks. Acidic, CO_2-bearing pore waters, injected from maturing coal-bearing rocks, had some potential to cause dissolution of feldspar and reversible cements. Hydrocarbons migrated into horizons of enhanced porosity. Oxidation of hydrocarbon compounds most likely caused bleaching by reduction of hematite, and may have produced organic acids and CO_2 within the reservoir sandstones. K-feldspars dissolved and provided the ions necessary for illite formation. Solid bitumen probably formed due to asphaltene precipitation and/or hydrocarbon oxidation reactions. Impregnation of pore surfaces by bitumen retarded further

cementation in some cases. Reduced iron was incorporated in Fe^{2+}-rich mesodiagenetic minerals. Local extensive late (post-bitumen) quartz cementation may have been related to petroleum migration, too, although the origin of this cement is still unclear. Such processes are not expected in areas, where red beds were not affected by petroleum migration during burial.

The comparison of two contrasting basin margins of the North German Basin can improve the understanding of organic-inorganic interactions during diagenesis of Rotliegend sandstone reservoirs. The results of this study may help to interpret the diagenetic evolution of red bed sandstones in more complex basin settings, where the distribution of source rocks and migration pathways of organic maturation products are less clear. However, further research including experimental studies is necessary to understand and finally to model the complex set of mineral reactions which are apparently controlled or influenced by organic maturation products.

9 References

Aagaard, P., Egeberg, P.K., Saigal, G.C., Morad, S. and Bjørlykke, K. (1990): Diagenetic albitization of detrital K-feldspars in Jurassic, Lower Cretaceous and Tertiary clastic reservoir rocks from offshore Norway, II. Formation water chemistry and kinetic considerations.– J. Sediment. Petrol., **60**: 575-581.

Aagaard, P., Jahren, J.S., Harstad, A.O., Nilsen, O. and Ramm, M. (2000): Formation of grain-coating chlorite in sandstones. Laboratory synthesized vs. natural occurrences.– Clay Min., **35**: 261-269.

Aigner, T. and Bachmann, G.H. (1992): Sequence-stratigraphic framework of the German Triassic.– Sed. Geol., **80**: 115-135.

Allen, P.A. and Allen, J.R. (1997): Basin Analysis: Principles and Applications.– 451 pp.; Oxford (Blackwell).

Allis, R., Chidsey, T., Gwynn, W., Morgan, C., White, S., Adams, M. and Moore, J. (2001): Natural CO_2 reservoirs on the Colorado Plateau and Southern Rocky Mountains: candidates for CO_2 sequestration.– Proceedings of the First National Conference on Carbon Sequestration, 1-19; Washington DC.

Almon, W.R. (1981): Depositional environment and diagenesis of Permian Rotliegendes sandstones in the Dutch sector of the Southern North Sea.– In: Longstaffe, F.J. (ed.), Clays and the Resource Geologist, Mineral. Assoc. Canada Short Course Handbook, **7**: 119-147; Calgary.

Andrews-Speed, C.P., Oxburgh, E.R. and Cooper, B.A. (1984): Temperatures and Depth-Dependent Heat Flow in Western North Sea.– AAPG Bull., **68**(11): 1764-1781.

April, R.H. (1981): Trioctahedral smectite and interstratified chlorite/smectite in Jurassic strata of the Connecticut Valley.– Clays Clay Min., **29**(1): 31-39.

Baccar, M.B., Fritz, B. and Madé, B. (1993): Diagenetic albitization of K-feldspar and plagioclase in sandstone reservoirs: thermodynamic and kinetic modeling.– J. Sediment. Petrol., **63**(6): 1100-1109.

Bachmann, G.H. and Grosse, S. (1989): Struktur und Entstehung des Norddeutschen Beckens - geologische und geophysikalische Interpretation einer verbesserten Bouger-Schwerekarte.– Nds. Akad. Geowiss. Veröfftl., **1989**(2): 23-47.

Bachmann, G.-H. and Hoffmann, N. (1997): Development of the Rotliegend Basin in Northern Germany.– Geol. Jb., **D103**: 9-31.

Bailey, S.W., Alietti, A., Brindley, G.W., Formosa, M.L.L., Jasmund, K., Konta, J., Mackenzie, R.S., Nagasawa, K., Rausell-Colom, R.A. and Zvyagin, B.B. (1980): Summary of recommendations of AIPEA Nomenclature Commitee.– Clays Clay Min., **28**: 73-78.

Baisert, D. (1975): Postsedimentäre Prozesse bei der Ausbildung von Granularspeichern.– Z. angew. Geol., **21**(11): 533-536.

Baisert, D. (1990): Zeitliche Fixierung diagenetischer Prozesse in Saxon-Sandsteinen der DDR.– Z. angew. Geol., **36**(7): 253-256.

Baldschuhn, R. (1979): Stratigraphie und Verbreitung des Dan (Tertiär) in Nordwestdeutschland.– Z. dt. geol. Ges., **130**: 201-209.

Baldschuhn, R., Best, G., Deneke, E., Frisch, U., Jürgens, U., Kockel, F., Schmitz, J., Sattler-Kosinowski, S., Stancu-Kristoff, G. and Zirngast, M. (1996): Geotektonischer Atlas von NW-Deutschland 1:300000.– Hannover (BGR).

Baldschuhn, R., Binot, F., Fleig, S. and Kockel, F. (2001): Geotektonischer Atlas von Nordwest-Deutschland und dem deutschen Nordsee-Sektor.– Geol. Jb., **A 153**: 3-95.

Bandlowa, T. (1990): Lagerstättenbildung in Teilgebieten der Mitteleuropäischen permokarbonischen Erdgasprovinz.– Z. angew. Geol., **36**(9): 336-341.

Bandlowa, T. (1998): Erdgasführung im Karbon-Perm-Trias-Komplex der Mitteleuropäischen Senke.– Geol. Jb., **A 151**: 3-65.

Barclay, S.A. and Worden, R.H. (2000): Geochemical modelling of diagenetic reactions in a sub-arkosic sandstone.– Clay Min., **35**: 57-67.

Barker, C. and Takach, N.E. (1992): Prediction of Natural Gas Composition in Ultradeep Sandstone Reservoirs.– AAPG Bull., **76**(12): 1859-1873.

Bath, A.H., Milodowski, A.E. and Spiro, B. (1987): Diagenesis of carbonate cements in Permo-Triassic sandstone in the Wessex and East Yorkshire - Lancashire basins, UK: a stable isotope study.– In: Marshall, J.D. (ed.), Diagenesis of sedimentary sequences, Geol. Soc. Spec. Pub., **36**: 173-190; London.

Bauer, A., Velde, B. and Gaupp, R. (2000): Experimental constraints on illite crystal morphology.– Clay Min., **35**: 587-597.

Baunack, C. (2002): Petrographische Untersuchungen und Modellierung der Quarzdiagenese in Rotliegend-Sandsteinen des Norddeutschen Beckens.– Diploma Thesis, Univ. Jena, 85 pp.

Beard, D.C. and Weyl, P.K. (1973): Influence of texture on porosity and permeability of unconsilidated sand.– AAPG Bull., **57**(2): 349-369.

Behar, F., Vandenbroucke, M., Tang, Y., Marquis, F. and Espitalie, J. (1997): Thermal cracking of kerogen in open and closed systems: determination of kinetic parameters and stoichiometric coefficients for oil and gas generation.– Org. Geochem., **26**(5-6): 321-339.

Beitler, B., Chan, M.A. and Parry, W.T. (2003): Bleaching of Jurassic Navajo Sandstone on Colorado Plateau Laramide highs: Evidence of exhumed hydrocarbon supergiants?– Geology, **31**(12): 1041-1044.

Bender, F. and Hedemann, H.-A. (1983): Zwanzig Jahre erfolgreiche Rotliegend-Exploration in Nordwestdeutschland - weitere Aussichten auch im Präperm?– Erdöl-Erdgas, **99**: 39-49.

Benek, R., Kramer, W., McCann, T., Scheck, M., Negendank, J.F.W., Korich, D., Huebscher, H.-D. and Bayer, U. (1996): Permo-Carboniferous magmatism of the Northeast German Basin.– Tectonophysics, **266**: 379-404.

Bentz, A. (1958): Relations between oil fields and sedimentary troughs in northwest German Basin.– In: Weeks, L.G. (ed.), Habitat of Oil, 1054-1066; Tulsa.

Berthelsen, A. (1992a): Mobile Europe.– In: Blundell, D., Freeman, R. and Mueller, S. (eds.), A Continent Revealed - The European Geotraverse, 11-32; Cambridge (Cambridge University Press).

Berthelsen, A. (1992b): From Precambrian to Variscan Europe.– In: Blundell, D., Freeman, R. and Mueller, S. (eds.), A Continent Revealed - The European Geotraverse, 153-164; Cambridge (Cambridge University Press).

Best, G., Kockel, F. and Schöneich, H. (1983): Geological history of the southern Horn Graben.– In: Kaasschieter, J.P.H. and Reijers, T.J.A. (eds.), Petroleum geology of the southeastern North Sea and the adjacent onshore areas, Geol. Mijnbouw, **62**: 25-33.

Betz, D., Führer, F., Greiner, G. and Plein, E. (1987): Evolution of the Lower Saxony Basin.– Tectonophysics, **137**: 127-170.

Beutler, G., Heunisch, N., Luppold, F.W., Rettig, B. and Röhling, H.-G. (1996): Muschelkalk, Keuper, Lias am Mittellandkanal bei Sehnde (Niedersachsen) und die regionale Stellung des Keupers.– Geol. Jb., **A 145**: 67-197.

Beutler, G., Hauschke, N. and Nitsch, E. (1999): Faziesentwicklung des Keupers im Germanischen Becken.– In: Hauschke, N. and Wilde, N. (eds.), Trias - Eine ganz andere Welt, 129-174; München (Pfeil).

Beutler, G. and Szulc, J. (1999): Die Paläogeographische Entwicklung des Germanischen Beckens in der Trias und die Verbindung zur Tethys.– In: Hauschke, N. and Wilde, N. (eds.), Trias - Eine ganz andere Welt, 71-80; München (Pfeil).

Bjørkum, P.A. and Gjelsvik, N. (1988): An isochemical model for formation of authigenic kaolinite, K-feldspar and illite in sediments.– J. Sediment. Petrol., **58**(3): 506-511.

Bjørlykke, K. (1983): Diagenetic reactions in sandstones.– In: Parker, A. and Sellwood, B.W. (eds.), Sediment Diagenesis, 169-213; Dordrecht, Boston, Lancaster (Reidel).

Bjørlykke, K. (1984): Formation of secondary porosity: How important is it?– In: Mcdonald, D.A. and Surdam, R.C. (eds.), Clastic Diagenesis, AAPG Mem., **37**: 277-289; Tulsa.

Bjørlykke, K. and Brendsdal, A. (1986): Diagenesis of the Brent Sandstone in the Statfjord Field, North Sea.– In: Gautier, D.L. (ed.), Roles of Organic Matter in Sediment Diagenesis, SEPM Spec. Pub., **38**: 157-167; Tulsa.

Bjørlykke, K., Ramm, M. and Saigal, G.C. (1989): Sandstone diagenesis and porosity modification during basin evolution.– Geol. Rundsch., **78**(1): 243-268.

Bjørlykke, K. and Aagaard, P. (1992): Clay minerals in North Sea sandstones.– In: Houseknecht, D.W. and Pittman, E.D. (eds.), Origin, Diagenesis, and Petrophysics of Clay Minerals in Sandstones, SEPM Spec. Pub., **47**: 65-80.

Bjørlykke, K., Aagaard, P., Egeberg, P.K. and Simmons, S.P. (1995): Geochemical constraints from formation water analyses from the North Sea and the Gulf Coast Basins on quartz, feldspar and illite precipation in reservoir rocks.– In: Cubitt, J.M. and England, W.A. (eds.), The Geochemistry of Reservoirs, Geol. Soc. Spec. Pub., **86**: 33-50; London.

Blair, T.C. and McPherson, J.G. (1994): Alluvial fans and their natural distiction from rivers based on morphology, hydraulic processes, sedimentary processes, and facies assemblages.– J. Sediment. Res., **A64**(3): 450-489.

Blake, R.E. and Walter, L.M. (1996): Effects of organic acids on the dissolution of orthoclase at 80°C and pH 6.– Chem. Geol., **132**: 91-102.

Blundell, D., Freeman, R. and Mueller, S.A. (eds.) (1992): A Continent Revealed -The European Geotraverse.– 261 pp.; Cambridge (Cambridge University Press).

Boigk, H., Stahl, W.J., Teichmüller, M. and Teichmüller, R. (1971): Inkohlung und Erdgas.– Fortschr. Geol. Rheinld. u. Westf., **19**: 101-108.

Boigk, H. (1981a): Die Erdöl- und Erdgaserschließung in Deutschland.– Oel, **1981**(10): 260-268.

Boigk, H. (1981b): Erdöl und Erdölgas in der Bundesrepublik Deutschland.– 330 pp.; Stuttgart (Enke).

Boles, J.R. and Franks, S.G. (1979): Clay diagenesis in Wilcox sandstones of southwest Texas: implications of smectite diagenesis on sandstone cementation.– J. Sediment. Petrol., **49**: 55-70.

Boles, J.R. (1981): Clay diagenesis and effects on sandstone cementation (case histories from the Gulf Coast Tertiary).– In: Longstaffe, F.J. (ed.), Clays and the Resource Geologist, Mineral. Assoc. Canada Short Course Handbook, **7**: 148-166; Calgary.

Boles, J.R. (1982): Active albitization of plagiclase in Gulf Coast Tertiary.– Am. J. Sci., **282**: 165-180.

Boles, J.R. and Ramseyer, K. (1987): Diagenetic Carbonate in Miocene Sandstone Reservoir, San Joaquin Basin, California.– AAPG Bull., **71**(12): 1475-1487.

Boreham, C.J. and Powell, T.G. (1993): Petroleum Source Rock Potential of Coal and Associated Sediments: Qualitative and Quantitative Aspects.– In: Law, B.E. and Rice, D.D. (eds.), Hydrocarbons from coal, AAPG Studies in Geology, **38**: 133-157; Tulsa.

Bouchet, A., Meunier, A. and Sardini, P. (2000): Minéraux argileux: Structure cristalline, Indentification par diffraction de rayon X.– Bull. Centres Rech. Explor.-Prod. Elf Aquitaine, Mem., **23**: 136.

Brand, E. and Hoffmann, K. (1963): Stratigraphie und Fazies des nordwestdeutschen Jura und Bildungsbedingungen seiner Erdöllagerstätten.– Erdöl und Kohle, Erdgas, Petrochemie, **16**(6): 437-450.

Breitkreuz, C. and Kennedy, A. (1999): Magmatic flare-up at the Carboniferous/Permian boundary in the NE German Basin revealed by SHRIMP zircon ages.– Tectonophysics, **302**(307-326).

Brindley, G.W. and Brown, G. (eds.) (1980): Crystal structures of clay minerals and their X-ray identification.– Mineral. Soc. Monograph, **5**, 495 pp.; London.

Brink, H.-J. (1984): Die Salzstockverteilung in Nordwestdeutschland.– Geowissenschaften in unserer Zeit, **2**(5): 160-166.

Brink, H.-J., Franke, D., Hoffmann, N., Horst, W. and Oncken, O. (1990): Structure and Evolution of the North German Basin.– In: Freeman, R., Giese, P. and Mueller, S. (eds.), The European Geotraverse: Integrated Studies, 195-212; Strasbourg (European Science Foundation).

Brink, H.-J., Dürschner, H. and Trappe, H. (1992): Some aspects of the late and post-Variscan development of the Northwestern German Basin.– Tectonophysics, **207**: 65-95.

Brown, B.E. and Bailey, S.W. (1962): Chlorite polytypism: I. Regular and semi-random one-layer structures.– Amer. Mineral., **47**(7-8): 819-850.

Budzinski, H. and Judersleben, G. (1980): Zur Diagenese tonarmer Sandsteine.– Z. angew. Geol., **26**: 302-308.

Burley, S.D. (1984): Patterns of diagenesis in the Sherwood Sandstone Group (Triassic), United Kindom.– Clay Min.,(19): 403-440.

Burley, S.D. (1986): The development and destruction of porosity within Upper Jurassic reservoir sandstones of the Piper and Tartan Fields, Outer Moray Firth, North Sea.– Clay Min., **21**: 649-694.

Burley, S.D., Mullis, J. and Matter, A. (1989): Timing diagenesis in the Tartan Reservoir (UK North Sea): constraints from combined cathodoluminescence microscopy and fluid inclusion studies.– Mar. Petrol. Geol., **6**: 98-120.

Burnham, A.K. (1989): A simple kinetic model of petroleum formation and cracking.– Lawrence Livermore National Laboratory Report UCID-21665, 11 pp.

Burton, J.H., Krinsley, D.H. and Pye, K. (1987): Authigenesis of kaolinite and chlorite in Texas Gulf Coast sediments.– Clays Clay Min., **35**(4): 291-296.

Campbell, K.A., Farmer, J.D. and Des Marais, D. (2002): Ancient hydrocarbon seeps from the Mesozoic convergent margin of California: carbonate geochemistry, fluids and palaeoenvironments.– Geofluids, **2**: 63-94.

Carothers, W.W. and Kharaka, Y.K. (1978): Aliphatic Acid Anions in Oil-Field Waters - Implications for Origin of Natural Gas.– AAPG Bull., **62**(12): 2441-2453.

Cermak, V. (1979): Heat flow map of Europe.– In: Rybach, L. (ed.), Terrestrial Heat Flow in Europe, 3-40; Berlin (Springer).

Cermák, V. (1979): Heat flow map of Europe.– In: Cermak, V. and Rybach, L. (eds.), Terrestrial Heat Flow in Europe, 3-40; Berlin (Springer).

Chan, M.A., Parry, W.T. and Bowman, J.R. (2000): Diagenetic Hematite and Manganese Oxides and Fault-Related Fluid Flow in Jurassic Sandstones, Southeastern Utah.– AAPG Bull., **84**(9): 1281-1310.

Chukhrov, F.V. (1973): On mineralogical and geochemical criteria in the genesis of red beds.– Chem. Geol., **12**: 67-75.

Claret, F., Bauer, A., Schäfer, T., Griffault, L. and Lanson, B. (2002): Experimental investigation of the interaction of clays with high-pH solutions: A case study from the Callovo-Oxfordian Formation, Meuse-Haute Marne Underground Laboratory (France).– Clays Clay Min., **50**(5): 633-646.

Clark, D.N. and Tallbacka, L. (1980): The Zechstein deposits of southern Denmark.– Contr. Sedimentology, **9**: 205-231.

Clauer, N., Zwingmann, H. and Chaudhuri, S. (1996): Extent and importance of the Liassic hydrothermal activity in Western Europe based on isotopic constraints from contemporaneous mica-type minerals.– Clay Min., **31**: 301-318.

Clauer, N., Rinckenbach, T., Weber, F., Sommer, F., Chaudhuri, S. and O'Neil, J.R. (1999): Diagenetic Evolution of Clay Minerals in Oil-Bearing Neogene Sandstones and Associated Shales, Mahakam Dalta Basin, Kalimantan, Indonesia.– AAPG Bull., **83**(1): 62-87.

Colson, I. and Cojan, I. (1996): Groundwater dolcretes in a lake-margin environment: an alternative model for dolocrete formation in continental settings (Danian of the Provence Basin, France).– Sedimentology, **43**: 175-188.

Connan, J. (1984): Biodegradation of crude oils in reservoirs.– In: Brooks, J. and Welte, D.H. (eds.), Advances in petroleum geochemistry, **1**: 299-335; New York (Academic Press).

Cookenboo, H.O. and Bustin, R.M. (1999): Pore water evolution in sandstones of the Groundhog Coalfield, northern Bower Basin, British Columbia.– Sed. Geol., **123**: 129-146.

Cord, M. (1994): Diagenese äolischer Sandsteine im Oberrotliegenden Norddeutschlands.– Diss., Univ. Mainz, 119 pp.

Cornell, R.M. and Schwertmann, U. (1996): The Iron Oxides.– 573 pp.; Weinheim (VCH).

Crossey, L.J., Hagen, E.S., Surdam, R.C. and Lapoint, T.W. (1986a): Correlation of organic parameters derived from elemental analysis and programmed pyrolysis of kerogen.– In: Gautier, D.L. (ed.), Roles of Organic Matter in Sediment Diagenesis, SEPM Spec. Pub., **38**: 35-45; Tulsa.

Crossey, L.J., Surdam, R.C. and Lahann, R. (1986b): Application of organic/inorganic diagenesis to porosity prediction.– In: Gautier, D.L. (ed.), Roles of Organic Matter in Sediment Diagenesis, SEPM Spec. Pub.,**38**: 147-155; Tulsa.

Crossey, L.J. and Larsen, D. (1992): Authigenic mineralogy of sandstones intercalated with organic-rich mudstones: integrating diagenesis and burial history of the Mesaverde Group, Piceance Basin, NW Colorado.– In: Houseknecht, D.W. and Pittman, E.D. (eds.), Origin, Diagenesis, and Petrophysics of Clay Minerals in Sandstones, SEPM Spec. Pub., **47**: 125-144; Tulsa.

Curtis, C.D. (1983): Link between aluminium mobility and destruction of secondary porosity.– AAPG Bull., **63**(3): 380-384.

Curtis, C.D., Ireland, B.J., Whiteman, J.A., Mulvaney, R. and Whittle, C.K. (1984): Authigenic chlorites: problems with chemical analysis and structural formula calculation.– Clay Min., **19**: 471-481.

Curtis, C.D., Hughes, C.R., Whiteman, J.A. and Whittle, C.K. (1985): Compositional variation within some sedimentary chlorites and some comments on their origin.– Mineral. Mag., **49**: 375-386.

Curtis, C.D. and Coleman, M.L. (1986): Controls on the precipitation of early diagenetic calcite, dolomite and siderite concretions in complex depositional sequences.– In: Gautier, D.L. (ed.), Roles of Organic Matter in Sediment Diagenesis, SEPM Spec. Pub., **38**: 23-33; Tulsa.

Dahm, H. (1966): Das marine Niveau über Flöz Finefrau Nebenbank (Obere Wittener Schichten, Westfal A) im niederrheinisch-westfälischen Steinkohlengebirge.– Fortschr. Geol. Rheinld. u. Westf., **13**: 39-124.

Darby, D., Wilkinson, M., Fallick, A.E. and Haszeldine, R.S. (1997): Illite dates record deep fluid movements in petroleum basins.– Petroleum Geoscience, **3**: 130-140.

Dean, W.E., Davis, G.R. and Anderson, R.Y. (1975): Sedimentological significance of nodular and laminated anhydrite.– Geology, **3**: 367-372.

Decker, J. and Helmold, K.P. (1985): The effect of grain size on detrial modes: a test of the Gazzi-Dickinson point-counting method - Discussion.– J. Sediment. Petrol., **55**(4): 618-619.

Deer, W.A., Howie, R.A. and Zussman, J. (1992): An Introduction to the Rock-Forming Minerals.– 2 ed., 696 pp.; Harlow, Essex, England (Longman).

Deutrich, T. (1993): Tonmineral-Diagenese in Rotliegend-Sandsteinen des Norddeutschen Beckens.– Diss., Univ. Mainz, 179 pp.

Deutsche Stratigraphische Kommission (ed.) (2002): Stratigraphische Tabelle von Deutschland 2002.– Potsdam.

Dickinson, W.R. (1985): Interpreting Provenance Relations from Detrital Modes of Sandstones.– In: Zuffa, G.G. (ed.), Provenance of Arenites, 333-361; Dordrecht (Reidel).

Dixon, S.A., Summers, D.M. and Surdam, R.C. (1989): Diagenesis and Preservation of Porosity in Northplet Formation (Upper Jurassic), Southern Alabama.– AAPG Bull., **73**(6): 707-728.

Donovan, T.J., Forgey, R.L. and Roberts, A.A. (1979): Aeromagnetic Detection of Diagenetic Magnetite over Oil Fields.– AAPG Bull., **63**(9): 245-248.

Donovan, T.J., Hendricks, J.D., Roberts, A.A. and Eliason, P.T. (1984): Low-altitude aeromagnetic reconnaissance for petroleum in the Arctic National Wildlife Refuge, Alaska.– Geophysics, **49**(8): 1338-1353.

Dowdle, W.L. and Cobb, W.M. (1975): Static formation temperatures from well logs - an empirical method.– J. Pet. Technol., **27**(11): 1326-1330.

Drever, J.I. (1997): The geochemistry of natural waters.– 3rd ed., Upper Saddle River, N.J. (Prentice-Hall).

Drong, H.J. (1979): Diagenetische Veränderungen in den Rotliegend Sandsteinen im NW-Deutschen Becken.– Geol. Rundsch., **68**: 1172-1183.

Drong, H.J., Plein, E., Sannemann, D., Schuepbach, M.A. and Zimdars, J. (1982): Der Schneverdingen-Sandstein des Rotliegenden - eine äolische Sedimentfüllung alter Grabenstrukturen.– Z. dt. geol. Ges., **133**: 699-725.

Drozdzewski, G. (1992): Zur Faziesentwicklung im Oberkarbon des Ruhrbeckens, abgeleitet aus Mächtigkeitskarten und lithostratigraphischen Gesamtprofilen.– Z. angew. Geol., **38**(1): 41-48.

Drozdzewski, G. and Wrede, V. (1997): Die Variscische Faltungsfront in Nordostdeutschland - Hypothese und Fakten.– Z. angew. Geol., **43**(2): 104-111.

Durand, B., Parratte, M. and Bertrand, P. (1983): Le potentiel en huile des charbons : une approche géochimique.– Revue de l'Institut Francais de Petrole, **38**: 709-721.

Dutton, S.P. and Land, L.S. (1988): Cementation and burial history of a low-permeability quartzarenite, Lower Cretaceous Travis Peak Formation, East Texas.– Geol. Soc. Am. Bull., **100**: 1271-1282.

Dvorák, J. and Paproth, E. (1988): Trends of the Variscan development near the SW border of the East European Platform.– Z. angew. Geol., **34**(12): 353-359.

Edman, J.D. and Surdam, R.C. (1986): Organic-inorganic interactions as a mechanism for porosity enhancement in the Upper Cretaceous Ericson Sandstone, Green River Basin, Wyoming.– In: Gautier, D.L. (ed.), Roles of Organic Matter in Sediment Diagenesis, SEPM Spec. Pub., **38**: 85-109; Tulsa.

Eglinton, T.I., Curtis, C.D. and Rowland, S.J. (1987): Generation of water-soluble organic acids from kerogen during hydrous pyrolysis: implications for porosity development.– Mineral. Mag., **51**: 495-503.

Ehrenberg, S.N. (1993): Preservation of anomalously high porosity in deeply buried sandstones by grain-coating chlorite, examples from the Norwegian Continental Shelf.– AAPG Bull., **77**: 1260-1286.

Ehrenberg, S.N. (1995): Measuring sandstone compaction from modal analyses of thin sections: How to do it and what the results mean.– J. Sediment. Res., **A65**(2): 369-379.

Ehrenberg, S.N., Skjevrak, I. and Gilje, A.E. (1995): Asphaltene-rich residues in sandstone reservoirs of Haltenbanken province, mid-Norwegian continental shelf.– Mar. Petrol. Geol., **12**(1): 53-69.

Emery, D., Myers, R.J. and Young, R. (1990): Ancient subaerial exposure and freshwater leaching in sandstones.– Geology, **18**: 1178-1181.

Evans, D., Graham, C., Armour, A. and Bathurst, P. (eds.) (2003): The Millennium Atlas: Petroleum Geology of the Central and Northern North Sea.– London (The Geological Society of London).

Faber, E., Schmitt, M. and Stahl, W.J. (1979): Geochemische Daten nordwestdeutscher Oberkarbon-, Zechstein- und Buntsandsteingase.– Erdöl und Kohle, Erdgas, Petrochemie, **32**(2): 65-70.

Fahrion, H. (1984): Zur Verbreitung und Fazies des Maastricht in Nordwestdeutschland.– Z. dt. geol. Ges., **135**: 573-583.

Falke, H. (1976): Problems of the continental Permian in the Federal Republic of Germany.– In: Falke, H. (ed.), The Continental Permian in Central, West, and South Europe, 38-52; Dordrecht (Reidel).

Folk, R.L. and Ward, C.R. (1957): Brazos River bar: a study in the significance of grain size parameters.– J. Sediment. Petrol., **27**: 3-26.

Folk, R.L. (1976): Reddening of desert sands: Simpson Desert, N.T., Australia.– J. Sediment. Petrol., **46**(3): 604-615.

Forbes, P.L., Ungerer, P.M., Kuhfuss, A.B., Riis, F. and Eggen, S. (1991): Compositional modeling of petroleum generation and expulsion: Trial application to a local mass balance in the Smørbukk Sør Field, Haltenbanken Area, Norway.– AAPG Bull., **75**(5): 873-893.

Foxford, K.A., Garden, I.R., Guscott, S.C., Burley, S.D., Lewis, J.J.M., Walsh, J.J. and Watterson, J. (1996): The Field Geology of the Moab Fault.– In: Huffman, A.C., Lund, W.R. and Godwin, L.H. (eds.), Geology and Resources of the Paradox Basin, Utah Geol. Assoc. Guidebook, **25**: 256-283.

Frank, F., Zinkernagel, U. and Füchtbauer, H. (1992): Zur Liefergebietsfrage der Sandsteine des Nordwestdeutschen Oberkarbons.– DGMK-Forschungsbericht, **384-8**: 1-167.

Franke, D. (1990): Der präpermische Untergrund der Mitteleuropäischen Senke - Fakten und Hypothesen.– Nds. Akad. Geowiss. Veröfftl., **1990**(4): 19-75.

Franke, D. and Oncken, O. (1990): Geodynamic Evolution of the North-Central Variscides - a Comic Strip.– In: Freeman, R., Giese, P. and Mueller, S. (eds.), The European Geotraverse: Intergrated Studies; Strasbourg (European Science Foundation).

Franke, D. (1995): The North Variscan Foreland.– In: Dallmeyer, R.D., Franke, W. and Weber, K. (eds.), Pre-Permian Geology of Central and Eastern Europe, 554-566; Berlin (Springer).

Franke, D., Hoffmann, N. and Lindert, W. (1995a): The Variscan Deformation Front in East Germany, Part 1: Geological and Geophysical Constraints.– Z. angew. Geol., **41**(2): 83-91.

Franke, D., Hoffmann, N. and Lindert, W. (1996): The Variscan Deformation Front in East Germany, Part 2: Tectonic Interpretation.– Z. angew. Geol., **42**(1): 44-56.

Franke, W., Dallmeyer, R.D. and Weber, K. (1995b): Geodynamic Evolution.– In: Franke, W., Dallmeyer, R.D. and Weber, K. (eds.), Pre-Permian Geology of Central and Eastern Europe, 579-593; Berlin (Springer).

Fraser, A.J., Nash, D.F., Steele, R.P. and Ebdon, C.C. (1990): A regional assessment of the intra-Carboniferous play of Northern England.– In: Brooks, J. (ed.), Classic Petroleum Provinces, Geol. Soc. Spec. Pub., **50**: 417-440; London.

Friberg, L.J. (2001): Untersuchungen zur Temperatur- und Absenkungsgeschichte sowie zur Bildung und Migration von Methan und molekularem Stickstoff im Nordostdeutschen Becken.– Ber. Forschungszentrum Jülich, **3914**: 1-247.

Frisch, U. and Kockel, F. (2004): Der Bremen-Knoten im Strukturnetz Nordwest-Deutschlands. Stratigraphie, Paläogeographie, Strukturgeologie.– Berichte, Fachbereich Geowissenschaften, Univ. Bremen, **223**: 1-379.

Füchtbauer, H. (1974): Zur Diagenese fluviatiler Sandsteine.– Geol. Rundsch., **63**: 904-924.

Füchtbauer, H. (1979): Die Sandsteindiagenese im Spiegel der neueren Literatur.– Geol. Rundsch., **68**: 1125-1151.

Füchtbauer, H. (1988): Sedimente und Sedimentgesteine.– Sediment-Petrologie Teil 2, 4 ed., 1141 pp.; Stuttgart (Schweizerbart).

Gaitzsch, B., Ellenberg, J., Lützner, H. and Benek, R. (1995): Flechtinger Scholle.– In: Plein, E. (ed.), Norddeutsches Rotliegendbecken, Rotliegend-Monographie Teil II, Cour. Forsch.-Inst. Senckenberg, **183**: 84-96; Frankfurt a.M.

Galloway, W.E. (1984): Hydrological regime of sandstone diagenesis.– In: Mcdonald, D.A. and Surdam, R.C. (eds.), Clastic Diagenesis, AAPG Mem., **37**: 3-13.

Garcia, A.J.V., Morad, S., De Ros, L.F. and Al-Aasm, I.S. (1998): Paleogeographical, paleoclimatic and burial history controls on the diagenetic evolution of Lower Cretaceous Serraria sandstones in Sergipe-Alagoas Basin, NE Brazil.– In: Morad, S. (ed.), Carbonate Cementation in Sandstones: Distribution Patterns and Geochemical Evolution, Int. Ass. Sed. Spec. Pub., **26**: 107-140; Oxford (Blackwell).

Garden, I.R., Guscott, S.C., Burley, S.D., Foxford, K.A., Walsh, J.J. and Marshall, J. (2001): An exhumed palaeo-hydrocarbon migration fairway in a faulted carrier system, Entrada Sandstone of SE Utah, USA.– Geofluids, **1**: 195-213.

Gast, R.E. (1988): Rifting im Rotliegenden Niedersachsens.– Die Geowissenschaften, **4**: 115-122.

Gast, R.E. (1991): The Perennial Rotliegend Saline Lake in NW Germany.– Geol. Jb., **A 119**: 25-59.

Gaupp, R., Matter, A., Platt, J., Ramseyer, K. and Walzebuck, J.P. (1993): Diagenesis and Fluid Evolution of Deeply Buried Permian (Rotliegende) Gas Reservoirs, Northwest Germany.– AAPG Bull., **77**(7): 1111-1128.

Gaupp, R. (1996): Diagenesis types and their application in diagenesis mapping.– Zbl. Geol. Paläont., Teil 1, **1994**(11/12): 1183-1199.

Gaupp, R., Clauer, N., Cord, M., Matter, A., Ramseyer, K. and Zwingmann, H. (1996): Silicification during hydrocarbon migration - evidence from Paleozoic sandstone reservoirs in Northern Germany.– Geofluids seminar series, 25; Belfast.

Gaupp, R., Voigt, T. and Lützner, H. (1998): Stratigraphy and sedimentological evolution of Lower and Middle Triassic deposits in the SE part of the Germanic Trassic basin.– In: Bachman, G.-H., Beutler, G. and Lerche, I. (eds.), Exkursions of the International Symposium on the Epicontnental Triassic, Halle (Saale), Hallesches Jb. Geowiss., **B, Beih. 6**: 99-120.

Gaupp, R., Gast, R. and Forster, C. (2000): Late Permian Playa Lake Deposits of the Southern Permian Basin (Central Europe).– In: Gierlowski-Kordesch, E.H. and Kelts, K.R. (eds.), Lake basins through space and time, AAPG Studies in Geology, **46**: 75-86; Tulsa.

Gaupp, R., Solms, M. and Deutrich, T. (2001): Einfluß der Tonmineralgenese auf das Speicherverhalten von Rotliegendsandsteinen des Nordwestdeutschen Beckens.– DGMK Tagungsbericht, **2001-2**: 61-68; Celle.

Gaupp, R. (2005): Model conclusions.– In: Gaupp, R., et al. (eds.), Palaeo Oil- and Gasfields in the Rotliegend of the North German Basin: Effects upon Hydrocarbon Reservoir Quality, DGMK-Forschungsbericht, **593-8**: 5.1-5.17; Hamburg.

Gaupp, R., Baunack, C., Pudlo, D., Solms, M., Trappe, H., Schubart-Engelschall, J., Samiee, R., Littke, R., Schwarzer, D., Oncken, O., Krawczyk, C.M. and Tanner, D. (2005): Paleo Oil- and Gasfields in the Rotliegend of the North German Basin: Effects upon Hydrocarbon Reservoir Quality.– DGMK-Forschungsbericht, **593-8**: 1-242.

Gaupp, R. and Solms, M. (2005): Sedimentological and Petrological Investigations.– In: Gaupp, R., et al. (eds.), Palaeo Oil- and Gasfields in the Rotliegend of the North German Basin: Effects upon Hydrocarbon Reservoir Quality, DGMK-Forschungsbericht, **593-8**: 1.1-1.44; Hamburg.

Gebhardt, U., Schneider, U. and Hoffmann, N. (1991): Modelle zur Stratigraphie und Beckenentwicklung im Rotliegenden der Norddeutschen Senke.– Geol. Jb., **A 127**: 405-427.

Gebhardt, U., Helmuth, H.-J., Kleditzsch, O. and Süssmuth, S. (1995): Havel-Subgroup.– In: Plein, E. (ed.), Norddeutsches Rotliegendbecken, Rotliegend-Monographie Teil II, Cour. Forsch.-Inst. Senckenberg, **183**: 110-121; Frankfurt a.M.

Geluk, M.C. and Röhling, H.-G. (1997): High-resolution sequence stratigraphy of the Lower Triassic "Buntsandstein" in the Netherlands and northwestern Germany.– Geol. Mijnbouw, **76**: 227-246.

Gemmer, L., Nielsen, S.B. and Bayer, U. (2003): Late Cretaceous-Cenozoic evolution of the North German Basin - results from 3-D geodynamic modelling.– Tectonophysics, **373**: 39-54.

Gerling, P., Piske, J., Rasch, H.-J. and Wehner, H. (1996): Paläogeographie, Organofazies und Genese von Kohlenwasserstoffen im Staßfurt-Karbonat Ostdeutschlands. (1) Sedimentationsverlauf und Muttergesteinsausbildung.– Erdöl Erdgas Kohle, **112**(1): 13-18.

Gerling, P., Gulek, M.C., Kockel, F., Lokhorst, A., Lott, G.K. and Nicholson, R.A. (1999a): NW European Gas Atlas - new implications for the Carboniferous gas plays in the western part of the Southern Permian Basin.– In: Fleet, A.J. and Boldy, S.A.R. (eds.), Petroleum Geology of Northwest Europe. Proceedings of the 5th Conference, 799-808; London (Geological Society).

Gerling, P., Kockel, F. and Krull, P. (1999b): Das Kohlenwasserstoff-Potential des Präwestfals im norddeutschen Becken.– DGMK-Forschungsbericht, **433**: 1-107.

Gieré, R. (1996): Formation of rare earth minerals in hydrothermal systems.– In: Jones, A.P., Wall, F. and Williams, C.T. (eds.), Rare earth minerals. Chemistry, origin and ore deposits, Mineral. Soc. Ser., **7**: 105-150; London (Chapman & Hall).

Giggenbach, W.F. (1997): Relative importance of thermodynamic and kinetic processes in governing the chemical and isotopic composition of carbon gases in high-heatflow sedimentary basins.– Geochim. Cosmochim. Acta, **61**(17): 3763-3785.

Giles, M.R. and Marshall, J.D. (1986): Constraints on the development of secondary porosity in the subsurface: re-evaluation of processes.– Mar. Petrol. Geol., **3**: 243-255.

Giles, M.R. and De Boer, R.B. (1990): Origin and significance of redistributional secondary porosity.– Mar. Petrol. Geol., **7**(4): 378-397.

Glasauer, S., Weidler, P.G., Langley, S. and Beveridge, T.J. (2003): Controls on Fe reduction and mineral formation by a subsurface bacterium.– Geochim. Cosmochim. Acta, **67**(7): 1277-1288.

Glasmann, J.R., Clark, R.A., Larter, S., Briedis, N.A. and Lundegard, P.D. (1989): Diagenesis and hydrocarbon accumulation, Brent Sandstone (Jurassic), Bergen High Area, North Sea.– AAPG Bull., **73**(11): 1341-1360.

Glennie, K.W. (1972): Permian Rotliegendes of Northwest Europe Interpreted in Light of Modern Desert Sedimentation Studies.– AAPG Bull., **56**(6): 1048-1071.

Glennie, K.W., Mudd, G. and Nagtegaal, P.J.C. (1978): Depositional environment and diagenesis of Permian Rotliegendes sandstones in Leman Bank and Sole Pit areas of the UK southern North Sea.– J. Geol. Soc. London, **135**: 25-34.

Glennie, K.W. and Provan, D.M.J. (1990): Lower Permian Rotliegend reservoir of the Southern North Sea gas province.– In: Brooks, J. (ed.), Classic Petroleum Provinces, Geol. Soc. Spec. Pub., **50**: 399-416; London.

Glennie, K.W. (1997): Recent advances in understanding the southern North Sea Basin: a summary.– In: Ziegler, K., Turner, P. and Daines, S.R. (eds.), Petroleum Geology of the Southern North Sea: Future Potential, Geol. Soc. Spec. Pub., **123**: 17-29; London.

Glennie, K.W. (ed.) (1998): Petroleum Geology of the North Sea: basic concepts and recent advances.– 4 ed., 636 pp.; Oxford (Blackwell Science).

Glennie, K.W. (2001): Exploration activities in the Netherlands and North-West-Europe since Groningen.– Geol. Mijnbouw / Neth. J. Geosciences, **80**(1): 33-52.

Gluyas, J. and Leonard, A. (1995): Diagenesis of the Rotliegend Sandstone: the answer ain't blowin' in the wind.– Mar. Petrol. Geol., **12**(5): 491-497.

Goodchild, M.W. and Whitaker, J.H.M. (1986): A petrographic study of the Rotliegendes Sandstone reservoir (Lower Permian) in the Rough Gas Field.– Clay Min., **21**: 459-477.

Gralla, P. (1988): Das Oberrotliegende in NW-Deutschland - Lithostratigraphie und Faziesanalyse.– Geol. Jb., **A 106**: 3-59.

Gramann, F. and Kockel, F. (1988): Paleogeographical, lithological, paleoecological and paleoclimatic development of the North West European Tertiary Basin.– In: Vinken, R. (ed.), The NW-European Tertiary Basin.- Results of the International Geological Correlation Program 124, Geol. Jb., **A 100**: 428-442.

Grigsby, J.D. (2001): Origin and growth mechanism of authigenic chlorite in sandstones of the Lower Vicksburg Fromation, South Texas.– J. Sediment. Res., **71**(1): 27-36.

Hall, B.D. and White, N. (1994): Origin of anomalous Tertiary subsidence adjacent to North Atlantic continental margins.– Mar. Petrol. Geol., **11**(6): 703-715.

Hamilton, P.J., Giles, M.R. and Ainsworth, P. (1992): K-Ar dating of illites in Brent Group reservoirs: a regional perspective.– In: Morton, A.C., et al. (eds.), Geology of the Brent Group, Geol. Soc. Spec. Pub., **61**: 377-400; London.

Hancock, N.J. (1978): Possible causes of Rotliegend sandstone diagenesis in northern W. Germany.– J. Geol. Soc. London, **135**: 35-40.

Handford, C.R. (1982): Sedimentology and evaporite genesis in a Holocene continental-sebkha playa basin, Bristol Dry Lake, California.– Sedimentology, **29**: 239-253.

Hansel, C.M., Benner, S.G., Nico, P. and Fendorf, S. (2004): Structural constraints of ferric (hydr)oxides on dissimilatory iron reduction and the fate of Fe(II).– Geochim. Cosmochim. Acta, **68**(15): 3217-3229.

Haq, B.U., Hardenbol, J. and Vail, P.R. (1987): Chronology of Fluctuating Sea Levels Since the Triassic.– Science, **235**: 1156-1167.

Hardie, L.A. (1968): The origin of recent non-marine evaporite deposits of Saline Valley, Inyo County, California.– Geochim. Cosmochim. Acta, **32**: 1279-301.

Harrel, J.A. and Eriksson, K.A. (1979): Empirical conversion equations for thin-section and sieve derived size distribution parameters.– J. Sediment. Petrol., **49**(1): 273-280.

Harrison, W.J. and Thyne, G.D. (1992): Prediction of diagenetic reactions in the presence of organic acids.– Geochim. Cosmochim. Acta, **56**: 565-586.

Hartmann, B. (1997): Mobilität von Seltenen-Erd-Elementen und deren Fixierung in Karbonatphasen am Beispiel von Rotliegend-Sandsteinen des Norddeutschen Beckens.– Diss., Univ. Mainz, 116 pp.

Hartmann, M. (1963): Einige geochemische Untersuchungen an Sandsteinen aus Perm und Trias.– Geochim. Cosmochim. Acta, **27**: 459-499.

Hasner, K. (2004): Untersuchungen an Hämatit-Tonmineralkrusten in Rotliegendsandsteinen des Norddeutschen Beckens.– Diploma Thesis, Univ. Jena, 145 pp.

Haszeldine, R.S., Quinn, O., England, G., Wilkinson, M., Shipton, Z.K., Evans, J.P., Heath, J., Crossey, L., Ballentine, C.J. and Graham, C.M. (2005): Natural geochemical analogues for carbon dioxide storage in deep geological porous reservoirs, a United Kingdom perspective.– Oil Gas Sci. Technol. / Rev. IFP, **60**(1): 33-49.

Hay, R.L. and Sheppard, R.A. (2001): Occurrence of zelites in sedimentary rocks: an overview.– In: Bish, D.L. and Ming, D.W. (eds.), Natural zeolites: occurence, properties, applications, Reviews in Mineralogy and Geochemistry, **45**: 217-234.

Hayes, J.B. (1970): Polytypism of chlorite in sedimentary rocks.– Clays Clay Min., **18**: 285-306.

Heald, M.T. and Larese, R.E. (1974): Influence of coatings on quartz cementation.– J. Sediment. Petrol., **44**: 1269-1274.

Hedemann, H.-A. and Teichmüller, R. (1971): Die paläogeographische Entwicklung des Oberkarbons.– Fortschr. Geol. Rheinld. u. Westf., **19**: 129-142.

Hedemann, H.-A., Maschek, W., Paulus, B. and Plein, E. (1984a): Mitteilung zur lithostratigraphischen Gliederung des Oberrotliegend im Norwestdeutschen Becken.– Nachr. dt. geol. Ges., **30**: 100-107.

Hedemann, H.-A., Schuster, A., Stancu-Kristoff, G. and Lösch, J. (1984b): Die Verbreitung der Kohleflöze des Oberkarbons in Nordwestdeutschland und ihre stratigraphische Einstufung.– Fortschr. Geol. Rheinld. u. Westf., **32**: 39-88.

Hedemann, H.-A. (1985): Energierohstoffe im Oberkarbon Nordwestdeutschlands.– Erdöl-Erdgas, **101**(4): 106-112.

Heide, K., Gerth, K. and Hartmann, E. (2000): The detection of an inorganic hydrocarbon formation in silicate melts by means of a direct-coupled-evolved-gas-analysis-system (DEGAS).– Thermochim. Acta, **354**: 165-172.

Hillier, S. and Velde, B. (1991): Octahedral occupancy and the chemical composition of diagenetic (low-temperature) chlorites.– Clay Min., **26**: 149-168.

Hillier, S. and Velde, B. (1992): Chlorite interstratified with a 7 Å mineral: An example from offshore Norway and possible implications for the interpretation of the composition of diagenetic chlorites.– Clay Min., **27**: 475-486.

Hillier, S. (1994): Pore-lining chlorites in siliciclastic reservoir sandstones: Electron microprobe, SEM and XRD data, and implications for their origin.– Clay Min., **29**: 665-679.

Hinsch, W. (1974): Das Tertär im Untergrund von Schleswig-Holstein (Das Nordwestdeusche Tertiärbecken, Beitrag 5).– Geol. Jb., **A 24**: 3-34.

Hinsch, W. (1986): Strukturell-halokinetische Gliederung Schleswig-Holsteins im Känozoikum.– In: Tobien, H. (ed.), Nordwestdeutschland im Tertiär, Beiträger zur regionalen Geologie der Erde, 603-609; Berlin, Stuttgart (Borntraeger).

Hoffmann, N., Kamps, H.J. and Schneider, J. (1989): Neuerkenntnisse zur Biostratigraphie und Paläodynamik des Perms in der Norddeutschen Senke - ein Diskussionsbeitrag.– Z. angew. Geol., **35**(7): 198-207.

Hoffmann, N., Jödicke, H., Fluche, B., Jording, A. and Müller, W. (1998): Modellvorstellungen zur Verbreitung potentieller präwestfalischer Erdgas-Muttergesteine in Norddeutschland - Ergebnisse neuer magnetotellurischer Messungen.– Z. angew. Geol., **44**(3): 140-158.

Hoffmann, N., Jödicke, H. and Gerling, P. (2001): The distribution of Pre-Westphalian source rocks in the North German Basin - Evidence from magnetotelluric and geochemical data.– Geol. Mijnbouw / Neth. J. Geoscience, **80**(1): 71-84.

Hoffmann, N., Jödicke, H. and Horejschi, L. (2005): Regional Distribution of the Lower Carboniferous Culm and Carboniferous limestone facies in the North German Basin - derived from magnetotelluric soundings.– Z. dt. Ges. Geowiss., **156**(2): 323-339.

Horsfield, B., Yordy, K.L. and Crelling, J.C. (1988): Determining the petroleum-generating potential of coal using organic geochemistry and organic petrology.– Org. Geochem., **13**(1-3): 121-129.

Horsfield, B., Schenk, H.-J., Mills, N. and Welte, D.H. (1992): An investigation of the in-reservoir conversion of oil to gas: compositional and kinetic findings from closed-system programmed-temperature pyrolysis.– Org. Geochem., **19**(1-3): 191-204.

Hoth, K., Huebscher, H.-D., Korich, D., Gabriel, W. and Enderlein, F. (1993): Die Lithostratigraphie der permokarbonen Effusiva im Zentralabschnitt der Mitteleuropäischen Senke.– Geol. Jb., **A 131**: 179-196.

Hoth, P. (1993): Fazies, Diagenese und schwache Metamorphose klastischer Prä-Perm-Sedimente zwischen Harz und Ostsee.– Diss., TU Berlin, 158 pp.

Houseknecht, D.W. (1987): Assessing the Relative Importance of Compaction Processes and Cementation to Reduction of Porosity in Sandstones.– AAPG Bull., **71**(6): 633-642.

Howarth, R.J. (1998): Improved estimators of uncertainty in proportions, point-counting, and pass-fail test results.– Am. J. Sci., **298**(7): 594-607.

Hug, N. (2004): Sedimentgenese und Paläogeographie des höheren Zechstein bis zur Basis des Buntsandstein in der Hessischen Senke.– Geol. Abh. Hessen, **113**, 238 pp.; Wiesbaden.

Humphreys, B., Smith, S.A. and Strong, G.E. (1989): Authigenic chlorite in late Triassic sandstones from the Central Graben, North Sea.– Clay Min., **24**: 427-444.

Humphreys, B., Kemp, S.J., Lott, G.K., Bermanto, Dharmayanti, D.A. and Samsori, I. (1994): Origin of grain-coating chlorite by smectite transformation: An example from Miocene sandstones, North Sumatra back-arc basin, Indonesia.– Clay Min., **29**: 681-692.

Hunt, J.M. (1979): Petroleum geochemistry and geology.– 617 pp.; San Francisco (Freeman).

Hurtig, E., Cermak, V., Haenel, R. and Zui, V. (eds.) (1992): Geothermal Atlas of Europe.– 156 pp.; Gotha (Haack).

Hutcheon, I., Oldershaw, A. and Ghent, E.D. (1980): Diagenesis of Cretaceous sandstones of the Kootenay Formation at Elk Valley (southeastern Britisch Colombia) and Mt Allan (southwestern Alberta).– Geochim. Cosmochim. Acta, **44**: 1425-1435.

Ingersoll, R.V., Bullard, T.F., Ford, R.L., Grimm, J.P., Pickle, J.D. and Sares, S.W. (1984): The effect of grain size on detrital modes: a test of the Gazzi-Dickinson point-counting method.– J. Sediment. Petrol., **54**(1): 103-116.

Irwin, H., Curtis, C. and Coleman, M. (1977): Isotopic evidence for source of diagenetic carbonates formed during burial of organic-rich sediments.– Nature, **269**: 209-213.

Jahren, J. and Ramm, M. (2000): The porosity-preserving effects of microcrystalline quartz coatings in arenitic sandstones: example from Norwegian continental shelf.– In: Worden, R.H. and Morad, S. (eds.), Quartz cementation in sandstones, 271-280.

Jahren, J.S. and Aagaard, P. (1989): Compositional variations in diagenetic chlorites and illites, and relationships with formation-water chemistry.– Clay Min., **24**: 157-170.

Jaritz, W. (1969): Epirogenese in Nordwestdeutschland im höheren Jura und in der Unterkreide.– Geol. Rundsch., **59**: 114-124.

Jaritz, W. (1973): Zur Entstehung der Salzstrukturen Nordwestdeutschlands.– Geol. Jb., **A 10**: 3-77.

Jaritz, W. (1980): Einige Aspekte der Entwicklungsgeschichte der nordwestdeutschen Salzstöcke.– Z. dt. geol. Ges., **131**: 387-408.

Kappelmeyer, O. (1985): Geothermik.– In: Bender, F. (ed.), Angewandte Geowissenschaften, Band II, 435-490; Stuttgart (Enke).

Kashefi, K. and Lovley, D.R. (2003): Extending the Upper Temperature Limit for Life.– Science, **301**: 934.

Kashefi, K., Holmes, D.E., Lovley, D.R. and Tor, J.M. (2004): Potential importance of dissimilatory Fe(III)-reducing microorganisms in hot sedimentary environments.– The Subseafloor Biosphere at Mid-Ocean Ridges, Geophysical Monograph Series, **144**: 199-211.

Katzung, G. (1975): Tektonik, Klima und Sedimentation in der Mitteleuropäischen Saxon-Senke und in angrenzenden Gebieten.– Z. geol. Wiss., **3**: 1453-1472.

Katzung, G., Sigeneger, W.-D., John, K.-H., Süssmuth, S. and Warncke, D. (1977): Die Saxongliederung im Zentralabschnitt der Mitteleuropäischen Senke.– Z. angew. Geol., **23**: 559-561.

Katzung, G. and Krull, P. (1984): Zur tektonischen Entwicklung Mittel- und Nordwesteuropas während des Jungpaläozoikums.– Z. angew. Geol., **30**(4): 163-173.

Katzung, G. (1988): Tectonics and Sedimentation of Variscan Molasses in Central Europe.– Z. geol. Wiss., **16**(9): 823-843.

Kawamura, K. and Kaplan, I.R. (1987): Dicarbolic acids generated by thermal alteration of kerogen and humic acids.– Geochim. Cosmochim. Acta, **51**: 3201-3207.

Kerr, S.D. and Thomson, A. (1963): Origin of nodular and bedded anhydrite in Permian shelf sediments, Texas and New Mexico.– AAPG Bull., **47**: 1726-1732.

Kettel, D. (1989): Upper Carboniferous source rocks north and south of the Variscan Front (NW and Central Europe).– Mar. Petrol. Geol., **6**: 170-181.

Kharaka, Y.K., Law, L.M., Carothers, W.W. and Goerlitz, D.F. (1986): Role of organic species dissolved in formation waters from sedimentary basins in mineral diagenesis.– In: Gautier, D.L. (ed.), Roles of Organic Matter in Sediment Diagenesis, SEPM Spec. Pub., **38**: 111-122; Tulsa.

Kiersnowski, H., Paul, J., Peryt, T.M. and Smith, D.B. (1995): Facies, Paleogeography, and Sedimentary History of the Southern Permian Basin in Europe.– In: Scholle, P.A., Peryt, T.M. and Ulmer-Scholle, D.S. (eds.), The Permian of Northern Pangea, Volume 2: Sedimentary Basins and Economic Resources, 119-136; Berlin (Springer).

Kilgore, B. and Elmore, R.D. (1989): A study of the relationship between hydrocarbon migration and the precipitacion of authigenic magnetic minerals in the Triassic Chugwater Formation, southern Montana.– Geol. Soc. Am. Bull., **101**: 1280-1288.

Koch, J., Kockel, F. and Krull, P. (1997): Coalification at the base Zechstein and the Pre-Permian surface in northern Germany.– Geol. Jb., **D 103**: 33-43.

Kockel, F. (1980): A Lithostratigraphic Scheme for the NW-European Tertiary Basin.– Newsl. Stratigr., **8**(3): 236-237.

Kockel, F. (2002): Rifting processes in NW-Germany and the German North Sea Sector.– Neth. J. Geosciences / Geol. Mijnbouw, **81**(2): 149-157.

Krooss, B.M., Littke, R., Müller, B., Frielingsdorf, J., Schwochau, K. and Idiz, E.F. (1995): Generation of nitrogen and methane from sedimentary organic matter: implications on the dynamics of natural gas accumulations.– Chem. Geol., **126**: 291-318.

Kutasov, I.M. and Eppelbaum, L.V. (2005): Determination of formation temperature from bottom-hole temperature logs—a generalized Horner method.– J. Geophys. Eng., **2**: 90-96.

Land, L.S. and Milliken, K.L. (1981): Feldspar diagenesis in the Frio Formation, Brazoria County, Texas Gulf Coast.– Geology, **9**: 314-318.

Lanson, B., Beaufort, D., Berger, G., Baradat, J. and Lacharpagne, J.-C. (1996): Illitization of diagenetic kaolinite-to-dickite conversion series: Late-stage diagenesis of the Lower Permian Rotliegend sandstone reservoir, offshore of the Netherlands.– J. Sediment. Res., **66**(3): 501-518.

Lanson, B., Beaufort, D., Berger, G., Bauer, A., Cassagnabère, A. and Meunier, A. (2002): Authigenic kaolin and illitic minerals during burial diagenesis of sandstones: a review.– Clay Min., **37**: 1-22.

Larter, S., Wilhelms, A., Head, I., Koopmany, M., Aplin, A., di Primio, R., Zwach, C., Erdmann, M. and Telnaes, N. (2003): The controls on the composition of biodegraded oils in the deep subsurface—part 1: biodegradation rates in petroleum reservoirs.– Org. Geochem., **34**(4): 601-613.

Lee, M., Aronson, J.L. and Savin, S.M. (1989): Timing and Conditions of Permian Rotliegende Sandstone Diagenesis, Southern North Sea: K/Ar and Oxygen Isotopic Data.– AAPG Bull., **73**(2): 195-215.

Lee, M.-K. and Bethke, C.M. (1994): Groundwater flow, late cementation, and petroleum accumulation in the Permian Lyons Sandstone, Denver Basin.– AAPG Bull., **78**(2): 217-237.

Legler, B., Gebhardt, U. and Schneider, J.W. (2005): Late Permian non-marine–marine transitional profiles in the central Southern Permian Basin, northern Germany.– Int. J. Earth Sci. / Geol. Rundsch.: in press.

Leveille, G.P., Primmer, T.J., Dudley, G., Ellis, D. and Allinson, G.J. (1997): Diagenetic controls on reservoir quality in Permian Rotliegendes sandstones, Jupiter Fields area, southern North Sea.– In: Ziegler, K., Turner, P. and Daines, S.R. (eds.), Petroleum geology of the Southern North Sea: Future and Potential, Geol. Soc. Spec. Pub., **123**: 105-122; London.

Leythaeuser, D., Schaefer, R.G. and Radke, M. (1985): Aspekte der Erkennung und Beurteilung der primären Migration des Erdöls - erläutert an einem Beispiel aus dem Ruhrkarbon.– Fortschr. Geol. Rheinld. u. Westf., **33**: 219-229.

Liang, L., McCarthy, J.F., Jollet, L.W., McNabb, J.A. and Mehlhorn, T.L. (1993): Iron dynamics: transformation of Fe(II)/Fe(III) during injection of natural organic matter in a sandy aquifer.– Geochim. Cosmochim. Acta, **57**: 1987-1999.

Liewig, N., Clauer, N. and Sommer, F. (1987): Rb-Sr and K-Ar Dating of Clay Diagenesis in Jurassic Sandstone Oil Reservoir, North Sea.– AAPG Bull., **71**(12): 1467-1474.

Liewig, N. and Clauer, N. (2000): K-Ar dating of varied microtextural illite in Permian gas reservoirs, northern Germany.– Clay Min., **35**: 271-281.

Littke, R., Horsfield, B. and Leythaeser, D. (1989): Hydrocarbon distribution in coals and in dispersed organic matter of different maceral compositions and maturity.– Geol. Rundsch., **78**(1): 391-410.

Littke, R. and Leythaeuser (1993): Migration of Oil and Gas in Coals.– In: Law, B.E. and Rice, D.D. (eds.), Hydrocarbons from coal, AAPG Studies in Geology, **38**: 219-236; Tulsa.

Littke, R., Büker, C., Lückge, A., Sachsenhofer, R.F. and Welte, D.H. (1994): A new evaluation of palaeo-heat flows and eroded thicknesses for the carboniferous Ruhr basin, western Germany.– Int. J. Coal Geol., **26**: 155-183.

Littke, R., Krooss, B., Idiz, E. and Frielingsdorf, J. (1995): Molecular Nitrogen in Natural Gas Accumulations: Generation from Sedimentary Organic Matter at High Temperatures.– AAPG Bull., **79**(3): 410-430.

Littke, R., Brauckmann, F.J., Radke, M. and Schaefer, R.G. (1996): Solid bitumen in Rotliegend gas reservoirs in northern Germany: implications for their thermal and filling history.– Zbl. Geol. Paläont., Teil 1, **1994**(11/12): 1275-1292.

Lokhorst, A. (ed.) (1998): Northwest European Gas Altas - Composition and Isotope Ratio of Natural Gases.– Haarlem (NITG-TNO).

Lovley, D.R. and Phillips, E.J.P. (1988): Novel mode of microbial energy metabolism: Organic carbon oxidation coupled to dissimilatory reduction of iron or manganese.– Appl. Environ. Microbiol., **54**(6): 1472-1480.

Lovley, D.R. (1991): Dissimilatory Fe(III) and Mn(IV) reduction.– Microb. Rev., **55**(2): 259-287.

Lovley, D.R. and Woodward, J.C. (1996): Mechanisms for chelator stimulation of microbial Fe(III) - oxide reduction.– Chem. Geol., **132**: 19-24.

Lundegard, P.D. and Land, L.S. (1986): Carbon dioxide and organic acids: their role in porosity enhancement and cementation, Paleogene of the Texas Gulf Coast.– In: Gautier, D.L. (ed.), Roles of Organic Matter in Sediment Diagenesis, SEPM Spec. Pub., **38**: 129-146; Tulsa.

Macaulay, C.I., Fallick, A.E., McLaughlin, O.M., Haszeldine, R.S. and Pearson, M.J. (1998): The significance of $\delta^{13}C$ of carbonate cements in reservoir sandstones: a regional perspective from the Jurassic of the northern North Sea.– In: Morad, S. (ed.), Carbonate cementation in sandstones: Distribution patterns and geochemical evolution, Int. Ass. Sed. Spec. Pub., **26**: 395-408; Oxford (Blackwell).

Macaulay, C.I., Fallick, A.E., Haszeldine, R.S. and McAulay, G.E. (2000): Oil migration makes the difference: regional distribution of carbonate cement $\delta^{13}C$ in northern North Sea Tertiary sandstones.– Clay Min., **35**: 69-76.

Machel, H.G., Krouse, H.R. and Sassen, R. (1995): Products and distinguishing criteria of bacterial and thermochemical sulfate reduction.– Appl. Geochem., **10**(4): 373-389.

Machel, H.G. (2001): Bacterial and thermodynamic sulfate reduction in diagenetic settings - old and new insights.– Sed. Geol., **140**: 143-175.

Mack, G.H. (1984): Exceptions to the relationship between plat tectonics and sandstone composition.– J. Sediment. Petrol., **54**: 212-220.

Magri, F., Bayer, U., Clausnitzer, V., Jahnke, C., Diersch, H.-J., Fuhrmann, J., Möller, P., Pekdeger, A., Tesmer, M. and Voigt, H.-J. (2005a): Deep-reaching fluid flow close to convective instability in the NE German Basin - results from water chemistry and numerical modelling.– Tectonophysics, **397**: 5-20.

Magri, F., Bayer, U., Jahnke, C., Clausnitzer, V., Diersch, H.-J., Fuhrmann, J., Möller, P., Pekdeger, A., Tesmer, M. and Voigt, H.-J. (2005b): Fluid-dynamics driving saline water in the North East German Basin.– Int. J. Earth Sci. / Geol. Rundsch.: in press.

Marchand, A.M.E., Macaulay, C.I., Haszeldine, R.S. and Fallick, A.E. (2002): Pore water evolution in oilfield sandstones: constraints from oxygen isotope microanalyses of quartz cement.– Chem. Geol., **191**: 285-304.

Marx, J., Huebscher, H.-D., Hoth, K., Korich, D. and Kramer, W. (1995): Vulkanostratigraphie und Geochemie der Eruptivkomplexe.– In: Plein, E. (ed.), Norddeutsches Rotliegendbecken, Rotliegend-Monographie Teil II, Cour. Forsch.-Inst. Senckenberg, **183**: 54-83; Frankfurt a.M.

Matlack, K.S., Houseknecht, D.W. and Applin, K.R. (1989): Emplacement of clay into sand by infiltration.– J. Sediment. Petrol., **59**: 77-87.

Mauthe, G. (2001): Salzzementation im Solling Sandstein von Hengstlage und Dötlingen (Mittlerer Buntsandstein; Oldenburg).– DGMK Tagungsbericht, **2001-2**: 69-77; Celle.

Maystrenko, Y., Bayer, U. and Scheck-Wenderoth, M. (2005): The Glueckstadt Graben, a sedimentary record between the North and Baltic Sea in north Central Europe.– Tectonophysics, **397**: 113-126.

McBride, E.F. (1963): A classification of common sandstones.– J. Sediment. Petrol., **33**(3): 664-669.

McBride, E.F. (1989): Quartz cement in sandstones: A review.– Earth-Sci. Rev., **26**: 69-112.

McCann, T. (1996): Pre-Permian of the north-east German Basin.– Geol. J., **31**: 159-177.

McCann, T. (1998): Lower Palaeozoic evolution of the northeast German Basin/Baltica borderland.– Geol. Mag., **135**(1): 129-142.

McCann, T. (1999): The tectonosedimentary evolution of the northern margin of the Carboniferous foreland basin of NE Germany.– Tectonophysics, **313**: 119-144.

McCollom, T.M. and Seewald, J.S. (2003): Experimental study of the hydrothermal reactivity of organic acids and acid anions: II. Acetic acid, acetate, and valeric acid.– Geochim. Cosmochim. Acta, **67**(19): 3645-3664.

McConnell, J.D.C. (1954): The hydrated calcium silicates riversideite, tobermorite, and plombierite.– Mineral. Mag., **30**: 293-305.

McKinley, J.M., Worden, R.H. and Ruffell, A.H. (2003): Smectite in sandstones: a review of the controls on occurence and behaviour during diagenesis.– In: Worden, R. and Morad, S. (eds.), Clay Mineral Cements in Sandstones, Int. Ass. Sed. Spec. Pub., **34**: 109-128; Oxford (Blackwell).

Meissner, R., Sadowiak, P. and Thomas, S. (1994): Eastern-Avalonia, the third partner in the Caledonian collisions: Evidence from deep seismic reflection data.– Geol. Rundsch., **83**: 186-196.

Menning, M., Katzung, G. and Lützner, H. (1988): Magnetostratigraphic Investigations in the Rotliegendes (300-252 Ma) of Central Europe.– Z. geol. Wiss., **16**(11/12): 1045-1063.

Menning, M. (1991): Rapid subsidence in the Central European Basin during the initial development (Permian-Triassic boundary sequences, 258-240 Ma).– Zbl. Geol. Paläont., Teil 1, **1991**(4): 809-824.

Menning, M. (1995): A Numerical Time Scale for the Permian and Triassic Periods: An Integrated Time Analysis.– In: Scholle, P.A., Peryt, T.M. and Ulmer-Scholle, D.S. (eds.), The Permian of Northern Pangea, Volume 1: Paleogeography, Paleoclimates, Stratigraphy, 77-97; Berlin (Springer).

Merlino, S., Bonaccorsi, E. and Armbruster, T. (2001): The real structure of tobermorite 11Å: normal and anomalous forms, OD character and polytypic modifications.– Eur. J. Mineral., **13**: 577-590.

Mertz, K.A.J. and Hubert, J.F. (1990): Cylces of sand-flat sandstone and playa-lacustrine mudstone in the Triassic-Jurassic Blomidon red beds, Fundy rift basin, Nova Scotia.– Can. J. Earth Sci., **27**: 442-451.

Meshri, I.D. (1986): On the reactivity of carbonic and organic acids and the generation of secondary porosity.– In: Gautier, D.L. (ed.), Roles of Organic Matter in Sediment Diagenesis, SEPM Spec. Pub., **38**: 123-128; Tulsa.

Metcalfe, R., Rochelle, C.A., Savage, D. and Higgo, J.W. (1994): Fluid-Rock interactions during continental red bed diagenesis: implications for theoretical models of mineralization in sedimentary basins.– In: Parnell, J. (ed.), Geofluids: Origin, Migration and Evolution of Fluids in Sedimentary Basins, Geol. Soc. Spec. Pub., **78**: 301-324; London.

Meunier, A. and Velde, B.D. (2004): Illite - Origins, Evolution and Metamorphism.– 286 pp.; Berlin (Springer).

Michelsen, O. (1971): Lower Carboniferous Foraminiferal Faunas of the Boring Ørslev No. 1, Island of Falster, Denmark.– Geol. Surv. Denmark, II Series, **98**: 1-86.

Milliken, K.L., Mack, G.H. and Land, L.S. (1994): Element mobility in sandstones during burial: Whole-rick chemical and isotopic data, Frio Formation, south Texas.– J. Sediment. Res., **A64**(4): 788-796.

Miyake, M., Niiya, S. and Matsuda, M. (2000): Microwave-assisted Al-substituted tobermorite synthesis.– J. Mater. Res., **15**(4): 850-853.

Mohr, M., Kukla, P.A., Urai, J.L. and Bresser, G. (2005): Multiphase salt tectonic evolution in NW Germany: seismic interpretation and retro-deformation.– Int. J. Earth Sci. / Geol. Rundsch.: in press.

Moore, D.M. and Reynolds, R.C. (1997): X-Ray Diffraction and the Identification and Analysis of Clay Minerals.– 2 ed., 373 pp.; Oxford (Oxford University Press).

Morad, S., Bergan, M., Knarud, R. and Nystuen, J.P. (1990): Albitization of detrital plagioclase in Triassic reservoir sandstones from the Snorre Field, Norwegian North Sea.– J. Sediment. Petrol., **60**: 411-425.

Morad, S., Ketzer, J.M. and De Ros, L.F. (2000): Spatial and temporal distribution of diagenetic alterations in siliciclastic rocks: implications for mass transfer in sedimentary basins.– Sedimentology, **47**(Suppl. 1): 95-120.

Muchez, P., Viaene, W. and Dusar, M. (1992): Diagenetic control on secondary porosity in flood plain deposits: an example of the Lower Triassic of northeastern Belgium.– Sed. Geol., **78**: 285-298.

Mücke, A. (1994): Part 1. Postdiagenetic ferruginization of sedimentary rocks (sandstones, oolitic ironstones, kaolins and bauxites).– In: Wolf, K.H. and Chilingarian, G.V. (eds.), Diagenesis, IV, Developments in Sedimentology, **51**: 361-423; Amsterdam.

Müller, E.P. (1990): Genetische Modelle der Bildung von Erdgaslagerstätten im Rotliegenden.– Nds. Akad. Geowiss. Veröfftl., **4**: 77-90.

Nairn, A.E.M. and Smithwick, M.E. (1976): Permian paleogeography and climatology.– In: Falke, H. (ed.), The Continental Permian in Central, West, and South Europe, 283-312; Dordrecht (Reidel).

Neunzert, G.H., Gaupp, R. and Littke, R. (1996): Absenkungs- und Temperaturgeschichte paläozoischer und mesozoischer Formationen im Nordwestdeutschen Becken.– Z. dt. geol. Ges., **147**(2): 183-208.

Neunzert, G.H. (1997): Simulation der Beckensubsidenz, der Temperaturgeschichte, der Reifung organischen Materials, und der Genese, Migration und Akkumulation von Methan und Stickstoff in Nordwestdeutschland auf der Basis seismischer Interpretationen.– Ber. Forschungszentrum Jülich, **3521**: 1-173.

Nielsen, L.H. and Japsen, P. (1991): Deep wells in Denmark 1935-1990.– Geol. Surv. Denmark, **A 31**: 1-177.

Odin, G.S., Bailey, S.W., Amouric, M., Fröhlich, F. and Waychunas, G. (1988): Mineralogy of the verdine facies.– In: Odin, G.S. (ed.), Green Marine Clays, 159-204; Amsterdam, New York (Elsevier).

Palandri, J.L. and Kharaka, Y.K. (2005): Ferric iron-bearing sediments as mineral trap for CO_2 sequestration: Iron reduction using sulfur-bearing waste gas.– Chem. Geol., **217**: 315-364.

Parnell, J. and Eakin, P. (1987): The replacement of sandstones by uraniferous hydrocarbons: significance for petroleum migration.– Mineral. Mag., **51**: 505-515.

Parnell, J. (1994): Hydrocarbons and other fluids: paragenesis, interactions and exploration potential inferred from petrographic studies.– In: Parnell, J. (ed.), Geofluids: Origin, Migration and Evolution of Fluids in Sedimentary Basins, Geol. Soc. Spec. Pub., **78**: 275-291; London.

Parnell, J., Carey, P. and Monson, B. (1996): Fluid inclusion constraints on temperatures of petroleum migration from authigenic quartz in bitumen veins.– Chem. Geol., **129**: 217-226.

Parry, W.T., Chan, M.A. and Beitler, B. (2004): Chemical bleaching indicates episodes of fluid flow in deformation bands in sandstone.– AAPG Bull., **88**(2): 175-191.

Pasternak, M., Brinkmann, S., Messner, J. and Sedlacek, R. (2004): Erdöl und Erdgas in der Bundesrepublik Deutschland 2003.– 48 pp.; Hannover (Niedersächsisches Landesamt für Bodenforschung).

Pepper, A.S. and Corvi, P.J. (1995): Simple kinetic models of petroleum formation. Part I: oil and gas generation from kerogen.– Mar. Petrol. Geol., **12**(3): 291-319.

Petschick, R. (2002): Röntgendiffraktometrie in der Sedimentologie.– Schriftenr. dt. geol. Ges., **18**: 99-118.

Pettijohn, F.J., Potter, P.E. and Siever, R. (1987): Sand and sandstone.– 2 ed., 553 pp.; New York (Springer).

Pharaoh, T.C. (1999): Paleozoic terranes and their lithospheric boundaries within the Trans-European Suture Zone (TESZ): a review.– Tectonophysics, **314**: 17-41.

Philipp, W. and Reinicke, K.M. (1982): Zur Entstehung und Erschließung der Gasprovinz Osthannover.– Erdöl-Erdgas, **98**: 85-90.

Pierre, C., Ortlieb, L. and Person, A. (1984): Supratidal evaporitic dolomite at Ojo de Liebre Lagoon; Mineralogical and isotopic arguments for primary crystallisation.– J. Sediment. Petrol., **54**(4): 1049-1061.

Pittman, E.D., Larese, R.E. and Heald, M.T. (1992): Clay coats: occurence and relevance to preservation of porosity in sandstones.– In: Houseknecht, D.W. and Pittman, E.D. (eds.), Origin, Diagenesis, and Petrophysics of Clay Minerals in Sandstones, SEPM Spec. Pub., **47**: 241-255.

Platt, J. (1991): The Diagenesis of Early Permian Rotliegend deposits from northwest Germany.– Diss., Univ. Bern, 367 pp.

Platt, J. (1993): Controls on clay mineral distribution and chemistry in the early Permian Rotliegend of Germany.– Clay Min., **28**: 393-416.

Platt, J. (1994): Geochemical evolution of pore waters in the Rotliegend (Early Permian) of northern Germany.– Mar. Petrol. Geol., **11**(1): 66-78.

Plein, E. (1978): Rotliegend-Ablagerungen im Norddeutschen Becken.– Z. dt. geol. Ges., **129**: 71-97.

Plein, E. (1993): Bemerkungen zum Ablauf der paläogeographischen Entwicklung im Stefan und Rotliegend des Norddeutschen Beckens.– Geol. Jb., **A 131**: 99-116.

Plein, E. (ed.) (1995): Norddeutsches Rotliegendbecken, Rotliegend-Monographie Teil II.– Cour. Forsch.-Inst. Senckenberg, **183**, 193 pp.; Frankfurt a.M.

Plummer, N.L. (1975): Mixing of sea water with calcium carbonate ground water.– Geol. Soc. Am. Mem., **142**: 219-236.

Poelchau, H.S., Baker, D.R., Hantschel, T., Horsfield, B. and Wygrala, B. (1997): Basin simulation and the design of the conceptual basin model.– In: Welte, D.H., Horsfield, B. and Baker, D.R. (eds.), Petroleum and Basin Evolution, 3-70; Berlin (Springer).

Powers, M.C. (1953): A new roundness scale for sedimentary particles.– J. Sediment. Petrol., **23**: 117-119.

Purvis, K. (1989): Zoned authigenic magnesites in the Rotliegend Lower Permian, southern North Sea.– Sed. Geol., **65**: 307-318.

Purvis, K. and Okkerman, J.A. (1996): Inversion of reservoir quality by early diagenesis: an example from the Triassic Buntsandstein, offshore the Netherlands.– In: Rondeel, H.E., Batjes, D.A.J. and Nieuwenhuijs, W.H. (eds.), Geology of Gas and Oil under the Netherlands, 179-189; Dordrecht (Kluwer).

Putnis, A. and Mauthe, G. (2001): The effect of pore size on cementation in porous rocks.– Geofluids, **1**: 37-41.

Pye, K. and Krinsley, D.H. (1986): Diagenetic carbonate and evaporite minerals in Rotliegend aeolian sandstones of the southern North Sea: Their nature and relationship to secondary porosity development.– Clay Min., **21**: 443-457.

Rabitz, A. (1966): Der marine Katharina-Horizont (Basis des Westphal B) im Ruhrrevier und seine Fauna.– Fortschr. Geol. Rheinld. u. Westf., **13**: 125-195.

Radies, D., Stollhofen, H., Hollmann, G. and Kukla, P. (2005): Synsedimenary faults and amalgamated unconformities: Insights from 3D-seismic and core analysis of the Lower Triassic Middle Buntsandstein, Ems Basin, Germany.– Int. J. Earth Sci. / Geol. Rundsch.: in press.

Radke, M., Schaefer, R.G., Leythaeuser, D. and Teichmüller, M. (1985): Bildung und Umwandlung schwerflüchtiger Kohlenwasserstoffe in Kohlen des Ruhrkarbons in Abhängigkeit vom Inkohlungsgrad.– Fortschr. Geol. Rheinld. u. Westf., **33**: 197-217.

Ramseyer, K., Baumann, J., Matter, A. and Mullis, J. (1988): Cathodoluminescence colours of α-quartz.– Mineral. Mag., **52**: 669-677.

Ramseyer, K., Amthor, J.E., Spötl, C., Terken, J.M.J., Matter, A., Vroon-ten Hove, M. and Borgomano, J.R.F. (2004): Impact of basin evolution, depositional environment, pore water evolution and diagenesis on reservoir-quality of Lower Paleozoic Haima Supergroup sandstones, Sultanate of Oman.– GeoArabia, **9**(4): 107-138.

Reynolds, R.L., Goldhaber, M. and Tuttle, M.L. (1993): Sulfidization and magnetization above hydrocarbon reservoirs.– In: Aissaoui, D.M., Mcneill, D.F. and Hurley, N.F. (eds.), Applications of Paleomagnetism to Sedimentary Geology, SEPM Spec. Pub., **49**: 167-179; Tulsa.

Rieke, H. (2001): Sedimentologie, Faziesarchitektur und Faziesentwicklung des kontinentalen Rotliegenden im Nordostdeutschen Becken (NEDB).– Diss., Univ. Potsdam, 138 pp.

Rieken, R. (1988): Lösungs-Zusammensetzung und Migrationsprozesse von Paläo-Fluidsystemen in Sedimentgesteinen des Norddeutschen Beckens (Mikrothermometrie, Laser-Raman-Spektroskopie und Isotopen-Geochemie).– Göttinger Arb. Geol. Paläont., **37**: 1-116.

Roden, E.E. and Zachara, J.M. (1996): Microbial reduction of crystalline iron(III) oxides: Influence of oxide surface area and potential for cell growth.– Environ. Sci. Technol., **30**: 1618-1628.

Roden, E.E. and Urrutia, M.M. (1999): Ferrous iron removal promotes microbial reduction of crystalline iron(III) oxides.– Environ. Sci. Technol., **33**: 1847-1853.

Rodon, S. and Littke, R. (2005): Thermal maturity in the Central European Basin system (Schleswig-Holstein area): results of 1D basin modelling and new maturity maps.– Int. J. Earth Sci. / Geol. Rundsch.: in press.

Röhling, H.-G. (1991): A Lithostratigraphic Subdivision of the Lower Triassic in the Northwest German Lowlands and the German Sector of the North Sea, Based on Gamma-Ray and Sonic Logs.– Geol. Jb., **119**: 3-24.

Rosenbaum, J. and Sheppard, S.M. (1986): An isotopic study of siderites, dolomites and ankerites at high temperatures.– Geochim. Cosmochim. Acta, **50**: 1147-1150.

Rossel, N.C. (1982): Clay mineral diagenesis in Rotliegend aeolian sandstones of the southern North Sea.– Clay Min., **17**: 69-77.

Rowe, J. and Burley, S.D. (1997): Faulting and porosity modification in the Sherwood Sandstone at Alderley Edge, northeastern Cheshire: an exhumed example of fault-related diagenesis.– In: Meadows, N.S., et al. (eds.), Petroleum Geology of the Irish Sea and Adjacent Areas, Geol. Soc. London Spec. Publ., **124**: 325-352; London.

Ryan, P.C. and Reynolds, R.C. (1996): The origin and diagenesis of grain-coating serpentine-chlorite in Tuscaloosa Formation sandstone, U.S. Gulf Coast.– Amer. Mineral., **81**: 213-225.

Ryan, P.C. and Hillier, S. (2002): Berthierine/chamosite, corrensite, and discrete chlorite from evolved verdine and evaporite-associated facies in the Jurassic Sundance Formation, Wyoming.– Amer. Mineral., **87**: 1607-1615.

Saigal, G.C., Morad, S., Bjørlykke, K., Egeberg, P.K. and Aagaard, P. (1988): Diagenetic albitization of detrital K-feldspars in Jurassic, Lower Cretaceous and Tertiary clastic reservoir rocks from offshore Norway, I.Textures and origin.– J. Sediment. Petrol., **58**: 1003-1013.

Saigal, G.C., Bjørlykke, K. and Larter, S. (1992): The Effects of Oil Emplacement on Diagenetic Processes - Examples from the Fulmar Reservoir Sandstones, Central North Sea.– AAPG Bull., **76**(7): 1024-1033.

Scheck, M., Bayer, U. and Lewerenz, B. (2003): Salt movements in the Northeast German Basin and its relation to major post-Permian tectonic phases - results from 3D structural modelling, backstripping and reflection seismic data.– Tectonophysics, **361**: 277-299.

Scheck-Wenderoth, M. and Lamarche, J. (2005): Crustal memory and basin evolution in the Central European Basin System - new insights from a 3D structural model.– Tectonophysics, **397**: 143-165.

Scheffer, F. and Schachtschabel, P. (2002): Lehrbuch der Bodenkunde.– 15 ed., 593 pp.; Heidelberg (Spektrum).

Schenk, H.-J., di Primio, R. and Horsfield, B. (1997): The conversion of oil into gas in petroleum reservoirs. Part 1: Comparative kinetic investigation of gas generation from crude oils of lacustrine, marine and fluviodeltaic origin by programmed-temperature closed-system pyrolysis.– Org. Geochem., **26**(7-8): 467-481.

Schluger, P.R. and Roberson, H.E. (1975): Mineralogy and Chemistry of the Patapsco Formation, Maryland, Related to the Ground-Water Geochemistry and Flow System: A Contribution to the Origin of Red Beds.– Geol. Soc. Am. Bull., **86**: 153-158.

Schmidt, C.M. and Heide, K. (2001): Thermal analysis of hydrocarbons in paleozoic black shales.– J. Therm. Anal. Cal., **64**: 1297-1302.

Schmidt, C.M. (2004): DEGAS - Untersuchungen zur Verwitterung von Schwarzpeliten.– Diss., Univ. Jena, 129 pp.

Schmidt, V. and McDonald, D.A. (1979): The role of secondary porosity in the course of sandstone diagenesis.– In: Scholle, P.A. and Schluger, P.R. (eds.), Aspects of diagenesis, SEPM Spec. Pub., **26**: 175-207; Tulsa.

Schneider, J., Gebhardt, U. and Gaitzsch, B. (1995): Fossilführung und Biostratigraphie.– In: Plein, E. (ed.), Norddeutsches Rotliegendbecken, Rotliegend-Monographie Teil II, Cour. Forsch.-Inst. Senckenberg, **183**: 25-39; Frankfurt a.M.

Schneider, J.W. and Gebhardt, U. (1993): Litho- und Biofaziesmuster in intra- und extramontanen Senken des Rotliegend (Perm, Nord- und Ostdeutschland).– Geol. Jb., **A 131**: 57-98.

Schöner, R. and Gaupp, R. (2004a): Diagenetic and thermal evolution of Rotliegend sandstones from onshore Schleswig-Holstein.– DGMK-Tagungsbericht, **2004-2**: 363-369; Celle.

Schöner, R. and Gaupp, R. (2004b): Hydrocarbon fluids and clastic diagenesis: Mineral reactions in redbed reservoir sandstones.– AAPG European Region Conference, Abstracts, 103; Prague.

Schöner, R. and Gaupp, R. (2004c): Diagenese permischer Rotsedimente am Süd- und Nordrand des Nordwestdeutschen Beckens: Ein Vergleich.– Schriftenr. dt. geol. Ges., **33**: 141.

Schöner, R. and Gaupp, R. (2005a): Contrasting red bed diagenesis: The southern and northern margin of the Central European Basin.– Int. J. Earth Sci. / Geol. Rundsch.: in press.

Schöner, R. and Gaupp, R. (2005b): Diagenetic reactions of Fe-species pre- and post petroleum migration: Examples from Permian sandstone reservoirs in northern Germany, Central European Basin System.– Geophysical Research Abstracts, **7**: 8628.

Schöner, R., Lippmann, R., Rusek, M., Ondrak, R. and Gaupp, R. (2005): Gemeinsamkeiten der Diageneseentwicklung in tiefliegenden klastischen Speichergesteinen: Beobachtungen aus der Nordsee, dem Norddeutschen und dem Polnischen Becken.– DGMK-Tagungsbericht 2005-1, 147-152; Celle.

Schott, W., Jaritz, W., Kockel, F., Sames, C.-W., v. Stackelberg, U., Stets, J. and Stoppel, D. (1967): Zur Paläogeographie der Unterkreide im nördlichen Mitteleuropa mit Detailstudien aus Nordwestdeutschland.– Erdöl Erdgas Kohle, **20**: 149-158.

Schröder, L., Plein, E., Bachmann, G.H., Gast, R.E., Gebhardt, U., Graf, R., Helmuth, H.J., Pasternak, M., Porth, H. and Süssmuth, S. (1995): Stratigraphische Neugliederung des Rotliegend im Norddeutschen Becken.– Geol. Jb., **A 148**: 3-21.

Schumacher, D. (1996): Hydrocarbon-induced alteration of soils and sediments.– In: Schumacher, D. and Abrams, M.A. (eds.), Hydrocarbon Migration and Its Near-Surface Expression, AAPG Mem., **66**: 71-89; Tulsa.

Schwarzer, D., Tanner, D., Littke, R., Krawczyk, C.M., Oncken, O., Solms, M., Gaupp, R., Schubart-Engelschall, J. and Trappe, H. (2003): Paläo-Öl- und -Gasfelder im Rotliegenden im Rotliegenden des Norddeutschen Beckens: Wirkung der KW-Migration auf die Speicherqualitäts-Entwicklung. Strukturelle Analyse (3D) und Beckenmodellierung (2D) im Bereich von Tight Gas Arealen am Südrand des Rotliegend Gas Plays.– DGMK-Tagungsbericht, **2003-1**: 17-30; Celle.

Schwarzer, D. and Littke, R. (2005): Petroleum Systems Modelling.– In: Gaupp, R., et al. (eds.), Palaeo Oil- and Gasfields in the Rotliegend of the North German Basin: Effects upon Hydrocarbon Reservoir Quality, DGMK-Forschungsbericht, **593-8**: 3.1-3.58; Hamburg.

Schwarzkopf, T. (1990): Relationship between petroleum generation, migration and sandstone diagenesis, Middle Jurassic, Gifhorn Trough, N Germany.– Mar. Petrol. Geol., **7**: 153-169.

Sedat, B. (1992): Petrographie und Diagenese von Sandsteinen im Nordwestdeutschen Oberkarbon.– DGMK-Forschungsbericht, **384-7**: 1-143.

Seemann, U. (1982): Depositional facies, diagenetic clay minerals and reservoir quality of Rotliegend sediments in the Southern Permian Basin (North Sea): A review.– Clay Min., **17**: 55-67.

Seewald, J.S. (2001a): Model for the origin of carboxylic acids in basinal brines.– Geochim. Cosmochim. Acta, **65**(21): 3779-3789.

Seewald, J.S. (2001b): Aqueous geochemistry of low molecular weight hydrocarbons at elevated temperatures and pressures: Constraints from mineral buffered laboratory experiments.– Geochim. Cosmochim. Acta, **65**(10): 1641-1664.

Seewald, J.S. (2003): Organic-inorganic interactions in petroleum-producing sedimentary basins.– Nature, **426**: 327-333.

Shaw, H.F. (1972): The preparation of orientated clay mineral specimens for X-ray diffraction analysis by a suction-onto-ceramic tile method.– Clay Min., **9**(3): 349-350.

Shebl, M.A. and Surdam, R.C. (1996): Redox reactions in hydrocarbon clastic reservoirs: experimental validation of this mechanism for porosity enhancement.– Chem. Geol., **132**: 103-117.

Small, J.S., Hamilton, D.L. and Habesch, S. (1992): Experimental simulation of clay precipitation within reservoir sandstones 1: techniques and examples.– J. Sediment. Petrol., **62**(3): 508-519.

Spötl, C., Houseknecht, D.W. and Riciputi, L.R. (2000): High-temperature quartz cement and the role of stylolites in a deep gas reservoir, Spiro Sandstone, Arkoma Basin, USA.– In: Worden, R. and Morad, S. (eds.), Quartz cementation in sandstones, Int. Ass. Sed. Spec. Pub., **29**: 281-297; Oxford (Blackwell).

Stahl, W.J. (1968): Zur Herkunft nordwestdeutscher Erdgase.– Erdöl und Kohle, Erdgas, Petrochemie, **21**: 514-518.

Stancu-Kristoff, G. and Stehn, O. (1984): Ein großregionaler Schnitt durch das nordwestdeutsche Oberkarbon-Becken vom Ruhrgebiet bis in die Nordsee.– Fortschr. Geol. Rheinld. u. Westf., **32**: 35-38.

Stelzner, T. and Heide, K. (1996): The study of weathering products of meteorites by means of evolved gas analysis.– Meteor. Planet. Sci., **31**: 249-254.

Strack, Ä. and Freudenberg, U. (1984): Schichtmächtigkeiten und Kohleninhalte im Westfal des Niederrheinisch-Westfälischen Steinkohlenreviers.– Fortschr. Geol. Rheinld. u. Westf., **32**: 243-256.

Strong, G.E. and Milodowski, A.E. (1987): Aspects of the diagenesis of the Sherwood Sandstone of the Wessex Basin and their influence on reservoir characteristics.– In: Marshall, J.D. (ed.), Diagenesis of sedimentary sequences, Geol. Soc. Spec. Pub., **36**: 325-337; London.

Sullivan, M.D., Haszeldine, R.S. and Fallick, A.E. (1990): Linear coupling of carbon and strontium isotopes in Rotliegend Sandstone, North Sea: Evidence for cross-formational fluid flow.– Geology, **18**(12): 1215-1218.

Surdam, R.C., Boese, S.W. and Crossey, L.J. (1984): The geochemistry of secondary porosity.– In: Mcdonald, D.A. and Surdam, R.C. (eds.), Clastic Diagenesis, AAPG Mem., **37**: 127-149; Tulsa.

Surdam, R.C. and Crossey, L.J. (1985): Mechanisms of organic/inorganic interactions in sandstone/shale sequences.– SEPM short course, **17**: 177-272.

Surdam, R.C., Crossey, L.J., Hagen, E.S. and Heasler, H.P. (1989a): Organic-Inorganic Interactions and Sandstone Diagenesis.– AAPG Bull., **73**(1): 1-23.

Surdam, R.C., Dunn, T.L., Heasler, H.P. and MacGowan, D.B. (1989b): Porosity evolution in sandstone/shale systems.– In: Hutcheon, I.E. (ed.), Burial Diagenesis, Mineral. Assoc. Canada Short Course Handbook, **15**: 61-134; Montreal.

Surdam, R.C., Jiao, Z.S. and MacGowan, D.B. (1993): Redox reactions involving hydrocarbons and mineral oxidants: A mechanism for significant porosity enhancement in sandstones.– AAPG Bull., **77**(9): 1509-1518.

Süss, M.P., Drozdzewski, G. and Schäfer, A. (2000): Sequenzstratigraphie des kohleführenden Oberkarbons im Ruhr-Becken.– Geol. Jb., **A 156**: 45-106.

Sweeny, J.J. and Burnham, A.K. (1990): Evaluation of a Simple Model of Vitrinite Reflectance Based on Chemical Kinetics.– AAPG Bull., **74**(10): 1559-1570.

Teichmüller, M. (1955): Anzeichen mariner Beeinflussung bei der Kohle aus Flöz Katharina der Zeche Frierich Heinrich.– N. Jb. Geol. Paläont., Mh., **1955**: 193-201.

Teichmüller, M. (1974): Entstehung und Veränderung bituminöser Substanzen in Kohlen in Beziehung zur Entstehung und Umwandlung des Erdöl.– Fortschr. Geol. Rheinld. u. Westf., **24**: 65-112.

Teichmüller, M., Teichmüller, R. and Bartenstein, H. (1979): Inkohlung und Erdgas in Nordwestdeutschland. Eine Inkohlungskarte der Oberfläche des Oberkarbons.– Fortschr. Geol. Rheinld. u. Westf., **27**: 137-170.

Teichmüller, M., Teichmüller, R. and Bartenstein, H. (1984): Inkohlung und Erdgas - eine neue Inkohlungskarte der Karbon-Oberfläche in Nordwestdeutschland.– Fortschr. Geol. Rheinld. u. Westf., **32**(1): 11-34.

Teinturier, S. and Pironon, J. (2004): Experimental growth of quartz in petroleum environment. Part I: Procedures and Fluid Trapping.– Geochim. Cosmochim. Acta, **68**(11): 2495-2507.

Thompson, A.M. (1970): Geochemistry of color genesis in red-bed sequence, Juniata and Bald Eagle Formations, Pennsylvania.– J. Sediment. Petrol., **40**(2): 599-615.

Thyne, G. (2001): A model for diagenetic mass transfer between adjacent sandstone and shale.– Mar. Petrol. Geol., **18**: 743-755.

Thyne, G., Boudreau, B.P., Ramm, M. and Midtbo, R.E. (2001): Simulation of potassium feldspar dissolution and illitization in the Statfjord Formation, North Sea.– AAPG Bull., **85**(4): 621-635.

Tissot, B.P. and Welte, D.H. (1984): Petroleum Formation and Occurence.– 2 ed., 699 pp.; Berlin (Springer).

Tompkins, R.E. (1981): Sanning electron microscopy of a regular chlorite/smectite (corrensite) from a hydrocarbon reservoirs sandstone.– Clays Clay Min., **29**(3): 233-235.

Torrent, J. and Schwertmann, U. (1987): Influence of hematite on the color of red beds.– J. Sediment. Petrol., **57**(4): 682-686.

Torsvik, T.H., Trench, A., Svensson, I. and Walderhaug, H.J. (1993): Palaeogeographic significance of mid-Silurian palaeomagnetic results from southern Britain - major revision of the apparent pole wander path for eastern Avalonia.– Geophys. J. Int., **113**: 651-668.

Torsvik, T.H. and Rehnström, E.F. (2003): The Tornquist Sea and Baltica-Avalonia docking.– Tectonophysics, **362**: 67-82.

Trask, P.D. (1932): Origin and environment of source sediments of petroleum.– 323 pp.; Houston (Gulf Publ. Co.).

Tröger, W.E. (1967): Optische Bestimmung der gesteinsbildenen Minerale. Teil 2: Textband.– 822 pp.; Stuttgart (Schweizerbart).

Trusheim (1957): Über Halokinese und ihre Bedeutung für die strukturelle Entwicklung Norddeutschlands.– Z. dt. geol. Ges., **109**: 111-157.

Tucker, M. (ed.) (1996): Methoden der Sedimentologie.– 366 pp.; Stuttgart (Enke).

Turner, P. (1980): Continental Red Beds.– Develop. Sediment., **29**, 562 pp.; Amsterdam.

Underhill, J.R. and Partington, M.A. (1993): Jurassic thermal doming and deflation in the North Sea: implications of the sequence stratigraphic evidence.– In: Parker, J.R. (ed.), Petroleum Geology of Northwest Europe: Proceedings of the 4th Conference, 337-345; London (The Geological Society).

Utada, M. (2001): Zeolites in burial diagenesis and low-grade metamorphic rocks.– In: Bish, D.L. and Ming, D.W. (eds.), Natural zeolites: occurence, properties, applications, Reviews in Mineralogy and Geochemistry, **45**: 277-322.

van Houten, F.B. (1968): Iron Oxides in Red Beds.– Geol. Soc. Am. Bull., **79**: 399-416.

van Keer, I., Muchez, P. and Viaene, W. (1998): Clay mineralogical variations and evolutions in sandstone sequences near a coal seam and shales in the Westphalian of the Campine Basin.– Clay Min., **33**: 159-169.

van Wees, J.D., Stephenson, R.A., Ziegler, P.A., Bayer, U., McCann, T., Dadlez, R., Gaupp, R., Narkiewicz, M., Bitzer, F. and Scheck, M. (2000): On the Origin of the Southern Permian Basin, Central Europe.– Mar. Petrol. Geol., **17**: 43-59.

Vandenbroucke, M., Behar, F. and Rudkiewicz, J.L. (1999): Kinetic modelling of petroleum formation and cracking: implications from the high pressure/high temperature Elgin Field (UK, North Sea). – Org. Geochem., 30: 1105-1125.– Org. Geochem., **30**(9): 1105-1125.

von der Gönna, J., Nover, G., Poelchau, M. and Schönbohm, D. (2003): Fluid flow and petrophysical properties of sedimentary rocks exposed to different stress regimes: Petrophysics.– Terra Nostra, **2003**(7): 94-97.

von Eynatten, H. and Gaupp, R. (1999): Provenance of Cretaceous synorogenic sandstones in the Eastern Alps: constraints from framework petrography, heavy mineral analysis, and mineral chemistry.– Sed. Geol., **124**: 81-111.

Wachter, E. and Hayes, J.M. (1985): Exchange of oxygen isotopes in carbon-dioxide - phosphoric acid systems.– Chem. Geol., **52**: 365-374.

Walderhaug, O. (1994): Temperatures of quartz cementation in Jurassic sandstones from the Norwegian continental shelf - Evidence from fluid inclusions.– J. Sediment. Res., **A64**(2): 311-323.

Walker, T.R. (1967): Formation of Red Beds in Modern and Ancient Deserts.– Geol. Soc. Am. Bull., **78**: 353-368.

Walker, T.R. and Honea, R.M. (1969): Iron content of modern deposits in the Sonoran desert: A contribution to the origin of red beds.– Geol. Soc. Am. Bull., **80**: 535-544.

Walker, T.R. (1976): Diagenetic origin of continental red beds.– In: Falke, H. (ed.), The continental Permian in Central, West and South Europe, NATO ASI series C, **22**: 240-282; Dordrecht (Reidel).

Walker, T.R., Waugh, B. and Grone, A.J. (1978): Diagenesis in first-cycle desert alluvium of Cenozoic age, southwestern united States and northwestern Mexico.– Geol. Soc. Am. Bull., **89**: 19-32.

Waples, D.W. (1994): Maturity Modeling: Thermal Indicators, Hydrocarbon Generation, and Oil Cracking.– In: Magoon, L.B. and Dow, W.G. (eds.), The Petroleum System - from source to trap, AAPG Mem.**60**: 285-306; Tulsa.

Warren, E.A. and Smalley, P.C. (eds.) (1994): North Sea Formation Waters Atlas.– Geol. Soc. Mem., **15**, 208 pp.; London.

Watts, N.L. (1980): Quaternary pedogenic calcretes from the Kalahari (south Afraica): mineralogy, genesis and diagenesis.– Sedimentology, **27**: 661-686.

Weber, H. (1977): Salzstrukturen, Erdöl und Kreidebasis in Schleswig-Holstein.– Übersichtskarten zur Geologie von Schleswig-Holstein, 106 pp.; Kiel (Geol. L.-A. Schleswig-Holstein).

Weibel, R. (1998): Diagenesis in oxidising and locally reducing conditions - an example from the Triassic Skagerrak Formation, Denmark.– Sed. Geol., **121**: 259-276.

Welte, D.H. and Yükler, M.A. (1981): Petroleum origin and accumulation in basin evolution - A quantitative model.– AAPG Bull., **65**: 1387-1396.

Welte, D.H. and Yalçin, M.N. (1988): Basin modelling - A new comprehensive method in petroleum geology.– Org. Geochem., **13**: 141-152.

Welte, D.H., Horsfield, B. and Baker, D.R. (eds.) (1997): Petroleum and Basin Evolution.– 535 pp.; Berlin (Springer).

Wilkinson, J.J., Lonergan, L., Fairs, T. and Herrington, R.J. (1998): Fluid inclusion constraints on conditions and timing of hydrocarbon migration and quartz cementation in Brent Group reservoir sandstones, Columba Terrace, northern North Sea.– In: Parnell, J. (ed.), Dating and Duration of Fluid Flow and Fluid-Rock Interaction, Geol. Soc. Spec. Pub., **144**: 69-89; London.

Wilkinson, M. and Haszeldine, R.S. (1996): Aluminium loss during sandstone diagenesis.– J. Geol. Soc. London, **153**: 657-660.

Wilkinson, M., Darby, D., Haszeldine, R.S. and Couples, G.D. (1997): Secondary porosity generation during deep burial associated with overpressure leak-off: Fulmar Formation, United Kingdom Central Graben.– AAPG Bull., **81**(5): 803-813.

Wilkinson, M., Milliken, K.L. and Haszeldine, R.S. (2001): Systematic destruction of K-feldspar in deeply buried rift and passive margin sandstones.– J. Geol. Soc., **158**: 675-683.

Wilkinson, M. and Haszeldine, R.S. (2002): Fibrous illite in oilfield sandstones - a nucleation kinetic theory of growth.– Terra Nova, **14**(1): 56-60.

Wilkinson, M., Haszeldine, R.S. and Milliken, K.L. (2003): Cross-formational flux of aluminium and potassium in Gulf Coast (USA) sediments.– In: Worden, R.H. and Morad, S. (eds.), Clay mineral cements in sandstones, Int. Ass. Sed. Spec. Pub., **34**: 147-160; Oxford (Blackwell).

Wilkinson, M., Haszeldine, R.S. and Fallick, A.E. (2004): Jurassic and Cretaceous clays of the northern and central North Sea hydrocarbon reservoirs reviewed.– In: Jeans, C.V. (ed.), Clay Stratigraphy for the UK, (Min. Soc.).

Williams-Jones, A.E. and Wood, S.A. (1992): A preliminary petrogenetic grid for REE fluorocarbonates and associated minerals.– Geochim. Cosmochim. Acta, **56**: 725-738.

Wilson, M.D. (1992): Inherited grain-rimming clays in sandstones from eolian and shelf environments: their origin and control on reservoir properties.– In: Houseknecht, D.W. and Pittman, E.D. (eds.), Origin, Diagenesis, and Petrophysiscs of Clay Minerals in Sandstones, SEPM Spec. Pub., **47**: 209-225; Tulsa.

Wolfgramm, M. and Schmidt-Mumm, A. (2002): Die zeitliche Einordnung diagenetischer und hydrothermaler Fluidphasen im Nordostdeutschen Becken (NEDB).– Zbl. Geol. Paläont., Teil 1, **2001**(3/4): 237-256.

Worden, R. (ed.) (2000): Quartz cementation in sandstones.– Int. Ass. Sed. Spec. Pub., **29**, 342 pp.; Oxford (Blackwell).

Worden, R. and Morad, S. (eds.) (2003a): Clay Mineral Cements in Sandstones.– Int. Ass. Sed. Spec. Pub., **34**, 520 pp.; Oxford (Blackwell).

Worden, R. and Morad, S. (2003b): Clay minerals in sandstones: control on formation, distribution and evolution.– In: Worden, R. and Morad, S. (eds.), Clay Mineral Cements in Sandstones, Int. Ass. Sed. Spec. Pub., **34**: 3-41; Oxford (Blackwell).

Worden, R.H., Smalley, P.C. and Oxtoby, N.H. (1995): Gas souring by thermochemical sulfate reduction.– AAPG Bull., **79**(6): 853-871.

Worden, R.H., Smalley, P.C. and Oxtoby, N.H. (1996): The effects of thermochemical sulfate reduction upon formation water salinity and oxygen isotopes in carbonate reservoirs.– Geochim. Cosmochim. Acta, **60**: 3925-3931.

Wygrala, B. (1989): Integrated study of an oil field in southern Po Basin, northern Italy.– Ber. Forschungszentrum Jülich, **2313**: 1-217.

Yalçin, M.N. (1991): Basin modeling and hydrocarbon exploration.– J. Petrol. Sci. Eng., **5**(4): 379-398.

Yalçin, M.N., Littke, R. and Sachsenhofer, R.F. (1997): Thermal history of sedimentary basins.– In: Welte, D.H., Horsfield, B. and Baker, D.R. (eds.), Petroleum and Basin Evolution, 71-168; Berlin (Springer).

Zachara, J.M., Fredrickson, J.K., Li, S., Kennedy, D.W., Smith, S.C. and Gassman, P.L. (1998): Bacterial reduction of crystalline Fe^{3+} oxides in single phase suspensions and subsurface materials.– Amer. Mineral., **83**: 1426-1443.

Zachara, J.M., Kukkadapu, R.K., Gassman, P.L., Dohnalkova, A., Fredrickson, J.K. and Anderson, T. (2004): Biogeochemical transformation of Fe minerals in a petroleum-contaminated aquifer.– Geochim. Cosmochim. Acta, **68**(8): 1791–1805.

Ziegler, K. (1993): Diagenetic and geochemical history of the Rotliegend of the Southern North Sea (UK Sector): A comparative study.– Diss., Univ. of Reading, 329 pp.

Ziegler, P.A. (1978): North-Western Europe: tectonics and basin development.– Geol. Mijnbouw, **57**: 589-626.

Ziegler, P.A. (1981): Evolution of Sedimentary Basins in North-West Europe.– In: Illing, L.V. and Hobson, G.D. (eds.), Petroleum Geology of the Continental Shelf of North West Europe, 3-39; London (Heyden).

Ziegler, P.A. (1990): Geological Atlas of Western and Central Europe.– Shell Intern. Petrol. Maatschappij B.V., 2 ed., 239 pp.; Amsterdam (Elsevier).

Zimmerle, W. and Tietze, K.-W. (1971): Erscheinungsformen von Leukoxen aus Sandsteinen unter dem Raster-Elektronenmikroskop.– Der Aufschluss, **22**(2): 61-68.

Zuffa, G.G. (1985): Optical analysis of arenites: influence of methodology on compositional results.– In: Zuffa, G.G. (ed.), Provenance of Arenites, 165-189; Dordrecht (Reidel).

Zwingmann, H., Clauer, N. and Gaupp, R. (1998): Timing and fluid flow in a sandstone reservoir of the north German Rotliegend (Permian) by K-Ar dating of related hydrothermal illite.– In: Parnell, J. (ed.), Dating and Duration of Fluid Flow and Fluid-Rock Interaction, Geol. Soc. Spec. Pub., **144**: 91-106; London.

Zwingmann, H., Clauer, N. and Gaupp, R. (1999): Structure-related geochemical (REE) and isotopic (K-Ar, Rb-Sr, $\delta^{18}O$) characteristics of clay minerals from Rotliegend sandstone reservoirs (Permian, northern Germany).– Geochim. Cosmochim. Acta, **63**(18): 2805-2823.

PLATES

Plate 1:
Rotliegend lithology at the northern margin of the NGB. Depth below base Zechstein.

Plate 2-5:
Rotliegend petrography at the northern margin of the NGB.

Plate 6-7:
Petrography and geochemistry of carbonate cements at the northern margin of the NGB.

Plate 8:
Representative examples of XRD patterns of sandstones from the northern basin margin.

Plate 9-11:
Rotliegend petrography at the southern margin of the NGB.

Plate 12-14:
Degassing profiles (DEGAS), northern margin of the NGB.

Plate 15-17:
Degassing profiles (DEGAS), southern margin of the NGB.

Plate 1: Rotliegend lithology at the northern margin of the NGB. Depth below base Zechstein.

A: Very poorly sorted, clast-supported breccia with sandy matrix. Angular to subangular porphyric volcanic fragments are the most frequent clast type. The photo displays the lower part of an approximately 0.7 m thick breccia layer. The breccia is not graded, but large clast are floating within the layer.
Well Schleswig Z1, 2071 m.

B: Cross bedded conglomerate layer of 18 cm thickness. The poorly sorted conglomerate contains abundant (well) rounded quartz pebbles, rock fragments, and red-brown mud flakes. It follows without evidence of erosion on top of cross-bedded sandstones. The conglomerate is graded and is covered by a thin mudstone layer.
Well Flensburg Z1, 1264 m.

C: Clast-supported conglomerate, overlaid by horizontally laminated sandstone. The conglomerate is poorly sorted in the lower part, where elongate clasts are imbricated. In the moderately sorted upper part, pore spaces are filled by carbonate cement (white). There is a sharp, non-erosive boundary to the laminated, fine to medium grained sandstones.
Well Fehmarn Z1, 837 m.

D: Cross-bedded, fine-medium grained, well sorted sandstone. Brown mud flakes are aligned parallel to the lamination and indicate fluvial deposition. Note the brown-grey rock colour in contrast to the typical red/red-brown colour of other Rotliegend clastics.
Well Flensburg Z1, 935 m.

E: Cross-bedded sandstone. The sandstone consists of alternating, well sorted laminae of fine grained and fine-medium grained sand. The uniform, apparently planar cross-bedded set is approximately 0.5 m thick in this case (only lower part visible here). This type of sandstone is most likely an eolian sediment.
Well Schleswig Z1, 2077 m.

F: Poorly sorted, fine-medium grained, pebbly sandstone. Elongate clasts in the lower part trace a low-angle cross bedding, while the upper part is flat laminated. This fluvial sandstone is overlaid by a fine-medium grained conglomerate layer.
Well Schleswig Z1, 2067 m.

G: Fine to coarse grained sandstone, containing silt and clay. In the lower part, a flat laminated, moderately sorted sandstone overlies a mm-thin, desiccated mudstone layer. The upper part, separated by a second thin mudstone layer, is and characterised by poor sorting, diffuse lamination and silt-clay rich areas. Such sandstones are part of the sandflat environment.
Well Fehmarn Z1, 777 m.

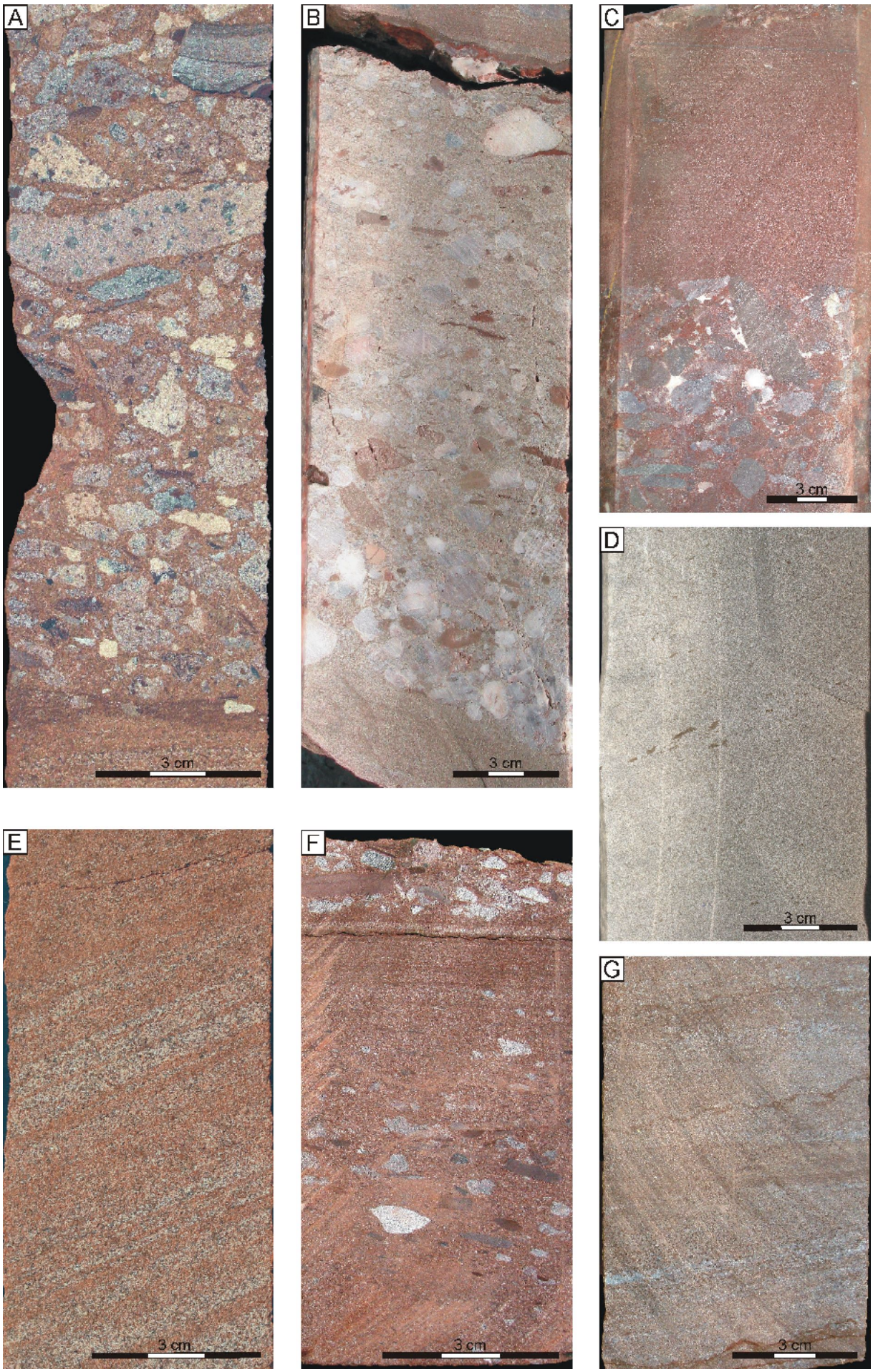
A
3 cm
B
3 cm
C
3 cm
D
3 cm
E
3 cm
F
3 cm
G
3 cm

Plate 2: Rotliegend petrography at the northern margin of the NGB.

A: Hematite (Hm, dark brown) and illite (IC, bright) grain coatings, and pore-filling calcite cement (Cc). Detrital grains are corroded.
Well Fehmarn Z1, sample Fe015, photomicrograph, plane polarised light.

B: Early dolomite (Do I), overgrown by later zoned dolomite (Do II) after a phase of dissolution. Growth bands of zoned dolomite separated by hematite layers (dark brown). Pore-lining radial chlorite (CR) partly overgrown by zoned dolomite. Open pore space is blue.
Well Flensburg Z1, sample Fb019, photomicrograph, plane polarised light.

C: Elongate Ti-oxide (Ti), overgrown by pore-filling calcite cement. The euhedral shape of the Ti-oxide indicates authigenic origin. Pore surfaces are coated by hematite (Hm) and illite (IC).
Well Fehmarn Z1, sample Fe030, photomicrograph, plane polarised light.

D: Typical cluster of Ti-oxides (Ti) in and around a dissolved grain. The outline of the former grain is still visible by a coating of radial chlorite (CR). Ti-oxides are probably partly detrital (relics of the dissolved grain), but the euhedral shape of some crystals (white arrows) suggests authigenic origin. Zoned, partly dissolved dolomite (Do), and hematite grain coating (Hm). Open pore space is blue.
Well Flensburg Z1, sample Fb035, photomicrograph, plane polarised light.

E: Early syntaxial quartz overgrowth (Qz I), post-dated by hematite-illite grain coating (Hm). Pore-space cemented by quartz (Qz II) and barite (Ba) after substantial compaction.
Well Schleswig Z1, sample Sw010, photomicrograph, plane polarised light.

F: Early syntaxial quartz overgrowth (Qz I) on almost every grain are difficult to distinguish from detrital quartz owing to the virtual absence of grain coatings. Examples are marked by arrows. Pore-space cemented by early dolomite (Do) and traces of calcite (Cc, red). The textural relation between dolomite and calcite is ambiguous here.
Well Flensburg Z1, sample Fb029, photomicrograph, cross polarised light.

G: Large pore space filled by albite (Ab), calcite (Cc) and barite (Ba). Early zoned calcite (bright grey and medium grey zones) is overgrown by apparently homogeneous calcite cement. Barite is typically found in coarse laminae of the sandstones.
Well Schleswig Z1, sample Sw016, BSE micrograph.

H: Early dolomite cement (Do) replacing a completely altered detrital grain ("pseudomatix", PM). The original, probably a clay-rich clast has been transformed to chlorite.
Well Flensburg Z1, sample Fb022, photomicrograph, plane polarised light.

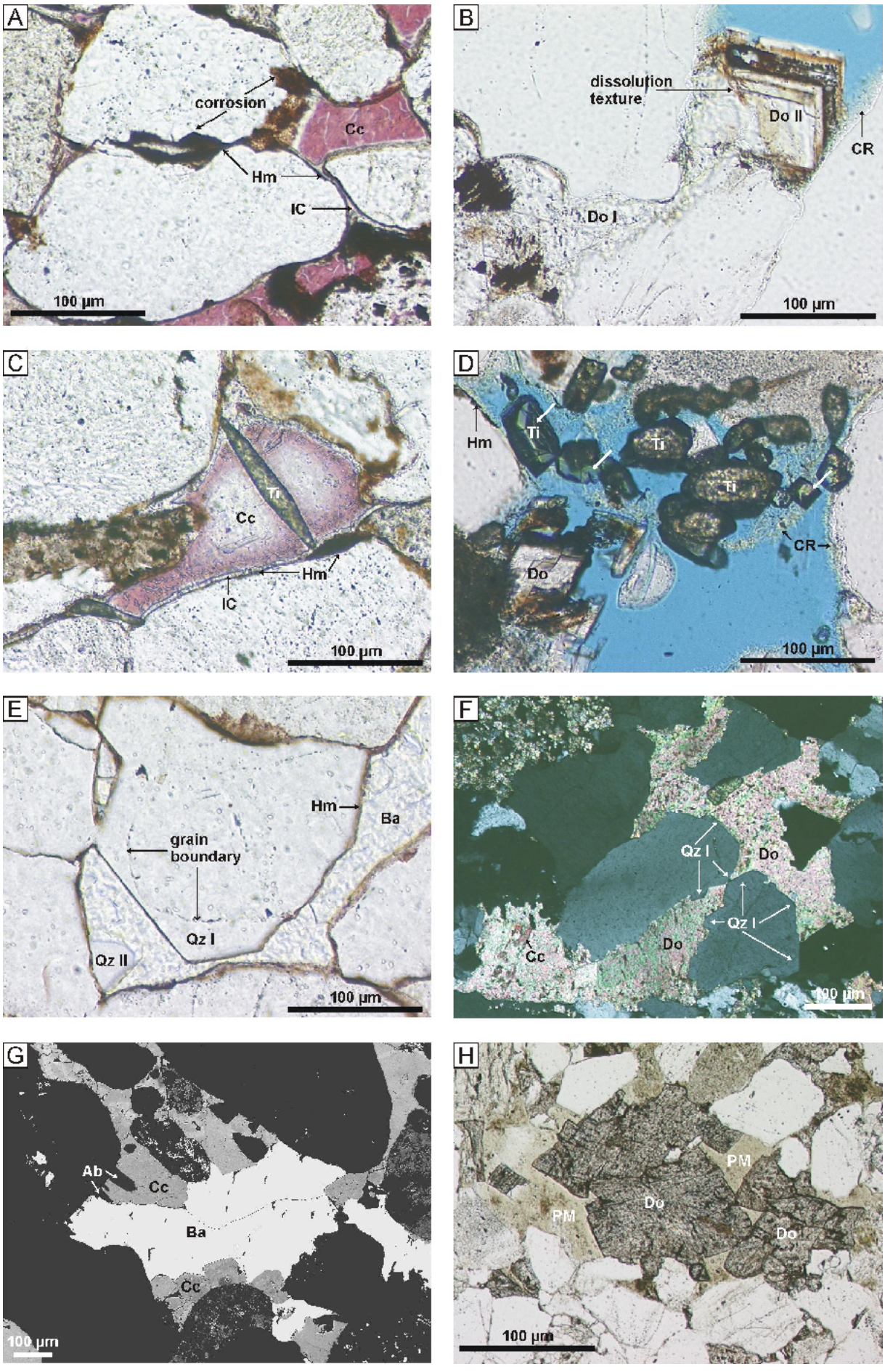
A
corrosion
Cc
Hm
IC
100 µm
B
dissolution texture
Do II
CR
Do I
100 µm
C
Ti
Cc
Hm
IC
100 µm
D
Hm
Ti
Ti
Ti
CR
Do
100 µm
E
Hm
Ba
grain boundary
Qz I
Qz II
100 µm
F
Qz I
Do
Qz I
Cc
Do
100 µm
G
Ab
Cc
Ba
Cc
100 µm
H
PM
Do
PM
Do
100 µm

Plate 3: Rotliegend petrography at the northern margin of the NGB.

A, B: Grain surfaces are partly covered by hematite (Hm, dark brown). Most of the pore space is cemented by syntaxial quartz cement (Qz).
Well Flensburg Z1, sample Fb019, photomicrograph, plane polarised light (A), cross polarised light (B).

C: Corroded quartz grain in the centre with hematite-illite coatings (Hm) and thick hematite aggregates in grain embayments. The IGV is cemented by euhedral, twinned albite (Ab) and subsequenc calcite (Cc) cement.
Well Schleswig Z1, sample Sw024, photomicrograph, linear polarised light.

D: Non-luminescent syntaxial quartz overgrowth (Qz I), blue luminescent pore-filling quartz cement with irreguar non-luminescent patches (Qz II).
Well Flensburg Z1, sample Fb008, CL micrograph.

E, F: Quartz cement (Qz) supporting a grain framework after substantial compaction. Calcite cement (Cc) with homogeneous orange luminescence colours fills remaining pore space. CL colours of quartz cannot be determined here owing to the intense luminescence of calcite.
Well Schleswig Z1, sample Sw016, photomicrograph, cross polarised light (E), Cl micrograph (F).

G: Pore-filling zoned calcite cement (Cc), showing bright orange to red luminescence colours. Calcite also replaces parts of detrital volcanic grains (white arrows). The relatively low IGV indicates substantial mechanical compaction prior to precipitation of calcite cements.
Well Fehmarn Z1, sample Fe011, CL micrograph.

H: Some pores are cemented by dolomite (Do) with red to red-brown luminescence colours, others are filled by zoned calcite cements (Cc). Calcite shows orange luminescent rims and brown or non-luminescent cores. Textural evidence suggests that dolomite was partly replaced by calcite (white arrow).
Well Flensburg Z1, sample Fb008, CL micrograph.

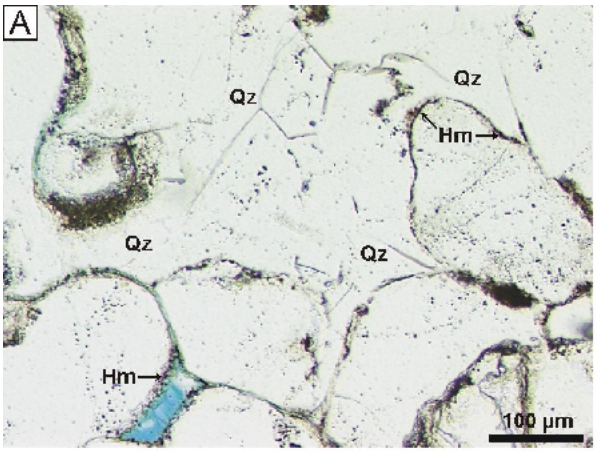
A
Qz
Qz
Hm
Qz
Qz
Hm
100 µm

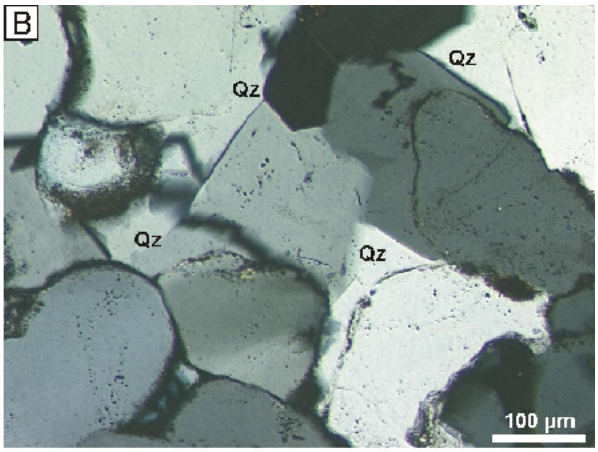
B
Qz
Qz
Qz
Qz
100 µm

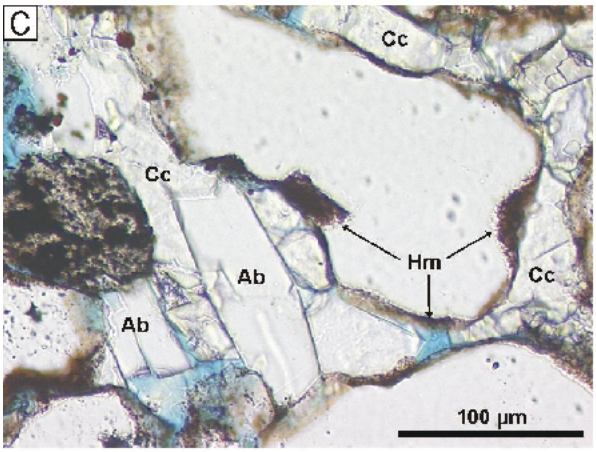
C
Cc
Cc
Hm
Ab
Cc
Ab
100 µm

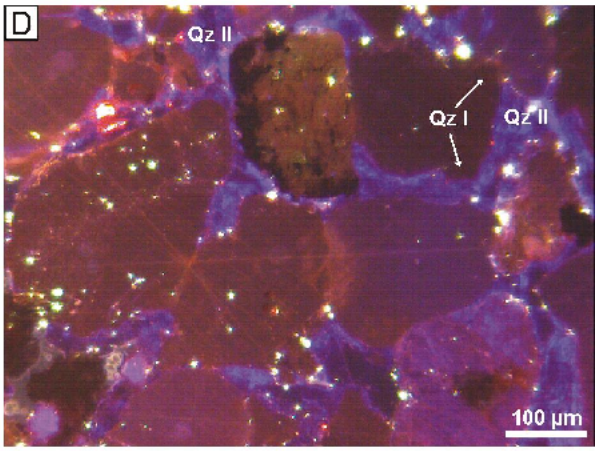
D
Qz II
Qz I
Qz II
100 µm

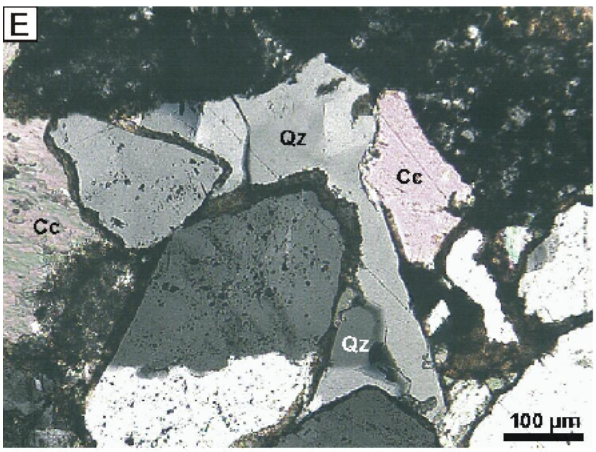
E
Qz
Cc
Cc
Qz
100 µm

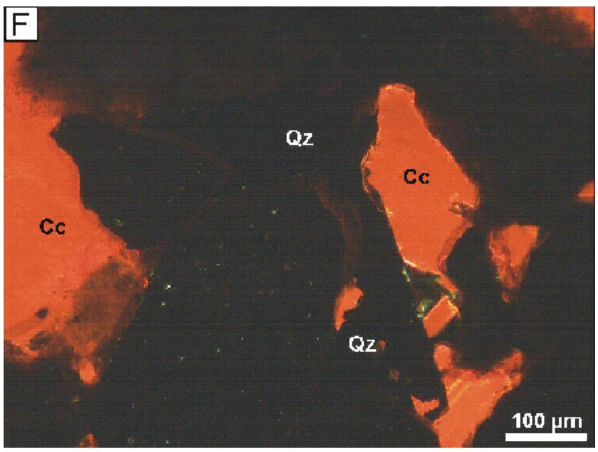
F
Qz
Cc
Cc
Qz
100 µm

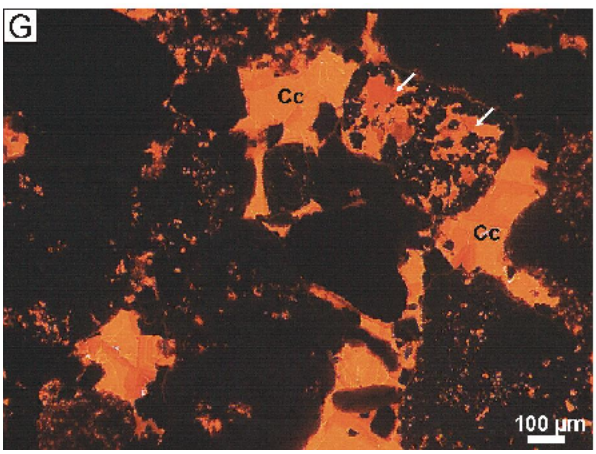
G
Cc
Cc
100 µm

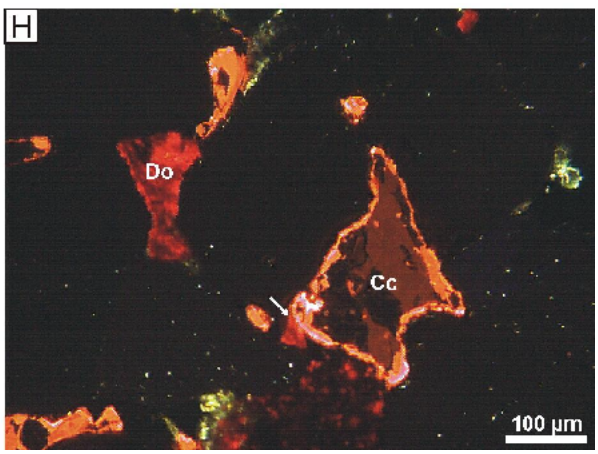
H
Do
Cc
100 µm

Plate 4: Rotliegend petrography at the northern margin of the NGB.

A: Albitisiation of detrital feldspar. Clear authigenic albite (Ab) with sharp crystal edges is evident in the lower part of the grain. Most feldspars in well Flensburg Z1 measured by EMP consist entirely of albite, so it is difficult to prove the original feldspar composition. Parts of the feldspar have been dissolved. The original outline of the grain is visible by tangential and radial chlorite coatings (CT/CR). Open pore space is blue.
Well Flensburg Z1, sample Fb035, photomicrograph, plane polarised light.

B: Detrital feldspar (Fs), partly dissolved, and partly replaced by authigenic albite (Ab). Feldspar dissolution and albite growth took place after formation of thick hematite-illite grain coatings (Hm). Calcite cement (Cc) fills parts of the IGV. Open pore space is blue.
Well Schleswig Z1, sample Sw015, photomicrograph, plane polarised light.

C: Detrital grain, probably a former feldspar (Fs), almost completely replaced by albite (Ab) and calcite (Cc). Individual detrial grains are covered by hematite (Hm) and chlorite coatings (CT).
Well Flensburg Z1, sample Fb023, photomicrograph, linear polarised light.

D: Dense meshwork of illite (IM) in a strongly compacted grain framework. Grain surfaces are coated by hematite (Hm) and tangential illite (IC). The IM in this case probably represents replacement of clay matrix, or replacement of a feldspar or lithic grain.
Well Fehmarn Z1, sample Fe019, photomicrograph, cross polarised light.

E: Illite meshwork (IM) replacing a strongly deformed grain, possibly a former feldspar or volcanic rock fragment. Relics of the grain are still visible (arrow). Hematite-illite grain coatings (Hm), minor intergranular calcite cement (Cc). Note the low IGV, suggesting strong mechanical compaction.
Well Schleswig Z1, sample Sw017, photomicrograph, plane polarised light.

F: Loose platy meshwork illite (IM) and relics of a corroded sedimentary or metasedimentary fragment (L_{sm}). Authigenic illite is only present in the vicinity of the corroded clast, and absent in adjacent pores (e.g. upper right corner). Open pore space is black.
Well Schleswig Z1, sample Sw027, BSE micrograph.

G: Vein-filling Mn-rich, zoned calcite (Cc) and zoned Mn-oxides/hydroxides (Mn). Minor anhydrite (An). Mn-oxides/hydroxides were only observed around veins in this locality. Volcanic fragments in the vicinity of this vein are completely replaced by these cements.
Well Fehmarn Z1, sample Fe011, BSE micrograph.

H: Quartz-rich sandstone cemented by radial chlorite (CR), authigenic quartz (Qz), and late halite (Ha). It is not clear whether halite is part of the diagenetic sequence or precipitated during drilling. Small hematite aggregates (Hm) are concentrated on grain surfaces, especially in grain indentations.
Well Flensburg Z1, sample Fb035, BSE micrograph.

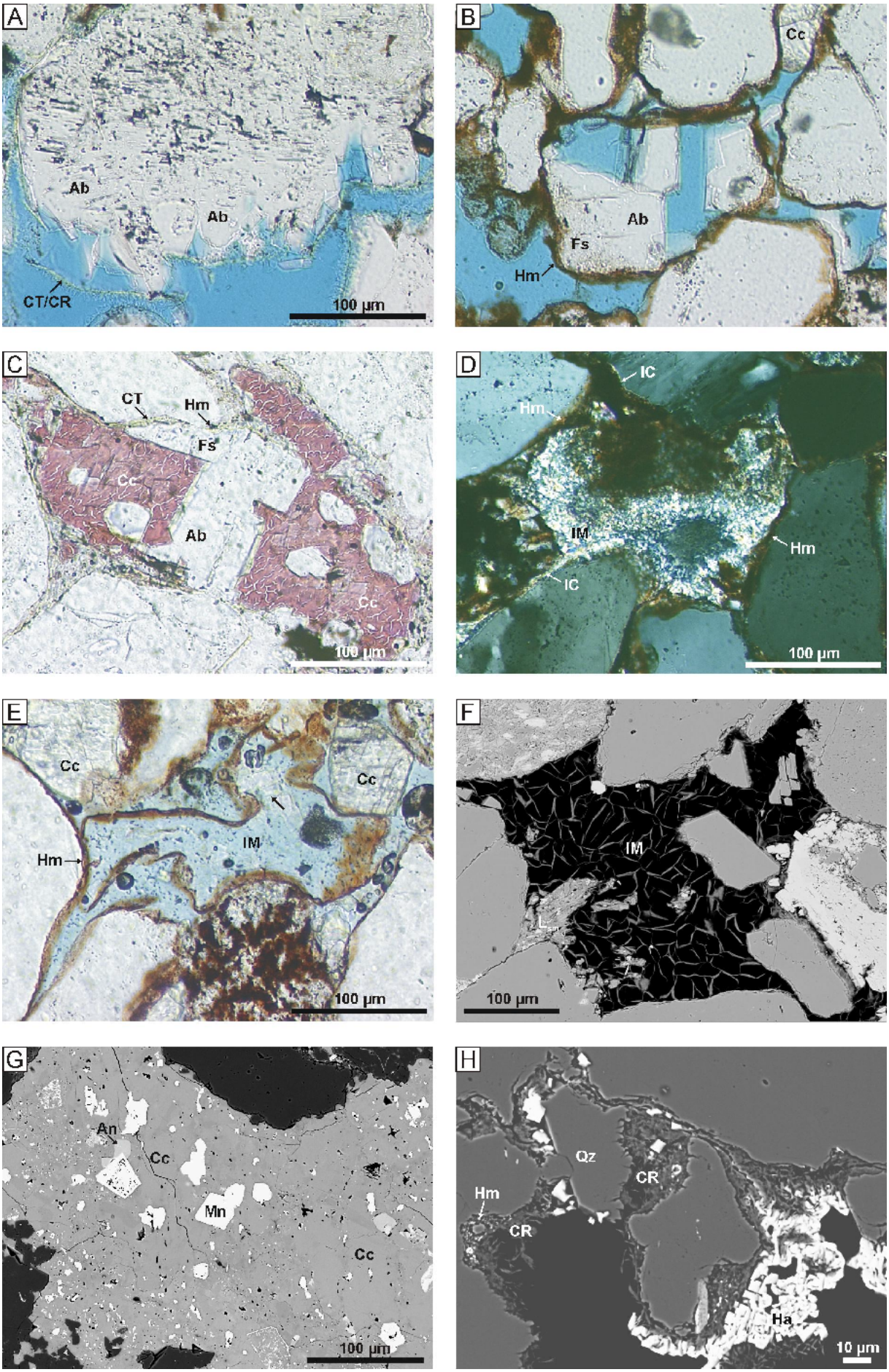
A
Ab
Ab
CT/CR
100 µm
B
Cc
Ab
Fs
Hm
C
CT
Hm
Fs
Cc
Ab
Cc
100 µm
D
IC
Hm
IM
Hm
IC
100 µm
E
Cc
Cc
IM
Hm
100 µm
F
IM
100 µm
G
An
Cc
Mn
Cc
100 µm
H
Qz
CR
Hm
CR
Ha
10 µm

Plate 5: Rotliegend petrography at the northern margin of the NGB.

A: Pore-lining radial chlorite, growing perpendicular to grain surfaces. Single crystals are about 5-10 µm in size and are arranged in a boxwork (honeycomb) texture. They partly have curved crystal faces.
Well Flensburg Z1, sample Fb041, SE micrograph, gold coating.

B: Pore-lining radial chlorite. Crystal faces are curved, crystals are strongly intergrown. Such textures point to an precursor mixed-layer/swelling clay minerals.
Well Flensburg Z1, sample Fb057, SE micrograph, gold coating.

C: Detrital quartz grain (Qz) coated by tangential chlorite (CT) of ≤3 µm thickness. The chlorite coating is overgrown by authigenic dolomite.
Well Flensburg Z1, sample Fb047, SE micrograph, carbon coating.

D: Pore-lining radial chlorite (CR), partly overgrown by authigenic quartz cement (Qz). Radial chlorite engulfs all grain surfaces with contact to open pore space.
Well Flensburg Z1, sample Fb009, SE micrograph, carbon coating.

E: Hematite-illite-coating (Hm-IC) and thick illite coating (IC) on quartz grain (Qz). The co-occurence of hematite and illite as thin layers on grain surfaces is typical for most Rotliegend sandstones. Thick illite coatings were observed in some poorly sorted, fluvial sandstones and conglomerates and most likely represent infiltrated clay.
Well Fehmarn Z1, sample Fe014, SE micrograph, carbon coating.

F: Surface of a detrital grain coated by hematite and illite (Hm+IC). The coating is only few µm thick and appear to post-date minor authigenic quartz overgrowths (Qz).
Well Schleswig Z1, sample Sw028, SE micrograph, carbon coating.

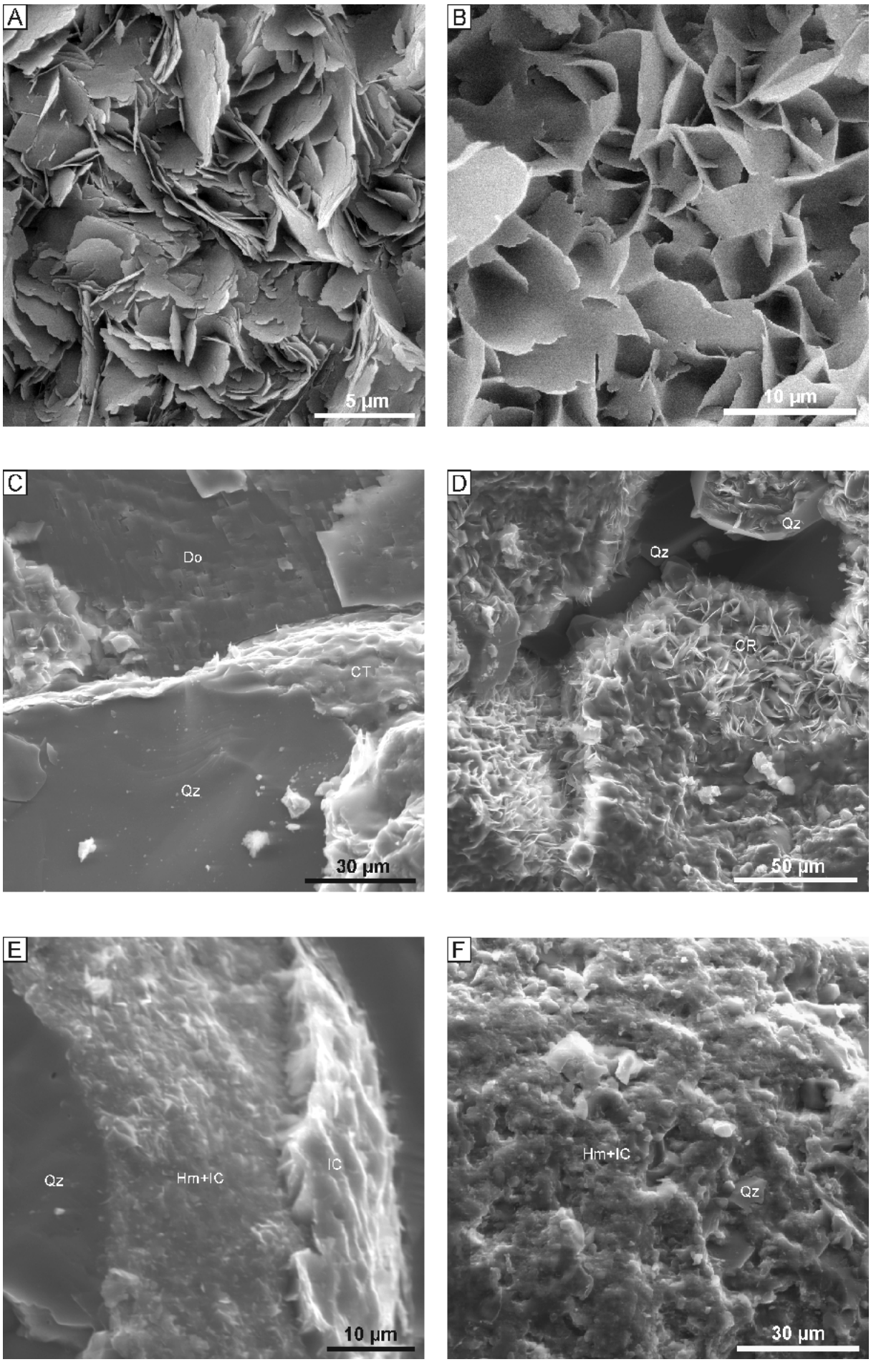
A
5 µm
B
10 µm
C
Do
CT
Qz
30 µm
D
Qz
Qz
CR
50 µm
E
Qz
Hm+IC
IC
10 µm
F
Hm+IC
Qz
30 µm

Plate 6: Petrography and geochemistry of carbonate cements at the northern margin of the NGB.

A, B: Pore-filling, zoned calcite cement. Calcite replaces a detrital grain (centre). Replacive calcite and early calcite overgrowth show similar BSE patterns and relatively low Fe, Mn, and Mg contents. Later calcite bands are enriched in Mn, and partly in Mg.
Well Schleswig Z1, sample Sw027, BSE micrograph (A), EMP analyses (B).

C, D: Pore-filling, zoned calcite and barite cement. Calcite replaces a detrital grain (centre). The early overgrowth is relatively pure calcite. Later calcite bands show different degrees of Mn and Mg enrichment. The iron content is low throughout.
Well Schleswig Z1, sample Sw031, BSE micrograph (C), EMP analyses (D).

E, F: Pore-filling authigenic albite and zoned Mn-rich calcite cement. 4-8 mol.-% $MnCO_3$ are among the highest Mn contents measured in calcite cements of the northern basin margin.
Well Fehmarn Z1, sample Fe011, BSE micrograph (E), EMP analyses (F).

G, H: Pore-lining radial chlorite (CR), post-dated by pore-filling, zoned calcite cement. Outer zones are enriched in Mn, inner zones are slightly enriched in Mg.
Well Flensburg Z1, sample Fb008, BSE micrograph (G), EMP analyses (H).

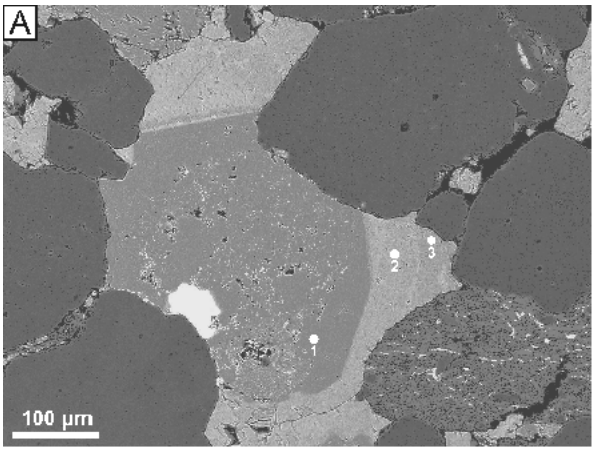
A
100 µm
1
2
3

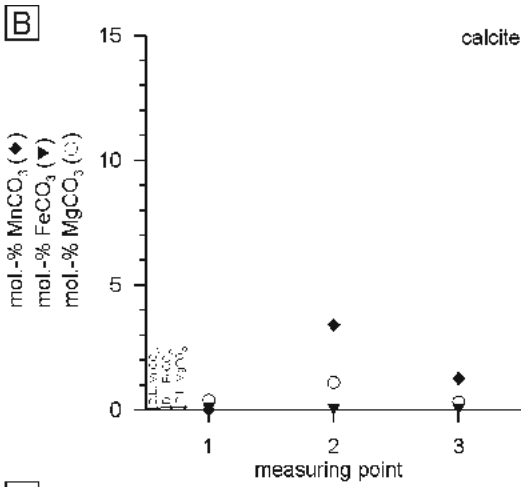
B
calcite
mol.-% MnCO3 (◆)
mol.-% FeCO3 (▶)
mol.-% MgCO3 (○)
15
10
5
0
1
2
3
measuring point

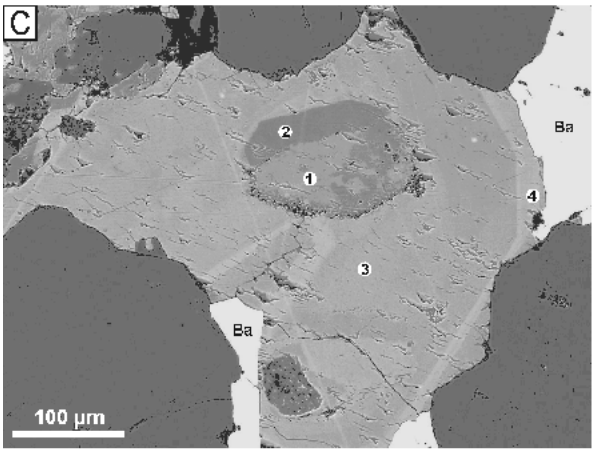
C
100 µm
Ba
Ba
1
2
3
4

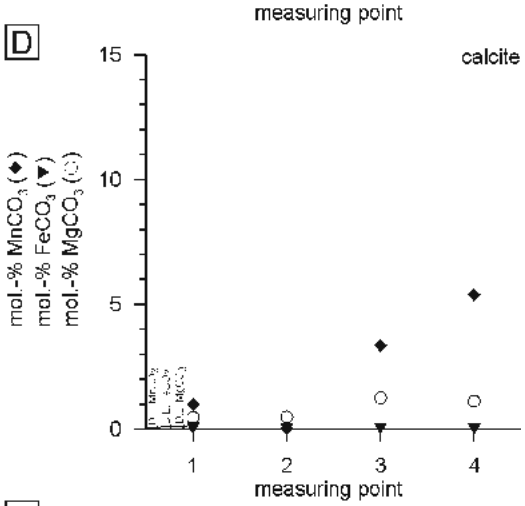
D
calcite
mol.-% MnCO3 (◆)
mol.-% FeCO3 (▶)
mol.-% MgCO3 (○)
15
10
5
0
1
2
3
4
measuring point

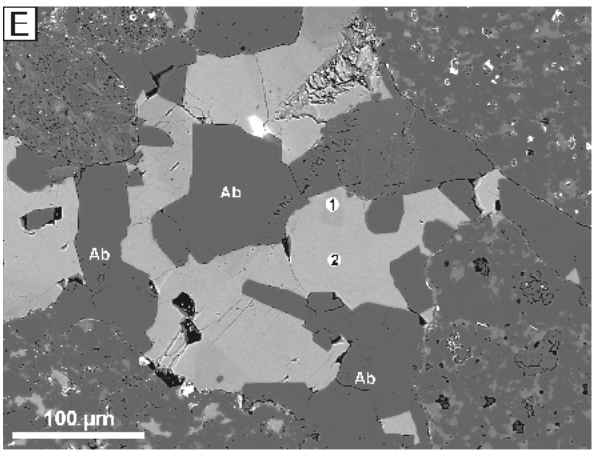
E
100 µm
Ab
Ab
Ab
1
2

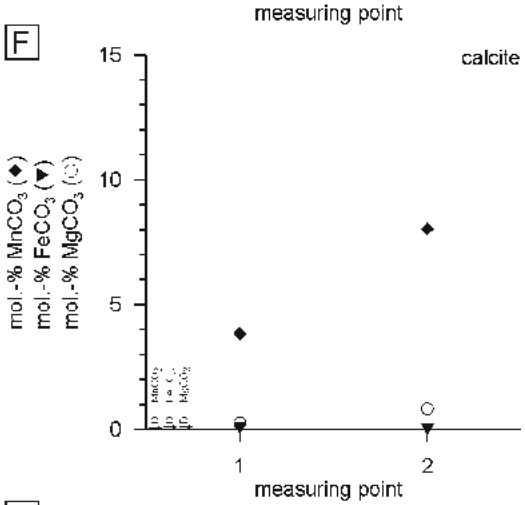
F
calcite
mol.-% MnCO3 (◆)
mol.-% FeCO3 (▶)
mol.-% MgCO3 (○)
15
10
5
0
1
2
measuring point

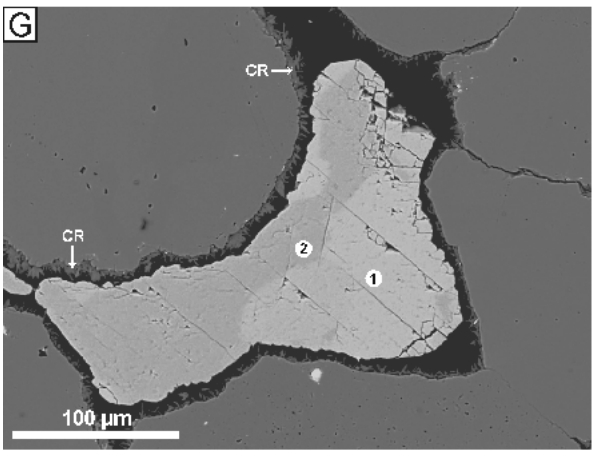
G
100 µm
CR
CR
1
2

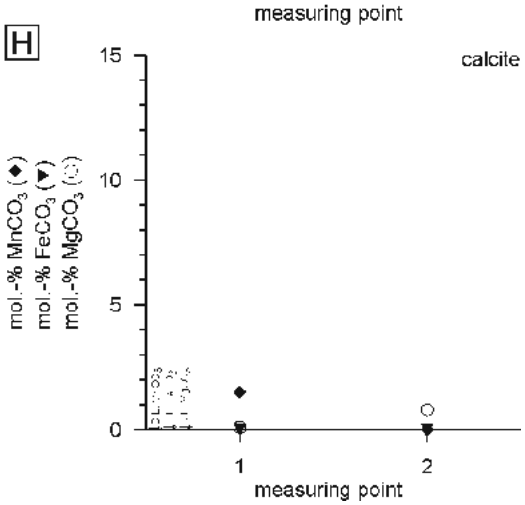
H
calcite
mol.-% MnCO3 (◆)
mol.-% FeCO3 (▶)
mol.-% MgCO3 (○)
15
10
5
0
1
2
measuring point

Plate 7: Petrography and geochemistry of carbonate cements at the northern margin of the NGB.

A, B: Rhombic, zoned dolomite cement. The central growth bands show varying, but overall similar chemical composition. The variations increase at the outer rims of the dolomite. The crystal is partly dissolved along the margins. White spots in the BSE micrograph (arrows) are discrete Fe-oxide crystals.
Well Flenburg Z1, sample Fb035, BSE micrograph (A), EMP analyses (B).

C, D: Rhombic, zoned dolomite cement. The outline of radial chlorite (CR) suggests that dolomite grows within a dissolved grain. The Ca content is increasing towards the outer rim of the crystal. A thin growth band, bright in the BSE micrograph, shows high Mn and Fe-contents. However, the measured Fe content is probably too high owing to µm-sized Fe-oxide crystals (arrows).
Well Flenburg Z1, sample Fb035, BSE micrograph (C), EMP analyses (D).

E, F: Rhombic, zoned dolomite, and subsequent calcite cement. The dolomite is relatively Mn-poor in the core and Mn-rich at the margin (about 13 mol.-% $MnCO_3$). Selected Mn-rich bands of the dolomite crystal are preferentially dissolved. Fe-oxide precipitates (arrows) are concentrated especially along these dissolved layers. The calcite cement is relatively pure $CaCO_3$. An authigenic quartz overgrowth (Qz) has developed on the quartz grain in the upper left corner. Some grain surfaces are covered by radial chlorite (CR).
Well Flenburg Z1, sample Fb041, BSE micrograph (E), EMP analyses (F).

G, H: Pore-filling dolomite and calcite cement. The dolomite is locally dissolved and slightly enriched in Mn and Fe. The calcite in the lower part of the BSE micrograph is very homogeneous and chemically almost pure $CaCO_3$. The calcite in the upper part is texturally similar to dolomite, but the chemistry is comparable to the calcite in the lower part. This calcite probably replaces earlier dolomite cement.
Well Flensburg Z1, sample Fb026, BSE micrograph (G), EMP analyses (H).

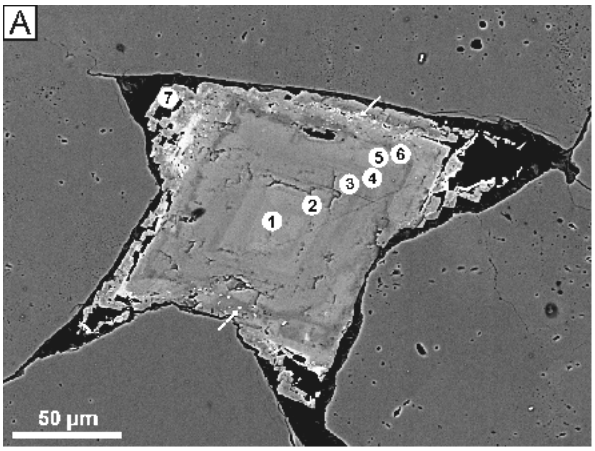
A
50 µm

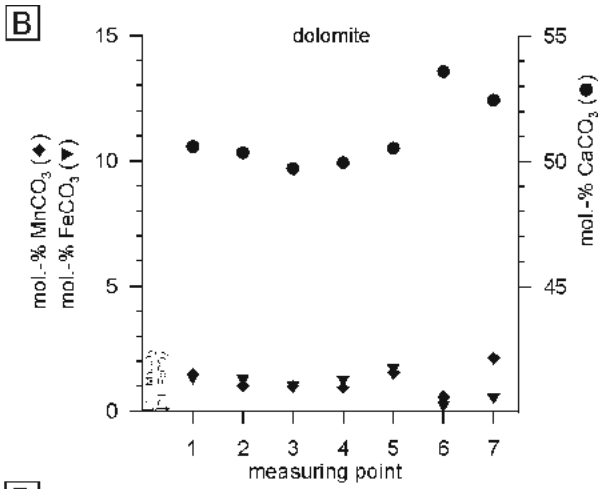
B
dolomite
mol.-% MnCO3 (◆)
mol.-% FeCO3 (▼)
mol.-% CaCO3 (●)
measuring point

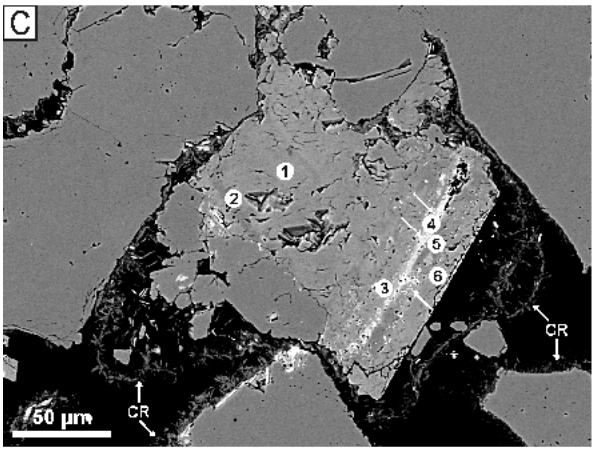
C
CR
CR
50 µm

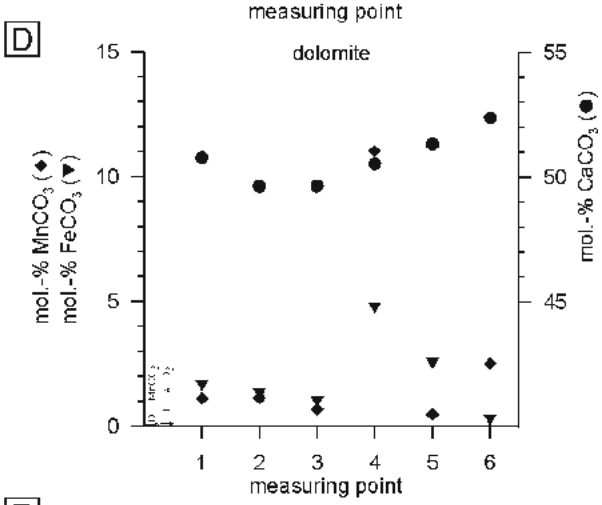
D
dolomite
mol.-% MnCO3 (◆)
mol.-% FeCO3 (▼)
mol.-% CaCO3 (●)
measuring point

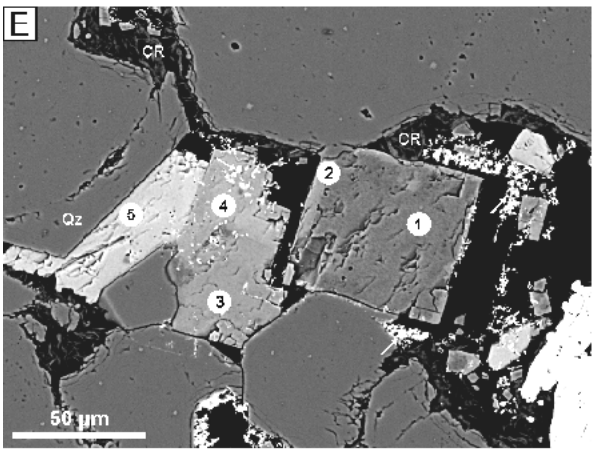
E
CR
CR
Qz
50 µm

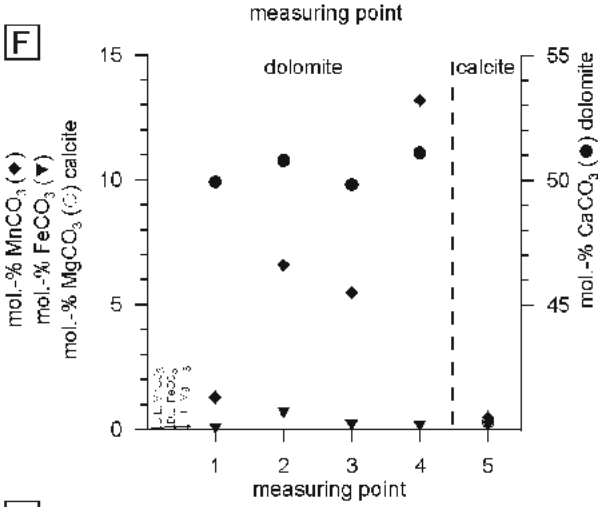
F
dolomite
calcite
mol.-% MnCO3 (◆)
mol.-% FeCO3 (▼)
mol.-% MgCO3 (○) calcite
mol.-% CaCO3 (●) dolomite
measuring point

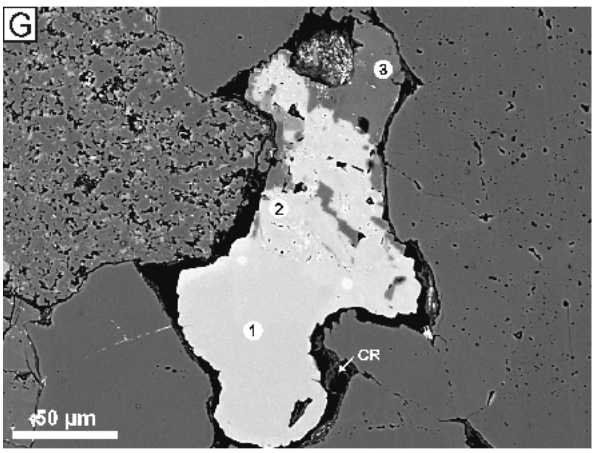
G
CR
50 µm

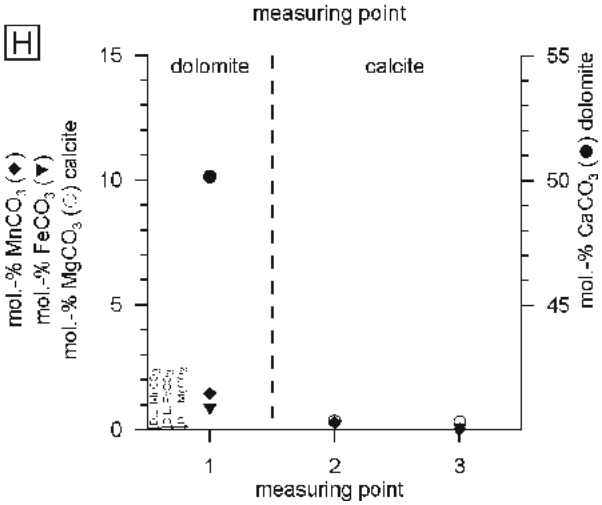
H
dolomite
calcite
mol.-% MnCO3 (◆)
mol.-% FeCO3 (▼)
mol.-% MgCO3 (○) calcite
mol.-% CaCO3 (●) dolomite
measuring point

Plate 8: Representative examples of XRD patterns of sandstones from the northern basin margin (air-dried whole rock powder samples).

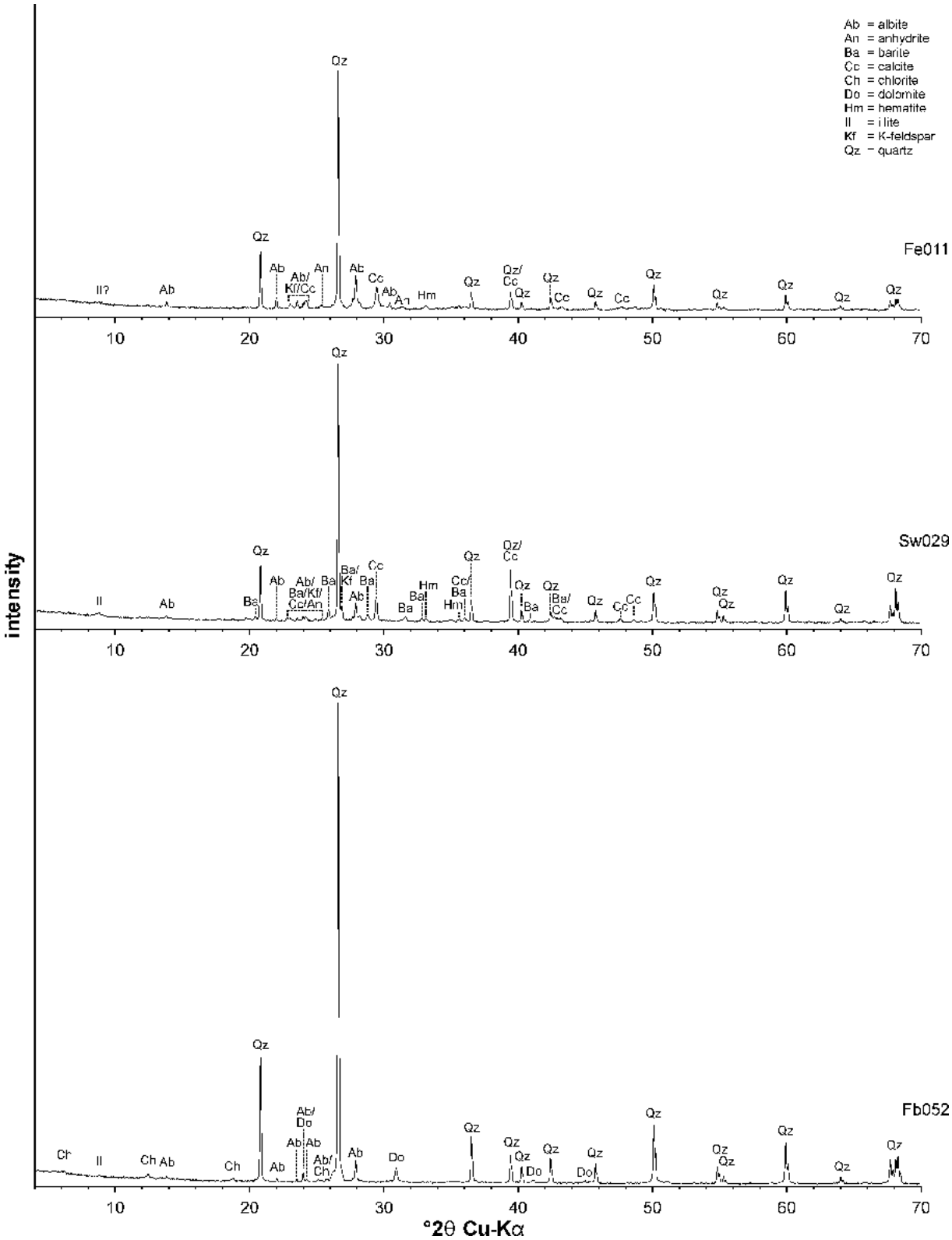
Ab = albite
An = anhydrite
Ba = barite
Cc = calcite
Ch = chlorite
Do = dolomite
Hm = hematite
Il = illite
Kf = K-feldspar
Qz = quartz
Fe011
Sw029
Fb052
intensity
°2θ Cu-Kα

Plate 9: Rotliegend petrography at the southern margin of the NGB.

A: Early diagenetic hematite (Hm, dark brown) and illite (IC, bright) grain coatings. Some pores remained open (blue), other were cemented by quartz (Qz) cement. (Minor meshwork illite IM)).
Well TG-1, sample 36682, photomicrograph, plane polarised light.

B: Hematite (Hm) and minor illite coating preserved beneath early quartz overgrowth (Qz). Hematite was removed along grain surfaces accessible to pore fluids after quartz precipitation. Instead, fibrous illite formed and was impregnated by bitumen (IM+B). Late pore-filling anhydrite (An).
Well TG-31, sample 18339, photomicrograph, plane polarised light.

C: Early diagenetic hematite-illite coatings (Hm+IC). Hematite is partly absent, however. Meshwork illite (IM) grew into open pore space (blue), and was impregnated by bitumen (B, brown).
Well TG-1, sample 36645, photomicrograph, plane polarised light.

D: Early diagenetic hematite-illite coatings (Hm+IC) and dolomite cement (Do). The relics of a dissolved feldspar (Fs) are surrounded by dense meshwork illite (IM) and green, fan-like chlorite (CF).
Well S-1, sample 23633, photomicrograph, plane polarised light.

E, F: Two detrital grains, most likely feldspars (Fs), were almost completely dissolved. Meshwork illite, impregnated by bitumen (IM+B) precipitated in intra- and intergranular pore space. Fan-like Fe-rich chlorite (CF) post-dates illite growths and fills secondary pore spaces. Only very little hematite (Hm) aggregates are present along pore surfaces. Blue is open pore space.
Well C-H, sample 26788, photomicrograph, plane polarised light (E), cross polarised light (F).

G: Small platelets and fan-like crystals of chlorite (white arrows) have been overgrown by fibrous illite (IM). The clay minerals were impregnated by a thin brown bitumen veil (B). Relics of hematite (Hm) are present in grain embayments and within tangential illite coatings (IC). Blue is open pore space.
Well Tg-41, sample 37393, photomicrograph, plane polarised light.

H: Bitumen coatings (B) along grain surfaces without visible authigenic illite, apart from traces of tangential illite coatings. The pore space is cemented by quartz (Qz), anhydrite (An), and calcite (Cc).
Well TG-43, sample 36860, photomicrograph, plane polarised light.

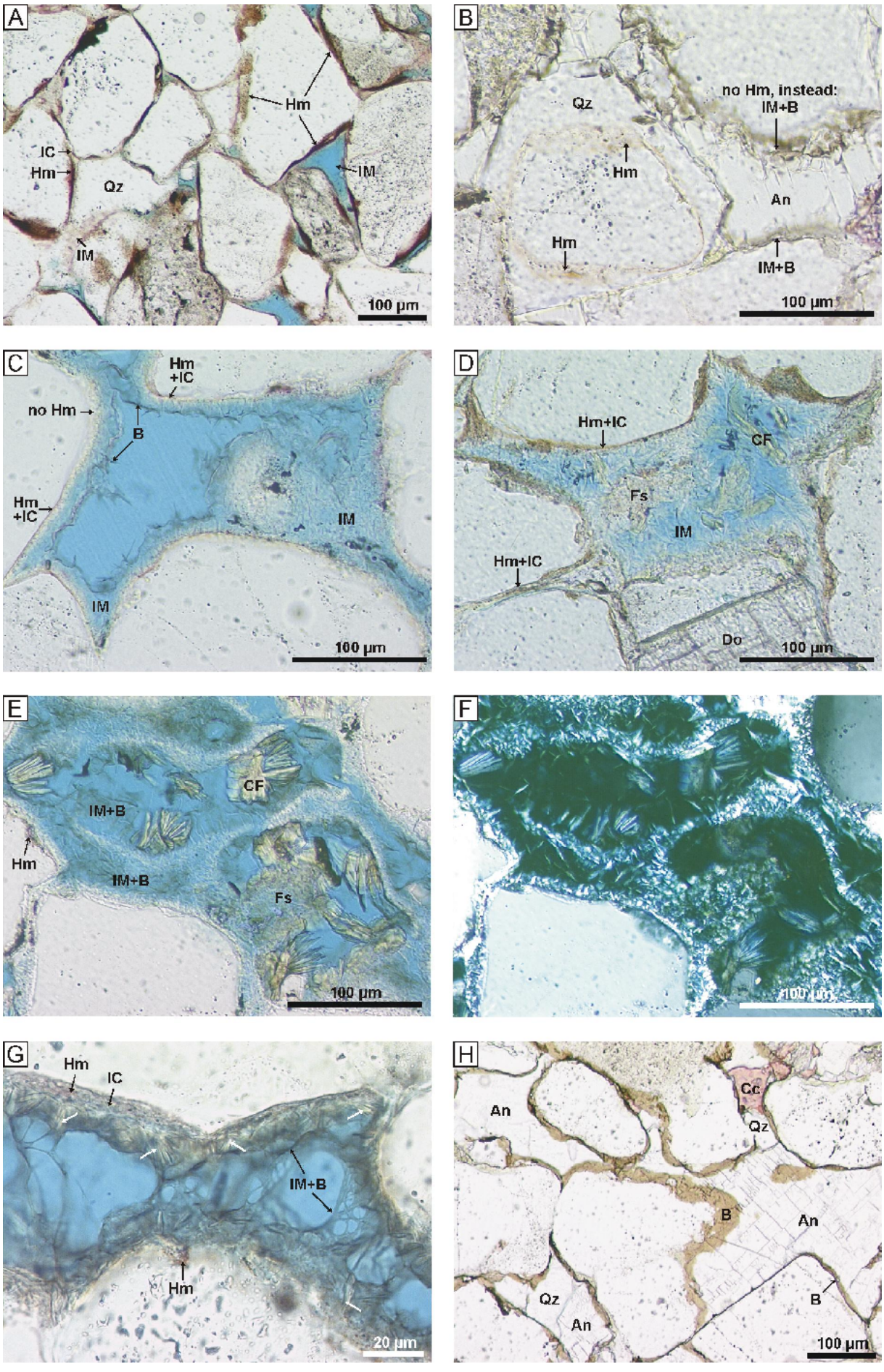
A
Hm
IC
Hm
Qz
IM
IM
100 µm
B
Qz
no Hm, instead:
IM+B
Hm
An
Hm
IM+B
100 µm
C
Hm
+IC
no Hm
B
Hm
+IC
IM
IM
100 µm
D
Hm+IC
CF
Fs
IM
Hm+IC
Do
100 µm
E
CF
IM+B
Hm
IM+B
Fs
100 µm
F
100 µm
G
Hm
IC
IM+B
Hm
20 µm
H
Cc
An
Qz
B
An
Qz
An
B
100 µm

Plate 10: Rotliegend petrography at the southern margin of the NGB.

A: Grey, totally bleached sandstone. Tangential illite coatings (IC) are bright in plane polarised light. Meshwork illite (IM) precipitated on pore surfaces. Blue is open pore space.
Well TG-2, sample 2080, photomicrograph, plane polarised light.

B: Bleached sandstone. Almost the entire grain surfaces are covered by meshwork illite (IM). Bitumen (B, greenish here) impregnated authigenic clay minerals in all places apart from grain contacts. Blue is open pore space.
Well D-B9, sample 45910, photomicrograph, plane polarised light.

C: Bleached sandstone with relics of hematite (Hm). Hematite appears to be lacking in most tangential illite coatings (IC). Fibrous, pore-bridging illite (IM) was impregnated by bitumen (B, black). Blue is open pore space.
Well TG-41, sample 37389, photomicrograph, plane polarised light.

D: Pore surfaces of a moderately compacted sandstone are covered by meshwork illite (IM), and by solid black bitumen (B). Such thick bitumen occurrences are rare, in contrast to bitumen impregnation of clay mineral surfaces. Secondary pore space of a partly dissolved feldspar is free of illite and bitumen, suggesting late feldspar dissolution. Blue is open pore space.
Well D-B9, sample 36991, photomicrograph, plane polarised light.

E: A euhedral, relatively early quartz crystal (Qz I) has been overgrown by hairy illite (IM). After bitumen (B) impregnation, quartz continued to grow (Qz II) and enclosed bitumen stained illite. Calcite (Cc) is the latest authigenic phase in this thin section micrograph.
Well TG-5, sample 41831, photomicrograph, plane polarised light.

F: Bleached sandstone with tangential illite coatings (IC). Relics of a corroded feldspar (Fs) are surrounded by bitumen stained meshwork illite (IM+B). Authigenic quartz cement encloses IM+B. Remaining pore space filled by late anhydrite (An).
Well TG-2, sample 1110, photomicrograph, plane polarised light.

G: Pore surfaces are lined by meshwork illite, which was impregnated by bitumen (IM+B), and subsequently overgrown by quartz cement (Qz). Authigenic quartz fills large, oversized pore volumes, suggesting preceding dissolution of detrital grains and framework supporting early cements.
Well TG-2, sample 1110, photomicrograph, plane polarised light.

H: Two almost completely dissolved feldspar grains (Fs). Precipitation of meshwork illite and bitumen impregnation (IM+B) took place after considerable compaction. The almost complete absence of illite and bitumen in the secondary pore space of feldspar and the lack of grain deformation at the corroded grains suggests late feldspar dissolution in a stabilised grain framework. Locally pore filling quartz (Qz) and calcite (Cc) cement. Blue is open pore space.
Well TG-41, sample 37393, photomicrograph, plane polarised light.

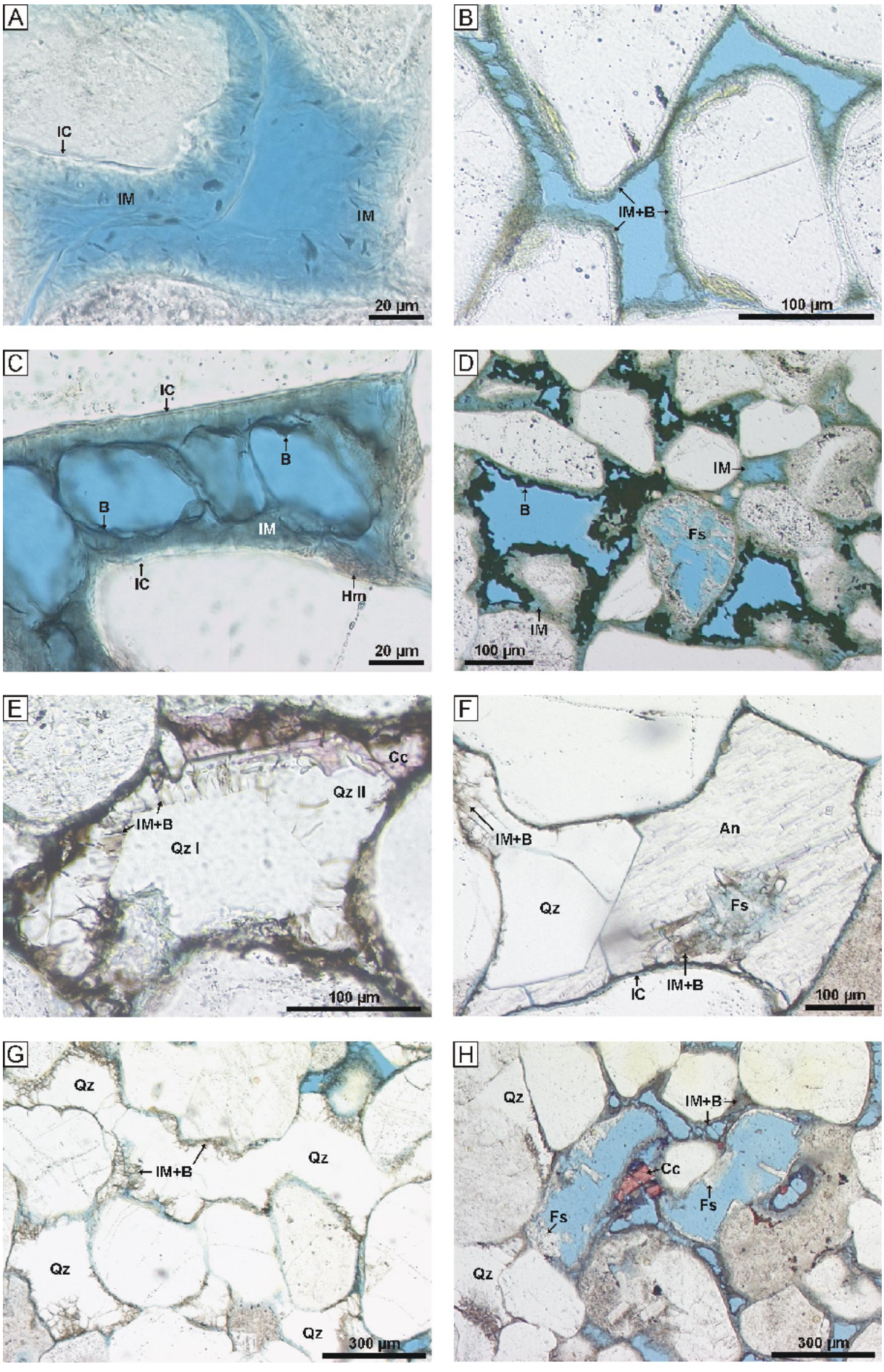
A
IC
IM
IM
20 µm
B
IM+B
100 µm
C
IC
B
B
IM
IC
Hm
20 µm
D
IM
B
Fs
IM
100 µm
E
Cc
Qz II
IM+B
Qz I
100 µm
F
IM+B
An
Qz
Fs
IC
IM+B
100 µm
G
Qz
IM+B
Qz
Qz
Qz
300 µm
H
Qz
IM+B
Cc
Fs
Fs
Qz
300 µm

Plate 11: Rotliegend petrography at the southern margin of the NGB.

A, B: Early sebkha-type cementation. Minor hematite grain coatings (brown in A), pore volume cemented by quartz (arrows), anhydrite (An) and calcite (Cc).
Well TG-31, sample 18387, photomicrograph, plane polarised light (A), cross polarised light (B).

C, D: Sebkha-type cementation (mainly anhydrite = An, minor calcite =Cc) prevails in the right part of the thin section micrograph. The left part is characterised by bitumen stained illite (brown grain coatings) and open pore space (blue colour). The IGV is smaller on the left compared to left right. It can be assumed that early cements similar to those preserved to the right were dissolved prior to illite formation and bitumen impregnation.
Well TG-5, sample 1099, photomicrograph, plane polarised light (C), cross polarised light (D).

E, F: Relatively large IGV cemented by calcite (Cc) in the left part of the thin section micrograph. The grains are coated by tangential illite and hematite. On the right hand side, calcite is lacking, hematite is less abundant, and the IGV is smaller than in the calcite-cemented area. Instead, meshwork illite and bitumen are widespread, and green chlorite fills the pore space of a dissolved grain. The texture suggest that the pore-filling calcite is the relic of and early cement. Calcite was probably dissolved in areas that are now cemented by illite. Blue is open pore space.
Well C-H, sample 26788, photomicrograph, plane polarised light (E), cross polarised light (F).

G: Bleached sandstone with meshwork illite (IM). Brown bitumen (B) staining on clay mineral surfaces. Apart from tangential illite, (IC) there are apparently no early diagenetic cements preserved. Some pore were cemented by post-bitumen calcite (Cc), other remained open (blue colour).
Well TG-5, sample 1099, photomicrograph, plane polarised light.

H: Hematite-illite grain coatings (Hm+IC), open pore space (blue colour). The open grain framework, oversized pores, and the absence of any pore-filling cement indicate dissolution of grains and framework-supporting cements.
Well TG-43, sample 37442, photomicrograph, plane polarised light.

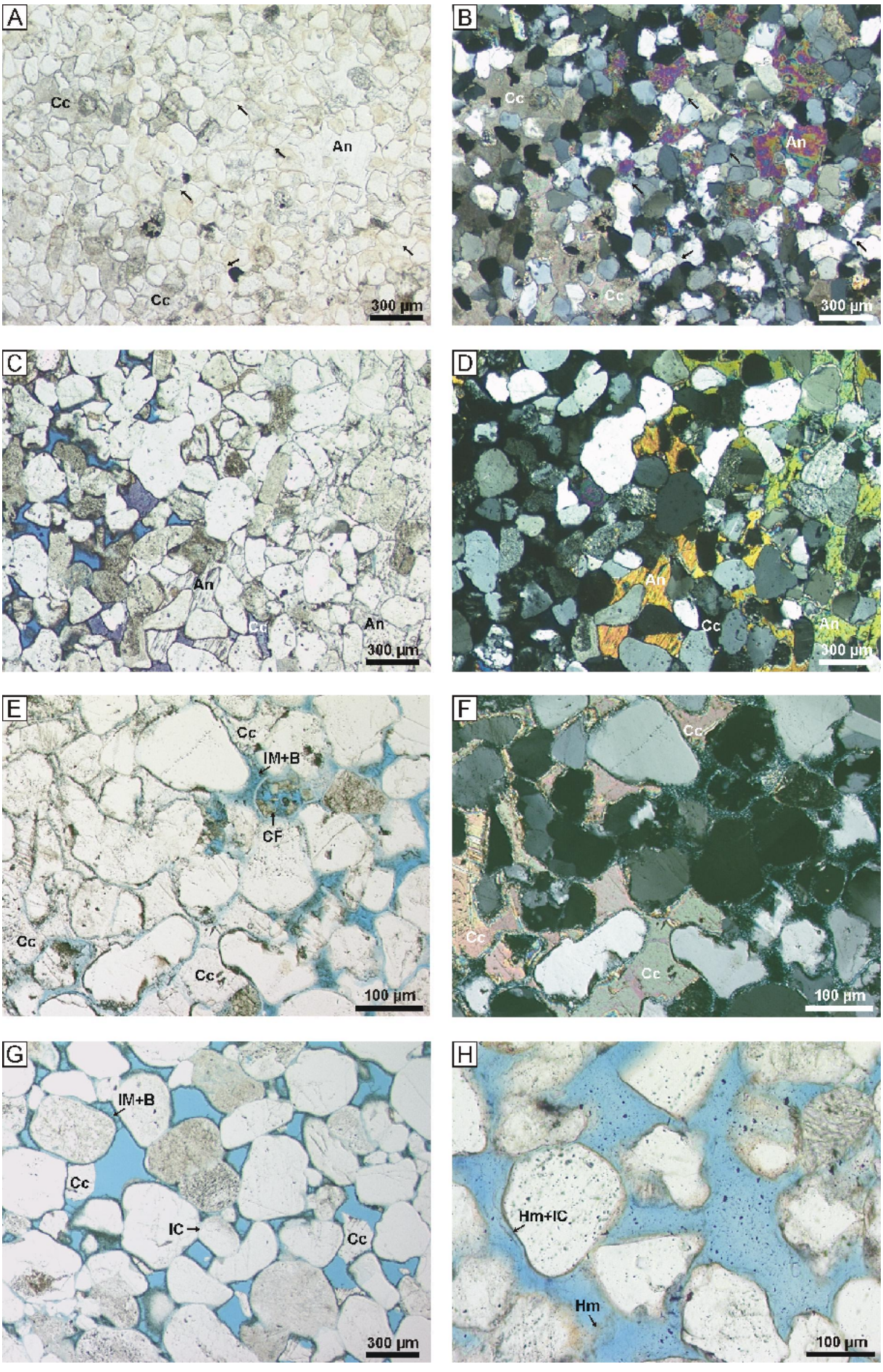
A
Cc
An
Cc
300 µm
B
Cc
An
Cc
300 µm
C
An
Cc
An
300 µm
D
An
Cc
An
300 µm
E
Cc
IM+B
CF
Cc
Cc
100 µm
F
Cc
Cc
Cc
100 µm
G
IM+B
Cc
IC
Cc
300 µm
H
Hm+IC
Hm
100 µm

Plate 12: Degassing profiles (DEGAS) and thermogravimetry curve (Tg) of a sandstone from the northern margin of the NGB, well Fehmarn Z1, sample Fe030.

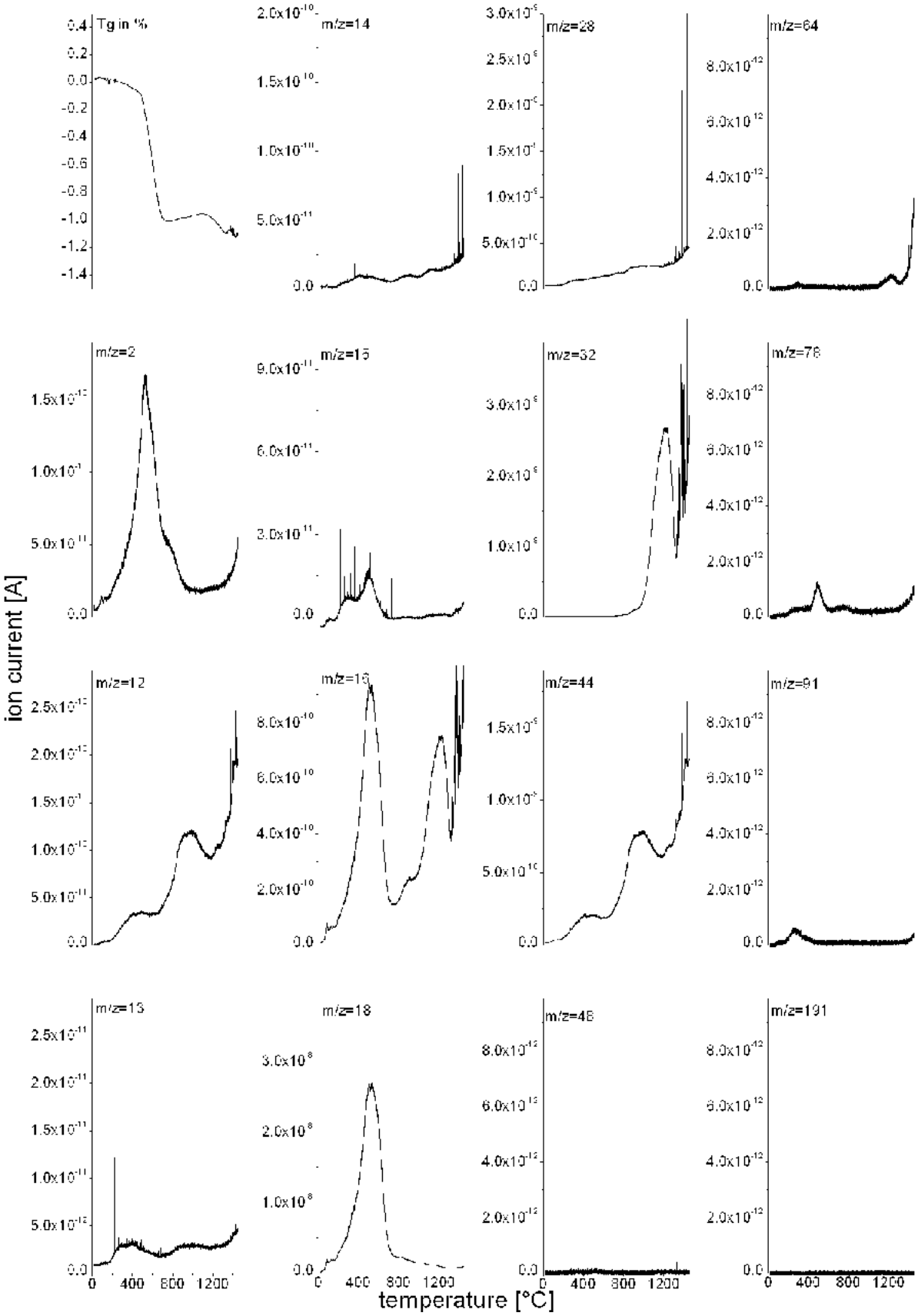

Plate 13: Degassing profiles (DEGAS) and thermogravimetry curve (Tg) of a sandstone from the northern margin of the NGB, well Schleswig Z1, sample Sw015.

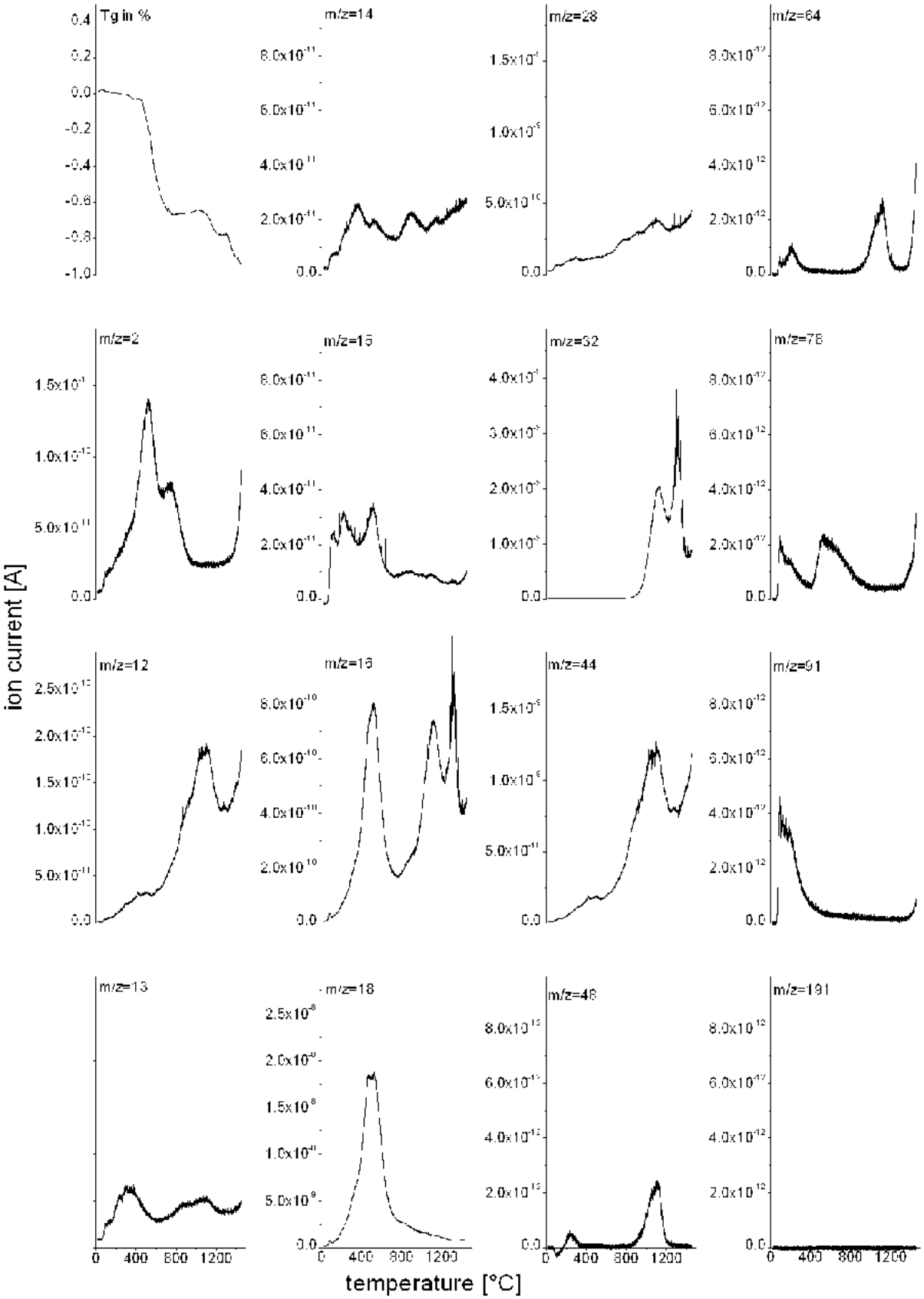

Plate 14: Degassing profiles (DEGAS) and thermogravimetry curve (Tg) of a sandstone from the northern margin of the NGB, well Flensburg Z1, sample Fb050.

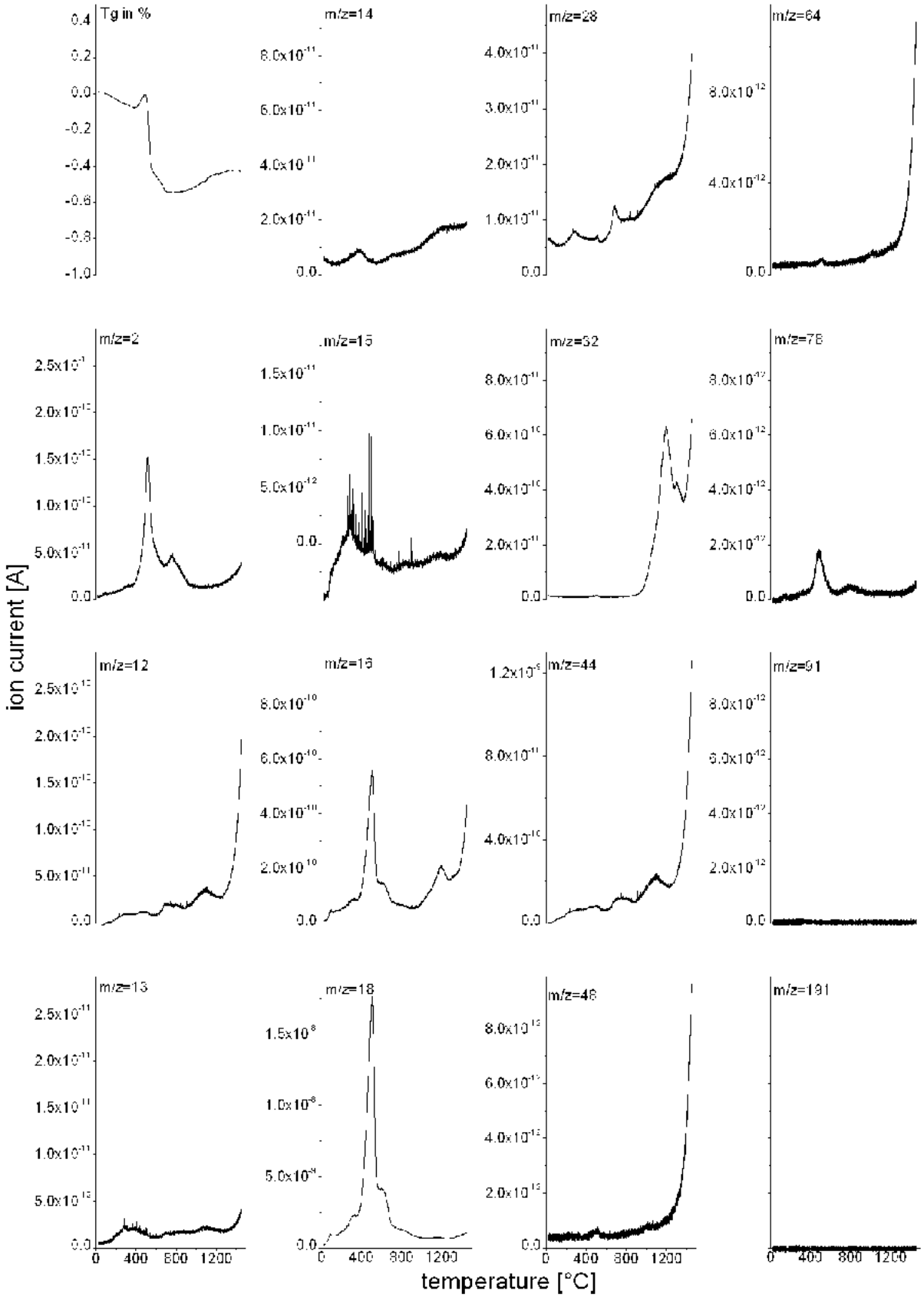

Plate 15: Degassing profiles (DEGAS) and thermogravimetry curve (Tg) of a sandstone from the southern margin of the NGB, well D-B9, sample 36991.

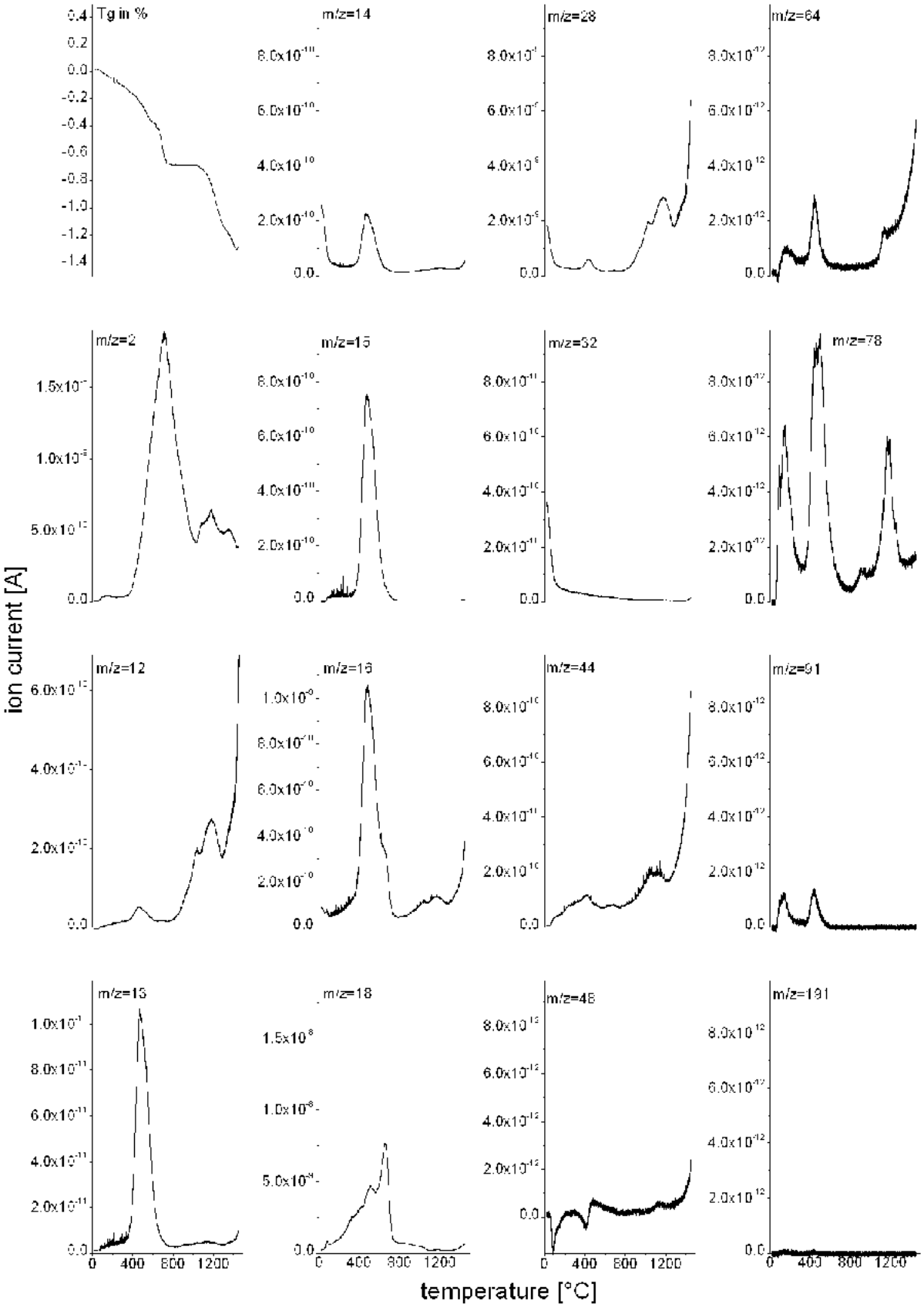

Plate 16: Degassing profiles (DEGAS) and thermogravimetry curve (Tg) of a sandstone from the southern margin of the NGB, well D-B9, sample 45908.

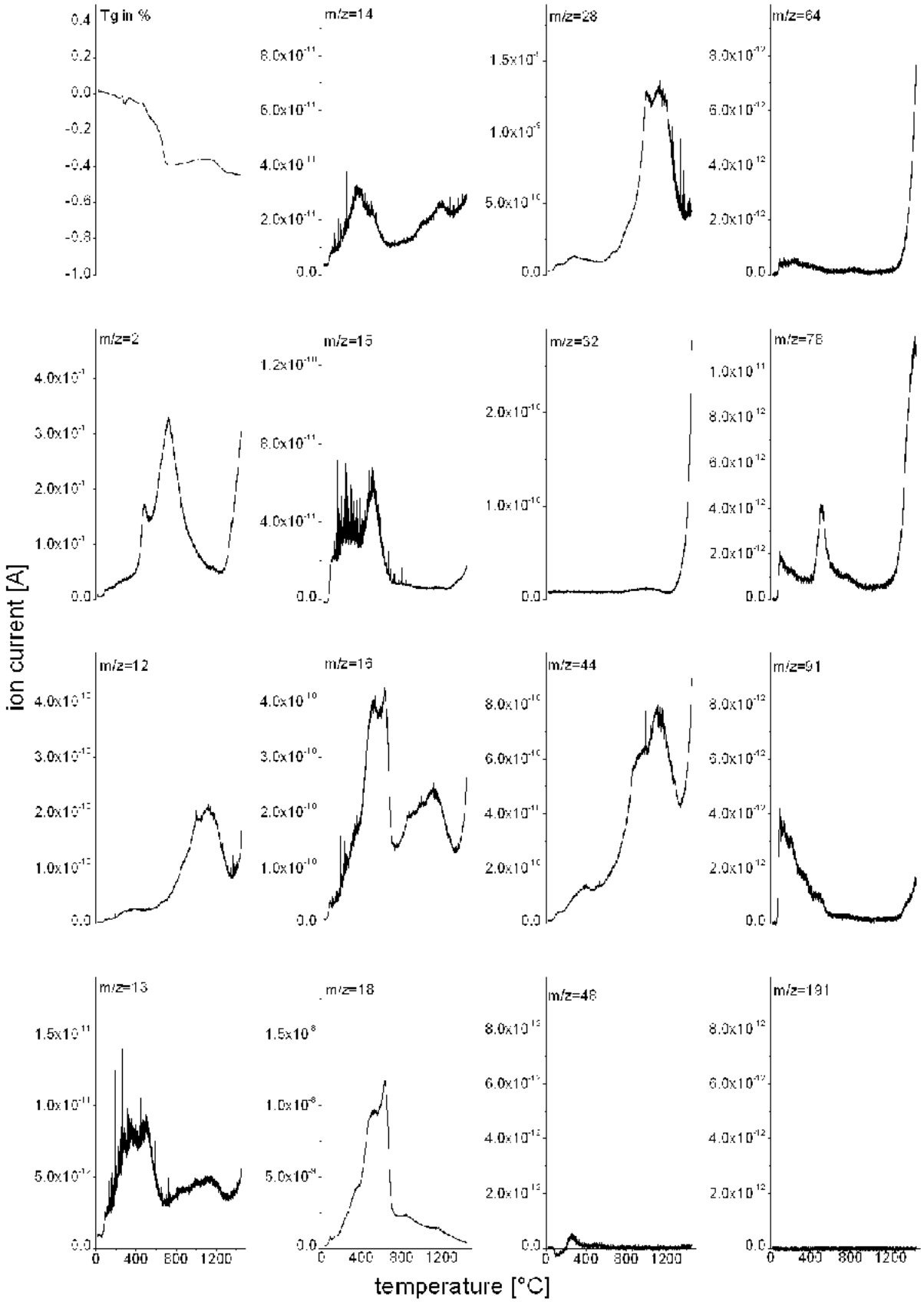

Plate 17: Degassing profiles (DEGAS) and thermogravimetry curve (Tg) of a sandstone from the southern margin of the NGB, well C-L, sample 42031.

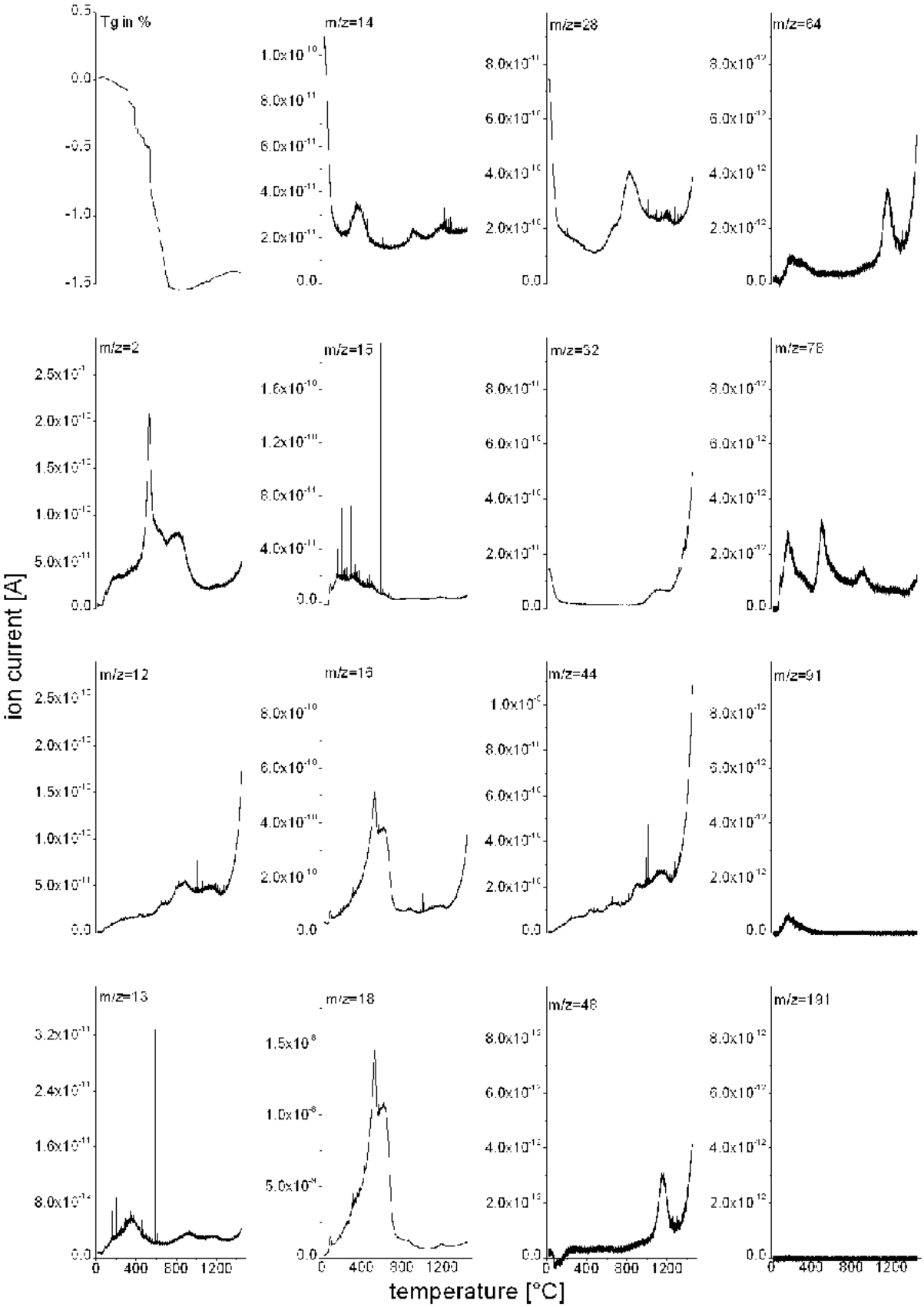

TABLES

Table A1:
Samples from the northern margin of the NGB investigated in this study.

Table A2:
Wells from the southern margin of the NGB used for this study.

Table A3:
Input data for well Fehmarn Z1.

Table A4:
Input data for well Schleswig Z1.

Table A5:
Input data for well Flensburg Z1.

Table A6:
Petrophysical properties of the lithologies used during for simulation.

Table A7:
Petrographic data of Rotliegend sandstones from the northern margin of the NGB.

Table A8:
Electron microprobe analyses of detrital and authigenic feldspar in sandstones from the northern margin of the NGB.

Table A9:
Electron microprobe analyses of authigenic calcite from the northern margin of the NGB.

Table A10:
Electron microprobe analyses of authigenic dolomite from the northern margin of the NGB.

Table A11:
Electron microprobe analyses of authigenic barite from the northern margin of the NGB.

Table A12:
Electron microprobe analyses of authigenic chlorite from the northern margin of the NGB.

Table A13:
Electron microprobe analyses of authigenic illite from the northern margin of the NGB.

Table A14:
X-ray fluorescence analyses of fine- to medium grained Rotliegend sandstones from the northern margin of the NGB.

Table A15:
Carbon and oxygen isotopic composition of calcite cements, dolomite cements, and vein calcites of Rotliegend and Carboniferous sandstones from the northern margin of the NGB.

Table A16:
Calculated masses of Fe for red and grey sandstones and for authigenic Fe-bearing minerals.

Table A1: Samples from the northern margin of the NGB investigated in this study, and overview over the methods applied. Depth in metres below base Zechstein. G = gravel, S_C =sand coarse, S_m = sand medium, S_f = sand fine, M = mud, V = volcanic rock, OM = optical microscopy, PC = point counting, other abbreviations see section 1 and list of abbreviations.

	sample-no.	depth [m]	lithology G	S_c	S_m	S_f	M	vein	V	colour	methods OM	PC	SEM	CL	XRD_{bulk}	XRD_{clay}	EMP	XRF	$d^{13}C$, $d^{18}C$	DEGAS
well Fehmarn Z1	Fe007	base Z.				x	x	x		red	x							x		
	Fe008	464.6				x	x	x		red	x									
	Fe009	470.0				x	x	x		red	x								x_{vein}	
	Fe010	770.1				x				red	x	x						x	x	
	Fe011	772.9		x	x					red	x	x	x	x	x		x	x	x	
	Fe012	774.3			x	x	x			red	x	x						x		
	Fe028	774.9			x	x	x			red	x	x						x	x	
	Fe029	777.2			x	x				red	x	x			x			x	x	
	Fe013	835.3	x		x					red	x	x						x		
	Fe014	835.8	x		x					red	x	x	x				x	x	x	
	Fe030	836.4	x		x					red	x	x								x
	Fe015	836.9	x		x	x				red	x	x			x			x	x	
	Fe016	838.0	x		x					red	x	x					x	x		
	Fe017	839.3	x					x		red	x		x	x					x_{vein}	
	Fe018	840.2	x		x					red	x	x			x			x	x	
	Fe019	840.8	x		x					red	x			x			x	x	x	
	Fe020	946.2						x	x	red	x		x							
	Fe021	948.7			x				x	red	x	x						x		
	Fe023	952.5						x	x	red									x_{vein}	
well Schleswig Z1	Sw001	1878.9				x	x			red	x									
	Sw002	1881.2				x	x			red	x							x		
	Sw003	1938.4			x	x				red	x							x		
	Sw004	1943.3				x	x			red	x									
	Sw005	1996.5			x	x	x	x		red	x							x		
	Sw006	1998.0			x	x	x			red	x									
	Sw007	1999.4			x	x	x			red	x									
	Sw008	2003.7			x	x	x			red	x									
	Sw009	2056.1	x		x	x				red	x	x								
	Sw010	2057.0			x					red	x	x						x	x	
	Sw011	2059.1	x	x	x					red	x	x								
	Sw012	2059.7	x	x	x	x				red	x	x						x		
	Sw013	2060.2	x	x	x	x				red	x	x						x	x	
	Sw014	2062.0			x					red	x	x								
	Sw015	2062.9			x					red	x	x			x		x	x	x	x
	Sw016	2063.6			x					red	x	x	x	x			x	x	x	
	Sw017	2063.9			x					red	x	x						x		
	Sw018	2065.1			x					red	x	x						x	x	
	Sw019	2066.0	x	x	x	x				red	x	x								
	Sw020	2067.4	x	x	x	x				red	x	x						x		
	Sw021	2069.2	x	x	x					red	x	x								
	Sw022	2070.4			x					red	x	x						x	x	
	Sw023	2071.7	x	x	x					red	x	x								
	Sw024	2073.7			x					red	x	x			x			x	x	
	Sw025	2074.8			x					red	x	x						x		
	Sw026	2076.5			x					red	x	x						x	x	
	Sw027	2077.2			x					red	x	x		x			x	x	x	
	Sw028	2077.8			x					red	x	x	x							
	Sw029	2078.4			x					red	x	x	x		x		x	x	x	x
	Sw030	2079.0			x					red	x	x						x		
	Sw031	2079.8			x					red	x	x	x				x	x	x	
	Sw032	2080.5			x					red	x	x						x		
	Sw033	2080.6			x	x	x			red	x	x	x		x					
additionally 31 Rotliegend thin sections between 1998 m and 2081 m (provided by EMPG)																				

Table A1: Samples, continuation.

	sample-no.	depth [m]	lithology G	S_c	S_m	S_f	U	vein	V	colour	methods OM	PC	SEM	CL	XRD_{bulk}	XRD_{clay}	EMP	XRF	$d^{13}C$, $d^{18}C$	DEGAS
well Flensburg Z1	Fb018	857.5	x		x					grey	x	x								
	Fb035	858.4			x	x				grey/red	x	x	x			x	x	x	x	x
	Fb036	859.2			x			x		grey/red								x	x	
	Fb019	859.5			x					grey	x	x	x							
	Fb038	862.1			x	x				grey/red								x		
	Fb039	863.6			x					red	x	x			x			x	x	
	Fb020	864.0			x					grey	x	x								
	Fb021	935.0			x					grey	x	x								
	Fb022	935.5			x					grey	x	x								
	Fb040	936.1			x					grey/red	x	x			x			x	x	
	Fb041	937.5			x	x				grey/red	x	x	x			x	x	x		
	Fb042	938.2			x	x		x		grey/red								x		
	Fb023	939.0			x			x		grey	x	x								
	Fb043	939.3			x					grey/red								x		
	Fb044	1030.8			x	x		x		red								x	x, x_{vein}	
	Fb045	1031.9			x			x		red	x	x			x			x		
	Fb024	1032.5	x		x	x				grey	x	x								
	Fb025	1033.0	x	x	x	x				grey	x	x								
	Fb046	1035.2			x	x				red								x		
	Fb047	1036.6			x	x				red	x	x	x			x		x		
	Fb026	1037.0			x					grey	x	x	x	x			x			
	Fb027	1143.0			x	x				grey/red	x	x								
	Fb028	1144.0			x	x				red	x	x								
	Fb049	1145.0			x	x				grey/red								x		
	Fb050	1145.9			x					red	x	x	x			x	x	x		x
	Fb008	1147.0		x	x					grey/red	x	x		x			x			
	Fb051	1147.7			x	x		x		grey/red								x		
	Fb009	1148.5			x					grey	x	x	x							
	Fb052	1149.1			x	x				grey/red	x	x			x		x	x	x, x_{vein}	
	Fb029	1149.5	x	x	x					grey	x	x								
	Fb010	1150.5		x	x					grey	x	x								
	Fb011	1252.0			x	x				red	x	x								
	Fb012	1252.5			x	x				grey/red	x	x								
	Fb054	1252.7			x	x				red	x	x			x			x	x	
	Fb013	1253.0			x	x				grey/red	x	x		x			x			
	Fb014	1262.0			x					grey/red	x	x								
	Fb055	1262.7			x	x				grey/red								x	x	
	Fb057	1266.6		x	x					grey/red	x	x	x			x	x	x	x	
	Fb058	1267.2			x					grey/red								x		
	Fb015	1267.5		x	x					grey/red	x	x								
	Fb059	1267.9			x					grey/red	x	x			x		x	x	x, x_{vein}	
	Fb016	1269.0				x	x			red	x									
	Fb030	1381.0				x	x			grey/red	x									
	Fb060	1381.8				x	x			red								x		
	additionally 42 Rotliegend thin sections between 860 m and 1269 m (provided by EMPG)																			
(*)	(*) well Westerland Z1																			
	Wl001	4.4			x	x				red	x	x								

Table A2: Wells from the southern margin of the NGB used for this study. HAV = Havel Subgroup; DET = Dethlingen Formation; HAN = Hannover Formation; P = Platt (1991); D = Deutrich (1993); C = Cord (1994); H = Hartmann (1997); TG = Tight Gas Study (Gaupp and Solms, 2005).

well name	stratigraphy			investigated by	petrographic data		chemical data	new data	
(coded)	HAV	DET	HAN		qualitative	quantitative	RFA	petrography	DEGAS
P-A				P	x				
P-B		x		P	x	x			
P-C		x		P	x	x			
P-D (=C-N)		x	x	P; C	x	x			
P-E		x	x	P	x	x			
P-F (=D-B6)	x	x	x	P; D	x	x		x	x
P-G	x	x	x	P	x	x			
P-H		x	x	P	x	x			
P-I	x	x	x	P	x				
D-B1 (=TG-3)		x	x	D; TG	x	x			
D-B2 (=TG-9)			x	D; TG	x	x	x	x	
D-B3		x	x	D; TG	x		x		
D-B4	x	x	x	D; TG	x		x		
D-B5 (=C-G =H-Z8)		x	x	D; C; H	x	x	x		
D-B7 (=H-Z9)	x	x	x	D; H	x		x	x	x
D-B8 (=H-Z10)	x	x	x	D; H	x		x		
D-B9		x	x	D	x		x	x	x
D-B10	x	x	x	D	x				
D-B11 (=H-Z11)	x	x	x	D; H	x		x	x	
D-B12			x	D	x		x		
C-A		x	x	C	x			x	
C-B		x		C	x	x		x	
C-C (=TG-10)	x	x	x	C; TG	x	x		x	x
C-D	x	x		C	x	x			
C-E	x	x		C	x	x		x	
C-F		x	x	C	x				
C-H	x	x		C	x	x		x	x
C-I		x		C	x				
C-J	x	x		C	x				
C-K		x		C	x	x			
C-L		x		C	x			x	x
C-M		x		C	x	x		x	
H-Z1		x		H	x		x		
H-Z3	x			H	x		x		
TG-1	x	x	x	TG	x	x		x	
TG-2		x	x	TG	x	x		x	
TG-4			x	TG	x	x			
TG-5			x	TG	x	x		x	x
TG-6		x	x	TG	x	x		x	
TG-11 (=H-Z2)	x	x	x	TG; H	x	x	x		
TG-12	x	x	x	TG	x	x			
TG-13	x		x	TG	x	x			
TG-14		x	x	TG	x	x			
TG-15		x	x	TG	x	x			
TG-16	x		x	TG	x	x			
TG-19			x	TG	x	x			
TG-20			x	TG	x	x			
TG-21		x	x	TG	x	x			
TG-22			x	TG	x	x			
TG-23			x	TG	x	x			
TG-24			x	TG	x	x			
TG-25			x	TG	x	x			
TG-26			x	TG	x	x			
TG-27		x	x	TG	x	x			
TG-29		x	x	TG	x	x			
TG-31			x	TG	x	x		x	
TG-32		x	x	TG	x				
TG-33		x	x	TG	x	x			
TG-34			x	TG	x	x			
TG-35			x	TG	x	x			
TG-37			x	TG	x	x			
TG-38			x	TG	x	x			
TG-40	x		x	TG	x				
TG-41	x	x	x	TG	x	x		x	
TG-43		x	x	TG	x	x		x	
TG-44	x	x	x	TG	x	x			
S-1		x		this study				x	

Table A3: Input data for well Fehmarn Z1. Eroded thicknesses were modified for simulation of different scenarios. *[1]Original thickness Zechstein 2 salt: 585 m. Salt migration: 100-65 Ma.

Event name	Top	Bottom	Present thickness	Eroded thickness	Deposition age from	Deposition age to	Erosion age from	Erosion age to	Lithology
	[m]	[m]	[m]	[m]	[Ma]	[Ma]	[Ma]	[Ma]	
Sediment Surface			0		0	0	0	0	
Pleistocene-Holocene	0	53	53		1	0			SANDcongl
Pliocene-Pleistocene	53	53	0		5	1			none
Oligocene-Miocene	53	53	0		34	5			none
U. Paleocene-Eocene	53	322	269	100	58	34	5	1	SHALEsand
M. Paleocene	322	322	0		61	58			none
Campanian-Danian	322	648	326	100	83	61	61	58	CHALK
Cenomanian-Santonian	648	903	255		99	83			CHALK&LIMEmarl
Aptian-Albian	903	935	32		121	99			SHALEcalc
M. Jurassic-L. Cretac.	935	935	0		175	121			none
L. Jurassic	935	935	0	200	200	175	175	121	SHALEcalcsand
Keuper 6	935	1015	80		209	200			SANDshaly
Keuper 2-5	1015	1370	355		232	209			SHALEevapsand
Keuper 1	1370	1476	106		235	232			SHALE
Muschelkalk	1476	1745	269		243	235			MARLcarb
Buntsandstein 6-7	1745	2061	316		245	243			SHALEevap
Buntsandstein 3-5	2061	2443	382		249	245			SHALEsand
Buntsandstein 1-2	2443	2856	413		251	249			SHALEsand
Zechstein 3-7	2856	3194	338		254	251			EVAPORITE
Zechstein 2 salt *[1]	3194	3723	529		255	254			SALT
Zechstein 1-2	3723	3798	75		258	255			ANHYD&CARB
Hannover mudst.-evap.	3798	4118	320		260	258			SILTevap.
Dethlingen mudst.-evap.	4118	4412	294		262	260			SILTevap.
Havel mudst.	4412	4630	218		264	262			SILTshaly
Havel sst.	4630	4723	93		266	264			SANDcongl
L. Rotliegend	4723	4723	0		297	266			none
L. Rotliegend rhyodacite	4723	4973	250	50	300	297	297	280	RHYOLITE
Stephanian	4973	4973	0		306	300			none
Westphalian D	4973	4973	0	200	308	306	306	305	SAND&SILT
Westphalian C	4973	4973	0	300	311	308	305	303	SHALE&SAND
Westphalian B	4973	4973	0	200	313	311	303	302	SAND&SHALE
Westphalian A	4973	4973	0	300	316	313	302	300	SAND&SILT
Namurian	4973	5373	400		326	316			SAND&SHALE
Tournaisian-Viséan	5373	5873	500		358	326			LIMEmarly
Devonian	5873	6173	300		400	358			SANDSTONE
Caledonian Hiatus	6173	6173	0		450	400			none
Basement	6173	7673	1500		545	450			BASEMENT

Table A4: Input data for well Schleswig Z1. Eroded thicknesses were modified for simulation of different scenarios. *[1]Original thickness Zechstein 2 salt: 600 m. Salt migration: 251-235 Ma.

Event name	Top	Bottom	Present thickness	Eroded thickness	Deposition age from	Deposition age to	Erosion age from	Erosion age to	Lithology
	[m]	[m]	[m]	[m]	[Ma]	[Ma]	[Ma]	[Ma]	
Sediment Surface			0		0	0	0	0	
Pleistocene-Holocene	0	25	25		1	0			SANDcongl
Pliocene-Pleistocene	25	25	0		5	1			none
Oligocene-Miocene	25	291	266	100	34	5	5	1	SANDshaly
Eocene	291	566	275		55	34			SHALEsand
M.-U. Paleocene	566	566	0		61	55			none
Campanian-Danian	566	963	397	50	83	61	61	55	CHALK
Cenomanian-Santonian	963	1212	249		99	83			CHALK&LIMEmarl
Hauterivian-Albian	1212	1257	45		132	99			SHALEcalc
M. Jurassic-L. Cretac.	1257	1257	0		175	132			none
L. Jurassic	1257	1257	0	400	200	175	175	132	SHALEcalcsand
Keuper 6	1257	1370	113		209	200			SHALEsand
Keuper 4-5	1370	1528	158		221	209			SHALEcarb
Keuper 4 salt	1528	1727	199		223	221			SALT
Keuper 2-4	1727	2444	717		232	223			SHALEevap
Keuper 1	2444	2817	373		235	232			SHALEcalc
Muschelkalk	2817	2817	0		243	235			none
Buntsandstein 6-7	2817	2817	0		245	243			none
Buntsandstein 3-5	2817	2817	0		249	245			none
Buntsandstein 1-2	2817	2817	0		251	249			none
Zechstein 3-7	2817	2817	0	300	254	251	251	235	EVAPORITE
Zechstein 2 salt *[1]	2817	3003	186		255	254			SALT
Zechstein 1-2	3003	3080	77		258	255			ANHYD&CARB
Hannover mudst.-evap.	3080	3775	695		260	258			SHALE&EVAP
Dethlingen mudst.-evap.	3775	4400	625		262	260			SHALE&EVAP
Havel mudst.	4400	5118	718		264	262			SHALEsilt
Havel sst.	5118	5161	43		266	264			SANDcongl
L. Rotliegend	5161	5161	0		300	266			none
Stephanian	5161	5161	0		306	300			none
Westphalian D	5161	5161	0	200	308	306	306	305	SAND&SILT
Westphalian C	5161	5161	0	300	311	308	305	303	SHALE&SAND
Westphalian B	5161	5161	0	200	313	311	303	302	SAND&SHALE
Westphalian A	5161	5161	0	300	316	313	302	300	SAND&SILT
Namurian	5161	5161	0	400	326	316	300	295	SAND&SHALE
Viséan b	5161	5282	121	100	330	326	295	280	SHALE
Rhyolite 3	5282	5552	270		300	297			RHYOLITE
Tournaisian b-Viséan a	5552	5705	153		350	330			SHALEcarbsand
Rhyolite 2	5705	5740	35		300	297			RHYOLITE
Tournaisian a	5740	5870	130		358	350			LIMEshaly
Rhyolite 1	5870	5890	20		300	297			RHYOLITE
Devonian	5890	6190	300		400	358			SANDSTONE
Caledonian Hiatus	6190	6190	0		450	400			none
Basement	6190	7690	1500		545	450			BASEMENT

Table A5: Input data for well Flensburg Z1. Eroded thicknesses were modified for simulation of different scenarios. *[1]Original thickness Zechstein 2 salt: 600 m. *[2]Original thickness Zechstein 3-4: 320 m. Salt migration: 235-144 Ma and 65-0 Ma.

Event name	Top	Bottom	Present thickness	Eroded thickness	Deposition age from	Deposition age to	Erosion age from	Erosion age to	Lithology
	[m]	[m]	[m]	[m]	[Ma]	[Ma]	[Ma]	[Ma]	
Sediment Surface			0		0	0	0	0	
Pleistocene-Holocene	0	55	55		1	0			SAND&SHALE
Pliocene-Pleistocene	55	55	0		5	1			none
Oligocene-Miocene	55	501	446		34	5			SHALE&SAND
U. Paleocene-Eocene	501	1017	516		58	34			MARL
M. Paleocene	1017	1017	0		61	58			none
Campanian-Danian	1017	1385	368		83	61			CHALK
Cenomanian-Santonian	1385	1700	315		99	83			CHALK&LIMEmarl
Hauterivian-Albian	1700	1760	60		132	99			SHALEcalcsilt
M. Jurassic-L. Cretac.	1760	1760	0		175	132			none
L. Jurassic	1760	1825	65	600	200	175	175	132	SHALEcalcsilt
Keuper 6	1825	1932	107		209	200			SHALEcalcsand
Keuper 2-5	1932	2310	378		232	209			SHALEcarb
Keuper 1	2310	2340	30		235	232			SHALEcarb
Muschelkalk	2340	2536	196		243	235			MARLcarb
Buntsandstein 6-7	2536	2776	240		245	243			SHALEevap
Buntsandstein 5/6	2776	2776	0		246	245			none
Buntsandstein 3-5	2776	2848	72	200	249	246	246	245	SAND&SHALE
Buntsandstein 1-2	2848	3148	300		251	249			SHALEcalcsand
Zechstein 3-7 *[2]	3148	3247	99		254	251			EVAPshaly
Zechstein 2 salt *[1]	3247	3303	56		255	254			SALT
Zechstein 1-2	3303	3386	83		258	255			ANHYD&CARB
Hannover mudst.-evap.	3386	3630	244		260	258			SHALE&EVAP
Dethlingen mudst.-evap.	3630	3956	326		262	260			SHALE&EVAP
Havel mudst.	3956	4236	280		264	262			SHALEsilt
Havel sst.	4236	4926	690		266	264			SANDshaly
L. Rotliegend	4926	4926	0		300	266			none
Stephanian	4926	4926	0		306	300			none
Westphalian D	4926	4926	0	200	308	306	306	305	SAND&SILT
Westphalian C	4926	4926	0	300	311	308	305	303	SHALE&SAND
Westphalian B	4926	4926	0	200	313	311	303	302	SAND&SHALE
Westphalian A	4926	4926	0	300	316	313	302	300	SAND&SILT
Namurian	4926	4926	0	400	326	316	300	295	SAND&SHALE
Tournaisian-Viséan	4926	4926	0	500	358	326	295	290	LIMEmarly
Devonian	4926	4926	0	300	400	358	290	280	SANDSTONE
Caledonian Hiatus	4926	4926	0		450	400			none
Basement	4926	6426	1500		545	450			BASEMENT

Table A6: Petrophysical properties of the lithologies used during for simulation. Standard lithologies are pre-defined in the software PetroMod v. 8. New lithologies were created by mixing of standard lithologies (% as stated).

Lithology	Source	Density	Initial porosity	Compressibility		Thermal conductivity		Heat capacity		Permeability at a porosity of	
		[kg/m³]	[%]	*10^{-10} [Pa^{-1}]		[W*m^{-1}*K^{-1}]		[kcal*kg^{-1}*K^{-1}]		[log mD]	
				min.	max.	20° C	100° C	20° C	100° C	5%	75%
SHALE	pre-defined	2680	65	10	60000	1.98	1.91	0.213	0.258	-5.5	-1.0
SHALEsilt	pre-defined	2677	62	10	25000	2.05	1.94	0.210	0.254	-5.4	-0.7
SHALEsand	pre-defined	2674	57	10	9000	2.32	2.12	0.205	0.248	-4.5	0.0
SHALE&SAND	pre-defined	2669	52	10	2800	2.65	2.38	0.197	0.236	-4.0	3.0
SHALEcalc	pre-defined	2688	52	10	5000	2.22	2.09	0.208	0.248	-2.5	8.5
SHALEcalcsilt	50% SHALEcalc 50% SHALEsilt	2683	57	10	11180	2.13	2.01	0.209	0.251	-3.9	3.9
SHALEcalcsand	50% SHALEcalc 50% SHALEsand	2681	55	10	6708	2.27	2.11	0.206	0.248	-3.5	4.3
SHALEcarb	pre-defined	2655	62	10	45000	1.50	1.43	0.212	0.258	-5.5	-1.0
SHALEcarbsand	50% SHALEcarb 50% SHALEsand	2665	60	10	20125	1.91	1.77	0.208	0.253	-5.0	-0.5
SHALEevap	pre-defined	2630	47	10	7000	2.93	2.61	0.210	0.247	-8.0	-4.0
SHALEevapsand	50% SHALEevap 50% SHALEsand	2652	52	10	7937	2.63	2.37	0.207	0.248	-6.3	-2.0
SHALE&EVAP	60% SHALE 40% SALT	2472	41	4	1282	3.46	3.05	0.210	0.240	-9.7	-7.0
SILTshaly	pre-defined	2675	58	10	15000	2.09	1.98	0.203	0.245	-5.2	-0.3
SILTevap	90% SILTshaly 10% SALT	2624	53	8	6587	2.45	2.26	0.203	0.242	-6.2	-1.9
SANDSTONE	pre-defined	2660	42	10	500	3.12	2.64	0.178	0.209	-2.0	0.0
SANDcongl	pre-defined	2663	35	10	330	2.93	2.63	0.184	0.217	-3.5	0.0
SAND&SILT	pre-defined	2665	50	10	1900	2.59	2.31	0.192	0.229	-3.5	3.0
SANDshaly	pre-defined	2666	48	10	1400	2.78	2.37	0.190	0.226	-4.0	0.0
SAND&SHALE	pre-defined	2669	52	10	2800	2.65	2.38	0.197	0.236	-4.0	3.0
LIMESTONE	pre-defined	2710	24	10	150	2.83	2.56	0.195	0.223	-4.3	13.3
LIMEdolom	pre-defined	2752	26	10	180	3.18	2.82	0.198	0.226	-3.3	14.3
LIMEmarly	pre-defined	2707	33	10	300	2.63	2.41	0.201	0.235	-4.3	13.3
MARLcarb	60% MARL 40% LIMEdolom	2713	39	10	485	2.61	2.39	0.204	0.239	-4.3	5.2
MARL	pre-defined	2687	47	10	940	2.23	2.11	0.208	0.248	-5.0	-0.9
CHALK	pre-defined	2700	65	45	700	2.85	2.51	0.197	0.226	-1.0	3.0
CHALK&LIMEmarl	50% CHALK 50% LIMEmarly	2704	49	21	458	2.74	2.46	0.199	0.230	-2.6	8.1
EVAPORITE	pre-defined	2540	10	1	10	4.69	3.91	0.194	0.210	-16.0	-16.0
EVAPshaly	pre-defined	2585	20	10	100	3.87	3.31	0.200	0.221	-13.0	-12.0
ANHYDRITE	pre-defined	2850	6	1	4	4.81	3.97	0.174	0.189	-16.0	-16.0
ANHYD&CARB	60% ANHYDRITE 40% LIMESTONE	2794	13	3	17	4.02	3.41	0.182	0.203	-11.3	-4.3
SALT	pre-defined	2160	6	1	4	5.69	4.76	0.206	0.212	-16.0	-16.0
BASEMENT	pre-defined	2750	5	1	2	2.72	2.35	0.188	0.223	-16.0	-16.0
RHYOLITE	modified from pre-defined	2700	5	1	2	3.00	2.65	0.188	0.233	-16.0	-16.0

Table A7: Petrographic data of Rotliegend sandstones from the northern margin of the NGB, derived from thin-section analysis (point counting, 300 points per thin section). Explanation of abbreviations:

sample: Fe = well Fehmarn Z1, Sw = well Schleswig Z1, Fb = well Flensburg Z1, Wl = well Westerland 1
depth: depth in metres below base Zechstein

detrital mineralogy:

Qz_m:	monocrystalline quartz grains
Qz_p:	polycrystalline quartz grains
Kf:	K-feldspar grains (fresh or partly altered to sericite/illite)
Pl:	plagioclase grains (fresh or partly altered to sericite/illite)
L_{vfe}:	felsic volcanic grains
L_{vma}:	mafic volcanic grains
L_{sm}:	sedimentary and metamorphic grains; rare quartz-feldspar aggregates of ambiguous origin (gneiss/granite) were included into this group (well Flensburg Z1 only)
L_{ch}:	chert grains: micro- to cryptocrystalline quartz
L_{ca}:	carbonate grains: calcite or dolomite micrites or sparites, often recrystallised, calcites partly biogenous, dolomites may contain clastic material (sand, silt)
L_{fe}:	Fe-oxide clasts: may be altered Fe-Mg-minerals, altered Fe-bearing HM, or fragments of intra-basinal Fe-oxide crust
HM:	heavy minerals: opaques, zircon, Ti-oxide, tourmaline, apatite, rare garnet
Ac:	accessories: mica, chlorite
PM:	"pseudomatrix": strongly altered and deformed grains or ambiguous origin (Lv, Kf, Pl, or L_{sm})
Re:	detrital components replaced by authigenic minerals (mainly carbonates, sulphates), detrital origin visible by relics of the former grains, grain coatings and/or opaque inclusions
M:	clay or silt matrix

authigenic mineralogy:

Qz:	quartz	Hm:	hematite
Fs:	feldspar	Lx:	leucoxene: aggregates of mainly Ti-oxides, e.g. anatase
Cc:	calcite		
Do:	dolomite	Il:	illite
An:	anhydrite	Ch:	chlorite
Ba:	barite	B:	bitumen

porosity:

P_{inter}:	intergranular porosity
P_{intra}:	intragranular porosity: mainly in feldspar or volcanic grains

detritus total: $Qz_m+Qz_p+Kf+Pl+L_{vfe}+L_{vma}+L_{sm}+L_{ch}+L_{ca}+L_{fe}+HM+Ac+PM+M$
cement total: Qz+Fs+Cc+Do+An+Ba+Hm+Lx+Il+Ch+B+Re
porosity total: $P_{inter}+P_{intra}$
IGV: intergranular volume, $Qz+Fs+Cc+Do+An+Ba+Hm+Lx+Il+Ch+B+P_{inter}$

grain coatings, clay minerals, feldspars, bitumen: 0 = not visible, 1 = poor, 2 = medium, 3 = strong

Hm:	hematite coatings on grain surfaces
IC:	illite coatings on grain surfaces
IM:	meshwork illite, including illites of fibrous, hairy, or platy morphology
CT:	tangential chlorite: chlorite coatings on grain surfaces
CR/CS:	radial/subtangantial chlorite: chlorite platelets growing on detrital grains perpendicular/subtangential to grain surfaces
CF:	fan-shaped chlorite, often pore-filling
Fs_{le}:	feldspar leaching
Fs_{al}:	feldspar alteration: illite/sericite
B	bitumen impregnation

granulometry:

$mean_1$/$median_1$:	mean/median grain size of the thin section; dominant layer, if two clearly defined layers present
$mean_2$/$median_2$:	mean/median grain size of the second layer, if present
$mode_{1a/b}$:	mode derived from bar charts (0.5 F class width), a/b for bimodal samples (only dominant layer)
$max_{ts.}$:	maximal grain size measured in thin section
sort.:	sorting, estimated according to the comparators of Beard and Weyl (1973), using the Trask (1932) sorting coefficient (So): 1.2 = very well sorted, 1.3 = well sorted, 1.7 = moderately well sorted, 2.4 = poorly sorted, 3 = very poorly sorted; note that this scale is not identical to the widely used sorting scale on the base of Folk and Ward (1957)
round.:	roundness, classified in 6 steps: 0 = very angular, 1 = angular, 2 = subangular, 3 = subrounded, 4 = rounded, 5 = well rounded; according to the roundness scale of Powers (1953)
grain c.:	grain contacts, classified in 5 steps: 0 = floating grains, 1 = point contacts, 2 = long contacts, 3 = concavo-convex contacts, 4 = sutured grains; according to Pettijohn et al. (1987)

Table A7: Petrographic data, continuation.

sample	detrital mineralogy													
[no.]	Qz_m [%]	Qz_p [%]	Kf [%]	Pl [%]	L_{vfe} [%]	L_{vma} [%]	L_{sm} [%]	L_{ch} [%]	L_{ca} [%]	L_{fe} [%]	HM [%]	Ac [%]	PM [%]	Re [%]
Fe010	23.0	6.0	2.0	6.3	31.3	0.7	2.7	0.3	0.3	0.0	2.3	0.3	0.3	1.7
Fe011	13.3	4.0	1.7	1.7	47.0	2.0	5.3	0.0	0.0	0.0	0.7	1.0	0.0	6.7
Fe012	18.0	6.7	1.0	4.7	37.3	0.3	5.3	0.7	0.0	0.7	0.3	0.3	0.7	2.0
Fe028	28.0	4.7	1.3	3.3	28.3	1.0	6.7	0.3	0.3	0.7	1.3	1.0	0.3	1.7
Fe029	27.3	3.0	2.3	4.7	24.3	0.7	7.0	0.7	0.7	1.7	1.0	0.7	0.0	3.0
Fe013	19.7	8.0	1.3	3.7	42.0	0.7	7.0	1.0	0.0	0.0	0.3	0.0	1.3	1.3
Fe014	34.7	5.7	0.7	4.7	24.7	0.3	8.0	0.0	0.3	0.7	2.3	0.0	4.0	0.3
Fe030	29.7	8.3	1.3	1.7	35.3	0.3	8.0	0.3	0.0	0.7	1.7	0.0	2.3	1.3
Fe015	29.0	7.3	3.3	4.0	32.3	0.0	5.0	0.0	0.0	2.7	1.0	0.0	2.0	1.0
Fe016	20.0	7.0	0.7	2.3	40.0	1.7	9.0	0.7	1.0	1.3	1.7	0.0	2.0	1.0
Fe018	13.0	10.0	0.7	0.7	30.7	0.7	27.0	0.0	0.0	1.7	1.3	0.0	0.7	1.3
Fe019	30.3	6.3	1.3	2.3	30.3	0.3	6.7	1.0	0.0	1.0	1.7	0.3	2.7	1.0
Fe021	35.3	9.7	1.7	3.3	30.7	0.0	3.7	0.3	0.0	0.0	1.7	0.0	1.0	1.0
Sw009	30.7	9.7	0.0	2.3	9.3	0.7	12.3	1.0	2.0	1.0	1.3	0.0	0.3	3.0
Sw010	33.7	7.0	0.0	2.7	11.7	2.7	11.7	1.0	2.0	1.0	0.7	0.0	0.3	3.3
Sw011	31.3	7.3	0.3	3.0	22.3	2.3	7.7	0.7	1.0	1.7	1.3	0.3	0.7	4.3
Sw012	34.7	7.0	1.3	6.3	14.3	3.3	9.3	0.3	0.0	0.7	0.3	0.3	1.7	2.3
Sw013	34.0	6.7	0.3	3.3	14.3	1.3	8.3	1.0	1.0	1.7	1.0	0.0	0.0	2.7
Sw014	32.3	7.0	0.7	3.7	10.0	1.7	16.7	1.7	0.7	0.7	0.0	0.0	0.3	4.3
Sw015	33.3	5.7	0.0	4.0	13.0	1.0	13.3	0.7	1.3	0.7	0.7	0.0	0.7	3.7
Sw016	35.7	7.7	0.3	3.0	12.7	1.7	12.0	0.7	1.7	2.0	0.0	0.0	1.0	1.7
Sw017	29.0	7.3	0.3	6.3	15.0	2.7	10.0	0.7	1.3	1.0	0.3	0.0	0.7	2.3
Sw018	33.7	8.0	0.0	4.0	14.3	1.0	12.0	0.3	0.3	0.3	1.0	0.0	2.3	1.7
Sw019	32.3	4.0	0.0	3.3	17.7	3.0	12.0	1.0	2.0	1.3	0.7	0.3	1.3	2.3
Sw020	35.3	3.3	0.0	2.3	14.0	1.7	12.7	1.3	3.0	1.7	1.0	0.0	1.0	1.7
Sw021	44.0	8.3	1.0	1.7	12.7	0.3	3.7	0.7	0.3	0.7	0.7	0.0	0.3	0.7
Sw022	46.3	5.7	0.0	2.0	10.3	0.0	5.0	0.7	1.7	0.7	0.7	0.0	0.7	1.7
Sw023	47.7	7.3	0.3	2.3	8.3	0.7	8.0	1.0	1.3	0.7	0.0	0.0	0.3	2.7
Sw024	29.3	8.0	0.0	1.3	18.3	1.0	14.7	0.7	1.7	0.7	0.3	0.0	0.3	0.7
Sw025	35.3	9.3	1.0	0.7	11.7	0.3	15.3	0.3	0.7	1.7	0.0	0.0	2.0	1.0
Sw026	44.0	5.7	1.0	1.3	9.7	1.3	12.7	0.3	1.0	2.0	0.0	0.0	0.7	1.3
Sw027	38.0	6.3	0.0	1.7	7.7	0.7	16.3	0.7	2.3	0.3	1.3	0.0	0.0	2.3
Sw028	43.3	10.0	0.0	2.3	7.3	0.3	11.0	1.0	1.7	1.7	0.0	0.0	1.3	1.0
Sw029	36.0	7.3	0.0	1.0	6.3	0.7	23.0	0.3	0.7	0.7	0.0	0.0	0.0	0.7
Sw030	44.7	9.7	0.3	1.7	3.7	1.0	13.3	0.7	2.0	1.7	0.3	0.0	0.3	1.0
Sw031	39.3	7.0	0.3	2.0	5.7	1.0	17.0	0.3	2.3	0.3	1.0	0.0	0.0	1.7
Sw032	38.3	8.3	0.0	1.7	6.7	0.3	24.3	0.3	0.0	1.0	0.0	0.0	1.3	0.0

Table A7: Petrographic data, continuation.

sample	authigenic mineralogy											matix	porosity	
[no.]	Qz [%]	Fs [%]	Cc [%]	Do [%]	An [%]	Ba [%]	Hm [%]	Lx [%]	Il [%]	Ch [%]	B [%]	M [%]	P_{inter} [%]	P_{intra} [%]
Fe010	2.3	4.3	9.3	0.0	0.0	0.0	5.3	0.0	0.0	0.0	0.0	0.3	1.0	0.0
Fe011	0.0	5.0	7.7	0.0	1.0	0.3	2.3	0.3	0.0	0.0	0.0	0.0	0.0	0.0
Fe012	1.7	3.7	8.0	0.0	0.3	0.0	6.0	0.0	0.0	0.0	0.0	1.7	0.7	0.0
Fe028	0.7	2.0	6.3	0.0	0.0	0.3	6.3	0.3	0.0	0.0	0.0	3.7	1.0	0.3
Fe029	2.3	7.7	9.3	0.0	0.0	0.0	3.7	0.0	0.0	0.0	0.0	0.0	0.0	0.0
Fe013	0.3	0.7	6.3	0.0	0.0	0.0	5.0	0.3	0.7	0.0	0.0	0.0	0.3	0.0
Fe014	1.3	0.0	2.7	0.0	0.0	0.0	6.7	0.3	2.0	0.0	0.0	0.3	0.3	0.0
Fe030	0.0	0.0	3.3	0.0	0.0	0.0	3.0	0.7	1.3	0.0	0.0	0.3	0.3	0.0
Fe015	0.7	0.3	4.7	0.0	0.0	0.0	4.7	0.3	1.3	0.0	0.0	0.0	0.3	0.0
Fe016	0.0	0.7	3.3	0.0	0.0	0.0	4.7	0.0	1.7	0.0	0.0	1.3	0.0	0.0
Fe018	0.3	0.0	7.3	0.0	0.0	0.0	2.7	0.7	0.7	0.0	0.0	0.0	0.3	0.3
Fe019	0.7	0.0	8.3	0.0	0.0	0.0	3.3	0.7	1.3	0.0	0.0	0.3	0.0	0.0
Fe021	0.0	0.0	6.0	0.0	0.3	0.0	2.0	0.3	0.3	0.0	0.0	2.3	0.3	0.0
Sw009	0.7	0.3	8.3	0.0	0.0	0.0	13.3	0.3	0.0	0.0	0.0	2.7	0.7	0.0
Sw010	2.0	1.0	13.3	0.0	0.0	0.3	4.7	0.3	0.0	0.0	0.0	0.0	0.7	0.0
Sw011	0.7	2.0	7.3	0.0	0.0	0.3	4.3	0.0	0.0	0.0	0.0	0.0	0.3	0.7
Sw012	0.3	0.3	8.7	0.0	0.0	0.0	6.0	0.0	0.0	0.0	0.0	0.7	1.7	0.3
Sw013	1.0	1.0	9.3	0.0	0.0	0.0	10.0	0.0	0.0	0.0	0.0	0.0	1.7	1.3
Sw014	0.7	1.0	10.7	0.0	0.0	0.0	6.3	0.0	0.0	0.0	0.0	0.3	1.0	0.3
Sw015	1.7	1.0	11.3	0.0	0.3	0.7	2.7	0.3	0.0	0.0	0.0	0.0	3.3	0.7
Sw016	0.7	1.0	8.0	0.0	0.0	3.0	3.7	0.7	0.0	0.0	0.0	0.0	2.3	0.7
Sw017	0.7	1.3	13.7	0.0	0.0	1.3	2.7	0.3	0.0	0.0	0.0	0.0	2.7	0.3
Sw018	0.3	1.0	13.7	0.0	0.0	0.0	4.7	0.3	0.0	0.0	0.0	0.3	0.7	0.0
Sw019	1.7	0.7	12.0	0.0	0.3	1.0	1.7	0.0	0.0	0.0	0.0	0.0	1.0	0.3
Sw020	1.0	0.7	12.7	0.0	0.0	0.0	3.7	0.7	0.0	0.0	0.0	0.0	1.7	0.7
Sw021	0.7	0.3	13.7	0.0	0.0	0.0	10.3	0.0	0.0	0.0	0.0	0.0	0.0	0.0
Sw022	2.3	0.3	16.7	0.0	0.0	0.3	4.0	0.3	0.0	0.0	0.0	0.0	0.0	0.7
Sw023	0.7	0.0	13.0	0.0	0.0	0.3	3.7	0.0	0.0	0.0	0.0	0.0	1.7	0.0
Sw024	0.3	0.3	16.7	0.0	0.0	0.3	3.7	0.0	0.0	0.0	0.0	0.0	1.0	0.7
Sw025	0.0	1.0	9.7	0.0	0.0	0.3	5.0	0.0	0.3	0.0	0.0	0.0	4.0	0.3
Sw026	0.3	0.7	9.0	0.0	0.0	0.3	3.3	0.0	0.0	0.0	0.0	0.0	5.0	0.3
Sw027	1.3	1.0	12.3	0.0	0.0	1.3	2.7	0.7	0.0	0.0	0.0	0.0	2.7	0.3
Sw028	1.0	0.7	9.3	0.0	0.0	0.0	3.0	0.3	0.0	0.0	0.0	0.3	3.7	0.7
Sw029	1.0	0.7	6.7	0.0	0.3	3.7	2.7	0.0	0.0	0.0	0.0	0.0	8.0	0.3
Sw030	0.3	1.0	8.0	0.0	0.3	0.3	3.7	0.3	0.0	0.0	0.0	0.0	5.0	0.7
Sw031	0.7	0.3	4.7	0.0	0.3	5.0	2.0	0.3	0.0	0.0	0.0	0.3	7.7	0.7
Sw032	2.0	0.7	1.0	0.0	0.7	1.0	3.0	0.0	0.0	0.0	0.0	0.3	7.7	1.3

Table A7: Petrographic data, continuation.

sample	detrius	cement	porosity	IGV	diage-	grain coatings, clay minerals, condition of feldspar, bitumen								
	total	total	total		nesis	Hm	IC	IM	CT	CR/CS	CF	Fs_{le}	Fs_{al}	B
[no.]	[%]	[%]	[%]	[%]	type	[0-3]	[0-3]	[0-3]	[0-3]	[0-3]	[0-3]	[0-3]	[0-3]	[0-3]
Fe010	76.0	23.0	1.0	22.3	H-SB	2.5	0.5	0.0	0.0	0.0	0.0	0.0	1.5	0.0
Fe011	76.7	23.3	0.0	16.7	H-SB	2.5	0.5	0.0	0.0	0.0	0.0	0.0	1.5	0.0
Fe012	77.7	21.7	0.7	20.3	H-SB	3.0	1.0	0.0	0.0	0.0	0.0	0.0	1.5	0.0
Fe028	81.0	17.7	1.3	17.0	H-SB	3.0	0.5	0.0	0.0	0.0	0.0	0.5	1.0	0.0
Fe029	74.0	26.0	0.0	23.0	H-SB	3.0	0.5	0.0	0.0	0.0	0.0	0.0	1.0	0.0
Fe013	85.0	14.7	0.3	13.7	H-SB	3.0	1.5	1.0	0.0	0.0	0.0	0.0	1.5	0.0
Fe014	86.3	13.3	0.3	13.3	H-SB	3.0	2.0	2.0	0.0	0.0	0.0	0.0	2.0	0.0
Fe030	90.0	9.7	0.3	8.7	H-SB	3.0	2.5	2.0	0.0	0.0	0.0	0.0	1.5	0.0
Fe015	86.7	13.0	0.3	12.3	H-SB	3.0	2.5	2.0	0.0	0.0	0.0	0.0	2.0	0.0
Fe016	88.7	11.3	0.0	10.3	H-SB	3.0	1.5	1.5	0.0	0.0	0.0	0.0	2.0	0.0
Fe018	86.3	13.0	0.7	12.0	H-SB	2.5	1.5	1.5	0.0	0.0	0.0	0.0	2.0	0.0
Fe019	84.7	15.3	0.0	14.3	H-SB	3.0	1.5	1.5	0.0	0.0	0.0	0.0	2.0	0.0
Fe021	89.7	10.0	0.3	9.3	H-SB	3.0	1.5	0.5	0.0	0.0	0.0	0.0	1.5	0.0
Sw009	73.3	26.0	0.7	23.7	H-SB	3.0	1.0	0.0	0.0	0.0	0.0	0.5	0.5	0.0
Sw010	74.3	25.0	0.7	22.3	H-SB	3.0	1.0	0.0	0.0	0.0	0.0	0.5	0.5	0.0
Sw011	80.0	19.0	1.0	15.0	H-SB	3.0	1.0	0.0	0.0	0.0	0.0	1.0	1.0	0.0
Sw012	80.3	17.7	2.0	17.0	H-SB	3.0	1.0	0.0	0.0	0.0	0.0	1.0	1.0	0.0
Sw013	73.0	24.0	3.0	23.0	H-SB	3.0	1.0	0.0	0.0	0.0	0.0	2.0	0.5	0.0
Sw014	75.7	23.0	1.3	19.7	H-SB	3.0	0.5	0.0	0.0	0.0	0.0	1.0	0.5	0.0
Sw015	74.3	21.7	4.0	21.3	H-SB	2.5	0.5	0.0	0.0	0.0	0.0	1.5	0.5	0.0
Sw016	78.3	18.7	3.0	19.3	H-SB	2.5	0.5	0.0	0.0	0.0	0.0	1.5	1.0	0.0
Sw017	74.7	22.3	3.0	22.7	H-SB	2.5	0.5	1.5	0.0	0.0	0.0	1.0	1.5	0.0
Sw018	77.7	21.7	0.7	20.7	H-SB	3.0	0.5	0.0	0.0	0.0	0.0	0.5	1.5	0.0
Sw019	79.0	19.7	1.3	18.3	H-SB	2.5	0.5	0.0	0.0	0.0	0.0	1.0	1.5	0.0
Sw020	77.3	20.3	2.3	20.3	H-SB	2.5	0.5	0.0	0.0	0.0	0.0	1.0	1.0	0.0
Sw021	74.3	25.7	0.0	25.0	H-SB	3.0	0.5	0.0	0.0	0.0	0.0	0.5	0.5	0.0
Sw022	73.7	25.7	0.7	24.0	H-SB	2.5	0.5	0.0	0.0	0.0	0.0	0.0	1.0	0.0
Sw023	78.0	20.3	1.7	19.3	H-SB	2.5	1.0	0.0	0.0	0.0	0.0	0.5	0.5	0.0
Sw024	76.3	22.0	1.7	22.3	H-SB	2.5	0.5	0.5	0.0	0.0	0.0	1.0	1.0	0.0
Sw025	78.3	17.3	4.3	20.3	H-SB	3.0	1.0	1.0	0.0	0.0	0.0	1.0	1.0	0.0
Sw026	79.7	15.0	5.3	18.7	H-SB	2.5	1.0	1.5	0.0	0.0	0.0	1.0	1.5	0.0
Sw027	75.3	21.7	3.0	22.0	H-SB	2.5	1.0	1.5	0.0	0.0	0.0	1.0	1.0	0.0
Sw028	80.3	15.3	4.3	18.0	H-SB	2.5	1.5	0.0	0.0	0.0	0.0	1.5	0.5	0.0
Sw029	76.0	15.7	8.3	23.0	H-SB	2.5	1.0	2.0	0.0	0.0	0.0	0.5	1.0	0.0
Sw030	79.3	15.0	5.7	19.0	H-SB	3.0	1.0	1.0	0.0	0.0	0.0	0.5	1.0	0.0
Sw031	76.7	15.0	8.3	21.0	H-SB	2.0	0.5	1.5	0.0	0.0	0.0	1.0	1.0	0.0
Sw032	82.7	8.3	9.0	16.0	H-SB	2.5	1.0	0.5	0.0	0.0	0.0	0.5	0.5	0.0

Table A7: Petrographic data, continuation.

sample	depth	granulometry									
		$mean_1$	$mean_2$	$median_1$	$median_2$	$mode_{1a}$	$mode_{1b}$	max_{ts}	sort.	round.	grain c.
[no.]	[m]	[µm]	[µm]	[µm]	[µm]	[µm]	[µm]	[mm]	[So]	[0-5]	[0-4]
Fe010	770.1	96	71	75	75	90	350	1.6	2.4	3.0	3.0
Fe011	772.9	230		214		500	90	1.6	1.7	3.5	2.5
Fe012	774.3	112		112		90	500	1.5	2.4	3.5	3.0
Fe028	774.9	130		112		90		1.2	1.7	2.5	3.0
Fe029	777.2	135	81	131	75	180		0.8	1.7	2.5	3.0
Fe013	835.3	195		210		180		11.5	3.0	2.5	3.5
Fe014	835.8	155		187		180		13.6	1.7	2.0	3.5
Fe030	836.4	218		247		350		5.5	2.4	2.5	3.5
Fe015	836.9	109		131		180		0.7	1.3	2.5	3.0
Fe016	838.0	177		187		180		4.0	2.4	2.5	3.5
Fe018	840.2	244		261		350	2800	11.0	2.4	2.5	3.0
Fe019	840.8	129		149		180		1.9	1.7	2.0	3.0
Fe021	948.7	117		121		90		3.0	2.4	2.5	3.0
Sw009	2056.1	148		149		125		4.0	1.7	2.5	2.5
Sw010	2057.0	148		187		250	90	7.0	1.7	3.0	2.5
Sw011	2059.1	111		121		125		15.0	2.4	2.0	2.5
Sw012	2059.7	136	96	145	93	180		4.5	2.4	2.0	3.0
Sw013	2060.2	130		135		180		6.0	2.4	2.0	2.5
Sw014	2062.0	168		168		180		3.2	1.7	2.5	3.0
Sw015	2062.9	112		126		180		0.7	1.3	2.5	2.5
Sw016	2063.6	221		224		180		3.0	1.3	3.0	2.5
Sw017	2063.9	206	186	205	187	180		1.5	1.3	2.5	2.0
Sw018	2065.1	140		149		180		2.0	1.3	2.0	2.5
Sw019	2066.0	124		131		180		12.0	2.4	2.0	2.5
Sw020	2067.4	104		112		180		6.0	2.4	2.5	2.5
Sw021	2069.2	132		131		180		20.0	1.3	2.5	2.5
Sw022	2070.4	126		140		180		0.6	1.3	2.5	2.5
Sw023	2071.7	118		126		180		2.0	1.3	2.5	2.5
Sw024	2073.7	155		163		180		8.0	1.3	2.0	2.5
Sw025	2074.8	119		112		125	350	3.7	1.7	2.0	2.0
Sw026	2076.5	145	105	135	103	125		1.0	1.3	2.0	2.0
Sw027	2077.2	137		131		125		1.4	1.3	2.5	2.5
Sw028	2077.8	124		112		90	350	1.5	1.7	2.0	2.5
Sw029	2078.4	178	130	177	131	90	350	2.8	1.3	3.0	2.0
Sw030	2079.0	128	95	112	89	90		1.2	1.7	2.5	2.0
Sw031	2079.8	221	132	243	112	250		1.2	1.3	2.5	2.0
Sw032	2080.5	138	111	140	98	90	250	2.5	1.7	2.5	2.0

Table A7: Petrographic data, continuation.

sample	detrital mineralogy													
[no.]	Qz_m [%]	Qz_p [%]	Kf [%]	Pl [%]	L_{vfe} [%]	L_{vma} [%]	L_{sm} [%]	L_{ch} [%]	L_{ca} [%]	L_{fe} [%]	HM [%]	Ac [%]	PM [%]	Re [%]
Fb018	44.0	14.7	0.0	2.3	2.0	0.0	8.7	1.0	1.7	0.0	1.7	0.3	0.3	1.0
Fb035	43.7	14.0	0.0	1.7	3.0	0.0	12.3	0.7	1.0	0.3	1.0	0.3	0.0	0.7
Fb019	45.0	17.7	0.3	2.7	1.7	0.0	6.3	1.7	0.7	0.0	0.0	0.7	0.0	0.3
Fb039	52.7	13.0	0.3	3.3	1.7	0.0	5.7	1.0	0.3	0.3	1.0	1.3	0.0	0.3
Fb020	40.0	17.3	0.0	1.7	1.0	0.0	7.0	1.0	2.3	0.0	0.0	0.0	0.0	1.7
Fb021	44.3	21.0	0.0	4.3	0.3	0.0	7.0	1.0	0.3	0.0	0.7	0.7	1.7	0.3
Fb022	45.3	14.3	0.0	2.0	0.7	0.0	12.0	1.0	0.7	0.0	0.7	0.0	0.3	0.7
Fb040	53.7	8.3	0.0	1.3	0.3	0.0	13.3	1.0	0.3	0.0	1.3	1.0	0.0	0.3
Fb041	47.7	7.3	0.0	4.3	1.0	0.0	10.7	0.7	0.3	0.0	0.7	0.0	0.3	1.0
Fb023	52.3	16.0	0.0	1.3	2.3	0.0	7.7	1.3	0.7	0.0	0.0	0.3	0.0	0.3
Fb045	48.3	12.7	0.0	2.7	0.7	0.0	11.0	1.3	0.3	0.0	0.3	0.3	0.0	1.0
Fb024	36.0	26.0	0.0	0.7	0.0	0.0	4.0	0.7	2.0	0.0	0.0	0.0	0.0	2.7
Fb025	32.0	18.0	0.0	2.0	0.7	0.0	17.3	2.7	3.3	0.0	0.0	0.7	0.0	2.0
Fb047	39.7	11.3	0.0	5.7	2.0	0.0	10.7	1.3	3.3	0.0	0.7	0.3	0.0	1.3
Fb026	40.7	21.0	0.0	3.0	1.3	0.0	8.7	0.7	1.3	0.0	1.3	0.7	0.0	0.7
Fb027	52.0	10.3	0.0	2.7	0.7	0.0	11.0	1.0	0.0	0.7	1.3	4.0	0.0	0.0
Fb028	52.0	16.3	0.0	4.3	2.3	0.0	8.3	0.3	0.7	0.3	1.0	0.3	0.0	0.7
Fb050	41.0	10.7	0.0	3.7	1.7	0.0	16.0	1.7	1.7	0.3	0.0	0.3	0.0	1.3
Fb008	46.7	11.3	0.0	4.0	1.3	0.0	9.7	1.0	0.3	0.0	0.3	0.0	0.0	0.3
Fb009	45.0	17.7	0.0	2.0	0.7	0.0	10.7	0.3	0.7	0.0	0.3	0.0	1.0	1.0
Fb052	37.7	22.7	0.0	3.0	1.0	0.0	19.0	1.0	0.0	0.0	0.7	0.3	0.0	0.3
Fb029	36.0	28.3	0.0	0.7	1.7	0.0	6.0	0.3	2.7	0.0	0.3	0.7	0.0	1.3
Fb010	47.0	21.3	0.0	1.7	1.0	0.0	4.3	1.3	1.3	0.0	0.0	0.0	0.0	0.0
Fb011	53.7	13.7	0.0	3.0	1.0	0.0	11.3	0.7	0.0	0.0	1.0	1.3	0.0	0.0
Fb012	50.0	12.3	0.0	2.0	0.0	0.0	6.3	0.3	1.0	0.7	0.7	0.3	0.0	0.3
Fb054	47.7	12.0	0.0	4.0	2.3	0.0	13.3	1.0	0.0	0.0	1.3	0.3	0.0	0.7
Fb013	42.0	17.0	0.3	4.0	1.3	0.0	11.7	1.0	0.0	0.3	0.7	0.7	0.0	0.3
Fb014	43.0	12.7	0.0	5.7	3.3	0.0	11.3	1.3	0.0	1.0	0.7	0.3	0.0	0.7
Fb057	44.7	16.7	0.0	2.0	2.7	0.0	11.0	0.7	0.3	0.7	1.3	0.0	0.7	1.0
Fb015	40.3	20.0	0.0	2.3	1.7	0.0	10.3	0.3	0.3	0.0	0.3	0.3	0.0	0.7
Fb059	47.3	17.0	0.0	3.3	0.7	0.0	14.7	1.3	0.3	0.3	1.0	0.3	0.0	0.0
Wl001	28.3	4.3	1.3	7.3	5.3	0.7	7.7	0.0	2.7	0.7	0.7	0.0	0.0	1.0

Table A7: Petrographic data, continuation.

sample	authigenic mineralogy											matix	porosity	
[no.]	Qz [%]	Fs [%]	Cc [%]	Do [%]	An [%]	Ba [%]	Hm [%]	Lx [%]	Il [%]	Ch [%]	B [%]	M [%]	P_{inter} [%]	P_{intra} [%]
Fb018	6.0	0.3	0.0	10.3	0.0	0.0	0.7	0.0	0.0	1.3	0.0	0.0	3.3	0.3
Fb035	5.7	0.3	0.0	7.7	0.0	0.0	1.0	0.3	0.0	1.7	0.0	0.0	4.3	0.3
Fb019	5.7	0.3	0.0	11.0	0.0	0.0	0.3	0.3	0.0	1.0	0.0	0.0	4.0	0.3
Fb039	4.3	0.7	0.0	7.3	0.0	0.0	0.7	0.0	0.0	0.3	0.0	0.0	5.3	0.3
Fb020	6.0	0.0	0.0	18.7	0.0	0.0	0.3	0.0	0.0	0.3	0.0	0.0	2.7	0.0
Fb021	6.3	0.3	0.0	3.3	0.0	0.0	0.3	0.3	0.0	2.7	0.0	2.7	2.3	0.0
Fb022	11.7	0.3	0.0	6.7	0.0	0.0	0.7	0.3	0.0	0.7	0.0	0.0	1.7	0.3
Fb040	5.7	0.3	0.3	8.7	0.0	0.0	1.0	0.0	0.0	1.0	0.0	0.0	2.0	0.0
Fb041	8.3	0.7	1.7	9.7	0.0	0.0	1.3	0.3	0.0	1.3	0.0	0.0	2.0	0.7
Fb023	7.3	0.3	0.7	4.7	0.0	0.0	0.0	0.3	0.0	0.7	0.0	0.0	3.3	0.3
Fb045	8.7	0.3	2.0	9.7	0.0	0.0	0.3	0.0	0.0	0.0	0.0	0.0	0.3	0.0
Fb024	10.0	0.0	0.0	13.3	0.0	0.0	0.0	0.0	0.0	1.3	0.0	0.0	2.7	0.7
Fb025	3.3	0.7	1.3	10.7	0.0	0.0	0.0	0.0	0.0	0.7	0.0	4.7	0.0	0.0
Fb047	10.7	0.3	1.0	8.7	0.0	0.0	0.7	0.3	0.0	0.3	0.0	0.0	1.7	0.0
Fb026	4.7	0.3	2.7	9.0	0.0	0.0	1.0	0.0	0.0	0.3	0.0	0.0	2.3	0.3
Fb027	2.3	0.3	0.0	0.0	0.0	0.0	7.0	0.0	0.0	1.3	0.0	4.0	1.0	0.3
Fb028	7.0	1.0	0.3	1.0	0.0	0.0	1.3	0.3	0.0	0.0	0.0	0.0	1.7	0.7
Fb050	11.3	1.0	0.3	4.0	0.0	0.0	1.3	0.0	0.0	0.7	0.0	0.0	2.7	0.3
Fb008	7.0	1.3	0.7	4.0	0.0	0.0	0.7	0.3	0.0	1.3	0.0	0.0	8.3	1.3
Fb009	6.3	0.7	0.0	5.3	0.0	0.0	0.0	0.3	0.0	3.0	0.0	0.0	4.3	0.7
Fb052	8.3	0.0	0.0	2.3	0.0	0.0	1.0	0.0	0.0	1.0	0.0	0.0	1.7	0.0
Fb029	5.0	0.3	1.0	14.7	0.0	0.0	0.7	0.0	0.0	0.3	0.0	0.0	0.0	0.0
Fb010	10.7	0.0	0.0	6.3	0.0	0.0	0.3	0.0	0.0	0.7	0.0	0.0	3.0	1.0
Fb011	4.0	0.3	0.0	0.0	0.0	0.0	8.7	0.3	0.0	0.0	0.0	0.3	0.7	0.0
Fb012	16.3	1.0	4.0	2.3	0.0	0.0	1.7	0.3	0.0	0.0	0.0	0.0	0.3	0.0
Fb054	3.0	0.7	8.3	0.0	0.0	0.0	4.3	0.0	0.0	0.0	0.0	0.0	0.7	0.3
Fb013	1.7	2.0	10.3	0.0	0.0	0.0	4.3	0.7	0.0	0.0	0.0	0.0	1.3	0.3
Fb014	10.3	1.0	0.3	4.7	0.0	0.0	2.3	0.3	0.0	0.0	0.0	0.0	0.7	0.3
Fb057	5.7	0.3	0.0	6.7	0.0	0.0	1.3	0.3	0.0	0.7	0.0	0.0	2.7	0.7
Fb015	8.3	0.7	0.0	7.3	0.0	0.0	0.7	0.3	0.0	0.3	0.0	0.0	4.7	1.0
Fb059	5.7	0.3	0.0	4.3	0.0	0.0	1.0	0.0	0.0	0.0	0.0	0.0	1.7	0.7
Wl001	1.7	0.3	17.3	0.0	17.3	0.0	2.0	0.0	0.0	0.0	0.0	0.0	1.3	0.0

Table A7: Petrographic data, continuation.

sample	detrius	cement	porosity	IGV	diage-	grain coatings, clay minerals, feldspars, bitumen								
	total	total	total		nesis	Hm	IC	IM	CT	CR/CS	CF	Fs_{le}	Fs_{al}	B
[no.]	[%]	[%]	[%]	[%]	type	[0-3]	[0-3]	[0-3]	[0-3]	[0-3]	[0-3]	[0-3]	[0-3]	[0-3]
Fb018	76.7	19.7	3.7	22.0	C-D	1.0	0.5	0.0	1.0	2.5	0.0	1.0	0.5	0.0
Fb035	78.0	17.3	4.7	21.0	C-D	1.5	0.5	0.0	1.0	2.5	0.0	1.5	1.5	0.0
Fb019	76.7	19.0	4.3	22.7	C-D	1.5	0.5	0.0	0.5	2.0	0.0	1.0	0.0	0.0
Fb039	80.7	13.7	5.7	18.7	C-D	1.5	0.0	0.0	1.0	1.5	0.0	1.0	0.5	0.0
Fb020	70.3	27.0	2.7	28.0	C-D	1.0	0.0	0.0	1.5	2.0	0.0	0.5	0.5	0.0
Fb021	84.0	13.7	2.3	15.7	C-D	1.0	0.5	0.0	2.0	2.5	0.0	1.0	1.0	0.0
Fb022	77.0	21.0	2.0	22.0	C-D	1.5	0.5	0.0	0.5	1.0	0.0	1.0	0.0	0.0
Fb040	80.7	17.3	2.0	19.0	C-D	1.0	0.0	0.0	1.0	1.0	0.0	1.0	0.5	0.0
Fb041	73.0	24.3	2.7	25.3	C-D	1.0	0.0	0.0	0.5	1.5	0.0	1.0	1.5	0.0
Fb023	82.0	14.3	3.7	17.3	C-D	1.0	0.5	0.0	1.5	1.0	0.0	1.0	1.0	0.0
Fb045	77.7	22.0	0.3	21.3	C-D	1.0	0.0	0.0	0.5	0.0	0.0	0.5	0.5	0.0
Fb024	69.3	27.3	3.3	27.3	C-D	0.5	0.5	0.0	1.0	1.0	0.0	1.0	0.0	0.0
Fb025	81.3	18.7	0.0	16.7	C-D	0.5	0.0	0.0	2.0	0.0	0.0	0.5	0.0	0.0
Fb047	75.0	23.3	1.7	23.7	C-D	1.0	0.0	0.0	0.5	1.0	0.0	1.5	1.0	0.0
Fb026	78.7	18.7	2.7	20.3	C-D	1.0	0.0	0.0	0.5	1.0	0.0	0.5	0.5	0.0
Fb027	87.7	11.0	1.3	12.0	C-D	2.5	0.5	0.0	1.0	1.0	0.0	0.0	0.0	0.0
Fb028	86.0	11.7	2.3	12.7	C-D	2.0	0.5	0.0	0.0	0.0	0.0	0.5	0.0	0.0
Fb050	77.0	20.0	3.0	21.3	C-D	1.5	0.0	0.0	0.0	1.0	0.0	1.5	0.5	0.0
Fb008	74.7	15.7	9.7	23.7	C-D	1.5	0.0	0.0	1.0	2.5	0.0	2.0	0.5	0.0
Fb009	78.3	16.7	5.0	20.0	C-D	1.0	0.0	0.0	1.5	2.5	0.0	0.5	1.5	0.0
Fb052	85.3	13.0	1.7	14.3	C-D	1.5	0.5	0.0	0.5	1.0	0.0	1.0	1.0	0.0
Fb029	76.7	23.3	0.0	22.0	C-D	1.0	0.0	0.0	1.0	0.0	0.0	0.5	0.5	0.0
Fb010	78.0	18.0	4.0	21.0	C-D	1.0	0.0	0.0	1.5	2.0	0.0	1.0	0.5	0.0
Fb011	86.0	13.3	0.7	14.0	C-D	3.0	1.0	0.0	0.0	0.0	0.0	0.0	0.5	0.0
Fb012	73.7	26.0	0.3	26.0	H-SB	1.5	0.5	0.0	0.0	0.0	0.0	0.0	0.0	0.0
Fb054	82.0	17.0	1.0	17.0	H-SB	2.5	0.5	0.0	0.0	0.0	0.0	0.5	0.0	0.0
Fb013	79.0	19.3	1.7	20.3	H-SB	3.0	0.5	0.0	0.0	0.0	0.0	0.0	0.5	0.0
Fb014	79.3	19.7	1.0	19.7	C-D	2.0	0.5	0.0	0.5	0.0	0.0	0.5	0.0	0.0
Fb057	80.7	16.0	3.3	17.7	C-D	1.5	0.5	0.0	0.5	1.0	0.0	2.0	0.5	0.0
Fb015	76.0	18.3	5.7	22.3	C-D	1.5	0.0	0.0	0.0	0.5	0.0	1.0	0.5	0.0
Fb059	86.3	11.3	2.3	13.0	C-D	1.5	0.0	0.0	0.0	0.0	0.0	1.0	1.5	0.0
Wl001	59.0	39.7	1.3	40.0	H-SB	2.0	0.5	0.0	0.0	0.0	0.0	0.0	2.0	0.0

Table A7: Petrographic data, continuation.

sample	**depth**	**granulometry**									
[no.]	[m]	$mean_1$ [µm]	$mean_2$ [µm]	$median_1$ [µm]	$median_2$ [µm]	$mode_{1a}$ [µm]	$mode_{1b}$ [µm]	max_{ts} [mm]	sort. [So]	round. [0-5]	grain c. [0-4]
Fb018	857.5	212		238		350		3.3	1.3	3.5	2.0
Fb035	858.4	194		224		250		0.6	1.2	2.5	2.5
Fb019	859.5	203		224		250		1.0	1.3	2.5	2.5
Fb039	863.6	176		196		250		1.0	1.2	3.5	2.5
Fb020	864.0	241		275		350		3.1	1.7	3.0	2.0
Fb021	935.0	158		168		180		4.0	1.3	2.5	2.5
Fb022	935.5	163		191		250		3.2	1.3	3.0	2.5
Fb040	936.1	163		168		180		0.5	1.3	2.5	2.5
Fb041	937.5	170		177		180		0.7	1.3	2.5	2.5
Fb023	939.0	173		177		180		0.7	1.3	3.0	2.5
Fb045	1031.9	176		187		250		1.4	1.3	2.5	2.0
Fb024	1032.5	289		308		350		15.0	2.4	3.5	2.5
Fb025	1033.0	161		168		250		21.0	2.4	2.5	2.0
Fb047	1036.6	230		224		180		5.6	1.7	2.0	3.0
Fb026	1037.0	181		215		250		1.0	1.3	3.0	2.5
Fb027	1143.0	56		56		90		0.6	1.7	2.5	3.0
Fb028	1144.0	132		149		180		0.6	1.3	2.5	2.5
Fb050	1145.9	216		224		250		2.5	1.3	2.5	2.5
Fb008	1147.0	197		205		180		2.6	1.3	2.5	2.5
Fb009	1148.5	253		285		350		2.2	1.7	3.0	3.0
Fb052	1149.1	183		205		180		0.9	1.3	3.0	2.5
Fb029	1149.5	263		261		250		4.8	2.4	3.0	2.0
Fb010	1150.5	235		257		350		2.4	1.3	3.0	2.0
Fb011	1252.0	106		112		180		0.7	1.7	2.0	3.0
Fb012	1252.5	137		131		180		0.6	1.3	2.5	2.5
Fb054	1252.7	147		168		180		0.8	1.3	2.5	2.5
Fb013	1253.0	130		145		180		0.5	1.3	2.0	2.5
Fb014	1262.0	121		117		90		1.1	1.3	2.5	2.5
Fb057	1266.6	267		303		350		2.5	1.3	2.5	3.0
Fb015	1267.5	254		275		350		1.2	1.3	2.5	3.0
Fb059	1267.9	212		205		180		1.6	1.3	2.5	2.5
Wl001	4.4	228		233		250		1.3	1.2	4.0	1.0

Table A8: Electron microprobe analyses of detrital and authigenic feldspar in sandstones from the northern basin margin. Ab = albite, Kf = K-feldspar, <d.l. = below detection limit.

sample-no.		chemical composition [wt.-%]										
		SiO_2	TiO_2	Al_2O_3	CaO	Na_2O	K_2O	FeO	MnO	MgO	BaO	SrO	Total
detrital feldspar													
Fe014_10	Ab	69.05	0.07	19.87	0.09	11.63	0.10	<d.l.	0.05	<d.l.	<d.l.	<d.l.	100.86
Fe016_4	Ab	65.93	<d.l.	20.69	1.30	10.47	0.80	0.07	<d.l.	<d.l.	<d.l.	<d.l.	99.26
Fe016_7	Ab	67.14	<d.l.	20.10	0.43	11.48	0.05	<d.l.	<d.l.	<d.l.	<d.l.	<d.l.	99.20
Fe019_10	Ab	65.74	<d.l.	19.93	0.31	11.17	0.71	0.15	<d.l.	0.12	<d.l.	<d.l.	98.13
Fe019_18	Ab	67.11	<d.l.	19.06	0.05	11.68	0.10	<d.l.	<d.l.	<d.l.	<d.l.	<d.l.	98.00
Sw031_6	Ab	67.95	<d.l.	19.73	<d.l.	11.75	0.04	0.06	<d.l.	<d.l.	<d.l.	<d.l.	99.53
Sw031_10	Ab	65.89	<d.l.	20.94	1.34	11.06	0.03	<d.l.	<d.l.	<d.l.	<d.l.	0.10	99.36
Sw031_13	Ab	67.46	<d.l.	19.92	<d.l.	11.90	0.12	0.08	<d.l.	<d.l.	0.07	<d.l.	99.54
Fb008_22	Ab	67.56	<d.l.	18.92	<d.l.	12.12	<d.l.	<d.l.	<d.l.	<d.l.	<d.l.	<d.l.	98.60
Fb008_25	Ab	67.26	<d.l.	18.89	<d.l.	11.88	<d.l.	<d.l.	<d.l.	<d.l.	<d.l.	<d.l.	98.03
Fb013_3	Ab	67.67	<d.l.	19.70	0.07	11.79	0.03	<d.l.	<d.l.	<d.l.	<d.l.	<d.l.	99.26
Fb013_5	Ab	67.50	<d.l.	19.61	<d.l.	12.04	<d.l.	0.06	<d.l.	<d.l.	<d.l.	<d.l.	99.21
Fb013_9	Ab	67.28	<d.l.	19.81	<d.l.	11.78	0.03	<d.l.	<d.l.	0.20	<d.l.	<d.l.	99.10
Fb013_14	Ab	67.88	<d.l.	19.87	<d.l.	11.81	0.03	0.06	<d.l.	<d.l.	<d.l.	<d.l.	99.64
Fb013_17	Ab	68.07	<d.l.	19.66	0.09	12.17	<d.l.	<d.l.	<d.l.	<d.l.	<d.l.	<d.l.	99.99
Fb013_22	Ab	67.84	<d.l.	19.79	0.07	11.74	<d.l.	<d.l.	<d.l.	<d.l.	<d.l.	<d.l.	99.44
Fb013_25	Ab	67.67	<d.l.	19.85	<d.l.	11.81	<d.l.	<d.l.	<d.l.	<d.l.	<d.l.	<d.l.	99.33
Fb035_4	Ab	67.77	<d.l.	19.20	0.15	11.72	0.05	<d.l.	<d.l.	<d.l.	<d.l.	<d.l.	98.88
Fb035_10	Ab	67.70	<d.l.	19.09	0.06	11.90	<d.l.	<d.l.	<d.l.	<d.l.	<d.l.	<d.l.	98.75
Fb057_6	Ab	68.54	<d.l.	19.69	<d.l.	11.63	0.03	<d.l.	<d.l.	<d.l.	<d.l.	<d.l.	99.89
Fb057_16	Ab	67.58	<d.l.	19.66	<d.l.	11.78	0.03	0.06	<d.l.	<d.l.	<d.l.	<d.l.	99.11
Fe016_6	Kf	63.68	<d.l.	18.62	0.10	0.19	16.08	0.14	<d.l.	0.15	0.35	<d.l.	99.30
Fe016_8	Kf	63.88	<d.l.	18.71	0.05	0.14	16.49	<d.l.	<d.l.	<d.l.	0.19	<d.l.	99.47
Fe016_13	Kf	63.74	<d.l.	18.61	<d.l.	1.20	14.82	0.11	<d.l.	<d.l.	0.59	0.12	99.19
Fe019_7	Kf	63.54	<d.l.	18.02	0.07	0.13	16.43	<d.l.	<d.l.	<d.l.	0.16	<d.l.	98.35
Fe019_12	Kf	63.72	<d.l.	17.93	<d.l.	0.60	15.87	<d.l.	<d.l.	<d.l.	0.18	<d.l.	98.30
Fe019_20	Kf	63.27	<d.l.	17.91	0.09	1.08	14.96	<d.l.	<d.l.	<d.l.	0.65	<d.l.	97.96
detrital feldspar within volcanic clasts													
Fe014_1	Ab	68.48	<d.l.	19.85	<d.l.	11.83	<d.l.	0.07	<d.l.	<d.l.	<d.l.	<d.l.	100.23
Fe014_2	Kf	64.77	<d.l.	18.74	<d.l.	0.36	16.38	<d.l.	<d.l.	<d.l.	0.27	<d.l.	100.52
Fe014_3	Kf	63.72	<d.l.	19.35	0.05	0.37	15.48	0.53	<d.l.	0.33	0.32	<d.l.	100.14
Fe016_18	Kf	64.02	<d.l.	18.67	<d.l.	0.23	16.26	0.16	<d.l.	<d.l.	0.27	<d.l.	99.60
Fe019_19	Kf	63.83	<d.l.	17.75	0.06	0.95	15.47	0.06	<d.l.	<d.l.	0.16	<d.l.	98.28
Sw015_11	Kf	67.85	<d.l.	19.21	0.04	12.10	0.04	<d.l.	<d.l.	<d.l.	<d.l.	<d.l.	99.24
authigenic feldspar overgrowths													
Fe011_6a	Ab	67.38	<d.l.	19.17	0.05	11.97	<d.l.	<d.l.	<d.l.	<d.l.	<d.l.	0.09	98.66
Fe016_7	Ab	67.63	<d.l.	19.79	0.15	11.88	0.04	<d.l.	<d.l.	<d.l.	<d.l.	<d.l.	99.49
Sw027_13	Ab	67.43	<d.l.	18.82	0.04	11.66	0.05	<d.l.	<d.l.	<d.l.	<d.l.	<d.l.	98.00
Fb008_19	Ab	67.53	<d.l.	18.83	<d.l.	11.84	<d.l.	<d.l.	<d.l.	<d.l.	<d.l.	<d.l.	98.20
Fb013_9	Ab	67.60	<d.l.	19.79	0.08	11.84	0.03	0.07	<d.l.	<d.l.	<d.l.	<d.l.	99.41
Fb013_14	Ab	67.96	<d.l.	19.69	<d.l.	11.77	<d.l.	<d.l.	<d.l.	<d.l.	<d.l.	<d.l.	99.42
Fb035_10	Ab	67.96	<d.l.	19.21	<d.l.	11.63	<d.l.	<d.l.	<d.l.	0.21	<d.l.	<d.l.	99.01
Fb057_16	Ab	67.85	<d.l.	19.65	<d.l.	12.09	<d.l.	<d.l.	<d.l.	<d.l.	<d.l.	<d.l.	99.59
authigenic feldspar													
Fe011_3a	Ab	67.83	<d.l.	19.24	0.05	11.93	0.03	<d.l.	<d.l.	<d.l.	<d.l.	<d.l.	99.08
Fe011_6b	Ab	67.59	<d.l.	19.38	0.13	11.87	0.03	<d.l.	0.06	<d.l.	<d.l.	<d.l.	99.05
Fe011_1d	Ab	67.70	<d.l.	19.81	0.11	11.00	0.03	0.06	<d.l.	<d.l.	<d.l.	<d.l.	98.72
Fe016_14	Ab	67.04	<d.l.	19.86	0.13	12.06	0.03	<d.l.	<d.l.	<d.l.	<d.l.	<d.l.	99.13
Sw016_1a	Ab	67.87	<d.l.	19.36	0.13	11.78	<d.l.	<d.l.	<d.l.	<d.l.	<d.l.	<d.l.	99.14
Sw016_3	Ab	68.13	<d.l.	19.27	<d.l.	12.02	0.03	<d.l.	<d.l.	<d.l.	<d.l.	<d.l.	99.45
Sw016_7	Ab	67.93	<d.l.	19.38	<d.l.	11.96	<d.l.	0.06	<d.l.	0.04	<d.l.	<d.l.	99.37
Fb008_25	Ab	67.51	<d.l.	18.97	<d.l.	12.08	<d.l.	<d.l.	<d.l.	<d.l.	<d.l.	<d.l.	98.56
Fb013_2	Ab	67.79	<d.l.	19.71	<d.l.	11.67	<d.l.	<d.l.	<d.l.	<d.l.	<d.l.	<d.l.	99.17
Fb013_27	Ab	67.87	<d.l.	19.60	0.11	11.99	<d.l.	<d.l.	<d.l.	<d.l.	<d.l.	<d.l.	99.57
Fb041_3	Ab	67.60	<d.l.	19.01	<d.l.	11.92	<d.l.	<d.l.	<d.l.	<d.l.	<d.l.	<d.l.	98.53
Fb057_7	Ab	68.70	<d.l.	19.63	<d.l.	11.72	<d.l.	0.06	<d.l.	<d.l.	<d.l.	<d.l.	100.11

Table A8: EMP feldspar, continuation.

sample-no.		stuctural formula [apfu], number of ions on the basis of 24 oxygen equivalents											
		Si	Ti	Al	Ca	Na	K	Fe	Mn	Mg	Ba	Sr	Total
detrital feldspar													
Fe014_10	Ab	8.964	0.007	3.040	0.013	2.927	0.016	<d.l.	0.006	<d.l.	<d.l.	<d.l.	14.973
Fe016_4	Ab	8.761	<d.l.	3.241	0.185	2.697	0.136	0.008	<d.l.	<d.l.	<d.l.	<d.l.	15.028
Fe016_7	Ab	8.879	<d.l.	3.134	0.061	2.943	0.008	<d.l.	<d.l.	<d.l.	<d.l.	<d.l.	15.026
Fe019_10	Ab	8.830	<d.l.	3.155	0.045	2.910	0.122	0.016	<d.l.	0.023	<d.l.	<d.l.	15.102
Fe019_18	Ab	8.976	<d.l.	3.004	0.008	3.030	0.017	<d.l.	<d.l.	<d.l.	<d.l.	<d.l.	15.035
Sw031_6	Ab	8.944	<d.l.	3.061	<d.l.	3.000	0.007	0.007	<d.l.	<d.l.	<d.l.	<d.l.	15.019
Sw031_10	Ab	8.734	<d.l.	3.272	0.190	2.843	0.006	<d.l.	<d.l.	<d.l.	<d.l.	0.008	15.053
Sw031_13	Ab	8.901	<d.l.	3.099	<d.l.	3.045	0.019	0.008	<d.l.	<d.l.	0.003	<d.l.	15.076
Fb008_22	Ab	8.989	<d.l.	2.968	<d.l.	3.126	<d.l.	<d.l.	<d.l.	<d.l.	<d.l.	<d.l.	15.083
Fb008_25	Ab	8.995	<d.l.	2.977	<d.l.	3.080	<d.l.	<d.l.	<d.l.	<d.l.	<d.l.	<d.l.	15.052
Fb013_3	Ab	8.938	<d.l.	3.066	0.009	3.019	0.005	<d.l.	<d.l.	<d.l.	<d.l.	<d.l.	15.038
Fb013_5	Ab	8.928	<d.l.	3.057	<d.l.	3.087	<d.l.	0.007	<d.l.	<d.l.	<d.l.	<d.l.	15.079
Fb013_9	Ab	8.900	<d.l.	3.089	<d.l.	3.020	0.005	<d.l.	<d.l.	0.039	<d.l.	<d.l.	15.053
Fb013_14	Ab	8.928	<d.l.	3.081	<d.l.	3.012	0.005	0.006	<d.l.	<d.l.	<d.l.	<d.l.	15.032
Fb013_17	Ab	8.937	<d.l.	3.042	0.013	3.099	<d.l.	<d.l.	<d.l.	<d.l.	<d.l.	<d.l.	15.091
Fb013_22	Ab	8.936	<d.l.	3.072	0.010	2.999	<d.l.	<d.l.	<d.l.	<d.l.	<d.l.	<d.l.	15.017
Fb013_25	Ab	8.926	<d.l.	3.086	<d.l.	3.021	<d.l.	<d.l.	<d.l.	<d.l.	<d.l.	<d.l.	15.033
Fb035_4	Ab	8.981	<d.l.	2.999	0.021	3.013	0.008	<d.l.	<d.l.	<d.l.	<d.l.	<d.l.	15.022
Fb035_10	Ab	8.985	<d.l.	2.986	0.008	3.063	<d.l.	<d.l.	<d.l.	<d.l.	<d.l.	<d.l.	15.042
Fb057_6	Ab	8.977	<d.l.	3.040	<d.l.	2.954	0.005	<d.l.	<d.l.	<d.l.	<d.l.	<d.l.	14.976
Fb057_16	Ab	8.939	<d.l.	3.066	<d.l.	3.021	0.006	0.006	<d.l.	<d.l.	<d.l.	<d.l.	15.038
Fe016_6	Kf	8.921	<d.l.	3.075	0.014	0.051	2.873	0.017	<d.l.	0.031	0.019	<d.l.	15.001
Fe016_8	Kf	8.930	<d.l.	3.083	0.008	0.037	2.942	<d.l.	<d.l.	<d.l.	0.011	<d.l.	15.011
Fe016_13	Kf	8.924	<d.l.	3.070	<d.l.	0.325	2.647	0.013	<d.l.	<d.l.	0.033	0.009	15.021
Fe019_7	Kf	8.985	<d.l.	3.003	0.010	0.036	2.964	<d.l.	<d.l.	<d.l.	0.009	<d.l.	15.007
Fe019_12	Kf	8.998	<d.l.	2.984	<d.l.	0.164	2.858	<d.l.	<d.l.	<d.l.	0.010	<d.l.	15.014
Fe019_20	Kf	8.975	<d.l.	2.994	0.014	0.297	2.708	<d.l.	<d.l.	<d.l.	0.036	<d.l.	15.024
detrital feldspar within volcanic clasts													
Fe014_1	Ab	8.951	<d.l.	3.058	<d.l.	2.997	<d.l.	0.008	<d.l.	<d.l.	<d.l.	<d.l.	15.014
Fe014_2	Kf	8.952	<d.l.	3.054	<d.l.	0.096	2.888	<d.l.	<d.l.	<d.l.	0.015	<d.l.	15.005
Fe014_3	Kf	8.838	<d.l.	3.164	0.008	0.100	2.739	0.061	<d.l.	0.068	0.017	<d.l.	14.995
Fe016_18	Kf	8.939	<d.l.	3.073	<d.l.	0.061	2.896	0.018	<d.l.	<d.l.	0.015	<d.l.	15.002
Fe019_19	Kf	9.011	<d.l.	2.954	0.009	0.260	2.786	0.008	<d.l.	<d.l.	0.009	<d.l.	15.036
Sw015_11	Kf	8.974	<d.l.	2.994	0.005	3.102	0.007	<d.l.	<d.l.	<d.l.	<d.l.	<d.l.	15.082
authigenic feldspar overgrowths													
Fe011_6a	Ab	8.964	<d.l.	3.006	0.008	3.088	<d.l.	<d.l.	<d.l.	<d.l.	<d.l.	0.007	15.072
Fe016_7	Ab	8.918	<d.l.	3.076	0.022	3.037	0.007	<d.l.	<d.l.	<d.l.	<d.l.	<d.l.	15.059
Sw027_13	Ab	9.011	<d.l.	2.965	0.006	3.020	0.009	<d.l.	<d.l.	<d.l.	<d.l.	<d.l.	15.010
Fb008_19	Ab	9.007	<d.l.	2.961	<d.l.	3.062	<d.l.	<d.l.	<d.l.	<d.l.	<d.l.	<d.l.	15.030
Fb013_9	Ab	8.921	<d.l.	3.078	0.012	3.029	0.005	0.008	<d.l.	<d.l.	<d.l.	<d.l.	15.053
Fb013_14	Ab	8.950	<d.l.	3.056	<d.l.	3.006	<d.l.	<d.l.	<d.l.	<d.l.	<d.l.	<d.l.	15.012
Fb035_10	Ab	8.984	<d.l.	2.993	<d.l.	2.982	<d.l.	<d.l.	<d.l.	0.042	<d.l.	<d.l.	15.001
Fb057_16	Ab	8.938	<d.l.	3.052	<d.l.	3.089	<d.l.	<d.l.	<d.l.	<d.l.	<d.l.	<d.l.	15.079
authigenic feldspar													
Fe011_3a	Ab	8.975	<d.l.	3.001	0.007	3.061	0.005	<d.l.	<d.l.	<d.l.	<d.l.	<d.l.	15.049
Fe011_6b	Ab	8.953	<d.l.	3.025	0.018	3.048	0.005	<d.l.	0.006	<d.l.	<d.l.	<d.l.	15.055
Fe011_1d	Ab	8.960	<d.l.	3.091	0.016	2.823	0.006	0.007	<d.l.	<d.l.	<d.l.	<d.l.	14.902
Fe016_14	Ab	8.886	<d.l.	3.103	0.019	3.099	0.005	<d.l.	<d.l.	<d.l.	<d.l.	<d.l.	15.112
Sw016_1a	Ab	8.967	<d.l.	3.015	0.018	3.018	<d.l.	<d.l.	<d.l.	<d.l.	<d.l.	<d.l.	15.018
Sw016_3	Ab	8.980	<d.l.	2.994	<d.l.	3.073	0.005	<d.l.	<d.l.	<d.l.	<d.l.	<d.l.	15.052
Sw016_7	Ab	8.965	<d.l.	3.015	<d.l.	3.060	<d.l.	0.007	<d.l.	0.008	<d.l.	<d.l.	15.055
Fb008_25	Ab	8.985	<d.l.	2.976	<d.l.	3.117	<d.l.	<d.l.	<d.l.	<d.l.	<d.l.	<d.l.	15.078
Fb013_2	Ab	8.949	<d.l.	3.067	<d.l.	2.987	<d.l.	<d.l.	<d.l.	<d.l.	<d.l.	<d.l.	15.003
Fb013_27	Ab	8.942	<d.l.	3.044	0.015	3.063	<d.l.	<d.l.	<d.l.	<d.l.	<d.l.	<d.l.	15.064
Fb041_3	Ab	8.989	<d.l.	2.980	<d.l.	3.073	<d.l.	<d.l.	<d.l.	<d.l.	<d.l.	<d.l.	15.042
Fb057_7	Ab	8.983	<d.l.	3.025	<d.l.	2.972	<d.l.	0.007	<d.l.	<d.l.	<d.l.	<d.l.	14.987

Table A9: Electron microprobe analyses of authigenic calcite, northern NGB. <d.l. = below detection limit.

	sample_no.	chemical composition [wt.-%]							
		CaO	MgO	MnO	FeO	SrO	BaO	SiO_2	Total
early calcite	Fe011_1ah	54.44	0.23	1.80	<d.l.	<d.l.	<d.l.	<d.l.	56.46
	Fe011_1ad	56.57	0.09	<d.l.	<d.l.	<d.l.	<d.l.	<d.l.	56.65
	Fe011_1c1	55.03	<d.l.	0.70	<d.l.	0.05	<d.l.	<d.l.	55.78
	Fe011_1c2	54.87	0.21	1.54	<d.l.	<d.l.	<d.l.	<d.l.	56.62
	Fe011_3b1	50.06	0.33	5.58	<d.l.	<d.l.	<d.l.	<d.l.	55.96
	Fe011_3b2	53.70	0.11	2.73	<d.l.	0.04	<d.l.	<d.l.	56.58
	Fe011_7	54.93	0.13	1.42	<d.l.	<d.l.	<d.l.	<d.l.	56.49
	Fe014_5	53.59	0.64	2.61	<d.l.	<d.l.	<d.l.	<d.l.	56.85
	Fe014_6	54.47	0.25	1.41	<d.l.	<d.l.	<d.l.	<d.l.	56.13
	Fe014_7	53.91	0.26	1.55	<d.l.	<d.l.	<d.l.	0.12	55.84
	Fe016_5	53.68	0.46	1.69	<d.l.	<d.l.	<d.l.	<d.l.	55.83
	Fe016_14	53.65	0.30	1.63	<d.l.	<d.l.	<d.l.	<d.l.	55.58
	Fe016_20	52.75	0.64	2.01	<d.l.	<d.l.	<d.l.	<d.l.	55.40
	Fe016_28	53.75	0.53	1.67	<d.l.	<d.l.	<d.l.	<d.l.	55.96
	Fe016_31	53.22	0.59	1.90	<d.l.	<d.l.	<d.l.	<d.l.	55.71
	Fe019_1	53.27	0.55	1.68	<d.l.	<d.l.	<d.l.	<d.l.	55.50
	Fe019_3	53.87	0.46	1.82	<d.l.	0.05	<d.l.	<d.l.	56.20
	Fe019_7	53.71	0.60	1.98	<d.l.	0.04	<d.l.	<d.l.	56.33
	Fe019_8	53.81	0.66	1.97	<d.l.	<d.l.	<d.l.	<d.l.	56.44
	Fe019_9	53.41	0.75	1.81	<d.l.	<d.l.	<d.l.	<d.l.	55.96
	Fb013_1	52.83	0.93	3.23	<d.l.	<d.l.	<d.l.	<d.l.	56.99
	Fb013_6	56.06	0.11	0.32	<d.l.	<d.l.	<d.l.	<d.l.	56.49
	Fb013_8	51.45	0.99	3.00	<d.l.	<d.l.	<d.l.	<d.l.	55.43
	Fb013_11	55.15	0.15	0.45	0.08	<d.l.	<d.l.	<d.l.	55.83
	Fb013_17	54.74	0.32	0.70	0.08	<d.l.	<d.l.	<d.l.	55.85
	Fb013_17d	54.85	0.19	0.51	<d.l.	0.05	<d.l.	<d.l.	55.61
	Fb013_17d2	56.64	0.13	0.10	<d.l.	<d.l.	<d.l.	<d.l.	56.87
	Fb013_23d	56.85	0.13	<d.l.	<d.l.	<d.l.	<d.l.	<d.l.	56.98
	Fb013_23h	55.80	0.20	0.53	0.08	<d.l.	<d.l.	<d.l.	56.61
	Fb013_30	52.23	0.96	2.80	<d.l.	<d.l.	<d.l.	<d.l.	55.99
	Fb013_32d	56.58	0.12	<d.l.	0.06	<d.l.	<d.l.	<d.l.	56.76
	Fb013_32h	55.52	0.12	0.40	<d.l.	<d.l.	<d.l.	<d.l.	56.05
	Fb026_6b	56.58	<d.l.	0.08	<d.l.	<d.l.	<d.l.	<d.l.	56.67
	Fb041_4a	56.60	0.36	<d.l.	<d.l.	<d.l.	<d.l.	<d.l.	56.96
	Fb041_4b	56.23	0.28	<d.l.	<d.l.	<d.l.	<d.l.	<d.l.	56.51
	Fb041_6	56.34	0.36	<d.l.	<d.l.	<d.l.	<d.l.	<d.l.	56.70
	Fb041_10a	56.76	0.18	<d.l.	<d.l.	0.04	<d.l.	<d.l.	56.98
	Fb041_10h	55.64	0.06	0.48	<d.l.	0.05	<d.l.	<d.l.	56.23
	Sw015_1	52.98	0.45	2.45	<d.l.	<d.l.	<d.l.	<d.l.	55.88
	Sw015_2d	55.80	<d.l.	<d.l.	<d.l.	<d.l.	<d.l.	<d.l.	55.80
	Sw015_2h	53.66	0.62	2.52	<d.l.	<d.l.	<d.l.	<d.l.	56.80
	Sw015_5a	53.71	0.45	1.49	<d.l.	<d.l.	<d.l.	<d.l.	55.65
	Sw015_5b	54.49	0.28	1.12	0.09	0.03	<d.l.	<d.l.	56.01
	Sw015_15z1	56.60	0.12	<d.l.	<d.l.	<d.l.	<d.l.	<d.l.	56.72
	Sw015_15z2	53.66	0.44	1.88	<d.l.	<d.l.	<d.l.	<d.l.	55.98
	Sw015_24g1	51.64	0.51	3.41	<d.l.	<d.l.	<d.l.	<d.l.	55.55
	Sw015_24g2	52.15	0.61	3.29	<d.l.	<d.l.	<d.l.	<d.l.	56.04
	Sw016_1a	53.64	0.49	2.31	<d.l.	0.04	0.07	<d.l.	56.56
	Sw016_1c1	53.76	0.71	1.98	<d.l.	<d.l.	<d.l.	<d.l.	56.46
	Sw016_1c2	52.71	0.65	3.41	<d.l.	<d.l.	<d.l.	<d.l.	56.76
	Sw016_2	55.24	0.27	0.96	<d.l.	<d.l.	<d.l.	0.22	56.68
	Sw027_4h	53.16	0.44	2.40	<d.l.	<d.l.	<d.l.	<d.l.	56.01
	Sw027_4m	54.55	0.13	0.89	<d.l.	0.05	<d.l.	<d.l.	55.62
	Sw027_6h1	53.68	0.42	1.84	<d.l.	0.03	<d.l.	<d.l.	55.98
	Sw027_6h2	53.34	0.64	2.33	<d.l.	<d.l.	<d.l.	<d.l.	56.31
	Sw027_6m	53.94	0.37	1.69	<d.l.	<d.l.	<d.l.	<d.l.	56.00
	Sw027_7	54.60	0.30	1.55	0.07	<d.l.	<d.l.	<d.l.	56.52
	Sw027_8d	56.61	0.18	<d.l.	<d.l.	<d.l.	<d.l.	0.13	56.91
	Sw027_8h	54.96	0.28	1.10	0.11	<d.l.	<d.l.	<d.l.	56.44
	Sw027_9	52.84	0.55	3.08	<d.l.	<d.l.	<d.l.	<d.l.	56.47
	Sw029_6	54.13	0.48	1.66	<d.l.	0.03	<d.l.	<d.l.	56.30

Table A9: EMP authigenic calcite, continuation.

	sample_no.	stuctural formula [apfu], number of ions on the basis of 6 oxygen equivalents						
		Ca	Mg	Mn	Fe	Sr	Ba	Total
early calcite	Fe011_1ah	1.955	0.011	0.051	<d.l.	<d.l.	<d.l.	2.017
	Fe011_1ad	2.032	0.004	<d.l.	<d.l.	<d.l.	<d.l.	2.036
	Fe011_1c1	1.963	<d.l.	0.020	<d.l.	0.001	<d.l.	1.984
	Fe011_1c2	1.973	0.011	0.044	<d.l.	<d.l.	<d.l.	2.027
	Fe011_3b1	1.797	0.016	0.158	<d.l.	<d.l.	<d.l.	1.972
	Fe011_3b2	1.935	0.005	0.078	<d.l.	0.001	<d.l.	2.018
	Fe011_7	1.973	0.007	0.040	<d.l.	<d.l.	<d.l.	2.020
	Fe014_5	1.931	0.032	0.074	<d.l.	<d.l.	<d.l.	2.038
	Fe014_6	1.950	0.013	0.040	<d.l.	<d.l.	<d.l.	2.002
	Fe014_7	1.924	0.013	0.044	<d.l.	<d.l.	<d.l.	1.980
	Fe016_5	1.916	0.023	0.048	<d.l.	<d.l.	<d.l.	1.987
	Fe016_14	1.910	0.015	0.046	<d.l.	<d.l.	<d.l.	1.971
	Fe016_20	1.875	0.032	0.057	<d.l.	<d.l.	<d.l.	1.963
	Fe016_28	1.920	0.027	0.047	<d.l.	<d.l.	<d.l.	1.993
	Fe016_31	1.897	0.029	0.054	<d.l.	<d.l.	<d.l.	1.980
	Fe019_1	1.894	0.027	0.047	<d.l.	<d.l.	<d.l.	1.969
	Fe019_3	1.930	0.023	0.052	<d.l.	0.001	<d.l.	2.005
	Fe019_7	1.926	0.030	0.056	<d.l.	0.001	<d.l.	2.013
	Fe019_8	1.930	0.033	0.056	<d.l.	<d.l.	<d.l.	2.019
	Fe019_9	1.908	0.037	0.051	<d.l.	<d.l.	<d.l.	1.996
	Fb013_1	1.908	0.047	0.092	<d.l.	<d.l.	<d.l.	2.046
	Fb013_6	2.013	0.006	0.009	<d.l.	<d.l.	<d.l.	2.027
	Fb013_8	1.830	0.049	0.084	<d.l.	<d.l.	<d.l.	1.963
	Fb013_11	1.967	0.007	0.013	0.002	<d.l.	<d.l.	1.989
	Fb013_17	1.952	0.016	0.020	0.002	<d.l.	<d.l.	1.990
	Fb013_17d	1.952	0.009	0.015	<d.l.	0.001	<d.l.	1.977
	Fb013_17d2	2.038	0.006	0.003	<d.l.	<d.l.	<d.l.	2.047
	Fb013_23d	2.049	0.007	<d.l.	<d.l.	<d.l.	<d.l.	2.055
	Fb013_23h	2.004	0.010	0.015	0.002	<d.l.	<d.l.	2.031
	Fb013_30	1.868	0.048	0.079	<d.l.	<d.l.	<d.l.	1.995
	Fb013_32d	2.034	0.006	<d.l.	0.002	<d.l.	<d.l.	2.042
	Fb013_32h	1.984	0.006	0.011	<d.l.	<d.l.	<d.l.	2.001
	Fb026_6b	2.035	<d.l.	0.002	<d.l.	<d.l.	<d.l.	2.037
	Fb041_4a	2.037	0.018	<d.l.	<d.l.	<d.l.	<d.l.	2.055
	Fb041_4b	2.017	0.014	<d.l.	<d.l.	<d.l.	<d.l.	2.031
	Fb041_6	2.023	0.018	<d.l.	<d.l.	<d.l.	<d.l.	2.041
	Fb041_10a	2.044	0.009	<d.l.	<d.l.	0.001	<d.l.	2.054
	Fb041_10h	1.991	0.003	0.014	<d.l.	0.001	<d.l.	2.009
	Sw015_1	1.893	0.022	0.069	<d.l.	<d.l.	<d.l.	1.985
	Sw015_2d	1.989	<d.l.	<d.l.	<d.l.	<d.l.	<d.l.	1.989
	Sw015_2h	1.933	0.031	0.072	<d.l.	<d.l.	<d.l.	2.036
	Sw015_5a	1.913	0.022	0.042	<d.l.	<d.l.	<d.l.	1.977
	Sw015_5b	1.947	0.014	0.032	0.003	0.001	<d.l.	1.996
	Sw015_15z1	2.034	0.006	<d.l.	<d.l.	<d.l.	<d.l.	2.040
	Sw015_15z2	1.918	0.022	0.053	<d.l.	<d.l.	<d.l.	1.993
	Sw015_24g1	1.843	0.025	0.096	<d.l.	<d.l.	<d.l.	1.964
	Sw015_24g2	1.867	0.030	0.093	<d.l.	<d.l.	<d.l.	1.990
	Sw016_1a	1.929	0.025	0.066	<d.l.	0.001	0.001	2.021
	Sw016_1c1	1.929	0.035	0.056	<d.l.	<d.l.	<d.l.	2.020
	Sw016_1c2	1.900	0.032	0.097	<d.l.	<d.l.	<d.l.	2.030
	Sw016_2	1.984	0.013	0.027	<d.l.	<d.l.	<d.l.	2.024
	Sw027_4h	1.903	0.022	0.068	<d.l.	<d.l.	<d.l.	1.993
	Sw027_4m	1.943	0.007	0.025	<d.l.	0.001	<d.l.	1.975
	Sw027_6h1	1.918	0.021	0.052	<d.l.	0.001	<d.l.	1.992
	Sw027_6h2	1.913	0.032	0.066	<d.l.	<d.l.	<d.l.	2.011
	Sw027_6m	1.929	0.018	0.048	<d.l.	<d.l.	<d.l.	1.995
	Sw027_7	1.961	0.015	0.044	0.002	<d.l.	<d.l.	2.022
	Sw027_8d	2.036	0.009	<d.l.	<d.l.	<d.l.	<d.l.	2.045
	Sw027_8h	1.972	0.014	0.031	0.003	<d.l.	<d.l.	2.020
	Sw027_9	1.900	0.027	0.088	<d.l.	<d.l.	<d.l.	2.015
	Sw029_6	1.939	0.024	0.047	<d.l.	0.001	<d.l.	2.011

Table A9: EMP authigenic calcite, continuation.

	sample_no.	chemical composition [wt.-%]							
		CaO	MgO	MnO	FeO	SrO	BaO	SiO_2	Total
early calcite	Sw029_9	54.59	0.23	1.14	<d.l.	0.05	<d.l.	<d.l.	56.01
	Sw029_10	54.21	0.19	1.15	0.08	<d.l.	<d.l.	<d.l.	55.62
	Sw029_12	54.25	0.28	1.33	0.10	<d.l.	<d.l.	0.49	56.45
	Sw029_13	54.48	0.35	1.47	0.07	<d.l.	<d.l.	<d.l.	56.38
	Sw031_1	55.78	0.13	<d.l.	<d.l.	0.06	<d.l.	<d.l.	55.97
	Sw031_1h	51.73	0.34	3.20	<d.l.	<d.l.	<d.l.	0.25	55.52
	Sw031_1m	53.54	0.28	2.42	<d.l.	<d.l.	<d.l.	<d.l.	56.23
	Sw031_7	53.70	0.34	1.41	0.09	<d.l.	<d.l.	0.11	55.65
	Sw031_8d	55.07	0.17	1.00	<d.l.	<d.l.	<d.l.	<d.l.	56.24
	Sw031_8h	51.72	0.39	3.96	<d.l.	<d.l.	<d.l.	<d.l.	56.06
	Sw031_11d	56.17	0.18	<d.l.	<d.l.	<d.l.	<d.l.	<d.l.	56.35
	Sw031_11h	53.39	0.46	1.89	<d.l.	<d.l.	<d.l.	<d.l.	55.74
	Sw031_14	51.82	0.51	3.97	<d.l.	0.04	<d.l.	<d.l.	56.34
	Sw031_17	53.67	0.26	1.73	<d.l.	<d.l.	<d.l.	<d.l.	55.67
	Sw031_19h	51.27	0.44	3.75	<d.l.	<d.l.	<d.l.	<d.l.	55.46
	Sw031_19m	53.29	0.51	2.37	<d.l.	<d.l.	<d.l.	<d.l.	56.17
	Sw031_23Zd	56.13	0.36	<d.l.	<d.l.	0.04	<d.l.	<d.l.	56.53
	Sw031_23Zh	53.55	0.37	2.26	<d.l.	<d.l.	<d.l.	<d.l.	56.18
	Sw031_26h1	51.93	0.40	3.39	0.07	<d.l.	<d.l.	<d.l.	55.79
	Sw031_26h2	52.68	0.45	3.42	<d.l.	<d.l.	<d.l.	<d.l.	56.55
	Sw031_26m	53.03	0.28	2.08	<d.l.	<d.l.	<d.l.	<d.l.	55.39
	Sw031_27	52.26	0.45	3.42	<d.l.	<d.l.	<d.l.	<d.l.	56.13
	Sw031_27d	52.82	0.50	2.31	<d.l.	<d.l.	<d.l.	<d.l.	55.64
	Sw031_27m	53.37	0.48	2.34	<d.l.	<d.l.	<d.l.	<d.l.	56.19
	Sw031_31	53.75	0.29	1.29	<d.l.	<d.l.	0.06	<d.l.	55.39
late calcite	Fb008_3	56.36	0.38	<d.l.	<d.l.	<d.l.	<d.l.	<d.l.	56.74
	Fb008_5	56.60	0.07	0.18	<d.l.	<d.l.	<d.l.	<d.l.	56.85
	Fb008_10	56.35	0.11	<d.l.	<d.l.	<d.l.	<d.l.	<d.l.	56.46
	Fb008_14	56.47	<d.l.	0.14	0.09	<d.l.	<d.l.	<d.l.	56.69
	Fb008_16	55.05	<d.l.	1.07	<d.l.	<d.l.	<d.l.	<d.l.	56.12
	Fb026_4a1	56.53	0.13	<d.l.	<d.l.	<d.l.	0.05	<d.l.	56.71
	Fb026_4a2	55.98	0.14	0.22	0.15	<d.l.	<d.l.	<d.l.	56.49
	Fb026_7a2	56.09	0.27	0.12	<d.l.	<d.l.	<d.l.	<d.l.	56.48
	Fb026_8a3	55.77	0.36	<d.l.	<d.l.	<d.l.	<d.l.	<d.l.	56.13
	Fb041_10i	55.97	0.34	0.26	0.41	<d.l.	<d.l.	<d.l.	56.98
	Fb041_14	56.47	0.30	<d.l.	<d.l.	<d.l.	<d.l.	<d.l.	56.76
	Fb041_21	55.71	0.12	0.35	0.12	<d.l.	<d.l.	<d.l.	56.30
calcite replacement	Fe011_2V	49.92	0.32	6.07	<d.l.	<d.l.	<d.l.	<d.l.	56.31
	Fe016_31V	53.44	0.66	1.77	<d.l.	<d.l.	<d.l.	<d.l.	55.86
	Fe019_7V	52.32	0.28	3.24	<d.l.	<d.l.	<d.l.	<d.l.	55.83
	Fb013_4V	56.11	0.12	0.22	<d.l.	<d.l.	<d.l.	<d.l.	56.45
	Fb013_11V	55.65	0.28	0.51	<d.l.	0.05	<d.l.	<d.l.	56.50
	Sw016_1dV	55.67	0.34	<d.l.	0.12	0.05	<d.l.	<d.l.	56.18
	Sw016_6aV	55.16	0.40	0.07	0.40	0.11	<d.l.	0.16	56.30
	Sw027_4V	56.11	0.16	<d.l.	<d.l.	<d.l.	<d.l.	<d.l.	56.27
	Sw027_5V	56.29	0.54	<d.l.	<d.l.	0.05	<d.l.	<d.l.	56.88
	Sw027_6Vd	56.43	0.15	<d.l.	<d.l.	<d.l.	<d.l.	<d.l.	56.58
	Sw027_6Vh	53.60	0.18	2.35	0.11	<d.l.	<d.l.	<d.l.	56.24
	Sw031_8V	55.05	0.46	0.09	0.23	0.04	<d.l.	<d.l.	55.88
	Sw031_11V	56.19	0.20	0.11	<d.l.	0.04	<d.l.	<d.l.	56.54
	Sw031_17V	55.25	0.42	<d.l.	0.12	0.04	<d.l.	<d.l.	55.82
	Sw031_19V	55.05	0.19	0.71	<d.l.	0.07	<d.l.	<d.l.	56.02
vein calcite	Fe011_2aK	52.51	0.20	3.08	<d.l.	<d.l.	<d.l.	<d.l.	55.80
	Fb052_1K	56.06	<d.l.	0.15	<d.l.	<d.l.	<d.l.	<d.l.	56.21
	Fb052_2K	56.72	<d.l.	0.08	<d.l.	<d.l.	<d.l.	<d.l.	56.80
	Fb052_3K	56.21	0.06	0.16	0.11	<d.l.	0.09	<d.l.	56.63
	Fb052_5K	56.67	<d.l.	0.15	0.06	<d.l.	<d.l.	<d.l.	56.88
	Fb052_7K	55.16	0.20	0.66	<d.l.	0.07	<d.l.	<d.l.	56.09
	Fb059_1K	54.91	0.07	1.05	<d.l.	<d.l.	<d.l.	<d.l.	56.02
	Fb059_2K	55.06	0.09	1.14	<d.l.	<d.l.	<d.l.	<d.l.	56.29
	Fb059_3K	55.48	0.10	1.20	<d.l.	<d.l.	<d.l.	<d.l.	56.78

Table A9: EMP authigenic calcite, continuation.

	sample_no.	stuctural formula [apfu], number of ions on the basis of 6 oxygen equivalents						
		Ca	Mg	Mn	Fe	Sr	Ba	Total
early calcite	Sw029_9	1.951	0.011	0.032	<d.l.	0.001	<d.l.	1.996
	Sw029_10	1.931	0.010	0.032	0.002	<d.l.	<d.l.	1.975
	Sw029_12	1.942	0.014	0.038	0.003	<d.l.	<d.l.	1.996
	Sw029_13	1.954	0.018	0.042	0.002	<d.l.	<d.l.	2.015
	Sw031_1	1.991	0.007	<d.l.	<d.l.	0.001	<d.l.	1.999
	Sw031_1h	1.842	0.017	0.090	<d.l.	<d.l.	<d.l.	1.949
	Sw031_1m	1.921	0.014	0.069	<d.l.	<d.l.	<d.l.	2.003
	Sw031_7	1.912	0.017	0.040	0.002	<d.l.	<d.l.	1.971
	Sw031_8d	1.973	0.008	0.028	<d.l.	<d.l.	<d.l.	2.009
	Sw031_8h	1.855	0.019	0.112	<d.l.	<d.l.	<d.l.	1.987
	Sw031_11d	2.012	0.009	<d.l.	<d.l.	<d.l.	<d.l.	2.021
	Sw031_11h	1.906	0.023	0.053	<d.l.	<d.l.	<d.l.	1.982
	Sw031_14	1.863	0.026	0.113	<d.l.	0.001	<d.l.	2.002
	Sw031_17	1.914	0.013	0.049	<d.l.	<d.l.	<d.l.	1.975
	Sw031_19h	1.829	0.022	0.106	<d.l.	<d.l.	<d.l.	1.956
	Sw031_19m	1.909	0.025	0.067	<d.l.	<d.l.	<d.l.	2.001
	Sw031_23Zd	2.013	0.018	<d.l.	<d.l.	0.001	<d.l.	2.031
	Sw031_23Zh	1.918	0.018	0.064	<d.l.	<d.l.	<d.l.	2.000
	Sw031_26h1	1.856	0.020	0.096	0.002	<d.l.	<d.l.	1.974
	Sw031_26h2	1.897	0.023	0.097	<d.l.	<d.l.	<d.l.	2.017
	Sw031_26m	1.887	0.014	0.059	<d.l.	<d.l.	<d.l.	1.959
	Sw031_27	1.874	0.023	0.097	<d.l.	<d.l.	<d.l.	1.993
	Sw031_27d	1.882	0.025	0.065	<d.l.	<d.l.	<d.l.	1.973
	Sw031_27m	1.911	0.024	0.066	<d.l.	<d.l.	<d.l.	2.002
	Sw031_31	1.912	0.014	0.036	<d.l.	<d.l.	0.001	1.963
late calcite	Fb008_3	2.025	0.019	<d.l.	<d.l.	<d.l.	<d.l.	2.044
	Fb008_5	2.037	0.004	0.005	<d.l.	<d.l.	<d.l.	2.045
	Fb008_10	2.020	0.006	<d.l.	<d.l.	<d.l.	<d.l.	2.026
	Fb008_14	2.030	<d.l.	0.004	0.003	<d.l.	<d.l.	2.036
	Fb008_16	1.971	<d.l.	0.030	<d.l.	<d.l.	<d.l.	2.001
	Fb026_4a1	2.030	0.007	<d.l.	<d.l.	<d.l.	0.001	2.038
	Fb026_4a2	2.008	0.007	0.006	0.004	<d.l.	<d.l.	2.025
	Fb026_7a2	2.011	0.014	0.003	<d.l.	<d.l.	<d.l.	2.028
	Fb026_8a3	1.992	0.018	<d.l.	<d.l.	<d.l.	<d.l.	2.010
	Fb041_10i	2.017	0.017	0.007	0.011	<d.l.	<d.l.	2.053
	Fb041_14	2.029	0.015	<d.l.	<d.l.	<d.l.	<d.l.	2.044
	Fb041_21	1.995	0.006	0.010	0.003	<d.l.	<d.l.	2.014
calcite replacement	Fe011_2V	1.799	0.016	0.173	<d.l.	<d.l.	<d.l.	1.988
	Fe016_31V	1.906	0.033	0.050	<d.l.	<d.l.	<d.l.	1.989
	Fe019_7V	1.871	0.014	0.092	<d.l.	<d.l.	<d.l.	1.977
	Fb013_4V	2.011	0.006	0.006	<d.l.	<d.l.	<d.l.	2.023
	Fb013_11V	1.997	0.014	0.015	<d.l.	0.001	<d.l.	2.027
	Sw016_1dV	1.989	0.017	<d.l.	0.003	0.001	<d.l.	2.011
	Sw016_6aV	1.973	0.020	0.002	0.011	0.002	<d.l.	2.008
	Sw027_4V	2.009	0.008	<d.l.	<d.l.	<d.l.	<d.l.	2.017
	Sw027_5V	2.023	0.027	<d.l.	<d.l.	0.001	<d.l.	2.051
	Sw027_6Vd	2.028	0.008	<d.l.	<d.l.	<d.l.	<d.l.	2.036
	Sw027_6Vh	1.923	0.009	0.067	0.003	<d.l.	<d.l.	2.002
	Sw031_8V	1.962	0.023	0.003	0.006	0.001	<d.l.	1.995
	Sw031_11V	2.016	0.010	0.003	<d.l.	0.001	<d.l.	2.030
	Sw031_17V	1.968	0.021	<d.l.	0.003	0.001	<d.l.	1.993
	Sw031_19V	1.967	0.009	0.020	<d.l.	0.001	<d.l.	1.998
vein calcite	Fe011_2aK	1.877	0.010	0.087	<d.l.	<d.l.	<d.l.	1.975
	Fb052_1K	2.006	<d.l.	0.004	<d.l.	<d.l.	<d.l.	2.010
	Fb052_2K	2.041	<d.l.	0.002	<d.l.	<d.l.	<d.l.	2.044
	Fb052_3K	2.019	0.003	0.005	0.003	<d.l.	0.001	2.031
	Fb052_5K	2.040	<d.l.	0.004	0.002	<d.l.	<d.l.	2.046
	Fb052_7K	1.972	0.010	0.019	<d.l.	0.001	<d.l.	2.002
	Fb059_1K	1.962	0.003	0.030	<d.l.	<d.l.	<d.l.	1.995
	Fb059_2K	1.973	0.005	0.032	<d.l.	<d.l.	<d.l.	2.010
	Fb059_3K	1.998	0.005	0.034	<d.l.	<d.l.	<d.l.	2.037

Table A10: Electron microprobe analyses of authigenic dolomite, northern NGB. <d.l. = below detection limit.

sample_no.	chemical composition [wt.-%]							
	CaO	MgO	MnO	FeO	SrO	BaO	SiO_2	Total
early pore-filling dolomite								
Fb008_2m1	30.94	20.53	0.37	1.45	<d.l.	<d.l.	<d.l.	53.29
Fb008_2m2	30.55	21.22	0.85	<d.l.	<d.l.	<d.l.	<d.l.	52.62
Fb008_6	30.55	20.71	0.73	0.49	<d.l.	<d.l.	<d.l.	52.48
Fb008_12	30.94	21.11	0.49	0.30	<d.l.	<d.l.	<d.l.	52.85
Fb026_3a	30.18	20.46	0.86	0.38	<d.l.	0.05	<d.l.	51.93
Fb026_3a1	30.48	20.60	0.99	0.18	<d.l.	<d.l.	<d.l.	52.24
Fb026_3a2	29.95	19.63	2.65	0.38	<d.l.	<d.l.	<d.l.	52.60
Fb026_3a3	30.16	18.78	3.80	0.35	<d.l.	<d.l.	<d.l.	53.09
Fb026_3b1	30.45	21.38	1.00	<d.l.	<d.l.	<d.l.	<d.l.	52.83
Fb026_3b2	31.25	20.98	0.15	<d.l.	<d.l.	<d.l.	<d.l.	52.37
Fb026_3c	30.36	20.47	0.94	0.12	<d.l.	<d.l.	<d.l.	51.89
Fb035_3	30.59	20.04	0.66	0.77	<d.l.	<d.l.	<d.l.	52.07
Fb057_14	30.51	20.86	0.85	0.19	<d.l.	<d.l.	<d.l.	52.41
Fb057_21	30.91	21.09	0.67	0.18	<d.l.	<d.l.	<d.l.	52.85
Fb059_6	29.92	20.70	1.03	0.76	<d.l.	<d.l.	0.11	52.53
zoned dolomite								
Fb008_2d	31.57	21.31	0.04	<d.l.	<d.l.	<d.l.	<d.l.	52.92
Fb008_2h	29.79	17.63	5.41	0.88	<d.l.	<d.l.	<d.l.	53.71
Fb008_10h	30.02	19.28	2.84	0.54	<d.l.	<d.l.	<d.l.	52.68
Fb008_14d	31.33	20.95	0.12	1.02	<d.l.	<d.l.	<d.l.	53.42
Fb008_14m	29.60	19.12	3.81	0.18	<d.l.	<d.l.	<d.l.	52.71
Fb008_15d	31.13	21.31	0.57	<d.l.	<d.l.	<d.l.	<d.l.	53.00
Fb008_15h	29.83	19.30	3.17	1.25	<d.l.	<d.l.	<d.l.	53.55
Fb008_15m	29.79	20.80	0.68	0.59	<d.l.	<d.l.	<d.l.	51.86
Fb026_4a	30.13	20.53	1.11	0.63	<d.l.	<d.l.	<d.l.	52.40
Fb026_4c	30.14	20.42	1.42	0.48	<d.l.	<d.l.	<d.l.	52.46
Fb026_7a1	30.32	20.89	1.09	0.08	<d.l.	<d.l.	<d.l.	52.38
Fb026_8a1	30.33	20.49	1.00	0.29	<d.l.	<d.l.	<d.l.	52.12
Fb026_8a2	29.08	15.45	7.57	2.43	<d.l.	<d.l.	0.11	54.64
Fb035_2z1	29.70	20.27	0.98	0.97	<d.l.	<d.l.	<d.l.	51.92
Fb035_2z2	30.05	20.83	0.70	0.93	<d.l.	<d.l.	<d.l.	52.51
Fb035_2z3	29.90	21.04	0.71	0.73	<d.l.	0.05	<d.l.	52.43
Fb035_3d	30.22	21.08	0.56	0.63	<d.l.	<d.l.	<d.l.	52.49
Fb035_5	29.62	20.89	0.70	0.97	<d.l.	<d.l.	<d.l.	52.18
Fb035_5zh	29.98	12.75	10.97	0.80	<d.l.	<d.l.	<d.l.	54.49
Fb035_5zr	31.47	18.92	1.55	1.97	<d.l.	<d.l.	0.10	54.01
Fb035_8zh	30.03	21.11	0.57	0.69	<d.l.	<d.l.	<d.l.	52.39
Fb035_8zr	31.79	20.31	0.71	0.20	<d.l.	<d.l.	0.29	53.29
Fb035_10d1	32.44	19.57	0.52	0.11	<d.l.	<d.l.	<d.l.	52.63
Fb035_10d3	29.69	20.82	0.73	0.85	<d.l.	<d.l.	<d.l.	52.09
Fb035_10h2	29.95	20.14	1.24	0.95	<d.l.	<d.l.	<d.l.	52.28
Fb035_10h3	29.80	20.30	0.97	0.99	<d.l.	<d.l.	<d.l.	52.07
Fb035_12	29.72	20.83	0.76	0.77	<d.l.	<d.l.	<d.l.	52.07
Fb035_12zr	31.51	19.77	1.31	0.42	<d.l.	<d.l.	<d.l.	53.00
Fb035_18	30.37	19.97	0.84	1.24	<d.l.	<d.l.	<d.l.	52.41
Fb035_18d1	29.55	20.50	0.86	0.98	<d.l.	<d.l.	<d.l.	51.89
Fb035_18h2	29.86	21.03	0.53	0.75	<d.l.	<d.l.	<d.l.	52.17
Fb035_18h3b	29.35	14.07	8.10	3.51	<d.l.	<d.l.	0.12	55.16
Fb035_18zh	31.21	19.21	1.89	0.19	<d.l.	<d.l.	<d.l.	52.49
Fb035_21z1	30.04	19.90	1.10	0.99	<d.l.	<d.l.	<d.l.	52.04
Fb035_21z2	30.41	20.56	0.79	0.96	<d.l.	<d.l.	<d.l.	52.73
Fb035_21z3	29.80	20.80	0.76	0.76	<d.l.	<d.l.	<d.l.	52.12
Fb035_21z4	29.98	20.66	0.72	0.93	<d.l.	<d.l.	<d.l.	52.29
Fb035_21z5	30.06	19.77	1.16	1.27	<d.l.	<d.l.	<d.l.	52.26
Fb035_21z6	32.41	19.84	0.44	0.14	<d.l.	<d.l.	<d.l.	52.82
Fb035_21z7	31.73	19.52	1.63	0.39	<d.l.	<d.l.	<d.l.	53.27

Table A10: EMP authigenic dolomite, continuation.

sample_no.	stuctural formula [apfu], number of ions on the basis of 6 oxygen equivalents						
	Ca	Mg	Mn	Fe	Sr	Ba	Total
early pore-filling dolomite							
Fb008_2m1	1.032	0.952	0.010	0.038	<d.l.	<d.l.	2.032
Fb008_2m2	1.010	0.977	0.022	<d.l.	<d.l.	<d.l.	2.009
Fb008_6	1.010	0.953	0.019	0.013	<d.l.	<d.l.	1.995
Fb008_12	1.025	0.973	0.013	0.008	<d.l.	<d.l.	2.019
Fb026_3a	0.994	0.938	0.022	0.010	<d.l.	0.001	1.965
Fb026_3a1	1.006	0.946	0.026	0.005	<d.l.	<d.l.	1.983
Fb026_3a2	0.996	0.908	0.070	0.010	<d.l.	<d.l.	1.984
Fb026_3a3	1.011	0.876	0.101	0.009	<d.l.	<d.l.	1.996
Fb026_3b1	1.009	0.986	0.026	<d.l.	<d.l.	<d.l.	2.021
Fb026_3b2	1.031	0.963	0.004	<d.l.	<d.l.	<d.l.	1.998
Fb026_3c	1.000	0.938	0.024	0.003	<d.l.	<d.l.	1.965
Fb035_3	1.010	0.921	0.017	0.020	<d.l.	<d.l.	1.968
Fb057_14	1.008	0.959	0.022	0.005	<d.l.	<d.l.	1.994
Fb057_21	1.025	0.973	0.017	0.005	<d.l.	<d.l.	2.019
Fb059_6	0.990	0.953	0.027	0.020	<d.l.	<d.l.	1.990
zoned dolomite							
Fb008_2d	1.045	0.982	0.001	<d.l.	<d.l.	<d.l.	2.028
Fb008_2h	1.009	0.831	0.145	0.023	<d.l.	<d.l.	2.009
Fb008_10h	1.001	0.894	0.075	0.014	<d.l.	<d.l.	1.984
Fb008_14d	1.044	0.972	0.003	0.026	<d.l.	<d.l.	2.045
Fb008_14m	0.988	0.888	0.101	0.005	<d.l.	<d.l.	1.981
Fb008_15d	1.033	0.983	0.015	<d.l.	<d.l.	<d.l.	2.031
Fb008_15h	1.003	0.903	0.084	0.033	<d.l.	<d.l.	2.022
Fb008_15m	0.980	0.952	0.018	0.015	<d.l.	<d.l.	1.965
Fb026_4a	0.997	0.945	0.029	0.016	<d.l.	<d.l.	1.987
Fb026_4c	0.998	0.941	0.037	0.013	<d.l.	<d.l.	1.989
Fb026_7a1	1.001	0.960	0.028	0.002	<d.l.	<d.l.	1.992
Fb026_8a1	1.001	0.941	0.026	0.008	<d.l.	<d.l.	1.976
Fb026_8a2	1.002	0.741	0.206	0.065	<d.l.	<d.l.	2.014
Fb035_2z1	0.980	0.930	0.026	0.025	<d.l.	<d.l.	1.960
Fb035_2z2	0.994	0.959	0.018	0.024	<d.l.	<d.l.	1.996
Fb035_2z3	0.988	0.967	0.019	0.019	<d.l.	0.001	1.994
Fb035_3d	0.999	0.969	0.015	0.016	<d.l.	<d.l.	1.999
Fb035_5	0.977	0.959	0.018	0.025	<d.l.	<d.l.	1.979
Fb035_5zh	1.040	0.615	0.301	0.022	<d.l.	<d.l.	1.978
Fb035_5zr	1.061	0.888	0.041	0.052	<d.l.	<d.l.	2.042
Fb035_8zh	0.992	0.970	0.015	0.018	<d.l.	<d.l.	1.994
Fb035_8zr	1.058	0.941	0.019	0.005	<d.l.	<d.l.	2.023
Fb035_10d1	1.076	0.903	0.014	0.003	<d.l.	<d.l.	1.996
Fb035_10d3	0.979	0.955	0.019	0.022	<d.l.	<d.l.	1.975
Fb035_10h2	0.991	0.928	0.032	0.025	<d.l.	<d.l.	1.976
Fb035_10h3	0.984	0.933	0.025	0.026	<d.l.	<d.l.	1.968
Fb035_12	0.980	0.956	0.020	0.020	<d.l.	<d.l.	1.976
Fb035_12zr	1.050	0.916	0.035	0.011	<d.l.	<d.l.	2.012
Fb035_18	1.007	0.921	0.022	0.032	<d.l.	<d.l.	1.982
Fb035_18d1	0.974	0.940	0.022	0.025	<d.l.	<d.l.	1.961
Fb035_18h2	0.985	0.965	0.014	0.019	<d.l.	<d.l.	1.983
Fb035_18h3b	1.021	0.681	0.223	0.095	<d.l.	<d.l.	2.019
Fb035_18zh	1.037	0.888	0.050	0.005	<d.l.	<d.l.	1.980
Fb035_21z1	0.993	0.915	0.029	0.026	<d.l.	<d.l.	1.962
Fb035_21z2	1.009	0.949	0.021	0.025	<d.l.	<d.l.	2.004
Fb035_21z3	0.983	0.954	0.020	0.020	<d.l.	<d.l.	1.976
Fb035_21z4	0.991	0.950	0.019	0.024	<d.l.	<d.l.	1.983
Fb035_21z5	0.996	0.911	0.030	0.033	<d.l.	<d.l.	1.971
Fb035_21z6	1.076	0.917	0.012	0.004	<d.l.	<d.l.	2.008
Fb035_21z7	1.061	0.908	0.043	0.010	<d.l.	<d.l.	2.022

Table A10: EMP authigenic dolomite, continuation.

sample_no.	chemical composition [wt.-%]							
	CaO	MgO	MnO	FeO	SrO	BaO	SiO_2	Total
zoned dolomite								
Fb041_2d	30.89	20.92	0.44	<d.l.	<d.l.	<d.l.	<d.l.	52.25
Fb041_2h	29.38	17.35	6.13	<d.l.	0.04	<d.l.	<d.l.	52.90
Fb041_8zd	30.18	20.79	1.35	<d.l.	<d.l.	<d.l.	<d.l.	52.32
Fb041_13zd	30.72	21.08	1.13	<d.l.	<d.l.	<d.l.	<d.l.	52.92
Fb041_14z1	29.50	19.49	3.09	0.42	<d.l.	<d.l.	0.58	53.07
Fb041_21i	29.87	20.93	0.98	<d.l.	<d.l.	0.09	<d.l.	51.86
Fb041_21zd	29.27	18.78	4.08	0.14	<d.l.	<d.l.	<d.l.	52.26
Fb057_8	30.40	20.88	0.78	0.38	<d.l.	<d.l.	<d.l.	52.44
Fb057_8a	30.01	20.67	0.92	0.34	<d.l.	<d.l.	0.10	52.05
Fb057_8m	30.38	20.74	0.98	0.86	<d.l.	<d.l.	<d.l.	52.97
dolomite replacement								
Fb008_18V	31.37	20.82	0.11	1.23	<d.l.	<d.l.	<d.l.	53.52
Fb057_10V	30.75	21.08	0.72	<d.l.	0.03	<d.l.	<d.l.	52.58

Table A11: Electron microprobe analyses of authigenic barite. <d.l. = below detection limit.

sample_no.	chemical composition [wt.-%]								
	BaO	SrO	CaO	MgO	K_2O	Na_2O	SiO_2	SO_3	Total
Fe011_2c_Ba	66.34	1.36	0.23	<d.l.	<d.l.	0.26	<d.l.	32.18	100.37
Fe011_7_Ba	66.05	1.48	<d.l.	<d.l.	<d.l.	0.20	<d.l.	32.60	100.33
Sw016_1a_Ba	65.86	2.23	<d.l.	<d.l.	0.04	0.09	<d.l.	32.53	100.75
Sw016_5a_Ba	65.38	2.39	0.05	<d.l.	<d.l.	<d.l.	<d.l.	32.77	100.59

Table A10: EMP authigenic dolomite, continuation.

sample_no.	stuctural formula [apfu], number of ions on the basis of 6 oxygen equivalents						
	Ca	Mg	Mn	Fe	Sr	Ba	Total
zoned dolomite							
Fb041_2d	1.019	0.960	0.011	<d.l.	<d.l.	<d.l.	1.990
Fb041_2h	0.989	0.812	0.163	<d.l.	0.001	<d.l.	1.964
Fb041_8zd	0.997	0.956	0.035	<d.l.	<d.l.	<d.l.	1.989
Fb041_13zd	1.019	0.973	0.030	<d.l.	<d.l.	<d.l.	2.022
Fb041_14z1	0.983	0.904	0.082	0.011	<d.l.	<d.l.	1.979
Fb041_21i	0.983	0.958	0.025	<d.l.	<d.l.	0.001	1.967
Fb041_21zd	0.974	0.869	0.107	0.004	<d.l.	<d.l.	1.954
Fb057_8	1.005	0.960	0.020	0.010	<d.l.	<d.l.	1.995
Fb057_8a	0.989	0.948	0.024	0.009	<d.l.	<d.l.	1.969
Fb057_8m	1.010	0.959	0.026	0.022	<d.l.	<d.l.	2.017
dolomite replacement							
Fb008_18V	1.047	0.967	0.003	0.032	<d.l.	<d.l.	2.049
Fb057_10V	1.017	0.970	0.019	<d.l.	0.001	<d.l.	2.007

Table A11: EMP authigenic barite, continuation.

sample_no.	stuctural formula [apfu], number of ions on the basis of 4 oxygen equivalents							
	Ba	Sr	Ca	Mg	K	Na	S	Total
Fe011_2c_Ba	1.041	0.032	0.010	<d.l.	<d.l.	0.020	0.967	2.069
Fe011_7_Ba	1.032	0.034	<d.l.	<d.l.	<d.l.	0.016	0.975	2.056
Sw016_1a_Ba	1.026	0.052	<d.l.	<d.l.	0.002	0.007	0.970	2.056
Sw016_5a_Ba	1.016	0.055	0.002	<d.l.	<d.l.	<d.l.	0.975	2.047

Table A12: Electron microprobe analyses of authigenic chlorite from the northern margin of the NGB, mean and standard deviation of n analyses. <d.l. = below detection limit. Fb052_12-16 are radial chlorites, Fb008_repl. are grain replacing chlorites. Structural formula of clay fractions <0.4 µm calculated assuming contamination of 20% quartz (Qz), and alternatively of 20% quartz, 5% illite (Il), and 3% Albite (Ab) and hematite (Hm) each.

sample_no.	n	contamination	chemical composition [wt.-%]				
			SiO_2	TiO_2	Al_2O_3	FeO	MgO
direct analyses (thin section)							
Fb052_12-16	3		32.63 ± 1.07	<d.l.	22.19 ± 1.54	6.17 ± 0.42	22.32 ± 0.64
Fb008_repl.	2		25.13 ± 1.59	<d.l.	19.94 ± 1.48	23.27 ± 4.19	15.98 ± 3.94
analyses of clay fractions <0.4 µm equivalent grain diameter							
Fb035_frac	8	Qz, Il, Ab, Hm	46.01 ± 6.36	0.27 ± 0.16	18.60 ± 2.24	5.32 ± 1.55	15.74 ± 1.72
Fb041_frac	8	Qz, Il, Ab, Hm	44.08 ± 2.54	0.18 ± 0.10	21.83 ± 0.37	6.46 ± 1.20	12.42 ± 1.01
Fb057_frac	8	Qz, Il, Ab, Hm	43.15 ± 3.00	0.18 ± 0.08	18.97 ± 0.63	5.76 ± 0.78	16.12 ± 1.04

sample_no.	n	assumed contamination	stuctural formula [apfu], number of ions on the basis of 28 oxygen equivalents				
			Si	Al (IV)	AL (VI)	Ti	Fe^{2+}
direct analyses (thin section)							
Fb052_12-16	3		6.37 ± 0.06	1.63 ± 0.06	3.47 ± 0.29	<d.l.	1.01 ± 0.09
Fb008_repl.	2		5.44 ± 0.22	2.56 ± 0.22	2.53 ± 0.27	<d.l.	4.22 ± 0.85
analyses of clay fractions <0.4 µm equivalent grain diameter							
Fb035_frac	8	20% Qz	6.31 ± 1.25	1.69 ± 1.25	3.70 ± 0.43	0.05 ± 0.03	1.10 ± 0.37
		20% Qz, 5% Il, 3% Ab, 3% Hm	6.03 ± 1.46	1.97 ± 1.46	3.63 ± 0.50	0.06 ± 0.04	0.61 ± 0.40
Fb041_frac	8	20% Qz	5.96 ± 0.46	2.04 ± 0.46	4.34 ± 0.25	0.03 ± 0.02	1.34 ± 0.26
		20% Qz, 5% Il, 3% Ab, 3% Hm	5.63 ± 0.54	2.37 ± 0.54	4.37 ± 0.29	0.04 ± 0.02	0.88 ± 0.30
Fb057_frac	8	20% Qz	5.85 ± 0.58	2.15 ± 0.58	3.53 ± 0.32	0.03 ± 0.02	1.22 ± 0.19
		20% Qz, 5% Il, 3% Ab, 3% Hm	5.50 ± 0.68	2.50 ± 0.68	3.42 ± 0.38	0.04 ± 0.02	0.73 ± 0.21

Table A13: Electron microprobe analyses of authigenic illite from the northern margin of the NGB, mean and standard deviation of n analyses. <d.l. = below detection limit.

sample_no.	n	chemical composition [wt.-%]				
		SiO_2	TiO_2	Al_2O_3	Fe_2O_3	MgO
Fe014_11-15	4	52.49 ± 0.71	<d.l.	25.53 ± 0.52	2.58 ± 0.07	4.14 ± 0.18
Sw029_5-14	2	41.39 ± 1.77	0.09 ± 0.05	24.40 ± 1.20	1.21 ± 0.18	1.65 ± 0.67

sample_no.	n	stuctural formula [apfu], number of ions on the basis of 22 oxygen equivalents				
		Si	Al (IV)	AL (VI)	Ti	Fe^{3+}
Fe014_11-15	4	6.98 ± 0.06	1.02 ± 0.06	2.99 ± 0.03	<d.l.	0.29 ± 0.01
Sw029_5-14	2	6.73 ± 0.15	1.27 ± 0.15	3.40 ± 0.17	0.01 ± 0.01	0.16 ± 0.02

Table A12: EMP authigenic chlorite, continuation.

MnO	CaO	Na_2O	K_2O	Total
0.06 ± 0.02	0.22 ± 0.10	<d.l.	0.22 ± 0.23	83.89 ± 1.33
0.54 ± 0.06	<d.l.	<d.l.	<d.l.	84.93 ± 0.22
0.09 ± 0.02	<d.l.	0.73 ± 0.38	0.74 ± 0.15	87.55 ± 1.29
0.13 ± 0.06	0.05 ± 0.02	0.84 ± 0.21	1.56 ± 0.11	87.58 ± 1.32
0.11 ± 0.03	0.13 ± 0.13	0.85 ± 0.20	0.70 ± 0.03	85.99 ± 1.00

Mg	Mn	OCT.	Fe/(Fe+Mg)	Ca	Na	K
6.50 ± 0.34	0.01 ± 0.00	10.99 ± 0.14	0.13 ± 0.01	0.05 ± 0.02	<d.l.	0.06 ± 0.06
5.14 ± 1.16	0.10 ± 0.01	12.00 ± 0.02	0.45 ± 0.11	<d.l.	<d.l.	<d.l.
5.77 ± 0.88	0.02 ± 0.01	10.65 ± 0.85	0.16 ± 0.03	<d.l.	0.34 ± 0.17	0.23 ± 0.06
6.64 ± 1.07	0.02 ± 0.01	10.96 ± 0.99	0.08 ± 0.04	<d.l.	0.21 ± 0.19	0.10 ± 0.06
4.60 ± 0.48	0.03 ± 0.01	10.35 ± 0.35	0.23 ± 0.04	0.01 ± 0.01	0.40 ± 0.10	0.49 ± 0.04
5.29 ± 0.58	0.03 ± 0.02	10.62 ± 0.41	0.14 ± 0.04	0.01 ± 0.01	0.26 ± 0.11	0.40 ± 0.05
6.11 ± 0.55	0.02 ± 0.01	10.92 ± 0.44	0.17 ± 0.01	0.04 ± 0.04	0.41 ± 0.09	0.23 ± 0.01
7.06 ± 0.67	0.03 ± 0.01	11.28 ± 0.52	0.09 ± 0.02	0.04 ± 0.04	0.27 ± 0.11	0.09 ± 0.01

Table A13: EMP authigenic illite, continuation.

MnO	CaO	Na_2O	K_2O	Total
<d.l.	0.11 ± 0.02	0.05 ± 0.01	10.43 ± 0.12	95.34 ± 0.60
<d.l.	0.77 ± 0.30	0.42 ± 0.42	7.19 ± 0.49	77.08 ± 1.71

Mg	Mn	OCT.	Si/Al	Ca	Na	K
0.82 ± 0.04	<d.l.	4.10 ± 0.01	1.75 ± 0.06	0.02 ± 0.00	0.01 ± 0.00	1.77 ± 0.01
0.40 ± 0.16	<d.l.	3.98 ± 0.00	1.44 ± 0.13	0.13 ± 0.05	0.13 ± 0.14	1.49 ± 0.07

Table A14: X-ray fluorescence analyses of fine- to medium grained Rotliegend sandstones from the northern margin of the NGB. <d.l. = below detection limit. *Ba measured as trace element, but calculated as BaO to allow for partly high Ba contents.

sample-	main elements [wt.-%]													
no.	SiO_2	TiO_2	Al_2O_3	Fe_2O_3	MnO	MgO	CaO	Na_2O	K_2O	P_2O_5	BaO*	SO_3	LOI	Total
Fe010	68.21	0.56	8.74	4.04	0.35	1.35	5.35	2.89	1.19	0.10	0.04	0.01	5.63	98.45
Fe011	66.39	0.47	7.67	3.48	0.73	0.86	7.26	2.92	1.12	0.08	0.23	0.17	6.82	98.18
Fe029	68.47	0.60	9.36	4.29	0.31	1.60	4.23	2.62	1.63	0.11	0.02	<d.l.	4.93	98.18
Fe013	70.35	0.44	9.63	3.97	0.15	1.19	2.88	1.63	3.33	0.10	0.05	<d.l.	3.76	97.48
Fe014	70.15	0.62	9.98	4.74	0.15	0.95	2.38	1.74	3.52	0.12	0.05	<d.l.	3.28	97.68
Fe015	70.32	0.80	9.02	5.74	0.16	0.85	2.58	1.60	2.89	0.12	0.06	0.01	3.44	97.58
Fe016	71.10	0.71	9.37	5.62	0.12	0.88	1.77	1.56	3.21	0.12	0.04	<d.l.	2.61	97.11
Fe018	69.41	0.58	10.39	5.61	0.15	1.22	2.29	1.54	3.74	0.13	0.05	<d.l.	3.23	98.34
Fe019	73.09	0.48	8.79	3.86	0.14	0.79	2.84	1.52	2.95	0.10	0.03	<d.l.	3.53	98.11
Fe021	71.84	0.24	9.26	1.92	0.68	2.98	3.67	1.18	2.58	0.06	0.06	0.08	5.75	100.28
Sw003	62.07	0.54	7.73	3.67	0.52	1.89	9.10	3.04	0.61	0.08	0.09	1.18	9.33	99.85
Sw010	67.64	0.34	5.93	2.96	0.18	0.49	6.48	1.48	0.99	0.07	4.23	0.71	7.65	99.15
Sw012	71.62	0.41	8.43	4.21	0.16	0.60	5.03	1.92	1.61	0.08	0.15	0.03	6.10	100.35
Sw013	73.60	0.43	7.47	3.48	0.15	0.62	4.87	1.42	1.61	0.07	0.18	0.04	6.27	100.21
Sw015	71.55	0.30	6.22	2.91	0.20	0.42	7.34	1.66	0.95	0.07	0.53	0.12	7.79	100.07
Sw016	66.14	0.27	5.25	2.59	0.17	0.37	7.70	1.58	0.72	0.06	4.70	1.37	8.03	98.95
Sw017	68.96	0.33	5.80	3.23	0.20	0.43	7.74	1.58	0.83	0.06	1.33	0.28	8.23	99.00
Sw018	70.17	0.32	6.32	3.05	0.25	0.50	8.09	1.48	1.04	0.06	0.20	0.03	8.34	99.86
Sw020	71.05	0.46	7.73	3.67	0.21	0.60	5.92	1.68	1.54	0.08	0.05	<d.l.	6.96	99.95
Sw022	70.08	0.22	4.70	1.86	0.30	0.42	9.66	0.88	0.93	0.05	0.84	0.33	9.23	99.50
Sw024	70.96	0.29	4.72	2.40	0.29	0.39	9.45	1.09	0.85	0.06	0.28	0.14	8.96	99.88
Sw025	74.24	0.47	6.35	3.23	0.18	0.48	5.43	1.42	1.22	0.09	0.14	0.02	6.39	99.66
Sw026	77.21	0.29	4.83	2.18	0.14	0.33	5.71	1.21	0.76	0.07	0.48	0.08	6.71	100.01
Sw027	73.56	0.21	4.21	1.87	0.21	0.30	7.98	1.06	0.59	0.05	0.59	0.08	8.57	99.29
Sw029	75.19	0.23	4.50	1.87	0.10	0.30	4.75	1.23	0.75	0.06	3.69	1.02	6.21	99.89
Sw030	76.42	0.31	4.98	2.54	0.14	0.34	6.14	1.25	0.83	0.07	0.19	0.03	7.06	100.29
Sw031	67.44	0.23	4.45	1.69	0.07	0.33	4.22	1.02	0.82	0.06	11.91	1.58	6.21	100.01
Sw032	81.80	0.37	6.28	3.18	0.03	0.41	0.48	1.35	1.33	0.09	0.78	0.12	3.04	99.25
Fb035	78.95	0.39	2.82	1.87	0.16	3.63	3.88	0.66	0.18	0.03	0.00	<d.l.	6.86	99.44
Fb036	82.67	0.28	3.47	1.44	0.12	2.69	2.47	1.00	0.22	0.04	0.00	<d.l.	4.72	99.11
Fb038	83.43	0.26	3.09	1.42	0.10	2.70	2.48	0.82	0.20	0.03	0.00	<d.l.	4.77	99.31
Fb039	83.15	0.33	3.14	1.50	0.10	2.67	2.35	0.86	0.21	0.04	0.00	<d.l.	4.59	98.94
Fb040	79.72	0.46	4.50	1.80	0.13	3.23	2.38	0.89	0.39	0.05	0.01	<d.l.	4.89	98.45
Fb041	83.24	0.21	3.40	0.88	0.17	2.38	2.96	1.00	0.22	0.02	0.00	<d.l.	4.98	99.46
Fb042	83.86	0.44	3.19	1.71	0.12	2.28	2.38	0.72	0.21	0.02	0.00	<d.l.	4.23	99.17
Fb043	83.33	0.17	3.06	0.94	0.18	2.78	3.16	0.74	0.21	0.03	0.00	<d.l.	5.39	99.98
Fb044	79.17	0.51	5.96	2.57	0.10	2.96	2.04	1.38	0.49	0.04	0.01	<d.l.	4.42	99.64
Fb045	79.26	0.09	2.24	1.13	0.24	3.08	5.58	0.73	0.17	0.03	0.00	<d.l.	7.93	100.48
Fb046	81.02	0.49	5.80	2.23	0.08	2.75	1.84	1.52	0.38	0.05	0.00	<d.l.	4.06	100.23
Fb047	79.59	0.28	3.37	1.49	0.18	3.09	4.01	1.12	0.21	0.02	0.00	<d.l.	6.60	99.96
Fb049	87.74	0.16	2.99	1.17	0.10	1.84	1.66	0.91	0.18	0.03	0.00	<d.l.	3.23	100.02
Fb050	88.40	0.12	2.90	1.09	0.08	1.78	1.39	0.83	0.19	0.02	0.01	<d.l.	3.01	99.81
Fb051	88.07	0.25	3.07	1.24	0.05	2.25	1.20	0.65	0.19	0.04	0.00	<d.l.	2.85	99.87
Fb052	87.33	0.14	2.63	0.82	0.09	2.32	1.91	0.67	0.15	0.02	0.00	<d.l.	3.78	99.87
Fb054	81.61	0.33	4.77	1.70	0.11	1.44	4.02	1.48	0.30	0.03	0.01	<d.l.	4.31	100.10
Fb055	79.54	0.50	4.88	2.18	0.13	3.00	2.57	1.45	0.34	0.06	0.00	<d.l.	4.98	99.64
Fb057	85.63	0.23	2.02	1.13	0.13	2.37	2.61	0.54	0.13	0.02	0.00	<d.l.	4.66	99.50
Fb058	86.90	0.38	2.35	1.49	0.10	2.17	1.97	0.60	0.16	0.03	0.00	<d.l.	3.73	99.87
Fb059	87.47	0.21	2.25	1.06	0.11	2.00	2.03	0.69	0.16	0.03	0.00	<d.l.	3.82	99.83

Table A14: XFR sandstones, continuation.

sample-	trace elements [ppm]												
no.	Cl	V	Cr	Co	Ni	Cu	Zn	Rb	Sr	Y	Zr	Ba	Pb
Fe010	548	72	147	12	31	22	121	57	100	32	214	317	15
Fe011	538	65	157	11	22	23	70	46	136	36	221	2036	15
Fe029	547	68	206	15	34	21	109	78	92	29	232	217	14
Fe013	541	55	94	10	24	13	63	138	84	40	212	418	12
Fe014	596	58	179	5	19	14	101	153	86	48	238	471	14
Fe015	631	73	467	5	20	21	149	147	96	42	283	499	16
Fe016	599	66	273	5	21	12	98	152	83	43	253	375	14
Fe018	661	61	176	8	25	18	75	153	84	46	243	406	15
Fe019	485	50	198	5	16	12	83	138	84	42	202	235	12
Fe021	348	14	21	11	16	25	66	145	61	38	143	517	145
Sw003	528	69	131	8	21	20	51	28	202	31	314	793	10
Sw010	2195	96	156	11	48	51	81	56	2088	13	351	37852	15
Sw012	2301	60	141	8	28	22	49	78	131	31	240	1326	14
Sw013	3082	59	166	10	25	28	69	75	173	20	297	1643	14
Sw015	3655	52	97	8	20	26	58	48	278	19	118	4777	14
Sw016	4276	98	118	10	37	56	67	39	2265	9	191	42089	18
Sw017	3434	64	126	7	26	28	59	48	546	21	169	11946	16
Sw018	2343	49	96	8	21	20	41	54	160	22	131	1762	13
Sw020	3612	58	110	9	24	22	49	76	123	25	257	444	14
Sw022	2099	40	69	7	17	19	37	53	349	23	92	7553	9
Sw024	3548	42	104	9	17	20	41	45	169	24	168	2465	10
Sw025	3506	57	123	8	22	24	71	59	157	21	421	1285	13
Sw026	4859	43	82	7	16	23	80	43	263	14	180	4315	13
Sw027	4115	37	70	7	16	23	64	39	296	17	122	5304	13
Sw029	10966	82	95	13	31	61	109	49	1441	8	219	33065	19
Sw030	5429	46	89	8	17	23	73	45	170	16	193	1658	13
Sw031	4877	189	125	12	70	117	122	41	6778	<d.l.	526	106673	22
Sw032	3770	61	95	9	24	34	67	64	345	15	284	6980	16
Fb035	829	36	263	7	17	13	60	13	34	17	245	<d.l.	8
Fb036	1465	30	144	8	17	12	46	6	39	2	173	9	5
Fb038	1212	27	118	6	17	10	40	13	39	13	181	41	5
Fb039	1127	30	156	6	17	10	42	13	28	17	300	<d.l.	6
Fb040	547	42	214	6	25	6	83	20	33	20	492	68	7
Fb041	864	21	77	7	15	2	33	14	36	11	129	<d.l.	8
Fb042	769	35	328	7	16	2	112	13	27	16	368	<d.l.	6
Fb043	542	22	73	6	14	1	31	13	26	14	108	23	5
Fb044	790	46	222	8	33	4	81	23	41	20	423	87	8
Fb045	440	20	24	6	10	1	12	12	24	14	43	<d.l.	6
Fb046	718	43	207	8	28	4	77	20	38	17	396	39	7
Fb047	639	28	145	6	14	2	48	14	26	14	195	<d.l.	7
Fb049	1336	22	44	6	14	5	23	13	33	11	69	<d.l.	7
Fb050	935	19	29	5	14	4	18	13	32	10	56	80	6
Fb051	1000	27	63	6	18	4	32	13	33	10	93	9	7
Fb052	522	22	47	6	13	2	30	11	22	11	82	<d.l.	7
Fb054	407	33	154	7	29	5	56	17	29	22	161	75	8
Fb055	674	40	249	8	32	7	76	20	29	18	385	19	9
Fb057	877	25	146	6	16	2	49	11	25	18	141	<d.l.	7
Fb058	894	34	278	8	17	5	87	12	29	19	226	<d.l.	7
Fb059	784	23	117	6	15	4	43	12	26	15	127	<d.l.	6

Table A15: Carbon and oxygen isotopic composition of calcite cements, dolomite cements, and vein calcites of Rotliegend and Carboniferous sandstones from the northern margin of the NGB, analysed from bulk rock samples.

calcite cement (Rotliegend)		
sample-no.	**$d^{13}C$**	**$d^{18}O$**
	[‰ V-PDB]	**[‰ V-PDB]**
Fe010	-0.03	-10.29
Fe011	0.44	-10.06
Fe014	0.28	-11.13
Fe015	0.19	-11.67
Fe018	0.40	-11.58
Fe019	0.42	-11.70
Fe028	0.37	-9.48
Fe029	0.34	-10.25
Sw010	-1.32	-7.95
Sw013	-1.28	-8.09
Sw015	-1.79	-8.38
Sw016	-1.57	-8.35
Sw018	-1.84	-8.35
Sw022	-2.39	-7.55
Sw024	-2.38	-8.27
Sw026	-2.52	-7.76
Sw027	-2.79	-8.18
Sw029	-2.90	-7.81
Sw031	-2.91	-7.44
Fb054	-6.29	-10.97

calcite cement (Carboniferous)		
sample-no.	**$d^{13}C$**	**$d^{18}O$**
	[‰ V-PDB]	**[‰ V-PDB]**
Sw034	-1.38	-10.84
Sw036b	1.44	-10.99

dolomite cement (Rotliegend)		
sample-no.	**$d^{13}C$**	**$d^{18}O$**
	[‰ V-PDB]	**[‰ V-PDB]**
Fb035	-5.78	-10.85
Fb036	-4.89	-7.62
Fb039	-5.29	-8.76
Fb040	-5.10	-4.71
Fb044	-5.38	-4.39
Fb052	-5.19	-4.60
Fb055	-5.63	-8.99
Fb057	-5.78	-7.45
Fb059	-5.68	-7.52

vein calcite (Rotliegend)		
sample-no.	**$d^{13}C$**	**$d^{18}O$**
	[‰ V-PDB]	**[‰ V-PDB]**
Fe009	0.86	-9.96
Fe017	-1.28	-11.64
Fe023	-0.08	-11.03
Fb044-K	-5.56	-3.48
Fb052-K	-6.03	-7.19
Fb059-K	-6.79	-7.79

vein calcite (Carboniferous)		
sample-no.	**$d^{13}C$**	**$d^{18}O$**
	[‰ V-PDB]	**[‰ V-PDB]**
Sw034b	-1.06	-11.98
Sw039	-0.51	-11.01

Table A16: Calculated masses of Fe for red and grey sandstones and for authigenic Fe-bearing minerals in the sandstones of the NGB. The calculations are based on available petrographic and geochemical data. *) No detailed quantitative data about the percentage of ankerite in Rotliegend sandstones available.

	kg Fe per m³ sandstone			
	min	mean	max	
total Fe of red sandstones	10	30	80	
total Fe of grey sandstones	6	19	36	
Fe available due to bleaching, assuming dissolution of 0.3 to 1 wt.-% hematite	6	to	17	
Fe stored in hematite coatings	6	21	37	
Fe stored in late Fe-rich chlorite	0	8	38	
Fe stored in ankerite		locally up to	~35	(assumed) *)
Fe stored in siderite		locally up to	115	

Selbständigkeitserklärung

Ich erkläre, dass ich die vorliegende Arbeit selbständig und unter Verwendung der angegebenen Hilfsmittel, persönlichen Mitteilungen und Quellen angefertigt habe.

.....

Jena, 1. Mai 2006 Robert Schöner